László P. Kollár
George S. Springer

MECHANICS OF
Composite Structures

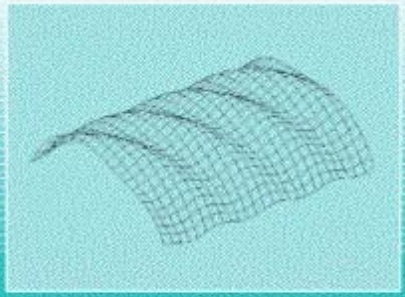

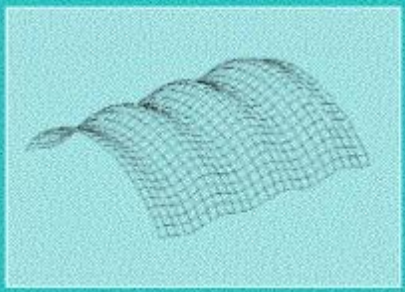

CAMBRIDGE

CAMBRIDGE
More information - www.cambridge.org/9780521801652

MECHANICS OF COMPOSITE STRUCTURES

An increase in the use of composite materials in many areas of engineering has led to a greater demand for engineers versed in the design of structures made from such materials. Although numerous books offer introductions to composites, few demonstrate advanced concepts or emphasize structures.

This book addresses that need by offering students and engineers tools for designing practical composite structures. The focus is on fiber-reinforced composites composed of fibers embedded in a matrix. Among the topics of interest to the designer are stress–strain relationships for a wide range of anisotropic materials; bending, buckling, and vibration of plates; bending, torsion, buckling, and vibration of solid as well as thin-walled beams; shells; hygrothermal stresses and strains; finite element formulation; and failure criteria. The emphasis is on analyses that lead to methods applicable to a variety of structural design problems. The expressions resulting from the analyses are either readily usable or can be translated into a computer algorithm. More than 300 illustrations, 50 fully worked problems, and material properties data sets are included. Some knowledge of composites, differential equations, and matrix algebra is helpful but not necessary, for the book is self-contained.

This book will be of great practical use to graduate students, researchers, and practicing engineers seeking to acquire advanced knowledge of the mechanics of composites and of the applications of composite materials.

László P. Kollár is Professor in the Department of Architecture at the Budapest University of Technology and Economics.

George S. Springer is Paul Pigott Professor of Engineering in the Department of Aeronautics and Astronautics at Stanford University.

CAMBRIDGE UNIVERSITY PRESS
Cambridge, New York, Melbourne, Madrid, Cape Town, Singapore, São Paulo

Cambridge University Press
The Edinburgh Building, Cambridge CB2 2RU, United Kingdom

Published in the United States of America by Cambridge University Press, New York

www.cambridge.org

Information on this title: www.cambridge.org/9780521801652

© Cambridge University Press 2003

This book is in copyright. Subject to statutory exception and to the provision of relevant collective licensing agreements, no reproduction of any part may take place without the written permission of Cambridge University Press.

First published in print format 2003

ISBN-13 978-0-511-05703-8 eBook (Adobe Reader)
ISBN-10 0-511-05703-2 eBook (Adobe Reader)

ISBN-13 978-0-521-80165-2 hardback
ISBN-10 0-521-80165-6 hardback

Cambridge University Press has no responsibility for the persistence or accuracy of URLs for external or third-party internet websites referred to in this book, and does not guarantee that any content on such websites is, or will remain, accurate or appropriate.

Contents

Preface *page* xi
List of Symbols xiii

1 Introduction 1

2 Displacements, Strains, and Stresses 3
2.1 Strain–Displacement Relations 4
2.2 Equilibrium Equations 6
2.3 Stress-Strain Relationships 8
2.3.1 Generally Anisotropic Material 8
2.3.2 Monoclinic Material 11
2.3.3 Orthotropic Material 14
2.3.4 Transversely Isotropic Material 19
2.3.5 Isotropic Material 20
2.4 Plane–Strain Condition 22
2.4.1 Free End – Generally Anisotropic Material 28
2.4.2 Free End – Monoclinic Material 30
2.4.3 Free End – Orthotropic, Transversely Isotropic, or Isotropic Material 34
2.4.4 Built-In Ends – Generally Anisotropic Material 35
2.4.5 Built-In Ends – Monoclinic Material 36
2.4.6 Built-In Ends – Orthotropic, Transversely Isotropic, or Isotropic Material 38
2.5 Plane-Stress Condition 38
2.6 Hygrothermal Strains and Stresses 44
2.6.1 Plane-Strain Condition 47
2.6.2 Plane-Stress Condition 47
2.7 Boundary Conditions 47
2.8 Continuity Conditions 48
2.9 Stress and Strain Transformations 49
2.9.1 Stress Transformation 50
2.9.2 Strain Transformation 52
2.9.3 Transformation of the Stiffness and Compliance Matrices 53

2.10 Strain Energy 55
2.10.1 The Ritz Method 55
2.11 Summary 56
2.11.1 Note on the Compliance and Stiffness Matrices 56

3 Laminated Composites 63
3.1 Laminate Code 63
3.2 Stiffness Matrices of Thin Laminates 65
3.2.1 The Significance of the [A], [B], and [D] Stiffness Matrices 72
3.2.2 Stiffness Matrices for Selected Laminates 74

4 Thin Plates 89
4.1 Governing Equations 90
4.1.1 Boundary Conditions 92
4.1.2 Strain Energy 92
4.2 Deflection of Rectangular Plates 93
4.2.1 Pure Bending and In-Plane Loads 93
4.2.2 Long Plates 94
4.2.3 Simply Supported Plates – Symmetrical Layup 100
4.2.4 Plates with Built-In Edges – Orthotropic and Symmetrical Layup 107
4.3 Buckling of Rectangular Plates 112
4.3.1 Simply Supported Plates – Symmetrical Layup 112
4.3.2 Plates with Built-In and Simply Supported Edges – Orthotropic and Symmetrical Layup 118
4.3.3 Plates with One Free Edge – Orthotropic and Symmetrical Layup 124
4.3.4 Plates with Rotationally Restrained Edges – Orthotropic and Symmetrical Layup 127
4.3.5 Long Plates 132
4.4 Free Vibration of Rectangular Plates 141
4.4.1 Long Plates 141
4.4.2 Simply Supported Plates – Symmetrical Layup 144
4.4.3 Plates with Built-In and Simply Supported Edges – Orthotropic and Symmetrical Layup 149
4.5 Hygrothermal Effects 151
4.5.1 Change in Thickness Due to Hygrothermal Effects 161
4.6 Plates with a Circular or an Elliptical Hole 163
4.7 Interlaminar Stresses 166

5 Sandwich Plates 169
5.1 Governing Equations 170
5.1.1 Boundary Conditions 172
5.1.2 Strain Energy 173
5.1.3 Stiffness Matrices of Sandwich Plates 174
5.2 Deflection of Rectangular Sandwich Plates 178
5.2.1 Long Plates 178
5.2.2 Simply Supported Sandwich Plates – Orthotropic and Symmetrical Layup 182

5.3 Buckling of Rectangular Sandwich Plates 185
5.3.1 Long Plates 185
5.3.2 Simply Supported Plates – Orthotropic and Symmetrical Layup 187
5.3.3 Face Wrinkling 190
5.4 Free Vibration of Rectangular Sandwich Plates 196
5.4.1 Long Plates 196
5.4.2 Simply Supported Plates – Orthotropic and Symmetrical Layup 199

6 Beams 203
6.1 Governing Equations 203
6.1.1 Boundary Conditions 205
6.1.2 Stiffness Matrix 205
6.1.3 Compliance Matrix 209
6.1.4 Replacement Stiffnesses 210
6.2 Rectangular, Solid Beams Subjected to Axial Load and Bending 210
6.2.1 Displacements – Symmetrical Layup 211
6.2.2 Displacements – Unsymmetrical Layup 213
6.2.3 Stresses and Strains 214
6.3 Thin-Walled, Open-Section Orthotropic or Symmetrical Cross-Section Beams Subjected to Axial Load and Bending 217
6.3.1 Displacements of T-Beams 217
6.3.2 Displacements of L-Beams 221
6.3.3 Displacements of Arbitrary Cross-Section Beams 226
6.3.4 Stresses and Strains 233
6.4 Thin-Walled, Closed-Section Orthotropic Beams Subjected to Axial Load and Bending 243
6.5 Torsion of Thin-Walled Beams 248
6.5.1 Thin Rectangular Cross Section 248
6.5.2 Open-Section Orthotropic Beams 250
6.5.3 Closed-Section Orthotropic Beams – Single Cell 252
6.5.4 Closed-Section Orthotropic Beams – Multicell 260
6.5.5 Restrained Warping – Open-Section Orthotropic Beams 261
6.5.6 Restrained Warping – Closed-Section Orthotropic Beams 264
6.6 Thin-Walled Beams with Arbitrary Layup Subjected to Axial Load, Bending, and Torsion 265
6.6.1 Displacements of Open- and Closed-Section Beams 267
6.6.2 Stresses and Strains in Open- and Closed-Section Beams 268
6.6.3 Centroid 271
6.6.4 Restrained Warping 271
6.7 Transversely Loaded Thin-Walled Beams 274
6.7.1 Beams with Orthotropic Layup or with Symmetrical Cross Section 276
6.7.2 Beams with Arbitrary Layup 280
6.7.3 Shear Center 283
6.8 Stiffened Thin-Walled Beams 288

6.9 Buckling of Beams 290
6.9.1 Beams Subjected to Axial Load (Flexural–Torsional Buckling) 291
6.9.2 Lateral–Torsional Buckling of Orthotropic Beams with Symmetrical Cross Section 296
6.9.3 Local Buckling 300
6.10 Free Vibration of Beams (Flexural–Torsional Vibration) 306
6.10.1 Doubly Symmetrical Cross Sections 306
6.10.2 Beams with Symmetrical Cross Sections 309
6.10.3 Beams with Unsymmetrical Cross Sections 309
6.11 Summary 312

7 Beams with Shear Deformation 313
7.1 Governing Equations 314
7.1.1 Strain–Displacement Relationships 315
7.1.2 Force–Strain Relationships 315
7.1.3 Equilibrium Equations 320
7.1.4 Summary of Equations 320
7.1.5 Boundary Conditions 321
7.2 Stiffnesses and Compliances of Beams 321
7.2.1 Shear Stiffnesses and Compliances of Thin-Walled Open-Section Beams 322
7.2.2 Shear Stiffnesses and Compliances of Thin-Walled Closed-Section Beams 325
7.2.3 Stiffnesses of Sandwich Beams 326
7.3 Transversely Loaded Beams 329
7.4 Buckling of Beams 334
7.4.1 Axially Loaded Beams with Doubly Symmetrical Cross Sections (Flexural and Torsional Buckling) 335
7.4.2 Axially Loaded Beams with Symmetrical or Unsymmetrical Cross Sections (Flexural–Torsional Buckling) 341
7.4.3 Lateral–Torsional Buckling of Beams with Symmetrical Cross Section 345
7.4.4 Summary 346
7.5 Free Vibration of Beams 347
7.5.1 Beams with Doubly Symmetrical Cross Sections 347
7.5.2 Beams with Symmetrical or Unsymmetrical Cross Sections 356
7.5.3 Summary 359
7.6 Effect of Shear Deformation 359

8 Shells 365
8.1 Shells of Revolution with Axisymmetrical Loading 367
8.2 Cylindrical Shells 368
8.2.1 Membrane Theory 368
8.2.2 Built-In Ends 370
8.2.3 Temperature – Built-In Ends 379
8.3 Springback 380
8.3.1 Springback of Cylindrical Shells 380
8.3.2 Doubly Curved Shells 384

8.4 Buckling of Shells 384
8.4.1 Buckling of Cylinders 387

9 Finite Element Analysis 395
9.1 Three-Dimensional Element 396
9.2 Plate Element 397
9.3 Beam Element 397
9.4 Sublaminate 398
9.4.1 Step 1. Elements of $[J]$ due to In-Plane Stresses 400
9.4.2 Step 2. Elements of $[J]$ due to Out-of-Plane Normal Stresses 403
9.4.3 Step 3. Elements of $[J]$ due to Out-of-Plane Shear Stresses 405
9.4.4 Step 4. The Stiffness Matrix 407

10 Failure Criteria 411
10.1 Quadratic Failure Criterion 413
10.1.1 Orthotropic Material 414
10.1.2 Transversely Isotropic Material 420
10.1.3 Isotropic Material 421
10.1.4 Plane-Strain and Plane-Stress Conditions 422
10.1.5 Proportional Loading – Stress Ratio 423
10.2 "Maximum Stress" Failure Criterion 425
10.3 "Maximum Strain" Failure Criterion 426
10.4 Plate with a Hole or a Notch 430
10.4.1 Plate with a Circular Hole 431
10.4.2 Plate with a Notch 434
10.4.3 Characteristic Length 434

11 Micromechanics 436
11.1 Rule of Mixtures 436
11.1.1 Longitudinal Young Modulus E_1 438
11.1.2 Transverse Young Modulus E_2 439
11.1.3 Longitudinal Shear Modulus G_{12} 439
11.1.4 Transverse Shear Modulus G_{23} 440
11.1.5 Longitudinal Poisson Ratio ν_{12} 441
11.1.6 Transverse Poisson Ratio ν_{23} 442
11.1.7 Thermal Expansion Coefficients 443
11.1.8 Moisture Expansion Coefficients 445
11.1.9 Thermal Conductivity 446
11.1.10 Moisture Diffusivity 447
11.1.11 Specific Heat 448
11.2 Modified Rule of Mixtures 448
11.3 Note on the Micromechanics Models 449

Appendix A. Cross-Sectional Properties of Thin-Walled Composite Beams 453

Appendix B. Buckling Loads and Natural Frequencies of Orthotropic Beams with Shear Deformation 461

Appendix C. Typical Material Properties 464

Index 469

Preface

The increased use of composites in aerospace, land, and marine applications has resulted in a growing demand for engineers versed in the design of structures made of fiber-reinforced composite materials. To satisfy this demand, and to introduce engineers to the subject of composites, numerous excellent texts have been published dealing with the mechanics of composites. These texts deal with those fundamental aspects needed by engineers new to the subject. Our book addresses topics not generally covered by existing texts but that are necessary for designing practical structures. Among the topics in this book of special interest to the designer, but that usually are not included in standard texts, are stress–strain relationships for a wide range of anisotropic materials; bending, buckling, and vibration of plates; bending, torsion, buckling, and vibration of solid as well as thin-walled beams; shells; hygrothermal stresses and strains; and finite element formulation. The material is presented in sufficient detail to enable the reader to follow the developments leading to the final results. The expressions resulting from the analyses are either readily usable or can be translated into a computer algorithm. Thus, the book should be useful to students and researchers wishing to acquire knowledge of some of the advanced concepts of the mechanics of composites as well as to engineers engaged in the design of structures made of composite materials.

The emphasis is on analyses built on fundamental concepts that are applicable to a variety of structural design problems. In presenting the material we have strived to follow the outline commonly used in texts dealing with the analysis of structures made of isotropic materials. We have consciously omitted empirical approaches. Test results are certainly of value to the engineer. However, for composites, these mostly apply only under specific circumstances and cannot readily be generalized to different materials and different applications. We have included material properties data to help the designer perform calculations without the need to search the literature.

The book is self-contained. Nevertheless, the reader will find it helpful to have a background in mechanics and in composites and some knowledge of differential

equations and matrix algebra. We have made an effort to keep the notation as uniform as practicable and reasonably consistent with accepted usage. The principal symbols are summarized in a list of symbols.

We are grateful to Professor István Hegedűs for his constructive comments. We thank Dr. Rita Kiss, Gabriella Tarján, and Anikó Pluzsik for proofreading portions of the manuscript, Gabriella Tarján for preparing the illustrations, and Eric Allison and Sarah Brennan for their help in compiling the index.

László P. Kollár
Budapest

George S. Springer
Stanford

List of Symbols

We have used, wherever possible, notation standard in elasticity, structural analysis, and composite materials. We tried to avoid duplication, although there is some repetition of those symbols that are used only locally. In the following list we have not included those symbols that pertain only to the local discussion. Below, we give a verbal description of each symbol and, when appropriate, the number of the equation in which the symbol is first used.

Latin letters

A	area
A^{iso}	tensile stiffness of an isotropic laminate (Eq. 3.42)
$[A]$, A_{ij}	tensile stiffness of a laminate (Eqs. 3.18, 3.19)
$[a]$, a_{ij}	inverse of the $[A]$ matrix for symmetric laminates (Eq. 3.29)
$[B]$, B_{ij}	stiffness of a laminate (Eqs. 3.18, 3.19)
$[C]$, C_{ij}	3D stiffness matrix in the x_1, x_2, x_3 coordinate system (Eq. 2.22)
$[\overline{C}]$, $\overline{C}_{ij}$	3D stiffness matrix in the x, y, z coordinate system (Eq. 2.19)
c	moisture concentration (Eq. 2.154); core thickness (Fig. 5.2)
$[D]$, D_{ij}	bending stiffness of a laminate (Eqs. 3.18, 3.19)
$[D]^*$, D^*_{ij}	reduced bending stiffness of a laminate (Eq. 4.1)
D^{iso}	bending stiffness of an isotropic laminate (Eq. 3.42)
D, $\overline{D}$, $\widehat{D}$	parameters (Table 6.2, page 222, Eq. 6.157)
$[d]$, d_{ij}	inverse of the $[D]$ matrix for symmetrical laminates (Eq. 3.30)
d, d^{t}, d^{b}	distances for sandwich plates (Fig. 5.2)
E_1, E_2, E_3	Young's moduli in the x_1, x_2, x_3 coordinate system (Table 2.5)
$[E]$	stiffness matrix in the FE calculation (Eq. 9.4)
$\widehat{EA}$	tensile stiffness of a beam (Eq. 6.8)
$\widehat{EI}$	bending stiffness of a beam (Eq. 6.8)
$\widehat{EI}_\omega$	warping stiffness of a beam (Eq. 6.244)
F_i, F_{ij}	strength parameters in the quadratic failure criterion (Eq. 10.2)

f_{ij}	constants in the quadratic failure criterion (Eq. 10.25)
f, f_{ij}	frequency (Eq. 4.190)
f_x, f_y, f_z,	body forces per unit volume (Eq. 2.13)
G_{23}, G_{13}, G_{12}	shear moduli in the x_1, x_2, x_3 coordinate system (Table 2.5)
$\widehat{GI}_t$	torsional stiffness of a beam (Eq. 6.8)
h	plate thickness
h_b, h_t	distances of the bottom and top surfaces of a plate from the reference plane (Eq. 3.9)
i_ω	polar radius of gyration (Eq. 6.340)
$[J]$	inverse of the material stiffness matrix $[E]$ (Eq. 9.16)
K	number of layers in a laminate; number of wall segments; stiffness parameter of a plate (Eq. 4.153)
$\widetilde{k}$	rotational spring constant (Eq. 4.149)
k	equivalent length factor (Eq. 6.340)
L_x, L_y	dimensions of a plate
L	length; number of cells in a multicell beam (Eq. 6.222)
L_i, L_i^f	load and failure load (Eq. 10.42)
l_x, l_x^o	half buckling length (Eq. 4.142), half buckling length corresponding to the lowest buckling load of a long plate (Eq. 4.173)
M_x, M_y, M_{xy}	bending and twist moments per unit length acting on a laminate (Eq. 3.9)
M_x^{ht}, M_y^{ht}, M_{xy}^{ht}	hygrothermal moments per unit length (Eq. 4.247)
$\widehat{M}_y$, $\widehat{M}_z$	bending moments acting on a beam (Fig. 6.2)
$\widehat{M}_\omega$	bimoment acting on a beam (Eq. 6.232)
N_x, N_y, N_{xy}	in-plane forces per unit length acting on a laminate (Eq. 3.9)
N_{x0}, N_{y0}, N_{xy0}	in-plane compressive forces per unit length (Eq. 4.109)
N_x^{ht}, N_y^{ht}, N_{xy}^{ht}	hygrothermal forces per unit length (Eq. 4.246)
$N_{x,cr}$	buckling load of a uniaxially loaded plate (Eq. 4.141)
$\widehat{N}$	axial force acting on a beam (Fig. 6.2)
$\widehat{N}_{cr}$, $\widehat{N}_{cr}^B$	buckling load and buckling load due to bending deformation (Eq. 6.337)
$\widehat{N}_{cry}$, $\widehat{N}_{crz}$	buckling load in the x–z and x–y planes, respectively (Eqs. 6.337, 7.110)
$\widehat{N}_{cr\phi}$	buckling load under torsional buckling (Eqs. 6.337, 7.110)
$[P]$, $[\overline{P}]$	stiffness matrix of a beam (Eqs. 6.2, 6.250). Without bar refers to the centroid; with bar to an arbitrarily chosen coordinate system
p	transverse load per unit area; distance between the origin and the tangent of the wall of a beam (Eq. 6.190)
p_x, p_y, p_z	axial and transverse loads (per unit length) acting on a beam (Fig. 6.1); surface forces per unit area (Eq. 2.166)
$[Q]$, Q_{ij}	2D plane-stress stiffness matrix in the x_1, x_2 coordinate system (Eq. 2.134)

$[\overline{Q}]$, $\overline{Q}_{ij}$	2D plane-stress stiffness matrix in the x, y coordinate system (Eq. 2.126)
$\widehat{Q}_{cr}$	buckling load resulting in lateral buckling (Eq. 6.359)
q	shear flow (Eq. 6.189).
R	stiffness parameter (Eq. 3.46)
$\widetilde{R}$	stress ratio (Eq. 10.42)
R_x, R_y, R_{xy}	radii of curvatures of a shell (Eq. 8.1)
$[R]$, R_{ij}	compliance matrix under plane-strain condition in the x_1, x_2 coordinate system (Eq. 2.79)
$[\overline{R}]$, $\overline{R}_{ij}$	compliance matrix under plane-strain condition in the x, y coordinate system (Eq. 2.65)
$[S]$, S_{ij}	3D compliance matrix in the x_1, x_2, x_3 coordinate system (Eq. 2.23)
$[\overline{S}]$, $\overline{S}_{ij}$	3D compliance matrix in the x, y, z coordinate system (Eq. 2.21)
$\widehat{S}_{ij}$	shear stiffness of a beam, i, $j = z, y, \omega$ (Eqs. 7.13, 7.36)
$\widetilde{S}_{ij}$	shear stiffness of a plate, i, $j = 1, 2$ (Eq. 5.15)
$\widehat{s}_{ij}$	shear compliance of a beam, i, $j = z, y, \omega$ (Eq. 7.38)
s_1^+, s_2^+, s_3^+	tensile strengths (Eq. 10.13)
s_1^-, s_2^-, s_3^-	compression strengths (Eq. 10.13)
s_{23}, s_{13}, s_{12}	shear strengths (Eq. 10.15)
$\widehat{T}$	torque acting on a beam (Fig. 6.2)
$\widehat{T}_\omega$	restrained warping-induced torque (Eq. 6.235)
$\widehat{T}_{sv}$	Saint-Venant torque (Eq. 6.239)
$[T_\sigma]$	2D stress transformation matrix (Eq. 2.182)
$[\hat{T}_\sigma]$	3D stress transformation matrix (Eq. 2.179)
$[T_\epsilon]$	2D strain transformation matrix (Eq. 2.188)
$[\hat{T}_\epsilon]$	3D strain transformation matrix (Eq. 2.185)
t	torque load acting on a beam (Fig. 6.1)
t^t, t^b	thicknesses of the top and bottom facesheets (Eq. 5.26)
U	strain energy (Eq. 2.200)
U	displacement in the x direction; varies with the x and y coordinates only (Eq. 2.50)
u	displacement in the x direction
u^o	displacement of the reference surface in the x direction
u_1, u_2, u_3	displacements in the x_1, x_2, and x_3 direction
V	displacement in the y direction; varies with the x and y coordinates only (Eq. 2.51)
V_f, V_m, V_v	volume of fibers, matrix, and void
V_x, V_y	out-of-plane shear forces per unit length (Eq. 3.10)
$\widehat{V}_y$, $\widehat{V}_z$	transverse shear forces acting on a beam (Fig. 6.2)
v	displacement in the y direction
v^o	displacement of the reference surface in the y direction
v_f, v_m, v_v	volume fraction of fibers, matrix, and void

W	displacement in the z direction; varies with the x and y coordinates only (Eq. 2.52)
$[W]$, $[\overline{W}]$	compliance matrix of a beam (Eq. 6.17). No bar refers to the centroid; bar to an arbitrarily chosen coordinate system
w	deflection in the z direction
$\widetilde{w}$	maximum deflection in the z direction (Eq. 4.29)
w^{o}	deflection of the reference surface in the z direction
w^{B}, w^{S}	deflections due to bending and shear deformations (Eq. 7.85)
y_{c}, z_{c}	coordinates of the centroid of a beam (Eqs. 6.54, 6.73)
y_{sc}, z_{sc}	coordinates of the shear center of a beam (Eq. 6.311)
z_k, z_{k-1}	coordinates of the top and bottom surfaces of the kth ply in a laminate (Eq. 3.20)

Greek letters

α	parameter describing shear deformation (Eq. 7.253)
α_i	parameter describing shear deformation, $i = w, \psi, N, \omega$ (Eq. 7.244)
$[\alpha]$, α_{ij}	compliance matrix of a laminate (Eq. 3.23)
α, β	parameters describing buckled shape of a shell (Eq. 8.78)
$\widehat{\alpha}_{ij}$	compliances for closed-section beams (Eq. 6.156)
$\widetilde{\alpha}_i$, $\widetilde{\alpha}_{ij}$	thermal expansion coefficients (Eqs. 2.153, 2.158)
β, λ	parameters in the displacements of a cylinder (Eq. 8.30)
$[\beta]$, β_{ij}	compliance matrix of a laminate (Eq. 3.23)
$\overline{\beta}_{ij}$	compliance of symmetrical cross-section beams (Table 6.2)
$\widehat{\beta}_{ij}$	compliance of closed-section beams (Eq. 6.156)
$\widetilde{\beta}_i$, $\widetilde{\beta}_{ij}$	moisture expansion coefficients in the x, y, z directions (Eqs. 2.154, 2.159)
β_1	property of the cross section (Eq. 6.360)
γ_y, γ_z	shear strain in a beam in the x–y and x–z planes (Eq. 7.2)
γ_{yz}, γ_{xz}, γ_{xy}	engineering shear strain in the x, y, z coordinate system (Eq. 2.9)
γ_{23}, γ_{13}, γ_{12}	engineering shear strain in the x_1, x_2, x_3 coordinate system
Δh	change in thickness (Eq. 4.282)
ΔT	temperature change (Eq. 2.153)
$[\delta]$, δ_{ij}	compliance matrix of a laminate (Eq. 3.23)
$\widehat{\delta}_{ij}$	compliance of closed-section beams (Eq. 6.157)
$\overline{\epsilon}_x, \ldots$	average strains in a sublaminate (Eq. 9.14)
$\epsilon_x, \epsilon_y, \epsilon_z$	engineering normal strains in the x, y, z coordinate system
$\epsilon_1, \epsilon_2, \epsilon_3$	engineering normal strains in the x_1, x_2, x_3 coordinate system
$\epsilon_x^{\mathrm{o}}, \epsilon_y^{\mathrm{o}}, \gamma_{xy}^{\mathrm{o}}$	strains of the reference surface
$\epsilon_x^{\mathrm{o,ht}}, \epsilon_y^{\mathrm{o,ht}}, \gamma_{xy}^{\mathrm{o,ht}}$	hygrothermal strains in a laminate (Eq. 4.250)
ζ	parameter of restraint (Eq. 4.152)
Θ	polar moment of mass (Eq. 6.411)

Θ_k	ply orientation
ϑ	rate of twist (Eq. 6.1)
$\vartheta^{\mathrm{B}}, \vartheta^{\mathrm{S}}$	rate of twist due to bending and shear deformation (Eq. 7.5)
$\kappa_x, \kappa_y, \kappa_{xy}$	curvatures of the reference surface (Eq. 3.8)
$\kappa_x^{\mathrm{ht}}, \kappa_y^{\mathrm{ht}}, \kappa_{xy}^{\mathrm{ht}}$	hygrothermal curvatures of a laminate (Eq. 4.250)
$\lambda, \lambda_{\mathrm{cr}}, \lambda_{ij}$	load parameter (Eq. 4.109); buckling load parameter (Eq. 4.121); eigenvalue (Eq. 4.225)
$\mu_{Bi}, \mu_{Gi}, \mu_{\mathrm{Si}}$	parameters in the calculation of natural frequencies (Eqs. 6.398, 6.400, 7.203)
ν_{ij}	Poisson's ratio
ξ, η, ζ	coordinates attached to the wall of a beam (Fig. 6.13)
ξ, ξ'	parameters in the expressions of the buckling loads of plates with rotationally restrained edges (Eq. 4.151)
π_{p}	potential energy (Eq. 2.204)
ρ_x, ρ_y, ρ_z	radius of curvature in the y–z , x–z, and x–y planes (Eq. 2.45)
ρ_1, ρ_2, ρ_3	radius of curvature in the x_2–x_3 , x_1–x_3, and x_1–x_2 planes (Eq. 2.53)
$\rho_{\mathrm{comp}}, \rho_{\mathrm{f}}, \rho_{\mathrm{m}}$	densities of composite, fiber, and matrix
ρ	mass per unit area or per unit length
$\sigma_1, \sigma_2, \sigma_3$	normal stresses in the x_1, x_2, x_3 coordinate system
$\sigma_x, \sigma_y, \sigma_z$	normal stresses in the x, y, z coordinate system
$\overline{\sigma}$	average stress
$\tau_{23}, \tau_{13}, \tau_{12}$	shear stresses in the x_1, x_2, x_3 coordinate system
$\tau_{yz}, \tau_{xz}, \tau_{yx}$	shear stresses in the x, y, z coordinate system
χ_{xz}, χ_{yz}	rotation of the normal of a plate in the x–z and x–y planes (Eqs. 3.2 and 5.1)
χ_y, χ_z	rotation of the cross section of a beam in the x–y and x–z planes (Eq. 7.2)
ψ	angle of rotation of the cross section about the beam axis (twist) (Fig. 6.3)
Ψ	bending stiffness of an unsymmetrical long plate (Eq. 4.52)
Ω	potential energy of the external loads (Eq. 2.203)
ω	circular frequency (Eq. 4.190)
$\omega^{\mathrm{B}}, \omega^{\mathrm{S}}$	circular frequency of a beam due to bending and shear deformation (Eq. 7.198)
ω_y, ω_z	circular frequency of a freely vibrating beam in the x–z and x–y planes, respectively (Eq. 6.398)
ω_ψ	circular frequency of a freely vibrating beam under torsional vibration (Eq. 6.400)
$\varrho, \widetilde{\varrho}, \bar{\varrho}, \widehat{\varrho}$	distances between the new and the old reference surfaces (Eqs. 3.47, 6.105, 6.107, A.3)

Introduction

In this book we focus on fiber-reinforced composites composed of fibers embedded in a matrix. The fibers may be short or long, continuous or discontinuous, and may be in one or in multiple directions (Fig. 1.1). Such materials offer advantages over conventional isotropic structural materials such as steel, aluminum, and other types of metal. These advantages include high strength, low weight, and good fatigue and corrosion resistance. In addition, by changing the arrangements of the fibers, the properties of the material can be tailored to meet the requirements of a specific design.

The excellent properties of composites are achieved by the favorable characteristics of the two major constituents, namely the fiber and the matrix. In low-performance composites, the reinforcements, usually in the form of short or chopped fibers (or particles), provide some stiffening but very little strengthening; the load is mainly carried by the matrix. In high-performance composites, continuous fibers provide the desirable stiffness and strength, whereas the matrix provides protection and support for the fibers, and, importantly, helps redistribute the load from broken to adjacent intact fibers.

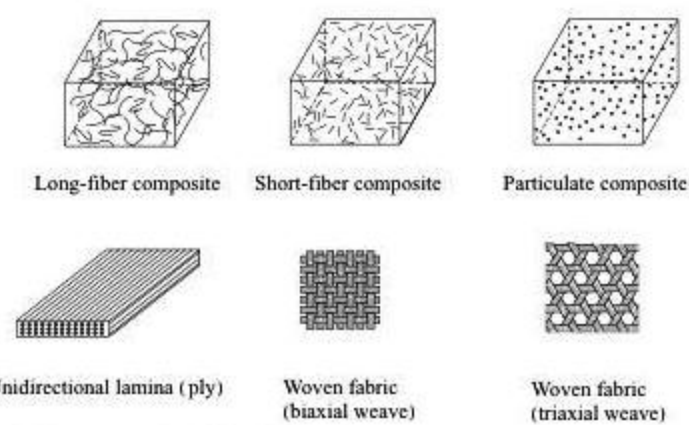

Figure 1.1: Composite material systems.

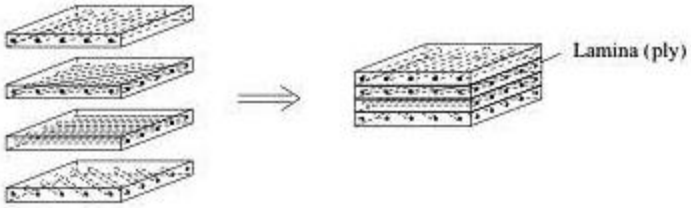

Figure 1.2: Laminated composite.

The arrangement of the fibers in a structure is governed by the structural requirements and by the process used to fabricate the part. Frequently, though not always, composite structures are made of thin layers called laminae or plies. Within each lamina, the fibers may be aligned in the same direction (unidirectional ply, Fig. 1.1) or in different directions. The latter configuration is produced, for example, by weaving the fibers in two or more directions (woven fabric). The lamina may also contain short fibers either oriented in the same direction or distributed randomly. Several laminae are then combined into a laminate to form the desired structure (Fig. 1.2).

The mechanical and thermal behaviors of a structure depend on the properties of the fibers and the matrix and on the amount and orientations of the fibers. In this book, we consider the design steps from micromechanics (which takes into account the fiber and matrix properties) through macromechanics (which treats the properties of the composite) to structural analysis. These steps are illustrated in Figure 1.3 for a structure made of laminated composite.

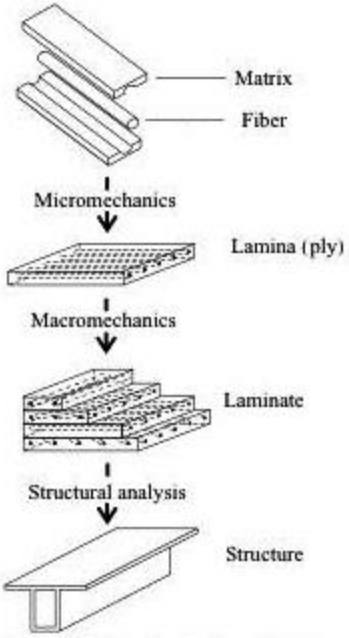

Figure 1.3: The levels of analysis for a structure made of laminated composite.

CHAPTER TWO

Displacements, Strains, and Stresses

We consider composite materials consisting of continuous or discontinuous fibers embedded in a matrix. Such a composite is heterogeneous, and the properties vary from point to point. On a scale that is large with respect to the fiber diameter, the fiber and matrix properties may be averaged, and the material may be treated as homogeneous. This assumption, commonly employed in macromechanical analyses of composites, is adopted here. Hence, the material is considered to be quasi-homogeneous, which implies that the properties are taken to be the same at every point. These properties are not the same as the properties of either the fiber or the matrix but are a combination of the properties of the constituents.

In this chapter, equations are presented for calculating the displacements, stresses, and strains when the structure undergoes only small deformations and the material behaves in a linearly elastic manner.

Continuous fiber-reinforced composite materials (and structures made of such materials) often have easily identifiable preferred directions associated with fiber orientations or symmetry planes. It is therefore convenient to employ two coordinate systems: a local coordinate system aligned, at a point, either with the fibers or with axes of symmetry, and a global coordinate system attached to a fixed reference point (Fig. 2.1). In this book the local and global Cartesian coordinate systems are designated respectively by x_1, x_2, x_3 and the x, y, z axes. In the x, y, z directions the displacements at a point A are denoted by u, v, w, and in the x_1, x_2, x_3 directions by u_1, u_2, u_3 (Fig. 2.2).

In the x, y, z coordinate system the normal stresses are denoted by σ_x, σ_y, and σ_z and the shear stresses by τ_{yz}, τ_{xz}, and τ_{xy} (Fig. 2.3). The corresponding normal and shear strains are $\epsilon_x, \epsilon_y, \epsilon_z$ and $\gamma_{yz}, \gamma_{xz}, \gamma_{xy}$, respectively.

In the x_1, x_2, x_3 coordinate system the normal stresses are denoted by σ_1, σ_2, and σ_3 and the shear stresses by τ_{23}, τ_{13}, and τ_{12} (Fig. 2.3). The corresponding normal and shear strains are $\epsilon_1, \epsilon_2, \epsilon_3$, and $\gamma_{23}, \gamma_{13}, \gamma_{12}$, respectively. The symbol γ represents engineering shear strain that is twice the tensorial shear strain, $\gamma_{ij} = 2\epsilon_{ij}$ ($i, j = x, y, z$ or $i, j = 1, 2, 3$).

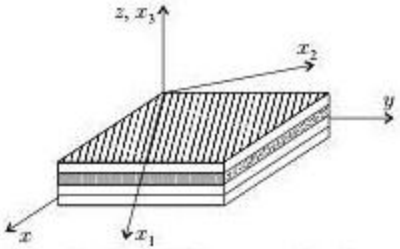

Figure 2.1: The global x, y, z and local x_1, x_2, x_3 coordinate systems.

A stress is taken to be positive when it acts on a positive face in the positive direction. According to this definition, all the stresses shown in Figure 2.3 are positive.

The preceding stress and strain notations, referred to as engineering notations, are used throughout this book. Other notations, most notably tensorial and contracted notations, can frequently be found in the literature. The stresses and strains in different notations are summarized in Tables 2.1 and 2.2.

2.1 Strain–Displacement Relations

We consider a Δx long segment that undergoes a change in length, the new length being denoted by $\Delta x'$. From Figure 2.4 it is seen that

$$u + \Delta x' = \Delta x + \left(u + \frac{\partial u}{\partial x}\Delta x\right), \tag{2.1}$$

where u and $u + \frac{\partial u}{\partial x}\Delta x$ are the displacements of points A and B, respectively, in the x direction. Accordingly, the normal strain in the x direction is

$$\epsilon_x = \frac{\Delta x' - \Delta x}{\Delta x} = \frac{\partial u}{\partial x}. \tag{2.2}$$

Similarly, in the y and z directions the normal strains are

$$\epsilon_y = \frac{\partial v}{\partial y} \tag{2.3}$$

$$\epsilon_z = \frac{\partial w}{\partial z}, \tag{2.4}$$

where v and w are the displacements in the y and z directions, respectively.

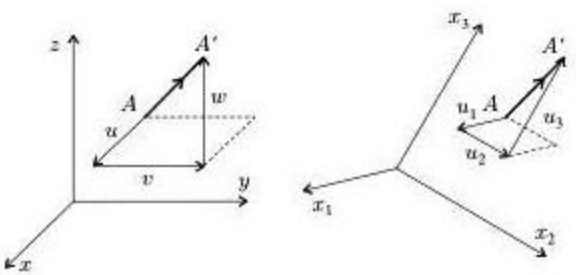

Figure 2.2: The x, y, z and x_1, x_2, x_3 coordinate systems and the corresponding displacements.

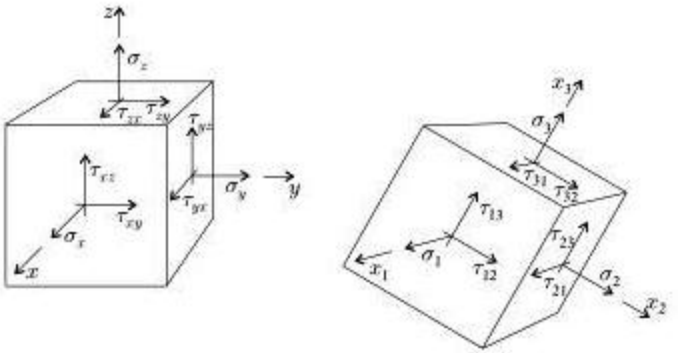

Figure 2.3: The stresses in the global x, y, z and the local x_1, x_2, x_3 coordinate systems.

For angular (shear) deformation the tensorial shear strain is the average change in the angle between two mutually perpendicular lines (Fig. 2.5)

$$\epsilon_{xy} = \frac{\alpha + \beta}{2}. \tag{2.5}$$

For small deformations we have

$$\alpha \approx \tan\alpha = \frac{\left(v + \frac{\partial v}{\partial x}\Delta x\right) - v}{\Delta x} = \frac{\partial v}{\partial x}. \tag{2.6}$$

Similarly $\beta = \partial u/\partial y$, and the xy component of the tensorial shear strain is

$$\epsilon_{xy} = \frac{1}{2}\left(\frac{\partial u}{\partial y} + \frac{\partial v}{\partial x}\right). \tag{2.7}$$

In a similar manner we obtain the following expressions for the ϵ_{yz} and ϵ_{xz} components of the tensorial shear strains:

$$\epsilon_{yz} = \frac{1}{2}\left(\frac{\partial v}{\partial z} + \frac{\partial w}{\partial y}\right) \qquad \epsilon_{xz} = \frac{1}{2}\left(\frac{\partial u}{\partial z} + \frac{\partial w}{\partial x}\right). \tag{2.8}$$

Table 2.1. Stress notations

	Normal stress			Shear stress		
x, y, z coordinate system						
Tensorial stress	σ_{xx}	σ_{yy}	σ_{zz}	σ_{yz}	σ_{xz}	σ_{xy}
Engineering stress	σ_x	σ_y	σ_z	τ_{yz}	τ_{xz}	τ_{xy}
Contracted notation	σ_x	σ_y	σ_z	σ_q	σ_r	σ_s
x_1, x_2, x_3 coordinate system						
Tensorial stress	σ_{11}	σ_{22}	σ_{33}	σ_{23}	σ_{13}	σ_{12}
Engineering stress	σ_1	σ_2	σ_3	τ_{23}	τ_{13}	τ_{12}
Contracted notation	σ_1	σ_2	σ_3	σ_4	σ_5	σ_6

Table 2.2. Strain notations (the engineering and contracted notation shear strains are twice the tensorial shear strain)

	Normal strain			Shear strain		
x, y, z coordinate system						
Tensorial strain	ϵ_{xx}	ϵ_{yy}	ϵ_{zz}	ϵ_{yz}	ϵ_{xz}	ϵ_{xy}
Engineering strain	ϵ_x	ϵ_y	ϵ_z	γ_{yz}	γ_{xz}	γ_{xy}
Contracted notation	ϵ_x	ϵ_y	ϵ_z	ϵ_q	ϵ_r	ϵ_s
x_1, x_2, x_3 coordinate system						
Tensorial strain	ϵ_{11}	ϵ_{22}	ϵ_{33}	ϵ_{23}	ϵ_{13}	ϵ_{12}
Engineering strain	ϵ_1	ϵ_2	ϵ_3	γ_{23}	γ_{13}	γ_{12}
Contracted notation	ϵ_1	ϵ_2	ϵ_3	ϵ_4	ϵ_5	ϵ_6

The engineering shear strains are twice the tensorial shear strains:

$$\gamma_{yz} = 2\epsilon_{yz} = \frac{\partial v}{\partial z} + \frac{\partial w}{\partial y} \tag{2.9}$$

$$\gamma_{xz} = 2\epsilon_{xz} = \frac{\partial u}{\partial z} + \frac{\partial w}{\partial x} \tag{2.10}$$

$$\gamma_{xy} = 2\epsilon_{xy} = \frac{\partial u}{\partial y} + \frac{\partial v}{\partial x}. \tag{2.11}$$

In the x_1, x_2, x_3 coordinate system the strain–displacement relationships are also given by Eqs. (2.2)–(2.4) and (2.9)–(2.11) with x, y, z replaced by x_1, x_2, x_3, the subscripts x, y, z by 1, 2, 3, and u, v, w by u_1, u_2, u_3.

2.2 Equilibrium Equations

The equilibrium equations at a point O are obtained by considering force and moment balances on a small $\Delta x \Delta y \Delta z$ cubic element located at point O. (The point O is at the center of the element, Fig. 2.6.) We relate the stresses at one face to those at the opposite face by the Taylor series. By using only the first term of the Taylor series, force balance in the x direction gives

$$-\sigma_x \Delta z \Delta y - \tau_{zx} \Delta x \Delta y - \tau_{yx} \Delta x \Delta z + \left(\sigma_x + \frac{\partial \sigma_x}{\partial x} \Delta x\right) \Delta z \Delta y$$
$$+ \left(\tau_{zx} + \frac{\partial \tau_{zx}}{\partial z} \Delta z\right) \Delta x \Delta y + \left(\tau_{yx} + \frac{\partial \tau_{yx}}{\partial y} \Delta y\right) \Delta x \Delta z + f_x \Delta x \Delta y \Delta z = 0, \tag{2.12}$$

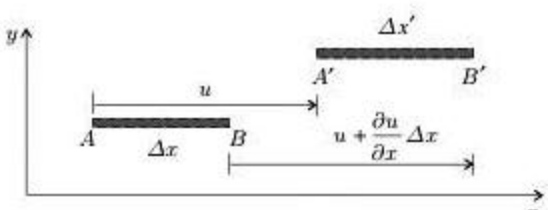

Figure 2.4: Displacement of the AB line segment.

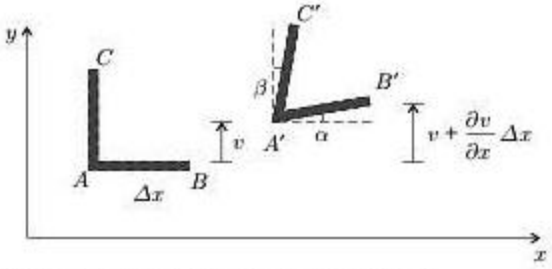

Figure 2.5: Displacement of the *ABC* segment.

where f_x is the body force per unit volume in the x direction. After simplification, this equation becomes

$$\frac{\partial \sigma_x}{\partial x} + \frac{\partial \tau_{yx}}{\partial y} + \frac{\partial \tau_{zx}}{\partial z} + f_x = 0. \tag{2.13}$$

By similar arguments, the equilibrium equations in the y and z directions are

$$\frac{\partial \tau_{xy}}{\partial x} + \frac{\partial \sigma_y}{\partial y} + \frac{\partial \tau_{zy}}{\partial z} + f_y = 0, \tag{2.14}$$

$$\frac{\partial \tau_{xz}}{\partial x} + \frac{\partial \tau_{yz}}{\partial y} + \frac{\partial \sigma_z}{\partial z} + f_z = 0, \tag{2.15}$$

where f_y and f_z are the body forces per unit volume in the y and z directions.

A moment balance about an axis parallel to x and passing through the center (point O) gives (Fig. 2.7)

$$\begin{aligned} &\tau_{yz}\Delta x\Delta z\frac{\Delta y}{2} - \tau_{zy}\Delta x\Delta y\frac{\Delta z}{2} \\ &+\left(\tau_{yz} + \frac{\partial \tau_{yz}}{\partial y}\Delta y\right)\Delta x\Delta z\frac{\Delta y}{2} - \left(\tau_{zy} + \frac{\partial \tau_{zy}}{\partial z}\Delta z\right)\Delta x\Delta y\frac{\Delta z}{2} = 0. \end{aligned} \tag{2.16}$$

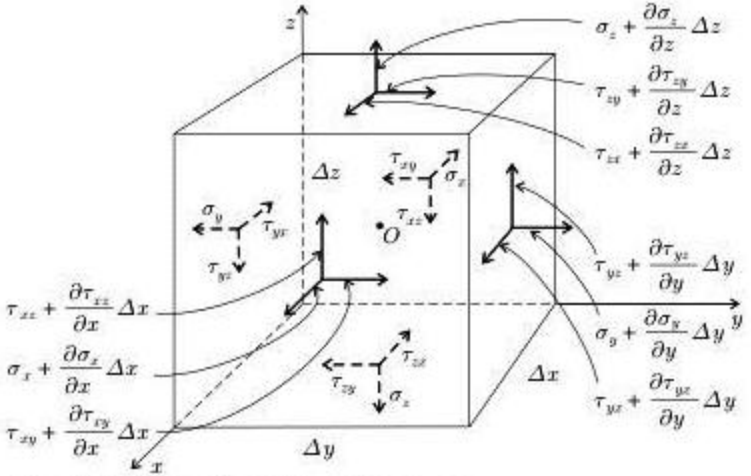

Figure 2.6: Stresses on the $\Delta x\Delta y\Delta z$ cubic element.

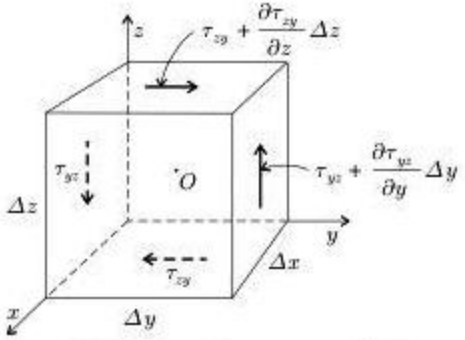

Figure 2.7: Stresses on the $\Delta x \Delta y \Delta z$ cubic element that appear in the moment balance about an axis parallel to x and passing through the center (point O).

By omitting higher order terms, which vanish in the limit $\Delta x \to 0, \Delta y \to 0, \Delta z \to 0$, this equation becomes

$$\tau_{yz} = \tau_{zy}. \tag{2.17}$$

Similarly, we obtain the following equalities:

$$\tau_{xz} = \tau_{zx} \qquad \tau_{xy} = \tau_{yx}. \tag{2.18}$$

By virtue of Eqs. (2.17) and (2.18), the three equilibrium equations (Eqs. 2.13–2.15) contain six unknowns, namely, the three normal stresses ($\sigma_x, \sigma_y, \sigma_z$) and the three shear stresses ($\tau_{yz}, \tau_{xz}, \tau_{xy}$).

In the x_1, x_2, x_3 coordinate system the equilibrium equations are also given by Eqs. (2.13)–(2.15) with x, y, z replaced by x_1, x_2, x_3 and the subscripts x, y, z by 1, 2, 3.

2.3 Stress–Strain Relationships

In a composite material the fibers may be oriented in an arbitrary manner. Depending on the arrangements of the fibers, the material may behave differently in different directions. According to their behavior, composites may be characterized as generally anisotropic, monoclinic, orthotropic, transversely isotropic, or isotropic. In the following, we present the stress–strain relationships for these types of materials under linearly elastic conditions.

2.3.1 Generally Anisotropic Material

When there are no symmetry planes with respect to the alignment of the fibers the material is referred to as generally anisotropic. A fiber-reinforced composite material is, for example, generally anisotropic when the fibers are aligned in three nonorthogonal directions (Fig. 2.8).

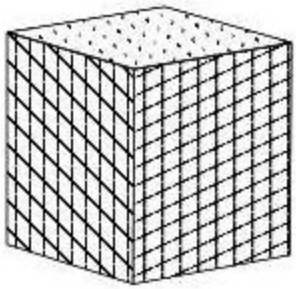

Figure 2.8: Example of a generally anisotropic material.

For a generally anisotropic linearly elastic material, in the x, y, z global coordinate system, the stress–strain relationships are

$$\begin{aligned}
\sigma_x &= \overline{C}_{11}\epsilon_x + \overline{C}_{12}\epsilon_y + \overline{C}_{13}\epsilon_z + \overline{C}_{14}\gamma_{yz} + \overline{C}_{15}\gamma_{xz} + \overline{C}_{16}\gamma_{xy} \\
\sigma_y &= \overline{C}_{21}\epsilon_x + \overline{C}_{22}\epsilon_y + \overline{C}_{23}\epsilon_z + \overline{C}_{24}\gamma_{yz} + \overline{C}_{25}\gamma_{xz} + \overline{C}_{26}\gamma_{xy} \\
\sigma_z &= \overline{C}_{31}\epsilon_x + \overline{C}_{32}\epsilon_y + \overline{C}_{33}\epsilon_z + \overline{C}_{34}\gamma_{yz} + \overline{C}_{35}\gamma_{xz} + \overline{C}_{36}\gamma_{xy} \\
\tau_{yz} &= \overline{C}_{41}\epsilon_x + \overline{C}_{42}\epsilon_y + \overline{C}_{43}\epsilon_z + \overline{C}_{44}\gamma_{yz} + \overline{C}_{45}\gamma_{xz} + \overline{C}_{46}\gamma_{xy} \\
\tau_{xz} &= \overline{C}_{51}\epsilon_x + \overline{C}_{52}\epsilon_y + \overline{C}_{53}\epsilon_z + \overline{C}_{54}\gamma_{yz} + \overline{C}_{55}\gamma_{xz} + \overline{C}_{56}\gamma_{xy} \\
\tau_{xy} &= \overline{C}_{61}\epsilon_x + \overline{C}_{62}\epsilon_y + \overline{C}_{63}\epsilon_z + \overline{C}_{64}\gamma_{yz} + \overline{C}_{65}\gamma_{xz} + \overline{C}_{66}\gamma_{xy}.
\end{aligned} \tag{2.19}$$

Equation (2.19) may be written in the form

$$\begin{Bmatrix} \sigma_x \\ \sigma_y \\ \sigma_z \\ \tau_{yz} \\ \tau_{xz} \\ \tau_{xy} \end{Bmatrix} = \begin{bmatrix} \overline{C}_{11} & \overline{C}_{12} & \overline{C}_{13} & \overline{C}_{14} & \overline{C}_{15} & \overline{C}_{16} \\ \overline{C}_{21} & \overline{C}_{22} & \overline{C}_{23} & \overline{C}_{24} & \overline{C}_{25} & \overline{C}_{26} \\ \overline{C}_{31} & \overline{C}_{32} & \overline{C}_{33} & \overline{C}_{34} & \overline{C}_{35} & \overline{C}_{36} \\ \overline{C}_{41} & \overline{C}_{42} & \overline{C}_{43} & \overline{C}_{44} & \overline{C}_{45} & \overline{C}_{46} \\ \overline{C}_{51} & \overline{C}_{52} & \overline{C}_{53} & \overline{C}_{54} & \overline{C}_{55} & \overline{C}_{56} \\ \overline{C}_{61} & \overline{C}_{62} & \overline{C}_{63} & \overline{C}_{64} & \overline{C}_{65} & \overline{C}_{66} \end{bmatrix} \begin{Bmatrix} \epsilon_x \\ \epsilon_y \\ \epsilon_z \\ \gamma_{yz} \\ \gamma_{xz} \\ \gamma_{xy} \end{Bmatrix}, \tag{2.20}$$

where $\overline{C}_{ij}$ are the elements of the stiffness matrix $[\overline{C}]$ in the x, y, z coordinate system.

Inversion of Eq. (2.20) results in the following strain–stress relationships:

$$\begin{Bmatrix} \epsilon_x \\ \epsilon_y \\ \epsilon_z \\ \gamma_{yz} \\ \gamma_{xz} \\ \gamma_{xy} \end{Bmatrix} = \begin{bmatrix} \overline{S}_{11} & \overline{S}_{12} & \overline{S}_{13} & \overline{S}_{14} & \overline{S}_{15} & \overline{S}_{16} \\ \overline{S}_{21} & \overline{S}_{22} & \overline{S}_{23} & \overline{S}_{24} & \overline{S}_{25} & \overline{S}_{26} \\ \overline{S}_{31} & \overline{S}_{32} & \overline{S}_{33} & \overline{S}_{34} & \overline{S}_{35} & \overline{S}_{36} \\ \overline{S}_{41} & \overline{S}_{42} & \overline{S}_{43} & \overline{S}_{44} & \overline{S}_{45} & \overline{S}_{46} \\ \overline{S}_{51} & \overline{S}_{52} & \overline{S}_{53} & \overline{S}_{54} & \overline{S}_{55} & \overline{S}_{56} \\ \overline{S}_{61} & \overline{S}_{62} & \overline{S}_{63} & \overline{S}_{64} & \overline{S}_{65} & \overline{S}_{66} \end{bmatrix} \begin{Bmatrix} \sigma_x \\ \sigma_y \\ \sigma_z \\ \tau_{yz} \\ \tau_{xz} \\ \tau_{xy} \end{Bmatrix}, \tag{2.21}$$

where $\overline{S}_{ij}$ are the elements of the compliance matrix $[\overline{S}]$ in the x, y, z coordinate system and are defined in Table 2.3 (page 10). In this table tests are illustrated that, in principle, could provide means of determining the different compliance matrix elements.

Table 2.3. The elements of the compliance matrix $[\bar{S}]$ in the x, y, z coordinate system. The elements S_{ij} (without bar) in the x_1, x_2, x_3 coordinate system are obtained by replacing x, y, z by 1, 2, 3 on the right-hand sides of the expressions.

Test	Elements of the compliance matrix	
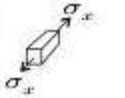	$\bar{S}_{11} = \epsilon_x/\sigma_x$ $\bar{S}_{21} = \epsilon_y/\sigma_x$ $\bar{S}_{31} = \epsilon_z/\sigma_x$	$\bar{S}_{41} = \gamma_{yz}/\sigma_x$ $\bar{S}_{51} = \gamma_{xz}/\sigma_x$ $\bar{S}_{61} = \gamma_{xy}/\sigma_x$
	$\bar{S}_{12} = \epsilon_x/\sigma_y$ $\bar{S}_{22} = \epsilon_y/\sigma_y$ $\bar{S}_{32} = \epsilon_z/\sigma_y$	$\bar{S}_{42} = \gamma_{yz}/\sigma_y$ $\bar{S}_{52} = \gamma_{xz}/\sigma_y$ $\bar{S}_{62} = \gamma_{xy}/\sigma_y$
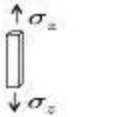	$\bar{S}_{13} = \epsilon_x/\sigma_z$ $\bar{S}_{23} = \epsilon_y/\sigma_z$ $\bar{S}_{33} = \epsilon_z/\sigma_z$	$\bar{S}_{43} = \gamma_{yz}/\sigma_z$ $\bar{S}_{53} = \gamma_{xz}/\sigma_z$ $\bar{S}_{63} = \gamma_{xy}/\sigma_z$
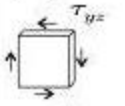	$\bar{S}_{14} = \epsilon_x/\tau_{yz}$ $\bar{S}_{24} = \epsilon_y/\tau_{yz}$ $\bar{S}_{34} = \epsilon_z/\tau_{yz}$	$\bar{S}_{44} = \gamma_{yz}/\tau_{yz}$ $\bar{S}_{54} = \gamma_{xz}/\tau_{yz}$ $\bar{S}_{64} = \gamma_{xy}/\tau_{yz}$
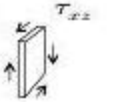	$\bar{S}_{15} = \epsilon_x/\tau_{xz}$ $\bar{S}_{25} = \epsilon_y/\tau_{xz}$ $\bar{S}_{35} = \epsilon_z/\tau_{xz}$	$\bar{S}_{45} = \gamma_{yz}/\tau_{xz}$ $\bar{S}_{55} = \gamma_{xz}/\tau_{xz}$ $\bar{S}_{65} = \gamma_{xy}/\tau_{xz}$
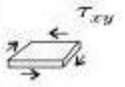	$\bar{S}_{16} = \epsilon_x/\tau_{xy}$ $\bar{S}_{26} = \epsilon_y/\tau_{xy}$ $\bar{S}_{36} = \epsilon_z/\tau_{xy}$	$\bar{S}_{46} = \gamma_{yz}/\tau_{xy}$ $\bar{S}_{56} = \gamma_{xz}/\tau_{xy}$ $\bar{S}_{66} = \gamma_{xy}/\tau_{xy}$

In the x_1, x_2, x_3 coordinate system the stress–strain relationships are

$$\begin{Bmatrix} \sigma_1 \\ \sigma_2 \\ \sigma_3 \\ \tau_{23} \\ \tau_{13} \\ \tau_{12} \end{Bmatrix} = \begin{bmatrix} C_{11} & C_{12} & C_{13} & C_{14} & C_{15} & C_{16} \\ C_{21} & C_{22} & C_{23} & C_{24} & C_{25} & C_{26} \\ C_{31} & C_{32} & C_{33} & C_{34} & C_{35} & C_{36} \\ C_{41} & C_{42} & C_{43} & C_{44} & C_{45} & C_{46} \\ C_{51} & C_{52} & C_{53} & C_{54} & C_{55} & C_{56} \\ C_{61} & C_{62} & C_{63} & C_{64} & C_{65} & C_{66} \end{bmatrix} \begin{Bmatrix} \epsilon_1 \\ \epsilon_2 \\ \epsilon_3 \\ \gamma_{23} \\ \gamma_{13} \\ \gamma_{12} \end{Bmatrix}, \tag{2.22}$$

where C_{ij} are the elements of the stiffness matrix $[C]$ in the x_1, x_2, x_3 coordinate system.

By inverting Eq. (2.22) we obtain the following strain–stress relationships:

$$\begin{Bmatrix} \epsilon_1 \\ \epsilon_2 \\ \epsilon_3 \\ \gamma_{23} \\ \gamma_{13} \\ \gamma_{12} \end{Bmatrix} = \begin{bmatrix} S_{11} & S_{12} & S_{13} & S_{14} & S_{15} & S_{16} \\ S_{21} & S_{22} & S_{23} & S_{24} & S_{25} & S_{26} \\ S_{31} & S_{32} & S_{33} & S_{34} & S_{35} & S_{36} \\ S_{41} & S_{42} & S_{43} & S_{44} & S_{45} & S_{46} \\ S_{51} & S_{52} & S_{53} & S_{54} & S_{55} & S_{56} \\ S_{61} & S_{62} & S_{63} & S_{64} & S_{65} & S_{66} \end{bmatrix} \begin{Bmatrix} \sigma_1 \\ \sigma_2 \\ \sigma_3 \\ \tau_{23} \\ \tau_{13} \\ \tau_{12} \end{Bmatrix}, \tag{2.23}$$

where S_{ij} are the elements of the compliance matrix $[S]$ in the x_1, x_2, x_3 coordinate system.

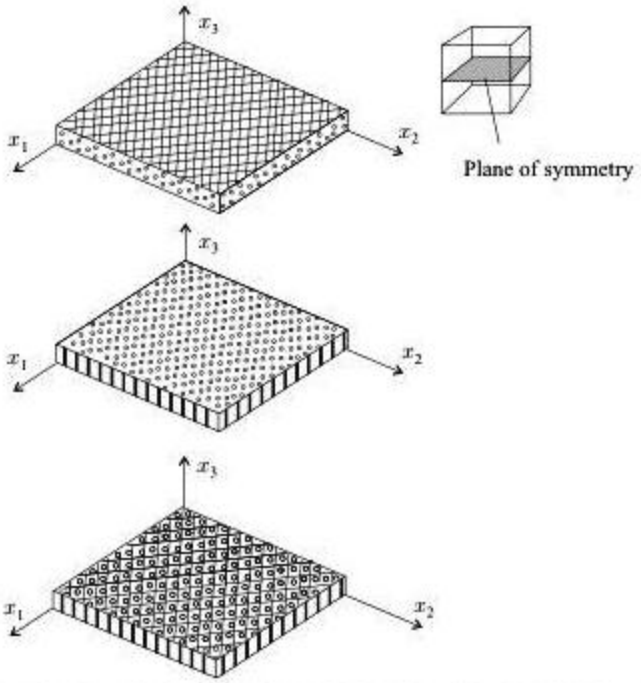

Figure 2.9: Illustrations of fiber-reinforced monoclinic materials. The fibers are only in planes parallel to the x_1–x_2 plane of symmetry (top), only perpendicular to the plane of symmetry (middle), and in the plane of symmetry and perpendicular to the plane of symmetry (bottom).

It is evident from Eqs. (2.20)–(2.23) that the compliance matrix $[S]$ is the inverse of the stiffness matrix $[C]$:

$$[\overline{S}] = [\overline{C}]^{-1} \qquad [S] = [C]^{-1}. \tag{2.24}$$

It can be shown (see Section 2.11.1) that for an elastic material the stiffness and compliance matrices are symmetrical in both the x, y, z and x_1, x_2, x_3 coordinate systems as follows:

$$\overline{S}_{ij} = \overline{S}_{ji} \qquad S_{ij} = S_{ji} \qquad \overline{C}_{ij} = \overline{C}_{ji} \qquad C_{ij} = C_{ji} \quad i, j = 1, 2, \ldots, 6. \tag{2.25}$$

Because of this symmetry, in both the $[\overline{S}]$ and the $[\overline{C}]$ matrices only 21 of the 36 elements are independent.

2.3.2 Monoclinic Material

When there is a symmetry plane with respect to the alignment of the fibers, the material is referred to as monoclinic. Examples of monoclinic fiber-reinforced composites are shown in Figure 2.9.

For a monoclinic material we specify the compliance $[S]$ and stiffness $[C]$ matrices in an x_1, x_2, x_3 coordinate system chosen in such a way that x_1 and x_2 are in the plane of symmetry, whereas x_3 is perpendicular to this plane.

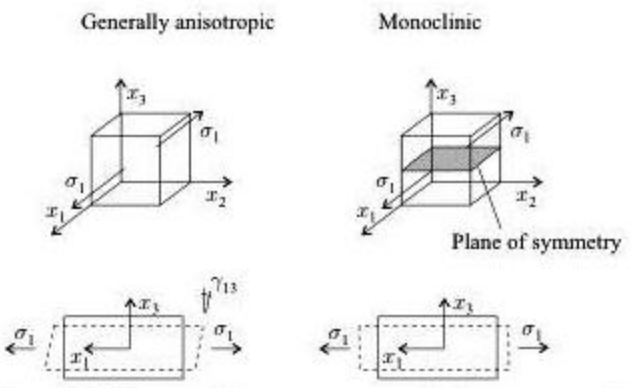

Figure 2.10: The normal stress σ_1 causes shear strain γ_{13} in a generally anisotropic material (left) and no shear strain in a monoclinic material (right).

The elements of the compliance matrix for a monoclinic material are obtained by modifying the compliance matrix of a generally anisotropic material. We observe that in a generally anisotropic material a normal stress σ_1 causes an out-of-plane shear strain γ_{13} (Fig. 2.10 left), but in a monoclinic material subjected to a normal stress σ_1 (σ_1 being in the plane of symmetry) the out-of-plane shear strain γ_{13} is zero (Fig. 2.10 right). Consequently, for a monoclinic material the S_{51} element of the compliance matrix is zero. By similar arguments it can be shown that

Table 2.4. The elements of the compliance matrix for monoclinic materials. For orthotropic, transversely isotropic, and isotropic materials $S_{16} = S_{61} = 0$, $S_{26} = S_{62} = 0$, $S_{36} = S_{63} = 0$, $S_{45} = S_{54} = 0$

Test	Elements of the compliance matrix	
σ_1	$S_{11} = \epsilon_1/\sigma_1$	$S_{41} = \gamma_{23}/\sigma_1 = 0$
	$S_{21} = \epsilon_2/\sigma_1$	$S_{51} = \gamma_{13}/\sigma_1 = 0$
σ_1	$S_{31} = \epsilon_3/\sigma_1$	$S_{61} = \gamma_{12}/\sigma_1$
σ_2 σ_2	$S_{12} = \epsilon_1/\sigma_2$	$S_{42} = \gamma_{23}/\sigma_2 = 0$
	$S_{22} = \epsilon_2/\sigma_2$	$S_{52} = \gamma_{13}/\sigma_2 = 0$
	$S_{32} = \epsilon_3/\sigma_2$	$S_{62} = \gamma_{12}/\sigma_2$
σ_3	$S_{13} = \epsilon_1/\sigma_3$	$S_{43} = \gamma_{23}/\sigma_3 = 0$
	$S_{23} = \epsilon_2/\sigma_3$	$S_{53} = \gamma_{13}/\sigma_3 = 0$
σ_3	$S_{33} = \epsilon_3/\sigma_3$	$S_{63} = \gamma_{12}/\sigma_3$
τ_{23}	$S_{14} = \epsilon_1/\tau_{23} = 0$	$S_{44} = \gamma_{23}/\tau_{23}$
	$S_{24} = \epsilon_2/\tau_{23} = 0$	$S_{54} = \gamma_{13}/\tau_{23}$
	$S_{34} = \epsilon_3/\tau_{23} = 0$	$S_{64} = \gamma_{12}/\tau_{23} = 0$
τ_{13}	$S_{15} = \epsilon_1/\tau_{13} = 0$	$S_{45} = \gamma_{23}/\tau_{13}$
	$S_{25} = \epsilon_2/\tau_{13} = 0$	$S_{55} = \gamma_{13}/\tau_{13}$
	$S_{35} = \epsilon_3/\tau_{13} = 0$	$S_{65} = \gamma_{12}/\tau_{13} = 0$
τ_{12}	$S_{16} = \epsilon_1/\tau_{12}$	$S_{46} = \gamma_{23}/\tau_{12} = 0$
	$S_{26} = \epsilon_2/\tau_{12}$	$S_{56} = \gamma_{13}/\tau_{12} = 0$
	$S_{36} = \epsilon_3/\tau_{12}$	$S_{66} = \gamma_{12}/\tau_{12}$

for a monoclinic material the S_{41}, S_{42}, S_{52}, S_{43}, S_{53}, S_{64}, S_{65} elements are also zero. (Since the compliance matrix is symmetrical the elements S_{14}, S_{24}, S_{25}, S_{34}, S_{35}, S_{46}, S_{56} are also zero.) The elements of the compliance matrix are listed in Table 2.4.

The elements of the compliance matrix may be expressed in terms of the engineering constants defined in Table 2.5. In Tables 2.4 and 2.5 the types of tests are also illustrated that, at least in principle, could provide the elements of the compliance matrix and the engineering constants. The relationships between the elements of the compliance matrix and the engineering constants are shown in Tables 2.6 and 2.7.

The nonzero and zero elements of the compliance matrix can best be seen when the matrix is written in the form

$$[S] = \begin{bmatrix} S_{11} & S_{12} & S_{13} & 0 & 0 & S_{16} \\ S_{12} & S_{22} & S_{23} & 0 & 0 & S_{26} \\ S_{13} & S_{23} & S_{33} & 0 & 0 & S_{36} \\ 0 & 0 & 0 & S_{44} & S_{45} & 0 \\ 0 & 0 & 0 & S_{45} & S_{55} & 0 \\ S_{16} & S_{26} & S_{36} & 0 & 0 & S_{66} \end{bmatrix}. \tag{2.26}$$

Table 2.5. The engineering constants for monoclinic materials. For orthotropic, transversely isotropic, and isotropic materials $\nu_{16} = \nu_{61} = 0$, $\nu_{26} = \nu_{62} = 0$, $\nu_{36} = \nu_{63} = 0$, $\nu_{45} = \nu_{54} = 0$

Test	Engineering constants	
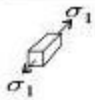	Young's modulus in the x_1 direction	$E_1 = \sigma_1/\epsilon_1$
	Poisson's ratio in the x_1–x_2 plane	$\nu_{12} = -\epsilon_2/\epsilon_1$
	Poisson's ratio in the x_1–x_3 plane	$\nu_{13} = -\epsilon_3/\epsilon_1$
	Poisson parameter	$\nu_{16} = \gamma_{12}/\epsilon_1$
	Young's modulus in the x_2 direction	$E_2 = \sigma_2/\epsilon_2$
	Poisson's ratio in the x_2–x_1 plane	$\nu_{21} = -\epsilon_1/\epsilon_2$
	Poisson's ratio in the x_2–x_3 plane	$\nu_{23} = -\epsilon_3/\epsilon_2$
	Poisson parameter	$\nu_{26} = \gamma_{12}/\epsilon_2$
	Young's modulus in the x_3 direction	$E_3 = \sigma_3/\epsilon_3$
	Poisson's ratio in the x_3–x_1 plane	$\nu_{31} = -\epsilon_1/\epsilon_3$
	Poisson's ratio in the x_3–x_2 plane	$\nu_{32} = -\epsilon_2/\epsilon_3$
	Poisson parameter	$\nu_{36} = \gamma_{12}/\epsilon_3$
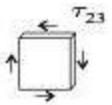	Shear modulus in the x_2–x_3 plane	$G_{23} = \tau_{23}/\gamma_{23}$
	Poisson parameter	$\nu_{45} = \gamma_{13}/\gamma_{23}$
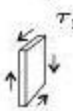	Shear modulus in the x_1–x_3 plane	$G_{13} = \tau_{13}/\gamma_{13}$
	Poisson parameter	$\nu_{54} = \gamma_{23}/\gamma_{13}$
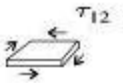	Shear modulus in the x_1–x_2 plane	$G_{12} = \tau_{12}/\gamma_{12}$
	Poisson parameter	$\nu_{61} = \epsilon_1/\gamma_{12}$
	Poisson parameter	$\nu_{62} = \epsilon_2/\gamma_{12}$
	Poisson parameter	$\nu_{63} = \epsilon_3/\gamma_{12}$

$\frac{\nu_{ij}}{E_i} = \frac{\nu_{ji}}{E_j}$, $\frac{\nu_{45}}{G_{23}} = \frac{\nu_{54}}{G_{13}}$, $\frac{\nu_{16}}{E_1} = \frac{\nu_{61}}{G_{12}}$ $(i, j = 1, 2, 3)$

Table 2.6. Elements of the compliance matrix in terms of the engineering constants for monoclinic materials. The expressions are also valid for orthotropic, transversely isotropic, and isotropic materials with $S_{16} = S_{61} = 0$, $S_{26} = S_{62} = 0$, $S_{36} = S_{63} = 0$, $S_{45} = S_{54} = 0$.

$S_{11} = \epsilon_1/\sigma_1 = \epsilon_1/(E_1\epsilon_1) = \frac{1}{E_1}$	$S_{41} = 0$
$S_{21} = \epsilon_2/\sigma_1 = \epsilon_2/(E_1\epsilon_1) = -\frac{\nu_{12}}{E_1}$	$S_{51} = 0$
$S_{31} = \epsilon_3/\sigma_1 = \epsilon_3/(E_1\epsilon_1) = -\frac{\nu_{13}}{E_1}$	$S_{61} = \gamma_{12}/\sigma_1 = \gamma_{12}/(E_1\epsilon_1) = \frac{\nu_{16}}{E_1}$
$S_{12} = \epsilon_1/\sigma_2 = \epsilon_1/(E_2\epsilon_2) = -\frac{\nu_{21}}{E_2}$	$S_{42} = 0$
$S_{22} = \epsilon_2/\sigma_2 = \epsilon_2/(E_2\epsilon_2) = \frac{1}{E_2}$	$S_{52} = 0$
$S_{32} = \epsilon_3/\sigma_2 = \epsilon_3/(E_2\epsilon_2) = -\frac{\nu_{23}}{E_2}$	$S_{62} = \gamma_{12}/\sigma_2 = \gamma_{12}/(E_2\epsilon_2) = \frac{\nu_{26}}{E_2}$
$S_{13} = \epsilon_1/\sigma_3 = \epsilon_1/(E_3\epsilon_3) = -\frac{\nu_{31}}{E_3}$	$S_{43} = 0$
$S_{23} = \epsilon_2/\sigma_3 = \epsilon_2/(E_3\epsilon_3) = -\frac{\nu_{32}}{E_3}$	$S_{53} = 0$
$S_{33} = \epsilon_3/\sigma_3 = \epsilon_3/(E_3\epsilon_3) = \frac{1}{E_3}$	$S_{63} = \gamma_{12}/\sigma_3 = \gamma_{12}/(E_3\epsilon_3) = \frac{\nu_{36}}{E_3}$
$S_{14} = 0$	$S_{44} = \gamma_{23}/\tau_{23} = \gamma_{23}/(G_{23}\gamma_{23}) = \frac{1}{G_{23}}$
$S_{24} = 0$	$S_{54} = \gamma_{13}/\tau_{23} = \gamma_{13}/(G_{23}\gamma_{23}) = \frac{\nu_{45}}{G_{23}}$
$S_{34} = 0$	$S_{64} = 0$
$S_{15} = 0$	$S_{45} = \gamma_{23}/\tau_{13} = \gamma_{23}/(G_{13}\gamma_{13}) = \frac{\nu_{54}}{G_{13}}$
$S_{25} = 0$	$S_{55} = \gamma_{13}/\tau_{13} = \gamma_{13}/(G_{13}\gamma_{13}) = \frac{1}{G_{13}}$
$S_{35} = 0$	$S_{65} = 0$
$S_{16} = \epsilon_1/\tau_{12} = \epsilon_1/(G_{12}\gamma_{12}) = \frac{\nu_{61}}{G_{12}}$	$S_{46} = 0$
$S_{26} = \epsilon_2/\tau_{12} = \epsilon_2/(G_{12}\gamma_{12}) = \frac{\nu_{62}}{G_{12}}$	$S_{56} = 0$
$S_{36} = \epsilon_3/\tau_{12} = \epsilon_3/(G_{12}\gamma_{12}) = \frac{\nu_{63}}{G_{12}}$	$S_{66} = \gamma_{12}/\tau_{12} = \gamma_{12}/(G_{12}\gamma_{12}) = \frac{1}{G_{12}}$

The stiffness matrix is obtained by inverting the compliance matrix as follows:

$$[C] = \begin{bmatrix} C_{11} & C_{12} & C_{13} & 0 & 0 & C_{16} \\ C_{12} & C_{22} & C_{23} & 0 & 0 & C_{26} \\ C_{13} & C_{23} & C_{33} & 0 & 0 & C_{36} \\ 0 & 0 & 0 & C_{44} & C_{45} & 0 \\ 0 & 0 & 0 & C_{45} & C_{55} & 0 \\ C_{16} & C_{26} & C_{36} & 0 & 0 & C_{66} \end{bmatrix}. \tag{2.27}$$

Because the $[S]$ and $[C]$ matrices are symmetrical (Eq. 2.25) only 13 of the elements are independent (Table 2.8).

2.3.3 Orthotropic Material

When there are three mutually perpendicular symmetry planes with respect to the alignment of the fibers the material is referred to as orthotropic (Fig. 2.11). Examples of orthotropic fiber-reinforced composites are shown in Figure 2.12. For an orthotropic material we specify the stiffness and compliance matrices in the x_1, x_2, x_3 coordinate system defined in such a way that the axes are perpendicular to the three planes of symmetry (Fig. 2.11).

We apply a normal stress σ_1 (Fig. 2.13). Because σ_1 is in the x_1–x_2 symmetry (orthotropy) plane the out-of-plane shear strains are zero, ($\gamma_{13} = \gamma_{23} = 0$); and

Table 2.7. The compliance matrices in terms of the engineering constants for monoclinic, orthotropic, transversely isotropic, and isotropic materials

$$[S] = \begin{bmatrix} \frac{1}{E_1} & -\frac{\nu_{21}}{E_2} & -\frac{\nu_{31}}{E_3} & 0 & 0 & \frac{\nu_{61}}{G_{12}} \\ -\frac{\nu_{12}}{E_1} & \frac{1}{E_2} & -\frac{\nu_{32}}{E_3} & 0 & 0 & \frac{\nu_{62}}{G_{12}} \\ -\frac{\nu_{13}}{E_1} & -\frac{\nu_{23}}{E_2} & \frac{1}{E_3} & 0 & 0 & \frac{\nu_{63}}{G_{12}} \\ 0 & 0 & 0 & \frac{1}{G_{23}} & \frac{\nu_{54}}{G_{13}} & 0 \\ 0 & 0 & 0 & \frac{\nu_{45}}{G_{23}} & \frac{1}{G_{13}} & 0 \\ \frac{\nu_{16}}{E_1} & \frac{\nu_{26}}{E_2} & \frac{\nu_{36}}{E_3} & 0 & 0 & \frac{1}{G_{12}} \end{bmatrix} \quad \text{monoclinic}$$

$$[S] = \begin{bmatrix} \frac{1}{E_1} & -\frac{\nu_{21}}{E_2} & -\frac{\nu_{31}}{E_3} & 0 & 0 & 0 \\ -\frac{\nu_{12}}{E_1} & \frac{1}{E_2} & -\frac{\nu_{32}}{E_3} & 0 & 0 & 0 \\ -\frac{\nu_{13}}{E_1} & -\frac{\nu_{23}}{E_2} & \frac{1}{E_3} & 0 & 0 & 0 \\ 0 & 0 & 0 & \frac{1}{G_{23}} & 0 & 0 \\ 0 & 0 & 0 & 0 & \frac{1}{G_{13}} & 0 \\ 0 & 0 & 0 & 0 & 0 & \frac{1}{G_{12}} \end{bmatrix} \quad \text{orthotropic}$$

$$[S] = \begin{bmatrix} \frac{1}{E_1} & -\frac{\nu_{21}}{E_2} & -\frac{\nu_{21}}{E_2} & 0 & 0 & 0 \\ -\frac{\nu_{12}}{E_1} & \frac{1}{E_2} & -\frac{\nu_{32}}{E_2} & 0 & 0 & 0 \\ -\frac{\nu_{12}}{E_1} & -\frac{\nu_{23}}{E_2} & \frac{1}{E_2} & 0 & 0 & 0 \\ 0 & 0 & 0 & \frac{2(1+\nu_{23})}{E_2} & 0 & 0 \\ 0 & 0 & 0 & 0 & \frac{1}{G_{13}} & 0 \\ 0 & 0 & 0 & 0 & 0 & \frac{1}{G_{13}} \end{bmatrix} \quad \text{transversely isotropic}$$

$$[S] = \begin{bmatrix} \frac{1}{E} & -\frac{\nu}{E} & -\frac{\nu}{E} & 0 & 0 & 0 \\ -\frac{\nu}{E} & \frac{1}{E} & -\frac{\nu}{E} & 0 & 0 & 0 \\ -\frac{\nu}{E} & -\frac{\nu}{E} & \frac{1}{E} & 0 & 0 & 0 \\ 0 & 0 & 0 & \frac{2(1+\nu)}{E} & 0 & 0 \\ 0 & 0 & 0 & 0 & \frac{2(1+\nu)}{E} & 0 \\ 0 & 0 & 0 & 0 & 0 & \frac{2(1+\nu)}{E} \end{bmatrix} \quad \text{isotropic}$$

because σ_1 is also in the x_1–x_3 symmetry plane, the $\gamma_{12} = 0$ shear strain is zero. This implies that S_{14}, S_{15}, S_{16} are zero. By similar arguments it can be shown that for an orthotropic material the S_{24}, S_{25}, S_{26}, S_{34}, S_{35}, S_{36}, S_{45}, S_{46}, S_{56} elements are also zero. Accordingly, the compliance matrix is

$$[S] = \begin{bmatrix} S_{11} & S_{12} & S_{13} & 0 & 0 & 0 \\ S_{12} & S_{22} & S_{23} & 0 & 0 & 0 \\ S_{13} & S_{23} & S_{33} & 0 & 0 & 0 \\ 0 & 0 & 0 & S_{44} & 0 & 0 \\ 0 & 0 & 0 & 0 & S_{55} & 0 \\ 0 & 0 & 0 & 0 & 0 & S_{66} \end{bmatrix}. \tag{2.28}$$

The elements of the compliance matrix are listed in Table 2.4. In terms of the engineering constants, the compliance matrix is given in Table 2.7. The stiffness

Table 2.8. The nonzero engineering constants for monoclinic, orthotropic, transversely isotropic, and isotropic materials ($\frac{\nu_{ij}}{E_i} = \frac{\nu_{ji}}{E_j}$, see Table 2.7)

	Nonzero engineering constants	
Material	Independent	Dependent
Monoclinic	E_1, E_2, E_3 G_{23}, G_{13}, G_{12} $\nu_{12}, \nu_{13}, \nu_{23}$ $\nu_{16}, \nu_{26}, \nu_{45}, \nu_{36}$	
Orthotropic	E_1, E_2, E_3 G_{23}, G_{13}, G_{12} $\nu_{12}, \nu_{13}, \nu_{23}$	
Transversely isotropic	E_1, E_2 G_{12} ν_{12}, ν_{23}	$E_3 = E_2, G_{13} = G_{12}$ $G_{23} = \frac{E_2}{2(1+\nu_{23})}$ $\nu_{13} = \nu_{12}$
Isotropic	$E_1 \quad (= E)$ $\nu_{12} \quad (= \nu)$	$E_2 = E_3 = E, \nu_{13} = \nu_{23} = \nu$ $G_{23} = G_{13} = G_{12} = \frac{E}{2(1+\nu)}$

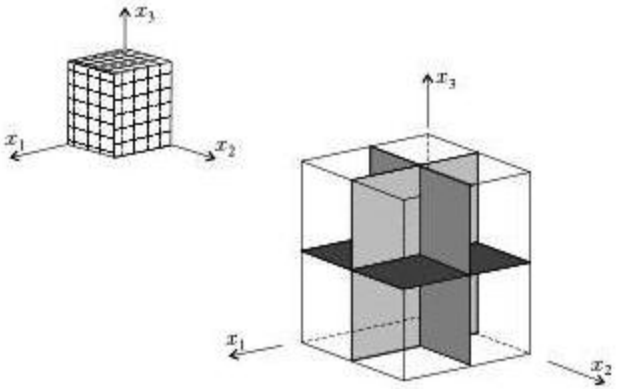

Figure 2.11: Material with three planes of symmetry.

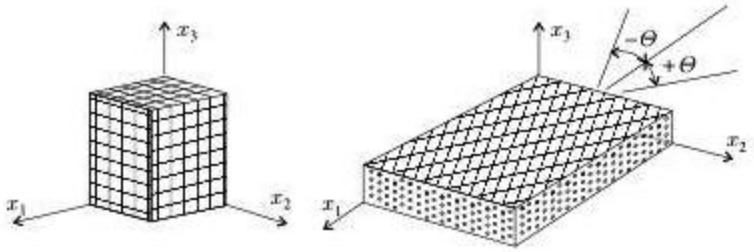

Figure 2.12: Illustrations of fiber-reinforced orthotropic composites.The fibers are oriented in three mutually perpendicular directions (left); the fibers are distributed equally in the $+\Theta$ and $-\Theta$ directions in planes parallel to the x_1–x_2 plane (right).

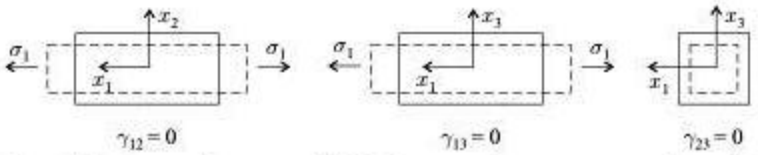

Figure 2.13: A normal stress σ_1 applied in the x_1–x_2 and x_1–x_3 symmetry planes of an orthotropic material.

matrix is obtained by inverting the compliance matrix. The nonzero terms of the stiffness matrix are

$$[C] = \begin{bmatrix} C_{11} & C_{12} & C_{13} & 0 & 0 & 0 \\ C_{12} & C_{22} & C_{23} & 0 & 0 & 0 \\ C_{13} & C_{23} & C_{33} & 0 & 0 & 0 \\ 0 & 0 & 0 & C_{44} & 0 & 0 \\ 0 & 0 & 0 & 0 & C_{55} & 0 \\ 0 & 0 & 0 & 0 & 0 & C_{66} \end{bmatrix}. \tag{2.29}$$

In the $[S]$ and $[C]$ matrices of the 12 nonzero elements only 9 are independent (Table 2.8). Equation (2.29) can be written in the form

$$[C] = \begin{bmatrix} & [L] & & \begin{bmatrix} 0 & 0 & 0 \\ 0 & 0 & 0 \\ 0 & 0 & 0 \end{bmatrix} \\ \begin{bmatrix} 0 & 0 & 0 \\ 0 & 0 & 0 \\ 0 & 0 & 0 \end{bmatrix} & & [M] \end{bmatrix}. \tag{2.30}$$

The submatrices $[L]$ and $[M]$ are given in Tables 2.9 and 2.10 in terms of the engineering constants.

With the compliance matrix given by Eq. (2.28), the strain–stress relationships (Eq. 2.23) become

$$\begin{Bmatrix} \epsilon_1 \\ \epsilon_2 \\ \epsilon_3 \\ \gamma_{23} \\ \gamma_{13} \\ \gamma_{12} \end{Bmatrix} = \begin{bmatrix} S_{11} & S_{12} & S_{13} & 0 & 0 & 0 \\ S_{12} & S_{22} & S_{23} & 0 & 0 & 0 \\ S_{13} & S_{23} & S_{33} & 0 & 0 & 0 \\ 0 & 0 & 0 & S_{44} & 0 & 0 \\ 0 & 0 & 0 & 0 & S_{55} & 0 \\ 0 & 0 & 0 & 0 & 0 & S_{66} \end{bmatrix} \begin{Bmatrix} \sigma_1 \\ \sigma_2 \\ \sigma_3 \\ \tau_{23} \\ \tau_{13} \\ \tau_{12} \end{Bmatrix}. \tag{2.31}$$

This equation shows an important feature of orthotropic materials, namely, that normal stresses do not produce shear deformations when these stresses are in the x_1, x_2, x_3 orthotropy directions. Note, however, that normal stresses applied in the x, y, z directions (which do not coincide with the x_1, x_2, x_3 orthotropy directions) result in shear deformations, as illustrated in Figure 2.14. In this case (in the x, y, z coordinate system) none of the elements of the compliance and stiffness matrices is zero.

Table 2.9. The $[L]$ submatrix in Eq. (2.30) for orthotropic, transversely isotropic, and isotropic materials

Orthotropic

$$[L] = \frac{1}{D}\begin{bmatrix} E_1\left(1-\frac{E_3}{E_2}\nu_{23}^2\right) & E_2\left(\nu_{12}+\frac{E_3}{E_2}\nu_{13}\nu_{23}\right) & E_3\left(\nu_{13}+\nu_{12}\nu_{23}\right) \\ E_2\left(\nu_{12}+\frac{E_3}{E_2}\nu_{13}\nu_{23}\right) & E_2\left(1-\frac{E_3}{E_1}\nu_{13}^2\right) & E_3\left(\nu_{23}+\frac{E_2}{E_1}\nu_{12}\nu_{13}\right) \\ E_3\left(\nu_{13}+\nu_{12}\nu_{23}\right) & E_3\left(\nu_{23}+\frac{E_2}{E_1}\nu_{12}\nu_{13}\right) & E_3\left(1-\frac{E_2}{E_1}\nu_{12}^2\right) \end{bmatrix}$$

$$D = \frac{E_1E_2E_3-\nu_{23}^2E_1E_3^2-\nu_{12}^2E_2^2E_3-2\nu_{12}\nu_{13}\nu_{23}E_2E_3^2-\nu_{13}^2E_2E_3^2}{E_1E_2E_3}$$

Transversely isotropic

$$[L] = \frac{1}{D}\begin{bmatrix} E_1\left(1-\nu_{23}^2\right) & E_2\nu_{12}\left(1+\nu_{23}\right) & E_2\nu_{12}\left(1+\nu_{23}\right) \\ E_2\nu_{12}\left(1+\nu_{23}\right) & E_2\left(1-\frac{E_2}{E_1}\nu_{12}^2\right) & E_2\left(\nu_{23}+\frac{E_2}{E_1}\nu_{12}^2\right) \\ E_2\nu_{12}\left(1+\nu_{23}\right) & E_2\left(\nu_{23}+\frac{E_2}{E_1}\nu_{12}^2\right) & E_2\left(1-\frac{E_2}{E_1}\nu_{12}^2\right) \end{bmatrix}$$

$$D = 1-\nu_{23}^2-2\left(1+\nu_{23}\right)\frac{E_2}{E_1}\nu_{12}^2$$

Isotropic

$$[L] = \frac{E}{(1+\nu)(1-2\nu)}\begin{bmatrix} 1-\nu & \nu & \nu \\ \nu & 1-\nu & \nu \\ \nu & \nu & 1-\nu \end{bmatrix}$$

Table 2.10. The $[M]$ submatrix in Eq. (2.30) for orthotropic, transversely isotropic, and isotropic materials

Orthotropic

$$[M] = \begin{bmatrix} G_{23} & 0 & 0 \\ 0 & G_{13} & 0 \\ 0 & 0 & G_{12} \end{bmatrix}$$

Transversely isotropic

$$[M] = \begin{bmatrix} \frac{E_2}{2(1+\nu_{23})} & 0 & 0 \\ 0 & G_{12} & 0 \\ 0 & 0 & G_{12} \end{bmatrix}$$

Isotropic

$$[M] = \begin{bmatrix} \frac{E}{2(1+\nu)} & 0 & 0 \\ 0 & \frac{E}{2(1+\nu)} & 0 \\ 0 & 0 & \frac{E}{2(1+\nu)} \end{bmatrix}$$

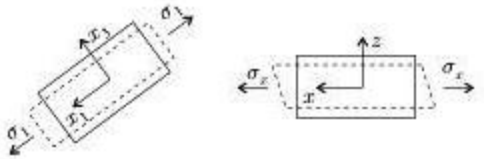

Figure 2.14: Orthotropic material subjected to a normal stress. There is no shear strain when the stress is applied in one of the orthotropy directions (left), but there is shear strain when the stress is not along an orthotropy direction (right).

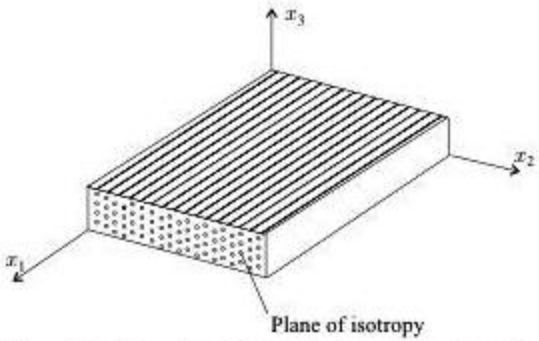

Figure 2.15: Example of a fiber-reinforced, transversely isotropic composite material.

2.3.4 Transversely Isotropic Material

A transversely isotropic material has three planes of symmetry (Fig. 2.11) and, as such, it is orthotropic. In one of the planes of symmetry the material is treated as isotropic. An example of transversely isotropic material is a composite reinforced with continuous unidirectional fibers with all the fibers aligned in the x_1 direction (Fig. 2.15). In this case the material in the plane perpendicular to the fibers (x_2–x_3 plane) is treated as isotropic.

For a transversely isotropic material we specify the stiffness and compliance matrices in an x_1, x_2, x_3 coordinate system chosen in such a way that the axes are perpendicular to the planes of symmetry and x_1 is perpendicular to the plane of isotropy (Fig. 2.15). In this coordinate system, because of material symmetry four of the Poisson ratios are zero ($\nu_{16} = \nu_{26} = \nu_{36} = \nu_{45} = 0$). Furthermore, because of isotropy the following engineering constants are related:

$$E_3 = E_2, \qquad G_{13} = G_{12}, \qquad \nu_{13} = \nu_{12}. \tag{2.32}$$

For an isotropic material the shear modulus is[1]

$$G = \frac{E}{2(1+\nu)}. \tag{2.33}$$

Correspondingly, for a material that is isotropic in the x_2–x_3 plane we write

$$G_{23} = \frac{E_2}{2(1+\nu_{23})}. \tag{2.34}$$

Equations (2.32) and (2.34), together with the expressions in Table 2.6 (page 14), yield the compliance matrix in terms of the engineering constants. The

[1] E. P. Popov, *Engineering Mechanics of Solids*. Prentice-Hall, Englewood Cliffs, New Jersey, 1990, p. 151.

results are given in Table 2.7 (page 15). The zero and nonzero elements of the compliance matrix are

$$[S] = \begin{bmatrix} S_{11} & S_{12} & S_{12} & 0 & 0 & 0 \\ S_{12} & S_{22} & S_{23} & 0 & 0 & 0 \\ S_{12} & S_{23} & S_{22} & 0 & 0 & 0 \\ 0 & 0 & 0 & 2(S_{22} - S_{23}) & 0 & 0 \\ 0 & 0 & 0 & 0 & S_{66} & 0 \\ 0 & 0 & 0 & 0 & 0 & S_{66} \end{bmatrix}. \tag{2.35}$$

The stiffness matrix is obtained by inverting the compliance matrix. The zero and nonzero elements of the stiffness matrix are

$$[C] = \begin{bmatrix} C_{11} & C_{12} & C_{12} & 0 & 0 & 0 \\ C_{12} & C_{22} & C_{23} & 0 & 0 & 0 \\ C_{12} & C_{23} & C_{22} & 0 & 0 & 0 \\ 0 & 0 & 0 & \frac{C_{22}-C_{23}}{2} & 0 & 0 \\ 0 & 0 & 0 & 0 & C_{66} & 0 \\ 0 & 0 & 0 & 0 & 0 & C_{66} \end{bmatrix}. \tag{2.36}$$

In terms of the engineering constants, the elements of the stiffness matrix are given by Eq. (2.30).

In both the compliance and stiffness matrices, of the 12 nonzero elements only 5 are independent (Table 2.8, page 16).

2.3.5 Isotropic Material

In an isotropic material there are no preferred directions and every plane is a plane of symmetry. For example, a composite containing a large number of randomly oriented fibers behaves in an isotropic manner. For an isotropic material the coordinate system may be chosen arbitrarily. Here, we present the compliance and the stiffness matrices in the x_1, x_2, and x_3 coordinate system.

Because of material symmetry four of the Poisson ratios are zero ($\nu_{16} = \nu_{26} = \nu_{36} = \nu_{45} = 0$). Also, because of isotropy some of the engineering constants are related as follows:

$$\begin{aligned} &E_1 = E_2 = E_3 = E \qquad G_{23} = G_{13} = G_{12} = G \\ &\nu_{23} = \nu_{13} = \nu_{12} = \nu \end{aligned} \tag{2.37}$$

$$G = \frac{E}{2(1+\nu)}. \tag{2.38}$$

Equations (2.37) and (2.38), together with the expressions in Table 2.6 (page 14), give the compliance matrix in terms of the engineering constants. The

results are in Table 2.7. The elements of the compliance matrix are

$$[S] = \begin{bmatrix} S_{11} & S_{12} & S_{12} & 0 & 0 & 0 \\ S_{12} & S_{11} & S_{12} & 0 & 0 & 0 \\ S_{12} & S_{12} & S_{11} & 0 & 0 & 0 \\ 0 & 0 & 0 & 2(S_{11}-S_{12}) & 0 & 0 \\ 0 & 0 & 0 & 0 & 2(S_{11}-S_{12}) & 0 \\ 0 & 0 & 0 & 0 & 0 & 2(S_{11}-S_{12}) \end{bmatrix}. \tag{2.39}$$

The stiffness matrix is obtained by inverting the compliance matrix. The elements of the stiffness matrix are

$$[C] = \begin{bmatrix} C_{11} & C_{12} & C_{12} & 0 & 0 & 0 \\ C_{12} & C_{11} & C_{12} & 0 & 0 & 0 \\ C_{12} & C_{12} & C_{11} & 0 & 0 & 0 \\ 0 & 0 & 0 & \frac{C_{11}-C_{12}}{2} & 0 & 0 \\ 0 & 0 & 0 & 0 & \frac{C_{11}-C_{12}}{2} & 0 \\ 0 & 0 & 0 & 0 & 0 & \frac{C_{11}-C_{12}}{2} \end{bmatrix}. \tag{2.40}$$

In terms of the engineering constants, the elements of the stiffness matrix are given by Eq. (2.30).

In both the compliance and stiffness matrices, of the 12 nonzero elements only 2 are independent (Table 2.8, page 16).

2.1 Example. *Calculate the elements of the stiffness and compliance matrices of a graphite epoxy unidirectional ply. The engineering constants are given as* $E_1 = 148 \times 10^9$ *N/m*^{2}, $E_2 = 9.65 \times 10^9$ *N/m*^{2}, $G_{12} = 4.55 \times 10^9$ *N/m*^{2}, $\nu_{12} = 0.3$, *and* $\nu_{23} = 0.6$.

Solution. For a transversely isotropic material the compliance matrix is given in Table 2.7 (page 15, third row). By substituting the engineering constants into the expression in Table 2.7, and by using the condition that $\nu_{ij}/E_i = \nu_{ji}/E_j$ (see Table 2.8, page 16) we obtain

$$[S] = \begin{bmatrix} 6.76 & -2.03 & -2.03 & 0 & 0 & 0 \\ -2.03 & 103.63 & -62.18 & 0 & 0 & 0 \\ -2.03 & -62.18 & 103.63 & 0 & 0 & 0 \\ 0 & 0 & 0 & 331.61 & 0 & 0 \\ 0 & 0 & 0 & 0 & 219.78 & 0 \\ 0 & 0 & 0 & 0 & 0 & 219.78 \end{bmatrix} 10^{-12} \frac{\text{m}^2}{\text{N}}. \tag{2.41}$$

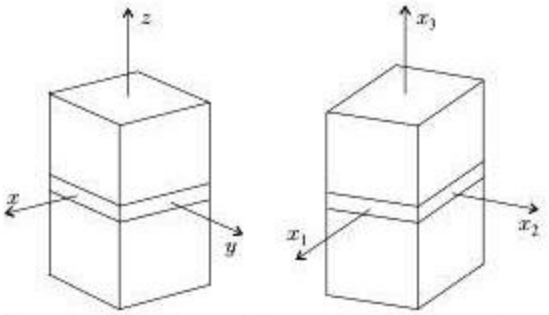

Figure 2.16: The x, y, z and the x_1, x_2, x_3 coordinate systems.

The elements of the stiffness matrix are obtained by inverting the compliance matrix

$$[C] = [S]^{-1} = \begin{bmatrix} 152.47 & 7.46 & 7.46 & 0 & 0 & 0 \\ 7.46 & 15.44 & 9.41 & 0 & 0 & 0 \\ 7.46 & 9.41 & 15.44 & 0 & 0 & 0 \\ 0 & 0 & 0 & 3.016 & 0 & 0 \\ 0 & 0 & 0 & 0 & 4.55 & 0 \\ 0 & 0 & 0 & 0 & 0 & 4.55 \end{bmatrix} 10^9 \frac{\text{N}}{\text{m}^2}. \tag{2.42}$$

2.4 Plane-Strain Condition

There are circumstances when the stresses and strains do not vary in a certain direction. This direction is designated by either the x_3 or the z axis (Fig. 2.16). Although the stresses and strains do not vary along x_3 (or z), they may vary in planes perpendicular to the x_3 (or z) axis. This condition is referred to as plane-strain condition.

When plane-strain condition exists in a body made of an isotropic material the x_1–x_2 (or x–y) planes of the cross section remain plane and perpendicular to the x_3 (or z) axis. In a body made of an anisotropic material these planes do not necessarily remain plane.

Plane-strain condition may exist far from the edges in a long body with constant cross section when both the material properties and the applied loads are uniform

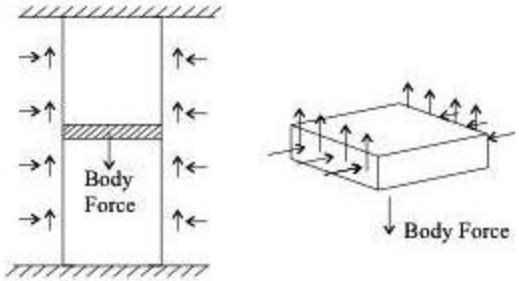

Figure 2.17: Surface and body forces that may be applied under plane-strain condition. The applied forces must be uniform along the longitudinal axis and must be in equilibrium for each segment.

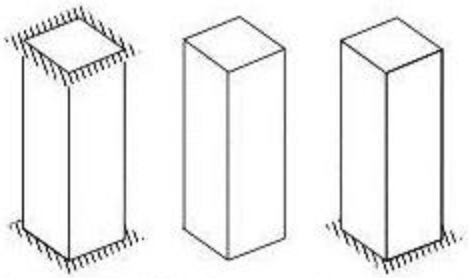

Figure 2.18: Possible end supports for structures analyzed by plane-strain condition.

along the longitudinal axis and, in addition, the loads are in equilibrium on any plane segment (Fig. 2.17).

When the aforementioned plane-strain condition exists, the three-dimensional analysis simplifies considerably. For an isotropic material, the normal strain ϵ_3 (or ϵ_z) in the axial direction (x_3 or z) and the out-of-plane shear strains γ_{13} and γ_{23} (or γ_{xz} and γ_{yz}) are zero. For fiber-reinforced composites these strains are not necessarily zero. Nonetheless, as is discussed in this chapter, plane-strain condition introduces simplifications that facilitate the analysis.

Geometry. The cross section perpendicular to the axis and the material properties must not vary along the length. Both ends of the body may be built-in or may be free, or one end may be built-in while the other one is free (Fig. 2.18). When both ends are built-in, the longitudinal axis (x_3 or z) remains straight and its length remains constant. When one or both ends are free, the longitudinal axis may become curved and its length may change.

Fiber orientation. On the basis of fiber orientation, the body is analyzed as generally anisotropic, monoclinic, orthotropic, transversely isotropic, or isotropic (Fig. 2.19).

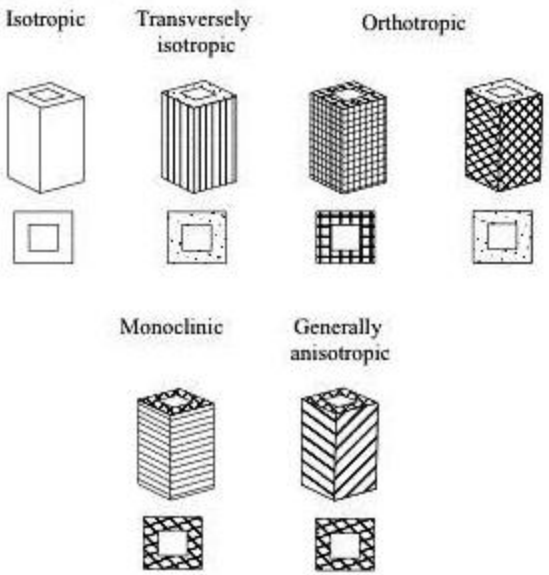

Figure 2.19: Illustrations of possible fiber orientations for plane-strain condition.

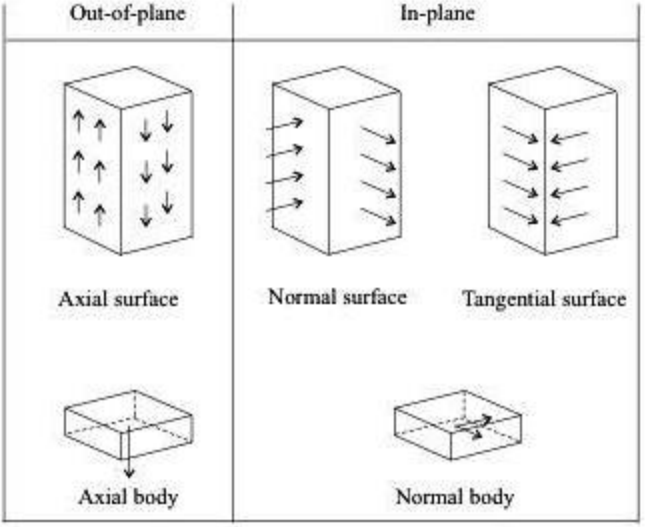

Figure 2.20: Illustrations of surface and body forces that may be applied under plane-strain condition.

In addition to the fiber arrangements shown in Figure 2.19, the composite may contain any combination of the fiber arrangements shown in this figure. The important fact is that the analysis must be performed according to the most complex fiber arrangement inside the body. A body that contains at least one generally anisotropic fiber arrangement must be treated as generally anisotropic; a body that consists of monoclinic, orthotropic, and transversely isotropic fiber arrangements must be treated as monoclinic; a body that consists of orthotropic and transversely isotropic fiber arrangements must be treated as orthotropic.

For monoclinic, orthotropic, and transversely isotropic materials the analysis simplifies considerably when one of the material symmetry planes coincides with the plane of plane-strain.

Loads. Normal, tangential, and axial forces may act on the surface, and body forces may act parallel and normal to the longitudinal axis (Fig. 2.20). These

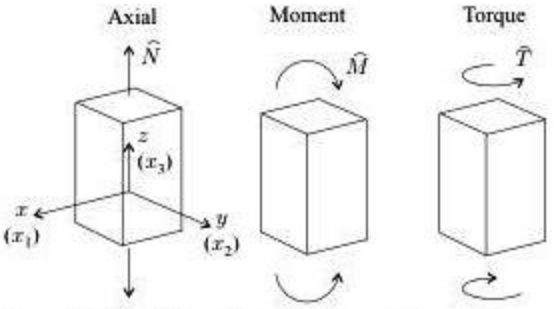

Figure 2.21: Possible end loads for plane-strain condition.

Table 2.11. Relationships between the stresses and the end loads

Load	x, y, z coordinate system	x_1, x_2, x_3 coordinate system
End axial	$\widehat{N} = \int_A \sigma_z dA$	$\widehat{N} = \int_A \sigma_3 dA$
End moment	$\widehat{M}_y = \int_A x\sigma_z dA$	$\widehat{M}_2 = \int_A x_1\sigma_3 dA$
End moment	$\widehat{M}_x = \int_A y\sigma_z dA$	$\widehat{M}_1 = \int_A x_2\sigma_3 dA$
Torque	$\widehat{T} = \int_A (y\tau_{xz} + x\tau_{yz})\, dA$	$\widehat{T} = \int_A (x_2\tau_{13} + x_1\tau_{23})\, dA$

applied forces (loads) may not vary along the length. In addition, an axial force, moment, and torque may be applied at the ends (Fig. 2.21). The forces acting perpendicular and parallel to the longitudinal axis are referred to as in-plane and out-of-plane.

Each of the loads shown in Figures 2.20 and 2.21 may act in combination. As stated previously, the only requirement is that the loads be in equilibrium on each segment (Fig. 2.17) of the body.

The end loads shown in Figure 2.21 are related the to the stresses by the expressions given in Table 2.11.

When two or more types of loads are applied, the stresses and strains can independently be calculated for each type of load. The stresses and strains thus obtained are then superimposed to obtain the final results.

Displacements. Plane-strain condition requires that the strains do not vary along the longitudinal axis. Thus, in the x, y, z coordinate system we have

$$\begin{aligned} &\frac{\partial \epsilon_x}{\partial z} = 0 \qquad \frac{\partial \epsilon_y}{\partial z} = 0 \qquad \frac{\partial \epsilon_z}{\partial z} = 0 \\ &\frac{\partial \gamma_{yz}}{\partial z} = 0 \qquad \frac{\partial \gamma_{xz}}{\partial z} = 0 \qquad \frac{\partial \gamma_{xy}}{\partial z} = 0. \end{aligned} \tag{2.43}$$

The following displacements satisfy these conditions[2]

$$\begin{aligned} u &= U(x, y) - C_1 yz - \frac{1}{2} C_2 z^2 \\ v &= V(x, y) + C_1 xz - \frac{1}{2} C_3 z^2 \\ w &= W(x, y) + (C_2 x + C_3 y + C_4)\, z, \end{aligned} \tag{2.44}$$

where U, V, and W are functions that depend only on x and y, and C_1, C_2, C_3, and C_4 are constants. For small displacements we have the following relationships[3]:

$$\epsilon_z^o = \frac{\partial w}{\partial z} \qquad \frac{1}{\rho_y} = -\frac{\partial^2 u}{\partial z^2} \qquad \frac{1}{\rho_x} = -\frac{\partial^2 v}{\partial z^2}. \tag{2.45}$$

[2] S. G. Lekhnitskii, *Theory of Elasticity of an Anisotropic Body*. Mir Publishers, Moscow, 1981, p. 104.

[3] T. H. G. Megson, *Aircraft Structures for Engineering Students*. 3d edition. Halsted Press, John Wiley & Sons, New York, 1999, p. 284.

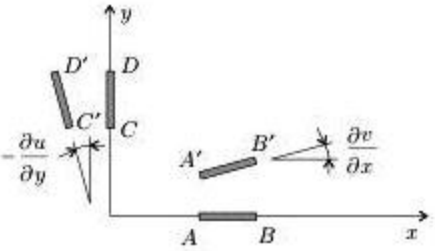

Figure 2.22: Illustration of the rotations of line elements parallel with the x- and y-axes.

where ϵ_z^o is the strain along the longitudinal axis; $1/\rho_y$, $1/\rho_x$ are the curvatures of the longitudinal axis in the x–z and y–z planes, respectively. By virtue of $\partial\gamma_{xy}/\partial z = 0$ (Eq. 2.43), we have (Eq. 2.11)

$$\frac{\partial^2 u}{\partial y \partial z} + \frac{\partial^2 v}{\partial x \partial z} = 0. \tag{2.46}$$

We define

$$\vartheta \equiv \frac{\partial}{\partial z}\left(\frac{\partial v}{\partial x}\right) = -\frac{\partial}{\partial z}\left(\frac{\partial u}{\partial y}\right). \tag{2.47}$$

As is illustrated in Figure 2.22, ϑ represents the rate of twist of the cross section.

The constants in Eq. (2.44) are determined as follows. From Eqs. (2.47) and (2.44) we have

$$\vartheta \equiv \frac{\partial^2 v}{\partial x \partial z} = -\frac{\partial^2 u}{\partial y \partial z} = C_1. \tag{2.48}$$

From Eqs. (2.45) and (2.44) we write

$$\begin{aligned} \epsilon_z^o &= \frac{\partial w}{\partial z} = C_4 \\ \frac{1}{\rho_y} &= -\frac{\partial^2 u}{\partial z^2} = C_2 \\ \frac{1}{\rho_x} &= -\frac{\partial^2 v}{\partial z^2} = C_3. \end{aligned} \tag{2.49}$$

We can now write the displacements as

$$u = U(x, y) - \vartheta yz - \frac{1}{2}\frac{1}{\rho_y} z^2 \tag{2.50}$$

$$v = V(x, y) + \vartheta xz - \frac{1}{2}\frac{1}{\rho_x} z^2 \tag{2.51}$$

$$w = W(x, y) + \left(\frac{1}{\rho_y} x + \frac{1}{\rho_x} y + \epsilon_z^o\right) z. \tag{2.52}$$

These represent the following five deformations (Fig. 2.23):

- Planar – planes perpendicular to the longitudinal axis remain plain and perpendicular to the axis
- Nonplanar – planes perpendicular to the longitudinal axis deform out of the plane

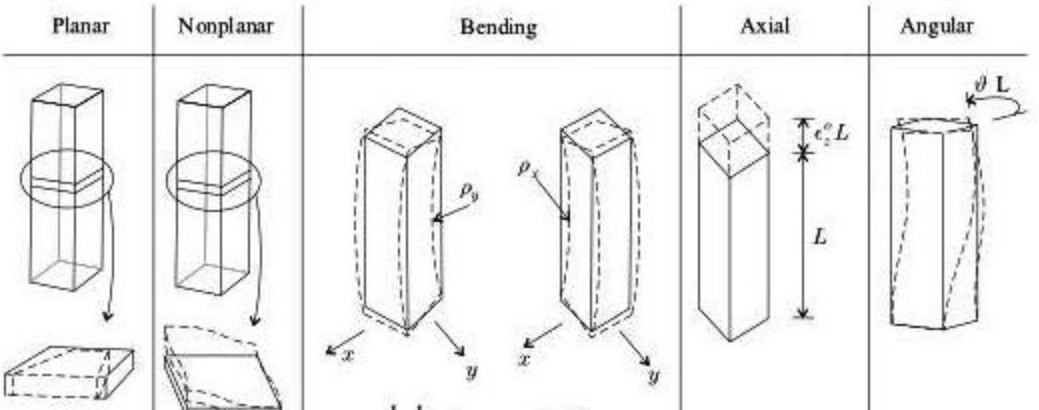

Planar	Nonplanar	Bending		Axial	Angular
$u = U(x,y)$	$u = 0$	$u = -\frac{1}{2}\frac{1}{\rho_y}z^2$	$u = 0$	$u = 0$	$u = -\vartheta yz$
$v = V(x,y)$	$v = 0$	$v = 0$	$v = -\frac{1}{2}\frac{1}{\rho_x}z^2$	$v = 0$	$v = \vartheta xz$
$w = 0$	$w = W(x,y)$	$w = \frac{1}{\rho_y}xz$	$w = \frac{1}{\rho_x}yz$	$w = \epsilon_z^o z$	$w = 0$

Figure 2.23: Deformations and displacements under plane-strain condition. In the x_1, x_2, x_3 coordinate system u, v, w are replaced by u_1, u_2, u_3; U, V, W by U_1, U_2, U_3; and ρ_x, ρ_y by ρ_1, ρ_2.

- Bending – the straight longitudinal axis becomes curved
- Axial – the straight longitudinal axis remains straight and undergoes axial elongation
- Angular – planes perpendicular to the longitudinal axis rotate about the axis.

The u, v, w components of the displacements corresponding to each of the deformations are shown in Figure 2.23.

We again use the x, y, z coordinate system for generally anisotropic materials. For monoclinic, orthotropic, transversely isotropic, and isotropic materials we use the x_1, x_2, x_3 coordinate system, with x_3 being along the longitudinal axis of the body (Fig. 2.16). In the x_1, x_2, x_3 coordinate system the displacements are

$$\begin{aligned} u_1 &= U_1(x_1, x_2) - \vartheta x_2 x_3 - \frac{1}{2}\frac{1}{\rho_2}x_3^2 \\ u_2 &= U_2(x_1, x_2) + \vartheta x_1 x_3 - \frac{1}{2}\frac{1}{\rho_1}x_3^2 \\ u_3 &= U_3(x_1, x_2) + \left(\frac{1}{\rho_2}x_1 + \frac{1}{\rho_1}x_2 + \epsilon_3^\circ\right)x_3, \end{aligned} \tag{2.53}$$

where ϵ_3° is the elongation of the longitudinal axis; $1/\rho_2, 1/\rho_1$ are the curvatures of this axis in the x_1–x_3 and x_2–x_3 planes, respectively; ϑ represents the rate of twist of the cross section.

In the following, we present the equilibrium equations, the strain–displacement relationships, and the stress–strain relationships when the aforementioned conditions of plane-strain are satisfied. The analyses are applicable in regions away from the two ends of the body.

We treat problems in two groups: (i) when one or both ends are free and (ii) when both ends are built-in (Fig. 2.18).

2.4.1 Free End – Generally Anisotropic Material

We consider a generally anisotropic body with one or both ends free. This body may undergo every deformation shown in Figure 2.23, and the displacements are the sum of all possible displacements shown in this figure. The strains are then obtained from the strain–displacement relationships given by Eqs. (2.2)–(2.4) and (2.9)–(2.11). By introducing Eqs. (2.50)–(2.52) we have

$$\epsilon_x = \frac{\partial U}{\partial x} \qquad \epsilon_y = \frac{\partial V}{\partial y} \tag{2.54}$$

$$\epsilon_z = \frac{1}{\rho_y}x + \frac{1}{\rho_x}y + \epsilon_z^\circ \tag{2.55}$$

$$\gamma_{yz} = \frac{\partial W}{\partial y} + \vartheta x \qquad \gamma_{xz} = \frac{\partial W}{\partial x} - \vartheta y \tag{2.56}$$

$$\gamma_{xy} = \frac{\partial U}{\partial y} + \frac{\partial V}{\partial x}. \tag{2.57}$$

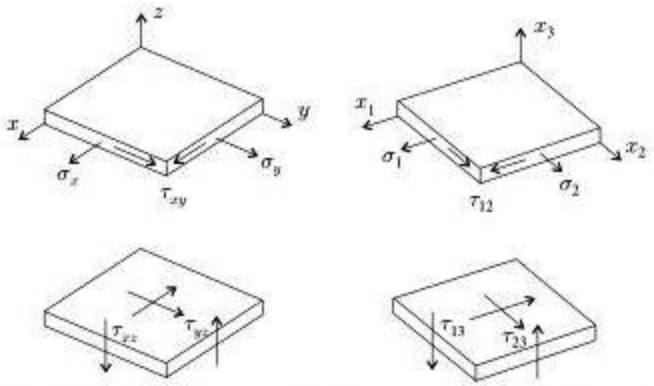

Figure 2.24: The stress components that appear in the equilibrium equations under plane-strain condition.

Since the strain components are independent of z, the stress components are also independent of z, and we have

$$\frac{\partial \sigma_z}{\partial z} = 0 \qquad \frac{\partial \tau_{yz}}{\partial z} = 0 \qquad \frac{\partial \tau_{xz}}{\partial z} = 0. \tag{2.58}$$

By utilizing Eq. (2.58), the equilibrium equations (Eqs. 2.13–2.15) become

$$\frac{\partial \sigma_x}{\partial x} + \frac{\partial \tau_{xy}}{\partial y} + f_x = 0 \tag{2.59}$$

$$\frac{\partial \tau_{xy}}{\partial x} + \frac{\partial \sigma_y}{\partial y} + f_y = 0 \tag{2.60}$$

$$\frac{\partial \tau_{xz}}{\partial x} + \frac{\partial \tau_{yz}}{\partial y} + f_z = 0. \tag{2.61}$$

The five stress components $\sigma_x, \sigma_y, \tau_{xy}, \tau_{yz}, \tau_{xz}$ that appear in these equilibrium equations are illustrated in Figure 2.24.

For a generally anisotropic material the stress–strain relationships (Eq. 2.20) may be written in partitioned form, as follows:

$$\begin{Bmatrix} \sigma_x \\ \sigma_y \\ \tau_{yz} \\ \tau_{xz} \\ \tau_{xy} \end{Bmatrix} = \begin{bmatrix} \overline{C}_{11} & \overline{C}_{12} & \overline{C}_{14} & \overline{C}_{15} & \overline{C}_{16} \\ \overline{C}_{12} & \overline{C}_{22} & \overline{C}_{24} & \overline{C}_{25} & \overline{C}_{26} \\ \overline{C}_{14} & \overline{C}_{24} & \overline{C}_{44} & \overline{C}_{45} & \overline{C}_{46} \\ \overline{C}_{15} & \overline{C}_{25} & \overline{C}_{45} & \overline{C}_{55} & \overline{C}_{56} \\ \overline{C}_{16} & \overline{C}_{26} & \overline{C}_{46} & \overline{C}_{56} & \overline{C}_{66} \end{bmatrix} \begin{Bmatrix} \epsilon_x \\ \epsilon_y \\ \gamma_{yz} \\ \gamma_{xz} \\ \gamma_{xy} \end{Bmatrix} + \begin{Bmatrix} \overline{C}_{13} \\ \overline{C}_{23} \\ \overline{C}_{34} \\ \overline{C}_{35} \\ \overline{C}_{36} \end{Bmatrix} \epsilon_z \tag{2.62}$$

$$\sigma_z = [\overline{C}_{13} \quad \overline{C}_{23} \quad \overline{C}_{34} \quad \overline{C}_{35} \quad \overline{C}_{36}] \begin{Bmatrix} \epsilon_x \\ \epsilon_y \\ \gamma_{yz} \\ \gamma_{xz} \\ \gamma_{xy} \end{Bmatrix} + \overline{C}_{33} \epsilon_z, \tag{2.63}$$

where, we recall, ϵ_z is (Eq. 2.55)

$$\epsilon_z = \frac{1}{\rho_y}x + \frac{1}{\rho_x}y + \epsilon_z^o. \tag{2.64}$$

The stiffness matrix $[\overline{C}]$ is the inverse of the compliance matrix $[\overline{S}]$ defined in Table 2.3 (page 10). The strain–stress relationships are obtained by inverting Eq. (2.62) as follows:

$$\begin{Bmatrix} \epsilon_x \\ \epsilon_y \\ \gamma_{yz} \\ \gamma_{xz} \\ \gamma_{xy} \end{Bmatrix} = \begin{bmatrix} \overline{R}_{11} & \overline{R}_{12} & \overline{R}_{14} & \overline{R}_{15} & \overline{R}_{16} \\ \overline{R}_{12} & \overline{R}_{22} & \overline{R}_{24} & \overline{R}_{25} & \overline{R}_{26} \\ \overline{R}_{14} & \overline{R}_{24} & \overline{R}_{44} & \overline{R}_{45} & \overline{R}_{46} \\ \overline{R}_{15} & \overline{R}_{25} & \overline{R}_{45} & \overline{R}_{55} & \overline{R}_{56} \\ \overline{R}_{16} & \overline{R}_{26} & \overline{R}_{46} & \overline{R}_{56} & \overline{R}_{66} \end{bmatrix} \left(\begin{Bmatrix} \sigma_x \\ \sigma_y \\ \tau_{yz} \\ \tau_{xz} \\ \tau_{xy} \end{Bmatrix} - \begin{Bmatrix} \overline{C}_{13} \\ \overline{C}_{23} \\ \overline{C}_{34} \\ \overline{C}_{35} \\ \overline{C}_{36} \end{Bmatrix} \epsilon_z \right), \tag{2.65}$$

where $\overline{R}_{ij}$ $(i, j = 1, 2, 4, 5, 6)$ are the in-plane elements of the compliance matrix under plane-strain condition calculated from the relationship

$$\begin{bmatrix} \overline{R}_{11} & \overline{R}_{12} & \overline{R}_{14} & \overline{R}_{15} & \overline{R}_{16} \\ \overline{R}_{12} & \overline{R}_{22} & \overline{R}_{24} & \overline{R}_{25} & \overline{R}_{26} \\ \overline{R}_{14} & \overline{R}_{24} & \overline{R}_{44} & \overline{R}_{45} & \overline{R}_{46} \\ \overline{R}_{15} & \overline{R}_{25} & \overline{R}_{45} & \overline{R}_{55} & \overline{R}_{56} \\ \overline{R}_{16} & \overline{R}_{26} & \overline{R}_{46} & \overline{R}_{56} & \overline{R}_{66} \end{bmatrix} = \begin{bmatrix} \overline{C}_{11} & \overline{C}_{12} & \overline{C}_{14} & \overline{C}_{15} & \overline{C}_{16} \\ \overline{C}_{12} & \overline{C}_{22} & \overline{C}_{24} & \overline{C}_{25} & \overline{C}_{26} \\ \overline{C}_{14} & \overline{C}_{24} & \overline{C}_{44} & \overline{C}_{45} & \overline{C}_{46} \\ \overline{C}_{15} & \overline{C}_{25} & \overline{C}_{45} & \overline{C}_{55} & \overline{C}_{56} \\ \overline{C}_{16} & \overline{C}_{26} & \overline{C}_{46} & \overline{C}_{56} & \overline{C}_{66} \end{bmatrix}^{-1}. \tag{2.66}$$

2.4.2 Free End – Monoclinic Material

We consider a body made of a monoclinic material (Fig. 2.9) with the plane of material symmetry coinciding with the x_1–x_2 plane shown in Figure 2.16. One or both ends of the body are free. The displacements resulting from specified loads are summarized in Figure 2.25.

In-plane loads. The body is subjected to the in-plane loads shown in Figure 2.20. Under these loads the body may undergo only planar, bending, and axial deformations (Fig. 2.25). Accordingly, Eq. (2.53) reduces to (see Fig. 2.23)

$$\begin{aligned} u_1 &= U_1(x_1, x_2) - \frac{1}{2}\frac{1}{\rho_2}x_3^2 \\ u_2 &= U_2(x_1, x_2) - \frac{1}{2}\frac{1}{\rho_1}x_3^2 \\ u_3 &= \left(\frac{1}{\rho_2}x_1 + \frac{1}{\rho_1}x_2 + \epsilon_3^o\right)x_3. \end{aligned} \tag{2.67}$$

The strain–displacement relationships (Eqs. 2.2–2.4, 2.9–2.11) show that for these displacements the strains are

$$\epsilon_1 = \frac{\partial U_1}{\partial x_1} \qquad \epsilon_2 = \frac{\partial U_2}{\partial x_2} \tag{2.68}$$

$$\epsilon_3 = \frac{1}{\rho_2}x_1 + \frac{1}{\rho_1}x_2 + \epsilon_3^o \tag{2.69}$$

$$\gamma_{23} = 0 \qquad \gamma_{13} = 0 \tag{2.70}$$

$$\gamma_{12} = \frac{\partial U_1}{\partial x_2} + \frac{\partial U_2}{\partial x_1}. \tag{2.71}$$

Deformation / Load	Planar	Nonplanar	Bending		Axial	Angular
In-plane			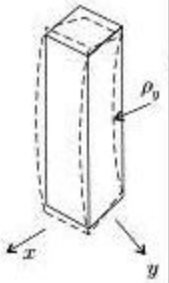	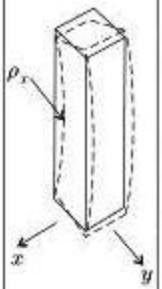	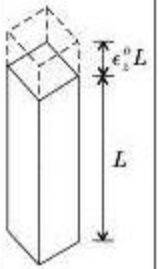	
End axial						
End moment						
Out-of-plane		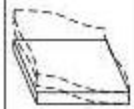				
Torque						

Figure 2.25: Deformations of a monoclinic body under plane-strain condition for different loads. One or both ends are free.

Since $\gamma_{23} = 0$ and $\gamma_{13} = 0$, Eqs. (2.22) and (2.27) give

$$\tau_{23} = 0 \qquad \tau_{13} = 0. \tag{2.72}$$

Furthermore, since the strain and stress components are independent of x_3, we have

$$\frac{\partial \sigma_3}{\partial x_3} = 0. \tag{2.73}$$

With these stresses the relevant equilibrium equations (Eqs. 2.13 and 2.14) – in the x_1, x_2, x_3 coordinate system – reduce to

$$\frac{\partial \sigma_1}{\partial x_1} + \frac{\partial \tau_{12}}{\partial x_2} + f_1 = 0 \tag{2.74}$$

$$\frac{\partial \tau_{12}}{\partial x_1} + \frac{\partial \sigma_2}{\partial x_2} + f_2 = 0. \tag{2.75}$$

The stress components σ_1, σ_2, τ_{12}, which appear in the equilibrium equations, are illustrated in Figure 2.24 (top, right).

By substituting Eq. (2.70) into Eq. (2.22) and by utilizing Eq. (2.27) we obtain the following stress–strain relationships for in-plane loads:

$$\begin{Bmatrix} \sigma_1 \\ \sigma_2 \\ \tau_{12} \end{Bmatrix} = \begin{bmatrix} C_{11} & C_{12} & C_{16} \\ C_{12} & C_{22} & C_{26} \\ C_{16} & C_{26} & C_{66} \end{bmatrix} \begin{Bmatrix} \epsilon_1 \\ \epsilon_2 \\ \gamma_{12} \end{Bmatrix} + \begin{Bmatrix} C_{13} \\ C_{23} \\ C_{36} \end{Bmatrix} \epsilon_3 \tag{2.76}$$

$$\sigma_3 = \begin{bmatrix} C_{31} & C_{32} & C_{36} \end{bmatrix} \begin{Bmatrix} \epsilon_1 \\ \epsilon_2 \\ \gamma_{12} \end{Bmatrix} + C_{33}\epsilon_3, \tag{2.77}$$

where, we recall, ϵ_3 is (Eq. 2.69)

$$\epsilon_3 = \frac{1}{\rho_2} x_1 + \frac{1}{\rho_1} x_2 + \epsilon_3^o. \tag{2.78}$$

The strain–stress relationships are obtained from Eq. (2.76) by inversion

$$\begin{Bmatrix} \epsilon_1 \\ \epsilon_2 \\ \gamma_{12} \end{Bmatrix} = \begin{bmatrix} R_{11} & R_{12} & R_{16} \\ R_{12} & R_{22} & R_{26} \\ R_{16} & R_{26} & R_{66} \end{bmatrix} \left(\begin{Bmatrix} \sigma_1 \\ \sigma_2 \\ \tau_{12} \end{Bmatrix} - \begin{Bmatrix} C_{13} \\ C_{23} \\ C_{36} \end{Bmatrix} \epsilon_3 \right), \tag{2.79}$$

where R_{ij} $(i, j = 1, 2, 6)$ are the in-plane elements of the compliance matrix in the x_1, x_2 coordinate system calculated from the relationship

$$\begin{bmatrix} R_{11} & R_{12} & R_{16} \\ R_{12} & R_{22} & R_{26} \\ R_{16} & R_{26} & R_{66} \end{bmatrix} = \begin{bmatrix} C_{11} & C_{12} & C_{16} \\ C_{12} & C_{22} & C_{26} \\ C_{16} & C_{26} & C_{66} \end{bmatrix}^{-1}. \tag{2.80}$$

Out-of-plane loads. The body is subjected to the out-of-plane loads shown in Figure 2.20. Under these loads the body may undergo only nonplanar and angular deformations (Fig. 2.25), and the displacements (in the x_1, x_2, x_3 coordinate system) are (see Eq. 2.53 and Fig. 2.23)

$$\begin{aligned} u_1 &= -\vartheta x_2 x_3 \\ u_2 &= \vartheta x_1 x_3 \\ u_3 &= U_3(x_1, x_2). \end{aligned} \tag{2.81}$$

For these displacements the strains are (see Eqs. 2.2–2.4, 2.9–2.11)

$$\epsilon_1 = 0 \qquad \epsilon_2 = 0 \tag{2.82}$$

$$\epsilon_3 = 0 \tag{2.83}$$

$$\gamma_{23} = \frac{\partial U_3}{\partial x_2} + \vartheta x_1 \qquad \gamma_{13} = \frac{\partial U_3}{\partial x_1} - \vartheta x_2 \tag{2.84}$$

$$\gamma_{12} = 0. \tag{2.85}$$

Only γ_{23} and γ_{13} are nonzero. Correspondingly, the only nonzero stresses are τ_{13} and τ_{23}. Thus, two of the equilibrium equations (Eqs. 2.13 and 2.14) become trivial, and the third (Eq. 2.15) – in the x_1, x_2, x_3 coordinate system – reduces to

$$\frac{\partial \tau_{13}}{\partial x_1} + \frac{\partial \tau_{23}}{\partial x_2} + f_3 = 0. \tag{2.86}$$

The τ_{23}, τ_{13} stress components, which appear in the equilibrium equation, are illustrated in Figure 2.24 (bottom, right).

From Eqs. (2.22) and (2.27) we obtain the following stress–strain relationships for out-of-plane loads:

$$\begin{Bmatrix} \tau_{23} \\ \tau_{13} \end{Bmatrix} = \begin{bmatrix} C_{44} & C_{45} \\ C_{45} & C_{55} \end{bmatrix} \begin{Bmatrix} \gamma_{23} \\ \gamma_{13} \end{Bmatrix}. \tag{2.87}$$

The strain–stress relationships are obtained from Eq. (2.87) by inversion

$$\begin{Bmatrix} \gamma_{23} \\ \gamma_{13} \end{Bmatrix} = \begin{bmatrix} S_{44} & S_{45} \\ S_{45} & S_{55} \end{bmatrix} \begin{Bmatrix} \tau_{23} \\ \tau_{13} \end{Bmatrix}, \tag{2.88}$$

where the compliance matrix $[S]$ is the inverse of the stiffness matrix in Eq. (2.87)

$$\begin{bmatrix} S_{44} & S_{45} \\ S_{45} & S_{55} \end{bmatrix} = \begin{bmatrix} C_{44} & C_{45} \\ C_{45} & C_{55} \end{bmatrix}^{-1}. \tag{2.89}$$

End axial loads. Axial loads are applied at the ends (Fig. 2.21). Under such loads the body may undergo only planar, bending, and axial deformations

(Fig. 2.25), and the displacements are (see Eq. 2.53 and Fig. 2.23)

$$u_1 = U_1(x_1, x_2) - \frac{1}{2}\frac{1}{\rho_2}x_3^2 \tag{2.90}$$

$$u_2 = U_2(x_1, x_2) - \frac{1}{2}\frac{1}{\rho_1}x_3^2 \tag{2.91}$$

$$u_3 = \left(\frac{1}{\rho_2}x_1 + \frac{1}{\rho_1}x_2 + \epsilon_3^o\right)x_3. \tag{2.92}$$

These displacements are the same as those for in-plane loads (Eq. 2.67). Hence, the strain–displacement, equilibrium, and stress–strain relationships are the same as those given by Eqs. (2.68)–(2.80).

End moment. A bending moment is applied at each end (Fig. 2.21). Under this loading the body may undergo only planar, bending, and axial deformations (Fig. 2.25), and the displacements are (see Eq. 2.53 and Fig. 2.23)

$$\begin{aligned} u_1 &= U_1(x_1, x_2) - \frac{1}{2}\frac{1}{\rho_2}x_3^2 \\ u_2 &= U_2(x_1, x_2) - \frac{1}{2}\frac{1}{\rho_1}x_3^2 \\ u_3 &= \left(\frac{1}{\rho_2}x_1 + \frac{1}{\rho_1}x_2 + \epsilon_3^o\right)x_3. \end{aligned} \tag{2.93}$$

These displacements are the same as those for in-plane loads (Eq. 2.67). Hence, the strain–displacement, equilibrium, and stress–strain relationships are the same as those given by Eqs. (2.68)–(2.80).

Torque. A torque is applied at each end (Fig. 2.21). Under this load the body may undergo only nonplanar and angular deformations (Fig. 2.25), and the displacements are (see Eq. 2.53 and Fig. 2.23)

$$u_1 = -\vartheta x_2 x_3 \qquad u_2 = \vartheta x_1 x_3 \qquad u_3 = U_3(x_1, x_2). \tag{2.94}$$

These displacements are the same as those for out-of-plane loads (Eq. 2.81). Hence, the strain–displacement, equilibrium, and stress–strain relationships are the same as those given by Eqs. (2.81)–(2.88).

2.4.3 Free End – Orthotropic, Transversely Isotropic, or Isotropic Material

When at least one end of the body is free, the expressions given in Section 2.4.2 are also applicable to bodies treated as orthotropic, transversely isotropic, or isotropic provided that one of the material symmetry planes coincides with the x_1–x_2 plane shown in Figure 2.16. For such bodies the following simplifications apply:

Orthotropic

$$C_{16} = C_{26} = C_{36} = 0 \qquad R_{16} = R_{26} = 0. \tag{2.95}$$

Transversely isotropic

$$\begin{aligned} &C_{16} = C_{26} = C_{36} = 0 \qquad R_{16} = R_{26} = 0 \\ &C_{13} = C_{12}. \end{aligned} \tag{2.96}$$

Isotropic

$$\begin{aligned} &C_{16} = C_{26} = C_{36} = 0 \qquad R_{16} = R_{26} = 0 \\ &C_{22} = C_{11} \qquad\qquad R_{22} = R_{11} \\ &C_{66} = \tfrac{1}{2}(C_{11} - C_{12}) \qquad R_{66} = 2(R_{11} - R_{12}) \\ &C_{13} = C_{23} = C_{12}. \end{aligned} \tag{2.97}$$

2.4.4 Built-In Ends – Generally Anisotropic Material

When both ends of a generally anisotropic body are built-in (Fig. 2.18), in-plane as well as out-of-plane loads may be applied (Fig. 2.20). The body may undergo only planar and nonplanar deformations (Fig. 2.23). However, the longitudinal axis of the body remains straight ($1/\rho_y = 1/\rho_x = 0$), its length remains constant ($\epsilon_z^o = 0$), and the body does not twist ($\vartheta = 0$). The permissible deformations are summarized in Figure 2.26 and the displacements are (see Fig. 2.23)

$$u = U(x, y) \qquad v = V(x, y) \qquad w = W(x, y). \tag{2.98}$$

These displacements are the same as the displacements given by Eqs. (2.50)–(2.52) for a body with free ends, when $1/\rho_y$, $1/\rho_x$, ϵ_z^o, and ϑ are set equal to zero. Thus, the strain–displacement, the stress–strain, and the equilibrium equations are obtained by setting $1/\rho_y$, $1/\rho_x$, ϵ_z^o, and ϑ equal to zero in the equations of Section 2.4.1. The strain–displacement relationships (Eqs. 2.54–2.57) become

$$\epsilon_x = \frac{\partial U}{\partial x} \qquad \epsilon_y = \frac{\partial V}{\partial y} \tag{2.99}$$

$$\epsilon_z = 0 \tag{2.100}$$

$$\gamma_{yz} = \frac{\partial W}{\partial y} \qquad \gamma_{xz} = \frac{\partial W}{\partial x} \tag{2.101}$$

$$\gamma_{xy} = \frac{\partial U}{\partial y} + \frac{\partial V}{\partial x}. \tag{2.102}$$

The equilibrium equations are identical with Eqs. (2.59)–(2.61).

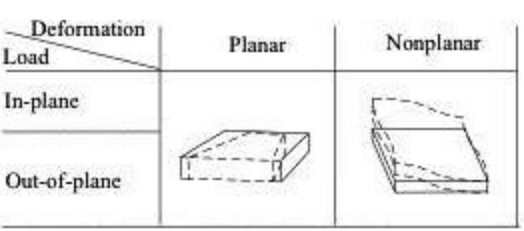

Figure 2.26: Deformations of a generally anisotropic body under plane-strain condition for different loads; built-in ends.

The stress–strain relationships (Eqs. 2.62 and 2.63) become

$$\begin{Bmatrix} \sigma_x \\ \sigma_y \\ \tau_{yz} \\ \tau_{xz} \\ \tau_{xy} \end{Bmatrix} = \begin{bmatrix} \overline{C}_{11} & \overline{C}_{12} & \overline{C}_{14} & \overline{C}_{15} & \overline{C}_{16} \\ \overline{C}_{12} & \overline{C}_{22} & \overline{C}_{24} & \overline{C}_{25} & \overline{C}_{26} \\ \overline{C}_{14} & \overline{C}_{24} & \overline{C}_{44} & \overline{C}_{45} & \overline{C}_{46} \\ \overline{C}_{15} & \overline{C}_{25} & \overline{C}_{45} & \overline{C}_{55} & \overline{C}_{56} \\ \overline{C}_{16} & \overline{C}_{26} & \overline{C}_{46} & \overline{C}_{56} & \overline{C}_{66} \end{bmatrix} \begin{Bmatrix} \epsilon_x \\ \epsilon_y \\ \gamma_{yz} \\ \gamma_{xz} \\ \gamma_{xy} \end{Bmatrix} \tag{2.103}$$

$$\sigma_z = [\overline{C}_{13} \quad \overline{C}_{23} \quad \overline{C}_{34} \quad \overline{C}_{35} \quad \overline{C}_{36}] \begin{Bmatrix} \epsilon_x \\ \epsilon_y \\ \gamma_{yz} \\ \gamma_{xz} \\ \gamma_{xy} \end{Bmatrix}. \tag{2.104}$$

By inverting Eq. (2.103), we obtain the strain–stress relationships

$$\begin{Bmatrix} \epsilon_x \\ \epsilon_y \\ \gamma_{yz} \\ \gamma_{xz} \\ \gamma_{xy} \end{Bmatrix} = \begin{bmatrix} \overline{R}_{11} & \overline{R}_{12} & \overline{R}_{14} & \overline{R}_{15} & \overline{R}_{16} \\ \overline{R}_{12} & \overline{R}_{22} & \overline{R}_{24} & \overline{R}_{25} & \overline{R}_{26} \\ \overline{R}_{14} & \overline{R}_{24} & \overline{R}_{44} & \overline{R}_{45} & \overline{R}_{46} \\ \overline{R}_{15} & \overline{R}_{25} & \overline{R}_{45} & \overline{R}_{55} & \overline{R}_{56} \\ \overline{R}_{16} & \overline{R}_{26} & \overline{R}_{46} & \overline{R}_{56} & \overline{R}_{66} \end{bmatrix} \begin{Bmatrix} \sigma_x \\ \sigma_y \\ \tau_{yz} \\ \tau_{xz} \\ \tau_{xy} \end{Bmatrix}, \tag{2.105}$$

where $[\overline{R}]$ is defined by Eq. (2.66).

2.4.5 Built-In Ends – Monoclinic Material

We consider a body made of a monoclinic material with the plane of material symmetry coinciding with the x_1–x_2 plane shown in Figure 2.16. Both ends of the body are built-in. The longitudinal axis of the body remains straight ($1/\rho_y = 1/\rho_x = 0$), its length remains constant ($\epsilon_z^o = 0$), and the body does not twist ($\vartheta = 0$); hence, the body may undergo only planar and nonplanar deformations (Fig. 2.23). The deformations resulting from specified loads are summarized in Figure 2.27.

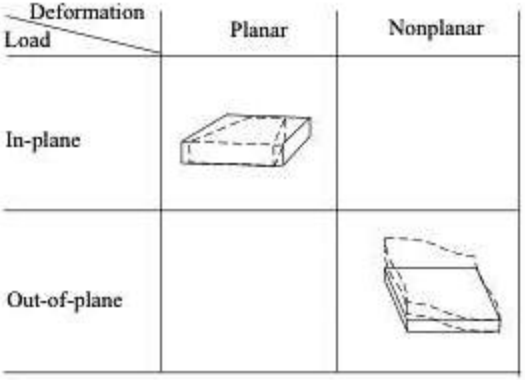

Figure 2.27: Deformations of a monoclinic body under plane-strain condition for different loads; built-in ends.

In-plane loads. The body is subjected to the in-plane loads shown in Figure 2.20. Under these loads the body undergoes planar deformations (Fig. 2.27), and the displacements are (see Eq. 2.53 and Fig. 2.23)

$$u_1 = U_1(x_1, x_2) \qquad u_2 = U_2(x_1, x_2) \qquad u_3 = 0. \tag{2.106}$$

These displacements are the same as the displacements of a body with free ends with $1/\rho_2$, $1/\rho_1$, and ϵ_3^0 set equal to zero in Eq. (2.67). Thus, the strain–displacement, the stress–strain, and the equilibrium equations are obtained by setting $1/\rho_2$, $1/\rho_1$, and ϵ_3^0 equal to zero in the equations of Section 2.4.2. The strain–displacement relationships (see Eqs. 2.68–2.71) are

$$\epsilon_1 = \frac{\partial U_1}{\partial x_1} \qquad \epsilon_2 = \frac{\partial U_2}{\partial x_2} \tag{2.107}$$

$$\epsilon_3 = 0 \tag{2.108}$$

$$\gamma_{23} = 0 \qquad \gamma_{13} = 0 \tag{2.109}$$

$$\gamma_{12} = \frac{\partial U_1}{\partial x_2} + \frac{\partial U_2}{\partial x_1}. \tag{2.110}$$

The equilibrium equations are identical to Eqs. (2.74) and (2.75).

The stress–strain relationships (Eqs. 2.76 and 2.77) become

$$\begin{Bmatrix} \sigma_1 \\ \sigma_2 \\ \tau_{12} \end{Bmatrix} = \begin{bmatrix} C_{11} & C_{12} & C_{16} \\ C_{12} & C_{22} & C_{26} \\ C_{16} & C_{26} & C_{66} \end{bmatrix} \begin{Bmatrix} \epsilon_1 \\ \epsilon_2 \\ \gamma_{12} \end{Bmatrix} \tag{2.111}$$

$$\sigma_3 = \begin{bmatrix} C_{31} & C_{32} & C_{36} \end{bmatrix} \begin{Bmatrix} \epsilon_1 \\ \epsilon_2 \\ \gamma_{12} \end{Bmatrix}. \tag{2.112}$$

By inverting Eq. (2.111), we obtain the strain–stress relationships

$$\begin{Bmatrix} \epsilon_1 \\ \epsilon_2 \\ \gamma_{12} \end{Bmatrix} = \begin{bmatrix} R_{11} & R_{12} & R_{16} \\ R_{12} & R_{22} & R_{26} \\ R_{16} & R_{26} & R_{66} \end{bmatrix} \begin{Bmatrix} \sigma_1 \\ \sigma_2 \\ \tau_{12} \end{Bmatrix}. \tag{2.113}$$

The in-plane elements of the compliance matrix R_{ij} are defined in Eq. (2.80).

Out-of-plane loads. The body is subjected to out-of-plane loads shown in Figure 2.20. Under these loads the body may undergo only nonplanar deformations (Fig. 2.27), and the displacements (in the x_1, x_2, x_3 coordinate system) are (see Eq. 2.53 and Fig. 2.23)

$$u_1 = 0 \qquad u_2 = 0 \qquad u_3 = U_3(x_1, x_2). \tag{2.114}$$

These displacements are the same as the displacements of a body with free ends with ϑ set equal to zero in Eq. (2.81). Thus, the strain–displacement and the stress–strain relations as well as the equilibrium equations can be obtained by setting ϑ equal to zero in the equations of Section 2.4.2. The strain–displacement

relationships (see Eqs. 2.82–2.85) are

$$\epsilon_1 = 0 \qquad \epsilon_2 = 0 \tag{2.115}$$

$$\epsilon_3 = 0 \tag{2.116}$$

$$\gamma_{23} = \frac{\partial U_3}{\partial x_2} \qquad \gamma_{13} = \frac{\partial U_3}{\partial x_1} \tag{2.117}$$

$$\gamma_{12} = 0. \tag{2.118}$$

The equilibrium equation is identical to Eq. (2.86).
The stress–strain relationships (see Eq. 2.87) are

$$\begin{Bmatrix} \tau_{23} \\ \tau_{13} \end{Bmatrix} = \begin{bmatrix} C_{44} & C_{45} \\ C_{45} & C_{55} \end{bmatrix} \begin{Bmatrix} \gamma_{23} \\ \gamma_{13} \end{Bmatrix}. \tag{2.119}$$

By inverting this equation, we obtain the strain–stress relationships

$$\begin{Bmatrix} \gamma_{23} \\ \gamma_{13} \end{Bmatrix} = \begin{bmatrix} S_{44} & S_{45} \\ S_{45} & S_{55} \end{bmatrix} \begin{Bmatrix} \tau_{23} \\ \tau_{13} \end{Bmatrix}, \tag{2.120}$$

where the compliance matrix is given by Eq. (2.89).

2.4.6 Built-In Ends – Orthotropic, Transversely Isotropic, or Isotropic Material

The expressions given in Section 2.4.5 for monoclinic bodies with both ends built-in are applicable to bodies treated as orthotropic, transversely isotropic, or isotropic provided that one of the material symmetry planes coincides with the x_1–x_2 plane shown in Figure 2.16. However, for such bodies the simplifications given by Eqs. (2.95)–(2.97) must be employed.

2.5 Plane-Stress Condition

Under plane-stress condition one of the normal stresses and both out-of-plane shear stresses are zero. We select the normal stress to be zero in the z (or x_3) coordinate direction and the out-of-plane shear stresses to be zero in the x–y (or x_1–x_2) plane (Fig. 2.28)

$$\sigma_z = 0 \qquad \tau_{yz} = 0 \qquad \tau_{xz} = 0. \tag{2.121}$$

Plane-stress condition may approximate the stresses in a thin fiber-reinforced composite plate when the fibers are parallel to the x–y plane and the plate is loaded by forces along the edges such that the forces are parallel to the plane of the plate and are distributed uniformly over the thickness (Fig. 2.29). The plane-stress condition does not provide the stresses exactly, not even for this thin-plate problem. Nevertheless, for many thin wall structures it is a useful approximation, yielding answers within reasonable accuracy.

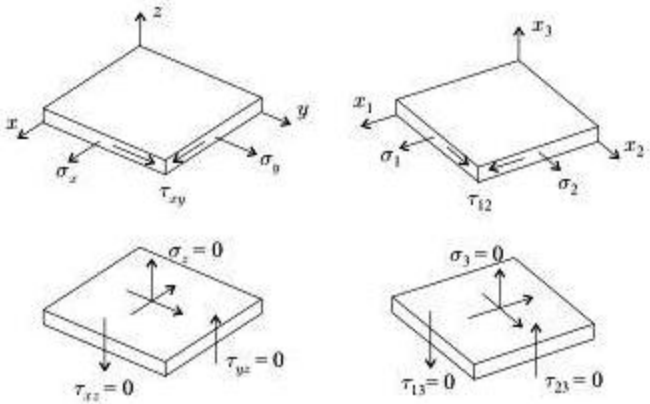

Figure 2.28: The stresses under plane-stress condition.

With the stipulations of Eq. (2.121), the equilibrium equations (Eqs. 2.13–2.15) become

$$\frac{\partial \sigma_x}{\partial x} + \frac{\partial \tau_{xy}}{\partial y} + f_x = 0 \tag{2.122}$$

$$\frac{\partial \tau_{xy}}{\partial x} + \frac{\partial \sigma_y}{\partial y} + f_y = 0. \tag{2.123}$$

Equations (2.121) and Eq. (2.21) give

$$\begin{Bmatrix} \epsilon_x \\ \epsilon_y \\ \gamma_{xy} \end{Bmatrix} = \begin{bmatrix} \overline{S}_{11} & \overline{S}_{12} & \overline{S}_{16} \\ \overline{S}_{12} & \overline{S}_{22} & \overline{S}_{26} \\ \overline{S}_{16} & \overline{S}_{26} & \overline{S}_{66} \end{bmatrix} \begin{Bmatrix} \sigma_x \\ \sigma_y \\ \tau_{xy} \end{Bmatrix} \tag{2.124}$$

$$\begin{Bmatrix} \epsilon_z \\ \gamma_{yz} \\ \gamma_{xz} \end{Bmatrix} = \begin{bmatrix} \overline{S}_{13} & \overline{S}_{23} & \overline{S}_{36} \\ \overline{S}_{14} & \overline{S}_{24} & \overline{S}_{46} \\ \overline{S}_{15} & \overline{S}_{25} & \overline{S}_{56} \end{bmatrix} \begin{Bmatrix} \sigma_x \\ \sigma_y \\ \tau_{xy} \end{Bmatrix}. \tag{2.125}$$

The elements of the compliance matrix $\overline{S}_{ij}$ are given in Table 2.3 (page 10). The stress–strain relationships are obtained from Eq. (2.124) by inversion

$$\begin{Bmatrix} \sigma_x \\ \sigma_y \\ \tau_{xy} \end{Bmatrix} = \begin{bmatrix} \overline{Q}_{11} & \overline{Q}_{12} & \overline{Q}_{16} \\ \overline{Q}_{12} & \overline{Q}_{22} & \overline{Q}_{26} \\ \overline{Q}_{16} & \overline{Q}_{26} & \overline{Q}_{66} \end{bmatrix} \begin{Bmatrix} \epsilon_x \\ \epsilon_y \\ \gamma_{xy} \end{Bmatrix}, \tag{2.126}$$

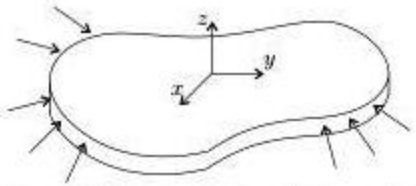

Figure 2.29: In-plane loads applied to a thin plate, resulting in plane-stress condition.

where $\overline{Q}_{ij}$ are the in-plane elements of the stiffness matrix in the x, y coordinate system under plane-stress condition:

$$\begin{bmatrix} \overline{Q}_{11} & \overline{Q}_{12} & \overline{Q}_{16} \\ \overline{Q}_{12} & \overline{Q}_{22} & \overline{Q}_{26} \\ \overline{Q}_{16} & \overline{Q}_{26} & \overline{Q}_{66} \end{bmatrix} = \begin{bmatrix} \overline{S}_{11} & \overline{S}_{12} & \overline{S}_{16} \\ \overline{S}_{12} & \overline{S}_{22} & \overline{S}_{26} \\ \overline{S}_{16} & \overline{S}_{26} & \overline{S}_{66} \end{bmatrix}^{-1}. \tag{2.127}$$

The stress–strain and strain–stress relationships simplify considerably when the fiber orientations are such that the material can be treated as monoclinic (Fig. 2.9), orthotropic (Fig. 2.12), transversely isotropic (Fig. 2.15), or isotropic. In the following we consider problems involving these material types and use an x_1, x_2, x_3 coordinate system with the x_1, x_2 coordinates being in one of the symmetry planes and x_3 being perpendicular to this plane. In this coordinate system, under plane-stress condition, we have (Fig. 2.28, right)

$$\sigma_3 = 0 \qquad \tau_{23} = 0 \qquad \tau_{13} = 0. \tag{2.128}$$

Monoclinic materials. By substituting Eq. (2.128) into Eq. (2.23) and by employing the compliance matrix of a monoclinic material (Eq. 2.26), we obtain

$$\gamma_{23} = 0 \qquad \gamma_{13} = 0. \tag{2.129}$$

With the stipulations in Eq. (2.128), the equilibrium equations (Eqs. 2.13–2.15) in the x_1, x_2, x_3 coordinate system become

$$\frac{\partial \sigma_1}{\partial x_1} + \frac{\partial \tau_{12}}{\partial x_2} + f_1 = 0 \tag{2.130}$$

$$\frac{\partial \tau_{12}}{\partial x_1} + \frac{\partial \sigma_2}{\partial x_2} + f_2 = 0. \tag{2.131}$$

By substituting Eq. (2.128) into Eq. (2.23), we obtain the following strain–stress relationships:

$$\begin{Bmatrix} \epsilon_1 \\ \epsilon_2 \\ \gamma_{12} \end{Bmatrix} = \begin{bmatrix} S_{11} & S_{12} & S_{16} \\ S_{12} & S_{22} & S_{26} \\ S_{16} & S_{26} & S_{66} \end{bmatrix} \begin{Bmatrix} \sigma_1 \\ \sigma_2 \\ \tau_{12} \end{Bmatrix} \tag{2.132}$$

$$\epsilon_3 = \begin{bmatrix} S_{13} & S_{23} & S_{36} \end{bmatrix} \begin{Bmatrix} \sigma_1 \\ \sigma_2 \\ \tau_{12} \end{Bmatrix}. \tag{2.133}$$

The elements of the compliance matrix S_{ij} are given in Table 2.7 (page 15). The stress–strain relationships are obtained from Eq. (2.132) by inversion

$$\begin{Bmatrix} \sigma_1 \\ \sigma_2 \\ \tau_{12} \end{Bmatrix} = \begin{bmatrix} Q_{11} & Q_{12} & Q_{16} \\ Q_{12} & Q_{22} & Q_{26} \\ Q_{16} & Q_{26} & Q_{66} \end{bmatrix} \begin{Bmatrix} \epsilon_1 \\ \epsilon_2 \\ \gamma_{12} \end{Bmatrix}, \tag{2.134}$$

where Q_{ij} are the in-plane elements of the stiffness matrix in the x_1, x_2 coordinate system under plane-stress condition:

$$\begin{bmatrix} Q_{11} & Q_{12} & Q_{16} \\ Q_{12} & Q_{22} & Q_{26} \\ Q_{16} & Q_{26} & Q_{66} \end{bmatrix} = \begin{bmatrix} S_{11} & S_{12} & S_{16} \\ S_{12} & S_{22} & S_{26} \\ S_{16} & S_{26} & S_{66} \end{bmatrix}^{-1}. \tag{2.135}$$

The expressions presented in this section for monoclinic materials also apply to orthotropic, transversely isotropic, and isotropic materials. However, for these types of materials the stiffness and compliance matrices further simplify, as shown below.

Orthotropic. For an orthotropic material the following elements of the compliance matrix are zero (Table 2.7, page 15):

$$S_{16} = S_{26} = 0. \tag{2.136}$$

Also, from Table 2.7 we have

$$S_{11} = \frac{1}{E_1} \qquad S_{12} = -\frac{\nu_{12}}{E_1} \qquad S_{22} = \frac{1}{E_2} \qquad S_{66} = \frac{1}{G_{12}}. \tag{2.137}$$

From Eqs. (2.135) and (2.136) we obtain

$$Q_{16} = Q_{26} = 0. \tag{2.138}$$

Accordingly, the elements of the stiffness matrix $[Q]$ in terms of the engineering constants are (Eqs. 2.135, 2.137, and 2.138)

$$[Q] = \begin{bmatrix} \frac{E_1}{D} & \frac{\nu_{12}E_2}{D} & 0 \\ \frac{\nu_{12}E_2}{D} & \frac{E_2}{D} & 0 \\ 0 & 0 & G_{12} \end{bmatrix}, \quad \text{where} \quad D = 1 - \frac{E_2}{E_1}\nu_{12}^2 = 1 - \nu_{12}\nu_{21}. \tag{2.139}$$

A woven, or filament wound, layer is orthotropic when there is the same number of fibers in the $+\Theta$ and $-\Theta$ directions in the x_1–x_2 plane (Fig. 2.30). For such a layer the elements of the stiffness matrix are calculated from

$$Q_{ij}^{\text{woven}} = \frac{1}{2}\left[(\overline{Q}_{ij})_{\Theta} + (\overline{Q}_{ij})_{-\Theta}\right], \quad i, j = 1, 2, 6, \tag{2.140}$$

where $(\overline{Q}_{ij})_{\Theta}$ and $(\overline{Q}_{ij})_{-\Theta}$ are the elements of the stiffness matrices of plies oriented in the $+\Theta$ and $-\Theta$ directions, respectively. The elements of the stiffness

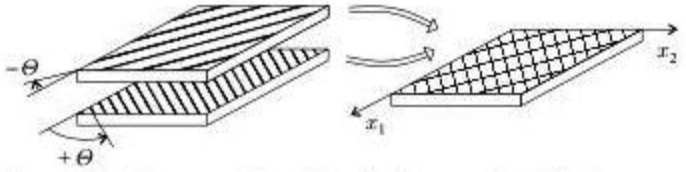

Figure 2.30: A layer consisting of fibers in the $+\Theta$ and $-\Theta$ directions.

Table 2.12. Elements of the stiffness matrix of a woven layer with the fibers oriented in the $\pm\Theta$ directions

$$
\begin{aligned}
Q_{11}^{\text{woven}} &= c^4 Q_{11} + s^4 Q_{22} + 2c^2 s^2 (Q_{12} + 2Q_{66}) \\
Q_{22}^{\text{woven}} &= s^4 Q_{11} + c^4 Q_{22} + 2c^2 s^2 (Q_{12} + 2Q_{66}) \\
Q_{12}^{\text{woven}} &= c^2 s^2 (Q_{11} + Q_{22} - 4Q_{66}) + (c^4 + s^4) Q_{12} \\
Q_{66}^{\text{woven}} &= c^2 s^2 (Q_{11} + Q_{22} - 2Q_{12}) + (c^2 - s^2)^2 Q_{66} \\
Q_{16}^{\text{woven}} &= 0 \\
Q_{26}^{\text{woven}} &= 0 \\
& c = \cos\Theta \qquad s = \sin\Theta
\end{aligned}
$$

matrix in the Θ direction $(\overline{Q}_{ij})_{\Theta}$ are obtained by the transformation described in Section 2.9.3 and summarized in Table 3.1 (page 70). The elements $(\overline{Q}_{ij})_{-\Theta}$ are calculated by replacing Θ by $-\Theta$ in Table 3.1. By performing these steps, we obtain the elements Q_{ij}^{woven} given in Table 2.12.

Transversely isotropic. For a transversely isotropic material we have (Table 2.7, page 15)

$$S_{16} = S_{26} = 0 \tag{2.141}$$

$$S_{13} = S_{12}. \tag{2.142}$$

By substituting these values, together with the expressions in Table 2.7 (page 15), into Eq. (2.135), we obtain the $[Q]$ matrix in terms of the engineering constants. The results are identical to those of Eq. (2.139).

Isotropic. For an isotropic material the following relationships hold (Table 2.7, page 15):

$$
\begin{aligned}
S_{22} &= S_{11} & S_{16} &= S_{26} = 0 \\
S_{13} &= S_{23} = S_{12} & S_{66} &= 2(S_{11} - S_{12}).
\end{aligned}
\tag{2.143}
$$

From Eq. (2.135) we obtain

$$
\begin{aligned}
Q_{22} &= Q_{11} & Q_{16} &= Q_{26} = 0 \\
Q_{66} &= \frac{1}{2}(Q_{11} - Q_{12}).
\end{aligned}
\tag{2.144}
$$

The elements of the stiffness matrix in terms of the engineering constants are

$$[Q] = \frac{E}{1-\nu^2}\begin{bmatrix} 1 & \nu & 0 \\ \nu & 1 & 0 \\ 0 & 0 & \frac{1-\nu}{2} \end{bmatrix}. \tag{2.145}$$

2.2 Example. *Calculate the elements of the stiffness matrix of a graphite epoxy unidirectional ply under plane-stress condition. The engineering constants are given as* $E_1 = 148 \times 10^9\, N/m^2$, $E_2 = 9.65 \times 10^9\, N/m^2$, $G_{12} = 4.55 \times 10^9\, N/m^2$, $\nu_{12} = 0.3$, *and* $\nu_{23} = 0.6$.

Solution. Under plane-stress condition the stiffness matrix is (Eq. 2.135)

$$\begin{bmatrix} Q_{11} & Q_{12} & Q_{16} \\ Q_{12} & Q_{22} & Q_{26} \\ Q_{16} & Q_{26} & Q_{66} \end{bmatrix} = \begin{bmatrix} S_{11} & S_{12} & S_{16} \\ S_{12} & S_{22} & S_{26} \\ S_{16} & S_{26} & S_{66} \end{bmatrix}^{-1}. \tag{2.146}$$

The elements of the compliance matrix are given in Example 2.1 (page 21). By substituting these values into the expression above we obtain

$$[Q] = \begin{bmatrix} 6.76 & -2.03 & 0 \\ -2.03 & 103.63 & 0 \\ 0 & 0 & 219.78 \end{bmatrix}^{-1} = \begin{bmatrix} 148.87 & 2.91 & 0 \\ 2.91 & 9.71 & 0 \\ 0 & 0 & 4.55 \end{bmatrix} 10^9 \frac{\mathrm{N}}{\mathrm{m}^2}. \tag{2.147}$$

The stiffness matrix may also be calculated by Eq. (2.139) with the engineering constants and with $D = 1 - \frac{E_2}{E_1}\nu_{12}^2 = 0.994$. Equation (2.139) gives

$$[Q] = \begin{bmatrix} \frac{E_1}{D} & \frac{\nu_{12}E_2}{D} & 0 \\ \frac{\nu_{12}E_2}{D} & \frac{E_2}{D} & 0 \\ 0 & 0 & G_{12} \end{bmatrix} = \begin{bmatrix} 148.87 & 2.91 & 0 \\ 2.91 & 9.71 & 0 \\ 0 & 0 & 4.55 \end{bmatrix} 10^9 \frac{\mathrm{N}}{\mathrm{m}^2}. \tag{2.148}$$

This is the same result as that given by Eq. (2.147).

2.3 Example. *Estimate the plane-stress stiffness matrix and the engineering constants of a* (±45) *woven fabric layer made of graphite fibers and epoxy resin.*

Solution. We approximate the woven fabric by a layer made of one 45° and one −45° ply. The properties of these plies are taken to be those of the graphite epoxy unidirectional ply given in Example 2.2. The stiffness matrix of a ply made of this material under plane-stress condition is (Eq. 2.147)

$$[Q] = \begin{bmatrix} 148.87 & 2.91 & 0 \\ 2.91 & 9.71 & 0 \\ 0 & 0 & 4.55 \end{bmatrix} 10^9 \frac{\mathrm{N}}{\mathrm{m}^2}. \tag{2.149}$$

We obtain the stiffness matrix of the woven fabric by substituting the elements of this matrix into the expressions in Table 2.12 (page 42) with $\Theta = 45°$. The result is

$$\begin{aligned} Q_{11}^{\pm 45} &= Q_{22}^{\pm 45} = 45.65 \times 10^9 \ \mathrm{N/m^2} & Q_{12}^{\pm 45} &= 36.55 \times 10^9 \ \mathrm{N/m^2} \\ Q_{16}^{\pm 45} &= Q_{26}^{\pm 45} = 0 & Q_{66}^{\pm 45} &= 38.19 \times 10^9 \ \mathrm{N/m^2}. \end{aligned} \tag{2.150}$$

The compliance matrix is

$$\begin{bmatrix} S_{11} & S_{12} & 0 \\ S_{12} & S_{22} & 0 \\ 0 & 0 & S_{66} \end{bmatrix}^{\pm 45} = \begin{bmatrix} Q_{11}^{\pm 45} & Q_{12}^{\pm 45} & 0 \\ Q_{12}^{\pm 45} & Q_{22}^{\pm 45} & 0 \\ 0 & 0 & Q_{66}^{\pm 45} \end{bmatrix}^{-1}$$

$$= \begin{bmatrix} 61.03 & -48.86 & 0 \\ -48.86 & 61.03 & 0 \\ 0 & 0 & 26.19 \end{bmatrix} 10^{-12} \frac{\text{m}^2}{\text{N}}. \tag{2.151}$$

The engineering constants of the woven fabric are (see Eq. 2.137)

$$\begin{aligned} E_1^{\pm 45} &= \frac{1}{S_{11}} = 16.39 \times 10^9 \frac{\text{N}^2}{\text{m}} & \nu_{12}^{\pm 45} &= -S_{12} E_1 = 0.801 \\ E_2^{\pm 45} &= \frac{1}{S_{22}} = 16.39 \times 10^9 \frac{\text{N}^2}{\text{m}} & G_{12}^{\pm 45} &= \frac{1}{S_{66}} = 38.19 \times 10^9 \frac{\text{N}^2}{\text{m}}. \end{aligned} \tag{2.152}$$

2.6 Hygrothermal Strains and Stresses

An unrestrained composite may change both its size and shape when the temperature is increased or decreased uniformly by ΔT. The corresponding strains in the x, y, z coordinate system are

$$\begin{aligned} \epsilon_x^T &= \tilde{\alpha}_x \Delta T & \epsilon_y^T &= \tilde{\alpha}_y \Delta T & \epsilon_z^T &= \tilde{\alpha}_z \Delta T \\ \gamma_{yz}^T &= \tilde{\alpha}_{yz} \Delta T & \gamma_{xz}^T &= \tilde{\alpha}_{xz} \Delta T & \gamma_{xy}^T &= \tilde{\alpha}_{xy} \Delta T. \end{aligned} \tag{2.153}$$

Similarly, moisture inside an unrestrained composite causes a change in size and shape. A uniform moisture concentration c in the material results in the following strains:

$$\begin{aligned} \epsilon_x^c &= \tilde{\beta}_x c & \epsilon_y^c &= \tilde{\beta}_y c & \epsilon_z^c &= \tilde{\beta}_z c \\ \gamma_{yz}^c &= \tilde{\beta}_{yz} c & \gamma_{xz}^c &= \tilde{\beta}_{xz} c & \gamma_{xy}^c &= \tilde{\beta}_{xy} c. \end{aligned} \tag{2.154}$$

Inside a dry material the moisture concentration c is zero. In Eqs. (2.153) and (2.154) $\tilde{\alpha}$ and $\tilde{\beta}$ are the temperature and moisture expansion coefficients, respectively. (Note that $\tilde{\alpha}$ and $\tilde{\beta}$ follow the same transformation rules as strains, Section 2.9.2.) In an unrestrained composite the strains induced by uniform temperature and moisture distributions (referred to as hygrothermal strains) are

$$\begin{Bmatrix} \epsilon_x^{\text{ht}} \\ \epsilon_y^{\text{ht}} \\ \epsilon_z^{\text{ht}} \\ \gamma_{yz}^{\text{ht}} \\ \gamma_{xz}^{\text{ht}} \\ \gamma_{xy}^{\text{ht}} \end{Bmatrix} = \begin{Bmatrix} \tilde{\alpha}_x \\ \tilde{\alpha}_y \\ \tilde{\alpha}_z \\ \tilde{\alpha}_{yz} \\ \tilde{\alpha}_{xz} \\ \tilde{\alpha}_{xy} \end{Bmatrix} \Delta T + \begin{Bmatrix} \tilde{\beta}_x \\ \tilde{\beta}_y \\ \tilde{\beta}_z \\ \tilde{\beta}_{yz} \\ \tilde{\beta}_{xz} \\ \tilde{\beta}_{xy} \end{Bmatrix} c. \tag{2.155}$$

For a generally anisotropic material, in the x, y, z coordinate system, the strain–stress relationships are obtained by combining the hygrothermal strains (Eq. 2.155) with the stress-induced strains (Eq. 2.21):

$$\begin{Bmatrix} \epsilon_x \\ \epsilon_y \\ \epsilon_z \\ \gamma_{yz} \\ \gamma_{xz} \\ \gamma_{xy} \end{Bmatrix} = \begin{bmatrix} \overline{S}_{11} & \overline{S}_{12} & \overline{S}_{13} & \overline{S}_{14} & \overline{S}_{15} & \overline{S}_{16} \\ \overline{S}_{21} & \overline{S}_{22} & \overline{S}_{23} & \overline{S}_{24} & \overline{S}_{25} & \overline{S}_{26} \\ \overline{S}_{31} & \overline{S}_{32} & \overline{S}_{33} & \overline{S}_{34} & \overline{S}_{35} & \overline{S}_{36} \\ \overline{S}_{41} & \overline{S}_{42} & \overline{S}_{43} & \overline{S}_{44} & \overline{S}_{45} & \overline{S}_{46} \\ \overline{S}_{51} & \overline{S}_{52} & \overline{S}_{53} & \overline{S}_{54} & \overline{S}_{55} & \overline{S}_{56} \\ \overline{S}_{61} & \overline{S}_{62} & \overline{S}_{63} & \overline{S}_{64} & \overline{S}_{65} & \overline{S}_{66} \end{bmatrix} \begin{Bmatrix} \sigma_x \\ \sigma_y \\ \sigma_z \\ \tau_{yz} \\ \tau_{xz} \\ \tau_{xy} \end{Bmatrix} + \begin{Bmatrix} \epsilon_x^{\mathrm{ht}} \\ \epsilon_y^{\mathrm{ht}} \\ \epsilon_z^{\mathrm{ht}} \\ \gamma_{yz}^{\mathrm{ht}} \\ \gamma_{xz}^{\mathrm{ht}} \\ \gamma_{xy}^{\mathrm{ht}} \end{Bmatrix}, \tag{2.156}$$

where $\epsilon_x, \ldots, \gamma_{xy}$ are the actual strains in the composite.

By inverting Eq. (2.156) we obtain the following stress–strain relationships:

$$\begin{Bmatrix} \sigma_x \\ \sigma_y \\ \sigma_z \\ \tau_{yz} \\ \tau_{xz} \\ \tau_{xy} \end{Bmatrix} = \begin{bmatrix} \overline{C}_{11} & \overline{C}_{12} & \overline{C}_{13} & \overline{C}_{14} & \overline{C}_{15} & \overline{C}_{16} \\ \overline{C}_{21} & \overline{C}_{22} & \overline{C}_{23} & \overline{C}_{24} & \overline{C}_{25} & \overline{C}_{26} \\ \overline{C}_{31} & \overline{C}_{32} & \overline{C}_{33} & \overline{C}_{34} & \overline{C}_{35} & \overline{C}_{36} \\ \overline{C}_{41} & \overline{C}_{42} & \overline{C}_{43} & \overline{C}_{44} & \overline{C}_{45} & \overline{C}_{46} \\ \overline{C}_{51} & \overline{C}_{52} & \overline{C}_{53} & \overline{C}_{54} & \overline{C}_{55} & \overline{C}_{56} \\ \overline{C}_{61} & \overline{C}_{62} & \overline{C}_{63} & \overline{C}_{64} & \overline{C}_{65} & \overline{C}_{66} \end{bmatrix} \left(\begin{Bmatrix} \epsilon_x \\ \epsilon_y \\ \epsilon_z \\ \gamma_{yz} \\ \gamma_{xz} \\ \gamma_{xy} \end{Bmatrix} - \begin{Bmatrix} \epsilon_x^{\mathrm{ht}} \\ \epsilon_y^{\mathrm{ht}} \\ \epsilon_z^{\mathrm{ht}} \\ \gamma_{yz}^{\mathrm{ht}} \\ \gamma_{xz}^{\mathrm{ht}} \\ \gamma_{xy}^{\mathrm{ht}} \end{Bmatrix} \right). \tag{2.157}$$

For a monoclinic material, in the x_1, x_2, x_3 local coordinate system (Fig. 2.9) temperature and moisture do not induce out-of-plane shear strains. Thus, the temperature- and moisture-induced strains are

$$\begin{aligned} &\epsilon_1^T = \widetilde{\alpha}_1 \Delta T \qquad \epsilon_2^T = \widetilde{\alpha}_2 \Delta T \qquad \epsilon_3^T = \widetilde{\alpha}_3 \Delta T \\ &\gamma_{23}^T = 0 \qquad\quad \gamma_{13}^T = 0 \qquad\quad \gamma_{12}^T = \widetilde{\alpha}_{12} \Delta T \end{aligned} \tag{2.158}$$

$$\begin{aligned} &\epsilon_1^c = \widetilde{\beta}_1 c \qquad \epsilon_2^c = \widetilde{\beta}_2 c \qquad \epsilon_3^c = \widetilde{\beta}_3 c \\ &\gamma_{23}^c = 0 \qquad\quad \gamma_{13}^c = 0 \qquad\quad \gamma_{12}^c = \widetilde{\beta}_{12} c, \end{aligned} \tag{2.159}$$

where $\widetilde{\alpha}$ and $\widetilde{\beta}$ are the temperature and moisture expansion coefficients, respectively, in the x_1, x_2, x_3 coordinate system ($\widetilde{\alpha}$ and $\widetilde{\beta}$ follow the same transformation rules as strains, Section 2.9.2). The hygrothermal strains are

$$\begin{Bmatrix} \epsilon_1^{\mathrm{ht}} \\ \epsilon_2^{\mathrm{ht}} \\ \epsilon_3^{\mathrm{ht}} \\ \gamma_{23}^{\mathrm{ht}} \\ \gamma_{13}^{\mathrm{ht}} \\ \gamma_{12}^{\mathrm{ht}} \end{Bmatrix} = \begin{Bmatrix} \widetilde{\alpha}_1 \\ \widetilde{\alpha}_2 \\ \widetilde{\alpha}_3 \\ 0 \\ 0 \\ \widetilde{\alpha}_{12} \end{Bmatrix} \Delta T + \begin{Bmatrix} \widetilde{\beta}_1 \\ \widetilde{\beta}_2 \\ \widetilde{\beta}_3 \\ 0 \\ 0 \\ \widetilde{\beta}_{12} \end{Bmatrix} c. \tag{2.160}$$

The stress–strain relationships are (Eq. 2.22)

$$\begin{Bmatrix} \sigma_1 \\ \sigma_2 \\ \sigma_3 \\ \tau_{23} \\ \tau_{13} \\ \tau_{12} \end{Bmatrix} = [C] \left(\begin{Bmatrix} \epsilon_1 \\ \epsilon_2 \\ \epsilon_3 \\ \gamma_{23} \\ \gamma_{13} \\ \gamma_{12} \end{Bmatrix} - \begin{Bmatrix} \epsilon_1^{\text{ht}} \\ \epsilon_2^{\text{ht}} \\ \epsilon_3^{\text{ht}} \\ 0 \\ 0 \\ \gamma_{12}^{\text{ht}} \end{Bmatrix} \right). \tag{2.161}$$

where $[C]$ is prescribed by Eq. (2.27). Note that $\epsilon_1, \ldots, \gamma_{12}$ are the *actual* strains in the composite.

By inverting Eq. (2.161), we obtain the following strain–stress relationships:

$$\begin{Bmatrix} \epsilon_1 \\ \epsilon_2 \\ \epsilon_3 \\ \gamma_{23} \\ \gamma_{13} \\ \gamma_{12} \end{Bmatrix} - \begin{Bmatrix} \epsilon_1^{\text{ht}} \\ \epsilon_2^{\text{ht}} \\ \epsilon_3^{\text{ht}} \\ 0 \\ 0 \\ \gamma_{12}^{\text{ht}} \end{Bmatrix} = [S] \begin{Bmatrix} \sigma_1 \\ \sigma_1 \\ \sigma_3 \\ \tau_{23} \\ \tau_{13} \\ \tau_{12} \end{Bmatrix}. \tag{2.162}$$

where $[S]$ is prescribed by Eq. (2.26).

In orthotropic, transversely isotropic, and isotropic materials temperature and moisture do not introduce γ_{23}, γ_{13}, and γ_{12} shear strains. Thus, for these types of materials the temperature- and moisture-induced strains are

$$\begin{aligned} &\epsilon_1^T = \tilde{\alpha}_1 \Delta T \qquad \epsilon_2^T = \tilde{\alpha}_2 \Delta T \qquad \epsilon_3^T = \tilde{\alpha}_3 \Delta T \\ &\gamma_{23}^T = 0 \qquad \gamma_{13}^T = 0 \qquad \gamma_{12}^T = 0 \end{aligned} \tag{2.163}$$

$$\begin{aligned} &\epsilon_1^c = \tilde{\beta}_1 c \qquad \epsilon_2^c = \tilde{\beta}_2 c \qquad \epsilon_3^c = \tilde{\beta}_3 c \\ &\gamma_{23}^c = 0 \qquad \gamma_{13}^c = 0 \qquad \gamma_{12}^c = 0. \end{aligned} \tag{2.164}$$

For orthotropic, transversely isotropic, and isotropic materials the stress–strain relationships given above for monoclinic material are valid (Eqs. 2.161 and 2.162) with $\gamma_{12}^{\text{ht}} = 0$ and the $[S]$ and $[C]$ matrices specified in Sections 2.3.4 and 2.3.5 (see also Table 2.13).

Table 2.13. The thermal and moisture expansion coefficients

Material	Thermal expansion coefficients	Moisture expansion coefficients
Generally anisotropic	$\tilde{\alpha}_x, \tilde{\alpha}_y, \tilde{\alpha}_z, \tilde{\alpha}_{xy}, \tilde{\alpha}_{xz}, \tilde{\alpha}_{xy}$	$\tilde{\beta}_x, \tilde{\beta}_y, \tilde{\beta}_z, \tilde{\beta}_{yz}, \tilde{\beta}_{xz}, \tilde{\beta}_{xy}$
Monoclinic	$\tilde{\alpha}_1, \tilde{\alpha}_2, \tilde{\alpha}_3, \tilde{\alpha}_{12}$	$\tilde{\beta}_1, \tilde{\beta}_2, \tilde{\beta}_3, \tilde{\beta}_{12}$
Orthotropic	$\tilde{\alpha}_1, \tilde{\alpha}_2, \tilde{\alpha}_3$	$\tilde{\beta}_1, \tilde{\beta}_2, \tilde{\beta}_3$
Transversely isotropic	$\tilde{\alpha}_1, \tilde{\alpha}_2 = \tilde{\alpha}_3$	$\tilde{\beta}_1, \tilde{\beta}_2 = \tilde{\beta}_3$
Isotropic	$\tilde{\alpha}_1 = \tilde{\alpha}_2 = \tilde{\alpha}_3$	$\tilde{\beta}_1 = \tilde{\beta}_2 = \tilde{\beta}_3$

2.6.1 Plane-Strain Condition

The hygrothermal stress–strain relationships under plane-strain condition can be obtained by making the following substitutions in the stress–strain relationships (*without* hygrothermal effects) given in Section 2.3:

$$\begin{aligned} \epsilon_i &\Rightarrow \epsilon_i - \widetilde{\alpha}_i \Delta T - \widetilde{\beta}_i c \\ \gamma_{ij} &\Rightarrow \gamma_{ij} - \widetilde{\alpha}_{ij} \Delta T - \widetilde{\beta}_{ij} c, \quad i \neq j \end{aligned} \tag{2.165}$$

where the subscripts ij represent x, y, z and $1, 2, 3$ in the x, y, z and x_1, x_2, x_3 coordinate systems, respectively.

2.6.2 Plane-Stress Condition

The hygrothermal stress–strain relationships under plane-stress condition can be obtained by replacing the strains ϵ_i and γ_{ij} in Eqs. (2.124) and (2.145) by those given in Eq. (2.165).

2.7 Boundary Conditions

To obtain solutions to the equilibrium, stress–strain, and strain–displacement equations, either the displacement or the applied force must be specified at every point on the surface. The relationships between the displacements and the strains are given by Eqs. (2.2)–(2.4) and (2.9)–(2.11). The surface forces per unit area are related to the stresses at the surface as follows.

We consider a small volume element ΔV (Fig. 2.31). A surface force per unit area p (with components p_x, p_y, p_z) is applied on the ΔA surface of this element. Force balance in the x direction gives

$$\sigma_x \frac{1}{2}\Delta z \Delta y + \tau_{zx} \frac{1}{2}\Delta x \Delta y + \tau_{yx} \frac{1}{2}\Delta x \Delta z = p_x \Delta A. \tag{2.166}$$

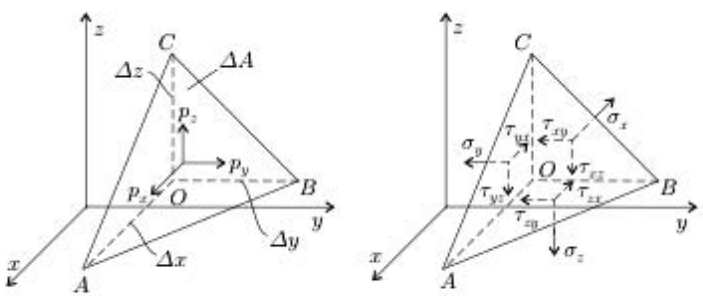

Figure 2.31: Components of the surface force p on the ΔA surface and the stresses on the OBC, OAC, and OAB surfaces.

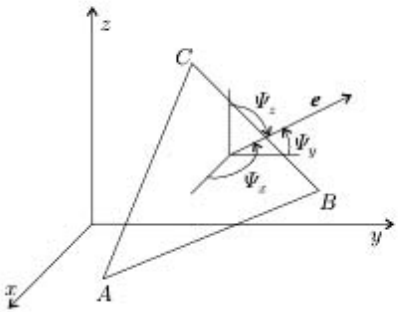

Figure 2.32: The angles Ψ_x, Ψ_y, Ψ_z.

By dividing both sides by ΔA, we obtain

$$p_x = \frac{1}{2\Delta A}(\sigma_x \Delta z \Delta y + \tau_{zx}\Delta x \Delta y + \tau_{yx}\Delta x \Delta z). \tag{2.167}$$

In the limit, when ΔA, Δx, Δy, Δz go to zero, Eq. (2.167) becomes

$$p_x = l\sigma_x + n\tau_{zx} + m\tau_{yx}, \tag{2.168}$$

where l, m, n are the direction cosines of the normal vector of the boundary surface (Fig. 2.32) as follows:

$$l = \frac{\Delta z \Delta y}{2\Delta A} = \cos(\Psi_x) \quad m = \frac{\Delta x \Delta z}{2\Delta A} = \cos(\Psi_y) \quad n = \frac{\Delta x \Delta y}{2\Delta A} = \cos(\Psi_z). \tag{2.169}$$

Similarly, we have

$$p_y = m\sigma_y + l\tau_{xy} + n\tau_{zy} \tag{2.170}$$

$$p_z = n\sigma_z + l\tau_{xz} + m\tau_{yz}. \tag{2.171}$$

2.8 Continuity Conditions

When composites are made of laminated layers, perfect bonding is assumed between each layer. Accordingly, at the interfaces of two adjacent layers the normal stresses are equal, the out-of-plane shear stresses are equal, and the displacements are equal. Thus, at two adjacent layers, denoted by k and $k+1$, we have (Fig. 2.33)

$$(\sigma_z)_{k,\mathrm{t}} = (\sigma_z)_{k+1,\mathrm{b}} \quad (\tau_{xz})_{k,\mathrm{t}} = (\tau_{xz})_{k+1,\mathrm{b}} \quad (\tau_{yz})_{k,\mathrm{t}} = (\tau_{yz})_{k+1,\mathrm{b}} \tag{2.172}$$

$$(u)_{k,\mathrm{t}} = (u)_{k+1,\mathrm{b}} \quad (v)_{k,\mathrm{t}} = (v)_{k+1,\mathrm{b}} \quad (w)_{k,\mathrm{t}} = (w)_{k+1,\mathrm{b}}. \tag{2.173}$$

The subscripts t and b refer to the top and bottom of a layer, respectively. The continuity conditions in terms of strains can be obtained from the preceding displacement continuity conditions (Eq. 2.173) together with Eqs. (2.2)–(2.4), (2.7), and (2.11) as follows:

$$(\epsilon_x)_{k,\mathrm{t}} = (\epsilon_x)_{k+1,\mathrm{b}} \quad (\epsilon_y)_{k,\mathrm{t}} = (\epsilon_y)_{k+1,\mathrm{b}} \quad (\gamma_{xy})_{k,\mathrm{t}} = (\gamma_{xy})_{k+1,\mathrm{b}}. \tag{2.174}$$

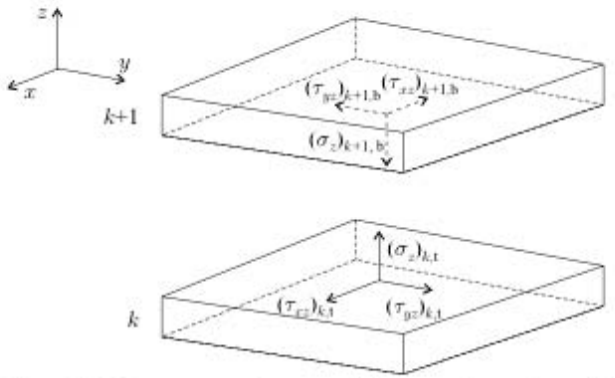

Figure 2.33: The stresses at the top and bottom surfaces of two adjacent layers that must match to satisfy continuity.

The $\sigma_x, \sigma_y, \tau_{xy}$ stress and the $\epsilon_z, \gamma_{xz}, \gamma_{yz}$ strain components are not necessarily continuous along two adjacent surfaces.

2.9 Stress and Strain Transformations

We consider two Cartesian coordinate systems with axes p, q, r and p', q', r'. The orientation of the primed coordinate system with respect to the unprimed coordinate system is given by the nine direction cosines (r_{11}, r_{21}, r_{31}), (r_{12}, r_{22}, r_{32}), (r_{13}, r_{23}, r_{33}) specified in Table 2.14.

The orientation of the primed p', q', r' coordinate system with respect to the unprimed coordinate system p, q, r can also be specified in terms of three

Table 2.14. Definitions of the direction cosines

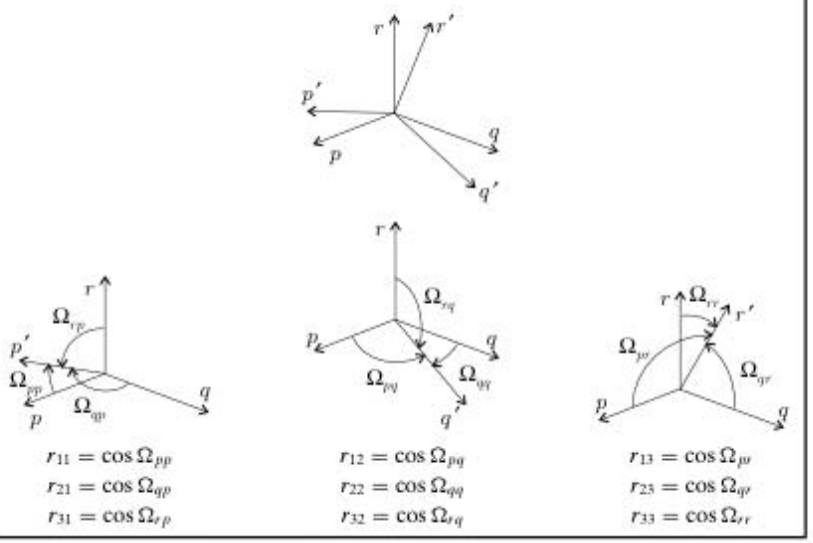

$r_{11} = \cos\Omega_{pp}$ $r_{12} = \cos\Omega_{pq}$ $r_{13} = \cos\Omega_{pr}$

$r_{21} = \cos\Omega_{qp}$ $r_{22} = \cos\Omega_{qq}$ $r_{23} = \cos\Omega_{qr}$

$r_{31} = \cos\Omega_{rp}$ $r_{32} = \cos\Omega_{rq}$ $r_{33} = \cos\Omega_{rr}$

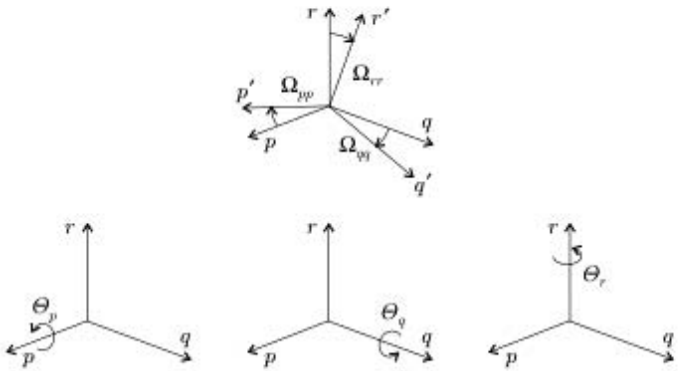

Figure 2.34: Consecutive rotations to arrive at the coordinate system p', q', and r'.

angles $\Theta_p, \Theta_q, \Theta_r$ (Fig. 2.34). These angles are consecutive rotations of the primed coordinate system about the p, q, r axes, as illustrated in Figure 2.34. The angles $\Theta_p, \Theta_q, \Theta_r$ are positive in the counterclockwise direction.

The $\Theta_p, \Theta_q, \Theta_r$ angles are related to the direction cosines by the following expressions[4]:

$$\begin{aligned}\Theta_q &= \text{Atan2}\left(-r_{31}, \sqrt{r_{11}^2 + r_{21}^2}\right)\\ \Theta_r &= \text{Atan2}(r_{21}/\cos\Theta_q, r_{11}/\cos\Theta_q)\\ \Theta_p &= \text{Atan2}(r_{32}/\cos\Theta_q, r_{33}/\cos\Theta_q),\end{aligned} \tag{2.175}$$

where $\text{Atan2}(y, x)$ is a two-argument arc tangent function as follows:

$$\text{Atan2}(y, x) = \tan^{-1}\left(\frac{y}{x}\right) \qquad \text{when} \quad x > 0 \tag{2.176}$$

$$\text{Atan2}(y, x) = \tan^{-1}\left(\frac{y}{x}\right) + \pi \quad \text{when} \quad x < 0. \tag{2.177}$$

When $\Theta_q = 90^\circ$, then Θ_r and Θ_p are

$$\Theta_r = 0 \qquad \Theta_p = \text{Atan2}(r_{12}, r_{22}). \tag{2.178}$$

2.9.1 Stress Transformation

The stresses in the primed coordinate system are calculated from the stresses in the unprimed coordinate system by the transformation

$$\begin{Bmatrix}\sigma'_p\\ \sigma'_q\\ \sigma'_r\\ \tau'_{qr}\\ \tau'_{pr}\\ \tau'_{pq}\end{Bmatrix} = \begin{bmatrix}T_{\sigma 11} & T_{\sigma 12} & T_{\sigma 13} & T_{\sigma 14} & T_{\sigma 15} & T_{\sigma 16}\\ T_{\sigma 21} & T_{\sigma 22} & T_{\sigma 23} & T_{\sigma 24} & T_{\sigma 25} & T_{\sigma 26}\\ T_{\sigma 31} & T_{\sigma 32} & T_{\sigma 33} & T_{\sigma 34} & T_{\sigma 35} & T_{\sigma 36}\\ T_{\sigma 41} & T_{\sigma 42} & T_{\sigma 43} & T_{\sigma 44} & T_{\sigma 45} & T_{\sigma 46}\\ T_{\sigma 51} & T_{\sigma 52} & T_{\sigma 53} & T_{\sigma 54} & T_{\sigma 55} & T_{\sigma 56}\\ T_{\sigma 61} & T_{\sigma 62} & T_{\sigma 63} & T_{\sigma 64} & T_{\sigma 65} & T_{\sigma 66}\end{bmatrix} \begin{Bmatrix}\sigma_p\\ \sigma_q\\ \sigma_r\\ \tau_{qr}\\ \tau_{pr}\\ \tau_{pq}\end{Bmatrix}. \tag{2.179}$$

[4] J. J. Craig, *Introduction to Robotics (Mechanics and Control)*. 2nd edition. Addison-Wesley, Reading, Massachusetts, 1989, pp. 43–56.

Table 2.15. The stress transformation matrices

$$[\hat{T}_\sigma^p] = \begin{bmatrix} 1 & 0 & 0 & 0 & 0 & 0 \\ 0 & c_p^2 & s_p^2 & 2c_p s_p & 0 & 0 \\ 0 & s_p^2 & c_p^2 & -2c_p s_p & 0 & 0 \\ 0 & -c_p s_p & c_p s_p & c_p^2 - s_p^2 & 0 & 0 \\ 0 & 0 & 0 & 0 & c_p & -s_p \\ 0 & 0 & 0 & 0 & s_p & c_p \end{bmatrix} \qquad \begin{aligned} c_p &= \cos\Theta_p \\ s_p &= \sin\Theta_p \end{aligned}$$

$$[\hat{T}_\sigma^q] = \begin{bmatrix} c_q^2 & 0 & s_q^2 & 0 & 2c_q s_q & 0 \\ 0 & 1 & 0 & 0 & 0 & 0 \\ s_q^2 & 0 & c_q^2 & 0 & -2c_q s_q & 0 \\ 0 & 0 & 0 & c_q & 0 & -s_q \\ -c_q s_q & 0 & c_q s_q & 0 & c_q^2 - s_q^2 & 0 \\ 0 & 0 & 0 & s_q & 0 & c_q \end{bmatrix} \qquad \begin{aligned} c_q &= \cos\Theta_q \\ s_q &= \sin\Theta_q \end{aligned}$$

$$[\hat{T}_\sigma^r] = \begin{bmatrix} c_r^2 & s_r^2 & 0 & 0 & 0 & 2c_r s_r \\ s_r^2 & c_r^2 & 0 & 0 & 0 & -2c_r s_r \\ 0 & 0 & 1 & 0 & 0 & 0 \\ 0 & 0 & 0 & c_r & -s_r & 0 \\ 0 & 0 & 0 & s_r & c_r & 0 \\ -c_r s_r & c_r s_r & 0 & 0 & 0 & c_r^2 - s_r^2 \end{bmatrix} \qquad \begin{aligned} c_r &= \cos\Theta_r \\ s_r &= \sin\Theta_r \end{aligned}$$

Equation (2.179) can also be written as

$$\boldsymbol{\sigma}' = [\hat{T}_\sigma]\,\boldsymbol{\sigma}, \tag{2.180}$$

where $[\hat{T}_\sigma]$ is the transformation matrix, which may be expressed as

$$[\hat{T}_\sigma] = [\hat{T}_\sigma^p]\,[\hat{T}_\sigma^q]\,[\hat{T}_\sigma^r], \tag{2.181}$$

where $[\hat{T}_\sigma^p]$, $[\hat{T}_\sigma^q]$, $[\hat{T}_\sigma^r]$ are given in Table 2.15. The subscript σ refers to the stress transformation, and the hat on T indicates that all six stress components are being transformed. The superscripts p, q, and r refer to the transformations about the p, q, and r axes, respectively.

Plane-strain and plane-stress. Under plane-strain and plane-stress conditions we are interested only in the stresses in the p–q and p'–q' planes. In this case the stresses in the primed coordinate system are obtained from the stresses in the unprimed coordinate system by rotation about the r-axis (see Fig. 2.35) as follows:

$$\begin{Bmatrix} \sigma_p' \\ \sigma_q' \\ \tau_{pq}' \end{Bmatrix} = \begin{bmatrix} c^2 & s^2 & 2cs \\ s^2 & c^2 & -2cs \\ -cs & cs & c^2 - s^2 \end{bmatrix} \begin{Bmatrix} \sigma_p \\ \sigma_q \\ \tau_{pq} \end{Bmatrix} \tag{2.182}$$

$$c = \cos\Theta \qquad s = \sin\Theta. \tag{2.183}$$

Equation (2.182) may be written as

$$\boldsymbol{\sigma}' = [T_\sigma]\,\boldsymbol{\sigma}. \tag{2.184}$$

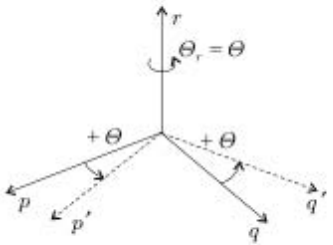

Figure 2.35: Rotation of the coordinate system around the r-axis.

The subscript σ refers to the stress transformation, and T without a hat indicates that only the three in-plane stress components are transformed.

2.9.2 Strain Transformation

The strains in the primed coordinate system are calculated from the strains in the unprimed coordinate system by

$$\begin{Bmatrix} \epsilon'_p \\ \epsilon'_q \\ \epsilon'_r \\ \gamma'_{qr} \\ \gamma'_{pr} \\ \gamma'_{pq} \end{Bmatrix} = \begin{bmatrix} T_{\epsilon 11} & T_{\epsilon 12} & T_{\epsilon 13} & T_{\epsilon 14} & T_{\epsilon 15} & T_{\epsilon 16} \\ T_{\epsilon 21} & T_{\epsilon 22} & T_{\epsilon 23} & T_{\epsilon 24} & T_{\epsilon 25} & T_{\epsilon 26} \\ T_{\epsilon 31} & T_{\epsilon 32} & T_{\epsilon 33} & T_{\epsilon 34} & T_{\epsilon 35} & T_{\epsilon 36} \\ T_{\epsilon 41} & T_{\epsilon 42} & T_{\epsilon 43} & T_{\epsilon 44} & T_{\epsilon 45} & T_{\epsilon 46} \\ T_{\epsilon 51} & T_{\epsilon 52} & T_{\epsilon 53} & T_{\epsilon 54} & T_{\epsilon 55} & T_{\epsilon 56} \\ T_{\epsilon 61} & T_{\epsilon 62} & T_{\epsilon 63} & T_{\epsilon 64} & T_{\epsilon 65} & T_{\epsilon 66} \end{bmatrix} \begin{Bmatrix} \epsilon_p \\ \epsilon_q \\ \epsilon_r \\ \gamma_{qr} \\ \gamma_{pr} \\ \gamma_{pq} \end{Bmatrix}. \tag{2.185}$$

Equation (2.185) may be written as

$$\epsilon' = [\hat{T}_\epsilon]\,\epsilon, \tag{2.186}$$

where the vector ϵ represents engineering strains. The strain transformation matrix $[\hat{T}_\epsilon]$ applies to engineering strains and thus is not the same as the stress transformation matrix $[\hat{T}_\sigma]$. (Tensorial strains transform by the same transformation matrix as the stresses.)

The transformation matrix $[\hat{T}_\epsilon]$ may be expressed as

$$[\hat{T}_\epsilon] = [\hat{T}_\epsilon^p][\hat{T}_\epsilon^q][\hat{T}_\epsilon^r], \tag{2.187}$$

where $[\hat{T}_\epsilon^p]$, $[\hat{T}_\epsilon^q]$, $[\hat{T}_\epsilon^r]$ are given in Table 2.16. The subscript ϵ refers to the strain transformation. The hat on T indicates that all six strain components are transformed. The superscripts p, q, and r refer to the transformations about the p-, q-, and r-axes, respectively.

Plane-strain and plane-stress. Under plane-strain and plane-stress conditions we are interested only in the strains in the p–q and p'–q' planes. In this case the strains in the primed coordinate system are obtained from the strains in the unprimed coordinate system by rotation about the r-axis (see Fig. 2.35) as follows:

$$\begin{Bmatrix} \epsilon'_p \\ \epsilon'_q \\ \gamma'_{pq} \end{Bmatrix} = \begin{bmatrix} c^2 & s^2 & cs \\ s^2 & c^2 & -cs \\ -2cs & 2cs & c^2 - s^2 \end{bmatrix} \begin{Bmatrix} \epsilon_p \\ \epsilon_q \\ \gamma_{pq} \end{Bmatrix}. \tag{2.188}$$

Table 2.16. The engineering strain transformation matrices

$$[\hat{T}_\epsilon^p] = \begin{bmatrix} 1 & 0 & 0 & 0 & 0 & 0 \\ 0 & c_p^2 & s_p^2 & c_p s_p & 0 & 0 \\ 0 & s_p^2 & c_p^2 & -c_p s_p & 0 & 0 \\ 0 & -2c_p s_p & 2c_p s_p & c_p^2 - s_p^2 & 0 & 0 \\ 0 & 0 & 0 & 0 & c_p & -s_p \\ 0 & 0 & 0 & 0 & s_p & c_p \end{bmatrix} \qquad \begin{aligned} c_p &= \cos\Theta_p \\ s_p &= \sin\Theta_p \end{aligned}$$

$$[\hat{T}_\epsilon^q] = \begin{bmatrix} c_q^2 & 0 & s_q^2 & 0 & c_q s_q & 0 \\ 0 & 1 & 0 & 0 & 0 & 0 \\ s_q^2 & 0 & c_q^2 & 0 & -c_q s_q & 0 \\ 0 & 0 & 0 & c_q & 0 & -s_q \\ -2c_q s_q & 0 & 2c_q s_q & 0 & c_q^2 - s_q^2 & 0 \\ 0 & 0 & 0 & s_q & 0 & c_q \end{bmatrix} \qquad \begin{aligned} c_q &= \cos\Theta_q \\ s_q &= \sin\Theta_q \end{aligned}$$

$$[\hat{T}_\epsilon^r] = \begin{bmatrix} c_r^2 & s_r^2 & 0 & 0 & 0 & c_r s_r \\ s_r^2 & c_r^2 & 0 & 0 & 0 & -c_r s_r \\ 0 & 0 & 1 & 0 & 0 & 0 \\ 0 & 0 & 0 & c_r & -s_r & 0 \\ 0 & 0 & 0 & s_r & c_r & 0 \\ -2c_r s_r & 2c_r s_r & 0 & 0 & 0 & c_r^2 - s_r^2 \end{bmatrix} \qquad \begin{aligned} c_r &= \cos\Theta_r \\ s_r &= \sin\Theta_r \end{aligned}$$

Equation (2.188) may be written as

$$\epsilon' = [T_\epsilon]\epsilon. \tag{2.189}$$

The subscript ϵ refers to the strain transformation. Without a hat, T indicates that only the three in-plane strain components are transformed.

2.9.3 Transformation of the Stiffness and Compliance Matrices

The stress–strain relationships in the unprimed and primed coordinate systems are (Eq. 2.22)

$$\sigma = [C]\epsilon \qquad \sigma' = [C']\epsilon'. \tag{2.190}$$

To obtain the relation between the stiffness matrices in the unprimed $[C]$ and primed $[C']$ coordinate systems, we multiply both sides of the stress–strain equation in the unprimed coordinate system by $[\hat{T}_\sigma]$

$$[\hat{T}_\sigma]\sigma = [\hat{T}_\sigma][C]\epsilon. \tag{2.191}$$

A matrix multiplied by its inverse $[\hat{T}_\epsilon]^{-1}[\hat{T}_\epsilon]$ is a unit matrix, and we may write

$$\underbrace{[\hat{T}_\sigma]\sigma}_{\sigma'} = \underbrace{[\hat{T}_\sigma][C][\hat{T}_\epsilon]^{-1}}_{[C']}\underbrace{[\hat{T}_\epsilon]\epsilon}_{\epsilon'}. \tag{2.192}$$

By comparing Eqs. (2.190) and (2.192), we see that the elements of the stiffness matrix $(C'_{11}, C'_{12}, \ldots, C'_{66})$ in the primed (p', q', r') coordinate system and

the elements of the stiffness matrix $(C_{11}, C_{12}, \ldots, C_{66})$ in the unprimed (p, q, r) coordinate system are related by the expression

$$[C'] = [T_\sigma][C][T_\epsilon]^{-1}. \tag{2.193}$$

The elements of the compliance matrix $(S'_{11}, S'_{12}, \ldots, S'_{66})$ in the primed (p', q', r') coordinate system and the elements of the compliance matrix $(S_{11}, S_{12}, \ldots, S_{66})$ in the unprimed (p, q, r) coordinate system are obtained by inverting Eq. (2.193) as follows:

$$[S'] = [T_\epsilon][S][T_\sigma]^{-1}. \tag{2.194}$$

Plane-stress and plane-strain conditions. Under plane-stress and plane-strain conditions we are interested in the stiffness and compliance matrices in the p–q and p'–q' planes.

For plane-stress, the elements of the stiffness matrix in the primed and unprimed coordinate systems are Q'_{ij} and Q_{ij}, where $i, j = 1, 2, 6$. The relationship between Q'_{ij} and Q_{ij} are given by the transformation specified by Eq. (2.193). The result is

$$\begin{bmatrix} Q'_{11} & Q'_{12} & Q'_{16} \\ Q'_{12} & Q'_{22} & Q'_{26} \\ Q'_{16} & Q'_{26} & Q'_{66} \end{bmatrix} = [T_\sigma] \begin{bmatrix} Q_{11} & Q_{12} & Q_{16} \\ Q_{12} & Q_{22} & Q_{26} \\ Q_{16} & Q_{26} & Q_{66} \end{bmatrix} [T_\epsilon]^{-1}, \tag{2.195}$$

where $[T_\sigma]$ and $[T_\epsilon]$ are (Eqs. 2.182 and 2.188)

$$[T_\sigma] = \begin{bmatrix} c^2 & s^2 & 2cs \\ s^2 & c^2 & -2cs \\ -cs & cs & c^2 - s^2 \end{bmatrix} \quad [T_\epsilon] = \begin{bmatrix} c^2 & s^2 & cs \\ s^2 & c^2 & -cs \\ -2cs & 2cs & c^2 - s^2 \end{bmatrix}. \tag{2.196}$$

The elements of the compliance matrix in the unprimed coordinate system are obtained by similar reasoning and are

$$\begin{bmatrix} S'_{11} & S'_{12} & S'_{16} \\ S'_{12} & S'_{22} & S'_{26} \\ S'_{16} & S'_{26} & S'_{66} \end{bmatrix} = [T_\epsilon] \begin{bmatrix} S_{11} & S_{12} & S_{16} \\ S_{12} & S_{22} & S_{26} \\ S_{16} & S_{26} & S_{66} \end{bmatrix} [T_\sigma]^{-1}. \tag{2.197}$$

Similarly, under plane-strain conditions the stiffness and compliance matrices are

$$\begin{bmatrix} C'_{11} & C'_{12} & C'_{16} \\ C'_{12} & C'_{22} & C'_{26} \\ C'_{16} & C'_{26} & C'_{66} \end{bmatrix} = [T_\sigma] \begin{bmatrix} C_{11} & C_{12} & C_{16} \\ C_{12} & C_{22} & C_{26} \\ C_{16} & C_{26} & C_{66} \end{bmatrix} [T_\epsilon]^{-1} \tag{2.198}$$

$$\begin{bmatrix} R'_{11} & R'_{12} & R'_{16} \\ R'_{12} & R'_{22} & R'_{26} \\ R'_{16} & R'_{26} & R'_{66} \end{bmatrix} = [T_\epsilon] \begin{bmatrix} R_{11} & R_{12} & R_{16} \\ R_{12} & R_{22} & R_{26} \\ R_{16} & R_{26} & R_{66} \end{bmatrix} [T_\sigma]^{-1}, \tag{2.199}$$

where $[T_\sigma]$ and $[T_\epsilon]$ are given by Eq. (2.196).

2.10 Strain Energy

In this section we define three parameters useful in the analyses of plates and beams. These are the strain energy, the potential of the external forces, and the total potential energy.

For a linearly elastic system, the strain energy of volume V is defined as

$$U=\frac{1}{2}\int\int\int(\epsilon_x\sigma_x+\epsilon_y\sigma_y+\epsilon_z\sigma_z+\gamma_{yz}\tau_{yz}+\gamma_{xz}\tau_{xz}+\gamma_{xy}\tau_{xy})\,dV. \tag{2.200}$$

This expression can be written as

$$U=\frac{1}{2}\int\int\int\{\epsilon_x\quad\epsilon_y\quad\epsilon_z\quad\gamma_{yz}\quad\gamma_{xz}\quad\gamma_{xy}\}\begin{Bmatrix}\sigma_x\\\sigma_y\\\sigma_z\\\tau_{yz}\\\tau_{xz}\\\tau_{xy}\end{Bmatrix}dV. \tag{2.201}$$

With the use of the stress–strain relationships (Eq. 2.20) this expression can be expressed in terms of the strains, as follows:

$$U=\frac{1}{2}\int\int\int\{\epsilon_x\quad\epsilon_y\quad\epsilon_z\quad\gamma_{yz}\quad\gamma_{xz}\quad\gamma_{xy}\}[\overline{C}]\begin{Bmatrix}\epsilon_x\\\epsilon_y\\\epsilon_z\\\gamma_{yz}\\\gamma_{xz}\\\gamma_{xy}\end{Bmatrix}dV, \tag{2.202}$$

where $[\overline{C}]$ is the stiffness matrix in the x, y, z coordinate system. The strain energy must be positive ($U > 0$) for any nonzero strain.

The potential of the external forces is defined as

$$\Omega=-\int\int\int(f_xu+f_yv+f_zw)\,dV-\int\int(p_xu+p_yv+p_zw)\,dA, \tag{2.203}$$

where, we recall, f_x, f_y, f_z are the body forces (per unit volume) and p_x, p_y, p_z are the surface forces (per unit area).

The total potential energy of the system is

$$\pi_p=U+\Omega. \tag{2.204}$$

2.10.1 The Ritz Method

In the Ritz method the displacements are assumed to be in the form

$$u=\sum_{i=1}^{I}A_iu_i\qquad v=\sum_{j=1}^{J}B_jv_j\qquad w=\sum_{k=1}^{K}C_kw_k. \tag{2.205}$$

The displacements u_i, v_j, w_k are conveniently chosen known functions that must satisfy the geometrical boundary conditions, whereas A_i, B_j, C_k are yet unknown constants. According to the principle of stationary potential energy, at equilibrium the potential energy (Eq. 2.204) must satisfy the conditions

$$\begin{aligned} \frac{\partial \pi_p}{\partial A_i} &= 0, \quad i = 1, \ldots, I \\ \frac{\partial \pi_p}{\partial B_j} &= 0, \quad j = 1, \ldots, J \\ \frac{\partial \pi_p}{\partial C_k} &= 0, \quad k = 1, \ldots, K. \end{aligned} \tag{2.206}$$

The constants are provided by the solution of these equations.

2.11 Summary

The equilibrium equations and the stress–strain and strain–displacement relationships presented in this chapter are summarized in Table 2.17 for generally anisotropic materials and in Table 2.18 for monoclinic materials. Equations for orthotropic, transversely isotropic, and isotropic materials are the same as for monoclinic materials (Table 2.18) with the elements of the stiffness and compliance matrices simplified according to Eqs. (2.95)–(2.97)

The unknowns of interest for generally anisotropic materials are summarized in Table 2.19 and for monoclinic, orthotropic, transversely isotropic, and isotropic materials in Table 2.20. It is evident that under plane-stress and plane-strain conditions the number of unknowns is reduced and the equations are simplified.

2.11.1 Note on the Compliance and Stiffness Matrices

In this section, we give proof of the important statement that the compliance matrix (and consequently its inverse the stiffness matrix) must be positive definite, and symmetrical.

We consider a small cube made of a linearly elastic material. This initially stress-free cube is deformed. During this deformation the internal energy (in this case, the strain energy) changes. Since initially the cube is stress free, the deformation results in a positive change in the strain energy[5] ($\Delta U \equiv U > 0$). This requirement may be expressed as (see Eq. 2.202)

$$[\epsilon_x \quad \epsilon_y \quad \epsilon_z \quad \gamma_{yz} \quad \gamma_{xz} \quad \gamma_{xy}][\overline{C}] \begin{Bmatrix} \epsilon_x \\ \epsilon_y \\ \epsilon_z \\ \gamma_{yz} \\ \gamma_{xz} \\ \gamma_{xy} \end{Bmatrix} > 0 \text{ when } \begin{Bmatrix} \epsilon_x \\ \epsilon_y \\ \epsilon_z \\ \gamma_{yz} \\ \gamma_{xz} \\ \gamma_{xy} \end{Bmatrix} \neq 0. \tag{2.207}$$

[5] L. E. Malvern, *Introduction to the Mechanics of a Continuous Medium*. Prentice-Hall, Englewood Cliffs, New Jersey, 1969, p. 292.

Table 2.17. The equations for a generally anisotropic material

	Equilibrium	Strain–displacement	Stress–strain
Three-dimensional	2.13, 2.14, 2.15	2.2, 2.3, 2.4, 2.9–2.11	2.20
Plane-strain			
Free end	2.59, 2.60, 2.61	2.54 2.56 2.57	2.62
Built-in ends	2.59, 2.60, 2.61	2.99 2.101, 2.102	2.103
Plane-stress	2.122, 2.123	2.2, 2.3, 2.11	2.126

Table 2.18. The equations for a monoclinic material. The equations for orthotropic, transversely isotropic, and isotropic materials are the same as for monoclinic materials with the stiffness and compliance matrix elements simplified as specified in Eqs. (2.95)–(2.97).

	Equilibrium	Strain–displacement	Stress–strain
Three-dimensional	2.13, 2.14, 2.15	2.2, 2.3, 2.4, 2.9–2.11	2.20
Plane-strain, free end			
In-plane load End axial load End moment	2.74, 2.75	2.68, 2.71	2.76
Out-of-plane load Torque	2.86	2.84	2.87
Plane-strain, built-in ends			
In-plane load	2.74, 2.75	2.107, 2.110	2.111
Out-of-plane load	2.86	2.117	2.119
Plane-stress	2.130, 2.131	2.2, 2.3, 2.11	2.134

Table 2.19. The unknowns in the equations for generally anisotropic materials.

	Displacements	Strains	Stresses
Three-dimensional	u, v, w	$\epsilon_x, \epsilon_y, \epsilon_z$ $\gamma_{yz}, \gamma_{xz}, \gamma_{xy}$	$\sigma_x, \sigma_y, \sigma_z$ $\tau_{yz}, \tau_{xz}, \tau_{xy}$
Plane-strain			
Free end	u, v, w	ϵ_x, ϵ_y $\gamma_{yz}, \gamma_{xz}, \gamma_{xy}$	σ_x, σ_y $\tau_{yz}, \tau_{xz}, \tau_{xy}$
Built-in ends	u, v, w	ϵ_x, ϵ_y $\gamma_{yz}, \gamma_{xz}, \gamma_{xy}$	σ_x, σ_y $\tau_{yz}, \tau_{xz}, \tau_{xy}$
Plane-stress	u, v	$\epsilon_x, \epsilon_y, \gamma_{xy}$	$\sigma_x, \sigma_y, \tau_{xy}$

Table 2.20. The unknowns in the equations for monoclinic, orthotropic, transversely isotropic, and isotropic materials

	Displacements	Strains	Stresses
Three-dimensional	u_1, u_2, u_3	$\epsilon_1, \epsilon_2, \epsilon_3$ $\gamma_{23}, \gamma_{13}, \gamma_{12}$	$\sigma_1, \sigma_2, \sigma_3$ $\tau_{23}, \tau_{13}, \tau_{12}$
Plane-strain, free end			
In-plane load End axial load End moment	u_1, u_2	$\epsilon_1, \epsilon_2, \gamma_{12}$	$\sigma_1, \sigma_2, \tau_{12}$
Out-of-plane load Torque	u_3	γ_{23}, γ_{13}	τ_{23}, τ_{13}
Plane-strain, built-in ends			
In-plane load	u_1, u_2	$\epsilon_1, \epsilon_2, \gamma_{12}$	$\sigma_1, \sigma_2, \tau_{12}$
Out-of-plane load	u_3	γ_{23}, γ_{13}	τ_{23}, τ_{13}
Plane-stress	u_1, u_2	$\epsilon_1, \epsilon_2, \gamma_{12}$	$\sigma_1, \sigma_2, \tau_{12}$

The preceding inequality requires that $[\overline{C}]$ be positive definite.[6] (Correspondingly, $[\overline{S}]$, $[C]$ and $[S]$ must also be positive definite.) The manner in which we can determine whether or not $[\overline{C}]$ is positive definite is discussed subsequently (page 59).

First we show that the compliance matrix must be symmetrical. To this end we apply loads in four steps (Fig. 2.36) to our initially stress-free cube made of an elastic material.

(a) A tensile load p (per unit area) is applied in the x direction. As the result of this load $\sigma_x = p$ is the only nonzero stress in the material. The strains are (see Eq. 2.21)

$$\epsilon_x^a = \overline{S}_{11} p \qquad \epsilon_y^a = \overline{S}_{21} p. \tag{2.208}$$

The work is

$$W^a = \int_0^{\epsilon_x^a} \sigma_x d\epsilon_x + \int_0^{\epsilon_y^a} \sigma_y d\epsilon_y = \frac{1}{2}\overline{S}_{11} p^2. \tag{2.209}$$

(b) An additional tensile load p is applied in the y direction. The stresses in the material become $\sigma_x = \sigma_y = p$, and the corresponding strains are

$$\epsilon_x^b = \overline{S}_{11} p + \overline{S}_{12} p \qquad \epsilon_y^b = \overline{S}_{21} p + \overline{S}_{22} p. \tag{2.210}$$

The work is

$$W^b = \int_{\epsilon_x^a}^{\epsilon_x^b} \sigma_x d\epsilon_x + \int_{\epsilon_y^a}^{\epsilon_y^b} \sigma_y d\epsilon_y = \overline{S}_{12} p^2 + \frac{1}{2}\overline{S}_{22} p^2. \tag{2.211}$$

[6] E. Kreyszig, *Advanced Engineering Mathematics*, 7th Edition. John Wiley & Sons, New York, 1993, p. 407.

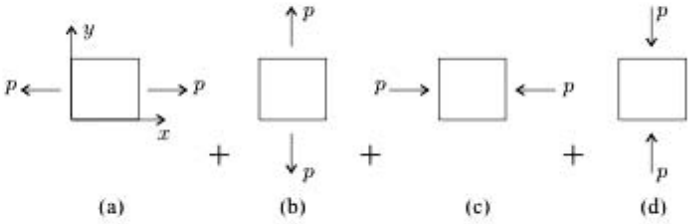

Figure 2.36: Illustration of the four load steps.

(c) An additional compressive load p is applied in the x direction. The stresses in the material become $\sigma_x = 0, \sigma_y = p$, and the corresponding strains are

$$\epsilon_x^c = \overline{S}_{12} p \qquad \epsilon_y^c = \overline{S}_{22} p. \tag{2.212}$$

The work is

$$W^c = \int_{\epsilon_x^b}^{\epsilon_x^c} \sigma_x d\epsilon_x + \int_{\epsilon_y^b}^{\epsilon_y^c} \sigma_y d\epsilon_y = -\frac{1}{2}\overline{S}_{11} p^2 - \overline{S}_{21} p^2. \tag{2.213}$$

(d) An additional compressive load p is applied in the y direction. The stresses in the material become $\sigma_x = \sigma_y = 0$, and the corresponding strains are $\epsilon_x^d = \epsilon_y^d = 0$. The work is

$$W^d = \int_{\epsilon_x^c}^{0} \sigma_x d\epsilon_x + \int_{\epsilon_y^c}^{0} \sigma_y d\epsilon_y = -\frac{1}{2}\overline{S}_{22} p^2. \tag{2.214}$$

The total work done on the cube is

$$W = W^a + W^b + W^c + W^d = (\overline{S}_{12} - \overline{S}_{21}) p^2. \tag{2.215}$$

For an elastic material the total work is zero. Accordingly, we must have

$$\overline{S}_{12} = \overline{S}_{21}. \tag{2.216}$$

By similar arguments it can be shown that

$$\overline{S}_{ij} = \overline{S}_{ji} \quad i, j = 1, 2, \ldots, 6. \tag{2.217}$$

Thus, the compliance matrix of an elastic material $[\overline{S}]$ (and correspondingly $[\overline{C}]$, $[C]$, and $[S]$) must be symmetrical.

Next we discuss the conditions that ensure a compliance matrix is positive definite. A symmetrical matrix is positive definite when each of its eigenvalues is positive.[7] Thus, to determine whether or not the matrix is positive definite we must examine the eigenvalues of the compliance (or stiffness) matrix.

For orthotropic, transversely isotropic, and isotropic materials there is a simpler method for determining whether or not the compliance (or stiffness) matrix

[7] F. B. Hildebrand, *Methods of Applied Mathematics*. 2nd edition. Prentice-Hall, Englewood Cliffs, New Jersey, 1965, p. 48.

is positive definite. The simpler method utilizes the condition that the matrix is positive definite when every subdeterminant of the main diagonal is positive.[8]

For an orthotropic material the compliance matrix is (Eq. 2.28)

$$[S] = \begin{bmatrix} S_{11} & S_{12} & S_{13} & 0 & 0 & 0 \\ S_{12} & S_{22} & S_{23} & 0 & 0 & 0 \\ S_{13} & S_{23} & S_{33} & 0 & 0 & 0 \\ 0 & 0 & 0 & S_{44} & 0 & 0 \\ 0 & 0 & 0 & 0 & S_{55} & 0 \\ 0 & 0 & 0 & 0 & 0 & S_{66} \end{bmatrix}. \tag{2.218}$$

The following subdeterminants must all be positive:

$$\begin{aligned} D_1 &= S_{11} > 0 \qquad D_2 = S_{22} > 0 \qquad D_3 = S_{33} > 0 \\ D_4 &= S_{44} > 0 \qquad D_5 = S_{55} > 0 \qquad D_6 = S_{66} > 0 \end{aligned} \tag{2.219}$$

$$D_{23} = \begin{vmatrix} S_{22} & S_{23} \\ S_{23} & S_{33} \end{vmatrix} > 0 \qquad D_{13} = \begin{vmatrix} S_{11} & S_{13} \\ S_{13} & S_{33} \end{vmatrix} > 0 \qquad D_{12} = \begin{vmatrix} S_{11} & S_{12} \\ S_{12} & S_{22} \end{vmatrix} > 0 \tag{2.220}$$

$$D_{123} = \begin{vmatrix} S_{11} & S_{12} & S_{13} \\ S_{12} & S_{22} & S_{23} \\ S_{13} & S_{23} & S_{33} \end{vmatrix} > 0, \tag{2.221}$$

where $|\ \ |$ denotes the determinant. Since the stiffness matrix is the inverse of the compliance matrix, according to the rules of matrix inversion the elements of the main diagonal of the stiffness matrix are

$$C_{11} = \frac{D_{23}}{D_{123}} \qquad C_{22} = \frac{D_{13}}{D_{123}} \qquad C_{33} = \frac{D_{12}}{D_{123}}, \tag{2.222}$$

where D_{23}, D_{13}, and D_{12} are positive when C_{11}, C_{22}, and C_{33} are positive,

$$C_{11} > 0 \qquad C_{22} > 0 \qquad C_{33} > 0, \tag{2.223}$$

and, at the same time, D_{123} is positive. Thus, the requirement for positive definiteness is met when all three of the following conditions are met:

- the elements of the main diagonal of the compliance matrix are positive (Eq. 2.219),
- the determinant of the compliance matrix is positive (Eq. 2.221), and
- the elements of the main diagonal of the stiffness matrix are positive (Eq. 2.223).

The same conditions apply for transversely isotropic and isotropic materials. If the relevant elements of the compliance and stiffness matrices are presented in

[8] E. Kreyszig, *Advanced Engineering Mathematics*. 7th edition. John Wiley & Sons, New York, 1993, p. 407.

Table 2.21. The constraints on the engineering constants.

Orthotropic	$E_1 > 0$	$E_2 > 0$	$E_3 > 0$
	$G_{23} > 0$	$G_{13} > 0$	$G_{12} > 0$
	$1 - \nu_{23}^2 \frac{E_3}{E_2} - \nu_{12}^2 \frac{E_2}{E_1} - 2\nu_{12}\nu_{13}\nu_{23}\frac{E_3}{E_1} - \nu_{13}^2 \frac{E_3}{E_1} > 0$		
	$\nu_{23}^2 < \frac{E_2}{E_3}$,	$\nu_{13}^2 < \frac{E_1}{E_3}$,	$\nu_{12}^2 < \frac{E_1}{E_2}$
Transversely isotropic	$E_1 > 0$,	$E_2 > 0$,	$G_{12} > 0$
	$-1 < \nu_{23} < 1 - 2\frac{E_2}{E_1}\nu_{12}^2$		
	$\nu_{12}^2 < \frac{E_1}{E_2}$		
Isotropic	$E_1 > 0$		
	$-1 < \nu_{12} < 0.5$		

terms of the engineering constants (see Tables 2.7 and 2.9, pages 15 and 18) the preceding conditions can be expressed in terms of the engineering constants. Details of the algebraic manipulations are not given here. The results are summarized in Table 2.21.[9]

2.4 Example. *The engineering constants of a graphite epoxy unidirectional ply are given as* $E_1 = 148 \times 10^9$ *N/m*^{2}, $E_2 = 9.65 \times 10^9$ *N/m*^{2}, $G_{12} = 4.55 \times 10^9$ *N/m*^{2}, $\nu_{12} = 0.3$, *and* $\nu_{23} = 0.6$. *Determine whether or not this set of constants is valid.*

Solution. There are two ways to find the answer to this problem.

Method 1. The compliance matrix is (Eq. 2.41)

$$[S] = \begin{bmatrix} 6.76 & -2.03 & -2.03 & 0 & 0 & 0 \\ -2.03 & 103.63 & -62.18 & 0 & 0 & 0 \\ -2.03 & -62.18 & 103.63 & 0 & 0 & 0 \\ 0 & 0 & 0 & 331.61 & 0 & 0 \\ 0 & 0 & 0 & 0 & 219.78 & 0 \\ 0 & 0 & 0 & 0 & 0 & 219.78 \end{bmatrix} 10^{-12} \frac{\text{m}^2}{\text{N}}. \tag{2.224}$$

The eigenvalues ($\lambda \times 10^{+9}$) of this matrix are

0.0065 0.0417 0.1658 0.2198 0.2198 0.3316.

Since every eigenvalue is positive, the specified set of engineering constants is valid.

Method 2. For a transversely isotropic material the engineering constants must satisfy the inequalities in Table 2.21. In terms of the engineering constants these inequalities are

$$-1 < \nu_{23} < 1 - 2\frac{E_2}{E_1}\nu_{12}^2 \qquad \nu_{12}^2 < \frac{E_1}{E_2} \tag{2.225}$$

[9] B. M. Lempriere, Poisson's Ratio in Orthotropic Materials. *AIAA Journal*, Vol. 7, 2226–2227, 1968.

or

$$-1 < 0.6 < 0.988 \qquad 0.09 < 15.3. \tag{2.226}$$

Since the inequalities are satisfied, the specified set of engineering constants is valid.

Let us now assume that $\nu_{21} = 0.3$. In this case $\nu_{12} = \frac{E_1}{E_2}\nu_{21} = 4.601$ (see Table 2.8, page 16), and the compliance matrix (Table 2.7, third row, page 15) is

$$[S] = \begin{bmatrix} 6.76 & -31.09 & -31.09 & 0 & 0 & 0 \\ -31.09 & 103.63 & -62.18 & 0 & 0 & 0 \\ -31.09 & -62.18 & 103.63 & 0 & 0 & 0 \\ 0 & 0 & 0 & 331.61 & 0 & 0 \\ 0 & 0 & 0 & 0 & 219.78 & 0 \\ 0 & 0 & 0 & 0 & 0 & 219.78 \end{bmatrix} 10^{-12}\frac{\text{m}^2}{\text{N}}. \tag{2.227}$$

The eigenvalues ($\lambda \times 10^{+9}$) are

$$-0.0232 \qquad 0.0714 \qquad 0.1658 \qquad 0.2198 \qquad 0.2198 \qquad 0.3316.$$

One of the eigenvalues is negative; hence, the specified set of engineering constants is invalid. We reach the same conclusion if we use the inequalities given by Eq. (2.225) since two of the inequalities are not satisfied:

$$-1 < 0.6 \not< -1.76 \qquad 21.2 \not< 15.3. \tag{2.228}$$

This example illustrates that care should be taken to use proper values of the Poisson ratios. The ν_{12} and ν_{21} Poisson ratios (referred to as the major and minor Poisson ratios) must not be interchanged.

Laminated Composites

Composites are frequently made of layers (plies) bonded together to form a laminate (Fig. 3.1). A layer may consist of short fibers, unidirectional continuous fibers, or woven or braided fibers embedded in a matrix (Figs. 1.1 and 1.2). A layer containing woven or braided fibers is referred to as fabric.

Adjacent plies having the same material and the same orientation are referred to as a ply group. Since the properties and the orientations are the same across the ply group, a ply group may be treated as one layer.

3.1 Laminate Code

An x, y, z orthogonal coordinate system is used in analyzing laminates with the z coordinate being perpendicular to the plane of the laminate (Fig. 3.2).

The orientations of continuous, unidirectional plies are specified by the angle Θ (in degree) with respect to the x-axis (Fig. 3.2). The angle Θ is positive in the counterclockwise direction. The number of plies within a ply group is specified by a numerical subscript. For example, the laminate consisting of unidirectional plies and shown in Figure 3.3 is designated as

$$[45_3/0_4/90_2/60]\,.$$

This laminate contains four ply groups, the first containing three plies in the 45-degree direction, the second containing four plies in the 0-degree direction, the third containing two plies in the 90-degree direction, the fourth containing one ply in the 60-degree direction.

Symmetrical laminate. When the laminate is symmetrical with respect to the midplane it is referred to as a symmetrical laminate. Examples of symmetrical laminates are shown in Figure 3.4. The laminates represented in Figure 3.4 are

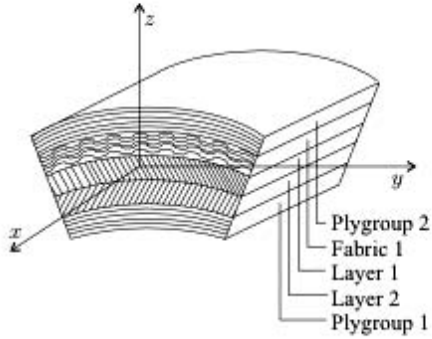

Figure 3.1: Laminated composite.

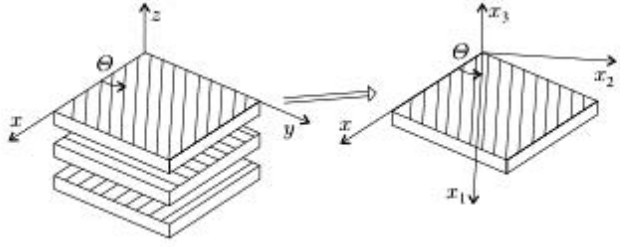

Figure 3.2: The x, y, z laminate coordinate system, the x_1, x_2, x_3 ply coordinate system, and the ply angle.

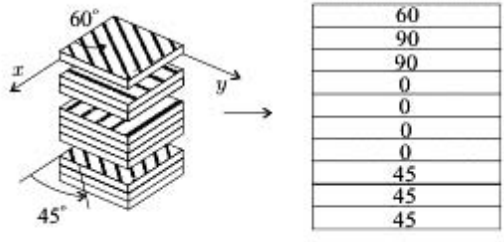

Figure 3.3: Description of the layup in a laminate consisting of unidirectional plies $[45_3/0_4/90_2/60]$.

–45
–45
0
0
0
0
–45
–45

$[-45_2/0_2]_s$

45
–45
–45
45
45
–45
–45
45

$[45/-45_2/45]_s$

Figure 3.4: Examples of symmetrical laminates.

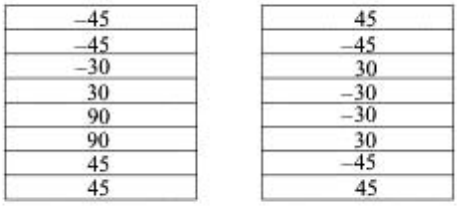

Figure 3.5: Examples of balanced laminates.

specified as

$$[-45_2/0_4/-45_2] \equiv [-45_2/0_2]_s$$
$$[45/-45_2/45_2/-45_2/45] \equiv [45/-45_2/45]_s .$$

The subscript s indicates symmetry about the midplane.

Balanced laminate. In balanced laminates, for every ply in the $+\Theta$ direction there is an identical ply in the $-\Theta$ direction. Examples of balanced laminates are shown in Figure 3.5.

Cross-ply laminates. In cross-ply laminates fibers are only in the 0- and 90-degree directions (Fig. 3.6). Cross-ply laminates may be symmetrical or unsymmetrical. Since there is no distinction between the $+0$ and -0 and between the $+90$- and -90-degree directions, cross-ply laminates are balanced.

Angle-ply laminate. Angle-ply laminates consist of plies in the $+\Theta$ and $-\Theta$ directions. Angle-ply laminates may by symmetrical or unsymmetrical, balanced or unbalanced. Examples of angle-ply laminates are shown in Figure 3.7.

$\pi/4$ laminate. $\pi/4$ laminates consist of plies in which the fibers are in the 0-, 45-, 90-, and -45-degree directions. The number of plies in each direction is the same (balanced laminate). In addition, the layup is also symmetrical.

3.2 Stiffness Matrices of Thin Laminates

Thin laminates are characterized by three stiffness matrices denoted by $[A]$, $[B]$, and $[D]$. In this section we determine these matrices for thin, flat laminates undergoing small deformations. The analyses are based on the laminate plate theory and are formulated using the approximations that the strains vary linearly across the

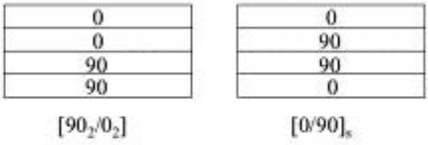

Figure 3.6: Examples of cross-ply laminates.

−45
−45
45
45
−45
−45

$[-45_2/45_2/-45_2]$

30
30
30
−30
−30
−30

$[-30_3/30_3]$

Figure 3.7: Examples of angle-ply laminates.

laminate, (out-of-plane) shear deformations are negligible, and the out-of-plane normal stress σ_z and the shear stresses τ_{xz}, τ_{yz} are small compared with the in-plane σ_x, σ_y, and τ_{xy} stresses. These approximations imply that the stress–strain relationships under plane-stress conditions may be applied. The x, y, z refer to a coordinate system with the x and y coordinates in a suitably chosen reference plane, and z is perpendicular to this reference plane (Fig. 3.8).

Frequently, though not always, for convenience the reference plane is taken to be the midplane of the laminate. Unless the laminate is symmetrical with respect to the reference plane, the reference plane is not a neutral plane, and the strains in the reference plane are not zero under pure bending. The strains in the reference plane are (see Eqs. 2.2, 2.3, and 2.11)

$$\epsilon_x^o = \frac{\partial u^o}{\partial x} \qquad \epsilon_y^o = \frac{\partial v^o}{\partial y} \qquad \gamma_{xy}^o = \frac{\partial u^o}{\partial y} + \frac{\partial v^o}{\partial x}, \tag{3.1}$$

where u and v are the x, y components of the displacement and the superscript 0 refers to the reference plane.

We adopt the Kirchhoff hypothesis, namely, that normals to the reference surface remain normal and straight (Fig. 3.9). Accordingly, for small deflections the angle of rotation of the normal of the reference plane χ_{xz} is

$$\chi_{xz} = \frac{\partial w^o}{\partial x}, \tag{3.2}$$

where w^o is the out-of-plane displacement of the reference plane. The total displacement in the x direction is

$$u = u^o - z\chi_{xz} = u^o - z\frac{\partial w^o}{\partial x}. \tag{3.3}$$

Similarly, the total displacement in the y direction is

$$v = v^o - z\frac{\partial w^o}{\partial y}. \tag{3.4}$$

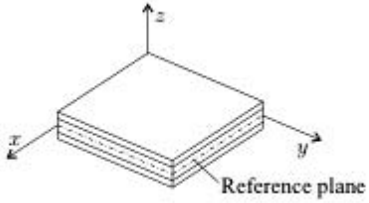

Figure 3.8: The coordinate system.

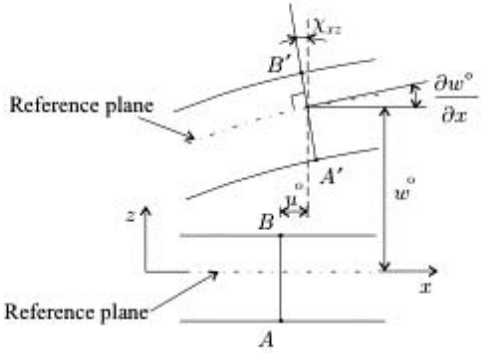

Figure 3.9: Deformation of a plate in the x–z plane.

By definition, the strains are (Eqs. 2.2, 2.3, 2.11)

$$\epsilon_x = \frac{\partial u}{\partial x} \qquad \epsilon_y = \frac{\partial v}{\partial y} \qquad \gamma_{xy} = \frac{\partial u}{\partial y} + \frac{\partial v}{\partial x}. \tag{3.5}$$

Substituting Eqs. (3.3) and (3.4) into these expressions, we obtain

$$\begin{aligned} \epsilon_x &= \frac{\partial u^o}{\partial x} - z\frac{\partial^2 w^o}{\partial x^2} \\ \epsilon_y &= \frac{\partial v^o}{\partial y} - z\frac{\partial^2 w^o}{\partial y^2} \\ \gamma_{xy} &= \frac{\partial u^o}{\partial y} + \frac{\partial v^o}{\partial x} - z\frac{2\partial^2 w^o}{\partial x \partial y}. \end{aligned} \tag{3.6}$$

These equations can be written in the following form:

$$\begin{Bmatrix} \epsilon_x \\ \epsilon_y \\ \gamma_{xy} \end{Bmatrix} = \begin{Bmatrix} \epsilon_x^o \\ \epsilon_y^o \\ \gamma_{xy}^o \end{Bmatrix} + z \begin{Bmatrix} \kappa_x \\ \kappa_y \\ \kappa_{xy} \end{Bmatrix}, \tag{3.7}$$

where ϵ_x^o, ϵ_y^o, γ_{xy}^o are the strains in the reference plane (Eq. 3.1), and κ_x, κ_y, and κ_{xy} are the curvatures of the reference plane of the plate (Fig. 3.10) defined as

$$\kappa_x = -\frac{\partial^2 w^o}{\partial x^2} \qquad \kappa_y = -\frac{\partial^2 w^o}{\partial y^2} \qquad \kappa_{xy} = -\frac{2\partial^2 w^o}{\partial x \partial y}. \tag{3.8}$$

The in-plane forces and moments acting on a small element are (Fig. 3.11)

$$\begin{aligned} N_x &= \int_{-h_b}^{h_t} \sigma_x dz \qquad N_y = \int_{-h_b}^{h_t} \sigma_y dz \qquad N_{xy} = \int_{-h_b}^{h_t} \tau_{xy} dz \\ M_x &= \int_{-h_b}^{h_t} z\sigma_x dz \qquad M_y = \int_{-h_b}^{h_t} z\sigma_y dz \qquad M_{xy} = \int_{-h_b}^{h_t} z\tau_{xy} dz, \end{aligned} \tag{3.9}$$

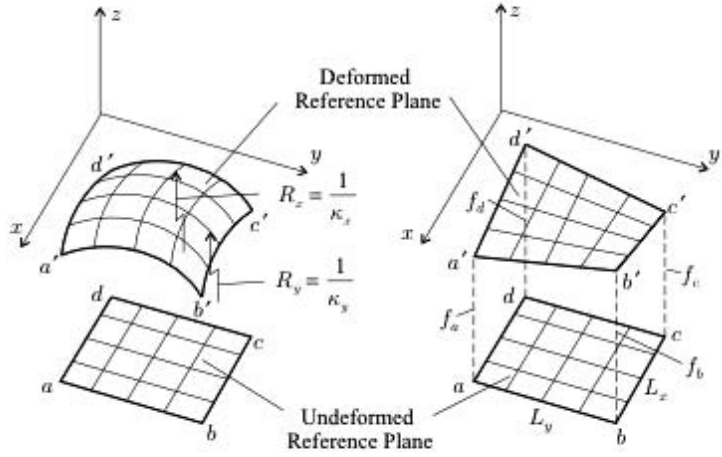

Figure 3.10: The curvatures κ_x, κ_y, and κ_{xy} of the reference plane.

where N and M are the in-plane forces and moments (per unit length), and h_t and h_b are the distances from the reference plane to the plate's surfaces (Fig. 3.12). The transverse shear forces (per unit length) are (Fig. 3.11, right)

$$V_x = \int_{-h_b}^{h_t} \tau_{xz} dz \qquad V_y = \int_{-h_b}^{h_t} \tau_{yz} dz. \tag{3.10}$$

We now recall that for plane-stress condition the stress–strain relationships *for each ply* are (Eq. 2.126)

$$\begin{Bmatrix} \sigma_x \\ \sigma_y \\ \tau_{xy} \end{Bmatrix} = \begin{bmatrix} \overline{Q}_{11} & \overline{Q}_{12} & \overline{Q}_{16} \\ \overline{Q}_{12} & \overline{Q}_{22} & \overline{Q}_{26} \\ \overline{Q}_{16} & \overline{Q}_{26} & \overline{Q}_{66} \end{bmatrix} \begin{Bmatrix} \epsilon_x \\ \epsilon_y \\ \gamma_{xy} \end{Bmatrix}. \tag{3.11}$$

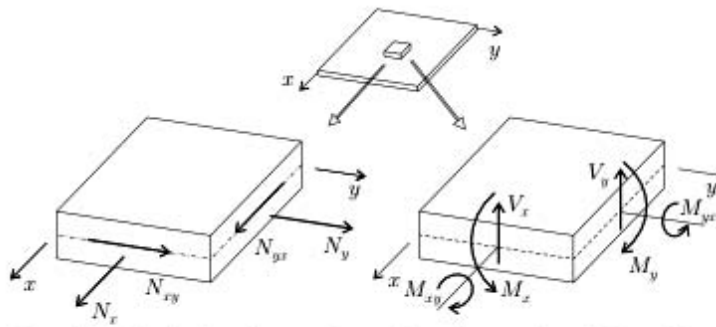

Figure 3.11: The in-plane forces acting at the reference plane (left) and the moments and the transverse shear forces (right).

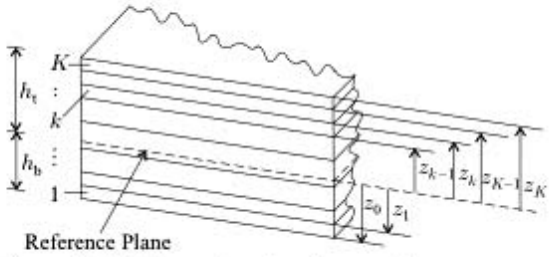

Figure 3.12: Distances from the reference plane.

By introducing the notation

$$[\overline{Q}] = \begin{bmatrix} \overline{Q}_{11} & \overline{Q}_{12} & \overline{Q}_{16} \\ \overline{Q}_{12} & \overline{Q}_{22} & \overline{Q}_{26} \\ \overline{Q}_{16} & \overline{Q}_{26} & \overline{Q}_{66} \end{bmatrix}, \tag{3.12}$$

we write the stress–strain relationships for a ply as

$$\begin{Bmatrix} \sigma_x \\ \sigma_y \\ \tau_{xy} \end{Bmatrix} = [\overline{Q}] \begin{Bmatrix} \epsilon_x \\ \epsilon_y \\ \gamma_{xy} \end{Bmatrix}, \tag{3.13}$$

where $[\overline{Q}]$ is the stiffness matrix of the ply in the x–y coordinate system. The elements of this stiffness matrix are obtained from the elements of the stiffness matrix $[Q]$ in the $x_1 - x_2$ coordinate system by the transformation given by Eq. (2.195). By replacing $[Q]$ and $[Q']$ by $[\overline{Q}]$ and $[Q]$, respectively, Eq. (2.195) yields

$$\begin{bmatrix} \overline{Q}_{11} & \overline{Q}_{12} & \overline{Q}_{16} \\ \overline{Q}_{12} & \overline{Q}_{22} & \overline{Q}_{26} \\ \overline{Q}_{16} & \overline{Q}_{26} & \overline{Q}_{66} \end{bmatrix} = [T_\sigma]^{-1} \begin{bmatrix} Q_{11} & Q_{12} & Q_{16} \\ Q_{12} & Q_{22} & Q_{26} \\ Q_{16} & Q_{26} & Q_{66} \end{bmatrix} [T_\epsilon], \tag{3.14}$$

where $[T_\sigma]$ and $[T_\epsilon]$ are given by Eq. (2.196) and are reiterated below,

$$[T_\sigma] = \begin{bmatrix} c^2 & s^2 & 2cs \\ s^2 & c^2 & -2cs \\ -cs & cs & c^2 - s^2 \end{bmatrix} \qquad [T_\epsilon] = \begin{bmatrix} c^2 & s^2 & cs \\ s^2 & c^2 & -cs \\ -2cs & 2cs & c^2 - s^2 \end{bmatrix}, \tag{3.15}$$

and $c = \cos\Theta$, $s = \sin\Theta$ with Θ defined in Figure 3.2. For an orthotropic ply the local coordinates x_1, x_2 are in the orthotropy directions. For transversely isotropic plies these local coordinates are parallel and perpendicular to the fibers (Fig. 2.15). For orthotropic and transversely isotropic materials the elements of the stiffness matrix in the global coordinate system are given in Table 3.1 in terms of the elements of the stiffness matrix in the local coordinate system.

Table 3.1. The elements of the $[\overline{Q}]$ matrix for an othotropic or transversely isotropic ply oriented in the $+\Theta$ direction (Fig 3.2)

$$\overline{Q}_{11} = c^4 Q_{11} + s^4 Q_{22} + 2c^2 s^2 (Q_{12} + 2Q_{66})$$
$$\overline{Q}_{22} = s^4 Q_{11} + c^4 Q_{22} + 2c^2 s^2 (Q_{12} + 2Q_{66})$$
$$\overline{Q}_{12} = c^2 s^2 (Q_{11} + Q_{22} - 4Q_{66}) + (c^4 + s^4) Q_{12}$$
$$\overline{Q}_{66} = c^2 s^2 (Q_{11} + Q_{22} - 2Q_{12}) + (c^2 - s^2)^2 Q_{66}$$
$$\overline{Q}_{16} = cs(c^2 Q_{11} - s^2 Q_{22} - (c^2 - s^2)(Q_{12} + 2Q_{66}))$$
$$\overline{Q}_{26} = cs(s^2 Q_{11} - c^2 Q_{22} + (c^2 - s^2)(Q_{12} + 2Q_{66}))$$
$$c = \cos\ \Theta \qquad s = \sin\ \Theta$$

By substituting Eqs. (3.7) and (3.13) into Eq. (3.9), we obtain

$$\begin{Bmatrix} N_x \\ N_y \\ N_{xy} \end{Bmatrix} = \int_{-h_b}^{h_t} \left\{ [\overline{Q}] \begin{Bmatrix} \epsilon_x^o \\ \epsilon_y^o \\ \gamma_{xy}^o \end{Bmatrix} + [\overline{Q}] z \begin{Bmatrix} \kappa_x \\ \kappa_y \\ \kappa_{xy} \end{Bmatrix} \right\} dz$$
$$= \int_{-h_b}^{h_t} [\overline{Q}] dz \begin{Bmatrix} \epsilon_x^o \\ \epsilon_y^o \\ \gamma_{xy}^o \end{Bmatrix} + \int_{-h_b}^{h_t} z[\overline{Q}] dz \begin{Bmatrix} \kappa_x \\ \kappa_y \\ \kappa_{xy} \end{Bmatrix} \tag{3.16}$$

$$\begin{Bmatrix} M_x \\ M_y \\ M_{xy} \end{Bmatrix} = \int_{-h_b}^{h_t} z \left\{ [\overline{Q}] \begin{Bmatrix} \epsilon_x^o \\ \epsilon_y^o \\ \gamma_{xy}^o \end{Bmatrix} + [\overline{Q}] z \begin{Bmatrix} \kappa_x \\ \kappa_y \\ \kappa_{xy} \end{Bmatrix} \right\} dz$$
$$= \int_{-h_b}^{h_t} z[\overline{Q}] dz \begin{Bmatrix} \epsilon_x^o \\ \epsilon_y^o \\ \gamma_{xy}^o \end{Bmatrix} + \int_{-h_b}^{h_t} z^2[\overline{Q}] dz \begin{Bmatrix} \kappa_x \\ \kappa_y \\ \kappa_{xy} \end{Bmatrix}. \tag{3.17}$$

The stiffness matrices of the laminate are defined as

$$[A] = \int_{-h_b}^{h_t} [\overline{Q}] dz$$
$$[B] = \int_{-h_b}^{h_t} z[\overline{Q}] dz \tag{3.18}$$
$$[D] = \int_{-h_b}^{h_t} z^2[\overline{Q}] dz.$$

The elements of these matrices are ($i, j = 1, 2, 6$)

$$A_{ij} = \int_{-h_0}^{h_1} \overline{Q}_{ij} dz \qquad B_{ij} = \int_{-h_0}^{h_1} z\overline{Q}_{ij} dz$$
$$D_{ij} = \int_{-h_0}^{h_1} z^2 \overline{Q}_{ij} dz. \tag{3.19}$$

The $[A]$, $[B]$, and $[D]$ matrices are the stiffness matrices of the laminate, and $[\overline{Q}]$ is the stiffness matrix of the ply. Since $[\overline{Q}]$ is constant across each ply, the integrals in the equations above (Eq. 3.19) may be replaced by summations (Fig. 3.12) as follows ($i, j = 1, 2, 6$):

$$A_{ij} = \sum_{k=1}^{K} (\overline{Q}_{ij})_k (z_k - z_{k-1})$$
$$B_{ij} = \frac{1}{2} \sum_{k=1}^{K} (\overline{Q}_{ij})_k (z_k^2 - z_{k-1}^2) \tag{3.20}$$
$$D_{ij} = \frac{1}{3} \sum_{k=1}^{K} (\overline{Q}_{ij})_k (z_k^3 - z_{k-1}^3),$$

where K is the total number of plies (or ply groups) in the laminate; z_k, z_{k-1} are the distances from the reference plane to the two surfaces of the kth ply; and $(\overline{Q}_{ij})_k$ are the elements of the stiffness matrix of the kth ply.

With the preceding definitions of the stiffness matrices, the expressions for the in-plane forces and moments (Eqs. 3.16 and 3.17) become

$$\begin{Bmatrix} N_x \\ N_y \\ N_{xy} \\ M_x \\ M_y \\ M_{xy} \end{Bmatrix} = \begin{bmatrix} A_{11} & A_{12} & A_{16} & B_{11} & B_{12} & B_{16} \\ A_{12} & A_{22} & A_{26} & B_{12} & B_{22} & B_{26} \\ A_{16} & A_{26} & A_{66} & B_{16} & B_{26} & B_{66} \\ B_{11} & B_{12} & B_{16} & D_{11} & D_{12} & D_{16} \\ B_{12} & B_{22} & B_{26} & D_{12} & D_{22} & D_{26} \\ B_{16} & B_{26} & B_{66} & D_{16} & D_{26} & D_{66} \end{bmatrix} \begin{Bmatrix} \epsilon_x^o \\ \epsilon_y^o \\ \gamma_{xy}^o \\ \kappa_x \\ \kappa_y \\ \kappa_{xy} \end{Bmatrix}. \tag{3.21}$$

The vectors on the left and right hand side represent generalized forces and strains. Hereafter, we simply refer to these as forces and strains.

By inverting Eqs. (3.21), we obtain the strains and curvatures in terms of the in-plane forces and moments:

$$\begin{Bmatrix} \epsilon_x^o \\ \epsilon_y^o \\ \gamma_{xy}^o \\ \kappa_x \\ \kappa_y \\ \kappa_{xy} \end{Bmatrix} = \begin{bmatrix} \alpha_{11} & \alpha_{12} & \alpha_{16} & \beta_{11} & \beta_{12} & \beta_{16} \\ \alpha_{12} & \alpha_{22} & \alpha_{26} & \beta_{21} & \beta_{22} & \beta_{26} \\ \alpha_{16} & \alpha_{26} & \alpha_{66} & \beta_{61} & \beta_{62} & \beta_{66} \\ \beta_{11} & \beta_{21} & \beta_{61} & \delta_{11} & \delta_{12} & \delta_{16} \\ \beta_{12} & \beta_{22} & \beta_{62} & \delta_{12} & \delta_{22} & \delta_{26} \\ \beta_{16} & \beta_{26} & \beta_{66} & \delta_{16} & \delta_{26} & \delta_{66} \end{bmatrix} \begin{Bmatrix} N_x \\ N_y \\ N_{xy} \\ M_x \\ M_y \\ M_{xy} \end{Bmatrix}. \tag{3.22}$$

The $[\alpha]$, $[\beta]$, and $[\delta]$ matrices are related to the $[A]$, $[B]$, and $[D]$ matrices by

$$\begin{bmatrix} \alpha_{11} & \alpha_{12} & \alpha_{16} & \beta_{11} & \beta_{12} & \beta_{16} \\ \alpha_{12} & \alpha_{22} & \alpha_{26} & \beta_{21} & \beta_{22} & \beta_{26} \\ \alpha_{16} & \alpha_{26} & \alpha_{66} & \beta_{61} & \beta_{62} & \beta_{66} \\ \beta_{11} & \beta_{21} & \beta_{61} & \delta_{11} & \delta_{12} & \delta_{16} \\ \beta_{12} & \beta_{22} & \beta_{62} & \delta_{12} & \delta_{22} & \delta_{26} \\ \beta_{16} & \beta_{26} & \beta_{66} & \delta_{16} & \delta_{26} & \delta_{66} \end{bmatrix} = \begin{bmatrix} A_{11} & A_{12} & A_{16} & B_{11} & B_{12} & B_{16} \\ A_{12} & A_{22} & A_{26} & B_{12} & B_{22} & B_{26} \\ A_{16} & A_{26} & A_{66} & B_{16} & B_{26} & B_{66} \\ B_{11} & B_{12} & B_{16} & D_{11} & D_{12} & D_{16} \\ B_{12} & B_{22} & B_{26} & D_{12} & D_{22} & D_{26} \\ B_{16} & B_{26} & B_{66} & D_{16} & D_{26} & D_{66} \end{bmatrix}^{-1} . \tag{3.23}$$

3.2.1 The Significance of the [A], [B], and [D] Stiffness Matrices

The $[A]$, $[B]$, and $[D]$ matrices represent the stiffnesses of a laminate and describe the response of the laminate to in-plane forces and moments.

A_{ij} are the in-plane stiffnesses that relate the in-plane forces N_x, N_y, N_{xy} to the in-plane deformations ϵ_x^o, ϵ_y^o, γ_{xy}^o.

D_{ij} are the bending stiffnesses that relate the moments M_x, M_y, M_{xy} to the curvatures κ_x, κ_y, κ_{xy}.

Table 3.2. Illustration of the coupling terms A_{16}, D_{16}, B_{16}, B_{11}, B_{12}, B_{66} for composite materials. When the element shown in the last column is zero, there is no coupling. (The coupling terms A_{26}, D_{26}, B_{26}, B_{22} can be illustrated in a similar manner by applying a force N_y and a moment M_y in the y–z plane.)

Coupling	No Coupling	Element
Extension–shear		
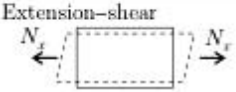		A_{16}
Bending–twist		
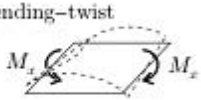		D_{16}
Extension–twist		
	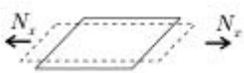	B_{16}
In-plane–out-of-plane		
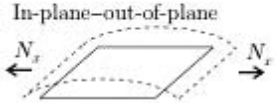	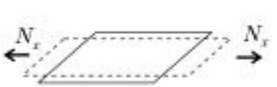	B_{11}
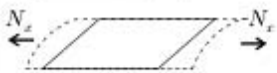		B_{12}
		B_{66}

Table 3.3. Illustration of the coupling terms A_{12}, D_{12} that may be present both in composite and in isotropic materials. When the element shown in the last column is zero, there is no coupling.

Coupling	No Coupling	Element
Extension–extension 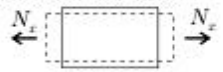		A_{12}
Bending–bending 		D_{12}

B_{ij} are the in-plane–out-of-plane coupling stiffnesses that relate the in-plane forces N_x, N_y, N_{xy} to the curvatures κ_x, κ_y, κ_{xy} and the moments M_x, M_y, M_{xy} to the in-plane deformations ϵ_x^o, ϵ_y^o, γ_{xy}^o.

Examination of the $[A]$, $[B]$, and $[D]$ matrices shows that different types of couplings may occur as discussed below and illustrated in Tables 3.2 and 3.3.

Extension–shear coupling. When the elements A_{16}, A_{26} are not zero, in-plane normal forces N_x, N_y cause shear deformation γ_{xy}^o, and a twist force N_{xy} causes elongations in the x and y directions.

Bending–twist coupling. When the elements D_{16}, D_{26} are not zero, bending moments M_x, M_y cause twist of the laminate κ_{xy}, and a twist moment M_{xy} causes curvatures in the x–z and y–z planes.

Extension–twist and bending–shear coupling. When the elements B_{16}, B_{26} are not zero, in-plane normal forces N_x, N_y cause twist κ_{xy}, and bending moments M_x, M_y result in shear deformation γ_{xy}^o.

In-plane–out-of-plane coupling. When the elements B_{ij} are not zero, in-plane forces N_x, N_y, N_{xy} cause out-of-plane deformations (curvatures) of the laminate, and moments M_x, M_y, M_{xy} cause in-plane deformations in the x–y plane.

The preceding four types of coupling are characteristic of composite materials and do not occur in homogeneous isotropic materials. The following two couplings occur in both composite and isotropic materials (Table 3.3):

Extension–extension coupling. When the element A_{12} is not zero, a normal force N_x causes elongation in the y direction ϵ_y^o, and a normal force N_y causes elongation in the x direction ϵ_x^o.

Bending–bending coupling. When the element D_{12} is not zero, a bending moment M_x causes curvature of the laminate in the y–z plane κ_y, and a bending moment M_y causes curvature of the laminate in the x–z plane κ_x.

3.2.2 Stiffness Matrices for Selected Laminates

For certain ply arrangements (layups), some of the couplings described do not occur, and the $[A]$, $[B]$, $[D]$ matrices become simpler.

Symmetrical laminate. In a symmetrical laminate the ply located at a position $+z$ is identical to the ply at $-z$. Correspondingly, the stiffness matrix $[\overline{Q}]$ of the ply at $+z$ is identical to the stiffness matrix of the ply at $-z$:

$$[\overline{Q}](z) = [\overline{Q}](-z). \tag{3.24}$$

By substituting these stiffnesses into Eq. (3.18), we find that the $[B]$ matrix is zero:

$$[B] = 0 \qquad \text{(symmetrical)}. \tag{3.25}$$

Thus, for a symmetrical laminate there is no in-plane–out-of-plane coupling, and Eq. (3.21) reduces to

$$\begin{Bmatrix} N_x \\ N_y \\ N_{xy} \end{Bmatrix} = \begin{bmatrix} A_{11} & A_{12} & A_{16} \\ A_{12} & A_{22} & A_{26} \\ A_{16} & A_{26} & A_{66} \end{bmatrix} \begin{Bmatrix} \epsilon_x^o \\ \epsilon_y^o \\ \gamma_{xy}^o \end{Bmatrix} \tag{3.26}$$

$$\begin{Bmatrix} M_x \\ M_y \\ M_{xy} \end{Bmatrix} = \begin{bmatrix} D_{11} & D_{12} & D_{16} \\ D_{12} & D_{22} & D_{26} \\ D_{16} & D_{26} & D_{66} \end{bmatrix} \begin{Bmatrix} \kappa_x \\ \kappa_y \\ \kappa_{xy} \end{Bmatrix}. \tag{3.27}$$

When the laminate is symmetrical, the compliance matrix is generally expressed as

$$\begin{bmatrix} \alpha_{11} & \alpha_{12} & \alpha_{16} \\ \alpha_{12} & \alpha_{22} & \alpha_{26} \\ \alpha_{16} & \alpha_{26} & \alpha_{66} \end{bmatrix} = \begin{bmatrix} a_{11} & a_{12} & a_{16} \\ a_{12} & a_{22} & a_{26} \\ a_{16} & a_{26} & a_{66} \end{bmatrix} \quad \begin{bmatrix} \delta_{11} & \delta_{12} & \delta_{16} \\ \delta_{12} & \delta_{22} & \delta_{26} \\ \delta_{16} & \delta_{26} & \delta_{66} \end{bmatrix} = \begin{bmatrix} d_{11} & d_{12} & d_{16} \\ d_{12} & d_{22} & d_{26} \\ d_{16} & d_{26} & d_{66} \end{bmatrix}, \tag{3.28}$$

where

$$\begin{bmatrix} a_{11} & a_{12} & a_{16} \\ a_{12} & a_{22} & a_{26} \\ a_{16} & a_{26} & a_{66} \end{bmatrix} = \begin{bmatrix} A_{11} & A_{12} & A_{16} \\ A_{12} & A_{22} & A_{26} \\ A_{16} & A_{26} & A_{66} \end{bmatrix}^{-1} \tag{3.29}$$

$$\begin{bmatrix} d_{11} & d_{12} & d_{16} \\ d_{12} & d_{22} & d_{26} \\ d_{16} & d_{26} & d_{66} \end{bmatrix} = \begin{bmatrix} D_{11} & D_{12} & D_{16} \\ D_{12} & D_{22} & D_{26} \\ D_{16} & D_{26} & D_{66} \end{bmatrix}^{-1}. \tag{3.30}$$

The relationships between the strains and curvatures and the forces and moments (Eq. 3.22) now simplify to

$$\begin{Bmatrix} \epsilon_x^o \\ \epsilon_y^o \\ \gamma_{xy}^o \end{Bmatrix} = \begin{bmatrix} a_{11} & a_{12} & a_{16} \\ a_{12} & a_{22} & a_{26} \\ a_{16} & a_{26} & a_{66} \end{bmatrix} \begin{Bmatrix} N_x \\ N_y \\ N_{xy} \end{Bmatrix} \tag{3.31}$$

$$\begin{Bmatrix} \kappa_x \\ \kappa_y \\ \kappa_{xy} \end{Bmatrix} = \begin{bmatrix} d_{11} & d_{12} & d_{16} \\ d_{12} & d_{22} & d_{26} \\ d_{16} & d_{26} & d_{66} \end{bmatrix} \begin{Bmatrix} M_x \\ M_y \\ M_{xy} \end{Bmatrix}. \tag{3.32}$$

Balanced laminate. In a balanced laminate, for every unidirectional ply in the $+\Theta$ direction (measured counterclockwise from the x coordinate) there is an identical ply in the $-\Theta$ direction. The elements of the stiffness matrix $[\overline{Q}]$ are given in Table 3.1 (page 70). From this table we deduce that the elements of the stiffness matrices of plies in the $+\Theta$ and $-\Theta$ directions are related as follows:

$$\begin{aligned} \overline{Q}_{11(+\Theta)} &= \overline{Q}_{11(-\Theta)} & \overline{Q}_{22(+\Theta)} &= \overline{Q}_{22(-\Theta)} \\ \overline{Q}_{12(+\Theta)} &= \overline{Q}_{12(-\Theta)} & \overline{Q}_{66(+\Theta)} &= \overline{Q}_{66(-\Theta)} \\ \overline{Q}_{16(+\Theta)} &= -\overline{Q}_{16(-\Theta)} & \overline{Q}_{26(+\Theta)} &= -\overline{Q}_{26(-\Theta)}. \end{aligned} \tag{3.33}$$

By substituting these elements into the expression of the stiffness matrix in Eq. (3.20), we find that

$$A_{16} = A_{26} = 0. \tag{3.34}$$

The structure of the stiffness matrix given in Table 3.4 shows that there is no extension–shear coupling in a balanced laminate (Table 3.5). (Note that A_{16} and A_{26} are zero only in the x–y coordinate system.)

Elements A_{16} and A_{26} are zero for symmetrical and unsymmetrical laminates. Correspondingly, for symmetrical balanced laminates the a_{16} and a_{26} elements of the compliance matrix are zero ($a_{16} = 0$ and $a_{26} = 0$). However, for unsymmetrical balanced laminates none of the elements of the compliance matrix is zero (see Eq. 3.22).

Orthotropic laminate. In orthotropic laminates we are interested in two mutually perpendicular directions, called orthotropy directions, in the plane of the laminate. Normal forces and bending moments applied in these directions do not cause shear or twist of the laminate. Hence, there are no extension–shear, bending–twist, and extension–twist couplings.

A laminate is orthotropic when every ply is orthotropic and the orthotropy directions coincide with the x and y directions. Fiber-reinforced plies are orthotropic under the following conditions:

- when the ply is made of unidirectional fibers and all the fibers are aligned with one of the laminate's orthotropy directions (Fig. 3.13);

Table 3.4. The $[A]$, $[B]$, $[D]$ matrices for laminates. When the laminate is symmetrical, the $[B]$ matrix is zero. Cross-ply laminates are orthotropic.

$[A]$	$[B]$	$[D]$
Symmetrical		
$\begin{bmatrix} A_{11} & A_{12} & A_{16} \\ A_{12} & A_{22} & A_{26} \\ A_{16} & A_{26} & A_{66} \end{bmatrix}$	$\begin{bmatrix} 0 & 0 & 0 \\ 0 & 0 & 0 \\ 0 & 0 & 0 \end{bmatrix}$	$\begin{bmatrix} D_{11} & D_{12} & D_{16} \\ D_{12} & D_{22} & D_{26} \\ D_{16} & D_{26} & D_{66} \end{bmatrix}$
Balanced		
$\begin{bmatrix} A_{11} & A_{12} & 0 \\ A_{12} & A_{22} & 0 \\ 0 & 0 & A_{66} \end{bmatrix}$	$\begin{bmatrix} B_{11} & B_{12} & B_{16} \\ B_{12} & B_{22} & B_{26} \\ B_{16} & B_{26} & B_{66} \end{bmatrix}$	$\begin{bmatrix} D_{11} & D_{12} & D_{16} \\ D_{12} & D_{22} & D_{26} \\ D_{16} & D_{26} & D_{66} \end{bmatrix}$
Orthotropic		
$\begin{bmatrix} A_{11} & A_{12} & 0 \\ A_{12} & A_{22} & 0 \\ 0 & 0 & A_{66} \end{bmatrix}$	$\begin{bmatrix} B_{11} & B_{12} & 0 \\ B_{12} & B_{22} & 0 \\ 0 & 0 & B_{66} \end{bmatrix}$	$\begin{bmatrix} D_{11} & D_{12} & 0 \\ D_{12} & D_{22} & 0 \\ 0 & 0 & D_{66} \end{bmatrix}$
Isotropic		
$\begin{bmatrix} A_{11} & A_{12} & 0 \\ A_{12} & A_{11} & 0 \\ 0 & 0 & \frac{A_{11}-A_{12}}{2} \end{bmatrix}$	$\begin{bmatrix} B_{11} & B_{12} & 0 \\ B_{12} & B_{11} & 0 \\ 0 & 0 & \frac{B_{11}-B_{12}}{2} \end{bmatrix}$	$\begin{bmatrix} D_{11} & D_{12} & 0 \\ D_{12} & D_{11} & 0 \\ 0 & 0 & \frac{D_{11}-D_{12}}{2} \end{bmatrix}$
Quasi-isotropic		
$\begin{bmatrix} A_{11} & A_{12} & 0 \\ A_{12} & A_{11} & 0 \\ 0 & 0 & \frac{A_{11}-A_{12}}{2} \end{bmatrix}$	$\begin{bmatrix} B_{11} & B_{12} & B_{16} \\ B_{12} & B_{22} & B_{26} \\ B_{16} & B_{26} & B_{66} \end{bmatrix}$	$\begin{bmatrix} D_{11} & D_{12} & D_{16} \\ D_{12} & D_{22} & D_{26} \\ D_{16} & D_{26} & D_{66} \end{bmatrix}$

Table 3.5. Couplings in selected laminates ("no" means that the indicated element of the stiffness matrix is zero and the corresponding coupling does not occur)

	Extension–shear A_{16}	Bending–twist D_{16}	Extension–twist B_{16}	In-plane–out-of-plane B_{ij}
Symmetrical			no	no
Balanced	no			
Orthotropic	no	no	no	
Quasi-isotropic	no			
Isotropic layered	no	no	no	
Isotropic single layer	no	no	no	no

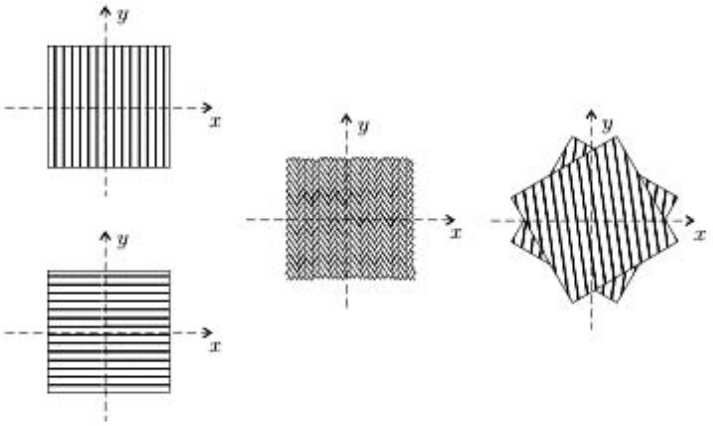

Figure 3.13: Ply arrangements in orthotropic laminates. The ply's symmetry axes (dashed lines) must coincide with the laminate's orthotropy x, y axes.

- when the ply is a woven fabric and the ply's symmetry axes are aligned with the laminates orthotropy directions;
- when two adjacent unidirectional plies (oriented in different directions) are treated as a single layer and the symmetry axes of this layer are aligned with the laminate's orthotropy directions.

For the orthotropic plies described above, the $\overline{Q}_{16}$ and $\overline{Q}_{26}$ elements of the ply stiffness matrix are zero (Eq. 2.138):

$$\overline{Q}_{16} = \overline{Q}_{26} = 0. \tag{3.35}$$

With these values, Eq. (3.20) gives that the 16 and 26 elements of the $[A]$, $[B]$, and $[D]$ matrices are zero:

$$A_{16} = A_{26} = 0 \qquad B_{16} = B_{26} = 0 \qquad D_{16} = D_{26} = 0. \tag{3.36}$$

Accordingly, there is no extension–shear, bending–twist, or extension–twist coupling in an orthotropic laminate (Table 3.5). On the other hand, when the laminate is not orthotropic, these couplings are present and result in unexpected deformations.

We observe that the 16 and 26 elements of the $[A]$, $[B]$, and $[D]$ matrices are zero only in the x–y coordinate system, where x and y are the orthotropy directions (Table 3.4, page 76).

For unsymmetrical orthotropic laminates the compliance matrix becomes (see Eq. 3.23)

$$\begin{bmatrix} \alpha_{11} & \alpha_{12} & 0 & \beta_{11} & \beta_{12} & 0 \\ \alpha_{12} & \alpha_{22} & 0 & \beta_{21} & \beta_{22} & 0 \\ 0 & 0 & \alpha_{66} & 0 & 0 & \beta_{66} \\ \beta_{11} & \beta_{21} & 0 & \delta_{11} & \delta_{12} & 0 \\ \beta_{12} & \beta_{22} & 0 & \delta_{12} & \delta_{22} & 0 \\ 0 & 0 & \beta_{66} & 0 & 0 & \delta_{66} \end{bmatrix}. \tag{3.37}$$

When the layup is orthotropic and symmetrical, the elements of the compliance matrices are (see Eqs. 3.29 and 3.30)

$$\begin{bmatrix} a_{11} & a_{12} & 0 \\ a_{12} & a_{22} & 0 \\ 0 & 0 & a_{66} \end{bmatrix} \quad \begin{bmatrix} d_{11} & d_{12} & 0 \\ d_{12} & d_{22} & 0 \\ 0 & 0 & d_{66} \end{bmatrix}. \tag{3.38}$$

Isotropic laminate. We consider a laminate in which each ply is isotropic. (The material may be different in each ply.) Since in isotropic materials there is no preferred direction, the $[\overline{Q}]$ matrix in the x–y coordinate system is the same as the $[Q]$ matrix in the x_1–x_2 coordinate system:

$$[\overline{Q}] = [Q]. \tag{3.39}$$

Consequently, the $[A]$, $[B]$, $[D]$ matrices are independent of the coordinate directions. By introducing the elements of the $[Q]$ matrix given by Eq. (2.145) into Eq. (3.20), we obtain the following elements of the $[A]$, $[B]$, and $[D]$ matrices:

$$\begin{aligned} &A_{11} && A_{22} = A_{11} && A_{12} \\ &A_{66} = \frac{A_{11} - A_{12}}{2} && A_{16} = 0 && A_{26} = 0 \\ &B_{11} && B_{22} = B_{11} && B_{12} \\ &B_{66} = \frac{B_{11} - B_{12}}{2} && B_{16} = 0 && B_{26} = 0 \\ &D_{11} && D_{22} = D_{11} && D_{12} \\ &D_{66} = \frac{D_{11} - D_{12}}{2} && D_{16} = 0 && D_{26} = 0. \end{aligned} \tag{3.40}$$

In isotropic laminates there are no extension–shear, bending–twist, or extension–twist couplings (Table 3.5, page 76), but there may be in-plane–out-of-plane coupling.

When the laminate consists of a single isotropic layer, the nonzero elements of the $[A]$, $[B]$, and $[D]$ matrices are (Eqs. 2.145 and 3.20)

$$\begin{aligned} &A_{11} = A_{22} = A^{\text{iso}} && A_{12} = \nu A^{\text{iso}} && A_{66} = \tfrac{1-\nu}{2} A^{\text{iso}} \\ &D_{11} = D_{22} = D^{\text{iso}} && D_{12} = \nu D^{\text{iso}} && D_{66} = \tfrac{1-\nu}{2} D^{\text{iso}}, \end{aligned} \tag{3.41}$$

where

$$A^{\text{iso}} = \frac{Eh}{1-\nu^2}, \qquad D^{\text{iso}} = \frac{Eh^3}{12(1-\nu^2)}, \tag{3.42}$$

E is the Young modulus, ν is the Poisson ratio, and h is the thickness. The preceding stiffnesses are identical to the stiffnesses of isotropic plates.[1]

[1] S. P. Timoshenko and S. Woinowsky-Krieger, *Theory of Plates and Shells*. 2nd edition. McGraw-Hill, New York, 1959, pp. 5 and 81.

Inversion of matrices $[A]$ and $[D]$ yields the compliance matrices $[a]$ and $[d]$ (see Eqs. 3.29 and 3.30). The nonzero elements are

$$\begin{aligned} a_{11} &= \frac{1}{Eh} \qquad a_{12} = -\nu a_{11} \qquad a_{66} = \frac{2(1+\nu)}{Eh} = \frac{1}{Gh} \\ d_{11} &= \frac{12}{Eh^3} \qquad d_{12} = -\nu d_{11} \qquad d_{66} = \frac{24(1+\nu)}{Eh^3} = \frac{12}{Gh^3}. \end{aligned} \tag{3.43}$$

Quasi-isotropic laminate. A laminate is quasi-isotropic when

- there are at least three fiber directions;
- the orientation (fiber angle Θ) of each ply is $\Theta = i\pi/I$, where i is an integer ($i = 1, 2, \ldots, I$), and I is the total number of fiber orientations ($I \geq 3$);
- the number of plies in each fiber direction is the same; and
- each ply is made of the same material and has the same thickness.

For example, in $\pi/4$ laminates (page 65) there are fibers in the $0°$, $45°$, $-45°$, and $90°$ directions, and $I = 4$.

For each ply, the elements of the $[\overline{Q}]$ matrix are obtained by substituting $\Theta = i180°/I$ into the expressions in Table 3.1 (page 70). Then, by substituting these elements into the expression for the $[A]$ matrix (see Eq. 3.20), we obtain the following nonzero elements of the $[A]$ matrix:

$$\begin{aligned} A_{11} &= \frac{3}{8}h(Q_{11} + Q_{22}) + \frac{1}{4}hQ_{12} + \frac{1}{2}hQ_{66} \\ A_{22} &= A_{11} \\ A_{12} &= \frac{1}{8}h(Q_{11} + Q_{22}) + \frac{3}{4}hQ_{12} - \frac{1}{2}hQ_{66} \\ A_{66} &= \frac{A_{11} - A_{12}}{2}. \end{aligned} \tag{3.44}$$

The stiffness matrix $[A]$ may be written as

$$[A] = \begin{bmatrix} A_{11} & A_{12} & 0 \\ A_{12} & A_{22} & 0 \\ 0 & 0 & A_{66} \end{bmatrix} = hR \begin{bmatrix} 1 & \nu^{iso} & \\ \nu^{iso} & 1 & \\ & & \frac{1-\nu^{iso}}{2} \end{bmatrix}, \tag{3.45}$$

where R and ν^{iso} are parameters defined as

$$\begin{aligned} R &= \frac{3}{8}(Q_{11} + Q_{22}) + \frac{1}{4}Q_{12} + \frac{1}{2}Q_{66} \\ \nu^{iso} &= \frac{1}{8R}(Q_{11} + Q_{22} + 6Q_{12} - 4Q_{66}), \end{aligned} \tag{3.46}$$

and h is the thickness of the laminate. It is stated here without proof that Eqs. (3.45) and (3.46) are valid[2] for all values of I as long as $I \geq 3$.

[2] S. W. Tsai and H. T. Hahn, *Introduction to Composite Materials*. Technomic, Lancaster, Pennsylvania, 1980, p. 145.

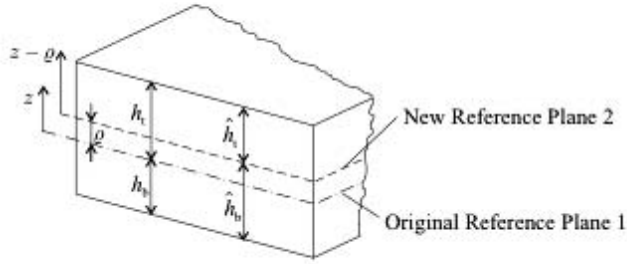

Figure 3.14: Definition of the new reference plane.

We observe that for both quasi-isotropic and isotropic laminates, A_{22} and A_{66} are $A_{22} = A_{11}$ and $A_{66} = (A_{11} - A_{12})/2$. Thus, under in-plane forces, quasi-isotropic laminates behave in the same way as isotropic laminates, that is, there is no extension–shear coupling (Table 3.5) and the $[A]$ matrix is independent of the coordinate directions. The $[B]$ and $[D]$ matrices do not simplify for quasi-isotropic laminates.

Elements A_{16} and A_{26} are zero and $A_{66} = (A_{11} - A_{12})/2$ for symmetrical and unsymmetrical quasi-isotropic laminates. Correspondingly, for symmetrical quasi-isotropic laminates, the a_{16} and a_{26} elements of the compliance matrix are zero ($a_{16} = 0$ and $a_{26} = 0$) and $a_{66} = 2(a_{11} - a_{12})$. For unsymmetrical quasi-isotropic laminates, none of the elements of the compliance matrix is zero (see Eq. 3.22).

Reference plane. The stiffness matrices $[A]$, $[B]$, and $[D]$ refer to Reference Plane 1. The stiffness matrices for Reference Plane 2 (located at a distance ϱ from Reference Plane 1, Fig. 3.14) are obtained from Eq. (3.20) by replacing z_k by $(z_k - \varrho)$ as follows:

$$
\begin{aligned}
A^{\varrho}_{ij} &= \sum_{k=1}^{K} (\overline{Q}_{ij})_k \left[(z_k - \varrho) - (z_{k-1} - \varrho)\right] \\
&= \sum_{k=1}^{K} (\overline{Q}_{ij})_k (z_k - z_{k-1}) = A_{ij} \\
B^{\varrho}_{ij} &= \frac{1}{2} \sum_{k=1}^{K} (\overline{Q}_{ij})_k [(z_k - \varrho)^2 - (z_{k-1} - \varrho)^2] \\
&= \sum_{k=1}^{K} (\overline{Q}_{ij})_k \left[\frac{z_k^2 - z_{k-1}^2}{2} - \varrho\,(z_k - z_{k-1})\right] = B_{ij} - \varrho A_{ij} \\
D^{\varrho}_{ij} &= \frac{1}{3} \sum_{k=1}^{K} (\overline{Q}_{ij})_k [(z_k - \varrho)^3 - (z_{k-1} - \varrho)^3] \\
&= \sum_{k=1}^{K} (\overline{Q}_{ij})_k \left[\frac{z_k^3 - z_{k-1}^3}{3} - 2\varrho \frac{z_k^2 - z_{k-1}^2}{2} + \varrho^2 (z_k - z_{k-1})\right] \\
&= D_{ij} - 2\varrho B_{ij} + \varrho^2 A_{ij}.
\end{aligned}
\tag{3.47}
$$

These equations correspond to the parallel axis theorem.

The superscript ϱ refers to Reference Plane 2. When the laminate is symmetrical and the reference plane coincides with the midplane, the matrix $[B]$ is zero. When the laminate is unsymmetrical, the matrix $[B]$ is not zero.

In general, there is no ϱ value that results in a nonzero $[B]$ matrix for an anisotropic composite laminate. In other words, for an unsymmetrical laminate there is no reference plane that is also a neutral plane.

The compliance matrices $[\alpha]$, $[\beta]$, and $[\delta]$ refer to Reference Plane 1. The elements of these matrices for Reference Plane 2 are obtained by introducing Eq. (3.47) into Eq. (3.23). After algebraic manipulations, we obtain

$$\begin{aligned} \alpha_{ij}^{\varrho} &= \alpha_{ij} + \varrho\,(\beta_{ij} + \beta_{ji}) + \varrho^2 \delta_{ij} \\ \beta_{ij}^{\varrho} &= \beta_{ij} + \varrho \delta_{ij} \\ \delta_{ij}^{\varrho} &= \delta_{ij}. \end{aligned} \tag{3.48}$$

The third of these equations shows that the bending compliance matrix $[\delta]$ is independent of the choice of the reference surface.

Curved laminates. The stiffness and compliance matrices derived in this chapter for flat laminates may be applied to thin curved laminates when the radius of curvature is large compared with the thickness.

Numerical values of the stiffness and compliance matrices of selected laminates. Below, we present numerical values of the stiffness and compliance matrices of laminates with different lay-ups. The engineering constants used to calculate the laminate stiffnesses and compliances are listed in Table 3.6. While the properties in this table are not intended to depict a particular material, they are characteristic of many graphite-epoxy composites. Therefore, the properties in Table 3.6 are used in the examples in the book.

3.1 Example. *Calculate the stiffness* $[A]$, $[B]$, $[D]$ *and the compliance* $[\alpha]$, $[\beta]$, $[\delta]$ *matrices of a* $[0_{10}/45_{10}]$ *laminate made of graphite epoxy unidirectional plies. The ply properties are given in Table 3.6.*

Solution. The stiffness matrix of a unidirectional ply with the fibers in the 0-degree direction is $[\overline{Q}]^0 = [Q]$. The stiffness matrix $[Q]$ is given by Eq. (2.147),

Table 3.6. Properties of the material used in the examples

		[0]	±45°
Longitudinal Young's modulus (GPa)	E_1	148	16.39
Transverse Young's modulus (GPa)	E_2	9.65	16.39
Longitudinal shear modulus (GPa)	G_{12}	4.55	38.19
Longitudinal Poission's ratio	ν_{12}	0.3	0.801
Thickness (mm)	h_0	0.1	0.2

and thus $[\overline{Q}]^0$ is

$$[\overline{Q}]^0 = [Q] = \begin{bmatrix} 148.87 & 2.91 & 0 \\ 2.91 & 9.71 & 0 \\ 0 & 0 & 4.55 \end{bmatrix} 10^9 \frac{\text{N}}{\text{m}^2}. \tag{3.49}$$

The stiffness matrix $[\overline{Q}]$ of a ply not in the 0-degree direction is (Eq. 3.14)

$$\begin{bmatrix} \overline{Q}_{11} & \overline{Q}_{12} & \overline{Q}_{16} \\ \overline{Q}_{12} & \overline{Q}_{22} & \overline{Q}_{26} \\ \overline{Q}_{16} & \overline{Q}_{26} & \overline{Q}_{66} \end{bmatrix} = [T_\sigma]^{-1}[Q][T_\epsilon], \tag{3.50}$$

where $[T_\sigma]$ and $[T_\epsilon]$ are given by Eq. (3.15). For the 45-degree ply $c = \cos 45^\circ = 0.707$ and $s = \sin 45^\circ = 0.707$, and we have

$$[T_\sigma] = \begin{bmatrix} 0.5 & 0.5 & 1.0 \\ 0.5 & 0.5 & -1.0 \\ -0.5 & 0.5 & 0 \end{bmatrix} \quad [T_\epsilon] = \begin{bmatrix} 0.5 & 0.5 & 0.5 \\ 0.5 & 0.5 & -0.5 \\ -1.0 & 1.0 & 0 \end{bmatrix}. \tag{3.51}$$

By substituting Eqs. (3.49) and (3.51) into Eq. (3.50), we obtain the stiffness matrix of the 45-degree ply as follows:

$$[\overline{Q}]^{45} = \begin{bmatrix} 45.65 & 36.55 & 34.79 \\ 36.55 & 45.65 & 34.79 \\ 34.79 & 34.79 & 38.19 \end{bmatrix} 10^9 \frac{\text{N}}{\text{m}^2}. \tag{3.52}$$

The layup is shown in Fig 3.15. In calculating the $[A]$, $[B]$, $[D]$ matrices we treat the ten 0-degree plies as one layer and the ten 45-degree plies as another layer. The $[A]$, $[B]$, $[D]$ matrices are (Eq. 3.20)

$$\begin{aligned} [A] &= [\overline{Q}]^0 (z_1 - z_0) + [\overline{Q}]^{45} (z_2 - z_1) \\ [B] &= [\overline{Q}]^0 \frac{z_1^2 - z_0^2}{2} + [\overline{Q}]^{45} \frac{z_2^2 - z_1^2}{2} \\ [D] &= [\overline{Q}]^0 \frac{z_1^3 - z_0^3}{3} + [\overline{Q}]^{45} \frac{z_2^3 - z_1^3}{3}. \end{aligned} \tag{3.53}$$

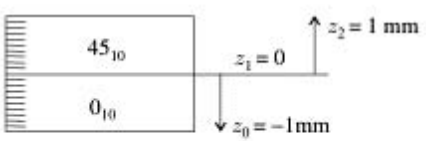

Figure 3.15: The $[0_{10}/45_{10}]$ laminate in Example 3.1.

The $[\overline{Q}]$ matrices are given by Eqs. (3.49) and (3.52). The distances (in meters) are $z_0 = -0.001$, $z_1 = 0$, $z_2 = 0.001$ (Fig. 3.15). With these values Eq. (3.53) yields

$$[A] = [\overline{Q}]^0[0-(-0.001)] + [\overline{Q}]^{45}(0.001-0) = \begin{bmatrix} 194.52 & 39.46 & 34.79 \\ 39.46 & 55.36 & 34.79 \\ 34.79 & 34.79 & 42.74 \end{bmatrix} 10^6 \frac{\text{N}}{\text{m}}$$

$$[B] = [\overline{Q}]^0 \frac{0^2-(-0.001)^2}{2} + [\overline{Q}]^{45} \frac{0.001^2-0^2}{2} = \begin{bmatrix} -51.61 & 16.82 & 17.40 \\ 16.82 & 17.97 & 17.40 \\ 17.40 & 17.40 & 16.82 \end{bmatrix} 10^3 \text{N}$$

$$[D] = [\overline{Q}]^0 \frac{0^3-(-0.001)^3}{3} + [\overline{Q}]^{45} \frac{0.001^3-0^3}{3} = \begin{bmatrix} 64.84 & 13.15 & 11.60 \\ 13.15 & 18.45 & 11.60 \\ 11.60 & 11.60 & 14.25 \end{bmatrix} \text{N}\cdot\text{m}. \tag{3.54}$$

The compliance matrices are (Eq. 3.23)

$$\begin{bmatrix} \alpha & \beta \\ \beta^T & \delta \end{bmatrix} = \begin{bmatrix} A & B \\ B & D \end{bmatrix}^{-1}. \tag{3.55}$$

Hence, we have

$$[\alpha] = \begin{bmatrix} 13.44 & -4.85 & -7.14 \\ -4.85 & 41.81 & -21.23 \\ -7.14 & -21.23 & 64.95 \end{bmatrix} 10^{-9} \frac{\text{m}}{\text{N}}$$

$$[\beta] = \begin{bmatrix} 17.07 & -6.01 & -11.06 \\ -6.01 & -5.04 & -11.06 \\ -11.06 & -11.06 & -24.05 \end{bmatrix} 10^{-6} \frac{1}{\text{N}} \tag{3.56}$$

$$[\delta] = \begin{bmatrix} 40.32 & -14.56 & -21.41 \\ -14.56 & 125.42 & -63.68 \\ -21.41 & -63.68 & 194.86 \end{bmatrix} 10^{-3} \frac{1}{\text{N}\cdot\text{m}}.$$

The compliance and stiffness matrices of $[45_2/-45_2/0_{12}/-45_2/45_2]$, $[-30_4/15_4/0_2]_s$, $[0_2/45_2/90_2/-45_2]_s$, $[45_6/0_4]_s$, and $[0_2/45_2/0_2/45_2]$ laminates are calculated similarly. The results are in Tables 3.7, 3.8, and 3.9 (pages 84–86). Note that, for symmetrical laminates, the following simplifications apply: $[B] = [\beta] = 0$ and $[\alpha] = [a]$, $[\delta] = [d]$.

3.2 Example. *Calculate the stiffness* $[A]$, $[B]$, $[D]$ *and the compliance* $[\alpha]$, $[\beta]$, $[\delta]$ *matrices of a* $[0_{20}]$ *laminate made of graphite epoxy unidirectional plies. The ply properties are given in Table 3.6 (page 81).*

Solution. The unidirectional laminate is symmetrical, and the $[B]$ matrix is zero:

$$[B] = 0. \tag{3.57}$$

Table 3.7. The $[A]$ and $[D]$ matrices for symmetrical laminates. The unit of $[A]$ is $10^6 \frac{N}{m}$ and the unit of $[D]$ is N · m. The material properties are given in Table 3.6 (page 81).

$[A]$	$[D]$
$[0_{20}]$ (orthotropic, symmetrical)	
$\begin{bmatrix} 297.75 & 5.82 & 0 \\ 5.82 & 19.41 & 0 \\ 0 & 0 & 9.10 \end{bmatrix}$	$\begin{bmatrix} 99.25 & 1.94 & 0 \\ 1.94 & 6.47 & 0 \\ 0 & 0 & 3.03 \end{bmatrix}$
$[\pm 45_2^t/0_{12}/\pm 45_2^t]$ (orthotropic, symmetrical)	
$\begin{bmatrix} 215.17 & 32.74 & 0 \\ 32.74 & 48.17 & 0 \\ 0 & 0 & 36.01 \end{bmatrix}$	$\begin{bmatrix} 45.30 & 19.52 & 0 \\ 19.52 & 25.26 & 0 \\ 0 & 0 & 20.62 \end{bmatrix}$
$[45_2/-45_2/0_{12}/-45_2/45_2]$ (balanced, symmetrical)	
$\begin{bmatrix} 215.17 & 32.74 & 0 \\ 32.74 & 48.17 & 0 \\ 0 & 0 & 36.01 \end{bmatrix}$	$\begin{bmatrix} 45.30 & 19.52 & 4.45 \\ 19.52 & 25.26 & 4.45 \\ 4.45 & 4.45 & 20.62 \end{bmatrix}$
$[-30_4/15_4/0_2]_s$ (symmetrical)	
$\begin{bmatrix} 235.54 & 32.74 & -10.19 \\ 32.74 & 27.79 & -10.19 \\ -10.19 & -10.19 & 36.01 \end{bmatrix}$	$\begin{bmatrix} 65.42 & 16.29 & -18.93 \\ 16.29 & 11.60 & -7.74 \\ -18.93 & -7.74 & 17.39 \end{bmatrix}$
$[0_2/45_2/90_2/-45_2]_s$ (quasi-isotropic, symmetrical)	
$\begin{bmatrix} 99.95 & 31.57 & 0 \\ 31.57 & 99.95 & 0 \\ 0 & 0 & 34.19 \end{bmatrix}$	$\begin{bmatrix} 34.61 & 4.58 & 3.34 \\ 4.58 & 12.34 & 3.34 \\ 3.34 & 3.34 & 5.14 \end{bmatrix}$
$[45_6/0_4]_s$ (symmetrical)	
$\begin{bmatrix} 173.88 & 46.19 & 41.75 \\ 46.19 & 62.55 & 41.75 \\ 41.75 & 41.75 & 49.47 \end{bmatrix}$	$\begin{bmatrix} 34.84 & 22.93 & 21.71 \\ 22.93 & 28.90 & 21.71 \\ 21.71 & 21.71 & 24.02 \end{bmatrix}$

By treating the 20 plies as a single layer, the $[A]$ and $[D]$ matrices are (Eq. 3.20)

$$[A] = h[\overline{Q}] \qquad [D] = \frac{h^3}{12}[\overline{Q}], \tag{3.58}$$

where $h = 0.002$ m is the thickness of the laminate.

By substituting Eqs. (3.20) and (2.139) into Eq. (3.58) and by using the engineering constants in Table 3.6 (page 81) ($E_1 = 148 \times 10^9\,\mathrm{N/m^2}$, $E_2 = 9.65 \times$

Table 3.8. The $[a]$ and $[d]$ matrices for symmetrical laminates. The unit of $[a]$ is $10^{-9}\frac{m}{N}$ and the unit of $[d]$ is $10^{-3}\frac{1}{N\cdot m}$. The material properties are given in Table 3.6 (page 81).

$[a]$	$[d]$
$[0_{20}]$ (orthotropic, symmetrical)	
$\begin{bmatrix} 3.38 & -1.01 & 0 \\ -1.01 & 51.81 & 0 \\ 0 & 0 & 109.89 \end{bmatrix}$	$\begin{bmatrix} 10.14 & -3.04 & 0 \\ -3.04 & 155.44 & 0 \\ 0 & 0 & 329.67 \end{bmatrix}$
$[\pm 45_2^t/0_{12}/\pm 45_2^t]$ (orthotropic, symmetrical)	
$\begin{bmatrix} 5.18 & -3.52 & 0 \\ -3.52 & 23.15 & 0 \\ 0 & 0 & 27.77 \end{bmatrix}$	$\begin{bmatrix} 33.10 & -25.59 & 0 \\ -25.59 & 59.37 & 0 \\ 0 & 0 & 48.51 \end{bmatrix}$
$[45_2/-45_2/0_{12}/-45_2/45_2]$ (balanced, symmetrical)	
$\begin{bmatrix} 5.18 & -3.52 & 0 \\ -3.52 & 23.15 & 0 \\ 0 & 0 & 27.77 \end{bmatrix}$	$\begin{bmatrix} 33.16 & -25.33 & -1.69 \\ -25.33 & 60.51 & -7.60 \\ -1.69 & -7.60 & 50.51 \end{bmatrix}$
$[-30_4/15_4/0_2]_s$ (symmetrical)	
$\begin{bmatrix} 5.08 & -6.09 & -0.29 \\ -6.09 & 47.44 & 11.70 \\ -0.29 & 11.70 & 31.00 \end{bmatrix}$	$\begin{bmatrix} 26.87 & -25.93 & 17.70 \\ -25.93 & 147.76 & 37.57 \\ 17.70 & 37.57 & 93.52 \end{bmatrix}$
$[0_2/45_2/90_2/-45_2]_s$ (quasi-isotropic, symmetrical)	
$\begin{bmatrix} 11.11 & -3.51 & 0 \\ -3.51 & 11.11 & 0 \\ 0 & 0 & 29.25 \end{bmatrix}$	$\begin{bmatrix} 31.38 & -7.44 & -15.55 \\ -7.44 & 100.06 & -60.17 \\ -15.55 & -60.17 & 243.70 \end{bmatrix}$
$[45_6/0_4]_s$ (symmetrical)	
$\begin{bmatrix} 7.45 & -2.99 & -3.77 \\ -2.99 & 37.81 & -29.39 \\ -3.77 & -29.39 & 48.20 \end{bmatrix}$	$\begin{bmatrix} 71.24 & -25.43 & -41.40 \\ -25.43 & 116.82 & -82.58 \\ -41.40 & -82.58 & 153.66 \end{bmatrix}$

$10^9\ \mathrm{N/m^2}$, $G_{12} = 4.55 \times 10^9\ \mathrm{N/m^2}$, $\nu_{12} = 0.3$), we obtain

$$A_{11} = \frac{E_1 h}{1-\nu_{12}^2\frac{E_2}{E_1}} = 297.75 \times 10^6\,\frac{\mathrm{N}}{\mathrm{m}} \qquad A_{22} = \frac{E_2 h}{1-\nu_{12}^2\frac{E_2}{E_1}} = 19.41 \times 10^6\,\frac{\mathrm{N}}{\mathrm{m}} \tag{3.59}$$

$$A_{12} = \nu_{12}A_{22} = 5.82 \times 10^6\,\frac{\mathrm{N}}{\mathrm{m}} \qquad A_{66} = G_{12}h = 9.10 \times 10^6\,\frac{\mathrm{N}}{\mathrm{m}}$$

$$D_{11} = \frac{E_1 h^3}{12\left(1-\nu_{12}^2\frac{E_2}{E_1}\right)} = 99.25\ \mathrm{N\cdot m} \qquad D_{22} = \frac{E_2 h^3}{12\left(1-\nu_{12}^2\frac{E_2}{E_1}\right)} = 6.47\ \mathrm{N\cdot m} \tag{3.60}$$

$$D_{12} = \nu_{12}D_{22} = 1.94\ \mathrm{N\cdot m} \qquad D_{66} = \frac{G_{12}h^3}{12} = 3.03\ \mathrm{N\cdot m}.$$

Table 3.9. The $[A]$, $[B]$, $[D]$ and the $[\alpha]$, $[\beta]$, and $[\delta]$ matrices for unsymmetrical laminates. $[A]$ is in $10^6 \frac{N}{m}$, $[B]$ is in 10^3N, $[D]$ is in N · m, $[\alpha]$ is in $10^{-9} \frac{m}{N}$, $[\beta]$ is in $10^{-6} \frac{1}{N}$, and $[\delta]$ is in $10^{-3} \frac{1}{N \cdot m}$. The material properties are given in Table 3.6 (page 81).

$[A]$	$[B]$	$[D]$
$[0_{10}/45_{10}]$		
$\begin{bmatrix} 194.52 & 39.46 & 34.79 \\ 39.46 & 55.36 & 34.79 \\ 34.79 & 34.79 & 42.74 \end{bmatrix}$	$\begin{bmatrix} -51.61 & 16.82 & 17.40 \\ 16.82 & 17.97 & 17.40 \\ 17.40 & 17.40 & 16.82 \end{bmatrix}$	$\begin{bmatrix} 64.84 & 13.15 & 11.60 \\ 13.15 & 18.45 & 11.60 \\ 11.60 & 11.60 & 14.25 \end{bmatrix}$
$[0_2/45_2/0_2/45_2]$		
$\begin{bmatrix} 77.81 & 15.79 & 13.92 \\ 15.79 & 22.14 & 13.92 \\ 13.92 & 13.92 & 17.10 \end{bmatrix}$	$\begin{bmatrix} -4.129 & 1.346 & 1.392 \\ 1.346 & 1.438 & 1.392 \\ 1.392 & 1.392 & 1.346 \end{bmatrix}$	$\begin{bmatrix} 4.150 & 0.842 & 0.742 \\ 0.842 & 1.181 & 0.742 \\ 0.742 & 0.742 & 0.912 \end{bmatrix}$
$[\pm 45_5^{\mathrm{f}}/0_{10}]$		
$\begin{bmatrix} 194.52 & 39.46 & 0 \\ 39.46 & 55.36 & 0 \\ 0 & 0 & 42.74 \end{bmatrix}$	$\begin{bmatrix} 51.61 & -16.82 & 0 \\ -16.82 & -17.97 & 0 \\ 0 & 0 & -16.82 \end{bmatrix}$	$\begin{bmatrix} 64.84 & 13.15 & 0 \\ 13.15 & 18.45 & 0 \\ 0 & 0 & 14.25 \end{bmatrix}$
$[\alpha]$	$[\beta]$	$[\delta]$
$[0_{10}/45_{10}]$		
$\begin{bmatrix} 13.44 & -4.85 & -7.14 \\ -4.85 & 41.81 & -21.23 \\ -7.14 & -21.23 & 64.95 \end{bmatrix}$	$\begin{bmatrix} 17.07 & -6.01 & -11.06 \\ -6.01 & -5.04 & -11.06 \\ -11.06 & -11.06 & -24.05 \end{bmatrix}$	$\begin{bmatrix} 40.32 & -14.56 & -21.41 \\ -14.56 & 125.42 & -63.68 \\ -21.41 & -63.68 & 194.86 \end{bmatrix}$
$[0_2/45_2/0_2/45_2]$		
$\begin{bmatrix} 17.88 & -7.14 & -8.79 \\ -7.14 & 96.35 & -69.68 \\ -8.79 & -69.68 & 128.51 \end{bmatrix}$	$\begin{bmatrix} 28.37 & -9.99 & -18.38 \\ -9.99 & -8.38 & -18.38 \\ -18.38 & -18.38 & -39.96 \end{bmatrix}$	$\begin{bmatrix} 335 & -134 & -165 \\ -134 & 1\,807 & -1\,306 \\ -165 & -1\,306 & 2\,410 \end{bmatrix}$
$[\pm 45_5^{\mathrm{f}}/0_{10}]$		
$\begin{bmatrix} 11.65 & -8.58 & 0 \\ -8.58 & 32.94 & 0 \\ 0 & 0 & 43.70 \end{bmatrix}$	$\begin{bmatrix} -13.97 & 12.22 & 0 \\ 12.22 & 15.55 & 0 \\ 0 & 0 & 51.60 \end{bmatrix}$	$\begin{bmatrix} 34.94 & -25.74 & 0 \\ -25.74 & 98.83 & 0 \\ 0 & 0 & 131.11 \end{bmatrix}$

The compliance matrices $[a]$ and $[d]$ are obtained by inverting the $[A]$ and $[D]$ stiffness matrices as follows:

$$[a] = [A]^{-1} \qquad [d] = [D]^{-1}. \tag{3.61}$$

Equations (3.59)–(3.61) give

$$a_{11} = \frac{1}{E_1 h} = 3.38 \times 10^{-9} \frac{\text{m}}{\text{N}} \qquad a_{22} = \frac{1}{E_2 h} = 51.81 \times 10^{-9} \frac{\text{m}}{\text{N}}$$
$$a_{12} = -\nu_{12} a_{11} = -1.01 \times 10^{-9} \frac{\text{m}}{\text{N}} \qquad a_{66} = \frac{1}{G_{12} h} = 109.89 \times 10^{-9} \frac{\text{m}}{\text{N}} \tag{3.62}$$

$$d_{11} = \frac{12}{E_1 h^3} = 10.14 \times 10^{-3} \frac{1}{\text{N} \cdot \text{m}} \qquad d_{22} = \frac{12}{E_2 h^3} = 155.44 \times 10^{-3} \frac{1}{\text{N} \cdot \text{m}}$$
$$d_{12} = -\nu_{12} d_{11} = -3.04 \times 10^{-3} \frac{1}{\text{N} \cdot \text{m}} \qquad d_{66} = \frac{12}{G_{12} h^3} = 329.67 \times 10^{-3} \frac{1}{\text{N} \cdot \text{m}}. \tag{3.63}$$

3.3 Example. *Calculate the stiffness and the compliance matrices of (i) a laminated composite consisting of two layers of ±45-degree woven fabric, twelve layers of 0-degree unidirectional plies, and two layers of ±45-degree woven fabric* ($[\pm 45^{\text{f}}_2/0_{12}/\pm 45^{\text{f}}_2]$)*; and (ii) a laminate consisting five layers of ±45-degree woven fabric and ten layers of 0-degree unidirectional plies* ($[\pm 45^{\text{f}}_5/0_{10}]$)*. The material properties are given in Table 3.6 (page 81).*

Solution. First we consider the laminate with ($[\pm 45^{\text{f}}_2/0_{12}/\pm 45^{\text{f}}_2]$) layup (Fig. 3.16). The laminate is symmetrical, and the $[B]$ matrix is zero:

$$[B] = 0. \tag{3.64}$$

The compliance matrix of a unidirectional ply with the fibers in the 0-degree direction is $[\overline{Q}]^0 = [Q]$. The stiffness matrix $[Q]$ is given by Eq. (2.147), and thus $[\overline{Q}]^0$ is

$$[\overline{Q}]^0 = [Q] = \begin{bmatrix} 148.87 & 2.91 & 0 \\ 2.91 & 9.71 & 0 \\ 0 & 0 & 4.55 \end{bmatrix} 10^9 \frac{\text{N}}{\text{m}^2}. \tag{3.65}$$

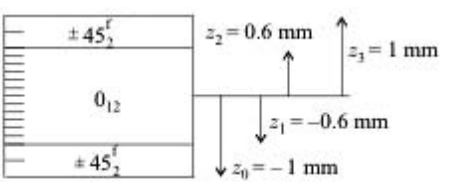

Figure 3.16: The layup of the laminate in Example 3.3. The supercript f denotes fabric.

For a ±45-degree woven fabric the stiffness matrix $[\overline{Q}]$ is (Eq. 2.150)

$$[\overline{Q}]^{\pm 45} = \begin{bmatrix} 45.65 & 36.55 & 0 \\ 36.55 & 45.65 & 0 \\ 0 & 0 & 38.19 \end{bmatrix} 10^9 \frac{\text{N}}{\text{m}^2}. \tag{3.66}$$

In calculating the $[A]$, $[B]$, $[D]$ matrices we treat the twelve 0-degree plies as one layer and each adjacent woven fabric as one layer. The $[A]$ and $[D]$ matrices are

$$\begin{aligned} [A] &= [\overline{Q}]^{\pm 45}(z_1 - z_0) + [\overline{Q}]^{0}(z_2 - z_1) + [\overline{Q}]^{\pm 45}(z_3 - z_2) \\ [D] &= [\overline{Q}]^{\pm 45}\frac{z_1^3 - z_0^3}{3} + [\overline{Q}]^{0}\frac{z_2^3 - z_1^3}{3} + [\overline{Q}]^{\pm 45}\frac{z_3^3 - z_2^3}{3}. \end{aligned} \tag{3.67}$$

The $[\overline{Q}]$ matrices are given by Eqs. (3.65) and (3.66). The distances (in meters) are $z_0 = -0.001$, $z_1 = -0.0006$, $z_2 = 0.0006$, and $z_3 = 0.001$ (Fig. 3.16). With these values Eq. (3.67) yields

$$[A] = \begin{bmatrix} 215.17 & 32.74 & 0 \\ 32.74 & 48.17 & 0 \\ 0 & 0 & 36.01 \end{bmatrix} 10^6 \frac{\text{N}}{\text{m}} \tag{3.68}$$

$$[D] = \begin{bmatrix} 45.30 & 19.52 & 0 \\ 19.52 & 25.26 & 0 \\ 0 & 0 & 20.62 \end{bmatrix} \text{N} \cdot \text{m}. \tag{3.69}$$

The compliance matrices $[a]$ and $[d]$ are (Eqs. 3.29 and 3.30)

$$[a] = [A]^{-1} = \begin{bmatrix} 5.18 & -3.52 & 0 \\ -3.52 & 23.15 & 0 \\ 0 & 0 & 27.77 \end{bmatrix} 10^{-9} \frac{\text{m}}{\text{N}} \tag{3.70}$$

$$[d] = [D]^{-1} = \begin{bmatrix} 33.10 & -25.59 & 0 \\ -25.59 & 59.37 & 0 \\ 0 & 0 & 48.51 \end{bmatrix} 10^{-3} \frac{1}{\text{N} \cdot \text{m}}. \tag{3.71}$$

The compliance and stiffness matrices of the $[\pm 45_5^{\text{f}}/0_{10}]$ laminate are calculated similarly. The results are given in Table 3.9.

CHAPTER FOUR

Thin Plates

In practice we frequently encounter "thin" plates whose thickness is small compared with all other dimensions. Such a plate, undergoing small displacements, may be analyzed with the approximations that the strains vary linearly across the plate, (out-of-plane) shear deformations are negligible, and the out-of-plane normal stress σ_z and shear stresses τ_{xz}, τ_{yz} are small compared with the in-plane normal σ_x, σ_y, and shear τ_{xy} stresses.

Under certain conditions, solutions may be obtained for thin plates either by the solution of the differential equations representing equilibrium or by energy methods.[1] Here we demonstrate the use of the first method via the example of long plates and the second method via examples of rectangular plates either with symmetrical layup or with orthotropic and symmetrical layup. (For orthotropic plates the directions of orthotropy are parallel to the edges of the plate.) We chose these three types of problems because (i) they illustrate the analytical approaches and the use of the relevant equations, (ii) solutions can be obtained without extensive numerical algorithms, and last, but not least, (iii) they are of practical interest. Additionally, and importantly, these problems provide insights that are useful when analyzing plates by numerical methods.

Although the specification of orthotropy may seem to be overly restrictive, in fact it does not unduly limit the applicability of the analyses. The reason for this is that plates are often made according to the 10-percent rule, and such plates behave similarly to orthotropic plates.[2] Therefore, solutions for orthotropic plates provide good approximations of the deflections, maximum bending moments, buckling loads, and natural frequencies of nonorthotropic plates that have symmetrical layup and are constructed according to the 10-percent rule. The 10-percent rule

[1] J. M. Whitney, *Structural Analysis of Laminated Anisotropic Plates*. Technomic, Lancaster, Pennsylvania, 1987.

[2] I. Veres and L. P. Kollár, Approximate Analysis of Mid-plane Symmetric Rectangular Composite Plates. *Journal of Composite Materials*, Vol. 36, 673–684, 2002.

requires that the plate satisfy the following conditions:

- The plate is made of unidirectional plies.
- There are at least three ply orientations.
- The angles between the fibers are at least 15°.
- The number of plies in each fiber direction is at least 10 percent of the total number of plies.

Plates conforming to the 10-percent rule have better load bearing capabilities than unidirectional or angle-ply laminates for the following reasons.

Unidirectional plies are stiffer and stronger in the 0-degree fiber direction than in the 90-degree direction perpendicular to the fibers. Thus, laminates made of unidirectional plies are ill-suited to carry load in the 90-degree direction. Angle-ply laminates with only two fiber directions do not resist well tensile loads applied along the symmetry axis. Plates made by the 10-percent rule minimize these shortcomings.

The specification of symmetrical layup is less restrictive than it may appear because the analyses of symmetrical plates (for which ($[B] = 0$) can readily be extended to unsymmetrical plates ($[B] \neq 0$) with the use of the reduced bending stiffness $[D]^*$, defined as [3,4,5]

$$[D]^* = [D] - [B][A]^{-1}[B]. \tag{4.1}$$

The deflections, maximum bending moments, buckling loads, and natural frequencies of unsymmetrical plates can be approximated by replacing $[D]$ by $[D]^*$ in the expressions derived for symmetrical plates.

4.1 Governing Equations

In this section we summarize the equations used in analyzing thin plates. We employ the x, y, z coordinate system. The origin is at the midplane for plates with symmetrical layup and at a suitably chosen reference plane for plates with unsymmetrical layup.

The strains and curvatures of the reference plane (Fig. 3.10) are (Eqs. 3.1, 3.8)

$$\epsilon_x^o = \frac{\partial u^o}{\partial x} \qquad \epsilon_y^o = \frac{\partial v^o}{\partial y} \qquad \gamma_{xy}^o = \frac{\partial u^o}{\partial y} + \frac{\partial v^o}{\partial x}$$
$$\kappa_x = -\frac{\partial^2 w^o}{\partial x^2} \qquad \kappa_y = -\frac{\partial^2 w^o}{\partial y^2} \qquad \kappa_{xy} = -\frac{2\partial^2 w^o}{\partial x \partial y}, \tag{4.2}$$

[3] J. M. Whitney, *Structural Analysis of Laminated Anisotropic Plates*. Technomic, Lancaster, Pennsylvania, 1987, p. 203.

[4] E. Reissner and Y. Stavsky, Bending and Stretching of Certain Types of Heterogeneous Aelotropic Elastic Plates. *Journal of Applied Mechanics*, Vol. 28, 402–408, 1961.

[5] J. E. Ashton, Approximate Solutions for Unsymmetrically Laminated Plates. *Journal of Composite Materials*, Vol. 3, 189–191, 1969.

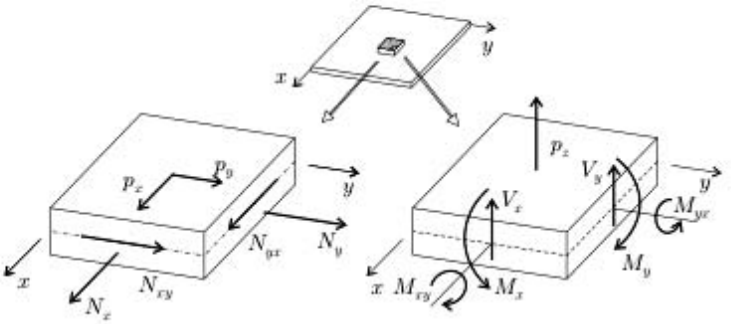

Figure 4.1: Forces and loads acting on an element of the plate.

where u^o and v^o are the displacements of the reference plane in the x and y directions, and w^o is the out-of-plane displacement (deflection) of this plane. The force–strain relationships are (Eq. 3.21)

$$\begin{Bmatrix} N_x \\ N_y \\ N_{xy} \\ M_x \\ M_y \\ M_{xy} \end{Bmatrix} = \begin{bmatrix} A_{11} & A_{12} & A_{16} & B_{11} & B_{12} & B_{16} \\ A_{12} & A_{22} & A_{26} & B_{12} & B_{22} & B_{26} \\ A_{16} & A_{26} & A_{66} & B_{16} & B_{26} & B_{66} \\ B_{11} & B_{12} & B_{16} & D_{11} & D_{12} & D_{16} \\ B_{12} & B_{22} & B_{26} & D_{12} & D_{22} & D_{26} \\ B_{16} & B_{26} & B_{66} & D_{16} & D_{26} & D_{66} \end{bmatrix} \begin{Bmatrix} \epsilon_x^o \\ \epsilon_y^o \\ \gamma_{xy}^o \\ \kappa_x \\ \kappa_y \\ \kappa_{xy} \end{Bmatrix}. \tag{4.3}$$

In the analyses we may employ either the equilibrium equations or the strain energy.

The equilibrium equations are[6]

$$\begin{aligned} \frac{\partial N_x}{\partial x} + \frac{\partial N_{xy}}{\partial y} &= -p_x \\ \frac{\partial N_y}{\partial y} + \frac{\partial N_{xy}}{\partial x} &= -p_y \\ \frac{\partial V_x}{\partial x} + \frac{\partial V_y}{\partial y} &= -p_z \end{aligned} \tag{4.4}$$

$$V_x = \frac{\partial M_x}{\partial x} + \frac{\partial M_{xy}}{\partial y} \qquad V_y = \frac{\partial M_y}{\partial y} + \frac{\partial M_{xy}}{\partial x}, \tag{4.5}$$

where p_x, p_y, and p_z are the components of the distributed surface load (per unit area); N_x, N_y, and N_{xy} are the in-plane forces (per unit length); V_x and V_y are the transverse shear forces (per unit length); M_x, M_y and M_{xy} are, respectively, the bending moments and the twist moment (per unit length) (Fig. 4.1).

[6] S. P. Timoshenko and S. Woinowsky-Krieger, *Theory of Plates and Shells*. 2nd edition. McGraw-Hill, New York, 1959, p. 80.

4.1.1 Boundary Conditions

The conditions along each edge of the plate must be specified. Boundary conditions for an edge parallel with the y-axis are given below.

Along a built-in edge, the deflection w^o, the rotation of the edge $\partial w^o/\partial x$, and the in-plane u^o, v^o displacements are zero:

$$w^o = 0 \qquad \frac{\partial w^o}{\partial x} = 0 \qquad u^o = v^o = 0. \tag{4.6}$$

Along a free edge, where no external loads are applied, the bending moment M_x, the replacement shear force[7] $V_x + \partial M_{xy}/\partial x$, and the in-plane forces N_x, N_{xy} are zero:

$$M_x = 0 \qquad V_x + \frac{\partial M_{xy}}{\partial y} = 0 \qquad N_x = N_{xy} = 0. \tag{4.7}$$

Along a simply supported edge, the deflection w^o, the bending moment M_x, and the in-plane forces N_x, N_{xy} are zero:

$$w^o = 0 \qquad M_x = 0 \qquad N_x = N_{xy} = 0. \tag{4.8}$$

When in-plane motions are prevented by the support, the in-plane forces are not zero ($N_x \neq 0$, $N_{xy} \neq 0$) whereas the in-plane displacements are zero:

$$u^o = 0 \qquad v^o = 0. \tag{4.9}$$

For an edge parallel with the x-axis, the preceding boundary conditions hold with x and y interchanged.

4.1.2 Strain Energy

As we noted previously, solutions to plate problems may be obtained by energy methods that require knowledge of the strain energy. For a linearly elastic material the strain energy is given by Eq. (2.200). Under plane-stress condition the stress components σ_z, τ_{xz}, and τ_{yz} are zero (Eq. 2.121), and the expression for the strain energy simplifies to

$$U = \frac{1}{2}\int_0^{L_x}\int_0^{L_y}\int_{-h_b}^{h_t} (\sigma_x\epsilon_x + \sigma_y\epsilon_y + \tau_{xy}\gamma_{xy})\, dzdydx, \tag{4.10}$$

where h_t and h_b are the distances from the reference plane to the plate's surfaces (Fig. 3.12). The strain components are (Eq. 3.7)

$$\begin{Bmatrix} \epsilon_x \\ \epsilon_y \\ \gamma_{xy} \end{Bmatrix} = \begin{Bmatrix} \epsilon_x^o \\ \epsilon_y^o \\ \gamma_{xy}^o \end{Bmatrix} + z \begin{Bmatrix} \kappa_x \\ \kappa_y \\ \kappa_{xy} \end{Bmatrix}. \tag{4.11}$$

[7] Ibid., p. 84.

The stresses and the strains at a point are related by (Eq. 3.13)

$$\begin{Bmatrix} \sigma_x \\ \sigma_y \\ \tau_{xy} \end{Bmatrix} = [\overline{Q}] \begin{Bmatrix} \epsilon_x \\ \epsilon_y \\ \gamma_{xy} \end{Bmatrix}. \tag{4.12}$$

By substituting Eqs. (4.11) and (4.12) into Eq. (4.10) and by utilizing the definitions of the $[A]$, $[B]$, $[D]$ matrices (Eq. 3.18), we obtain the following expression for the strain energy:

$$U = \frac{1}{2} \int_0^{L_x} \int_0^{L_y} \begin{Bmatrix} \epsilon_x^o \\ \epsilon_y^o \\ \gamma_{xy}^o \\ \kappa_x \\ \kappa_y \\ \kappa_{xy} \end{Bmatrix}^T \begin{bmatrix} A_{11} & A_{12} & A_{16} & B_{11} & B_{12} & B_{16} \\ A_{12} & A_{22} & A_{26} & B_{12} & B_{22} & B_{26} \\ A_{16} & A_{26} & A_{66} & B_{16} & B_{26} & B_{66} \\ B_{11} & B_{12} & B_{16} & D_{11} & D_{12} & D_{16} \\ B_{12} & B_{22} & B_{26} & D_{12} & D_{22} & D_{26} \\ B_{16} & B_{26} & B_{66} & D_{16} & D_{26} & D_{66} \end{bmatrix} \begin{Bmatrix} \epsilon_x^o \\ \epsilon_y^o \\ \gamma_{xy}^o \\ \kappa_x \\ \kappa_y \\ \kappa_{xy} \end{Bmatrix} dydx. \tag{4.13}$$

The superscript T denotes the transpose of the vector.

4.2 Deflection of Rectangular Plates

4.2.1 Pure Bending and In-Plane Loads

We consider an unsupported rectangular plate subjected to pure bending and to in-plane loads (Fig. 4.2). The in-plane forces and moments are related to the reference plane's strains and curvatures by Eq. (4.3). Six of the twelve quantities appearing in this equation must be specified as follows:

$$\begin{aligned} &N_x \text{ or } \epsilon_x^o \qquad M_x \text{ or } \kappa_x \\ &N_y \text{ or } \epsilon_y^o \qquad M_y \text{ or } \kappa_y \\ &N_{xy} \text{ or } \epsilon_{xy}^o \qquad M_{xy} \text{ or } \kappa_{xy}. \end{aligned} \tag{4.14}$$

With six of the quantities chosen (Eq. 4.14), the remaining six may be obtained by solving the six simultaneous equations given by Eq. (4.3). Once the curvatures

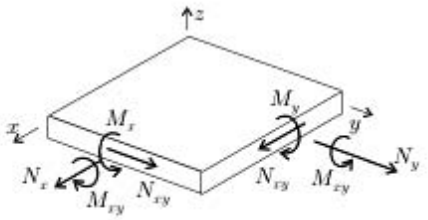

Figure 4.2: Rectangular plate subjected to bending and in-plane loads.

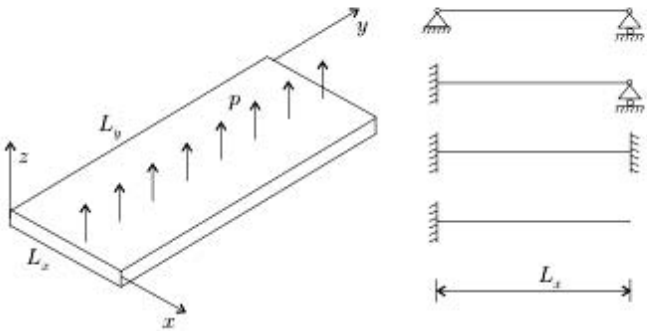

Figure 4.3: The different types of supports along the long edges of a transversely loaded long plate.

are known, the deflection of the reference surface w^o is calculated by using the relationships between the curvatures and the deflection (Eq. 4.2) as follows:

$$\kappa_x = -\frac{\partial^2 w^o}{\partial x^2} \qquad \kappa_y = -\frac{\partial^2 w^o}{\partial y^2} \qquad \kappa_{xy} = -\frac{2\partial^2 w^o}{\partial x \partial y}. \tag{4.15}$$

The following deflection satisfies these relationships:

$$w^o = -\frac{\kappa_x}{2}x^2 - \frac{\kappa_y}{2}y^2 - \frac{\kappa_{xy}}{2}xy. \tag{4.16}$$

This expression for w^o does not include the deflection of the reference plane due to rigid-body motion.

4.2.2 Long Plates

We consider a long rectangular plate whose length L_y is large compared with its width L_x. The long edges may be built-in, simply supported, or free, as shown in Figure 4.3. The plate is subjected to a distributed transverse load p. Neither this load nor the edge supports vary along the longitudinal y direction.

When the length of the plate is large compared with its width, away from the short edges the deflected surface may be assumed to be cylindrical (cylindrical deformation, Fig. 4.4), and the forces and moments do not vary appreciably along the length. With these approximations the analysis simplifies considerably. Before we undertake the analysis, we establish the length-to-width ratios for which a plate may be considered long.

For an isotropic plate the long-plate approximation for the deflection is reasonable when[8]

$$\frac{L'_y}{L'_x} > 3 \qquad \text{isotropic plate,} \tag{4.17}$$

where L'_y and L'_x are the length and the width of the isotropic plate, respectively. We now establish for orthotropic plates the length-to-width ratios at which the

[8] Ibid., p. 118.

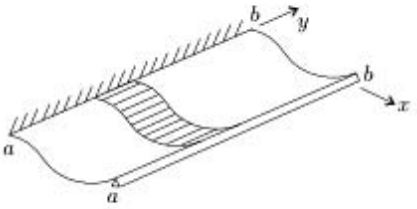

Figure 4.4: Cylindrical deformation of a long rectangular plate.

long-plate approximation may be applied. To this end we observe that the deflections of an orthotropic plate (with length L_y and width L_x) and an isotropic plate (with length L'_y and width L'_x) are similar when (page 109)

$$L'_x = \frac{L_x}{\sqrt[4]{\frac{D_{11}}{D_{22}}}} \qquad L'_y = L_y. \tag{4.18}$$

Thus, from Eqs. (4.17) and (4.18) we have that the long-plate approximation is reasonable when the following inequality is satisfied:

$$\frac{L_y}{L_x} > 3\sqrt[4]{\frac{D_{11}}{D_{22}}} \qquad \text{orthotropic plate.} \tag{4.19}$$

This formula, which is established for orthotropic plates, may also be used as a guide for plates whose layup is not orthotropic.

We now proceed with the analysis of long plates in cylindrical bending. The generator of this cylindrical surface is parallel to the longitudinal y-axis of the plate. The curvatures κ_y and κ_{xy} of the plate are zero

$$\kappa_y = 0 \qquad \kappa_{xy} = 0, \tag{4.20}$$

and κ_x is (Eq. 4.2)

$$\kappa_x = -\frac{\partial^2 w^o}{\partial x^2}. \tag{4.21}$$

Away from the short edges the forces and moments do not vary along the length of the plate. Thus, from the last of Eq. (4.4) and the first of Eq. (4.5) we have

$$\frac{dV_x}{dx} + p_z = 0 \tag{4.22}$$

$$\frac{dM_x}{dx} - V_x = 0. \tag{4.23}$$

The load is perpendicular to the surface, and for simplicity we replace p_z by p. Thus, by substituting V_x from Eq. (4.23) into Eq. (4.22) we obtain the equilibrium equation

$$\frac{d^2 M_x}{dx^2} + p = 0. \tag{4.24}$$

We note that this equation, representing equilibrium, is independent of the material.

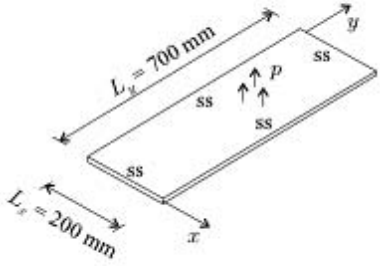

Figure 4.5: The plate in Example 4.1.

Symmetrical layup. The layup of the plate is symmetrical ($[B] = 0$). We now concern ourselves only with the bending moment M_x, which, from Eqs. (4.3) and (4.20), is

$$M_x = D_{11}\kappa_x. \tag{4.25}$$

The element D_{11} of the matrix $[D]$ is given by Eq. (3.20).

By substituting Eq. (4.25) into Eq. (4.24) and by using Eq. (4.21), we obtain the following equilibrium equation for the anisotropic long plate:

$$\frac{d^4 w^o}{dx^4} - \frac{p}{D_{11}} = 0 \qquad \begin{array}{l}\text{long plate} \\ \text{symmetrical layup.}\end{array} \tag{4.26}$$

The equation governing the deflection of a transversely loaded isotropic beam is[9]

$$\frac{d^4 w}{dx^4} - \frac{p'}{EI} = 0 \qquad \text{isotropic beam,} \tag{4.27}$$

where E is Young's modulus, I is the moment of inertia about the y-axis, and p' is the transverse load per unit length.

By comparing Eq. (4.26) and (4.27), we see that the equations describing the deflections of a long plate (symmetrical layup) and an isotropic beam are similar. Consequently, the deflection of a long plate (symmetrical layup) with bending stiffness D_{11} is the same as the deflection of an isotropic beam with bending stiffness EI when the numerical values of the loads are equal ($p = p'$). (Note however that p is per unit area and p' is per unit length.) Thus, the deflection of a long plate with symmetrical layup can be obtained by replacing EI/p' by D_{11}/p in the expression[10] given for the deflection of the corresponding isotropic beam.

4.1 Example. *A 0.7-m-long and 0.2-m-wide rectangular plate is made of graphite epoxy. The material properties are given in Table 3.6 (page 81). The layup is* $[\pm 45_2^f/0_{12}/\pm 45_2^f]$. *The 0-degree plies are parallel to the short edge of the plate. The plate is simply supported along all four edges and is subjected to a uniformly distributed transverse load* $p = 50\,000$ *N/m*^{2} *(Fig. 4.5). Calculate the maximum*

[9] E. P. Popov, *Engineering Mechanics of Solids*. Prentice-Hall, Englewood Cliffs, New Jersey, 1990, p. 505.

[10] W. D. Pilkey, *Formulas for Stresses, Strains, and Structural Matrices*. John Wiley & Sons, New York, 1994.

deflection, the maximum bending moments, and the stresses and strains in each layer.

Solution. The bending stiffnesses of the plate are (Table 3.7, page 84) $D_{11} = 45.30\ \text{N}\cdot\text{m}$ and $D_{22} = 25.26\ \text{N}\cdot\text{m}$. We may treat this plate as long when the following condition is met (Eq. 4.19):

$$\frac{L_y}{L_x} > 3\sqrt[4]{\frac{D_{11}}{D_{22}}}. \tag{4.28}$$

In the present problem the terms in this inequality are $L_y/L_x = 3.5$ and $3\sqrt[4]{D_{11}/D_{22}} = 3.47$. Thus, the preceding condition is satisfied and the long-plate expressions may be used.

The maximum deflection of a simply supported beam is (Table 7.3, page 332)

$$\widetilde{w} = \frac{5}{384}\frac{p'L^4}{EI}. \tag{4.29}$$

The maximum deflection of the plate is obtained by replacing EI/p' by D_{11}/p (see page 96). For the plate under consideration $D_{11} = 45.30\,\text{N}\cdot\text{m}$ and $L_x = 0.2\,\text{m}$, and we have

$$\widetilde{w} = \frac{5}{384}\frac{pL_x^4}{D_{11}} = 0.0230\ \text{m} = 23.0\ \text{mm}. \tag{4.30}$$

The bending moments are (Eq. 3.27)

$$M_x = D_{11}\kappa_x + D_{12}\kappa_y + D_{16}\kappa_{xy} \tag{4.31}$$

$$M_y = D_{12}\kappa_x + D_{22}\kappa_y + D_{26}\kappa_{xy}. \tag{4.32}$$

For a long plate κ_y and κ_{xy} are zero (Eq. 4.20), and M_x and M_y are

$$M_x = D_{11}\kappa_x \qquad M_y = D_{12}\kappa_x. \tag{4.33}$$

The maximum bending moment M_x, which arises at $L_x/2$, is (see Table 7.3, page 332)

$$M_x = \frac{pL_x^2}{8} = 250.00\,\frac{\text{N}\cdot\text{m}}{\text{m}}. \tag{4.34}$$

From Eqs. (4.33) and (4.34) we have

$$\kappa_x = \frac{M_x}{D_{11}} = 5.52\,\frac{1}{\text{m}}. \tag{4.35}$$

From Eqs. (4.33) and (4.34) the maximum bending moment M_y (at $L_x/2$) is

$$M_y = D_{12}\kappa_x = \underbrace{\frac{D_{12}}{D_{11}}}_{0.431} M_x = 107.75\,\frac{\text{N}\cdot\text{m}}{\text{m}}. \tag{4.36}$$

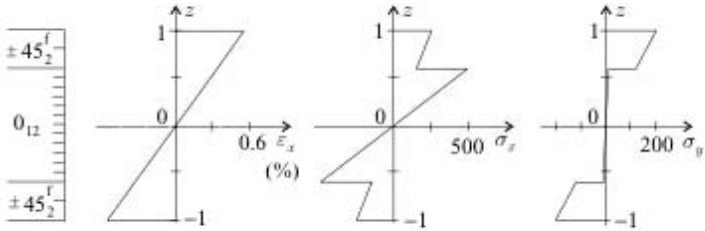

Figure 4.6: The nonzero strains and stresses across the thickness of the plate at $L_x/2$ in Example 4.1. The unit of σ is 10^6 N/m^2.

For the long plate ($\kappa_y = \kappa_{xy} = 0$) the strains at $L_x/2$ are (Eq. 3.7)

$$\begin{aligned} \epsilon_x &= \kappa_x z = 5.52z \\ \epsilon_y &= 0 \\ \gamma_{xy} &= 0. \end{aligned} \tag{4.37}$$

The strain distribution at $L_x/2$ is shown in Figure 4.6. The stresses are calculated by (Eq. 3.11)

$$\begin{Bmatrix} \sigma_x \\ \sigma_y \\ \tau_{xy} \end{Bmatrix} = \begin{bmatrix} \overline{Q}_{11} & \overline{Q}_{12} & \overline{Q}_{16} \\ \overline{Q}_{12} & \overline{Q}_{22} & \overline{Q}_{26} \\ \overline{Q}_{16} & \overline{Q}_{26} & \overline{Q}_{66} \end{bmatrix} \begin{Bmatrix} \epsilon_x \\ \epsilon_y \\ \gamma_{xy} \end{Bmatrix}. \tag{4.38}$$

The stiffness matrices for the fabric and for the unidirectional layer are given by Eqs. (3.65) and (3.66). The stresses in the top layer (where $z = h/2 = 0.001$ m) at $L_x/2$ are

$$\begin{Bmatrix} \sigma_x \\ \sigma_y \\ \tau_{xy} \end{Bmatrix} = \begin{bmatrix} \overline{Q}_{11} \\ \overline{Q}_{12} \\ \overline{Q}_{16} \end{bmatrix} \epsilon_x = \begin{bmatrix} 45.65 \\ 36.55 \\ 0 \end{bmatrix} 10^9 \times 5.52 \times 0.001 = \begin{bmatrix} 251.95 \\ 201.73 \\ 0 \end{bmatrix} 10^6 \frac{\text{N}}{\text{m}^2}. \tag{4.39}$$

The stresses in the other layers are calculated similarly. The results are shown in Figure 4.6.

Unsymmetrical layup. The layup of the plate is unsymmetrical. One of the long edges must be restrained along the lengthwise direction. With the plate thus restrained, the strain in the longitudinal y direction is zero throughout the plate:

$$\epsilon_y^o = 0. \tag{4.40}$$

Furthermore, we take the shear force N_{xy} to be zero:

$$N_{xy} = 0. \tag{4.41}$$

Equation (4.41) is valid when one of the long edges of the plate is free to move in the lengthwise y direction. It is only an approximation when the lengthwise motion

of both long edges of the plate is restricted, as in the top three configurations of Figure 4.3.

By substituting Eqs. (4.20), (4.40), and (4.41) into the third and fourth expressions of Eq. (4.3), we obtain

$$\begin{Bmatrix} 0 \\ M_x \end{Bmatrix} = \begin{bmatrix} A_{16} & A_{66} & B_{16} \\ B_{11} & B_{16} & D_{11} \end{bmatrix} \begin{Bmatrix} \epsilon_x^o \\ \gamma_{xy}^o \\ \kappa_x \end{Bmatrix}. \tag{4.42}$$

We now select a reference plane at a distance ϱ from the midplane (Fig. 3.14). The strain components and the stiffnesses referred to this reference plane are identified by the superscript ϱ. (The curvature and the M_x component of the moment are independent of the position of the reference plane and thus do not need to be identified by the superscript ϱ.) For the new reference plane Eq. (4.42) is written as

$$\begin{Bmatrix} 0 \\ M_x \end{Bmatrix} = \begin{bmatrix} A_{16}^\varrho & A_{66}^\varrho & B_{16}^\varrho \\ B_{11}^\varrho & B_{16}^\varrho & D_{11}^\varrho \end{bmatrix} \begin{Bmatrix} \epsilon_x^{o,\varrho} \\ \gamma_{xy}^{o,\varrho} \\ \kappa_x \end{Bmatrix}. \tag{4.43}$$

The first row of this equation gives

$$\gamma_{xy}^{o,\varrho} = -\epsilon_x^{o,\varrho} \frac{A_{16}^\varrho}{A_{66}^\varrho} - \kappa_x \frac{B_{16}^\varrho}{A_{66}^\varrho}. \tag{4.44}$$

Substitution of Eq. (4.44) into the second row of Eq. (4.43) yields

$$M_x = \left(B_{11}^\varrho - \frac{A_{16}^\varrho B_{16}^\varrho}{A_{66}^\varrho} \right) \epsilon_x^{o,\varrho} + \left(D_{11}^\varrho - \frac{B_{16}^{\varrho 2}}{A_{66}^\varrho} \right) \kappa_x. \tag{4.45}$$

In general, the bending moment M_x depends both on $\epsilon_x^{o,\varrho}$ and κ_x. However, there is a reference plane for which the term in the parentheses in front of $\epsilon_x^{o,\varrho}$ is zero:

$$B_{11}^\varrho - \frac{A_{16}^\varrho B_{16}^\varrho}{A_{66}^\varrho} = 0. \tag{4.46}$$

We recall that the stiffnesses in the midplane (Reference Plane 1) and the new reference plane (Reference Plane 2) are related by (Eq. 3.47)

$$\begin{aligned} A_{ij}^\varrho &= A_{ij} \\ B_{ij}^\varrho &= B_{ij} - \varrho A_{ij} \\ D_{ij}^\varrho &= D_{ij} - 2\varrho B_{ij} + \varrho^2 A_{ij}. \end{aligned} \tag{4.47}$$

Equations (4.46) and (4.47) give

$$B_{11} - \frac{A_{16} B_{16}}{A_{66}} - \varrho \left(A_{11} - \frac{A_{16}^2}{A_{66}} \right) = 0. \tag{4.48}$$

By rearranging this equation, we obtain the position of the reference plane where Eq. (4.46) is satisfied:

$$\varrho = \frac{B_{11} - \frac{A_{16}B_{16}}{A_{66}}}{A_{11} - \frac{A_{16}^2}{A_{66}}}. \tag{4.49}$$

For a reference plane at ϱ distance from the midplane, the moment M_x depends only on κ_x as follows:

$$M_x = \left[D_{11}^{\varrho} - \frac{\left(B_{16}^{\varrho}\right)^2}{A_{66}^{\varrho}} \right] \kappa_x. \tag{4.50}$$

Equations (4.50) and (4.24), together with Eq. (4.2), yield the following equilibrium equation for an anisotropic long plate:

$$\frac{d^4 w^o}{dx^4} - \frac{p}{\Psi} = 0 \qquad \begin{array}{l} \text{long plate} \\ \text{unsymmetrical layup,} \end{array} \tag{4.51}$$

where the symbol Ψ is the bending stiffness parameter

$$\Psi = D_{11}^{\varrho} - \frac{\left(B_{16}^{\varrho}\right)^2}{A_{66}^{\varrho}}. \tag{4.52}$$

By using Eq. (4.47), Ψ may be written as

$$\Psi = D_{11} - 2\varrho B_{11} + \varrho^2 A_{11} - \frac{\left(B_{16} - \varrho A_{16}\right)^2}{A_{66}}, \tag{4.53}$$

where ϱ is given by Eq. (4.49).

By comparing Eqs. (4.51) and (4.27), we again observe that the equations governing the deflections of long plates and isotropic beams are similar. Therefore, the deflection of a long plate with unsymmetrical layup can be obtained by replacing EI/p' by Ψ/p in the expression given for the deflection of the corresponding isotropic beam.

4.2.3 Simply Supported Plates – Symmetrical Layup

We consider a rectangular plate with dimensions L_x and L_y simply supported along its four edges (Fig. 4.7). The layup of the plate is symmetrical and $[B] = [0]$. The plate is subjected to a uniformly distributed load p.

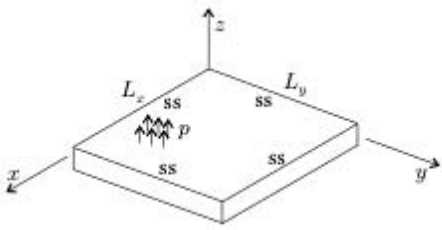

Figure 4.7: Rectangular simply supported (ss) plate subjected to a uniformly distributed transverse load.

Following Whitney,[11] we analyze the deflection of this plate by the energy method. For a simply supported plate (symmetrical layup) subjected to out-of-plane loads only, the in-plane strains in the midplane are zero, and Eq. (4.13) simplifies to

$$U = \frac{1}{2}\int_0^{L_x}\int_0^{L_y} \{\kappa_x \quad \kappa_y \quad \kappa_{xy}\} \begin{bmatrix} D_{11} & D_{12} & D_{16} \\ D_{12} & D_{22} & D_{26} \\ D_{16} & D_{26} & D_{66} \end{bmatrix} \begin{Bmatrix} \kappa_x \\ \kappa_y \\ \kappa_{xy} \end{Bmatrix} dydx. \tag{4.54}$$

By using the relationships between the curvatures and the deflections given by Eq. (4.2), we obtain

$$U = \frac{1}{2}\int_0^{L_x}\int_0^{L_y} \left[D_{11}\left(\frac{\partial^2 w^o}{\partial x^2}\right)^2 + D_{22}\left(\frac{\partial^2 w^o}{\partial y^2}\right)^2 + D_{66}\left(\frac{2\partial^2 w^o}{\partial x \partial y}\right)^2 + 2\left(D_{12}\frac{\partial^2 w^o}{\partial x^2}\frac{\partial^2 w^o}{\partial y^2} + D_{16}\frac{\partial^2 w^o}{\partial x^2}\frac{2\partial^2 w^o}{\partial x \partial y} + D_{26}\frac{\partial^2 w^o}{\partial y^2}\frac{2\partial^2 w^o}{\partial x \partial y} \right) \right] dydx. \tag{4.55}$$

For the applied transverse load p (per unit area) the potential of the external forces is (Eq. 2.203)

$$\Omega = -\int_0^{L_x}\int_0^{L_y} (pw^o) dydx. \tag{4.56}$$

We use the Ritz method and select an expression for the deflection that satisfies the geometrical boundary conditions. For the simply supported plate under consideration the geometrical boundary conditions require that the deflection be zero along the edges (see Eq. 4.8) as follows:

$$w^o = 0 \quad \text{at} \quad \begin{cases} x = 0 & \text{and} \quad 0 \le y \le L_y \\ x = L_x & \text{and} \quad 0 \le y \le L_y \\ 0 \le x \le L_x & \text{and} \quad y = 0 \\ 0 \le x \le L_x & \text{and} \quad y = L_y . \end{cases} \tag{4.57}$$

The following deflection satisfies these conditions:

$$w^o = \sum_{i=1}^{I}\sum_{j=1}^{J} w_{ij} \sin\frac{i\pi x}{L_x} \sin\frac{j\pi y}{L_y}, \tag{4.58}$$

where I and J are the number of terms, chosen arbitrarily, for the summations and w_{ij} are constants and are calculated from the principle of stationary potential energy (Eq. 2.206) expressed as

$$\frac{\partial \pi_p}{\partial w_{ij}} = \frac{\partial (U + \Omega)}{\partial w_{ij}} = 0. \tag{4.59}$$

[11] J. M. Whitney, *Structural Analysis of Laminated Anisotropic Plates*. Technomic, Lancaster, Pennsylvania, 1987, p. 133.

We now substitute w^o (from Eq. 4.58) into the expressions of U and Ω (Eqs. 4.55 and 4.56) and perform the differentiations indicated above. Lengthy but straightforward algebraic manipulations result in the following system of simultaneous algebraic equations:

$$\sum_{i=1}^{I}\sum_{j=1}^{J} G_{mnij} w_{ij} = p_{mn} \quad \begin{cases} i, m = 1, 2, 3, \ldots, I \\ j, n = 1, 2, 3, \ldots, J. \end{cases} \tag{4.60}$$

For convenience, we introduce the contracted notation

$$k = (i-1)J + j \quad \begin{cases} i = 1, 2, 3, \ldots, I \\ j = 1, 2, 3, \ldots, J \end{cases} \tag{4.61}$$

$$l = (m-1)J + n \quad \begin{cases} m = 1, 2, 3, \ldots, I \\ n = 1, 2, 3, \ldots, J. \end{cases} \tag{4.62}$$

Equation (4.60) may now be written as

$$\sum_{k=1}^{I\times J} G_{kl} w_k = p_l \quad l = 1, 2, 3, \ldots, I \times J, \tag{4.63}$$

where G_{kl} $(= G_{lk})$ is given in Table 4.1 and, for a uniformly distributed load, p_l is

$$p_l = \begin{cases} \frac{4pL_xL_y}{\pi^2 mn} & \text{if } m \text{ and } n \text{ are odd} \\ 0 & \text{if } m \text{ or } n \text{ is even} \end{cases}. \tag{4.64}$$

Table 4.1. The elements of the matrix [G]

$$G_{lk} = \tfrac{1}{4}L_xL_y\pi^4\left[D_{11}\left(\tfrac{i}{L_x}\right)^4 + 2(D_{12}+2D_{66})\left(\tfrac{i}{L_x}\right)^2\left(\tfrac{j}{L_y}\right)^2 + D_{22}\left(\tfrac{j}{L_y}\right)^4\right]\delta_{lk}$$

$$-2L_xL_y\pi^4 D_{16}\left[\left(\tfrac{i}{L_x}\right)^2\left(\tfrac{m}{L_x}\right)\left(\tfrac{n}{L_y}\right)r_{im}r_{jn} + \left(\tfrac{m}{L_x}\right)^2\left(\tfrac{i}{L_x}\right)\left(\tfrac{j}{L_y}\right)r_{mi}r_{nj}\right]$$

$$-2L_xL_y\pi^4 D_{26}\left[\left(\tfrac{j}{L_y}\right)^2\left(\tfrac{m}{L_x}\right)\left(\tfrac{n}{L_y}\right)r_{im}r_{jn} + \left(\tfrac{n}{L_y}\right)^2\left(\tfrac{i}{L_x}\right)\left(\tfrac{j}{L_y}\right)r_{mi}r_{nj}\right]$$

$$\delta_{lk} = \begin{cases} 1 & \text{if } k = l \\ 0 & \text{if } k \neq l \end{cases}$$

$$r_{ij} = \begin{cases} \frac{2i}{i^2-j^2}\frac{1}{\pi} & \text{if } (i-j) \text{ is odd} \\ 0 & \text{if } (i-j) \text{ is even} \end{cases}$$

$$k = (i-1)J + j \quad \begin{cases} i = 1, 2, 3, \ldots, I \\ j = 1, 2, 3, \ldots, J \end{cases}$$

$$l = (m-1)J + n \quad \begin{cases} m = 1, 2, 3, \ldots, I \\ n = 1, 2, 3, \ldots, J \end{cases}$$

In expanded form, Eq. (4.63) is

$$\begin{bmatrix} G_{11} & G_{12} & \cdots & G_{1(I\times J)} \\ G_{21} & G_{22} & & \\ \vdots & & \ddots & \\ G_{(I\times J)1} & & & G_{(I\times J)(I\times J)} \end{bmatrix} \begin{Bmatrix} w_1 \\ w_2 \\ \vdots \\ w_{(I\times J)} \end{Bmatrix} = \begin{Bmatrix} p_1 \\ p_2 \\ \vdots \\ p_{(I\times J)} \end{Bmatrix}. \tag{4.65}$$

By inverting this equation, we obtain the coefficients w_k

$$\begin{Bmatrix} w_1 \\ w_2 \\ \vdots \\ w_{(I\times J)} \end{Bmatrix} = \begin{bmatrix} G_{11} & G_{12} & \cdots & G_{1(I\times J)} \\ G_{21} & G_{22} & & \\ \vdots & & \ddots & \\ G_{(I\times J)1} & & & G_{(I\times J)(I\times J)} \end{bmatrix}^{-1} \begin{Bmatrix} p_1 \\ p_2 \\ \vdots \\ p_{(I\times J)} \end{Bmatrix}. \tag{4.66}$$

From Eqs. (4.2), (3.27), and (4.58) the moments are

$$\begin{Bmatrix} M_x \\ M_y \\ M_{xy} \end{Bmatrix} = [D] \begin{Bmatrix} \kappa_x \\ \kappa_y \\ \kappa_{xy} \end{Bmatrix} = [D] \begin{Bmatrix} \sum_{i=1}^{I}\sum_{j=1}^{J} w_{ij}\left(\frac{i\pi}{L_x}\right)^2 \sin\frac{i\pi x}{L_x}\sin\frac{j\pi y}{L_y} \\ \sum_{i=1}^{I}\sum_{j=1}^{J} w_{ij}\left(\frac{j\pi}{L_y}\right)^2 \sin\frac{i\pi x}{L_x}\sin\frac{j\pi y}{L_y} \\ -\sum_{i=1}^{I}\sum_{j=1}^{J} w_{ij} 2\frac{i\pi}{L_x}\frac{j\pi}{L_y}\cos\frac{i\pi x}{L_x}\cos\frac{j\pi y}{L_y} \end{Bmatrix}. \tag{4.67}$$

For an orthotropic plate $D_{16} = D_{26} = 0$, and Eq. (4.66) becomes

$$w_k = w_{ij} = \frac{16p}{\pi^6 ij\left[D_{11}\left(\frac{i}{L_x}\right)^4 + 2(D_{12}+2D_{66})\left(\frac{i}{L_x}\right)^2\left(\frac{j}{L_y}\right)^2 + D_{22}\left(\frac{j}{L_y}\right)^4\right]}, \tag{4.68}$$

where $i, j = 1, 3, 5, \ldots$ ($w_k = w_{ij} = 0$ when i or $j = 2, 4, 6, \ldots$).

Once the deflections are known, the moments can be calculated by Eq. (4.67).

4.2 Example. *A 0.7-m-long and 0.2-m-wide rectangular plate is made of graphite epoxy. The material properties are given in Table 3.6 (page 81). The layup is* $[\pm 45_2^f/0_{12}/\pm 45_2^f]$. *The 0-degree plies are parallel to the short edge of the plate. The plate is simply supported along all four edges and is subjected to a uniformly distributed transverse load* $p = 50\,000$ *N/m*^{2} *(Fig. 4.8). Calculate the maximum deflection and the maximum bending moments.*

Solution. The deflection of the plate is (Eq. 4.58)

$$w^o = \sum_{i=1}^{I}\sum_{j=1}^{J} w_{ij} \sin\frac{i\pi x}{L_x}\sin\frac{j\pi y}{L_y}. \tag{4.69}$$

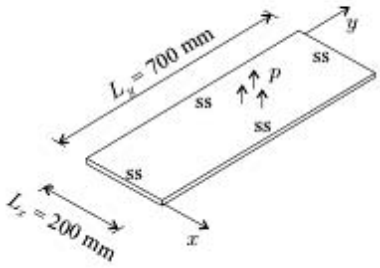

Figure 4.8: The plate in Example 4.2.

The plate is orthotropic, and the bending stiffnesses are (Table 3.7, page 84) $D_{11} = 45.30$ N · m, $D_{22} = 25.26$ N · m, $D_{12} = 19.52$ N · m, $D_{66} = 20.62$ N · m). The maximum deflection occurs at the center of the plate, where $x = L_x/2 = 0.1$ m and $y = L_y/2 = 0.35$ m. From Eq. (4.68), $w_{ij} \times 10^3$ are

$i \backslash j$	1	2	3	4	5	6	7
1	24.0389	0	2.9945	0	0.6683	0	0.2033
2	0	0	0	0	0	0	0
3	0.1181	0	0.0330	0	0.0148	0	0.0075
4	0	0	0	0	0	0	0
5	0.0093	0	0.0029	0	0.0015	0	0.0009
6	0	0	0	0	0	0	0
7	0.0017	0	0.0006	0	0.0003	0	0.0002.

At the center of the plate the deflection is

$$w^o = \sum_{i=1}^{7} \sum_{j=1}^{7} w_{ij} \sin \frac{i\pi}{2} \sin \frac{j\pi}{2}. \tag{4.70}$$

We chose to perform the summation up to $i = j = 7$. For $i, j = 2, 4, 6$, the sine is zero; for $i, j = 1, 5$ the sine is unity, and for $i, j = 3, 7$ the sine is minus one. The resulting deflection at the midpoint is

$$w^o = 0.0214 \text{ m} = 21.4 \text{ mm}. \tag{4.71}$$

We now assess the length-to-width ratios under which the long-plate approximation is reasonable. To this end, we calculated the maximum deflections of the plate, keeping the width L_x the same while changing the length L_y. In Figure 4.9 we plot the maximum deflections thus calculated versus L_y. In this figure we also included the deflection given by the long-plate approximation (Eq. 4.30). The results in this figure show that, in accordance with Eq. (4.19), the long-plate formula approximates the deflection well (within 8 percent) when L_y is greater than $3L_x\sqrt[4]{D_{11}/D_{22}} = 0.694$ m.

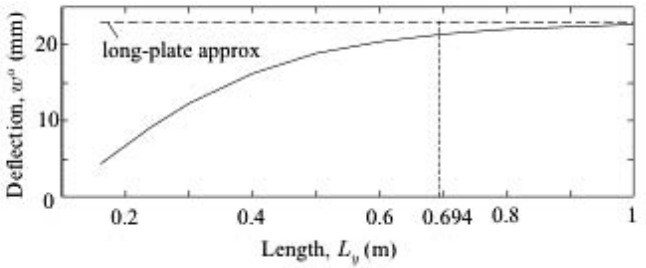

Figure 4.9: Maximum deflection of the plate in Example 4.2 as a function of the plate length.

The bending moments at the center of the plate are (Eq. 4.67)

$$\begin{Bmatrix} M_x \\ M_y \end{Bmatrix} = \begin{bmatrix} D_{11} & D_{12} \\ D_{12} & D_{22} \end{bmatrix} \begin{Bmatrix} \sum_{i=1}^{7}\sum_{j=1}^{7} w_{ij}\left(\frac{i\pi}{L_x}\right)^2 \sin\frac{i\pi}{2}\sin\frac{j\pi}{2} \\ \sum_{i=1}^{7}\sum_{j=1}^{7} w_{ij}\left(\frac{j\pi}{L_y}\right)^2 \sin\frac{i\pi}{2}\sin\frac{j\pi}{2} \end{Bmatrix}$$

$$= \begin{Bmatrix} 233.94 \\ 102.18 \end{Bmatrix} \frac{\text{N}\cdot\text{m}}{\text{m}}. \tag{4.72}$$

The twist moment at the corner of the plate ($x = y = 0$) is (Eq. 4.67)

$$M_{xy} = -D_{66}\sum_{i=1}^{7}\sum_{j=1}^{7} w_{ij} 2\frac{i\pi}{L_x}\frac{j\pi}{L_y}\cos\frac{i\pi x}{L_x}\cos\frac{j\pi y}{L_y}$$

$$= -D_{66}\sum_{i=1}^{7}\sum_{j=1}^{7} w_{ij} 2\frac{i\pi}{L_x}\frac{j\pi}{L_y} = -113.43\,\frac{\text{N}\cdot\text{m}}{\text{m}}. \tag{4.73}$$

4.3 Example. *A 0.2-m-long and 0.2-m-wide rectangular plate is made of graphite epoxy unidirectional plies. The material properties are given in Table 3.6 (page 81). The layup is* $[0_2/45_2/90_2/-45_2]_s$. *The plate, simply supported along the four edges (Fig. 4.10), is subjected to a uniformly distributed transverse load* $p = 50\,000\ \text{N/m}^2$. *Calculate the maximum deflection and the maximum moments.*

Solution. The layup of the plate is symmetrical but is not orthotropic. The bending stiffnesses are $D_{11} = 34.61\ \text{N}\cdot\text{m}$, $D_{22} = 12.34\ \text{N}\cdot\text{m}$, $D_{12} = 4.58\ \text{N}\cdot\text{m}$,

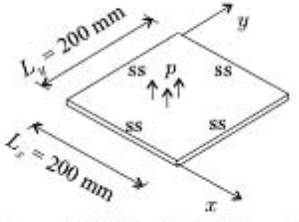

Figure 4.10: The plate in Example 4.3.

Table 4.2. The maximum deflection and the maximum bending and twist moments calculated by the numerical solution and by the orthotropic approximation for the plate in Example 4.3

	w^o	M_x	M_y	M_{xy} $x = y = 0$	M_{xy} $x = L_x, y = 0$
	mm			N · m/m	
numerical	17.60	160.65	64.53	−69.28	36.47
orthotropic approximation	16.93	154.07	63.21	−49.56	49.56

$D_{66} = 5.14$ N · m, $D_{16} = 3.34$ N · m, $D_{26} = 3.34$ N · m (Table 3.7, page 84). The maximum deflection and the maximum bending and twist moments must be calculated from Eqs. (4.58), (4.64), (4.66), and (4.67). With the preceding stiffnesses the calculations yield the results given in Table 4.2 (first row).

The layup follows the 10-percent rule (page 89), and we treat the plate as orthotropic. The deflection of the plate is (Eq. 4.58)

$$w^o = \sum_{i=1}^{I} \sum_{j=1}^{J} w_{ij} \sin \frac{i\pi x}{L_x} \sin \frac{j\pi y}{L_y}. \tag{4.74}$$

Since the plate is treated as orthotropic $D_{16} = D_{26} = 0$, and the relevant bending stiffnesses are $D_{11} = 34.61$ N · m, $D_{22} = 12.34$ N · m, $D_{12} = 4.58$ N · m, $D_{66} = 5.14$ N · m (Table 3.7, page 84). The maximum deflection occurs at the center of the plate, where $x = L_x/2 = 0.1$ m and $y = L_y/2 = 0.1$ m. From Eq. (4.68) $w_{ij} \times 10^3$ are

$i \backslash j$	1	2	3	4	5	6	7
1	17.3628	0	0.3409	0	0.0314	0	0.0061
2	0	0	0	0	0	0	0
3	0.1439	0	0.0238	0	0.0052	0	0.0014
4	0	0	0	0	0	0	0
5	0.0119	0	0.0030	0	0.0011	0	0.0004
6	0	0	0	0	0	0	0
7	0.0022	0	0.0007	0	0.0003	0	0.0001

At the center of the plate the deflection is

$$w^o = \sum_{i=1}^{7} \sum_{j=1}^{7} w_{ij} \sin \frac{i\pi}{2} \sin \frac{j\pi}{2}. \tag{4.75}$$

We perform the summation up to $i = j = 7$. For $i, j = 2, 4, 6$ the sine is zero, for $i, j = 1, 5$ the sine is unity, and for $i, j = 3, 7$ the sine is minus one. Thus, the resulting deflection at the center of the plate is

$$w^o = 0.01693 \text{ m} = 16.93 \text{ mm}. \tag{4.76}$$

The bending moments at the center of the plate are (Eq. 4.67)

$$\begin{Bmatrix} M_x \\ M_y \end{Bmatrix} = \begin{bmatrix} D_{11} & D_{12} \\ D_{12} & D_{22} \end{bmatrix} \begin{Bmatrix} \sum_{i=1}^{7}\sum_{j=1}^{7} w_{ij}\left(\frac{i\pi}{L_x}\right)^2 \sin\frac{i\pi}{2}\sin\frac{j\pi}{2} \\ \sum_{i=1}^{7}\sum_{j=1}^{7} w_{ij}\left(\frac{i\pi}{L_y}\right)^2 \sin\frac{i\pi}{2}\sin\frac{j\pi}{2} \end{Bmatrix}$$

$$= \begin{Bmatrix} 154.07 \\ 63.21 \end{Bmatrix} \frac{\text{N}\cdot\text{m}}{\text{m}}. \tag{4.77}$$

The twist moment at the corner of the plate ($x = y = 0$) is (Eq. 4.67)

$$M_{xy} = -D_{66}\sum_{i=1}^{7}\sum_{j=1}^{7} 2w_{ij}\frac{i\pi}{L_x}\frac{j\pi}{L_y}\cos\frac{i\pi x}{L_x}\cos\frac{j\pi y}{L_y}$$

$$= -D_{66}\sum_{i=1}^{7}\sum_{j=1}^{7} 2w_{ij}\frac{i\pi}{L_x}\frac{j\pi}{L_y} = -49.56\frac{\text{N}\cdot\text{m}}{\text{m}}. \tag{4.78}$$

The maximum deflection and the maximum moments thus calculated are included in Table 4.2 (second row). The maximum bending moments and the maximum deflections calculated by the numerical method and the orthotropic approximation are in close agreement, but the maximum twist moments differ significantly.

4.2.4 Plates with Built-In Edges – Orthotropic and Symmetrical Layup

We consider a rectangular plate with length L_x and width L_y built-in along its four edges (Fig. 4.11). The layup is orthotropic and symmetrical. The plate is subjected to a uniformly distributed load p.

The potential energy of the plate is obtained from Eqs. (4.55) and (4.56) by setting D_{16} and D_{26} equal to zero:

$$\pi_p = U + \Omega = \frac{1}{2}\int_0^{L_x}\int_0^{L_y}\left[D_{11}\left(\frac{\partial^2 w^o}{\partial x^2}\right)^2 + D_{22}\left(\frac{\partial^2 w^o}{\partial y^2}\right)^2 + D_{66}\left(\frac{2\partial^2 w^o}{\partial x\partial y}\right)^2 + 2D_{12}\frac{\partial^2 w^o}{\partial x^2}\frac{\partial^2 w^o}{\partial y^2} - pw^o\right]dydx. \tag{4.79}$$

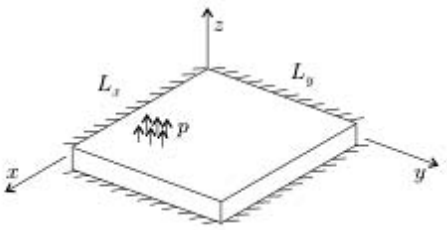

Figure 4.11: Rectangular plate with built-in edges.

The moments at a point x, y are (Eqs. 4.2 and 3.27)

$$\begin{aligned} M_x &= -D_{11}\frac{\partial^2 w^o}{\partial x^2} - D_{12}\frac{\partial^2 w^o}{\partial y^2} \\ M_y &= -D_{12}\frac{\partial^2 w^o}{\partial x^2} - D_{22}\frac{\partial^2 w^o}{\partial y^2} \\ M_{xy} &= -D_{66}\frac{2\partial^2 w^o}{\partial x \partial y}, \end{aligned} \tag{4.80}$$

where w^o is the deflection and D_{11}, D_{12}, D_{22}, D_{66} are the elements of the stiffness matrix in the x–y coordinate system.

The displacements and moments can be calculated when the plate's bending stiffnesses satisfy the following Huber orthotropy relationship[12] (see Eq. 4.153 with $K = 1$):

$$D_{66} = \frac{1}{2}(\sqrt{D_{11}D_{22}} - D_{12}). \tag{4.81}$$

Although this relationship may not hold exactly, we adopt it for calculating the displacements and the moments. Possible errors introduced by this relationship are discussed on page 111.

We introduce the variable

$$x' = \frac{x}{\alpha}, \tag{4.82}$$

where α is a constant defined as

$$\alpha = \sqrt[4]{\frac{D_{11}}{D_{22}}}. \tag{4.83}$$

Equations (4.79)–(4.83) yield the potential energy and the moments (per unit length) as follows:

$$\begin{aligned} \pi_p = \frac{1}{2}\int_0^{L_x/\alpha}\int_0^{L_y} D_{22}\Bigg[&\left(\frac{\partial^2 w^o}{\partial x'^2}\right)^2 + \left(\frac{\partial^2 w^o}{\partial y^2}\right)^2 + \frac{1}{2}\left(1 - \sqrt{\frac{D_{12}^2}{D_{11}D_{22}}}\right)\left(\frac{2\partial^2 w^o}{\partial x' \partial y}\right)^2 \\ &+ 2\sqrt{\frac{D_{12}^2}{D_{11}D_{22}}}\,\frac{\partial^2 w^o}{\partial x'^2}\frac{\partial^2 w^o}{\partial y^2} - pw^o\Bigg] dy dx' \end{aligned} \tag{4.84}$$

$$\begin{aligned} M_x &= \alpha^2\left[-D_{22}\frac{\partial^2 w^o}{\partial x'^2} - \sqrt{\frac{D_{12}^2}{D_{11}D_{22}}}\,\left(D_{22}\frac{\partial^2 w^o}{\partial y^2}\right)\right] \\ M_y &= \left[-\sqrt{\frac{D_{12}^2}{D_{11}D_{22}}}\,\left(D_{22}\frac{\partial^2 w^o}{\partial x'^2}\right) - D_{22}\frac{\partial^2 w^o}{\partial y^2}\right] \\ M_{xy} &= \alpha\left[-D_{22}\frac{1}{2}\left(1 - \sqrt{\frac{D_{12}^2}{D_{11}D_{22}}}\right)\frac{2\partial^2 w^o}{\partial x' \partial y}\right]. \end{aligned} \tag{4.85}$$

[12] S. P. Timoshenko and S. Woinowsky-Krieger, *Theory of Plates and Shells*. 2nd edition. McGraw-Hill, New York, 1959, p. 366.

We now consider a rectangular isotropic plate with dimensions L'_x and L_y. The potential energy and the moments (per unit length) of an isotropic plate are obtained by substituting into Eqs. (4.79) and (4.80) $D_{11} = D_{22} = D^{iso}$, $D_{12} = \nu^{iso} D^{iso}$, and $D_{66} = D^{iso}(1 - \nu^{iso})/2$ (see Eq. 3.41). In the x', y coordinate system the results are

$$\pi_p^{iso} = \frac{1}{2}\int_0^{L'_x}\int_0^{L_y} D^{iso}\left[\left(\frac{\partial^2 w^{iso}}{\partial x'^2}\right)^2 + \left(\frac{\partial^2 w^{iso}}{\partial y^2}\right)^2 + \frac{1}{2}(1-\nu^{iso})\left(\frac{2\partial^2 w^{iso}}{\partial x'\partial y}\right)^2 + 2\nu^{iso}\frac{\partial^2 w^{iso}}{\partial x'^2}\frac{\partial^2 w^{iso}}{\partial y^2} - pw^{iso}\right] dy dx' \tag{4.86}$$

$$M_{x'}^{iso} = -D^{iso}\frac{\partial^2 w^{iso}}{\partial x'^2} - \nu^{iso} D^{iso}\frac{\partial^2 w^{iso}}{\partial y^2}$$

$$M_y^{iso} = -\nu^{iso} D^{iso}\frac{\partial^2 w^{iso}}{\partial x'^2} - D^{iso}\frac{\partial^2 w^{iso}}{\partial y^2} \tag{4.87}$$

$$M_{x'y}^{iso} = -D^{iso}\frac{1-\nu^{iso}}{2}\frac{2\partial^2 w^{iso}}{\partial x'\partial y}.$$

The superscript "iso" refers to the isotropic plate.

From Eqs. (4.84) and (4.86) we see that the expressions for the potential energy for the Huber orthotropic plate (with dimensions L_x, L_y and stiffnesses D_{11}, D_{12}, D_{22}) and for an isotropic plate (with dimensions L'_x and L_y) are identical when

$$L'_x = L_x/\alpha \tag{4.88}$$

$$D^{iso} = D_{22} \qquad \nu^{iso} = \sqrt{\frac{D_{12}^2}{D_{11}D_{22}}}. \tag{4.89}$$

The deflections of the plate are obtained from the potential energy. Hence, when Eqs. (4.88) and (4.89) are satisfied, the deflection of the orthotropic plate at point x, y is the same as the deflection of the corresponding isotropic plate at point x', y, that is,

$$w^o(x, y) = w^{iso}(x', y). \tag{4.90}$$

Equations (4.85) and (4.87) show that the moments (per unit length) of a Huber orthotropic plate are related to the moments (per unit length) of the corresponding isotropic plate by

$$M_x(x, y) = \alpha^2 M_{x'}^{iso}(x', y)$$

$$M_y(x, y) = M_y^{iso}(x', y) \tag{4.91}$$

$$M_{xy}(x, y) = \alpha M_{x'y}^{iso}(x', y).$$

By the preceding method, the deflections and moments (per unit length) of an orthotropic plate can be obtained from the deflections and moments

Table 4.3. Maximum deflections and maximum moments of rectangular plates with built-in edges subjected to a uniformly distributed load p ($\nu^{iso} = 0.3$). The locations P_1, P_2, and P_3 are shown in Figure 4.12.

	$w^{iso} = \frac{1}{384}\frac{pL_x'^4}{D^{iso}}c_1$	$M_{x'}^{iso} = -\frac{pL_x'^2}{12}c_2$	$M_y^{iso} = -\frac{pL_x'^2}{12}c_3$	$M_{x'}^{iso} = \frac{pL_x'^2}{24}c_4$	$M_y^{iso} = \frac{pL_x'^2}{24}c_5$
$\frac{L_y}{L_x'}$	at P_1	at P_2	at P_3	at P_1	at P_1
	c_1	c_2	c_3	c_4	c_5
1.0	0.484	0.616	0.616	0.554	0.554
1.1	0.576	0.697	0.646	0.634	0.554
1.2	0.661	0.767	0.665	0.718	0.547
1.4	0.795	0.871	0.682	0.838	0.509
1.6	0.883	0.936	0.685	0.914	0.463
1.8	0.941	0.974	0.685	0.962	0.418
2.0	0.975	0.995	0.685	0.989	0.379
∞	1.000	1.000	0.685	1.000	0.300

(per unit length) of the corresponding isotropic plate. The calculation steps are as follows.

Step 1. We calculate the equivalent length L_x', stiffness D^{iso}, and Poisson's ratio ν^{iso} of the isotropic plate (width L_y):

$$L_x' = \frac{L_x}{\alpha} \qquad D^{iso} = D_{22} \qquad \nu^{iso} = \sqrt{\frac{D_{12}^2}{D_{11}D_{22}}}, \tag{4.92}$$

where

$$\alpha = \sqrt[4]{\frac{D_{11}}{D_{22}}}. \tag{4.93}$$

Step 2. We determine the deflections w^{iso} and moments (per unit length) $M_{x'}^{iso}$, M_y^{iso}, and $M_{x'y}^{iso}$ of the "equivalent" isotropic plate. Maximum deflections and maximum bending moments (per unit length) of isotropic plates (width a, length b, bending stiffness D) subjected to a uniformly distributed load are given by Timoshenko and Woinowsky-Krieger.[13] We modified these results and adopted them for Huber orthotropic plates. The resulting maximum deflections and maximum bending moments are given in Table 4.3.

Step 3. The deflection w^o and moments (per unit length) M_x, M_y, and M_{xy} of the orthotropic plate are calculated by (Eqs. 4.90 and 4.91)

$$w^o = w^{iso} \qquad M_x = \alpha^2 M_{x'}^{iso} \qquad M_y = M_y^{iso} \qquad M_{xy} = \alpha M_{x'y}^{iso}. \tag{4.94}$$

[13] Ibid., p. 202.

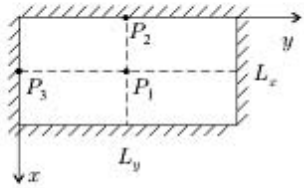

Figure 4.12: Locations where the moments and the deflection are calculated.

The preceding approximate procedure yields the deflections and bending moments of orthotropic plates with built-in edges within about 10 percent.[14]

4.4 Example. *A 0.2-m-long and 0.2-m-wide rectangular plate is made of graphite epoxy unidirectional plies. The material properties are given in Table 3.6 (page 81). The layup is* $[0_2/45_2/90_2/-45_2]_s$. *The plate, built-in along the four edges (Fig. 4.13), is subjected to a uniformly distributed transverse load* $p = 50\,000\ N/m^2$. *Calculate the maximum deflection and the maximum bending moments.*

Solution. We treat this plate as Huber orthotropic. The bending stiffnesses are $D_{11} = 34.61\ \text{N}\cdot\text{m}$, $D_{22} = 12.34\ \text{N}\cdot\text{m}$, $D_{12} = 4.58\ \text{N}\cdot\text{m}$, $D_{66} = 5.14\ \text{N}\cdot\text{m}$ (Table 3.7, page 84). From Eqs. (4.83) and (4.89) we have

$$\alpha = \sqrt[4]{\frac{D_{11}}{D_{22}}} = 1.29\ \text{N}\cdot\text{m} \qquad L_x' = \frac{L_x}{\alpha} = 0.155\ \text{m} \tag{4.95}$$

$$D^{\text{iso}} = D_{22} = 12.34\ \text{N}\cdot\text{m} \qquad \nu^{\text{iso}} = \sqrt{\frac{D_{12}^2}{D_{11}D_{22}}} = 0.222. \tag{4.96}$$

From Table 4.3 (at $L_y/L_x' = 1.29$) we obtain the constants $c_1 = 0.724$, $c_2 = 0.816$, $c_3 = 0.673$, $c_4 = 0.774$, and $c_5 = 0.529$. With the values of these constants the maximum deflection and the maximum bending moments of the corresponding isotropic plate are (Table 4.3)

$$w^{\text{iso}}\big|_{\text{at } P_1} = \frac{1}{384}\frac{pL_x'^4}{D^{\text{iso}}}c_1 = 0.0044\ \text{m} \tag{4.97}$$

$$M_{x'}^{\text{iso}}\big|_{\text{at } P_2} = -\frac{pL_x'^2}{12}c_2 = -81.21\ \frac{\text{N}\cdot\text{m}}{\text{m}} \tag{4.98}$$

$$M_y^{\text{iso}}\big|_{\text{at } P_3} = -\frac{pL_x'^2}{12}c_3 = -66.96\ \frac{\text{N}\cdot\text{m}}{\text{m}} \tag{4.99}$$

$$M_{x'}^{\text{iso}}\big|_{\text{at } P_1} = \frac{pL_x'^2}{24}c_4 = 38.52\ \frac{\text{N}\cdot\text{m}}{\text{m}} \tag{4.100}$$

$$M_y^{\text{iso}}\big|_{\text{at } P_1} = \frac{pL_x'^2}{24}c_5 = 26.33\ \frac{\text{N}\cdot\text{m}}{\text{m}}. \tag{4.101}$$

[14] I. Veres and L. P. Kollár, Approximate Analysis of Mid-plane Symmetric Rectangular Composite Plates. *Journal of Composite Materials*, Vol 36, 673–684, 2002.

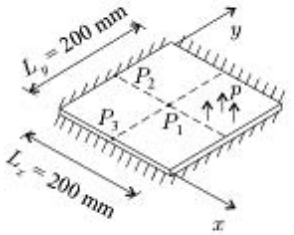

Figure 4.13: The plate in Example 4.4.

The points P_1–P_3 are shown in Figure 4.13. The maximum deflection and the maximum bending moments of the composite plate are (Eq. 4.94)

$$w^{\circ}|_{\text{at } P_1} = w^{\text{iso}}|_{\text{at } P_1} = 0.0044 \text{ m} \tag{4.102}$$

$$M_x|_{\text{at } P_2} = \alpha^2 \, M_{x'}^{\text{iso}}|_{\text{at } P_2} = -135.98 \frac{\text{N} \cdot \text{m}}{\text{m}} \tag{4.103}$$

$$M_y|_{\text{at } P_3} = M_y^{\text{iso}}|_{\text{at } P_3} = -66.96 \frac{\text{N} \cdot \text{m}}{\text{m}} \tag{4.104}$$

$$M_{x'}^{\text{iso}}|_{\text{at } P_1} = \alpha^2 \, M_{x'}^{\text{iso}}|_{\text{at } P_1} = 64.50 \frac{\text{N} \cdot \text{m}}{\text{m}} \tag{4.105}$$

$$M_y^{\text{iso}}|_{\text{at } P_1} = M_y^{\text{iso}}|_{\text{at } P_1} = 26.33 \frac{\text{N} \cdot \text{m}}{\text{m}}. \tag{4.106}$$

4.3 Buckling of Rectangular Plates

4.3.1 Simply Supported Plates – Symmetrical Layup

We consider a rectangular plate with dimensions L_x and L_y simply supported along its four edges (Fig. 4.14). The layup of the plate is symmetrical, $[B] = [0]$.

The plate is subjected to uniformly distributed in-plane loads N_{x0}, N_{y0}, and N_{xy0} around the edges. These loads are increased proportionally, that is, the loads are λN_{x0}, λN_{y0}, λN_{xy0}, where λ is the load parameter. For a buckled plate the load parameter is denoted by λ_{cr}. Following Whitney,[15] we obtain λ_{cr} by the energy method.

The strain energy is (Eq. 4.55)

$$U = \frac{1}{2} \int_0^{L_x} \int_0^{L_y} \left[D_{11} \left(\frac{\partial^2 w^{\circ}}{\partial x^2} \right)^2 + D_{22} \left(\frac{\partial^2 w^{\circ}}{\partial y^2} \right)^2 + D_{66} \left(\frac{2\partial^2 w^{\circ}}{\partial x \partial y} \right)^2 \right.$$
$$\left. + 2 \left(D_{12} \frac{\partial^2 w^{\circ}}{\partial x^2} \frac{\partial^2 w^{\circ}}{\partial y^2} + D_{16} \frac{\partial^2 w^{\circ}}{\partial x^2} \frac{2\partial^2 w^{\circ}}{\partial x \partial y} + D_{26} \frac{\partial^2 w^{\circ}}{\partial y^2} \frac{2\partial^2 w^{\circ}}{\partial x \partial y} \right) \right] dy dx. \tag{4.107}$$

[15] J. M. Whitney, *Structural Analysis of Laminated Anisotropic Plates*. Technomic, Lancaster, Pennsylvania, 1987, p. 151.

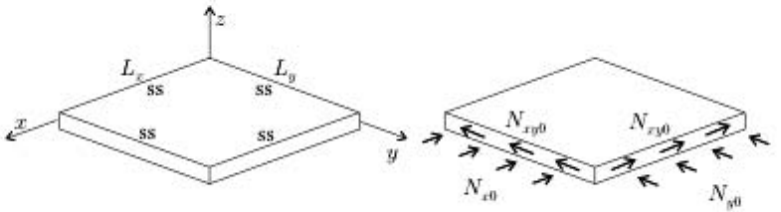

Figure 4.14: Rectangular simply supported (ss) plate subjected to compressive and shear edge loads.

For a plate subjected only to in-plane loads, which do not vary with x and y, the potential of the external forces is[16]

$$\Omega = \frac{1}{2}\int_0^{L_x}\int_0^{L_y}\left[N_x\left(\frac{\partial w^o}{\partial x}\right)^2 + N_y\left(\frac{\partial w^o}{\partial y}\right)^2 + 2N_{xy}\frac{\partial w^o}{\partial x}\frac{\partial w^o}{\partial y}\right]dydx, \quad (4.108)$$

where N_x, N_y, N_{xy} are the in-plane forces (per unit length) inside the plate. These internal in-plane forces are related to the edge loads λN_{x0}, λN_{y0}, λN_{xy0} by

$$N_x = -\lambda N_{x0} \qquad N_y = -\lambda N_{y0} \qquad N_{xy} = -\lambda N_{xy0}. \quad (4.109)$$

We use the Ritz method to obtain the deflection. For the simply supported plate under consideration the geometrical boundary conditions require that the deflection be zero along the edges (Eq. 4.57):

$$w^o = 0 \quad \text{at} \quad \begin{cases} x = 0 & \text{and} \quad 0 \le y \le L_y \\ x = L_x & \text{and} \quad 0 \le y \le L_y \\ 0 \le x \le L_x & \text{and} \quad y = 0 \\ 0 \le x \le L_x & \text{and} \quad y = L_y. \end{cases} \quad (4.110)$$

The following deflection satisfies these geometrical boundary conditions:

$$w^o = \sum_{i=1}^{I}\sum_{j=1}^{J} w_{ij} \sin\frac{i\pi x}{L_x}\sin\frac{j\pi y}{L_y}, \quad (4.111)$$

where I and J are the number of terms, chosen arbitrarily, in the summations; w_{ij} are constants and are calculated from the principle of stationary potential energy (Eq. 2.206) expressed as

$$\frac{\partial \pi_p}{\partial w_{ij}} = \frac{\partial (U + \Omega)}{\partial w_{ij}} = 0. \quad (4.112)$$

We now substitute w^o (from Eq. 4.111) into the expressions of U and Ω (Eqs. 4.107 and 4.108) and perform the differentiation indicated by Eq. (4.112).

[16] S. P. Timoshenko and J. Gere, *Theory of Elastic Stability*. 2nd edition. McGraw-Hill, New York, 1961, p. 349.

Algebraic manipulations result in the following system of simultaneous algebraic equations:

$$\sum_{i=1}^{I}\sum_{j=1}^{J}\left(G_{mnij}-\lambda b_{mnij}\right)w_{ij}=0 \quad \begin{cases} i,m=1,2,3,\ldots,I \\ j,n=1,2,3,\ldots,J. \end{cases} \tag{4.113}$$

For convenience, we introduce the contracted notation

$$k=(i-1)J+j \quad \begin{cases} i=1,2,3,\ldots,I \\ j=1,2,3,\ldots,J \end{cases} \tag{4.114}$$

$$l=(m-1)J+n \quad \begin{cases} m=1,2,3,\ldots,I \\ n=1,2,3,\ldots,J. \end{cases} \tag{4.115}$$

Equation (4.113) may now be written as

$$\sum_{k=1}^{I\times J}G_{kl}w_k=\lambda\sum_{k=1}^{I\times J}b_{kl}w_k, \quad l=1,2,3,\ldots,I\times J, \tag{4.116}$$

where G_{kl} $(=G_{lk})$ is given in Table 4.1 (page 102) and b_{kl} $(=b_{lk})$ is

$$\begin{aligned} b_{lk}=&\frac{1}{4}L_xL_y\pi^2\left[N_{x0}\left(\frac{i}{L_x}\right)^2+N_{y0}\left(\frac{j}{L_y}\right)^2\right]\delta_{lk} \\ &+L_xL_y\pi^2N_{xy0}\left(\frac{i}{L_x}\frac{n}{L_y}r_{mi}r_{jn}+\frac{j}{L_y}\frac{m}{L_x}r_{im}r_{nj}\right). \end{aligned} \tag{4.117}$$

The Kronecker delta δ_{lk} and the parameter r_{ij} are also given in Table 4.1. In expanded form Eq. (4.116) is

$$\left(\begin{bmatrix} G_{11} & \cdots & G_{1(I\times J)} \\ \vdots & \ddots & \\ G_{(I\times J)1} & & G_{(I\times J)(I\times J)} \end{bmatrix}-\lambda\begin{bmatrix} b_{11} & \cdots & b_{1(I\times J)} \\ \vdots & \ddots & \\ b_{(I\times J)1} & & b_{(I\times J)(I\times J)} \end{bmatrix}\right)\begin{Bmatrix} w_1 \\ \vdots \\ w_{(I\times J)} \end{Bmatrix}=\begin{Bmatrix} 0 \\ \vdots \\ 0 \end{Bmatrix}. \tag{4.118}$$

When the plate is not buckled, the deflection is zero, whereas for a buckled plate it is nonzero. The values of λ for the buckled plate (denoted by λ_{cr}) are the eigenvalues of Eq. (4.118), and these can be calculated by commercial software. There are $J\times I$ eigenvalues, of which the lowest gives the lowest buckling load.

We now consider an orthotropic plate subjected to N_{x0} and N_{y0} edge loads. The forces inside the plate are

$$N_x=-\lambda N_{x0} \qquad N_y=-\lambda N_{y0} \qquad N_{xy}=0. \tag{4.119}$$

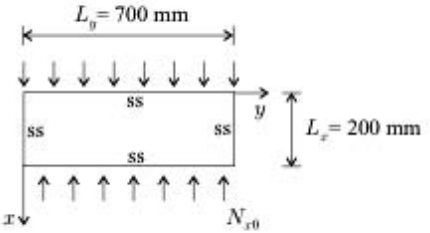

Figure 4.15: The plate in Example 4.5.

For orthotropic laminates we have (Table 3.4, page 76)

$$D_{16} = D_{26} = 0. \tag{4.120}$$

The eigenvalues of Eq. (4.118) can now be calculated directly. The result is

$$(\lambda_{cr})_{ij} = \frac{\pi^2\left[D_{11}\left(\frac{i}{L_x}\right)^4 + 2(D_{12}+2D_{66})\left(\frac{i}{L_x}\right)^2\left(\frac{j}{L_y}\right)^2 + D_{22}\left(\frac{j}{L_y}\right)^4\right]}{N_{x0}\left(\frac{i}{L_x}\right)^2 + N_{y0}\left(\frac{j}{L_y}\right)^2}. \tag{4.121}$$

$(\lambda_{cr})_{ij}$ must be calculated for different sets of i and j, ($i, j = 1, 2, \ldots$). The lowest resulting value of $(\lambda_{cr})_{ij}$ is the value of interest.

Libove[17] showed that, for simply supported orthotropic plates, the lowest buckling load corresponds to a mode that has a half wave in at least one direction. (In this direction either i or j is equal to unity.) When the plate is subjected to uniaxial compression, or to compression in one direction and tension in the other direction, buckling occurs with a half wave perpendicular to the compressive load.[18]

4.5 Example. *A 0.7-m-long and 0.2-m-wide rectangular plate is made of graphite epoxy. The material properties are given in Table 3.6 (page 81). The layup is* $[\pm 45_2^t/0_{12}/\pm 45_2^t]$. *The 0-degree plies are parallel to the short edge of the plate. The plate is simply supported along all four edges. (Fig. 4.15). The plate is subjected to uniform compressive loads along the long edges. Calculate the buckling load.*

Solution. From Eq. (4.121), with $N_{y0} = 0$ and with the stiffnesses $D_{11} = 45.30\,\text{N}\cdot\text{m}$, $D_{22} = 25.26\,\text{N}\cdot\text{m}$, $D_{12} = 19.52\,\text{N}\cdot\text{m}$, $D_{66} = 20.62\,\text{N}\cdot\text{m}$ (Table 3.7, page 84) we have

$$N_{x0}\,(\lambda_{cr})_{ij} = \pi^2\left[D_{11}\left(\frac{i}{L_x}\right)^2 + 2\,(D_{12}+2D_{66})\left(\frac{j}{L_y}\right)^2 + D_{22}\left(\frac{j}{L_y}\right)^4\left(\frac{L_x}{i}\right)^2\right]$$
$$= \left(11.18i^2 + 2.45j^2 + 0.0415\frac{j^4}{i^2}\right)10^3. \tag{4.122}$$

[17] C. Libove, Buckle Pattern for Biaxially Compressed Simply Supported Orthotropic Rectangular Plates. *Journal of Composite Materials*, Vol. 17, 45–48, 1983.

[18] T. K. Tung and J. Surdenas, Buckling of Rectangular Orthotropic Plates under Biaxial Loading. *Journal of Composite Materials*, Vol. 21, 124–128, 1987.

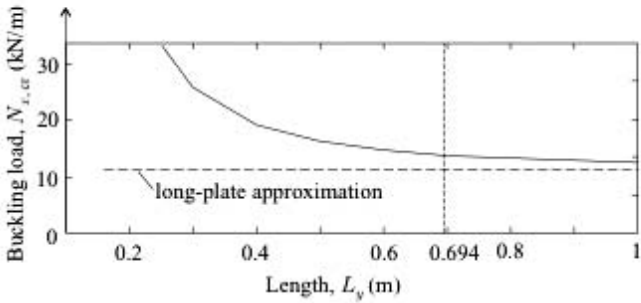

Figure 4.16: The lowest buckling load of the plate in Example 4.5 as a function of the plate length.

The values of $N_{x0}\,(\lambda_{cr})_{ij} \times 10^{-3}$ are

$i \setminus j$	1	2	3
1	13.67	21.63	36.57
2	47.17	54.66	67.58
3	103.04	110.46	122.99.

(4.123)

The lowest value is $N_{x0}\,(\lambda_{cr})_{ij} = 13.67$ kN/m, which corresponds to $i = j = 1$. Thus, the lowest buckling load is

$$N_{x,cr} = (\lambda_{cr})_{11}\, N_{x0} = 13.67 \text{ kN/m}. \tag{4.124}$$

We now assess the length-to-width ratios under which the long-plate approximation is reasonable. To this end, we calculate the lowest buckling loads of the plate, keeping the width L_x the same while changing the length L_y. In Figure 4.16 we plot the buckling loads thus calculated versus L_y. In this figure we also include the lowest buckling load given by the long-plate approximation (Eq. 4.170). The results in this figure show that, in accordance with Eq. (4.19), the long-plate formula is reasonable when L_y is greater than $3L_x\sqrt[4]{D_{11}/D_{22}} = 0.694$ m. At $L_y = 0.694$ m the long-plate formula underestimates the buckling load by about 18 percent.

4.6 Example. *A 0.2-m-long and 0.2-m-wide rectangular plate is made of graphite epoxy unidirectional plies. The material properties are given in Table 3.6 (page 81). The layup is* $[45_2/-45_2/0_{12}/-45_2/45_2]$. *The plate, simply supported along four edges, is subjected to uniform compressive loads along all four edges (Fig. 4.17). Determine the buckling load.*

Solution. The layup of the plate is symmetrical but is not orthotropic. The bending stiffnesses are $D_{11} = 45.30$ N · m, $D_{22} = 25.26$ N · m, $D_{12} = 19.52$ N · m, $D_{66} = 20.62$ N · m, $D_{16} = 4.45$ N · m, $D_{26} = 4.45$ N · m (Table 3.7, page 84). The buckling load is calculated from Eqs. (4.117) and (4.118). With the preceding stiffnesses and

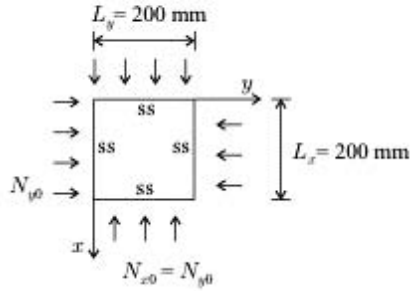

Figure 4.17: The plate in Example 4.6.

with $I = J = 7$, these calculations yield the following results for $(N_{cr})_{ij} \times 10^{-3}$:

$i \setminus j$	1	2	3
1	23.47	45.05	76.62
2	61.25	94.61	132.38
3	119.45	164.43	214.29.

(4.125)

The lowest buckling load is

$$N_{cr} = (N_{cr})_{ij} = 23.47 \text{ kN/m}. \tag{4.126}$$

The layup follows the 10-percent rule (page 89), and we may treat the plate as orthotropic. With $N_{x0} = N_{y0} = N_0$, from Eq. (4.121) we have

$$N_0(\lambda_{cr})_{ij} = \frac{\pi^2\left[D_{11}\left(\frac{i}{L_x}\right)^4 + 2(D_{12} + 2D_{66})\left(\frac{i}{L_x}\right)^2\left(\frac{j}{L_y}\right)^2 + D_{22}\left(\frac{j}{L_y}\right)^4\right]}{\left(\frac{i}{L_x}\right)^2 + \left(\frac{j}{L_y}\right)^2}$$
$$= \frac{(279.4i^4 + 749.5i^2j^2 + 155.8i^4)10^3}{25i^2 + 25j^2}. \tag{4.127}$$

The values of $N_0\,(\lambda_{cr})_{ij} \times 10^{-3}$ are

$i \setminus j$	1	2	3
1	23.70	46.16	78.58
2	61.00	94.78	135.61
3	118.14	160.34	213.26.

(4.128)

The lowest value is $N_0\,(\lambda_{cr})_{ij} = 23.70$ kN/m, which corresponds to $i = j = 1$. Thus, the lowest buckling load is

$$N_{cr} = (\lambda_{cr})_{11}\, N_0 = 23.70 \text{ kN/m}. \tag{4.129}$$

This buckling load, based on the orthotropy approximation, is within 1 percent of the buckling load given by Eq. (4.126).

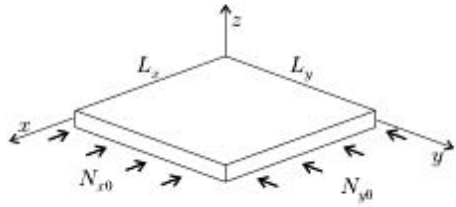

Figure 4.18: Rectangular plate subjected to uniform biaxial compressive edge loads.

4.3.2 Plates with Built-In and Simply Supported Edges – Orthotropic and Symmetrical Layup

We consider rectangular plates with length L_x and width L_y (Fig. 4.18). The layup of the plate is orthotropic and symmetrical. Each edge of the plate is either simply supported or built-in. Uniformly distributed in-plane loads N_{x0} and N_{y0} act along the edges.

The edge loads are increased proportionally to $\lambda N_{x0}, \lambda N_{y0}$, where λ is the load parameter. For the buckled plate the load parameter is denoted by λ_{cr}. We apply the Ritz method to find λ_{cr}.[19]

The expression of the potential energy is obtained by setting N_{xy} and D_{16} and D_{26} equal to zero (orthotropy) in Eqs. (4.107) and (4.108)

$$\pi_p = U + \Omega = \frac{1}{2}\int_0^{L_x}\int_0^{L_y}\left[D_{11}\left(\frac{\partial^2 w^o}{\partial x^2}\right)^2 + D_{22}\left(\frac{\partial^2 w^o}{\partial y^2}\right)^2 + D_{66}\left(\frac{2\partial^2 w^o}{\partial x \partial y}\right)^2 + 2D_{12}\frac{\partial^2 w^o}{\partial x^2}\frac{\partial^2 w^o}{\partial y^2} + N_x\left(\frac{\partial w^o}{\partial x}\right)^2 + N_y\left(\frac{\partial w^o}{\partial y}\right)^2\right] dydx, \tag{4.130}$$

where N_x and N_y are the in-plane loads (per unit length) inside the plate, which are related to the edge forces by

$$N_x = -\lambda N_{x0}, \qquad N_y = -\lambda N_{y0}, \tag{4.131}$$

and w^o is the deflection of the midplane, which is assumed to be of the form

$$w^o = AX_i(x)Y_j(y), \tag{4.132}$$

where A is an unknown amplitude. For the $X_i(x)$ and $Y_j(y)$ displacement functions we adopt the shape of a freely vibrating beam. (The $X_i(x)$ function is illustrated in Fig. 4.19.) For different end supports $X_i(x)$ and $Y_j(y)$ are given in Table 4.4 (page 119).

By virtue of the principle of stationary potential energy (Eq. 2.206), we have

$$\frac{\partial \pi_p}{\partial A} = 0. \tag{4.133}$$

[19] I. Veres and L. P. Kollár, Buckling of Orthotropic Plates with Different Edge Supports. *Journal of Composite Materials*, Vol. 35, 625–635, 2001.

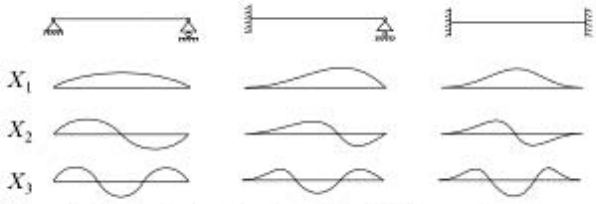

Figure 4.19: Freely vibrating beam. The displacements correspond to $X_i(x), i = 1, 2, 3$.

Equations (4.130) and (4.133), together with Eq. (4.132) and the expressions in Table 4.4, yield

$$\left[\frac{D_{11}}{L_x^4}\alpha_1^4 + \frac{D_{22}}{L_y^4}\alpha_3^4 + 2\left(D_{12}+2D_{66}\right)\frac{1}{L_x^2 L_y^2}\alpha_2 - \lambda_{cr}\left(\frac{N_{x0}}{L_x^2}\alpha_4 + \frac{N_{y0}}{L_y^2}\alpha_5\right)\right] = 0. \tag{4.134}$$

The parameters $\alpha_1, \alpha_2, \alpha_3, \alpha_4, \alpha_5$ are defined in Table 4.5 (page 120). The integrations indicated in Table 4.5 simplify when $X_i(x)$ and $Y_j(y)$ are calculated by the approximate expressions of μ_i given in Table 4.4. The resulting approximate expressions for α_1 through α_5 are given in Tables 4.6 and 4.7, and α_2 is

$$\alpha_2 = \alpha_4\alpha_5. \tag{4.135}$$

By rearranging Eq. (4.134), we obtain the following expression for λ_{cr}:

$$(\lambda_{cr})_{ij} = \frac{D_{11}\frac{\alpha_1^4}{L_x^4} + D_{22}\frac{\alpha_3^4}{L_y^4} + 2\left(D_{12}+2D_{66}\right)\frac{\alpha_4\alpha_5}{L_x^2 L_y^2}}{\left(N_{x0}\frac{\alpha_4}{L_x^2} + N_{y0}\frac{\alpha_5}{L_y^2}\right)}. \tag{4.136}$$

This equation applies when each edge is either simply supported or built-in. When all four edges are simply supported, Eq. (4.136) simplifies to Eq. (4.121).

Table 4.4. The displacement function X_i of a freely vibrating beam. The parameter μ_i is to be determined either from the exact or from the approximate expression. (Also: $\xi = \frac{x}{L_x}$.) For Y_j the same formulas apply with ξ, x, L_x, i replaced by η, y, L_y, j, respectively.

L_x	$X_i = \sin(i\pi\xi)$
L_x	$X_i = \gamma_i\cos(\mu_i\xi) - \gamma_i\cosh(\mu_i\xi) + \sin(\mu_i\xi) - \sinh(\mu_i\xi)$ $\tan\mu_i - \tanh\mu_i = 0$ (Exact) $\mu_i \approx (i+0.25)\pi$ (Approximate) $\gamma_i = \frac{\sin\mu_i - \sinh\mu_i}{\cosh\mu_i - \cos\mu_i}$
L_x	$X_i = \gamma_i\cos(\mu_i\xi) - \gamma_i\cosh(\mu_i\xi) + \sin(\mu_i\xi) - \sinh(\mu_i\xi)$ $\cos\mu_i\cosh\mu_i = 1$ (Exact) $\mu_i \approx (i+0.5)\pi$ (Approximate) $\gamma_i = \frac{\cos\mu_i - \cosh\mu_i}{\sin\mu_i + \sinh\mu_i}$

Table 4.5. The coefficients α_1 through α_5

$$\alpha_1 \equiv \sqrt[4]{\frac{1}{c_x^2}\int_0^1 \left(\frac{\partial^2 X_i}{\partial \xi^2}\right)^2 d\xi} \qquad \alpha_3 \equiv \sqrt[4]{\frac{1}{c_y^2}\int_0^1 \left(\frac{\partial^2 Y_j}{\partial \eta^2}\right)^2 d\eta}$$

$$\alpha_4 \equiv \frac{1}{c_x^2}\int_0^1 \left(\frac{\partial X_i}{\partial \xi}\right)^2 d\xi \qquad \alpha_5 \equiv \frac{1}{c_y^2}\int_0^1 \left(\frac{\partial Y_j}{\partial \eta}\right)^2 d\eta$$

$$\alpha_2 \equiv \frac{1}{c_x^2}\frac{1}{c_y^2}\int_0^1 \left(\frac{\partial X_i}{\partial \xi}\right)^2 d\xi \int_0^1 \left(\frac{\partial Y_j}{\partial \eta}\right)^2 d\eta$$

$$c_x \equiv \sqrt{\int_0^1 X_i^2 d\xi} \qquad c_y \equiv \sqrt{\int_0^1 Y_j^2 d\eta}$$

Table 4.6. Approximate expressions for the coefficients α_1 and α_4 (i represents the number of half waves in the x direction)

	α_1	α_4	i
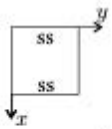	$i\pi$	$i^2\pi^2$	1, 2, 3, . . .
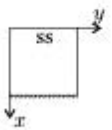	$(i+0.25)\,\pi$	$\alpha_1(\alpha_1-1)$	1, 2, 3, . . .
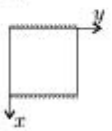	4.730 $(i+0.5)\,\pi$	$\alpha_1(\alpha_1-2)$ $\alpha_1(\alpha_1-2)$	1 2, 3, 4, . . .

Table 4.7. Approximate expressions for the coefficients α_3 and α_5 (j represents the number of half waves in the y direction)

	α_3	α_5	j
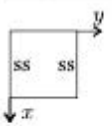	$j\pi$	$j^2\pi^2$	1, 2, 3, . . .
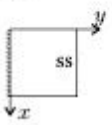	$(j+0.25)\,\pi$	$\alpha_3(\alpha_3-1)$	1, 2, 3, . . .
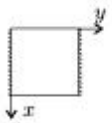	4.730 $(j+0.5)\,\pi$	$\alpha_3(\alpha_3-2)$ $\alpha_3(\alpha_3-2)$	1 2, 3, 4, . . .

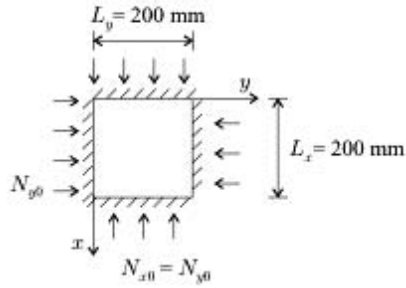

Figure 4.20: The plate in Example 4.7.

The critical load parameter must be calculated for different sets of i and j, $(i, j = 1, 2, \ldots)$. The lowest resulting value of λ_{cr} is the value of interest. The lowest buckling load (as in the case of simply supported plates) corresponds to a mode that has a half wave in at least one direction. (In this direction either i or j is equal to unity.) When the plate is subjected to uniaxial compression, or to compression in one direction and tension in the other direction, buckling occurs with a half wave perpendicular to the compressive load.

4.7 Example. *A 0.2-m-long and 0.2-m-wide rectangular plate is made of graphite epoxy unidirectional plies. The material properties are given in Table 3.6 (page 81). The layup is* $[45_2/-45_2/0_{12}/-45_2/45_2]$. *The plate, built-in along the four edges, is subjected to uniform compressive loads along all four edges (Fig. 4.20). Determine the buckling load.*

Solution. The layup follows the 10-percent rule (page 89), and we treat the plate as orthotropic. With the stiffnesses $D_{11} = 45.30\ \text{N}\cdot\text{m}$, $D_{22} = 25.26\ \text{N}\cdot\text{m}$, $D_{12} = 19.52\ \text{N}\cdot\text{m}$, $D_{66} = 20.62\ \text{N}\cdot\text{m}$ (Table 3.7, page 84) and with $N_{x0} = N_{y0} = N_0$, from Eq. (4.136) we have

$$N_0\,(\lambda_{cr})_{ij} = \frac{D_{11}\frac{\alpha_1^4}{L_x^4} + D_{22}\frac{\alpha_3^4}{L_y^4} + 2\,(D_{12} + 2D_{66})\,\frac{\alpha_4\alpha_5}{L_x^2 L_y^2}}{\frac{\alpha_4}{L_x^2} + \frac{\alpha_5}{L_y^2}}, \tag{4.137}$$

where α_1 and α_4 depend on i $(i = 1, 2, \ldots)$ and α_3 and α_5 depend on j $(j = 1, 2, \ldots)$ as given in Tables 4.6 and 4.7, third row. From these tables the values are

	$i=1$	$i=2$	$i=3$
α_1	4.73	7.85	11.00
α_4	12.91	45.98	98.91

	$j=1$	$j=2$	$j=3$
α_3	4.73	7.85	11.00
α_5	12.91	45.98	98.91 .

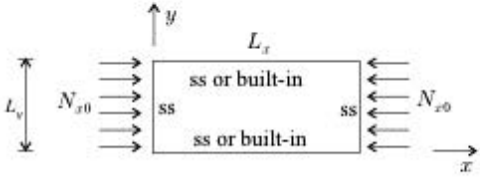

Figure 4.21: Uniaxially loaded rectangular plate.

The values of $N_0 (\lambda_{cr})_{ij} \times 10^{-3}$ are (Eq. 4.137)

$i \setminus j$	1	2	3
1	53.80	81.05	122.31
2	109.16	142.82	188.79
3	185.55	226.18	280.57.

The lowest value is $N_0 (\lambda_{cr})_{ij} = 53.80$ kN/m, which corresponds to $i = j = 1$, Thus, the lowest buckling load is

$$N_{cr} = (\lambda_{cr})_{11} N_0 = 53.80 \text{ kN/m}. \tag{4.138}$$

Uniform compressive load in the x direction. We consider a plate with the edges parallel to the y-axis simply supported and the edges parallel to the x-axis either simply supported or built-in (Fig. 4.21). The plate is subjected to a uniaxial compressive load N_{x0} in the x direction. By introducing the notation $N_{x,cr} = \lambda_{cr} N_{x0}$ and by setting $N_{y0} = 0$, Eq. (4.136) may be rearranged to yield

$$N_{x,cr} = D_{11} \frac{\alpha_1^4}{\alpha_4} \frac{1}{L_x^2} + D_{22} \frac{\alpha_3^4}{\alpha_4} \frac{L_x^2}{L_y^4} + 2 (D_{12} + 2D_{66}) \frac{\alpha_5}{L_y^2}, \tag{4.139}$$

where α_1 and α_4 depend on i ($i = 1, 2, \ldots$) and α_3 and α_5 depend on j ($j = 1, 2, \ldots$) (Tables 4.6 and 4.7). The values of i and j (and the corresponding values of $\alpha_1, \alpha_4, \alpha_3$, and α_5) that yield the lowest value of $N_{x,cr}$ are determined as follows.

To determine j, we observe that both α_3 and α_5 increase monotonically with j (Table 4.7). Hence, the right-hand side of Eq. (4.139) also increases with j. Thus, the lowest buckling load corresponds to $j = 1$. At this load the buckled shape is a half wave in the direction perpendicular to the load. This is illustrated in Figure 4.22 for a simply supported plate.

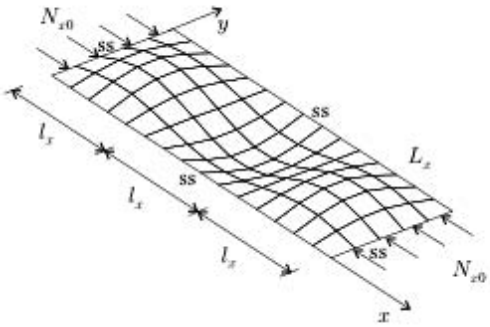

Figure 4.22: Buckled shape of a uniaxially loaded rectangular plate with simply supported edges.

Table 4.8. Buckling loads of unidirectionally loaded plates (orthotropic and symmetrical layup) with simply supported, built-in, and rotationally restrained edges ($l_x = L_x/i$, $i = 1, 2, \ldots$, $\xi = \frac{1}{1+10\zeta}$, $\zeta = \frac{D_{22}}{\tilde{k}L_y}$); L_x, L_y are the length and the width, respectively, and $\tilde{k}$ is the spring constant

Supports	Buckling load $N_{x,cr}$
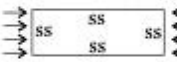	$\frac{\pi^2}{L_y^2}\left(D_{11}\frac{L_y^2}{l_i^2} + D_{22}\frac{l_i^2}{L_y^2} + 2(D_{12}+2D_{66})\right)$
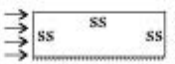	$\frac{\pi^2}{L_y^2}\left(D_{11}\frac{L_y^2}{l_i^2} + 2.441D_{22}\frac{l_i^2}{L_y^2} + 2.33(D_{12}+2D_{66})\right)$
	$\frac{\pi^2}{L_y^2}\left(D_{11}\frac{L_y^2}{l_i^2} + 5.139D_{22}\frac{l_i^2}{L_y^2} + 2.62(D_{12}+2D_{66})\right)$
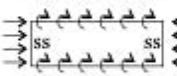	$\frac{\pi^2}{L_y^2}\left(D_{11}\frac{L_y^2}{l_i^2} + (1+4.139\xi)D_{22}\frac{l_i^2}{L_y^2} + (2+0.62\xi^2)(D_{12}+2D_{66})\right)$

To determine α_1 and α_4 we recall that the edges parallel to the y-axis are simply supported. The corresponding values of α_1 and α_4 are given in the first row of Table 4.6 and are

$$\alpha_1 = i\pi \qquad \alpha_4 = i^2\pi^2. \tag{4.140}$$

With these values of α_1 and α_4 Eq. (4.139) becomes

$$N_{x,cr} = D_{11}\pi^2\frac{1}{l_x^2} + D_{22}\frac{\alpha_3^4}{\pi^2}\frac{l_x^2}{L_y^4} + 2(D_{12}+2D_{66})\frac{\alpha_5}{L_y^2}, \tag{4.141}$$

where l_x is the length of the half buckling wave

$$l_x = \frac{L_x}{i}. \tag{4.142}$$

The values of α_3 and α_5 to be used are those given in Table 4.7 for $j = 1$. The resulting buckling loads are listed in the first three rows of Table 4.8.

The value of $N_{x,cr}$ must be calculated for different values of i ($i = 1, 2, \ldots$), and, generally the lowest resulting value is of interest.

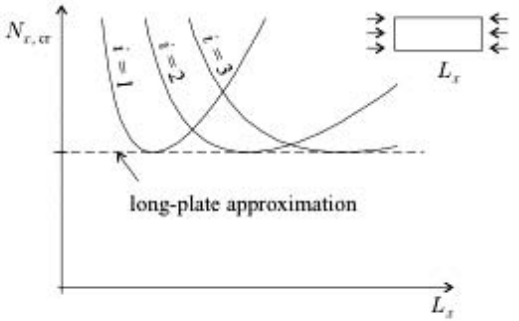

Figure 4.23: Buckling loads of unidirectionally loaded rectangular plates with simply supported or built-in edges. The plate's length is L_x.

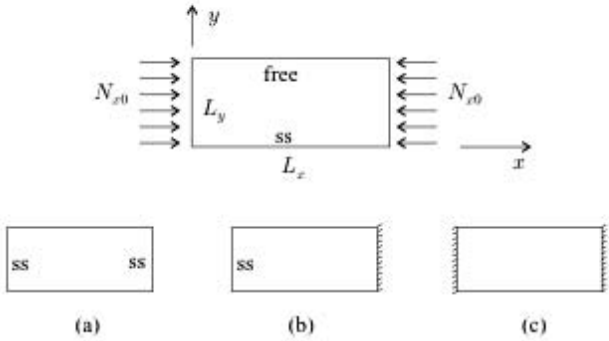

Figure 4.24: Supports along edges parallel (top) and perpendicular (bottom) to the load direction.

The buckling loads of plates with simply supported or built-in edges (Fig. 4.21) are illustrated in Figure 4.23. For each value of i the lowest buckling load is the same as the lowest buckling load of the corresponding long plate that will be given, subsequently, in the first three rows of Table 4.11 (page 136).

4.3.3 Plates with One Free Edge – Orthotropic and Symmetrical Layup

We consider a rectangular plate with length L_x and width L_y. The layup of the plate is orthotropic and symmetrical.

One Edge Parallel to the x Axis is Simply Supported; the Other is Free

The plate is simply supported along the $y = 0$ edge and is free along the $y = L_y$ edge (Fig. 4.24, top). The edges parallel to the y-axis may be either simply supported or built-in (Fig. 4.24, bottom). The plate is subjected to uniform uniaxial compression N_{x0} in the x direction (Fig. 4.24, top). We wish to determine the lowest value of the load at which the plate buckles.

Edges parallel to the y-axis are simply supported. We consider plates whose edges parallel to the y-axis are simply supported (Fig. 4.24, a). The buckling loads are denoted by $N_{x,cr}$. An exact analysis resulting in a transcendental equation for $N_{x,cr}$ is given by Whitney.[20] Here, we present an approximate analysis, which yields a closed-form expression for $N_{x,cr}$. In our analysis we apply the Ritz method and approximate the buckled shape (shown in Fig. 4.25) by

$$w^o = Ay \sin\left(\frac{\pi x}{L_x}\right). \tag{4.143}$$

where A is a constant and w^o is the deflection, which satisfies the geometrical boundary condition ($w^o = 0$) along the simply supported edges.

[20] J. M. Whitney, *Structural Analysis of Laminated Anisotropic Plates*. Technomic, Lancaster, Pennsylvania, 1987, p. 108.

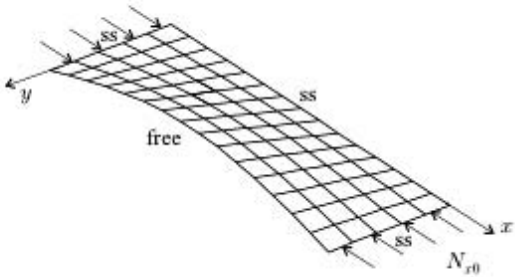

Figure 4.25: Buckled shape of a rectangular plate with one free and three simply supported edges.

We express the potential energy of the plate by setting $N_y = 0$ and $N_x = -N_{x0}$ in Eq. (4.130):

$$\pi_p = \frac{1}{2}\int_0^{L_x}\int_0^{L_y}\left[D_{11}\left(\frac{\partial^2 w^o}{\partial x^2}\right)^2 + D_{22}\left(\frac{\partial^2 w^o}{\partial y^2}\right)^2 + D_{66}\left(\frac{2\partial^2 w^o}{\partial x \partial y}\right)^2 + 2\left(D_{12}\frac{\partial^2 w^o}{\partial x^2}\frac{\partial^2 w^o}{\partial y^2}\right)\right]dydx - \frac{1}{2}\int_0^{L_x}\int_0^{L_y}\left[N_{x0}\left(\frac{\partial w^o}{\partial x}\right)^2\right]dydx. \quad (4.144)$$

By introducing Eq. (4.143) into Eq. (4.144), we arrive at the following expression for the potential energy:

$$\pi_p = \frac{A^2 L_x}{4}\left\{D_{11}\frac{L_y^3}{3}\frac{\pi^4}{L_x^4} + 4D_{66}L_y\frac{\pi^2}{L_x^2} - N_{x0}\frac{L_y^3}{3}\frac{\pi^2}{L_x^2}\right\}. \quad (4.145)$$

Table 4.9. Buckling loads of unidirectionally loaded plates (orthotropic and symmetrical layup) with one free edge ($l_x = L_x/i, i = 1, 2, \ldots, \zeta = \frac{D_{22}}{\widetilde{k}L_y}$); L_x, L_y are the length and the width, respectively, and $\widetilde{k}$ is the spring constant

Supports	Buckling load $N_{x,cr}$
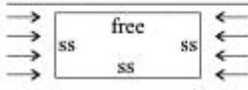	$\frac{\pi^2 D_{11}}{L_x^2} + \frac{12D_{66}}{L_y^2}$
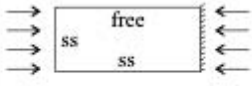	$\frac{\pi^2 D_{11}}{(0.7L_x)^2} + \frac{12D_{66}}{L_y^2}$
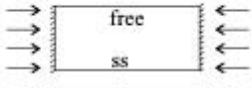	$\frac{\pi^2 D_{11}}{(0.5L_x)^2} + \frac{12D_{66}}{L_y^2}$
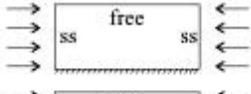	$\frac{1.25l_x^2 D_{22}}{L_y^4} + \frac{\pi^2 D_{11}}{l_x^2} + \frac{12D_{66}}{L_y^2}$
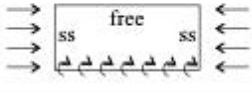	$\frac{1.25}{1+4.12\zeta}\frac{l_x^2 D_{22}}{L_y^4} + \frac{\pi^2 D_{11}}{l_x^2} + \frac{12D_{66}}{L_y^2}$

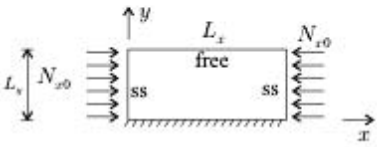

Figure 4.26: Support along the edges of a uniaxially loaded rectangular plate.

By virtue of the principle of stationary potential energy $\partial \pi_p / \partial A = 0$ (Eq. 2.206), and we have

$$N_{x,cr} = \frac{\pi^2 D_{11}}{L_x^2} + \frac{12 D_{66}}{L_y^2}. \tag{4.146}$$

One or Both Edges Parallel to the y-Axis are Built-in

The buckling loads of plates that have one or both edges parallel to the y-axis built-in (Fig. 4.24, b and c) can be derived in a way similar to that of Eq. (4.146). The details are not given here; the resulting buckling loads are given in Table 4.9.

One edge parallel to the x-axis is built-in; the other is free. The plate is built-in along the $y = 0$ edge, is free along the $y = L_y$ edge, and is simply supported along the $x = 0$ and $x = L_x$ edges (Fig. 4.26). The plate is subjected to uniform uniaxial compression N_{x0} in the x direction. We wish to determine the lowest value of the load at which the plate buckles (Fig. 4.27). An exact analysis, resulting in transcendental equations for the buckling loads $N_{x,cr}$, is given by Bank and Yin.[21] An approximate expression for $N_{x,cr}$ is[22]

$$N_{x,cr} = \frac{\pi^2 D_{11}}{l_x^2} + 1.25 \frac{l_x^2 D_{22}}{L_y^4} + \frac{12 D_{66}}{L_y^2}, \tag{4.147}$$

where $l_x = L_x / i$ is the length of the half buckling wave in the x direction and $i = 1, 2, \ldots$ is the number of half waves in the x direction.

Equation (4.147) underestimates the buckling loads by less than 14 percent.

The value of $N_{x,cr}$ must be calculated for different values of i ($i = 1, 2, \ldots$) and, in general, the lowest resulting value is of interest.

The buckling load is a function of the length of the plate L_x (Fig. 4.23). For each value of i the lowest buckling load is the same as the lowest buckling load of the corresponding long plate given subsequently in the fifth row of Table 4.11 (page 136).

4.8 Example. *A rectangular plate with length $L_x = 0.5$ m and width $L_y = 0.05$ m is made of graphite epoxy unidirectional plies with the fibers oriented along the x-axis of the plate (Fig. 4.28). The material properties are given in Table 3.6 (page 81). The layup is $[0_{20}]$. One of the long edges is built-in; the other long edge is free. The short edges are simply supported. The plate is subjected to uniform compressive loads in the x direction. Calculate the buckling load.*

[21] L. C. Bank and J. Yin, Buckling of Orthotropic Plates with Free and Rotationally Restrained Unloaded Edges. *Thin-Walled Structures*, Vol. 24, 83–96, 1996.

[22] L. P. Kollár, Buckling of Unidirectionally Loaded Composite Plates with One Free and One Rotationally Restrained Unloaded Edge. *Journal of Structural Engineering*, Vol. 128, 1202–1211, 2002.

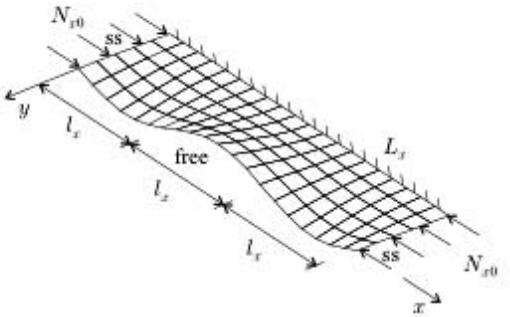

Figure 4.27: Buckled shape of a uniaxially loaded rectangular plate with a built-in and a free longitudinal edge.

Solution. The expression in Table 4.9, fourth row (page 125), together with the stiffnesses $D_{11} = 99.25\,\mathrm{N\cdot m}$, $D_{22} = 6.47\,\mathrm{N\cdot m}$, $D_{12} = 1.94\,\mathrm{N\cdot m}$, $D_{66} = 3.03\,\mathrm{N\cdot m}$ (Table 3.7, page 84) gives

$$N_{x,\mathrm{cr}} = \frac{\pi^2 D_{11}}{l_x^2} + 1.25\frac{l_x^2 D_{22}}{L_y^4} + \frac{12 D_{66}}{L_y^2}$$
$$= 979.5\frac{1}{l_x^2} + 1.294 \times 10^6 l_x^2 + 14\,560, \qquad (4.148)$$

where $l_x = L_x/i$. The buckling loads for $i = 1, 2, 3, 4, 5, 6$ are

i	1	2	3	4	5	6
$N_{x,\mathrm{cr}}$ (kN/m)	342.04	111.12	85.78	97.47	125.46	164.60

The lowest buckling load corresponds to $i = 3$ and is 85.78 kN/m.

The buckling loads of plates of the same width but with different lengths are given by solid lines in Figure 4.29. The buckling loads calculated by the equations of Bank and Yin[23] are also included in this figure. The approximate formula (Eq. 4.148) underestimates $N_{x,\mathrm{cr}}$, and, hence, is a conservative estimate.

The long-plate expression gives the lowest buckling load of this plate as 90.64 kN/m (Example 4.11, page 138). This value is also shown in Figure 4.29.

4.3.4 Plates with Rotationally Restrained Edges – Orthotropic and Symmetrical Layup

We consider a rectangular plate with length L_x and width L_y. The layup of the plate is orthotropic and symmetrical. The plate is simply supported along the edges parallel to the y-axis. The $y = 0$ edge is rotationally restrained, the $y = L_y$ edge is either rotationally restrained (Fig. 4.30, left) or free (Fig 4.30, right). Along a rotationally restrained edge the bending moment is proportional to the rotation

[23] L. C. Bank and J. Yin, Buckling of Orthotropic Plates with Free and Rotationally Restrained Unloaded Edges. *Thin-Walled Structures*, Vol. 24, 83–96, 1996.

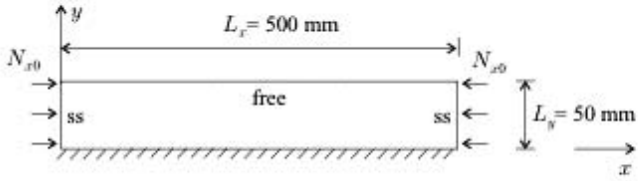

Figure 4.28: The plate in Example 4.8.

of the edge

$$M_y = \widetilde{k}\frac{\partial w}{\partial y}, \tag{4.149}$$

where $\widetilde{k}$ is the rotational spring constant. The rotational spring constant is further discussed in Section 6.9.3.

The plate is subjected to uniform uniaxial compression N_{x0} in the x direction. We wish to determine the lowest value of the load at which the plate buckles.

Both Unloaded Edges are Rotationally Restrained

We consider a plate that is rotationally restrained along the $y = 0$ and the $y = L_y$ edges (Fig. 4.30, left). An exact analysis resulting in a transcendental equation for the buckling loads $N_{x,\mathrm{cr}}$ is given by Qiao et al.[24] Here, we present an approximate analysis, which yields a closed-form expression for $N_{x,\mathrm{cr}}$.

The buckling load of a plate with rotationally restrained edges must be between the buckling load of a simply supported plate (Table 4.8, first row, page 123) and the buckling load of a plate with built-in edges (Table 4.8, third row). We combine the expressions for plates with simply supported and built-in edges and write

$$N_{x,\mathrm{cr}} = \frac{\pi^2}{L_y^2}\left(D_{11}\frac{L_y^2}{l_x^2} + (1+4.139\xi)\,D_{22}\frac{l_x^2}{L_y^2} + (2+0.62\xi')\,(D_{12}+2D_{66})\right), \tag{4.150}$$

where ξ and ξ' are parameters that depend on the support conditions along the unloaded edges. These parameters are zero for a plate with simply supported unloaded edges and are unity for a plate with built-in unloaded edges. The values of ξ and ξ' may be approximated by[25]

$$\xi = \frac{1}{1+10\zeta} \qquad \xi' = \xi^2, \tag{4.151}$$

where ζ is the parameter of restraint

$$\zeta = \frac{D_{22}}{\widetilde{k}L_y}. \tag{4.152}$$

[24] P. Qiao, J. F. Davalos, and J. Wang, Local Buckling of Composite FRP Shapes by Discrete Plate Analysis. *Journal of Structural Engineering*, Vol. 127, 245–255, 2001.

[25] L. P. Kollár, Discussion on the paper of Qiao, P. Davalos, J. F. and Wang, J.: Local Buckling of Composite FRP Shapes by Discrete Plate Analysis. *Journal of Structural Engineering*, Vol 128, 1091–1093, 2002.

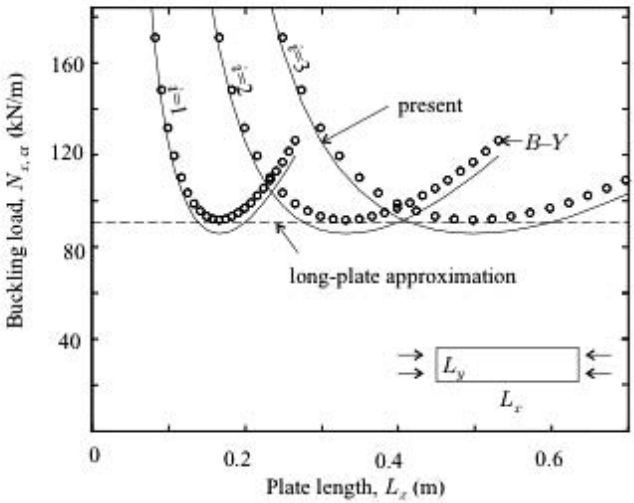

Figure 4.29: Buckling loads of the plate in Example 4.8. The results shown are by Eq. (4.148) (labeled as "present"), by Bank and Yin's equations, and by the long-plate approximation.

With these approximations of ξ and ξ', Eq. (4.150) overestimates the buckling load by less than 3.5 percent when $0 < K \leq 1$ and by less than 6.5 percent when $1 < K \leq 3$, where K is a stiffness parameter defined as

$$K = \frac{2D_{66} + D_{12}}{\sqrt{D_{11}D_{22}}}. \tag{4.153}$$

For most practical layups K is less than 3.

Equation (4.150) is included in Table 4.8 (page 123).

The value of $N_{x,cr}$ must be calculated for different values of i ($i = 1, 2, \ldots$), and, generally, the lowest resulting value is of interest.

The buckling load is a function of the length of the plate L_x (Fig. 4.23). For each value of i the lowest buckling load is the same as the lowest buckling load of the corresponding long plate given subsequently in the fourth row of Table 4.11 (page 136).

One Unloaded Edge is Rotationally Restrained; the Other is Free

The plate is rotationally restrained along the $y = 0$ edge and is free along the $y = L_y$ edge (Fig. 4.30, right). An exact analysis resulting in transcendental equations

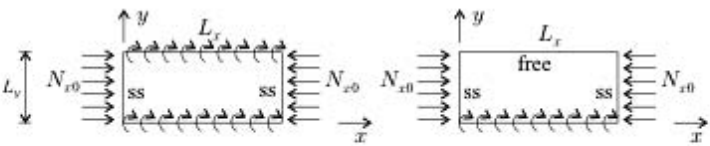

Figure 4.30: Uniaxially loaded rectangular plate with two rotationally restrained edges or with one rotationally restrained and one free edge.

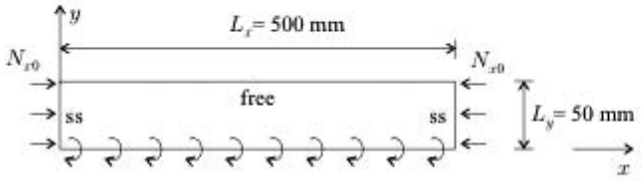

Figure 4.31: The plate in Example 4.9.

for the buckling loads $N_{x,cr}$ is given by Bank and Yin.[26] Here, we present an approximate analysis, which yields a closed-form expression for $N_{x,cr}$.

The buckling load of a plate with a rotationally restrained edge must be between the buckling load of a plate with a simply supported edge (Table 4.9, first row, page 125) and the buckling load of a plate with a built-in edge (Table 4.9, fourth row). We combine the expressions for plates with a simply supported and with a built-in edge and write

$$N_{x,cr} = \frac{\pi^2 D_{11}}{l_x^2} + \xi'' \frac{1.25 l_x^2 D_{22}}{L_y^4} + \frac{12 D_{66}}{L_y^2}, \tag{4.154}$$

where $l_x = L_x/i$ is the length of the half buckling wave in the x direction, $i = 1, 2, \ldots$ is the number of half waves in the x direction, and ξ'' is a parameter that depends on the supports along the unloaded edge. This parameter is zero for a plate with a simply supported unloaded edge and is equal to unity for a plate with a built-in unloaded edge. The value of ξ'' may be approximated by[27]

$$\xi'' = \frac{1}{1 + 4.12\zeta}, \tag{4.155}$$

where ζ is the parameter of restraint given by Eq. (4.152).

Equation (4.154) may underestimate the buckling load by up to 14 percent.

The value of $N_{x,cr}$ must be calculated for different values of i ($i = 1, 2, \ldots$), and, generally, the lowest resulting $N_{x,cr}$ is the value of interest.

The buckling load is a function of the length of the plate L_x (Fig. 4.23). For each value of i the lowest buckling load is the same as the lowest buckling load of the corresponding long plate given subsequently in the sixth row of Table 4.11 (page 136).

4.9 Example. *A rectangular plate with length $L_x = 0.5$ m and width $L_y = 0.05$ m is made of graphite epoxy unidirectional plies with the fibers oriented along the x-axis of the plate (Fig. 4.31). The material properties are given in Table 3.6 (page 81). The layup is $[0_{20}]$. One of the long edges is rotationally restrained while the other long edge is free. The short edges are simply supported. The rotational spring constant of the edge is $\widetilde{k} = 129.4$ N. The plate is subjected to uniform compressive loads in the x direction. Calculate the buckling load.*

[26] L. C. Bank and J. Yin, Buckling of Orthotropic Plates with Free and Rotationally Restrained Unloaded Edges. *Thin-Walled Structures*, Vol. 24, 83–96, 1996.

[27] L. P. Kollár, Buckling of Unidirectionally Loaded Composite Plates with One Free and One Rotationally Restrained Unloaded Edge. *Journal of Structural Engineering*, Vol 128, 1202–1211, 2002.

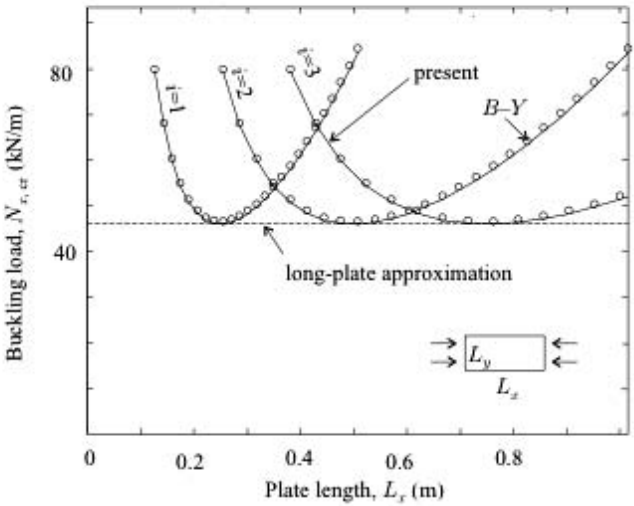

Figure 4.32: Buckling loads of the plate in Example 4.9. The results shown are by Eq. (4.156) (labeled as "present"), by Bank and Yin's equations, and by the long-plate approximation.

Solution. The expression in Table 4.9, fifth row (page 125), together with the stiffnesses $D_{11} = 99.25\,\mathrm{N\cdot m}$, $D_{22} = 6.47\,\mathrm{N\cdot m}$, $D_{12} = 1.94\,\mathrm{N\cdot m}$, $D_{66} = 3.03\,\mathrm{N\cdot m}$ (Table 3.7, page 84) gives

$$N_{x,cr} = \frac{\pi^2 D_{11}}{l_x^2} + \frac{1.25}{1+4.12\zeta}\frac{l_x^2 D_{22}}{L_y^4} + \frac{12 D_{66}}{L_y^2}$$
$$= 979.5\frac{1}{l_x^2} + 0.253\times 10^6 l_x^2 + 14\,560, \qquad (4.156)$$

where $l_x = L_x/i$ and ζ is the parameter of restraint (Eq. 4.152):

$$\zeta = \frac{D_{22}}{\widetilde{k} L_y} = 1. \qquad (4.157)$$

The buckling loads for $i = 1, 2, 3, 4, 5, 6$ are

i	1	2	3	4	5	6
$N_{x,cr}$ (kN/m)	81.67	46.03	56.85	81.20	115.04	157.37

The lowest buckling load corresponds to $i = 2$ and is 46.03 kN/m.

The buckling loads for plates with the same width but with different lengths are given by solid lines in Figure 4.32. The buckling loads calculated by the equations of Bank and Yin[28] are also included in this figure. The approximate expression (Eq. 4.156) underestimates $N_{x,cr}$, and, hence, is a conservative estimate.

The long-plate expression gives the buckling load of this plate as 46.16 kN/m (Example 4.12, page 139). This value is also shown in Figure 4.32.

[28] L. C. Bank and J. Yin, Buckling of Orthotropic Plates with Free and Rotationally Restrained Unloaded Edges. *Thin-Walled Structures*, Vol. 24, 83–96, 1996.

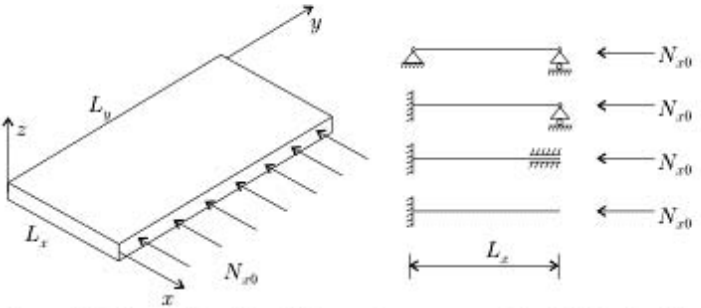

Figure 4.33: Long plate subjected to a uniform compressive edge load and the different types of supports along the long edges.

4.3.5 Long Plates

We consider a long rectangular plate of constant thickness whose length is large compared with its width.

Uniform Compressive Load Along the Long Edge

The length of the plate is L_y and the width is L_x ($L_y \gg L_x$). The supports along the long edges are as shown in Figure 4.33. A uniform compressive load N_{x0} is applied along one of the long edges of the plate. We wish to determine the lowest value of the applied under which the plate buckles.

We treat the plate as long and assume that it undergoes cylindrical deformation along its length (Fig. 4.4). This approximation is reasonable when $L_y > 3L_x\sqrt[4]{D_{11}/D_{22}}$ (Eq. 4.19).

When three in-plane loads N_{x0}, N_{y0}, and N_{xy0} act on the plate (Fig. 4.14, right), the equilibrium equations in the x, y, and z directions (Fig. 4.1) are[29]

$$\begin{aligned}
\frac{\partial N_x}{\partial x} + \frac{\partial N_{xy}}{\partial y} &= 0 \\
\frac{\partial N_y}{\partial y} + \frac{\partial N_{xy}}{\partial x} &= 0 \\
\frac{\partial V_x}{\partial x} + \frac{\partial V_y}{\partial y} &= N_{x0}\frac{d^2w^o}{dx^2} + N_{y0}\frac{d^2w^o}{dy^2} + 2N_{xy0}\frac{d^2w^o}{dxdy},
\end{aligned} \tag{4.158}$$

where N_x, N_y, and N_{xy} are the in-plane forces (per unit length), and V_x and V_y are the transverse shear forces (per unit length) (Fig. 4.1). Moment equilibria about the y- and z- axes give (Eq. 4.5)

$$V_x = \frac{\partial M_x}{\partial x} + \frac{\partial M_{xy}}{\partial y} \qquad V_y = \frac{\partial M_y}{\partial y} + \frac{\partial M_{xy}}{\partial x}, \tag{4.159}$$

where M_x and M_{xy} are, respectively, the bending moment and twist moment per unit length. Away from the short edges the forces and moments do not vary along

[29] S. P. Timoshenko and J. Gere, *Theory of Elastic Stability*. 2nd edition. McGraw-Hill, New York, 1961, pp. 333–334.

the length of the plate. Thus, from the last of Eq. (4.158) and from the first of Eq. (4.159) we have

$$\frac{dV_x}{dx} - N_{x0}\frac{d^2w^o}{dx^2} = 0 \tag{4.160}$$

$$\frac{dM_x}{dx} - V_x = 0. \tag{4.161}$$

By substituting V_x from Eq. (4.161) into Eq. (4.160) we obtain the equilibrium equation

$$\frac{d^2M_x}{dx^2} - N_{x0}\frac{d^2w^o}{dx^2} = 0. \tag{4.162}$$

As was shown in Section 4.2.2, when the plate is symmetrical, the bending moment M_x is (see Eq. 4.25)

$$M_x = D_{11}\kappa_x. \tag{4.163}$$

Equations (4.162), (4.21), and (4.163) yield

$$D_{11}\frac{d^4w^o}{dx^4} + N_{x0}\frac{d^2w^o}{dx^2} = 0 \qquad \begin{matrix}\text{long plate}\\ \text{symmetrical layup.}\end{matrix} \tag{4.164}$$

The equation describing the buckling of an isotropic beam subjected to an axial load $\widehat{N}_{x0}$ is[30]

$$EI\frac{d^4w}{dx^4} + \widehat{N}_{x0}\frac{d^2w}{dx^2} = 0 \qquad \text{isotropic beam.} \tag{4.165}$$

The structure of the two preceding equations is the same. Therefore, the buckling load of a long plate (symmetrical layup) may be obtained by substituting the value of D_{11} for EI in the expression for the buckling load of the corresponding isotropic beam.

It was shown in Section 4.2.2 that when the layup of the plate is unsymmetrical, the deflection may be obtained by replacing EI/p' by Ψ/p in the expression for the deflection of the corresponding isotropic beam. By similar arguments it can be shown that the buckling load of a long plate with unsymmetrical layup may be obtained by substituting the value of Ψ for EI in the expression for the buckling load of the corresponding isotropic beam. (Ψ is given by Eq. 4.52.)

4.10 Example. *A 0.7-m-long and 0.2-m-wide rectangular plate is made of graphite epoxy. The material properties are given in Table 3.6 (page 81). The layup is* $[\pm 45_2^t/0_{12}/\pm 45_2^t]$. *The 0-degree plies are parallel to the short edge of the plate. The plate is either simply supported or built-in along all four edges. The plate is subjected to uniform compressive loads along the long edges (Fig. 4.34). Calculate the buckling load.*

[30] Ibid., p. 2.

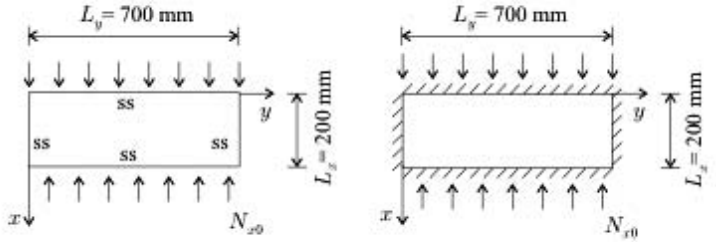

Figure 4.34: The plates in Example 4.10.

Solution. The plate may be treated as "long" (Example 4.1, page 96). The buckling loads of the corresponding beam are (Eq. 6.337)

$$\widehat{N}_{cr} = \frac{\pi^2 EI}{L^2} \qquad \text{(ss)} \tag{4.166}$$

$$\widehat{N}_{cr} = \frac{4\pi^2 EI}{L^2} \qquad \text{(built-in)}. \tag{4.167}$$

The buckling loads of the plate are obtained by replacing EI by D_{11} (see page 133) as follows:

$$N_{x,cr} = \frac{\pi^2 D_{11}}{L_x^2} \qquad \text{(ss)} \tag{4.168}$$

$$N_{x,cr} = \frac{4\pi^2 D_{11}}{L_x^2} \qquad \text{(built-in)}. \tag{4.169}$$

With the value of $D_{11} = 45.30$ N · m (Table 3.7, page 84) and with $L_x = 0.2$ m, the buckling loads are

$$N_{x,cr} = 11.18 \text{ kN/m} \qquad \text{(ss)} \tag{4.170}$$

$$N_{x,cr} = 44.71 \text{ kN/m} \qquad \text{(built-in)}. \tag{4.171}$$

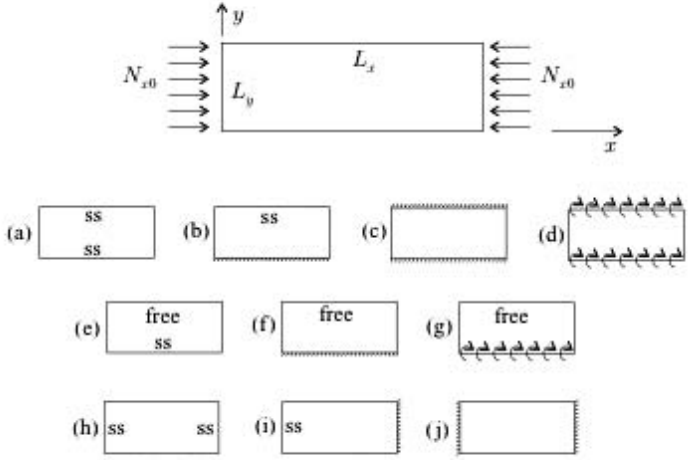

Figure 4.35: Long plate subjected to uniaxial load (top) and the supports along the long (a to g) and short edges (h to j).

Uniform Compressive Load Along the Short Edge – Orthotropic and Symmetrical Layup

We consider a plate with length L_x and width L_y ($L_x \gg L_y$) (Fig. 4.35). The layup of the plate is orthotropic and symmetrical. The possible edge supports are shown in Figure 4.35. The plate is subjected to a uniaxial compressive load N_{x0} (Fig. 4.35, top).

Simply supported and built-in edges. The buckling loads of long plates whose long edges are either simply supported or built-in (Fig. 4.35, a, b, c) are given below.

The buckled shape of a long plate away from the loaded edges is the same as the buckled shape of a plate simply supported along the loaded edges. Therefore, the buckling loads of the long plate are also given by Eq. (4.141). We are interested in the lowest buckling load. We denote the buckling length corresponding to this buckling load by l_x^o. With this notation, Eq. (4.141) becomes

$$N_{x,cr} = D_{11}\pi^2 \frac{1}{l_x^{o2}} + D_{22}\frac{\alpha_3^4}{\pi^2}\frac{l_x^{o2}}{L_y^4} + 2\left(D_{12} + 2D_{66}\right)\frac{\alpha_5}{L_y^2}. \tag{4.172}$$

The necessary condition that gives the lowest $N_{x,cr}$ is $d\left(N_{x,cr}\right)/d(l_x^o) = 0$. This condition and Eq. (4.172) give

$$l_x^o = \frac{\pi}{\alpha_3} L_y \sqrt[4]{\frac{D_{11}}{D_{22}}}. \tag{4.173}$$

Table 4.10. The buckling lengths corresponding to the lowest buckling load with unidirectionally loaded long plates (orthotropic and symmetrical layup, $\xi = \frac{1}{1+10\zeta}$, $\zeta = \frac{D_{22}}{\tilde{k}L_y}$); L_y is the width, and $\tilde{k}$ is the spring constant. Plates with one simply supported and one free long edge buckle with a long wave in the x direction, as illustrated in Figure 4.25.

Supports	Buckling length l_x^o
ss, ss	$L_y\sqrt[4]{\frac{D_{11}}{D_{22}}}$
ss	$0.8L_y\sqrt[4]{\frac{D_{11}}{D_{22}}}$
	$0.664L_y\sqrt[4]{\frac{D_{11}}{D_{22}}}$
	$\sqrt[4]{\frac{1}{1+4.139\xi}}L_y\sqrt[4]{\frac{D_{11}}{D_{22}}}$
free	$1.675L_y\sqrt[4]{\frac{D_{11}}{D_{22}}}$
free	$1.675\sqrt[4]{1+4.12\zeta}L_y\sqrt[4]{\frac{D_{11}}{D_{22}}}$
ss, ss	$0.707L_y\sqrt[4]{\frac{D_{11}}{D_{22}}}$

Table 4.11. The lowest buckling loads of long plates with orthotropic and symmetrical layup ($\xi = \frac{1}{1+10\zeta}$, $\zeta = \frac{D_{22}}{kL_y}$, $\nu = \frac{D_{12}}{2D_{66}+D_{12}}$, $K = \frac{2D_{66}+D_{12}}{\sqrt{D_{11}D_{22}}}$, $\eta = \frac{1}{\sqrt{1+(7.22-3.55\nu)\zeta}}$). L_y is the width, and $\tilde{k}$ is the spring constant. The buckling loads of long plates with one simply supported and one free long edge are given in the first three rows of Table 4.9 (page 125).

Supports	Buckling load $N_{x,cr}$ or $N_{xy,cr}$
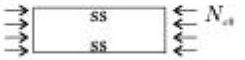	$\frac{\pi^2}{L_y^2}[2\sqrt{D_{11}D_{22}} + 2(D_{12}+2D_{66})]$
	$\frac{\pi^2}{L_y^2}[3.125\sqrt{D_{11}D_{22}} + 2.33(D_{12}+2D_{66})]$
	$\frac{\pi^2}{L_y^2}[4.53\sqrt{D_{11}D_{22}} + 2.62(D_{12}+2D_{66})]$
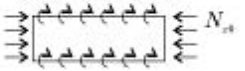	$\frac{\pi^2}{L_y^2}[2\sqrt{1+4.139\xi}\sqrt{D_{11}D_{22}} + (2+0.62\xi^2)(D_{12}+2D_{66})]$
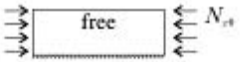	$\frac{\sqrt{D_{11}D_{22}}}{L_y^2}[15.1K\sqrt{1-\nu} + 7(1-K)]$ when $K \le 1$
	$\frac{\sqrt{D_{11}D_{22}}}{L_y^2}[15.1\sqrt{1-\nu} + (K-1)6(1-\nu)]$ when $1 < K$
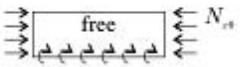	$\frac{\sqrt{D_{11}D_{22}}}{L_y^2}\left[K(\eta 15.1\sqrt{1-\nu} + (1-\eta)6(1-\nu)) + \frac{7(1-K)}{\sqrt{1+4.12\zeta}}\right]$ when $K \le 1$
	$\frac{\sqrt{D_{11}D_{22}}}{L_y^2}[\eta 15.1\sqrt{1-\nu} + (K-\eta)6(1-\nu)]$ when $1 < K$
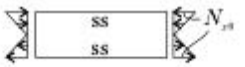	$\frac{\pi^2}{L_y^2}[13.9\sqrt{D_{11}D_{22}} + 11.1(D_{12}+2D_{66})]$
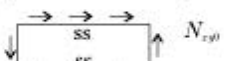	$\frac{4}{L_y^2}\sqrt[4]{D_{11}D_{22}^3}(8.125 + 5.045K)$ when $K \le 1$
	$\frac{4}{L_y^2}\sqrt{D_{22}(D_{12}+2D_{66})}\left(11.71 + \frac{1.46}{K^2}\right)$ when $1 < K$
	$\frac{4}{L_y^2}\sqrt[4]{D_{11}D_{22}^3}(15.07 + 7.08K)$ when $K \le 1$
	$\frac{4}{L_y^2}\sqrt{D_{22}(D_{12}+2D_{66})}\left(18.59 + \frac{3.56}{K^2}\right)$ when $1 < K$

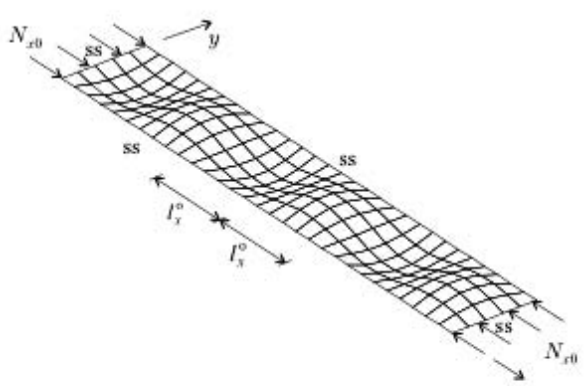

Figure 4.36: Buckled shape of a long plate with simply supported edges.

As before, the buckling length l_x^o is the half wavelength of the buckled shape. We obtain the lowest buckling load by introducing Eq. (4.173) into Eq. (4.172) as follows:

$$N_{x,cr} = \frac{2}{L_y^2}\left[\alpha_3^2\sqrt{D_{11}D_{22}} + \alpha_5\left(D_{12} + 2D_{66}\right)\right]. \tag{4.174}$$

The values of α_3 and α_5 to be used are those given in Table 4.7 (page 120) for $j = 1$. The resulting buckling lengths and buckling loads are listed in the first three rows of Tables 4.10 and 4.11.

Both long edges are rotationally restrained. The plate is rotationally restrained along the unloaded long edges (Fig. 4.35, d). The buckling load for a plate with arbitrary length is given by Eq. (4.150). The value of l_x that results in the lowest buckling load is denoted by l_x^o. When the plate is long, the necessary condition that gives the lowest $N_{x,cr}$ is $d\left(N_{x,cr}\right)/d\left(l_x^o\right) = 0$. This condition and Eq. (4.150), with l_x replaced by l_x^o, give

$$l_x^o = \sqrt[4]{\frac{1}{1+4.139\xi}}\,L_y\sqrt[4]{\frac{D_{11}}{D_{22}}}, \tag{4.175}$$

where ξ is given by Eq. (4.151). Equations (4.150), (4.151), and (4.175) yield

$$N_{x,cr} = \frac{\pi^2}{L_y^2}\left[2\sqrt{1+4.139\xi}\sqrt{D_{11}D_{22}} + \left(2+0.62\xi^2\right)\left(D_{12}+2D_{66}\right)\right]. \tag{4.176}$$

This result is included in Table 4.11.

One long edge is simply supported; the other is free. The buckling loads are given in the first three rows of Table 4.9 (page 125) for plates with one of the edges parallel to the load direction simply supported and the other edge free. These expressions are applicable regardless of the aspect ratio of the plate and hence may be used to calculate the buckling loads of long plates with one simply supported and one free long edge (Fig. 4.35, e).

One long edge is built-in; the other is free. The buckling loads of plates with one of the unloaded edges built-in and the other one free (Fig. 4.35, f) can be calculated by Eq. (4.147). The value of l_x that results in the lowest buckling load is denoted by l_x^o. When the plate is long, the necessary condition that gives the lowest $N_{x,cr}$ is $d\left(N_{x,cr}\right)/d\left(l_x^o\right) = 0$. This condition and Eq. (4.147), with l_x replaced by l_x^o,

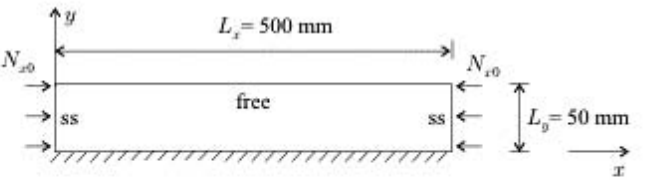

Figure 4.37: The plate in Example 4.11.

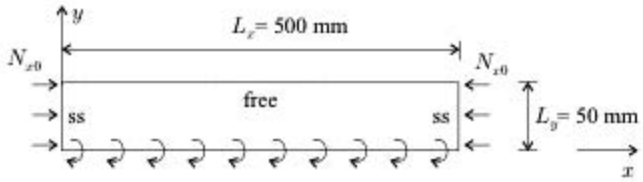

Figure 4.38: Illustration of the plate in Example 4.12.

give

$$l_x^o = 1.675 L_y \sqrt[4]{\frac{D_{11}}{D_{22}}}. \tag{4.177}$$

Equations (4.147) and (4.177) yield

$$N_{x,cr} = 7\frac{\sqrt{D_{11}D_{22}}}{L_y^2} + 12\frac{D_{66}}{L_y^2}. \tag{4.178}$$

This expression gives a conservative estimate of the buckling load and underestimates it by less than 14 percent. More accurate expressions, determined by Kollár,[31] are given in Table 4.11 (page 136). The accuracy of these equations is about 2 percent when $0 < K \leq 1$ and is about 5 percent when $1 < K \leq 3$.

4.11 Example. *A rectangular plate with length $L_x = 0.5$ m and width $L_y = 0.05$ m is made of graphite epoxy unidirectional plies with the fibers oriented along the x-axis of the plate (Fig. 4.37). The material properties are given in Table 3.6 (page 81). The layup is $[0_{20}]$. One of the long edges is built-in; the other long edge is free. The short edges are simply supported. The plate is subjected to uniform compressive loads in the x direction. Calculate the buckling load.*

Solution. The stiffnesses of the plate are $D_{11} = 99.25$ N·m, $D_{22} = 6.47$ N·m, $D_{12} = 1.94$ N·m, $D_{66} = 3.03$ N·m (Table 3.7, page 84). The buckling length l_x^o is (Eq. 4.177)

$$l_x^o = 1.675 L_y \sqrt[4]{\frac{D_{11}}{D_{22}}} = 0.166 \text{ m}. \tag{4.179}$$

Since the plate is longer than the buckling length ($L_x > l_x^o$), we may treat the plate as "long." From Table 4.11 (page 136), K and ν are

$$K = \frac{2D_{66} + D_{12}}{\sqrt{D_{11}D_{22}}} = 0.316 \qquad \nu = \frac{D_{12}}{2D_{66} + D_{12}} = 0.242. \tag{4.180}$$

[31] L. P. Kollár, Buckling of Unidirectionally Loaded Composite Plates with One Free and One Rotationally Restrained Unloaded Edge. *Journal of Structural Engineering*, Vol 128, 1202–1211, 2002.

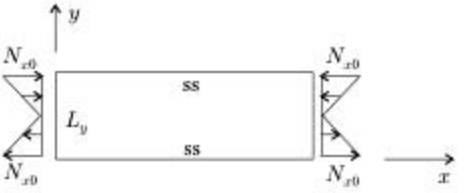

Figure 4.39: Long rectangular plate subjected to linearly varying load.

From Table 4.11 (fifth row) we obtain ($K < 1$)

$$N_{x,\mathrm{cr}} = \frac{\sqrt{D_{11}D_{22}}}{L_y^2}(15.1K\sqrt{1-\nu} + 7(1-K)) = 90.640 \text{ kN/m}. \tag{4.181}$$

One long edge is rotationally restrained the other is free. The buckling loads of plates with one of the unloaded edges rotationally restrained and the other one free (Fig. 4.35, g) can be calculated by Eq. (4.154). The value of l_x that results in the lowest buckling load is denoted by l_x^o. When the plate is long the necessary condition that gives the lowest $N_{x,\mathrm{cr}}$ is $d(N_{x,\mathrm{cr}})/d(l_x^o) = 0$. This condition and Eq. (4.154), with l_x replaced by l_x^o, give

$$l_x^o = 1.675 L_y \sqrt[4]{\frac{D_{11}}{D_{22}}(1 + 4.12\zeta)}, \tag{4.182}$$

where ζ is the parameter of restraint given by Eq. (4.152). Equations (4.154) and (4.182) yield

$$N_{x,\mathrm{cr}} = \frac{7}{\sqrt{1+4.12\zeta}}\frac{\sqrt{D_{11}D_{22}}}{L_y^2} + 12\frac{D_{66}}{L_y^2}. \tag{4.183}$$

This expression gives a conservative estimate of the buckling load and underestimates it by less than 14 percent. More accurate expressions, determined by Kollár,[32] are included in Table 4.11 (page 136). The accuracy of these equations is about 2 percent when $0 < K \leq 1$ and is about 5 percent when $1 < K \leq 3$.

4.12 Example. *A rectangular plate with length $L_x = 0.5\,m$ and width $L_y = 0.05\,m$ is made of graphite epoxy unidirectional plies with the fibers oriented along the x-axis of the plate (Fig. 4.38). The material properties are given in Table 3.6 (page 81). The layup is* $[0_{20}]$. *One of the long edges is rotationally restrained while the other long edge is free. The short edges are simply supported. The rotational spring constant of the edge is $\widetilde{k} = 129.4$ N. The plate is subjected to uniform compressive loads in the x direction. Calculate the buckling load.*

Solution. The bending stiffnesses of the plate are $D_{11} = 99.25$ N·m, $D_{22} = 6.47$ N·m, $D_{12} = 1.94$ N·m, $D_{66} = 3.03$ N·m (Table 3.7, page 84) and $\zeta = 1$

[32] Ibid.

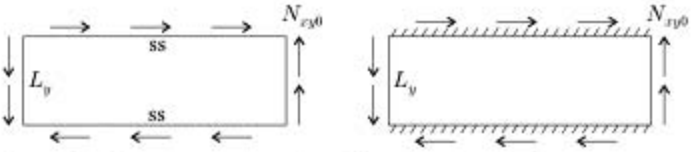

Figure 4.40: Long rectangular plate subjected to shear load.

(Eq. 4.157). The buckling length l_x^o is (Eq. 4.182)

$$l_x^o = 1.675 L_y \sqrt[4]{\frac{D_{11}}{D_{22}}(1 + 4.12\zeta)} = 0.249 \text{ m}. \tag{4.184}$$

Since the plate is longer than the buckling length ($L_x > l_x^o$), we may treat the plate as "long." With the parameters K and ν given by Eq. (4.180), from Table 4.11, sixth row (page 136) we obtain ($K < 1$)

$$\begin{aligned} N_{x,\text{cr}} &= \frac{\sqrt{D_{11} D_{22}}}{L_y^2}\left\{ K\left[\eta 15.1\sqrt{1-\nu} + (1-\eta)6(1-\nu)\right] + \frac{7(1-K)}{\sqrt{1+4.12\zeta}} \right\} \\ &= 46.16 \text{ kN/m}, \end{aligned} \tag{4.185}$$

where η is (Table 4.11)

$$\eta = \frac{1}{\sqrt{1 + (7.22 - 3.55\nu)\,\zeta}} = 0.369. \tag{4.186}$$

Linearly Varying Load Along the Short Edge – Orthotropic and Symmetrical Layup

The layup of the plate is orthotropic and symmetrical. The short edges of the plate are either simply supported or built-in, as shown in the bottom row of Figure 4.35. Both long edges are simply supported. Along the short edges the plate is subjected to a linearly varying normal load with maximum intensity N_{xo} (Fig. 4.39). The lowest buckling load $N_{x,\text{cr}}$ at which the plate buckles is given by Lekhnitskii[33]

$$N_{x,\text{cr}} = \frac{\pi^2}{L_y^2}\left[13.9\sqrt{D_{11} D_{22}} + 11.1(D_{12} + 2D_{66})\right]. \tag{4.187}$$

This result is included in Table 4.11 (page 136). The buckling length is given in Table 4.10 (page 135).

Shear Load – Orthotropic and Symmetrical Layup

The layup of the plate is orthotropic and symmetrical. Both long edges are either simply supported or built-in (Fig. 4.40). Regardless of the manner in which the long edges are supported, the short edges may be either simply supported or built-in.

[33] S. G. Lekhnitskii, *Anisotropic Plates*. Gordon and Breach Science Publishers, New York, 1968, pp. 462–463.

Table 4.12. The parameter β_1 in Eq. (4.188) as a function of $K = \frac{2D_{66}+D_{12}}{\sqrt{D_{11}D_{22}}}$

	$0 \le K \le 1$	$1 < K \le \infty$
Simply supported	$8.125 + 5.045K$	$11.71 + \frac{1.46}{K^2}$
Built-in	$15.07 + 7.08K$	$18.59 + \frac{3.56}{K^2}$

The plate is subjected to a uniform shear load N_{xy0}. We wish to determine the lowest value of the load $N_{xy,\,cr}$ at which the plate buckles.

Seydel derived the lowest buckling loads for infinitely long plates. The resulting expressions, as quoted by Whitney,[34] are

$$N_{xy,\,cr} = \begin{cases} \dfrac{4\beta_1}{L_y^2}\sqrt[4]{D_{11}D_{22}^3} & 0 \le K \le 1 \\ \dfrac{4\beta_1}{L_y^2}\sqrt{D_{22}\,(D_{12}+2D_{66})} & 1 < K \le \infty\,. \end{cases} \tag{4.188}$$

Seydel gave numerical values for β_1. These values can be approximated within 2 percent by the expressions in Table 4.12.

4.4 Free Vibration of Rectangular Plates

When a plate undergoes free, undamped vibration, the deflection of the plate is sinusoidal with respect to time t,

$$w^\circ = \overline{w}^\circ \sin(\omega t) = \overline{w}^\circ \sin(2\pi f t)\,, \tag{4.189}$$

where ω is the circular frequency and f is the natural frequency. The period of vibration T is

$$T = \frac{1}{f} \qquad \omega = 2\pi f = \frac{2\pi}{T}, \tag{4.190}$$

and $\overline{w}^\circ$ is the deflection of the plate at time $t = T/4$.

In this section we obtain the natural frequencies and, hence, the periods of vibration, of freely vibrating plates.

4.4.1 Long Plates

We consider a long rectangular plate whose length L_y is large compared with its width L_x. The mass of the plate is uniform. The edges may be built-in, simply supported, or free (Fig. 4.41).

[34] J. M. Whitney, *Structural Analysis of Laminated Anisotropic Plates*. Technomic, Lancaster, Pennsylvania, 1987, p. 118.

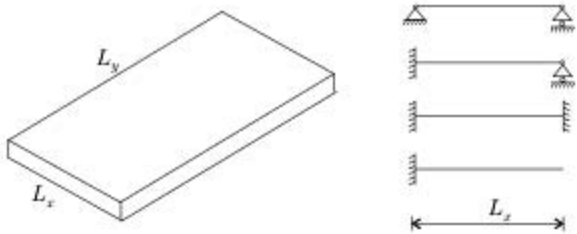

Figure 4.41: The different types of supports along the long edges of a freely vibrating long plate.

When $L_y > 3L_x\sqrt[4]{D_{11}/D_{22}}$ (Eq. 4.19), a laterally loaded plate may be approximated as a long plate undergoing cylindrical deformation (Fig. 4.4), and the equilibrium equations are (Eqs. 4.22 and 4.23)

$$\frac{dV_x}{dx} + p = 0 \tag{4.191}$$

$$\frac{dM_x}{dx} - V_x = 0, \tag{4.192}$$

where p is the lateral force (per unit area) acting on the plate. In the case of a freely vibrating plate, p is the inertia force, which, with the use of Eq. (4.189), is

$$p = -\rho\frac{\partial^2 w^o}{\partial t^2} = \rho\,(2\pi f)^2\,\overline{w}^o \sin(2\pi f t)\,, \tag{4.193}$$

where ρ is the mass of the plate per unit area. Equations (4.191)–(4.193) give

$$\frac{d^2M_x}{dx^2} + \rho\,(2\pi f)^2\,w^o = 0. \tag{4.194}$$

When the plate is symmetrical, the bending moment is (see Eqs. 4.25 and 4.21)

$$M_x = D_{11}\kappa_x = -D_{11}\frac{\partial^2 w^o}{\partial x^2}. \tag{4.195}$$

With this moment, Eq. (4.194) yields

$$\frac{d^4w^o}{dx^4} - \frac{\rho}{D_{11}}(2\pi f)^2\,w^o = 0 \qquad \begin{matrix}\text{long plate}\\ \text{symmetrical layup.}\end{matrix} \tag{4.196}$$

The equation of a freely vibrating isotropic beam is[35]

$$\frac{d^4w}{dx^4} - \frac{\rho'}{EI}(2\pi f)^2\,w = 0 \qquad \text{isotropic beam,} \tag{4.197}$$

where ρ' is the mass of the beam per unit length.

[35] W. Weaver, S. P. Timoshenko, and D. H. Young, *Vibration Problems in Engineering*. 5th edition. John Wiley & Sons, New York, 1990, p. 417.

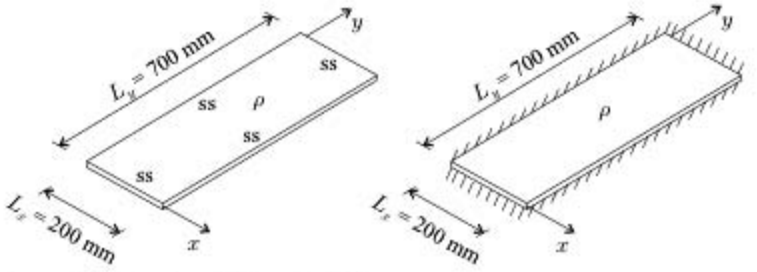

Figure 4.42: The plates in Example 4.13.

From Eqs. (4.196) and (4.197) we observe that the natural frequencies of a long plate (symmetrical layup) with bending stiffness D_{11} and mass ρ are the same as the natural frequencies of an isotropic beam with bending stiffness EI and mass ρ'. Thus, the natural frequencies of a long plate (symmetrical layup) may be obtained by replacing EI/ρ' by D_{11}/ρ in the expression for the natural frequencies of the corresponding isotropic beam.

The natural frequencies of a long plate with unsymmetrical layup may be obtained by replacing EI/ρ' by Ψ/ρ in the expression for the natural frequencies of the corresponding isotropic beam (where Ψ is given by Eq. 4.52).

4.13 Example. *A 0.7-m-long and 0.2-m-wide rectangular plate is made of graphite epoxy. The material properties are given in the Table 3.6 (page 81). The layup is* $[\pm 45_2^{\mathrm{t}}/0_{12}/\pm 45_2^{\mathrm{t}}]$. *The 0-degree plies are parallel to the short edge of the plate. The plate is either simply supported or built-in along all four edges (Fig. 4.42). The mass of the plate is uniform* ($\rho = 3.2$ *kg/m*^{2}). *Calculate the circular and natural frequencies.*

Solution. The plate may be treated as "long" (Example 4.1, page 96). The circular frequencies of the corresponding beam are (Eq. 6.398, and Table 6.13, page 308)

$$\omega_i = \sqrt{\frac{EI}{\rho'}}\frac{\mu_{Bi}^2}{L^2} \qquad \mu_{Bi} = \pi, 2\pi, 3\pi, \ldots \qquad \text{(ss)} \tag{4.198}$$

$$\omega_i = \sqrt{\frac{EI}{\rho'}}\frac{\mu_{Bi}^2}{L^2} \qquad \mu_{Bi} = 4.730, 7.853, 10.996, \ldots \qquad \text{(built-in).} \tag{4.199}$$

The circular frequencies of the plate are obtained by replacing EI/ρ' by D_{11}/ρ as follows:

$$\omega_i = \sqrt{\frac{D_{11}}{\rho}}\frac{\mu_{Bi}^2}{L_x^2} \qquad \mu_{Bi} = \pi, 2\pi, 3\pi, \ldots \qquad \text{(ss)} \tag{4.200}$$

$$\omega_i = \sqrt{\frac{D_{11}}{\rho}}\frac{\mu_{Bi}^2}{L_x^2} \qquad \mu_{Bi} = 4.730, 7.853, 10.996, \ldots \qquad \text{(built-in).} \tag{4.201}$$

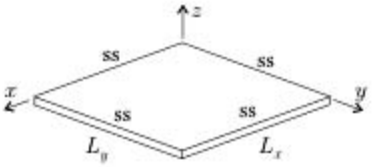

Figure 4.43: Rectangular simply supported (ss) plate.

With $D_{11} = 45.30$ N · m (Table 3.7, page 84) and $L_x = 0.2$ m, the circular frequencies are

$$\omega_1 = 928 \qquad \omega_2 = 3\,713 \qquad \omega_3 = 8\,355 \text{ 1/s} \qquad \text{(ss)} \tag{4.202}$$

$$\omega_1 = 2\,104 \qquad \omega_2 = 5\,801 \qquad \omega_3 = 11\,3731\text{/s} \qquad \text{(built-in).} \tag{4.203}$$

The natural frequencies are $f = \omega/2\pi$ (Eq. 6.397)

$$f_1 = 148 \qquad f_2 = 591 \qquad f_3 = 1\,330 \text{ Hz} \qquad \text{(ss)} \tag{4.204}$$

$$f_1 = 335 \qquad f_2 = 923 \qquad f_3 = 1\,810 \text{ Hz} \qquad \text{(built-in).} \tag{4.205}$$

4.4.2 Simply Supported Plates – Symmetrical Layup

We consider a rectangular plate with dimensions L_x and L_y simply supported along its four edges (Fig. 4.43). The layup of the plate is symmetrical, $[B] = [0]$. The mass of the plate is uniform.

Following Whitney,[36] we obtain the natural frequencies of this plate by the energy method. By introducing w^o (see Eq. 4.189) into the expression for U (Eq. 4.55), we obtain

$$U = \overline{U} \sin^2(2\pi f t), \tag{4.206}$$

where $\overline{U}$ is defined as

$$\overline{U} = \frac{1}{2}\int_0^{L_x}\int_0^{L_y}\left[D_{11}\left(\frac{\partial^2\overline{w}^o}{\partial x^2}\right)^2 + D_{22}\left(\frac{\partial^2\overline{w}^o}{\partial y^2}\right)^2 + D_{66}\left(\frac{2\partial^2\overline{w}^o}{\partial x\partial y}\right)^2 + 2\left(D_{12}\frac{\partial^2\overline{w}^o}{\partial x^2}\frac{\partial^2\overline{w}^o}{\partial y^2} + D_{16}\frac{\partial^2\overline{w}^o}{\partial x^2}\frac{2\partial^2\overline{w}^o}{\partial x\partial y} + D_{26}\frac{\partial^2\overline{w}^o}{\partial y^2}\frac{2\partial^2\overline{w}^o}{\partial x\partial y}\right)\right] dy dx. \tag{4.207}$$

The kinetic energy of the plate is

$$K = \frac{1}{2}\int_0^{L_x}\int_0^{L_y}\rho\left(\frac{dw^o}{dt}\right)^2 dy dx. \tag{4.208}$$

[36] J. M. Whitney, *Structural Analysis of Laminated Anisotropic Plates*. Technomic, Lancaster, Pennsylvania, 1987, p. 166.

Substitution of the deflection, given by Eq. (4.189), into this equation yields

$$K = \frac{1}{2}(2\pi f)^2 \cos^2(2\pi f t) \int_0^{L_x}\int_0^{L_y} \rho \overline{w}^{o2} dy dx. \tag{4.209}$$

According to the law of conservation of energy the change in strain energy from time $t = 0$ to time t equals the change in kinetic energy during this time

$$(U_t - U_{t=0}) = -(K_t - K_{t=0}). \tag{4.210}$$

Initially, at time $t = 0$ the strain energy is zero (Eq. 4.206), but at time $t = \frac{1}{4f}$ the kinetic energy is zero (Eq. 4.209). Thus, we have

$$U_{t=\frac{1}{4f}} = K_{t=0}. \tag{4.211}$$

Equation (4.211), together with Eqs. (4.206) and (4.209), yields

$$\frac{1}{2}(2\pi f)^2 \int_0^{L_x}\int_0^{L_y} \rho \overline{w}^{o2} dy dx = \overline{U}. \tag{4.212}$$

From this equation we obtain

$$(2\pi f)^2 = \frac{\overline{U}}{\frac{1}{2}\int_0^{L_x}\int_0^{L_y} \rho \overline{w}^{o2} dy dx}. \tag{4.213}$$

We use Rayleigh's energy method[37] to obtain the deflection. For the simply supported plate under consideration the geometrical boundary conditions require that the deflections be zero along the edges (Eq. 4.57) as follows:

$$w^o = 0 \quad \text{at} \quad \begin{cases} x = 0 & \text{and} \quad 0 \le y \le L_y \\ x = L_x & \text{and} \quad 0 \le y \le L_y \\ 0 \le x \le L_x & \text{and} \quad y = 0 \\ 0 \le x \le L_x & \text{and} \quad y = L_y. \end{cases} \tag{4.214}$$

The following deflection satisfies these geometrical boundary conditions:

$$w^o = \overline{w}^o \sin(2\pi f t), \tag{4.215}$$

where $\overline{w}^o$ is

$$\overline{w}^o = \sum_{i=1}^{I}\sum_{j=1}^{J} w_{ij} \sin\frac{i\pi x}{L_x} \sin\frac{j\pi y}{L_y}, \tag{4.216}$$

where I and J are the number of terms, chosen arbitrarily, for the summations and w_{ij} are constants. According to the Rayleigh principle the frequency of vibration of a conservative system has a minimum value in the neighborhood of the fundamental mode.[38] We express this principle in the form

$$\frac{\partial f}{\partial w_{ij}} = 0. \tag{4.217}$$

[37] L. Meirovitch, *Principles and Techniques of Vibrations*. Prentice-Hall, Upper Saddle River, New Jersey, 1997, pp. 518–522.

[38] Ibid., p. 520.

To determine the values of w_{ij}, we substitute Eqs. (4.207), (4.213), and (4.216) into this expression. Algebraic manipulations yield the following system of simultaneous algebraic equations:

$$\sum_{i=1}^{I}\sum_{j=1}^{J}\left(G_{mnij}-\lambda\delta_{mnij}\right)w_{ij}=0 \quad \begin{cases} i,m=1,2,3,\ldots,I \\ j,n=1,2,3,\ldots,J, \end{cases} \tag{4.218}$$

where λ is given by

$$\lambda=\frac{1}{4}(2\pi f)^2\rho L_x L_y. \tag{4.219}$$

For convenience, we introduce the contracted notation

$$k=(i-1)J+j \quad \begin{cases} i=1,2,3,\ldots,I \\ j=1,2,3,\ldots,J \end{cases} \tag{4.220}$$

$$l=(m-1)J+n \quad \begin{cases} m=1,2,3,\ldots,I \\ n=1,2,3,\ldots,J, \end{cases} \tag{4.221}$$

Equation (4.218) may now be written as

$$\sum_{k=1}^{I\times J}G_{kl}w_k=\lambda\sum_{k=1}^{I\times J}\delta_{kl}w_k \quad l=1,2,3,\ldots,I\times J, \tag{4.222}$$

where $G_{kl}\,(=G_{lk})$ and the Kronecker delta $\delta_{lk}\,(=\delta_{kl})$ are given in Table 4.1 (page 102). In expanded form Eq. (4.222) is

$$\left(\begin{bmatrix} G_{11} & \cdots & G_{1(I\times J)} \\ \vdots & \ddots & \\ G_{(I\times J)1} & & G_{(I\times J)(I\times J)} \end{bmatrix}-\lambda\begin{bmatrix} \delta_{11} & \cdots & \delta_{1(I\times J)} \\ \vdots & \ddots & \\ \delta_{(I\times J)1} & & \delta_{(I\times J)(I\times J)} \end{bmatrix}\right)\begin{Bmatrix} w_1 \\ \vdots \\ w_{(I\times J)} \end{Bmatrix}=\begin{Bmatrix} 0 \\ \vdots \\ 0 \end{Bmatrix}. \tag{4.223}$$

In the case of free vibration the deflection is nonzero. For nonzero deflections, Eq. (4.223) is satisfied when the determinant of the matrix in the parentheses is zero. At this condition λ is the eigenvalue of Eq. (4.223). There are $J\times I$ eigenvalues, denoted by λ_{ij}, which may readily be calculated by commercial software.

The natural frequencies are calculated from Eq. (4.219) as follows:

$$f_{ij}=\frac{1}{\pi}\sqrt{\frac{\lambda_{ij}}{\rho L_x L_y}}. \tag{4.224}$$

For an orthotropic plate $D_{16}=D_{26}=0$, and the eigenvalues of Eq. (4.223) can directly be calculated. The result is

$$\lambda_{ij}=\frac{1}{4}L_x L_y\pi^4\left[D_{11}\left(\frac{i}{L_x}\right)^4+2\left(D_{12}+2D_{66}\right)\left(\frac{i}{L_x}\right)^2\left(\frac{j}{L_y}\right)^2+D_{22}\left(\frac{j}{L_y}\right)^4\right]. \tag{4.225}$$

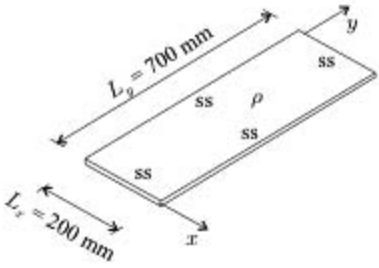

Figure 4.44: The plate in Example 4.14.

Equations (4.224) and (4.225) give the natural frequencies of an orthotropic plate as follows:

$$f_{ij} = \sqrt{\frac{\pi^2}{4\rho}\left\{D_{11}\left(\frac{i}{L_x}\right)^4 + 2\left(D_{12}+2D_{66}\right)\left(\frac{i}{L_x}\right)^2\left(\frac{j}{L_y}\right)^2 + D_{22}\left(\frac{j}{L_y}\right)^4\right\}}. \tag{4.226}$$

The values of f_{ij} must be calculated for different values of i and j.

4.14 Example. *A 0.7-m-long and 0.2-m-wide rectangular plate is made of graphite epoxy. The material properties are given in Table 3.6 (page 81). The layup is* $[\pm 45_2^t/0_{12}/\pm 45_2^t]$. *The 0-degree plies are parallel to the short edge of the plate. The plate is simply supported along all four edges (Fig. 4.44). The mass of the plate is uniform* ($\rho = 3.2$ *kg/m*^{2}). *Calculate the natural frequencies.*

Solution. From Eq. (4.226), with the stiffnesses $D_{11} = 45.30$ N·m, $D_{22} = 25.26$ N·m, $D_{12} = 19.52$ N·m, $D_{66} = 20.62$ N·m (Table 3.7, page 84) we have

$$f_{ij} = \sqrt{\frac{\pi^2}{4\rho}\left[D_{11}\left(\frac{i}{L_x}\right)^4 + 2\left(D_{12}+2D_{66}\right)\left(\frac{i}{L_x}\right)^2\left(\frac{j}{L_y}\right)^2 + D_{22}\left(\frac{j}{L_y}\right)^4\right]}$$

$$= \sqrt{21\,830 i^4 + 4\,780 i^2 j^2 + 81.11 j^4}. \tag{4.227}$$

This yields the following values of f_{ij} (Hz):

$i \setminus j$	1	2	3
1	163	205	267
2	607	653	727
3	1 346	1 393	1 470.

The lowest natural frequency corresponds to $i = j = 1$, and is

$$f_{11} = 163 \text{ Hz}. \tag{4.228}$$

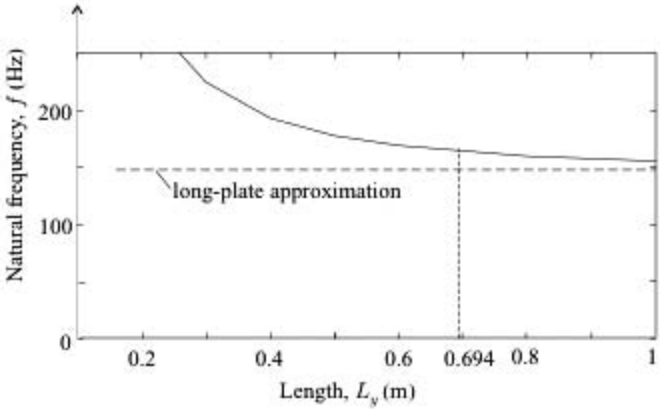

Figure 4.45: The lowest natural frequency of the plate in Example 4.14 as a function of the plate length.

We now assess the length-to-width ratios under which the long-plate approximation is reasonable. To this end, we calculated the lowest natural frequency of the plate, keeping the width L_x the same while changing the length L_y. In Figure 4.45 we plot the lowest natural frequency thus calculated versus L_y. In this figure we also included the lowest natural frequency given by the long-plate approximation (Eq. 4.204). The results in this figure show that, in accordance with Eq. (4.19), the long-plate formula approximates within 10 percent the natural frequency when L_y is greater than $3L_x\sqrt[4]{D_{11}/D_{22}} = 0.694$ m.

4.15 Example. *A 0.2-m-long and 0.2-m-wide rectangular plate is made of graphite epoxy unidirectional plies. The material properties are given in Table 3.6 (page 81). The layup is* $[0_2/45_2/90_2/-45_2]_s$. *The plate is simply supported along the four edges (Fig. 4.46). The mass of the plate is uniform* ($\rho = 2.56\ kg/m^2$). *Calculate the natural frequencies.*

Solution. The layup of the plate is symmetrical but not orthotropic. The bending stiffnesses are $D_{11} = 34.61$ N·m, $D_{22} = 12.34$ N·m, $D_{12} = 4.58$ N·m, $D_{66} = 5.14$ N·m, $D_{16} = 3.34$ N·m, $D_{26} = 3.34$ N·m (Table 3.7, page 84). The natural frequencies are calculated from Eqs. (4.224) and (4.223). With the preceding

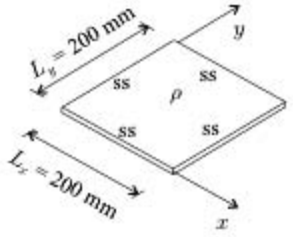

Figure 4.46: The plate in Example 4.15.

stiffnesses, and with $I = J = 7$, these calculations yield the following f_{ij} (Hz) values:

$i \setminus j$	1	2	3
1	211	446	910
2	640	797	1 179
3	1 359	1 569	1 955.

(4.229)

The layup follows the 10-percent rule (page 89), and we may treat the plate as orthotropic. From Eq. (4.226) we have

$$f_{ij} = \sqrt{\frac{\pi^2}{4\rho}\left[D_{11}\left(\frac{i}{L_x}\right)^4 + 2\left(D_{12}+2D_{66}\right)\left(\frac{i}{L_x}\right)^2\left(\frac{j}{L_y}\right)^2 + D_{22}\left(\frac{j}{L_y}\right)^4\right]}$$

$$= \sqrt{20\,850i^4 + 17\,910i^2j^2 + 7\,435j^4}. \tag{4.230}$$

The values of f_{ij} (Hz) are

$i \setminus j$	1	2	3
1	215	460	886
2	642	860	1 257
3	1 363	1 566	1 934.

(4.231)

We see that these natural frequencies (which are based on the orthotropy approximation) are within 8 percent of the natural frequencies resulting from the exact calculations (see Eq. 4.229).

4.4.3 Plates with Built-In and Simply Supported Edges – Orthotropic and Symmetrical Layup

We consider rectangular plates with length L_x and width L_y. Each edge of the plate is either simply supported or built-in. The layup of the plate is orthotropic and symmetrical. Following Hearmon[39] the natural frequencies of the plate are calculated by the Rayleigh energy method.

Under free vibration the deflection of the plate is (Eq. 4.189)

$$w^o = \overline{w}^o \sin(2\pi f t). \tag{4.232}$$

By introducing this w^o into the expression of the strain energy (Eq. 4.107), and by setting $D_{16} = D_{26} = 0$, we obtain

$$U = \overline{U} \sin^2(2\pi f t), \tag{4.233}$$

[39] R. F. S. Hearmon, The Frequency of Flexural Vibration of Rectangular Orthotropic Plates with Clamped or Simply Supported Edges. *Journal of Applied Mechanics*, Vol. 26, 537–540, 1959.

where $\overline{U}$ is defined as

$$\overline{U} = \frac{1}{2}\int_0^{L_x}\int_0^{L_y}\left[D_{11}\left(\frac{\partial^2\overline{w}^o}{\partial x^2}\right)^2 + D_{22}\left(\frac{\partial^2\overline{w}^o}{\partial y^2}\right)^2 + D_{66}\left(\frac{2\partial^2\overline{w}^o}{\partial x\partial y}\right)^2 + 2\left(D_{12}\frac{\partial^2\overline{w}^o}{\partial x^2}\frac{\partial^2\overline{w}^o}{\partial y^2}\right)\right]dydx. \tag{4.234}$$

By following the same steps as in Section 4.4.2, we arrive at

$$(2\pi f)^2 = \frac{\overline{U}}{\frac{1}{2}\int_0^{L_x}\int_0^{L_y}\rho\overline{w}^{o2}dydx}. \tag{4.235}$$

The deflection is assumed to be of the form

$$\overline{w}^o = AX_i(x)Y_j(y), \tag{4.236}$$

where A is the, as yet unknown, amplitude. For $X_i(x)$ and $Y_j(y)$ we adopt the shape of a freely vibrating beam. For different end supports these functions are given in Table 4.4 (page 119). The variables i and j represent the number of half waves in the x and y directions, respectively (Fig. 4.19).

By introducing Eq. (4.236) into Eq. (4.235), and by performing the integration, we obtain

$$\lambda_{ij} = \frac{1}{4}L_xL_y\left(D_{11}\frac{\alpha_1^4}{L_x^4} + D_{22}\frac{\alpha_3^4}{L_y^4} + 2(D_{12}+2D_{66})\frac{\alpha_2}{L_x^2L_y^2}\right). \tag{4.237}$$

where λ_{ij} is the eigenvalue, which is defined as

$$\lambda_{ij} = \frac{1}{4}(2\pi f_{ij})^2\rho L_xL_y. \tag{4.238}$$

The parameters α_1, α_2, α_3, α_4, α_5 are given in Table 4.5. The values of α_1 through α_5 must be calculated numerically. The integrations simlify when $X_i(x)$ and $Y_j(y)$ are calculated by the approximate expressions of μ_i given in Table 4.4. The resulting approximate expressions for α_1 through α_5 are given in Tables 4.6 and 4.7, whereas α_2 is

$$\alpha_2 = \alpha_4\alpha_5. \tag{4.239}$$

The parameters α_1–α_5 and the corresponding eigenvalues λ_{ij} must be calculated for different sets of i and j, ($i, j = 1, 2, \ldots$). The natural frequencies are then calculated by

$$f_{ij} = \frac{1}{\pi}\sqrt{\frac{\lambda_{ij}}{\rho L_xL_y}} = \frac{1}{2\pi}\sqrt{\frac{1}{\rho}\left(D_{11}\frac{\alpha_1^4}{L_x^4} + D_{22}\frac{\alpha_3^4}{L_y^4} + 2(D_{12}+2D_{66})\frac{\alpha_2}{L_x^2L_y^2}\right)}. \tag{4.240}$$

4.16 Example. *A 0.2-m-long and 0.2-m-wide rectangular plate is made of graphite epoxy unidirectional plies. The material properties are given in Table 3.6*

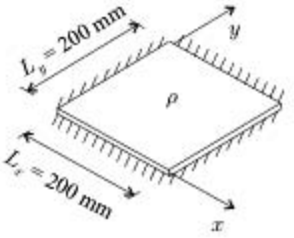

Figure 4.47: The plate in Example 4.16.

(page 81). The layup is $[0_2/45_2/90_2/-45_2]_s$. *The plate is built-in along the four edges (Fig. 4.47). The mass of the plate is uniform* ($\rho = 2.56$ *kg/m*^{2}). *Calculate the natural frequencies.*

Solution. The layup follows the 10-percent rule (page 89), and we treat the plate as orthotropic. With the stiffnesses $D_{11} = 34.61$ N·m, $D_{22} = 12.34$ N·m, $D_{12} = 4.58$ N·m, $D_{66} = 5.14$ N·m, $D_{16} = 3.34$ N·m, $D_{26} = 3.34$ N·m (Table 3.7, page 84) Eq. (4.240) yields

$$f_{ij} = \frac{1}{2\pi}\sqrt{\frac{1}{\rho}\left[D_{11}\frac{\alpha_1^4}{L_x^4} + D_{22}\frac{\alpha_3^4}{L_y^4} + 2\left(D_{12}+2D_{66}\right)\frac{\alpha_2}{L_x^2 L_y^2}\right]}$$
$$= \sqrt{214\alpha_1^4 + 184\alpha_3^4 + 76.3\alpha_4\alpha_5}, \qquad (4.241)$$

where α_1 and α_4 depend on i ($i = 1, 2, \ldots$) and α_3 and α_5 depend on j ($j = 1, 2, \ldots$) as given in Tables 4.6 and 4.7, third row. From these tables the values are

	$i=1$	$i=2$	$i=3$
α_1	4.73	7.85	11.00
α_4	12.91	45.98	98.91

	$j=1$	$j=2$	$j=3$
α_3	4.73	7.85	11.00
α_5	12.91	45.98	98.91 .

The values of f_{ij} (Hz) are (Eq. 4.241)

$i \setminus j$	1	2	3
1	420	712	1 207
2	981	1 222	1 663
3	1 844	2 063	2 458 .

4.5 Hygrothermal Effects

We consider a small element of a thin plate. The temperature and moisture concentration (both of which may vary across the thickness of the plate) are T and c,

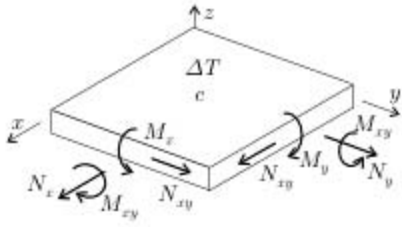

Figure 4.48: Hygrothermal and mechanical loads on a plate element.

respectively. In-plane forces and moments may also act on the element (Fig. 4.48). Owing to these hygrothermal and mechanical loads, under plane-stress condition, the strains at a point are (see Eqs. 2.155 and 2.156)

$$\begin{Bmatrix} \epsilon_x \\ \epsilon_y \\ \gamma_{xy} \end{Bmatrix} = \begin{bmatrix} \overline{S}_{11} & \overline{S}_{12} & \overline{S}_{16} \\ \overline{S}_{21} & \overline{S}_{22} & \overline{S}_{26} \\ \overline{S}_{61} & \overline{S}_{62} & \overline{S}_{66} \end{bmatrix} \begin{Bmatrix} \sigma_x \\ \sigma_y \\ \tau_{xy} \end{Bmatrix} + \Delta T \begin{Bmatrix} \widetilde{\alpha}_x \\ \widetilde{\alpha}_y \\ \widetilde{\alpha}_{xy} \end{Bmatrix} + c \begin{Bmatrix} \widetilde{\beta}_x \\ \widetilde{\beta}_y \\ \widetilde{\beta}_{xy} \end{Bmatrix}, \tag{4.242}$$

where ΔT is the temperature difference relative to a reference temperature

$$\Delta T = T - T_{\text{ref}}, \tag{4.243}$$

and $\widetilde{\alpha}$ and $\widetilde{\beta}$ are the thermal expansion and moisture expansion coefficients (Section 2.6). The stress at a point is obtained by inverting Eq. (4.242) as follows:

$$\begin{Bmatrix} \sigma_x \\ \sigma_y \\ \tau_{xy} \end{Bmatrix} = [\overline{Q}] \left(\begin{Bmatrix} \epsilon_x \\ \epsilon_y \\ \gamma_{xy} \end{Bmatrix} - \Delta T \begin{Bmatrix} \widetilde{\alpha}_x \\ \widetilde{\alpha}_y \\ \widetilde{\alpha}_{xy} \end{Bmatrix} - c \begin{Bmatrix} \widetilde{\beta}_x \\ \widetilde{\beta}_y \\ \widetilde{\beta}_{xy} \end{Bmatrix} \right). \tag{4.244}$$

By definition, the forces and moments are (Eq. 3.9)

$$\begin{Bmatrix} N_x \\ N_y \\ N_{xy} \end{Bmatrix} = \int_{-h_b}^{h_t} \begin{Bmatrix} \sigma_x \\ \sigma_y \\ \tau_{xy} \end{Bmatrix} dz \qquad \begin{Bmatrix} M_x \\ M_y \\ M_{xy} \end{Bmatrix} = \int_{-h_b}^{h_t} z \begin{Bmatrix} \sigma_x \\ \sigma_y \\ \tau_{xy} \end{Bmatrix} dz. \tag{4.245}$$

It is convenient to define the following equivalent generalized hygrothermal forces:

$$\begin{Bmatrix} N_x^{\text{ht}} \\ N_y^{\text{ht}} \\ N_{xy}^{\text{ht}} \end{Bmatrix} = \int_{-h_b}^{h_t} [\overline{Q}] \left(\Delta T \begin{Bmatrix} \widetilde{\alpha}_x \\ \widetilde{\alpha}_y \\ \widetilde{\alpha}_{xy} \end{Bmatrix} + c \begin{Bmatrix} \widetilde{\beta}_x \\ \widetilde{\beta}_y \\ \widetilde{\beta}_{xy} \end{Bmatrix} \right) dz \tag{4.246}$$

$$\begin{Bmatrix} M_x^{\text{ht}} \\ M_y^{\text{ht}} \\ M_{xy}^{\text{ht}} \end{Bmatrix} = \int_{-h_b}^{h_t} z[\overline{Q}] \left(\Delta T \begin{Bmatrix} \widetilde{\alpha}_x \\ \widetilde{\alpha}_y \\ \widetilde{\alpha}_{xy} \end{Bmatrix} + c \begin{Bmatrix} \widetilde{\beta}_x \\ \widetilde{\beta}_y \\ \widetilde{\beta}_{xy} \end{Bmatrix} \right) dz. \tag{4.247}$$

With the definitions of the $[A]$, $[B]$, and $[D]$ matrices (Section 3.2.2), Eqs. (4.244)–(4.247) may be combined to yield

$$\begin{Bmatrix} N_x \\ N_y \\ N_{xy} \\ M_x \\ M_y \\ M_{xy} \end{Bmatrix} = \begin{bmatrix} A_{11} & A_{12} & A_{16} & B_{11} & B_{12} & B_{16} \\ A_{12} & A_{22} & A_{26} & B_{12} & B_{22} & B_{26} \\ A_{16} & A_{26} & A_{66} & B_{16} & B_{26} & B_{66} \\ B_{11} & B_{12} & B_{16} & D_{11} & D_{12} & D_{16} \\ B_{12} & B_{22} & B_{26} & D_{12} & D_{22} & D_{26} \\ B_{16} & B_{26} & B_{66} & D_{16} & D_{26} & D_{66} \end{bmatrix} \begin{Bmatrix} \epsilon_x^o \\ \epsilon_y^o \\ \gamma_{xy}^o \\ \kappa_x \\ \kappa_y \\ \kappa_{xy} \end{Bmatrix} - \begin{Bmatrix} N_x^{ht} \\ N_y^{ht} \\ N_{xy}^{ht} \\ M_x^{ht} \\ M_y^{ht} \\ M_{xy}^{ht} \end{Bmatrix} \tag{4.248}$$

$$\begin{Bmatrix} \epsilon_x^o \\ \epsilon_y^o \\ \gamma_{xy}^o \\ \kappa_x \\ \kappa_y \\ \kappa_{xy} \end{Bmatrix} = \begin{bmatrix} \alpha_{11} & \alpha_{12} & \alpha_{16} & \beta_{11} & \beta_{12} & \beta_{16} \\ \alpha_{12} & \alpha_{22} & \alpha_{26} & \beta_{21} & \beta_{22} & \beta_{26} \\ \alpha_{16} & \alpha_{26} & \alpha_{66} & \beta_{61} & \beta_{62} & \beta_{66} \\ \beta_{11} & \beta_{21} & \beta_{61} & \delta_{11} & \delta_{12} & \delta_{16} \\ \beta_{12} & \beta_{22} & \beta_{62} & \delta_{12} & \delta_{22} & \delta_{26} \\ \beta_{16} & \beta_{26} & \beta_{66} & \delta_{16} & \delta_{26} & \delta_{66} \end{bmatrix} \left(\begin{Bmatrix} N_x \\ N_y \\ N_{xy} \\ M_x \\ M_y \\ M_{xy} \end{Bmatrix} + \begin{Bmatrix} N_x^{ht} \\ N_y^{ht} \\ N_{xy}^{ht} \\ M_x^{ht} \\ M_y^{ht} \\ M_{xy}^{ht} \end{Bmatrix} \right), \tag{4.249}$$

where α_{ij}, β_{ij}, and δ_{ij} are the elements of the compliance matrices (Eq. 3.22). We define the following generalized hygrothermal strains and curvatures:

$$\begin{Bmatrix} \epsilon_x^{o,ht} \\ \epsilon_y^{o,ht} \\ \gamma_{xy}^{o,ht} \\ \kappa_x^{ht} \\ \kappa_y^{ht} \\ \kappa_{xy}^{ht} \end{Bmatrix} = \begin{bmatrix} \alpha_{11} & \alpha_{12} & \alpha_{16} & \beta_{11} & \beta_{12} & \beta_{16} \\ \alpha_{12} & \alpha_{22} & \alpha_{26} & \beta_{21} & \beta_{22} & \beta_{26} \\ \alpha_{16} & \alpha_{26} & \alpha_{66} & \beta_{61} & \beta_{62} & \beta_{66} \\ \beta_{11} & \beta_{21} & \beta_{61} & \delta_{11} & \delta_{12} & \delta_{16} \\ \beta_{12} & \beta_{22} & \beta_{62} & \delta_{12} & \delta_{22} & \delta_{26} \\ \beta_{16} & \beta_{26} & \beta_{66} & \delta_{16} & \delta_{26} & \delta_{66} \end{bmatrix} \begin{Bmatrix} N_x^{ht} \\ N_y^{ht} \\ N_{xy}^{ht} \\ M_x^{ht} \\ M_y^{ht} \\ M_{xy}^{ht} \end{Bmatrix}. \tag{4.250}$$

These generalized hygrothermal strains would occur in the reference plane of an unrestrained plate subjected to changes in temperature and moisture content.

Expressions for calculating N^{ht}, M^{ht} (Eqs. 4.246 and 4.247) are given in Table 4.13 for piecewise linear, linear, and uniform temperature distributions (Fig. 4.49).

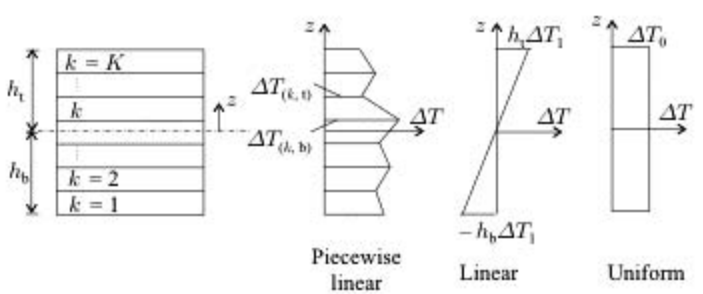

Figure 4.49: Piecewise linear, linear, and uniform temperature distributions across the plate.

Table 4.13. The hygrothermal forces N^{ht},M^{ht} for piecewise linear, linear, and uniform temperature distributions (Fig. 4.49). The $\Delta T_{(k,t)}$ and $\Delta T_{(k,b)}$ refer to the top and bottom of the kth layer. For piecewise linear, linear, and uniform moisture distributions ΔT and $\tilde{\alpha}$ are replaced by c and $\tilde{\beta}$.

Piecewise linear temperature distribution

$$\begin{Bmatrix} N_x^{ht} \\ N_y^{ht} \\ N_{xy}^{ht} \end{Bmatrix} = \sum_{k=1}^{K} \left(\frac{z_k - z_{k-1}}{2} [\overline{Q}]_k (\Delta T_{(k,t)} + \Delta T_{(k,b)}) \begin{Bmatrix} \tilde{\alpha}_x \\ \tilde{\alpha}_y \\ \tilde{\alpha}_{xy} \end{Bmatrix}_k \right)$$

$$\begin{Bmatrix} M_x^{ht} \\ M_y^{ht} \\ M_{xy}^{ht} \end{Bmatrix} = \sum_{k=1}^{K} \frac{z_k^3 - z_{k-1}^3}{3(z_k - z_{k-1})} [\overline{Q}]_k (\Delta T_{(k,t)} - \Delta T_{(k,b)}) \begin{Bmatrix} \tilde{\alpha}_x \\ \tilde{\alpha}_y \\ \tilde{\alpha}_{xy} \end{Bmatrix}_k + \sum_{k=1}^{K} \frac{z_k + z_{k-1}}{2} [\overline{Q}]_k (z_k \Delta T_{(k,b)} - z_{k-1} \Delta T_{(k,t)}) \begin{Bmatrix} \tilde{\alpha}_x \\ \tilde{\alpha}_y \\ \tilde{\alpha}_{xy} \end{Bmatrix}_k$$

Linear temperature distribution

$$\begin{Bmatrix} N_x^{ht} \\ N_y^{ht} \\ N_{xy}^{ht} \end{Bmatrix} = \Delta T_l \sum_{k=1}^{K} \frac{z_k^2 - z_{k-1}^2}{2} [\overline{Q}]_k \begin{Bmatrix} \tilde{\alpha}_x \\ \tilde{\alpha}_y \\ \tilde{\alpha}_{xy} \end{Bmatrix}_k$$

$$\begin{Bmatrix} M_x^{ht} \\ M_y^{ht} \\ M_{xy}^{ht} \end{Bmatrix} = \Delta T_l \sum_{k=1}^{K} \frac{z_k^3 - z_{k-1}^3}{3} [\overline{Q}]_k \begin{Bmatrix} \tilde{\alpha}_x \\ \tilde{\alpha}_y \\ \tilde{\alpha}_{xy} \end{Bmatrix}_k$$

Constant temperature distribution

$$\begin{Bmatrix} N_x^{ht} \\ N_y^{ht} \\ N_{xy}^{ht} \end{Bmatrix} = \Delta T_0 \sum_{k=1}^{K} \left((z_k - z_{k-1}) [\overline{Q}]_k \begin{Bmatrix} \tilde{\alpha}_x \\ \tilde{\alpha}_y \\ \tilde{\alpha}_{xy} \end{Bmatrix}_k \right)$$

$$\begin{Bmatrix} M_x^{ht} \\ M_y^{ht} \\ M_{xy}^{ht} \end{Bmatrix} = \Delta T_0 \sum_{k=1}^{K} \left(\frac{z_k^2 - z_{k-1}^2}{2} [\overline{Q}]_k \begin{Bmatrix} \tilde{\alpha}_x \\ \tilde{\alpha}_y \\ \tilde{\alpha}_{xy} \end{Bmatrix}_k \right)$$

With the preceding definition of the hygrothermal strains Eqs. (4.248) and (4.249) may be written in the following forms:

$$\begin{Bmatrix} N_x \\ N_y \\ N_{xy} \\ M_x \\ M_y \\ M_{xy} \end{Bmatrix} = \begin{bmatrix} A_{11} & A_{12} & A_{16} & B_{11} & B_{12} & B_{16} \\ A_{12} & A_{22} & A_{26} & B_{12} & B_{22} & B_{26} \\ A_{16} & A_{26} & A_{66} & B_{16} & B_{26} & B_{66} \\ B_{11} & B_{12} & B_{16} & D_{11} & D_{12} & D_{16} \\ B_{12} & B_{22} & B_{26} & D_{12} & D_{22} & D_{26} \\ B_{16} & B_{26} & B_{66} & D_{16} & D_{26} & D_{66} \end{bmatrix} \left(\begin{Bmatrix} \epsilon_x^o \\ \epsilon_y^o \\ \gamma_{xy}^o \\ \kappa_x \\ \kappa_y \\ \kappa_{xy} \end{Bmatrix} - \begin{Bmatrix} \epsilon_x^{o,ht} \\ \epsilon_y^{o,ht} \\ \gamma_{xy}^{o,ht} \\ \kappa_x^{ht} \\ \kappa_y^{ht} \\ \kappa_{xy}^{ht} \end{Bmatrix} \right) \tag{4.251}$$

$$\begin{Bmatrix} \epsilon_x^o \\ \epsilon_y^o \\ \gamma_{xy}^o \\ \kappa_x \\ \kappa_y \\ \kappa_{xy} \end{Bmatrix} = \begin{bmatrix} \alpha_{11} & \alpha_{12} & \alpha_{16} & \beta_{11} & \beta_{12} & \beta_{16} \\ \alpha_{12} & \alpha_{22} & \alpha_{26} & \beta_{21} & \beta_{22} & \beta_{26} \\ \alpha_{16} & \alpha_{26} & \alpha_{66} & \beta_{61} & \beta_{62} & \beta_{66} \\ \beta_{11} & \beta_{21} & \beta_{61} & \delta_{11} & \delta_{12} & \delta_{16} \\ \beta_{12} & \beta_{22} & \beta_{62} & \delta_{12} & \delta_{22} & \delta_{26} \\ \beta_{16} & \beta_{26} & \beta_{66} & \delta_{16} & \delta_{26} & \delta_{66} \end{bmatrix} \begin{Bmatrix} N_x \\ N_y \\ N_{xy} \\ M_x \\ M_y \\ M_{xy} \end{Bmatrix} + \begin{Bmatrix} \epsilon_x^{o,ht} \\ \epsilon_y^{o,ht} \\ \gamma_{xy}^{o,ht} \\ \kappa_x^{ht} \\ \kappa_y^{ht} \\ \kappa_{xy}^{ht} \end{Bmatrix}. \tag{4.252}$$

Rectangular plates with free edges. We consider a rectangular unsupported plate, that is, all four of the edges are free. The plate is subjected to pure bending, in-plane mechanical loads, and to hygrothermal loads. Such a plate can be analyzed by Eq. (4.248). In these equations the temperature and moisture distributions across the plate must be specified as well as 6 of the following 12 quantities (Table 4.14):

$$\begin{array}{llll} N_x & \text{or} & \epsilon_x^o & M_x \quad \text{or} \quad \kappa_x \\ N_y & \text{or} & \epsilon_y^o & M_y \quad \text{or} \quad \kappa_y \\ N_{xy} & \text{or} & \epsilon_{xy}^o & M_{xy} \quad \text{or} \quad \kappa_{xy}. \end{array} \tag{4.253}$$

The deflection of the plate is calculated by Eq. (4.16).

When the unsupported plate is subjected only to a temperature change ΔT and moisture c, the mechanical loads are zero (Table 4.14) as follows:

$$N_x = 0 \qquad N_y = 0 \qquad N_{xy} = 0 \tag{4.254}$$

$$M_x = 0 \qquad M_y = 0 \qquad M_{xy} = 0. \tag{4.255}$$

In this case the strains and curvatures are (see Eqs. 4.249 and 4.250)

$$\begin{Bmatrix} \epsilon_x^o \\ \epsilon_y^o \\ \gamma_{xy}^o \\ \kappa_x \\ \kappa_y \\ \kappa_{xy} \end{Bmatrix} = \begin{Bmatrix} \epsilon_x^{o,ht} \\ \epsilon_y^{o,ht} \\ \gamma_{xy}^{o,ht} \\ \kappa_x^{ht} \\ \kappa_y^{ht} \\ \kappa_{xy}^{ht} \end{Bmatrix}. \tag{4.256}$$

Rectangular plates with built-in edges. When a plate with built-in edges is subjected only to a temperature change ΔT and moisture c, the strains and curvatures are zero (Table 4.14) as follows:

$$\epsilon_x^o = 0 \qquad \epsilon_y^o = 0 \qquad \gamma_{xy}^o = 0 \tag{4.257}$$

$$\kappa_x = 0 \qquad \kappa_y = 0 \qquad \kappa_{xy} = 0. \tag{4.258}$$

The normal forces and moments are calculated by Eqs. (4.246)–(4.248).

Long rectangular plates. When the plate is long and is subjected only to a change in temperature ΔT and moisture content c, some of the strains, curvatures, moments, and in-plane loads are zero, as shown in Table 4.14. The response of the plate is then calculated by setting equal to zero in Eq. (4.248) the quantities indicated in this table. The deflections of the plate are calculated by Eq. (4.16).

Table 4.14. Rectangular plates subjected to hygrothermal and mechanical loads.

Loading	Conditions
	N_x or ϵ_x^o N_y or ϵ_y^o N_{xy} or ϵ_{xy}^o M_x or κ_x M_y or κ_y M_{xy} or κ_{xy}
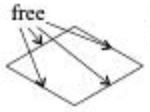	$N_x = 0 \quad N_y = 0 \quad N_{xy} = 0$ $M_x = 0 \quad M_y = 0 \quad M_{xy} = 0$
	$\epsilon_x^o = 0 \quad \epsilon_y^o = 0 \quad \gamma_{xy}^o = 0$ $\kappa_x = 0 \quad \kappa_y = 0 \quad \kappa_{xy} = 0$
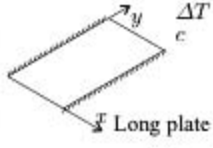	$\epsilon_x^o = 0 \quad \epsilon_y^o = 0 \quad \gamma_{xy}^o = 0$ $\kappa_x = 0 \quad \kappa_y = 0 \quad \kappa_{xy} = 0$
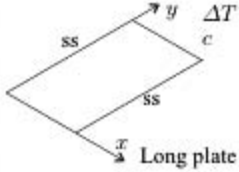	$\epsilon_y^o = 0 \quad \kappa_y = 0 \quad \kappa_{xy} = 0$ $N_x = 0 \quad N_{xy} = 0 \quad M_x = 0$
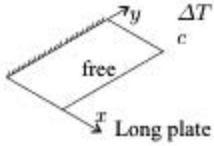	$\epsilon_y^o = 0 \quad \kappa_y = 0 \quad \kappa_{xy} = 0$ $N_x = 0 \quad N_{xy} = 0 \quad M_x = 0$

4.17 Example. *A 1-m-long and 1-m-wide plate is made of graphite epoxy unidirectional plies. The layup is* $[45_6/0_4]_s$. *The edges of the plate are free. The temperature of the bottom surface is raised by* 80 °C *and the top surface by* 120 °C *(Fig. 4.50). Estimate the temperature-induced change in the dimensions of the plate. The ply*

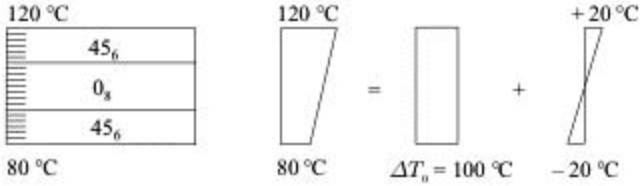

Figure 4.50: Illustration of the plate in Example 4.17.

properties are given in Table 3.6, (page 81) the thermal expansion coefficients are $\widetilde{\alpha}_1 = -0.7 \times 10^{-6} \frac{1}{°C}$ *and* $\widetilde{\alpha}_2 = 25 \times 10^{-6} \frac{1}{°C}$.

Solution. The temperature distribution across the plate is represented by the sum of a constant and a linearly varying temperature distribution, as shown in Figure 4.50. The temperature differences shown in this figure are

$$\Delta T_0 = \frac{80 + 120}{2} = 100\,°\text{C} \qquad \Delta T_1 = \frac{120 - 80}{h} = 20\,000\,°\text{C/m}, \tag{4.259}$$

where $h = 0.002$ m is the thickness of the plate. The hygrothermal forces are (Table 4.13, page 154)

$$\left\{\begin{matrix} N_x^{ht} \\ N_y^{ht} \\ N_{xy}^{ht} \end{matrix}\right\}_{\Delta T_0} = \Delta T_0 \sum_{k=1}^{K} \left((z_k - z_{k-1}) [\overline{Q}]_k \left\{\begin{matrix} \widetilde{\alpha}_x \\ \widetilde{\alpha}_y \\ \widetilde{\alpha}_{xy} \end{matrix}\right\}_k \right) \tag{4.260}$$

$$\left\{\begin{matrix} M_x^{ht} \\ M_y^{ht} \\ M_{xy}^{ht} \end{matrix}\right\}_{\Delta T_0} = \Delta T_0 \sum_{k=1}^{K} \left(\frac{z_k^2 - z_{k-1}^2}{2} [\overline{Q}]_k \left\{\begin{matrix} \widetilde{\alpha}_x \\ \widetilde{\alpha}_y \\ \widetilde{\alpha}_{xy} \end{matrix}\right\}_k \right) \tag{4.261}$$

$$\left\{\begin{matrix} N_x^{ht} \\ N_y^{ht} \\ N_{xy}^{ht} \end{matrix}\right\}_{\Delta T_1} = \Delta T_1 \sum_{k=1}^{K} \frac{z_k^2 - z_{k-1}^2}{2} [\overline{Q}]_k \left\{\begin{matrix} \widetilde{\alpha}_x \\ \widetilde{\alpha}_y \\ \widetilde{\alpha}_{xy} \end{matrix}\right\}_k \tag{4.262}$$

$$\left\{\begin{matrix} M_x^{ht} \\ M_y^{ht} \\ M_{xy}^{ht} \end{matrix}\right\}_{\Delta T_1} = \Delta T_1 \sum_{k=1}^{K} \frac{z_k^3 - z_{k-1}^3}{3} [\overline{Q}]_k \left\{\begin{matrix} \widetilde{\alpha}_x \\ \widetilde{\alpha}_y \\ \widetilde{\alpha}_{xy} \end{matrix}\right\}_k . \tag{4.263}$$

The stiffness matrices $[\overline{Q}]$ for the zero and 45-degree plies are (Eqs. 3.49 and 3.52)

$$[\overline{Q}]^0 = \begin{bmatrix} 148.87 & 2.91 & 0 \\ 2.91 & 9.71 & 0 \\ 0 & 0 & 4.55 \end{bmatrix} 10^9 \frac{\text{N}}{\text{m}^2} \quad [\overline{Q}]^{45} = \begin{bmatrix} 45.65 & 36.55 & 34.79 \\ 36.55 & 45.65 & 34.79 \\ 34.79 & 34.79 & 38.19 \end{bmatrix} 10^9 \frac{\text{N}}{\text{m}^2}. \tag{4.264}$$

The thermal expansion coefficients of the 0-degree plies are

$$\left\{\begin{matrix} \widetilde{\alpha}_x \\ \widetilde{\alpha}_y \\ 0 \end{matrix}\right\}^0 = \left\{\begin{matrix} \widetilde{\alpha}_1 \\ \widetilde{\alpha}_2 \\ 0 \end{matrix}\right\} = \left\{\begin{matrix} -0.7 \\ 25 \\ 0 \end{matrix}\right\} 10^{-6} \frac{1}{°\text{C}}, \tag{4.265}$$

where $\widetilde{\alpha}_1 = -0.7 \times 10^{-6} \frac{1}{°C}$ and $\widetilde{\alpha}_2 = 25 \times 10^{-6} \frac{1}{°C}$ are the thermal expansion coefficients parallel and perpendicular to the fibers. The thermal expansion coefficients

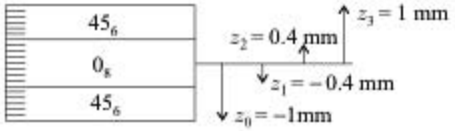

Figure 4.51: The layup of the plate in Example 4.17.

transform as the strains. By replacing ϵ by $\widetilde{\alpha}$ in Eq. (2.188) we obtain

$$\begin{Bmatrix} \widetilde{\alpha}_1 \\ \widetilde{\alpha}_2 \\ 0 \end{Bmatrix} = [T_\epsilon] \begin{Bmatrix} \widetilde{\alpha}_x \\ \widetilde{\alpha}_y \\ \widetilde{\alpha}_{xy} \end{Bmatrix}^{45}, \tag{4.266}$$

where $[T_\epsilon]$ is given by Eq. (3.51). Hence, in the 45-degree direction the thermal expression coefficients are

$$\begin{Bmatrix} \widetilde{\alpha}_x \\ \widetilde{\alpha}_y \\ \widetilde{\alpha}_{xy} \end{Bmatrix}^{45} = \begin{bmatrix} 0.5 & 0.5 & 0.5 \\ 0.5 & 0.5 & -0.5 \\ -1.0 & 1.0 & 0 \end{bmatrix}^{-1} \begin{Bmatrix} \widetilde{\alpha}_1 \\ \widetilde{\alpha}_2 \\ 0 \end{Bmatrix} = \begin{Bmatrix} 12.15 \\ 12.15 \\ -25.70 \end{Bmatrix} 10^{-6} \frac{1}{^\circ\text{C}}, \tag{4.267}$$

where z is the distance from the midplane (Fig. 4.51, $z_0 = -0.001$ m, $z_1 = -0.0004$ m, $z_2 = 0.0004$ m, $z_3 = 0.001$ m) and K is the number of ply groups ($K = 3$). With the preceding values of $[\overline{Q}]$ and $\widetilde{\alpha}$ the hygrothermal forces and moments are

$$\begin{Bmatrix} N_x^{ht} \\ N_y^{ht} \\ N_{xy}^{ht} \end{Bmatrix}_{\Delta T_0} = \begin{Bmatrix} 10\,041 \\ 31\,804 \\ -16\,323 \end{Bmatrix} \frac{\text{N}}{\text{m}} \qquad \begin{Bmatrix} M_x^{ht} \\ M_y^{ht} \\ M_{xy}^{ht} \end{Bmatrix}_{\Delta T_0} = \begin{Bmatrix} 0 \\ 0 \\ 0 \end{Bmatrix} \tag{4.268}$$

$$\begin{Bmatrix} N_x^{ht} \\ N_y^{ht} \\ N_{xy}^{ht} \end{Bmatrix}_{\Delta T_i} = \begin{Bmatrix} 0 \\ 0 \\ 0 \end{Bmatrix} \qquad \begin{Bmatrix} M_x^{ht} \\ M_y^{ht} \\ M_{xy}^{ht} \end{Bmatrix}_{\Delta T_i} = \begin{Bmatrix} 16.195 \\ 5.143 \\ -4.697 \end{Bmatrix} 10^6 \text{N}. \tag{4.269}$$

The hygrothermal strains are given by (Eq. 4.250)

$$\begin{Bmatrix} \epsilon_x^{0,ht} \\ \epsilon_y^{0,ht} \\ \gamma_{xy}^{0,ht} \\ \kappa_x^{ht} \\ \kappa_y^{ht} \\ \kappa_{xy}^{ht} \end{Bmatrix} = \begin{bmatrix} \alpha_{11} & \alpha_{12} & \alpha_{16} & \beta_{11} & \beta_{12} & \beta_{16} \\ \alpha_{12} & \alpha_{22} & \alpha_{26} & \beta_{21} & \beta_{22} & \beta_{26} \\ \alpha_{16} & \alpha_{26} & \alpha_{66} & \beta_{61} & \beta_{62} & \beta_{66} \\ \beta_{11} & \beta_{21} & \beta_{61} & \delta_{11} & \delta_{12} & \delta_{16} \\ \beta_{12} & \beta_{22} & \beta_{62} & \delta_{12} & \delta_{22} & \delta_{26} \\ \beta_{16} & \beta_{26} & \beta_{66} & \delta_{16} & \delta_{26} & \delta_{66} \end{bmatrix} \begin{Bmatrix} N_x^{ht} \\ N_y^{ht} \\ N_{xy}^{ht} \\ M_x^{ht} \\ M_y^{ht} \\ M_{xy}^{ht} \end{Bmatrix}. \tag{4.270}$$

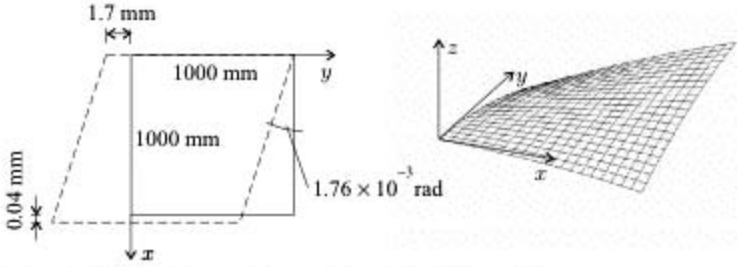

Figure 4.52: The deformed shape of the plate in Example 4.17.

The layup is symmetrical ($[\beta] = 0$), and the compliance matrices are (Table 3.8, page 85)

$$[\alpha] = [a] = \begin{bmatrix} 7.45 & -2.99 & -3.77 \\ -2.99 & 37.81 & -29.39 \\ -3.77 & -29.39 & 48.20 \end{bmatrix} 10^{-9} \frac{\text{m}}{\text{N}} \tag{4.271}$$

$$[\delta] = [d] = \begin{bmatrix} 71.24 & -25.43 & -41.40 \\ -25.43 & 116.82 & -82.58 \\ -41.40 & -82.58 & 153.66 \end{bmatrix} 10^{-3} \frac{1}{\text{N} \cdot \text{m}}. \tag{4.272}$$

Equations (4.270), (4.271), and (4.272) give the hygrothermal strains:

$$\begin{Bmatrix} \epsilon_x^{o,ht} \\ \epsilon_y^{o,ht} \\ \gamma_{xy}^{o,ht} \end{Bmatrix}_{\Delta T_0} = \begin{Bmatrix} 0.041 \\ 1.653 \\ -1.760 \end{Bmatrix} 10^{-3} \qquad \begin{Bmatrix} \kappa_x^{ht} \\ \kappa_y^{ht} \\ \kappa_{xy}^{ht} \end{Bmatrix}_{\Delta T_0} = \begin{Bmatrix} 0 \\ 0 \\ 0 \end{Bmatrix} \tag{4.273}$$

$$\begin{Bmatrix} \epsilon_x^{o,ht} \\ \epsilon_y^{o,ht} \\ \gamma_{xy}^{o,ht} \end{Bmatrix}_{\Delta T_i} = \begin{Bmatrix} 0 \\ 0 \\ 0 \end{Bmatrix} \qquad \begin{Bmatrix} \kappa_x^{ht} \\ \kappa_y^{ht} \\ \kappa_{xy}^{ht} \end{Bmatrix}_{\Delta T_i} = \begin{Bmatrix} 123.0 \\ 284.2 \\ -438.6 \end{Bmatrix} 10^{-3} \frac{1}{\text{m}}. \tag{4.274}$$

The sum $\{\}_{\Delta T_0} + \{\}_{\Delta T_i}$ gives the total hygrothermal strains

$$\begin{Bmatrix} \epsilon_x^{o,ht} \\ \epsilon_y^{o,ht} \\ \gamma_{xy}^{o,ht} \\ \kappa_x^{ht} \\ \kappa_y^{ht} \\ \kappa_{xy}^{ht} \end{Bmatrix} = \begin{Bmatrix} 0.041 \\ 1.653 \\ -1.760 \\ 123.0 \\ 284.2 \\ -438.6 \end{Bmatrix} 10^{-3}.$$

The deformed shape of the plate is illustrated in Figure 4.52.

4.18 Example. *A plate is made of graphite epoxy unidirectional plies. The layup is* $[45_6/0_4]_s$. *The 0-degree plies are parallel to the x axis. The plate is long in the y direction, and one of the long edges is built-in and the other one is free (Fig. 4.53). The temperature of the bottom surface is raised by 80 °C and the top surface by 120 °C (Fig. 4.50). Estimate the temperature-induced change in the dimensions of the plate. The ply properties are given in Table 3.6 (page 81), the thermal expansion coefficients are* $\widetilde{\alpha}_1 = -0.7 \times 10^{-6} \frac{1}{^\circ C}$ *and* $\widetilde{\alpha}_2 = 25 \times 10^{-6} \frac{1}{^\circ C}$.

Solution. The strains in the laminate are given by Eq. (4.249)

$$\begin{Bmatrix} \epsilon_x^o \\ \epsilon_y^o \\ \gamma_{xy}^o \\ \kappa_x \\ \kappa_y \\ \kappa_{xy} \end{Bmatrix} = \begin{bmatrix} \alpha_{11} & \alpha_{12} & \alpha_{16} & \beta_{11} & \beta_{12} & \beta_{16} \\ \alpha_{12} & \alpha_{22} & \alpha_{26} & \beta_{21} & \beta_{22} & \beta_{26} \\ \alpha_{16} & \alpha_{26} & \alpha_{66} & \beta_{61} & \beta_{62} & \beta_{66} \\ \beta_{11} & \beta_{21} & \beta_{61} & \delta_{11} & \delta_{12} & \delta_{16} \\ \beta_{12} & \beta_{22} & \beta_{62} & \delta_{12} & \delta_{22} & \delta_{26} \\ \beta_{16} & \beta_{26} & \beta_{66} & \delta_{16} & \delta_{26} & \delta_{66} \end{bmatrix} \left(\begin{Bmatrix} N_x \\ N_y \\ N_{xy} \\ M_x \\ M_y \\ M_{xy} \end{Bmatrix} + \begin{Bmatrix} N_x^{ht} \\ N_y^{ht} \\ N_{xy}^{ht} \\ M_x^{ht} \\ M_y^{ht} \\ M_{xy}^{ht} \end{Bmatrix} \right). \tag{4.275}$$

The hygrothermal forces are given in Eqs. (4.268) and (4.269). The compliance matrices are given in Eqs. (4.271) and (4.272). From Table 4.14, sixth row (page 156), we have

$$\epsilon_y^o = 0 \qquad \kappa_y = 0 \qquad \kappa_{xy} = 0 \tag{4.276}$$

$$N_x = 0 \qquad N_{xy} = 0 \qquad M_x = 0 \tag{4.277}$$

Equation (4.275) represents six equations that contain the six unknowns N_y, M_y, M_{xy}, ϵ_x^o, γ_{xy}^o, κ_x.

The temperature distribution across the plate is represented by the sum of a constant and a linearly varying temperature distribution, as shown in Figure 4.50. The temperature differences shown in this figure are

$$\Delta T_0 = \frac{80 + 120}{2} = 100\ ^\circ\text{C} \qquad \Delta T_1 = \frac{120 - 80}{h} = 20\,000\ ^\circ\text{C/m}. \tag{4.278}$$

The corresponding hygrothermal forces are given in Eqs. (4.268) and (4.269), respectively. By substituting the values of the hygrothermal forces given in these equations into Eq. (4.275) we obtain

$$(\epsilon_x^o)_{\Delta T_0} = 0.172 \times 10^{-3} \qquad (\gamma_{xy}^o)_{\Delta T_0} = -0.475 \times 10^{-3} \qquad (\kappa_x)_{\Delta T_0} = 0 \tag{4.279}$$

$$(\epsilon_x^o)_{\Delta T_1} = 0 \qquad (\gamma_{xy}^o)_{\Delta T_1} = 0 \qquad (\kappa_x)_{\Delta T_1} = 36.71 \times 10^{-3} \frac{1}{\text{m}}. \tag{4.280}$$

The sum $()_{\Delta T_0} + ()_{\Delta T_1}$ gives the hygrothermal strains

$$\epsilon_x^o = 0.172 \times 10^{-3} \qquad \gamma_{xy}^o = -0.475 \times 10^{-3} \qquad \kappa_x = 36.71 \times 10^{-3} \frac{1}{\text{m}}. \tag{4.281}$$

The deformed shape of the plate is illustrated in Figure 4.53.

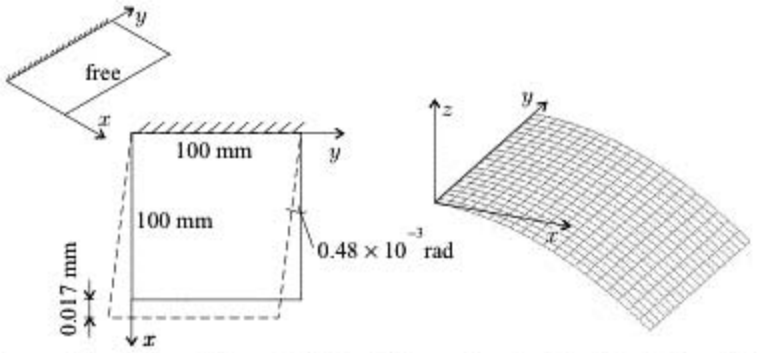

Figure 4.53: Deformed shape of a 100 by 100-mm element of the plate in Example 4.18.

4.5.1 Change in Thickness Due to Hygrothermal Effects

Owing to changes in temperature and moisture content the thickness of the plate changes. The change is (Fig. 4.54)

$$\Delta h = \int_{-h_b}^{h_t} \epsilon_z dz. \tag{4.282}$$

From Eqs. (2.133) and (2.165) the normal strain in a ply is

$$\epsilon_z = \epsilon_3 = [S_{13} \quad S_{23} \quad S_{36}] \begin{Bmatrix} \sigma_1 \\ \sigma_2 \\ \tau_{12} \end{Bmatrix} + \Delta T \widetilde{\alpha}_3 + c\widetilde{\beta}_3. \tag{4.283}$$

In the x_1, x_2 coordinate system the ply stresses are

$$\begin{Bmatrix} \sigma_1 \\ \sigma_2 \\ \tau_{12} \end{Bmatrix} = [T_\sigma] \begin{Bmatrix} \sigma_x \\ \sigma_y \\ \tau_{xy} \end{Bmatrix}, \tag{4.284}$$

where $[T_\sigma]$ is given by Eq. (2.182). In the x, y laminate coordinate system the

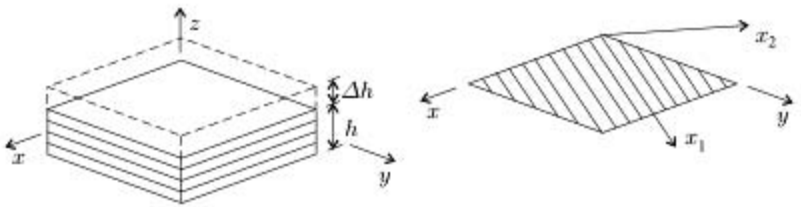

Figure 4.54: Change in thickness of a composite plate and the laminate and ply coordinate systems.

stresses in the ply are (Eqs. 2.126 and 2.165)

$$\begin{Bmatrix} \sigma_x \\ \sigma_y \\ \tau_{xy} \end{Bmatrix} = [\overline{Q}] \left(\begin{Bmatrix} \epsilon_x \\ \epsilon_y \\ \gamma_{xy} \end{Bmatrix} - \Delta T \begin{Bmatrix} \widetilde{\alpha}_x \\ \widetilde{\alpha}_y \\ \widetilde{\alpha}_{xy} \end{Bmatrix} - c \begin{Bmatrix} \widetilde{\beta}_x \\ \widetilde{\beta}_y \\ \widetilde{\beta}_{xy} \end{Bmatrix} \right). \tag{4.285}$$

The strains are (see Eq. 3.7)

$$\begin{Bmatrix} \epsilon_x \\ \epsilon_y \\ \gamma_{xy} \end{Bmatrix} = \begin{Bmatrix} \epsilon_x^o \\ \epsilon_y^o \\ \gamma_{xy}^o \end{Bmatrix} + z \begin{Bmatrix} \kappa_x \\ \kappa_y \\ \kappa_{xy} \end{Bmatrix}. \tag{4.286}$$

Equations (4.282)–(4.286) describe the change in thickness. For a plate subjected to a uniform ΔT_0 change in temperature these equations may be combined to yield

$$\Delta h = \sum_{k=1}^{K} \left\{ [S_{13} \quad S_{23} \quad S_{36}][T_\sigma]_k \left((z_k - z_{k-1})[\overline{Q}]_k \left(\begin{Bmatrix} \epsilon_x^o \\ \epsilon_y^o \\ \gamma_{xy}^o \end{Bmatrix} - \Delta T_0 \begin{Bmatrix} \widetilde{\alpha}_x \\ \widetilde{\alpha}_y \\ \widetilde{\alpha}_{xy} \end{Bmatrix}_k \right) \right. \right.$$
$$\left. \left. + \frac{z_k^2 - z_{k-1}^2}{2} [\overline{Q}]_k \begin{Bmatrix} \kappa_x \\ \kappa_y \\ \kappa_{xy} \end{Bmatrix} \right) + (z_k - z_{k-1})(\Delta T_0 (\widetilde{\alpha}_3)_k) \right\}, \tag{4.287}$$

where k is the ply number, K is the total number of plies, and z is the coordinate of the ply (Fig. 3.12). For uniform moisture distribution the change in thickness is calculated by replacing ΔT_0 and $\widetilde{\alpha}$ by c and $\widetilde{\beta}$, respectively.

When the mechanical loads are zero, the strains in, and the curvatures of the reference surface are due only to hygrothermal effects and, from Eq. (4.252), we have

$$\begin{Bmatrix} \epsilon_x^o \\ \epsilon_y^o \\ \gamma_{xy}^o \end{Bmatrix} = \begin{Bmatrix} \epsilon_x^{o,ht} \\ \epsilon_y^{o,ht} \\ \gamma_{xy}^{o,ht} \end{Bmatrix} \qquad \begin{Bmatrix} \kappa_x \\ \kappa_y \\ \kappa_{xy} \end{Bmatrix} = \begin{Bmatrix} \kappa_x^{ht} \\ \kappa_y^{ht} \\ \kappa_{xy}^{ht} \end{Bmatrix}, \tag{4.288}$$

where $\epsilon_x^{o,ht}, \epsilon_y^{o,ht}, \gamma_{xy}^{o,ht}, \kappa_x^{ht}, \kappa_y^{ht}, \kappa_{xy}^{ht}$ are obtained from Eq. (4.250).

4.19 Example. *A rectangular plate is made of graphite epoxy unidirectional plies. The layup is* $[45_6/0_4]_s$. *The edges of the plate are free. The temperature of the plate is raised by* $80\,^\circ C$. *Estimate the temperature-induced change in the thickness of the plate. The ply properties are given in Table 3.6 (page 81), the thermal expansion coefficients are* $\widetilde{\alpha}_1 = -0.7 \times 10^{-6} \frac{1}{^\circ C}$ *and* $\widetilde{\alpha}_2 = 25 \times 10^{-6} \frac{1}{^\circ C}$.

Solution. The temperature distribution across the plate is uniform and is

$$\Delta T_0 = 80\,^\circ\text{C}. \tag{4.289}$$

The change in thickness is (see Eq. 4.287)

$$\Delta h = \sum_{k=1}^{K} \left\{ [S_{13} \quad S_{23} \quad S_{36}][T_\sigma]_k \left((z_k - z_{k-1})[\overline{Q}]_k \left(\begin{Bmatrix} \epsilon_x^o \\ \epsilon_y^o \\ \gamma_{xy}^o \end{Bmatrix} - \Delta T_0 \begin{Bmatrix} \widetilde{\alpha}_x \\ \widetilde{\alpha}_y \\ \widetilde{\alpha}_{xy} \end{Bmatrix}_k \right) \right) \right.$$

$$\left. + (z_k - z_{k-1})(\Delta T_0 (\widetilde{\alpha}_3)_k) \right\}. \tag{4.290}$$

The stiffness matrices are (Eq. 4.264)

$$[\overline{Q}]^0 = \begin{bmatrix} 148.87 & 2.91 & 0 \\ 2.91 & 9.71 & 0 \\ 0 & 0 & 4.55 \end{bmatrix} 10^9 \frac{\mathrm{N}}{\mathrm{m}^2} \quad [\overline{Q}]^{45} = \begin{bmatrix} 45.65 & 36.55 & 34.79 \\ 36.55 & 45.65 & 34.79 \\ 34.79 & 34.79 & 38.19 \end{bmatrix} 10^9 \frac{\mathrm{N}}{\mathrm{m}^2}. \tag{4.291}$$

The thermal expansion coefficients are (Eqs. 4.265 and 4.267)

$$\begin{Bmatrix} \widetilde{\alpha}_x \\ \widetilde{\alpha}_y \\ \widetilde{\alpha}_{xy} \end{Bmatrix}^0 = \begin{Bmatrix} -0.7 \\ 25 \\ 0 \end{Bmatrix} 10^{-6} \frac{1}{^\circ\mathrm{C}} \quad \begin{Bmatrix} \widetilde{\alpha}_x \\ \widetilde{\alpha}_y \\ \widetilde{\alpha}_{xy} \end{Bmatrix}^{45} = \begin{Bmatrix} 12.15 \\ 12.15 \\ -25.70 \end{Bmatrix} 10^{-6} \frac{1}{^\circ\mathrm{C}}, \tag{4.292}$$

where z is the distance from the midplane: $z_0 = -0.001$ m, $z_1 = -0.0004$ m, $z_2 = 0.0004$ m, $z_3 = 0.001$ m (Fig. 4.51) and K is the number of ply groups ($K = 3$). The stress transformation matrix $[T_\sigma]$ in the 45-degree direction is obtained from Eq. (3.51)

$$[T_\sigma] = \begin{bmatrix} 0.5 & 0.5 & 1.0 \\ 0.5 & 0.5 & -1.0 \\ -0.5 & 0.5 & 0 \end{bmatrix}. \tag{4.293}$$

The strains and curvatures of the midplane are given by Eq. (4.273) as follows:

$$\begin{array}{lll} \epsilon_x^o = 0.041 \times 10^{-3} & \epsilon_y^o = 1.653 \times 10^{-3} & \gamma_{xy}^o = -1.760 \times 10^{-3} \\ \kappa_x = 0 & \kappa_y = 0 & \kappa_{xy} = 0. \end{array} \tag{4.294}$$

With these values Eq. (4.290) gives

$$\Delta h = 5.899 \times 10^{-6} \text{ m}. \tag{4.295}$$

4.6 Plates with a Circular or an Elliptical Hole

We consider a plate with symmetrical layup containing either a circular or an elliptical hole (Fig. 4.55). The dimensions of the hole are small compared with the dimensions of the plate. We assume that at some distance from the hole there is a region where the in-plane forces and strains are nearly uniform. These "farfield" forces and strains are taken to be those that would exist in the plate in the absence of the hole. We wish to determine the strains near the hole in terms of the farfield forces and strains.

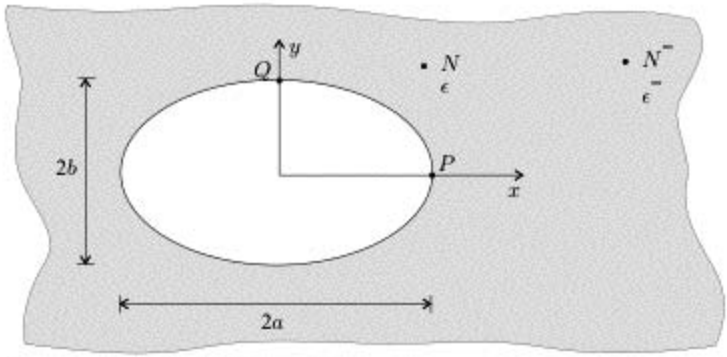

Figure 4.55: Elliptical hole in a plate.

Far from the hole the "farfield" in-plane forces are denoted by N_x^∞, N_y^∞, N_{xy}^∞ and the "farfield" in-plane strains are denoted by $\epsilon_x^{o,\infty}$, $\epsilon_y^{o,\infty}$, $\gamma_{xy}^{o,\infty}$. These forces and strains are related by (Eq. 3.26)

$$\begin{Bmatrix} N_x^\infty \\ N_y^\infty \\ N_{xy}^\infty \end{Bmatrix} = [A] \begin{Bmatrix} \epsilon_x^{o,\infty} \\ \epsilon_y^{o,\infty} \\ \gamma_{xy}^{o,\infty} \end{Bmatrix}. \tag{4.296}$$

At a point near the hole, the in-plane forces are

$$\begin{Bmatrix} N_x \\ N_y \\ N_{xy} \end{Bmatrix} = \begin{Bmatrix} N_x^\infty \\ N_y^\infty \\ N_{xy}^\infty \end{Bmatrix} + \begin{Bmatrix} N_x^* \\ N_y^* \\ N_{xy}^* \end{Bmatrix}, \tag{4.297}$$

where N_x^*, N_y^*, N_{xy}^* are modification terms that depend on x and y. Expressions

Table 4.15. The modification terms in Eq. (4.297)

$$N_x^* = 2\,\mathrm{Re}\left\{\mu_1^2\Phi_1'(Z_1) + \mu_2^2\Phi_2'(Z_2)\right\}$$
$$N_y^* = 2\,\mathrm{Re}\left\{\Phi_1'(Z_1) + \Phi_2'(Z_2)\right\}$$
$$N_{xy}^* = -2\,\mathrm{Re}\left\{\mu_1\Phi_1'(Z_1) + \mu_2\Phi_2'(Z_2)\right\}$$
$$\Phi_k(Z_k) = A_k\zeta_k^{-1} \quad (k = 1, 2)$$
$$\zeta_k = \frac{Z_k + \sqrt{Z_k^2 - a^2 - \mu_k^2 b^2}}{a - i\mu_k b} \quad \text{(at the interface } \zeta_k = e^{i\theta}\text{)}$$
$$Z_k = x + y\mu_k \quad (k = 1, 2)$$

μ_k's are the roots of the characteristic polynomial ($\mu_1 = \overline{\mu}_3$, $\mu_2 = \overline{\mu}_4$)

$$a_{11}\mu^4 - 2a_{16}\mu^3 + (2a_{12} + a_{66})\mu^2 - 2a_{26}\mu + a_{22} = 0,$$

where Re refers to the real part, i the imaginary unit;
$\overline{\mu}$ is the complex conjugate of μ;
$()'$ refers to the derivative with respect to Z_k;
a and b are shown in Figure 4.55;
$[a_{ij}] = [A_{ij}]^{-1}$ are the in-plane compliances of the plate.

for these parameters are given by Lekhnitskii[40] and are presented in Table 4.15. The modification terms depend on $\Phi_k(Z_k) = A_k \zeta_k^{-1}$, where A_k represents two unknown complex numbers whose real and imaginary parts constitute four unknown constants. These constants are determined from the condition that the surface traction is zero along the surface of the hole. It suffices to enforce this condition only at two points on the boundary

$$\begin{aligned} N_x \left(= N_x^{\infty} + N_x^*\right) &= 0 \qquad \text{at point } P \\ N_{xy} \left(= N_{xy}^{\infty} + N_{xy}^*\right) &= 0 \qquad \text{at point } P \\ N_y \left(= N_y^{\infty} + N_y^*\right) &= 0 \qquad \text{at point } Q \\ N_{xy} \left(= N_{xy}^{\infty} + N_{xy}^*\right) &= 0 \qquad \text{at point } Q. \end{aligned} \tag{4.298}$$

The four unknown constants in A_k are calculated by the following steps:

1. The constants A_k are assumed in the form

$$A_1 = C_1 + C_2 i \qquad A_2 = C_3 + C_4 i, \tag{4.299}$$

where $i = \sqrt{-1}$.

2. The roots μ_1 and μ_2 of the characteristic polynomial given in Table 4.15 are calculated.
3. Modification terms N_x^*, N_{xy}^* at point P and N_y^*, N_{xy}^* at point Q are calculated for four different sets of C_1, C_2, C_3, C_4.

Set 1 $C_1 = 1, C_2 = C_3 = C_4 = 0$, resulting in
$(N_x^*)_1^P$, $(N_{xy}^*)_1^P$ and $(N_y^*)_1^Q$, $(N_{xy}^*)_1^Q$

Set 2 $C_2 = 1, C_1 = C_3 = C_4 = 0$, resulting in
$(N_x^*)_2^P$, $(N_{xy}^*)_2^P$ and $(N_y^*)_2^Q$, $(N_{xy}^*)_2^Q$

Set 3 $C_3 = 1, C_1 = C_2 = C_4 = 0$, resulting in
$(N_x^*)_3^P$, $(N_{xy}^*)_3^P$ and $(N_y^*)_3^Q$, $(N_{xy}^*)_3^Q$

Set 4 $C_4 = 1, C_1 = C_2 = C_3 = 0$, resulting in
$(N_x^*)_4^P$, $(N_{xy}^*)_4^P$ and $(N_y^*)_4^Q$, $(N_{xy}^*)_4^Q$.

For arbitrary values of C_1–C_4 we have

$$\begin{Bmatrix} N_x^{*P} \\ N_{xy}^{*P} \\ N_y^{*Q} \\ N_{xy}^{*Q} \end{Bmatrix} = \begin{bmatrix} (N_x^*)_1^P & (N_x^*)_2^P & (N_x^*)_3^P & (N_x^*)_4^P \\ (N_{xy}^*)_1^P & (N_{xy}^*)_2^P & (N_{xy}^*)_3^P & (N_{xy}^*)_4^P \\ (N_y^*)_1^Q & (N_y^*)_2^Q & (N_y^*)_3^Q & (N_y^*)_4^Q \\ (N_{xy}^*)_1^Q & (N_{xy}^*)_2^Q & (N_{xy}^*)_3^Q & (N_{xy}^*)_4^Q \end{bmatrix} \begin{Bmatrix} C_1 \\ C_2 \\ C_3 \\ C_4 \end{Bmatrix}. \tag{4.300}$$

4. Equations (4.298) and (4.300) give

$$\begin{Bmatrix} N_x^{\infty} \\ N_{xy}^{\infty} \\ N_y^{\infty} \\ N_{xy}^{\infty} \end{Bmatrix} + \begin{bmatrix} (N_x^*)_1^P & (N_x^*)_2^P & (N_x^*)_3^P & (N_x^*)_4^P \\ (N_{xy}^*)_1^P & (N_{xy}^*)_2^P & (N_{xy}^*)_3^P & (N_{xy}^*)_4^P \\ (N_y^*)_1^Q & (N_y^*)_2^Q & (N_y^*)_3^Q & (N_y^*)_4^Q \\ (N_{xy}^*)_1^Q & (N_{xy}^*)_2^Q & (N_{xy}^*)_3^Q & (N_{xy}^*)_4^Q \end{bmatrix} \begin{Bmatrix} C_1 \\ C_2 \\ C_3 \\ C_4 \end{Bmatrix} = 0. \tag{4.301}$$

5. Equations (4.301) are solved for the C_1, C_2, C_3, C_4 constants.

[40] S. G. Lekhnitskii, *Anisotropic Plates*. Gordon and Breach Science Publishers, New York, 1968, p. 31.

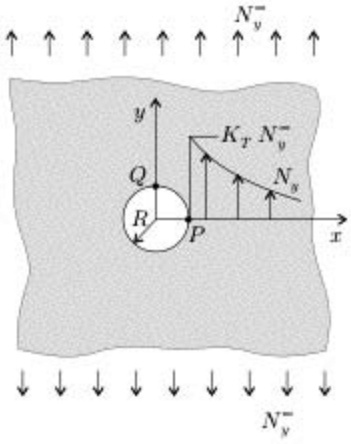

Figure 4.56: Orthotropic plate with a circular hole.

Next we apply the preceding equations to orthotropic plates containing a circular hole with radius R and subjected to a uniform tensile load N_y^∞ (Fig. 4.56). The maximum forces (per unit length) at the surface of the hole are[41]

$$N_y(R,0) = K_T N_y^\infty \qquad \text{force at point } P \tag{4.302}$$

$$N_x(0,R) = -\sqrt{\frac{A_{11}}{A_{22}}}\,N_y^\infty \qquad \text{force at point } Q, \tag{4.303}$$

where K_T is the stress intensity factor

$$K_T = 1 + \sqrt{\frac{2}{A_{11}}\left(\sqrt{A_{11}A_{22}} - A_{12} + \frac{A_{11}A_{22} - A_{12}^2}{2A_{66}}\right)}. \tag{4.304}$$

x and y are in the directions of orthotropy, and the elements of the stiffness matrix are to be calculated in this coordinate system. The force distribution N_y along the x-axis may be approximated by[42] (Fig 4.56)

$$N_y(x,0) = \frac{N_y^\infty}{2}\left\{2 + \left(\frac{R}{x}\right)^2 + 3\left(\frac{R}{x}\right)^4 - (K_T - 3)\left[5\left(\frac{R}{x}\right)^6 - 7\left(\frac{R}{x}\right)^8\right]\right\}. \tag{4.305}$$

4.7 Interlaminar Stresses

Laminate plate theory is formulated on the basis of the assumption that the laminate as well as all the layers are in a state of plane stress. Correspondingly, all

[41] Ibid., p. 175.

[42] H. J. Konish and J. M. Whitney, Approximate Stresses in an Orthotropic Plate Containing a Circular Hole. *Journal of Composite Materials*, Vol. 9, 157–166, 1975.

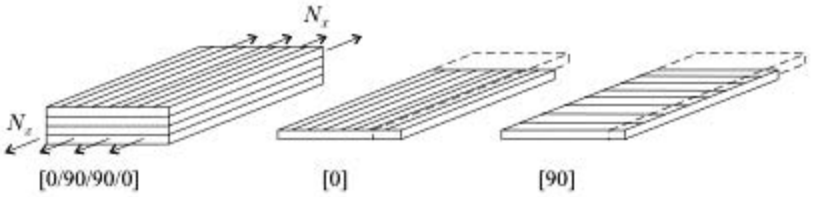

Figure 4.57: $[0/90]_s$ laminate loaded in tension and the deformations of unbonded 0- and 90-degree layers.

out-of-plane stress components are zero ($\sigma_z = 0$, $\tau_{yz} = 0$, $\tau_{xz} = 0$). This assumption is reasonable in regions away from free edges. Near free edges, both shear and normal stresses may arise between the layers. These interlaminar stresses may significantly alter the stress field existing away from the free edge and, importantly, may cause separation (delamination) of adjacent layers.

We illustrate the stresses near a free edge through the example of a $[0/90]_s$ cross-ply laminate (Fig. 4.57). The laminate is subjected to a unidirectional force (per unit length) N_x with x being in the direction of the 0-degree fibers. The axial load is shared by the plies, and the axial deformation of each ply is the same ($\epsilon_x^0 = \epsilon_x^{90}$). We now consider one of the 0-degree plies and the adjacent 90-degree ply. Their transverse Poisson ratios are different ($\nu_{xy}^0 \neq \nu_{xy}^{90}$). Hence, if the two plies were allowed to move freely, they would deform by different amounts in the transverse y direction (Fig. 4.57). In reality, the two plies are bonded together, and their transverse deformations (and transverse strains) are equal. Obviously, one of the plies (in this example the 0-degree ply) must be in tension, and the other one (90-degree ply) must be in compression.

The stresses on a 0-degree ply element are shown in Figure 4.58. Away from the free edge, on a small element the σ_y stresses equilibrate each other, and there is no interlaminar shear stress ($\tau_{yz} = 0$). At the free edge σ_y is unbalanced and is

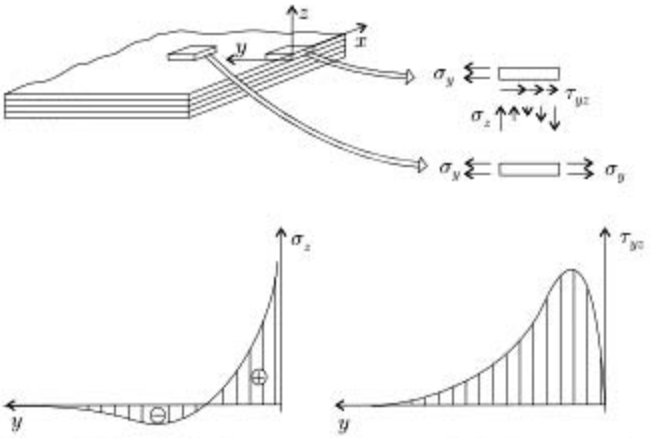

Figure 4.58: Free-body diagrams and the stress distributions near a free edge.

equilibrated by the interlaminar stresses ($\tau_{yz} \neq 0$). Furthermore, σ_y and τ_{yz} create a moment, which must be equilibrated by the interlaminar normal stress σ_z shown in Figure 4.58. The normal stress, as well as τ_{yz}, diminishes in regions away from the edge.

Care must be taken in calculating the interlaminar stresses. Under the assumption that the material is linearly elastic, the calculations result in infinite stresses at free edges.

Sandwich Plates

Sandwich plates, consisting of a core covered by facesheets, are frequently used instead of solid plates because of their high bending stiffness-to-weight ratio. The high bending stiffness is the result of the distance between the facesheets, which carry the load, and the light weight is due to the light weight of the core.

Here, we consider rectangular sandwich plates with facesheets on both sides of the core (Figs. 5.1 and 5.2). Each facesheet may be an isotropic material or a fiber-reinforced composite laminate but must be thin compared with the core. The core may be foam or honeycomb (Fig. 5.1) and must have a material symmetry plane parallel to its midplane; the core's in-plane stiffnesses must be small compared with the in-plane stiffnesses of the facesheets.

The behavior of thin plates undergoing small deformations may be analyzed by the Kirchhoff hypothesis, namely, by the assumptions that normals remain straight and perpendicular to the deformed reference plane. For a sandwich plate, consisting of a core covered on both sides by facesheets, the first assumption (normals remain straight) is reasonable. However, the second assumption may no longer be valid, because normals do not necessarily remain perpendicular to the reference plane (Fig. 5.3). In this case the x and y displacements of a point located at a distance z from an arbitrarily chosen reference plane are

$$u = u^{o} - z\chi_{xz} \qquad v = v^{o} - z\chi_{yz}, \tag{5.1}$$

where u^{o} and v^{o} are the x and y displacements at the reference plane (where $z = 0$) and χ_{xz}, χ_{yz} are the rotations of the normal in the x–z and y–z planes. The angle χ_{xz} is illustrated in Figure 5.3.

As shown in Figure 5.3, the first derivative of the deflection w^{o} of the reference plane with respect to x is

$$\frac{\partial w^{o}}{\partial x} = \chi_{xz} + \gamma_{xz}. \tag{5.2}$$

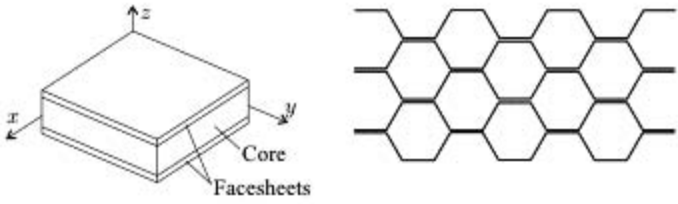

Figure 5.1: Illustration of the sandwich plate and the honeycomb core.

Similarly, the first derivative of the deflection w^o of the reference plane with respect to y is

$$\frac{\partial w^o}{\partial y} = \chi_{yz} + \gamma_{yz}. \tag{5.3}$$

5.1 Governing Equations

The strains at the reference plane are (Eq. 4.2)

$$\epsilon_x^o = \frac{\partial u^o}{\partial x} \qquad \epsilon_y^o = \frac{\partial v^o}{\partial y} \qquad \gamma_{xy}^o = \frac{\partial u^o}{\partial y} + \frac{\partial v^o}{\partial x}. \tag{5.4}$$

The transverse shear strains are (Eqs. 5.2 and 5.3)

$$\gamma_{xz} = \frac{\partial w^o}{\partial x} - \chi_{xz} \qquad \gamma_{yz} = \frac{\partial w^o}{\partial y} - \chi_{yz}. \tag{5.5}$$

For convenience we define κ_x, κ_y, and κ_{xy} as

$$\kappa_x = -\frac{\partial \chi_{xz}}{\partial x} \qquad \kappa_y = -\frac{\partial \chi_{yz}}{\partial y} \qquad \kappa_{xy} = -\frac{\partial \chi_{xz}}{\partial y} - \frac{\partial \chi_{yz}}{\partial x}. \tag{5.6}$$

We note that κ_x, κ_y, and κ_{xy} are not the curvatures of the reference plane. They are the reference plane's curvatures only in the absence of shear deformation.

The three equations above represent the strain–displacement relationships for a sandwich plate.

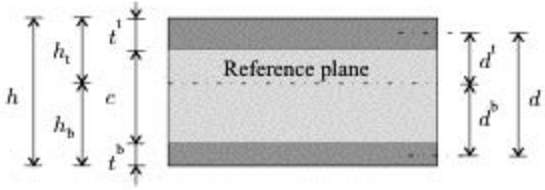

Figure 5.2: Sandwich-plate geometry.

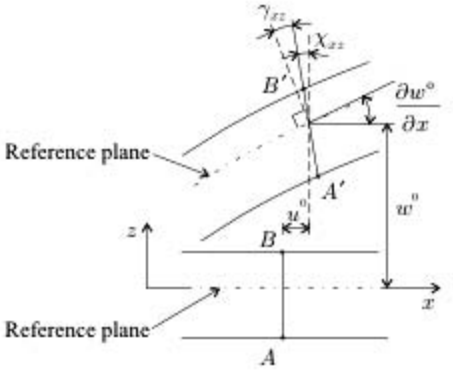

Figure 5.3: Deformation of a sandwich plate in the x–z plane.

Next we derive the force–strain relationships. The starting point of the analysis is the expressions for the forces and moments given by Eqs. (3.9) and (3.10)

$$N_x = \int_{-h_b}^{h_t} \sigma_x dz \qquad N_y = \int_{-h_b}^{h_t} \sigma_y dz \qquad N_{xy} = \int_{-h_b}^{h_t} \tau_{xy} dz$$

$$M_x = \int_{-h_b}^{h_t} z\sigma_x dz \qquad M_y = \int_{-h_b}^{h_t} z\sigma_y dz \qquad M_{xy} = \int_{-h_b}^{h_t} z\tau_{xy} dz \tag{5.7}$$

$$V_x = \int_{-h_b}^{h_t} \tau_{xz} dz \qquad V_y = \int_{-h_b}^{h_t} \tau_{yz} dz, \tag{5.8}$$

where N_i, M_i, and V_i are the in-plane forces, the moments, and the transverse shear forces per unit length (Fig. 3.11, page 68), respectively, and h_t and h_b are the distances from the arbitrarily chosen reference plane to the plate's surfaces (Fig. 5.2). The stresses (plane–stress condition) are (Eq. 2.126)

$$\begin{Bmatrix} \sigma_x \\ \sigma_y \\ \tau_{xy} \end{Bmatrix} = \begin{bmatrix} \overline{Q}_{11} & \overline{Q}_{12} & \overline{Q}_{16} \\ \overline{Q}_{12} & \overline{Q}_{22} & \overline{Q}_{26} \\ \overline{Q}_{16} & \overline{Q}_{26} & \overline{Q}_{66} \end{bmatrix} \begin{Bmatrix} \epsilon_x \\ \epsilon_y \\ \gamma_{xy} \end{Bmatrix}. \tag{5.9}$$

From Eqs. (2.2), (2.3), and (2.11) together with Eq. (5.1) the strains at a distance z from the reference plane are

$$\epsilon_x = \frac{\partial u}{\partial x} = \frac{\partial u^o}{\partial x} - z\frac{\partial \chi_{xz}}{\partial x}$$

$$\epsilon_y = \frac{\partial v}{\partial y} = \frac{\partial v^o}{\partial y} - z\frac{\partial \chi_{yz}}{\partial y} \tag{5.10}$$

$$\gamma_{xy} = \frac{\partial u}{\partial y} + \frac{\partial v}{\partial x} = \frac{\partial u^o}{\partial y} + \frac{\partial v^o}{\partial x} - z\left(\frac{\partial \chi_{xz}}{\partial y} + \frac{\partial \chi_{yz}}{\partial x}\right).$$

By combining Eqs. (5.4), (5.7), (5.9), and (5.10) and by utilizing the definitions of the $[A]$, $[B]$, $[D]$ matrices (Eq. 3.18), we obtain

$$\begin{Bmatrix} N_x \\ N_y \\ N_{xy} \end{Bmatrix} = [A] \begin{Bmatrix} \epsilon_x^o \\ \epsilon_y^o \\ \gamma_{xy}^o \end{Bmatrix} + [B] \begin{Bmatrix} -\frac{\partial \chi_{xz}}{\partial x} \\ -\frac{\partial \chi_{yz}}{\partial y} \\ -\frac{\partial \chi_{xz}}{\partial y} - \frac{\partial \chi_{yz}}{\partial x} \end{Bmatrix} \tag{5.11}$$

$$\begin{Bmatrix} M_x \\ M_y \\ M_{xy} \end{Bmatrix} = [B] \begin{Bmatrix} \epsilon_x^o \\ \epsilon_y^o \\ \gamma_{xy}^o \end{Bmatrix} + [D] \begin{Bmatrix} -\frac{\partial \chi_{xz}}{\partial x} \\ -\frac{\partial \chi_{yz}}{\partial y} \\ -\frac{\partial \chi_{xz}}{\partial y} - \frac{\partial \chi_{yz}}{\partial x} \end{Bmatrix}. \tag{5.12}$$

With the definitions in Eq. (5.6), these equations may be written as

$$\begin{Bmatrix} N_x \\ N_y \\ N_{xy} \end{Bmatrix} = [A] \begin{Bmatrix} \epsilon_x^o \\ \epsilon_y^o \\ \gamma_{xy}^o \end{Bmatrix} + [B] \begin{Bmatrix} \kappa_x \\ \kappa_y \\ \kappa_{xy} \end{Bmatrix} \tag{5.13}$$

$$\begin{Bmatrix} M_x \\ M_y \\ M_{xy} \end{Bmatrix} = [B] \begin{Bmatrix} \epsilon_x^o \\ \epsilon_y^o \\ \gamma_{xy}^o \end{Bmatrix} + [D] \begin{Bmatrix} \kappa_x \\ \kappa_y \\ \kappa_{xy} \end{Bmatrix}. \tag{5.14}$$

In addition we need the relationships between the transverse shear forces and the transverse shear strains. The relevant expressions are derived in Section 5.1.3. Here we quote the resulting expression, which is

$$\begin{Bmatrix} V_x \\ V_y \end{Bmatrix} = \begin{bmatrix} \widetilde{S}_{11} & \widetilde{S}_{12} \\ \widetilde{S}_{12} & \widetilde{S}_{22} \end{bmatrix} \begin{Bmatrix} \gamma_{xz} \\ \gamma_{yz} \end{Bmatrix}, \tag{5.15}$$

where $[\widetilde{S}]$ is the sandwich plate's shear stiffness matrix.

In the analyses we may employ either the equilibrium equations or the strain energy. The equilibrium equations are identical to those given for a thin plate (Eqs. 4.4 and 4.5).

5.1.1 Boundary Conditions

In order to determine the deflection, the conditions along the four edges of the plate must be specified. An edge may be built-in, free, or simply supported. Boundary conditions for an edge parallel with the y-axis (Fig. 5.4) are given below.

Along a built-in edge, the deflection w^o, the in-plane displacements u^o, v^o, and the rotations of normals χ_{xz}, χ_{yz} are zero:

$$w^o = 0 \qquad u^o = v^o = 0 \qquad \chi_{xz} = \chi_{yz} = 0. \tag{5.16}$$

Along a free edge, where no external loads are applied, the bending M_x and twist M_{xy} moments, the transverse shear force V_x, and the in-plane forces N_x,

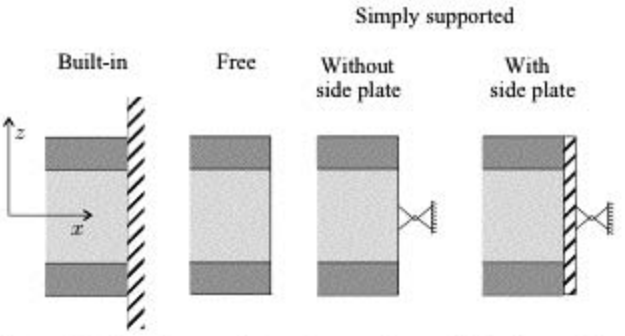

Figure 5.4: Boundary conditions for an edge parallel to the y-axis.

N_{xy} are zero:

$$M_x = M_{xy} = 0 \qquad V_x = 0 \qquad N_x = N_{xy} = 0. \tag{5.17}$$

Along a simply supported edge, the deflection w^o, the bending M_x and twist M_{xy} moments, and the in-plane forces N_x, N_{xy} are zero:

$$w^o = 0 \qquad M_x = M_{xy} = 0 \qquad N_x = N_{xy} = 0. \tag{5.18}$$

When in-plane motions are prevented by the support, the in-plane forces are not zero ($N_x \neq 0$, $N_{xy} \neq 0$), whereas the in-plane displacements are zero:

$$u^o = 0 \qquad v^o = 0. \tag{5.19}$$

When there is a rigid plate covering the side of the sandwich plate the normal cannot rotate in the y–z plane, and we have

$$\chi_{yz} = 0. \tag{5.20}$$

However, the twist moment is not zero ($M_{xy} \neq 0$).

For an edge parallel with the x-axis, the equations above hold with x and y interchanged.

5.1.2 Strain Energy

As we noted previously, solutions to plate problems may be obtained by the equations described above or via energy methods. The strain energy (for a linearly elastic material) is given by Eq. (2.200). The thickness of the sandwich plate is assumed to remain unchanged and, accordingly, $\epsilon_z = 0$. The expression for the strain energy (Eq. 2.200) simplifies to

$$U = \frac{1}{2}\int_0^{L_x}\int_0^{L_y}\int_{-h_b}^{h_t} (\sigma_x\epsilon_x + \sigma_y\epsilon_y + \tau_{xy}\gamma_{xy} + \tau_{xz}\gamma_{xz} + \tau_{yz}\gamma_{yz})\, dzdydx. \tag{5.21}$$

Substitution of Eqs. (5.4)–(5.15) and Eqs. (5.26)–(5.32) (derived on pages 175–176) into Eq. (5.21) gives

$$U = \frac{1}{2}\int_0^{L_x}\int_0^{L_y} \left\{ \begin{Bmatrix} \epsilon_x^o \\ \epsilon_y^o \\ \gamma_{xy}^o \\ \kappa_x \\ \kappa_y \\ \kappa_{xy} \end{Bmatrix}^T \begin{bmatrix} A_{11} & A_{12} & A_{16} & B_{11} & B_{12} & B_{16} \\ A_{12} & A_{22} & A_{26} & B_{12} & B_{22} & B_{26} \\ A_{16} & A_{26} & A_{66} & B_{16} & B_{26} & B_{66} \\ B_{11} & B_{12} & B_{16} & D_{11} & D_{12} & D_{16} \\ B_{12} & B_{22} & B_{26} & D_{12} & D_{22} & D_{26} \\ B_{16} & B_{26} & B_{66} & D_{16} & D_{26} & D_{66} \end{bmatrix} \begin{Bmatrix} \epsilon_x^o \\ \epsilon_y^o \\ \gamma_{xy}^o \\ \kappa_x \\ \kappa_y \\ \kappa_{xy} \end{Bmatrix} + \{\gamma_{xz} \quad \gamma_{yz}\} \begin{bmatrix} \widetilde{S}_{11} & \widetilde{S}_{12} \\ \widetilde{S}_{12} & \widetilde{S}_{22} \end{bmatrix} \begin{Bmatrix} \gamma_{xz} \\ \gamma_{yz} \end{Bmatrix} \right\} dydx, \tag{5.22}$$

where the superscript T denotes transpose of the vector.

5.1.3 Stiffness Matrices of Sandwich Plates

The stiffness matrices are evaluated by assuming that the thickness of the core remains constant under loading and the in-plane stiffnesses of the core are negligible. Under these assumptions the $[A]$, $[B]$, and $[D]$ stiffness matrices of a sandwich plate are governed by the stiffnesses of the facesheets and may be obtained by the parallel axes theorem (Eq. 3.47, page 80). The resulting expressions are given in Table 5.1. In this table the $[A]^t$, $[B]^t$, $[D]^t$ and $[A]^b$, $[B]^b$, $[D]^b$ are to be evaluated in a coordinate system whose origin is at each facesheet's reference plane. When the top and bottom facesheets are identical and their layup is symmetrical with respect to each facesheet's midplane, the $[B]$ matrix is zero and the $[A]$, $[D]$ matrices simplify, as shown in Table 5.1. (When the layup of each facesheet is symmetrical, the reference plane may conveniently be taken at the facesheets'

Table 5.1. The $[A]$, $[B]$, $[D]$ stiffness matrices of sandwich plates. The supersripts t and b refer to the top and bottom facesheets. The distances d, d^t, and d^b are shown in Figure 5.2.

	Layup of each facesheet with respect to the facesheet's midplane	
	Unsymmetrical	Symmetrical (identical facesheets)
$[A]$	$[A]^t + [A]^b$	$2[A]^t$
$[B]$	$d^t[A]^t - d^b[A]^b + [B]^t + [B]^b$	0
$[D]$	$(d^t)^2[A]^t + (d^b)^2[A]^b + [D]^t + [D]^b + 2d^t[B]^t - 2d^b[B]^b$	$\frac{1}{2}d^2[A]^t + 2[D]^t$

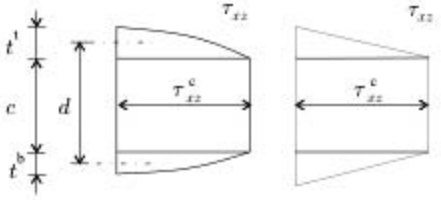

Figure 5.5: Shear stress distribution τ_{xz} (left) in a sandwich plate and the approximate distribution (right).

midplane.) When the top and bottom facesheets are unsymmetrical with respect to the facesheets' midplane but are symmetrical with respect to the midplane of the sandwich plate, then $[A]^t = [A]^b$, $[B]^t = -[B]^b$, $[D]^t = [D]^b$, and the $[A]$, $[B]$, $[D]$ matrices of the sandwich plate become

$$[A] = 2[A]^t \tag{5.23}$$

$$[B] = 0 \tag{5.24}$$

$$[D] = \frac{1}{2}d^2[A]^t + 2[D]^t + 2d[B]^t. \tag{5.25}$$

The shear stiffness matrix $[\widetilde{S}]$ is determined as follows. In the core, as a consequence of the assumption that the in-plane stiffnesses are negligible, the transverse shear stress τ_{xz} is uniform. In general, in the facesheets the shear stress distribution is as shown in Figure 5.5 (left). We approximate this distribution by the linear shear stress distribution shown in Figure 5.5 (right). Accordingly, the transverse shear force V_x is

$$V_x = \int_{-h_b}^{h_t} \tau_{xz}dz = \tau^c_{xz}c + \tau^c_{xz}\frac{t^t}{2} + \tau^c_{xz}\frac{t^b}{2} = \tau^c_{xz}d, \tag{5.26}$$

where the superscripts c, t, and b refer to the core, the top, and the bottom facesheets, respectively. The distance $d = c + t^t/2 + t^b/2$ is shown in Figure 5.5.

Similarly, we have

$$V_y = \tau^c_{yz}d. \tag{5.27}$$

The stress–strain relationship for the core material is given by Eqs. (2.20) and (2.27). With the superscript c identifying the core, these equations give

$$\begin{Bmatrix}\tau^c_{xz}\\ \tau^c_{yz}\end{Bmatrix} = \begin{bmatrix}\overline{\overline{C}}^c_{55} & \overline{\overline{C}}^c_{45}\\ \overline{\overline{C}}^c_{45} & \overline{\overline{C}}^c_{44}\end{bmatrix}\begin{Bmatrix}\gamma^c_{xz}\\ \gamma^c_{yz}\end{Bmatrix}, \tag{5.28}$$

where $\overline{\overline{C}}^c_{ij}$ are the elements of the core stiffnesses matrix.

We neglect the shear deformation of the thin facesheets. With this approximation the shear deformation γ^c_{xz} of the cross section is as shown in Figure 5.6 (left). We approximate this deformation by the average shear deformation γ_{xz} shown in

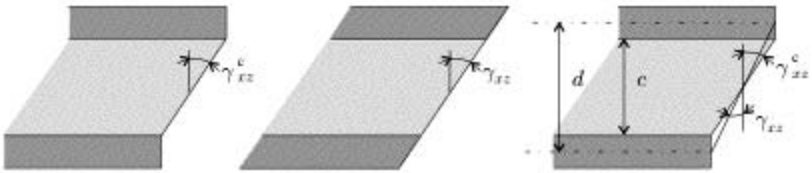

Figure 5.6: Shear deformation of a sandwich plate.

Figure 5.6 (middle). The relationship between this average shear deformation and the core deformation is given by (see Fig. 5.6, right)

$$\gamma_{xz}^c = \frac{d}{c}\gamma_{xz}. \tag{5.29}$$

Similarly, we have

$$\gamma_{yz}^c = \frac{d}{c}\gamma_{yz}. \tag{5.30}$$

Equations (5.26)–(5.30) yield the relationship between the transverse shear forces and the average shear deformation:

$$\begin{Bmatrix} V_x \\ V_y \end{Bmatrix} = \frac{d^2}{c}\begin{bmatrix} \overline{C}_{55}^c & \overline{C}_{45}^c \\ \overline{C}_{45}^c & \overline{C}_{44}^c \end{bmatrix}\begin{Bmatrix} \gamma_{xz} \\ \gamma_{yz} \end{Bmatrix}. \tag{5.31}$$

By comparing this equation with Eq. (5.15), we obtain

$$\begin{bmatrix} \widetilde{S}_{11} & \widetilde{S}_{12} \\ \widetilde{S}_{12} & \widetilde{S}_{22} \end{bmatrix} = \frac{d^2}{c}\begin{bmatrix} \overline{C}_{55}^c & \overline{C}_{45}^c \\ \overline{C}_{45}^c & \overline{C}_{44}^c \end{bmatrix}. \tag{5.32}$$

The preceding four elements of the matrix $[\overline{C}^c]$ characterize the core material, whereas $[\widetilde{S}]$ is the shear stiffness matrix of the sandwich plate. We point out that $[\widetilde{S}]$ is *not* the inverse of the $[\overline{C}]$ matrix.

Orthotropic sandwich plate. A sandwich plate is orthotropic when both facesheets as well as the core are orthotropic and the orthotropy directions are parallel to the edges. The facesheets may be different, and their layups may be unsymmetrical. For such an orthotropic sandwich plate there are no extension–shear, bending–twist, and extension–twist couplings. Accordingly, the following elements of the stiffness matrices are zero:

$$A_{16} = A_{26} = B_{16} = B_{26} = D_{16} = D_{26} = 0. \tag{5.33}$$

Furthermore, for an orthotropic sandwich plate the transverse shear force V_x acting in the x–z plane does not cause a shear strain γ_{yz} in the y–z plane. This condition gives

$$\widetilde{S}_{12} = 0. \tag{5.34}$$

Isotropic sandwich plate. A sandwich plate is isotropic when the core of the sandwich plate is made of an isotropic (such as foam) or transversely isotropic (such as honeycomb) material and the top and bottom facesheets are made of

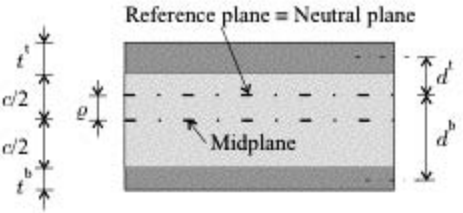

Figure 5.7: Neutral plane of an isotropic sandwich plate.

identical isotropic materials or are identical quasi-isotropic laminates. The thicknesses of the top and bottom facesheets may be different.

For isotropic facesheets the $[B]$ matrix is zero ($[B]^i = 0$). The $[A]$ and $[D]$ matrices for the isotropic facesheets are (Eqs. 3.41 and 3.42)

$$[A]^i = \frac{t^i E^f}{1-(\nu^f)^2}\begin{bmatrix} 1 & \nu^f & 0 \\ \nu^f & 1 & 0 \\ 0 & 0 & \frac{1-\nu^f}{2} \end{bmatrix} \qquad [D]^i = \frac{(t^i)^3 E^f}{12(1-(\nu^f)^2)}\begin{bmatrix} 1 & \nu^f & 0 \\ \nu^f & 1 & 0 \\ 0 & 0 & \frac{1-\nu^f}{2} \end{bmatrix}, \tag{5.35}$$

where the superscript i refers to the top ($i = \mathrm{t}$) or to the bottom ($i = \mathrm{b}$) facesheet (Fig. 5.7) and E^f and ν^f are the Young modulus and the Poisson ratio of the facesheets.

We now proceed to evaluate the $[A]$, $[B]$, $[D]$ matrices for the entire sandwich plate. To this end, we choose a reference plane located at the center of gravity of the two facesheets. The distance ϱ from the midplane of the core to the center of gravity is (Fig. 5.7)

$$\varrho = \frac{t^{\mathrm{t}}(c+t^{\mathrm{t}}) - t^{\mathrm{b}}(c+t^{\mathrm{b}})}{2(t^{\mathrm{t}}+t^{\mathrm{b}})}. \tag{5.36}$$

The distances d^{t} and d^{b} between the reference plane (passing through the center of gravity) and the midplanes of the facesheets are

$$d^{\mathrm{t}} = \frac{c}{2} + \frac{t^{\mathrm{t}}}{2} - \varrho \qquad d^{\mathrm{b}} = \frac{c}{2} + \frac{t^{\mathrm{b}}}{2} + \varrho\,. \tag{5.37}$$

By substituting Eqs. (5.35)–(5.37) into the expression for the $[B]$ matrix given in Table 5.1 (page 174) we obtain that for the entire sandwich plate the $[B]$ matrix is zero with reference to the ϱ reference plane. This means that for a sandwich plate with isotropic core and isotropic facesheets bending does not cause strains in this plane. Therefore, this reference plane is a "neutral plane."

By substituting the expressions of d^{t} and d^{b} (Eq. 5.37) into the expressions given in Table 5.1, we obtain the following $[A]$ and $[D]$ matrices for the sandwich

Table 5.2. The stiffnesses and the Poisson ratios of isotropic solid plates and isotropic sandwich plates; R is defined in Eq. (3.46).

		Isotropic sandwich plate	
	Isotropic solid plate	**Isotropic facesheets**	**Quasi-isotropic facesheets**
A^{iso}	$\frac{Eh}{1-\nu^2}$	$(t^{\text{f}}+t^{\text{b}})\frac{E^{\text{f}}}{1-(\nu^{\text{f}})^2}$	$(t^{\text{f}}+t^{\text{b}})R$
D^{iso}	$\frac{Eh^3}{12(1-\nu^2)}$	$\frac{(d^{\text{f}})^2t^{\text{f}}+(d^{\text{b}})^2t^{\text{b}}+\frac{(t^{\text{f}})^3+(t^{\text{b}})^3}{12}}{1-(\nu^{\text{f}})^2}E^{\text{f}}$	$\left[t^{\text{f}}(d^{\text{f}})^2+t^{\text{b}}(d^{\text{b}})^2\right]R$
ν^{iso}	ν	ν^{f}	$\frac{Q_{11}+Q_{22}+6Q_{12}-4Q_{66}}{8R}$

plate:

$$[A]=A^{\text{iso}}\begin{bmatrix}1 & \nu^{\text{f}} & \\ \nu^{\text{f}} & 1 & \\ & & \frac{1-\nu^{\text{f}}}{2}\end{bmatrix}\qquad [D]=D^{\text{iso}}\begin{bmatrix}1 & \nu^{\text{f}} & \\ \nu^{\text{f}} & 1 & \\ & & \frac{1-\nu^{\text{f}}}{2}\end{bmatrix}, \tag{5.38}$$

where A^{iso} and D^{iso} are defined in Table 5.2.

When the core is isotropic in the plane parallel to the facesheets from Eq. (2.40) we have $C_{45}=0$, $C_{44}=(C_{11}-C_{12})/2$, and the shear stiffnesses are (Eq. 5.32)

$$\bar{S}_{11}=\bar{S}_{22}=\bar{S}=\frac{d^2}{c}\frac{C^{\text{c}}_{11}-C^{\text{c}}_{12}}{2}\qquad \bar{S}_{12}=0. \tag{5.39}$$

The sandwich plate may also be treated as isotropic when the top and bottom facesheets are quasi-isotropic laminates (page 79) consisting of unidirectional plies made of the same material. For such sandwich plates the $[B]$ matrix is negligible, the $[A]$ and $[D]$ matrices are approximated by Eq. (5.38) (with the terms A^{iso} and D^{iso} defined in Table 5.2), and the elements of the shear stiffness matrix are given by Eq. (5.39).

5.2 Deflection of Rectangular Sandwich Plates

5.2.1 Long Plates

We consider a long rectangular sandwich plate whose length is large compared with its width ($L_y \gg L_x$). The long edges may be built-in, simply supported, or free, as shown in Figure 5.8. The sandwich plate is subjected to a transverse load p (per unit area). This load, as well as the edge supports, does not vary along the longitudinal y direction.

The deflected surface of the sandwich plate may be assumed to be cylindrical at a considerable distance from the short ends (Fig. 4.4). The generator of this cylindrical surface is parallel to the longitudinal y-axis of the plate, and hence the

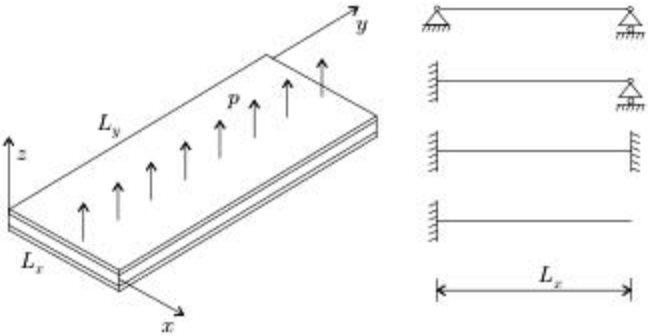

Figure 5.8: The different types of supports along the long edges of a long sandwich plate.

deflection of the plate w^o and the rotation χ_{xz} do not vary along y:

$$\frac{\partial w^o}{\partial y} = 0 \qquad \frac{\partial \chi_{xz}}{\partial y} = 0. \tag{5.40}$$

We neglect the shear deformation in the y–z plane ($\gamma_{yz} = 0$). Consequently, the rotation of the normal is zero (Eq. 5.3):

$$\chi_{yz} = 0. \tag{5.41}$$

The equilibrium equations are (Eqs. 4.22 and 4.23)

$$\frac{dV_x}{dx} + p = 0 \tag{5.42}$$

$$\frac{dM_x}{dx} - V_x = 0. \tag{5.43}$$

When the sandwich plate is symmetrical with respect to the midplane ($[B] = 0$) from Eqs. (5.12), (5.15), (5.40), and (5.41), we have

$$M_x = -D_{11}\frac{\partial \chi_{xz}}{\partial x} \qquad V_x = \widetilde{S}_{11}\gamma_{xz}. \tag{5.44}$$

Equations (5.42), (5.43), and (5.44), together with Eq. (5.2), give
sandwich plate, symmetrical layup:

$$-D_{11}\frac{d^3\chi_{xz}}{dx^3} + p = 0 \tag{5.45}$$

$$D_{11}\frac{d^2\chi_{xz}}{dx^2} + \widetilde{S}_{11}\left(\frac{dw^o}{dx} - \chi_{xz}\right) = 0. \tag{5.46}$$

For a transversely loaded isotropic sandwich beam the corresponding equations are (Eqs. 7.83 and 7.84)
isotropic sandwich beam:

$$-\widehat{EI}\frac{d^3\chi}{dx^3} + p' = 0 \tag{5.47}$$

$$\widehat{EI}\frac{d^2\chi}{dx^2} + \widehat{S}\left(\frac{dw}{dx} - \chi\right) = 0, \tag{5.48}$$

where $\widehat{EI}$ and $\widehat{S}$ are the bending and shear stiffnesses of the isotropic sandwich beam, respectively, and p' is the load per unit length.

The equations describing the deflections of long sandwich plates and isotropic sandwich beams are identical when in Eqs. (5.45) and (5.46), D_{11}, $\widetilde{S}_{11}$, and p are replaced, respectively, by $\widehat{EI}$, $\widehat{S}$, and p'. Therefore, the deflection of a long sandwich plate (symmetrical layup) may be obtained by substituting the values of D_{11}, $\widetilde{S}_{11}$, and p for $\widehat{EI}$, $\widehat{S}$, and p' in the expression, given in Section 7.3, for the deflection of the corresponding isotropic beam.

When the layup is unsymmetrical, the expression for the moment M_x can be derived analogously to the equation of a solid composite plate (Section 4.2.2). Here we only quote the result, which for sandwich plates is

$$M_x = -\underbrace{\left(D^o_{11} - \frac{B^{o2}_{16}}{A^o_{66}}\right)}_{\Psi} \frac{\partial \chi_{xz}}{\partial x}, \tag{5.49}$$

where χ_{xz} is shown in Figure 5.3. The term in parentheses is the bending stiffness parameter defined by Eq. (4.52). Equations (5.42), (5.43), (5.44, right), and (5.49), together with Eq. (5.2), give

sandwich plate, unsymmetrical layup:

$$-\Psi \frac{d^3 \chi_{xz}}{dx^3} 0 + p = 0 \tag{5.50}$$

$$\Psi \frac{d^2 \chi_{xz}}{dx^2} + \widetilde{S}_{11} \left(\frac{dw^o}{dx} - \chi_{xz}\right) = 0. \tag{5.51}$$

The preceding equations describing deflections of sandwich plates (unsymmetrical layup) become identical to the equations of sandwich beams (Eqs. 5.47 and 5.48) when Ψ, $\widetilde{S}_{11}$, and p are replaced, respectively, by $\widehat{EI}$, $\widehat{S}$, and p'. Therefore, the deflection of a long sandwich plate (unsymmetrical layup) may be obtained by substituting the values of Ψ, $\widetilde{S}_{11}$, and p for $\widehat{EI}$, $\widehat{S}$, and p' in the expression for the deflection of the corresponding isotropic beam.

5.1 Example. *A 0.9-m-long and 0.2-m-wide rectangular sandwich plate is made of a 0.02-m-thick core covered on both sides by graphite epoxy facesheets. The material properties are given in Table 3.6 (page 81). The layup of each facesheet is* $[\pm 45^t_2/0_{12}/\pm 45^t_2]$, *and the thickness of each facesheet is 0.002 m (Fig. 5.9). The 0-degree plies are parallel to the short edge of the plate. The plate is either simply supported or built-in along all four edges (Fig. 5.10). The plate is subjected to a*

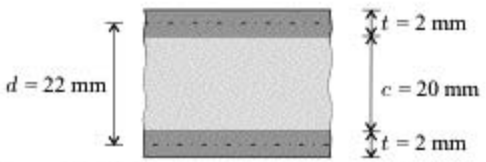

Figure 5.9: The cross section of the sandwich plate in Example 5.1.

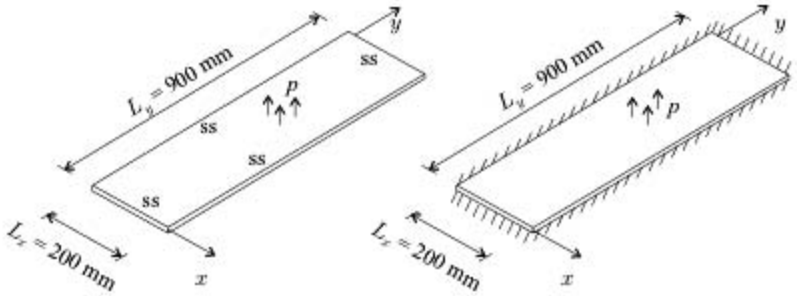

Figure 5.10: The sandwich plates in Example 5.1.

uniformly distributed transverse load $500\,kN/m^2$. *Calculate the maximum deflection. The core is isotropic* ($E_c = 2 \times 10^6\ kN/m^2$, $\nu_c = 0.3$).

Solution. The tensile and bending stiffnesses are calculated from Table 5.1 (page 174) as follows:

$$[A] = 2[A]^t = \begin{bmatrix} 430.34 & 65.47 & 0 \\ 65.47 & 96.34 & 0 \\ 0 & 0 & 72.02 \end{bmatrix} 10^3 \frac{\text{kN}}{\text{m}} \tag{5.52}$$

$$[D] = \frac{1}{2}d^2[A]^t + 2[D]^t = \begin{bmatrix} 52.16 & 7.96 & 0 \\ 7.96 & 11.71 & 0 \\ 0 & 0 & 8.76 \end{bmatrix} \text{kN} \cdot \text{m}, \tag{5.53}$$

where $[A]^t$ and $[D]^t$ are given in Table 3.7 (page 84) and $d = c + t = 0.022$ m. The shear stiffness matrix is (Eq. 5.32)

$$\begin{bmatrix} \widetilde{S}_{11} & \widetilde{S}_{12} \\ \widetilde{S}_{12} & \widetilde{S}_{22} \end{bmatrix} = \frac{d^2}{c}\begin{bmatrix} \overline{C}^c_{55} & \overline{C}^c_{45} \\ \overline{C}^c_{45} & \overline{C}^c_{44} \end{bmatrix} = \begin{bmatrix} 18\,615 & 0 \\ 0 & 18\,615 \end{bmatrix} \frac{\text{kN}}{\text{m}}, \tag{5.54}$$

where (see Eq. 2.30 and Table 2.10, page 18) $\overline{C}^c_{55} = \overline{C}^c_{44} = \frac{E_c}{2(1+\nu_c)} = 769\,231\ \text{kN/m}^2$, $\overline{C}^c_{45} = 0$.

We may treat this plate as long when (Eq. 4.19)

$$\frac{L_y}{L_x} > 3\sqrt[4]{\frac{D_{11}}{D_{22}}}. \tag{5.55}$$

In the present problem, $L_y/L_x = 4.5$ and $3\sqrt[4]{D_{11}/D_{22}} = 4.36$. Thus, the preceding condition is satisfied and the long plate expressions may be used. The maximum deflections of the corresponding beam are (Table 7.3, page 332)

$$\widetilde{w} = \frac{5}{384}\frac{p' L^4}{EI} + \frac{p' L^2}{8\widehat{S}} \qquad \text{(ss)} \tag{5.56}$$

$$\widetilde{w} = \frac{1}{384}\frac{p' L^4}{EI} + \frac{p' L^2}{8\widehat{S}} \qquad \text{(built-in)}. \tag{5.57}$$

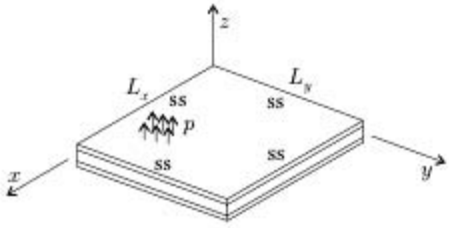

Figure 5.11: Rectangular simply supported (ss) sandwich plate subjected to transverse load.

The maximum deflections of the plate are obtained by replacing EI, $\widehat{S}$, p' by D_{11}, $\widetilde{S}_{11}$, p (see page 180)

$$\widetilde{w} = \frac{5}{384}\frac{pL_x^4}{D_{11}} + \frac{pL_x^2}{8\widetilde{S}_{11}} \qquad \text{(ss)} \tag{5.58}$$

$$\widetilde{w} = \frac{1}{384}\frac{pL_x^4}{D_{11}} + \frac{pL_x^2}{8\widetilde{S}_{11}} \qquad \text{(built-in).} \tag{5.59}$$

With the values of $D_{11} = 52.16\,\text{kN·m}$ and $\widetilde{S}_{11} = 18\,615\frac{\text{kN}}{\text{m}}$, and with $L_x = 0.2$ m, the maximum deflections are

$$\widetilde{w} = 0.000\,200 + 0.000\,134 = 0.000\,334\text{ m} = 0.334\text{ mm} \qquad \text{(ss)} \tag{5.60}$$

$$\widetilde{w} = 0.000\,040 + 0.000\,134 = 0.000\,174\text{ m} = 0.174\text{ mm} \qquad \text{(built-in).} \tag{5.61}$$

5.2.2 Simply Supported Sandwich Plates – Orthotropic and Symmetrical Layup

A simply supported rectangular sandwich plate with dimensions L_x and L_y is subjected to a uniformly distributed load p (Fig. 5.11). The layup of the plate is orthotropic (page 176) and symmetrical with respect to the plate's midplane.

For a simply supported symmetrical plate subjected to out-of-plane loads only, the in-plane strains in the midplane are zero (see Eq. 3.31) as follows:

$$\epsilon_x^o = 0 \qquad \epsilon_y^o = 0 \qquad \gamma_{xy}^o = 0. \tag{5.62}$$

Substitution of Eq. (5.62) into the expression of the strain energy (Eq. 5.22) gives

$$U = \frac{1}{2}\int_0^{L_x}\int_0^{L_y}\left\{ \{\kappa_x\kappa_y\kappa_{xy}\}\,[D]\begin{Bmatrix}\kappa_x\\ \kappa_y\\ \kappa_{xy}\end{Bmatrix} + \{\gamma_{xz}\gamma_{yz}\}\begin{bmatrix}\widetilde{S}_{11} & \widetilde{S}_{12}\\ \widetilde{S}_{12} & \widetilde{S}_{22}\end{bmatrix}\begin{Bmatrix}\gamma_{xz}\\ \gamma_{yz}\end{Bmatrix}\right\} dydx. \tag{5.63}$$

For orthotropic sandwich plates $D_{16} = D_{26} = \widetilde{S}_{12} = 0$ (Eqs. 5.33 and 5.34). With these values and the expressions in Eqs. (5.5) and (5.6), the strain energy becomes

$$U = \frac{1}{2}\int_0^{L_x}\int_0^{L_y}\left[\left(\frac{\partial \chi_{xz}}{\partial x}\right)^2 D_{11} + \left(\frac{\partial \chi_{yz}}{\partial y}\right)^2 D_{22} + 2\frac{\partial \chi_{xz}}{\partial x}\frac{\partial \chi_{yz}}{\partial y} D_{12} + \left(\frac{\partial \chi_{xz}}{\partial y} + \frac{\partial \chi_{yz}}{\partial x}\right)^2 D_{66} + \left(\frac{\partial w^o}{\partial x} - \chi_{xz}\right)^2 \widetilde{S}_{11} + \left(\frac{\partial w^o}{\partial y} - \chi_{yz}\right)^2 \widetilde{S}_{22}\right] dy dx. \tag{5.64}$$

For an applied transverse load p (per unit area), the potential of the external forces is (Eq. 4.56)

$$\Omega = -\int_0^{L_x}\int_0^{L_y} (pw^o)\, dx dy. \tag{5.65}$$

For a simply supported sandwich plate the deflection, bending moments, and rotations of the normals along the edges are zero, resulting in the following boundary conditions:

$$w^o = 0 \quad \text{at} \quad \begin{cases} x = 0 & \text{and} \quad 0 \le y \le L_y \\ x = L_x & \text{and} \quad 0 \le y \le L_y \\ 0 \le x \le L_x & \text{and} \quad y = 0 \\ 0 \le x \le L_x & \text{and} \quad y = L_y \end{cases} \tag{5.66}$$

$$M_x = 0 \quad \text{at} \quad \begin{cases} x = 0 & \text{and} \quad 0 \le y \le L_y \\ x = L_x & \text{and} \quad 0 \le y \le L_y \end{cases} \tag{5.67}$$

$$M_y = 0 \quad \text{at} \quad \begin{cases} 0 \le x \le L_x & \text{and} \quad y = 0 \\ 0 \le x \le L_x & \text{and} \quad y = L_y \end{cases} \tag{5.68}$$

$$\chi_{yz} = 0 \quad \text{at} \quad \begin{cases} x = 0 & \text{and} \quad 0 \le y \le L_y \\ x = L_x & \text{and} \quad 0 \le y \le L_y \end{cases} \tag{5.69}$$

$$\chi_{xz} = 0 \quad \text{at} \quad \begin{cases} 0 \le x \le L_x & \text{and} \quad y = 0 \\ 0 \le x \le L_x & \text{and} \quad y = L_y \end{cases}. \tag{5.70}$$

The following deflection and rotations satisfy these conditions:

$$\begin{aligned} w^o &= \sum_{i=1}^{I}\sum_{j=1}^{J} w_{ij} \sin\frac{i\pi x}{L_x}\sin\frac{j\pi y}{L_y} \\ \chi_{xz} &= \sum_{i=1}^{I}\sum_{j=1}^{J} (\chi_{xz})_{ij} \cos\frac{i\pi x}{L_x}\sin\frac{j\pi y}{L_y} \\ \chi_{yz} &= \sum_{i=1}^{I}\sum_{j=1}^{J} (\chi_{yz})_{ij} \sin\frac{i\pi x}{L_x}\cos\frac{j\pi y}{L_y}, \end{aligned} \tag{5.71}$$

Table 5.3. Elements of the coefficient matrix in Eq. (5.73)

$$F_{33} = D_{11}\left(\frac{i\pi}{L_x}\right)^4 + 2(D_{12}+2D_{66})\left(\frac{i\pi}{L_x}\right)^2\left(\frac{j\pi}{L_y}\right)^2 + D_{22}\left(\frac{j\pi}{L_y}\right)^4$$

$$F_{34} = -D_{11}\left(\frac{i\pi}{L_x}\right)^3 - (D_{12}+2D_{66})\frac{i\pi}{L_x}\left(\frac{j\pi}{L_y}\right)^2$$

$$F_{35} = -D_{22}\left(\frac{j\pi}{L_y}\right)^3 - (D_{12}+2D_{66})\left(\frac{i\pi}{L_x}\right)^2\frac{j\pi}{L_y}$$

$$F_{44} = D_{11}\left(\frac{i\pi}{L_x}\right)^2 + D_{66}\left(\frac{j\pi}{L_y}\right)^2 + \bar{S}_{11}$$

$$F_{45} = (D_{12}+2D_{66})\left(\frac{i\pi}{L_x}\right)\left(\frac{j\pi}{L_y}\right)$$

$$F_{55} = D_{22}\left(\frac{j\pi}{L_y}\right)^2 + D_{66}\left(\frac{i\pi}{L_x}\right)^2 + \bar{S}_{22}$$

where I and J are the number of terms, chosen arbitrarily, for the summations and w_{ij}, $(\chi_{xz})_{ij}$, and $(\chi_{yz})_{ij}$ are unknowns and are evaluated by the principle of stationary potential energy expressed as

$$\begin{aligned}
\frac{\partial(U+\Omega)}{\partial(\chi_{xz})_{ij}} &= 0 \\
\frac{\partial(U+\Omega)}{\partial(\chi_{yz})_{ij}} &= 0 \\
\frac{\partial(U+\Omega)}{\partial w_{ij}} &= 0.
\end{aligned} \tag{5.72}$$

We substitute w^0, χ_{xz}, χ_{yz} (from Eq. 5.71) into the expressions of U (Eq. 5.64) and Ω (Eq. 5.65) and perform the differentiations indicated above. Algebraic manipulations yield the following system of simultaneous algebraic equations:

$$\frac{L_x L_y}{4}\begin{bmatrix} F_{33} & F_{34} & F_{35} \\ F_{34} & F_{44} & F_{45} \\ F_{35} & F_{45} & F_{55} \end{bmatrix}\begin{Bmatrix} w_{ij} \\ (\gamma_{xz})_{ij} \\ (\gamma_{yz})_{ij} \end{Bmatrix} = \begin{Bmatrix} \frac{4pL_xL_y}{\pi^2 ij} \\ 0 \\ 0 \end{Bmatrix}, \tag{5.73}$$

where we have $i, j = 1, 3, 5, \ldots$ ($w_{ij} = (\gamma_{xz})_{ij} = (\gamma_{yz})_{ij} = 0$ when i or $j = 2, 4, 6\ldots$). The elements of the coefficient matrix are given in Table 5.3 and $(\gamma_{xz})_{ij}$ and $(\gamma_{yz})_{ij}$ are defined as

$$(\gamma_{xz})_{ij} = \frac{i\pi}{L_x}w_{ij} - (\chi_{xz})_{ij} \qquad (\gamma_{yz})_{ij} = \frac{j\pi}{L_y}w_{ij} - (\chi_{yz})_{ij}. \tag{5.74}$$

For each set of i, j values the three equations in Eq. (5.73) are solved simultaneously for the three unknowns w_{ij}, $(\gamma_{xz})_{ij}$, $(\gamma_{yz})_{ij}$. The deflection and the rotations are then calculated by Eqs. (5.71) and (5.74).

5.3 Buckling of Rectangular Sandwich Plates

5.3.1 Long Plates

We consider a long rectangular sandwich plate whose length L_y is large compared with its width L_x. The edges may be built-in, simply supported, or free, as shown in Figure 5.12. A uniform compressive force N_{x0} is applied along one of the long edges of the plate. This force, as well as the edge supports, does not vary along the longitudinal y direction. We are interested in the load at which the plate buckles.

The deflected surface of the plate may be assumed to be cylindrical at a considerable distance from the short edges (Fig. 4.4). The equilibrium equations are given by Eqs. (4.160) and (4.161) and for convenience are repeated here as follows:

$$\frac{dV_x}{dx} - N_{x0}\frac{d^2w^o}{dx^2} = 0 \tag{5.75}$$

$$\frac{dM_x}{dx} - V_x = 0. \tag{5.76}$$

We now consider a sandwich plate that is symmetrical with respect to the midplane. For this plate the bending moment and the transverse shear force are (Eq. 5.44)

$$M_x = -D_{11}\frac{\partial \chi_{xz}}{\partial x} \qquad V_x = \widetilde{S}_{11}\gamma_{xz}. \tag{5.77}$$

Equations (5.75), (5.76), (5.77), together with Eq. (5.2), give *sandwich plate, symmetrical layup:*

$$-D_{11}\frac{d^3\chi}{dx^3} - N_{x0}\frac{d^2w^o}{dx^2} = 0 \tag{5.78}$$

$$D_{11}\frac{d^2\chi}{dx^2} + \widetilde{S}_{11}\left(\frac{dw^o}{dx} - \chi\right) = 0. \tag{5.79}$$

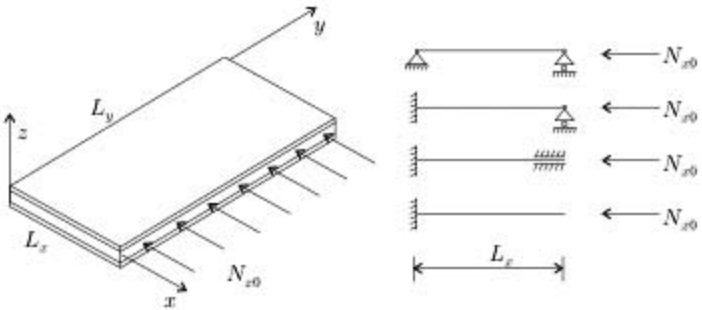

Figure 5.12: Long rectangular sandwich plate subjected to a uniform compressive edge load and the different types of supports along the long edges.

For an isotropic sandwich beam the corresponding equations are (Eqs. 7.113 and 7.114)

isotropic sandwich beam:

$$-\widehat{EI}\frac{d^3\chi}{dx^3} - \widehat{N}_{x0}\frac{d^2w}{dx^2} = 0 \tag{5.80}$$

$$\widehat{EI}\frac{d^2\chi}{dx^2} + \widehat{S}\left(\frac{dw}{dx} - \chi\right) = 0, \tag{5.81}$$

where $\widehat{EI}$ and $\widehat{S}$ are the bending and shear stiffnesses of the sandwich beam and $\widehat{N}_{x0}$ is the compressive load (per unit length).

The equations describing buckling of long sandwich plates (symmetrical layup) and isotropic sandwich beams are identical when in Eqs. (5.78) and (5.79) D_{11}, $\widetilde{S}_{11}$, and N_{x0} are replaced, respectively, by $\widehat{EI}$, $\widehat{S}$, and $\widehat{N}_{x0}$. Therefore, the buckling load (per unit length) of a long sandwich plate (symmetrical layup) may be obtained by substituting the values of D_{11} and $\widetilde{S}_{11}$ for $\widehat{EI}$ and $\widehat{S}$ in the expression for the buckling load of the corresponding isotropic sandwich beam (Section 7.4).

It was shown in Section 5.2.1 (page 180) that when the layup of the sandwich plate is unsymmetrical the deflection may be obtained by substituting the values of Ψ, $\widetilde{S}_{11}$, and p for $\widehat{EI}$, $\widehat{S}$, and p' in the expression for the deflection of the corresponding isotropic sandwich beam. Similarly, the buckling load of a long unsymmetrical sandwich plate may be obtained by substituting the values of Ψ and $\widetilde{S}_{11}$ for $\widehat{EI}$ and $\widehat{S}$ in the expression for the buckling load of the corresponding isotropic beam (where Ψ is given by Eq. 4.52).

5.2 Example. *A 0.9-m-long and 0.2-m-wide rectangular sandwich plate is made of a 0.02-m-thick core covered on both sides by graphite epoxy facesheets. The material properties are given in Table 3.6 (page 81). The layup of each facesheet is* $[\pm 45_2^t/0_{12}/\pm 45_2^t]$, *and the thickness of each facesheet is 0.002 m (Fig. 5.9). The 0-degree plies are parallel to the short edge of the plate. The plate is either simply supported or built-in along all four edges (Fig. 5.13). The plate is subjected to uniform compressive loads along the long edges. Calculate the buckling load. The core is isotropic* ($E_c = 2 \times 10^6$ *kN/m*^{2}, $\nu_c = 0.3$).

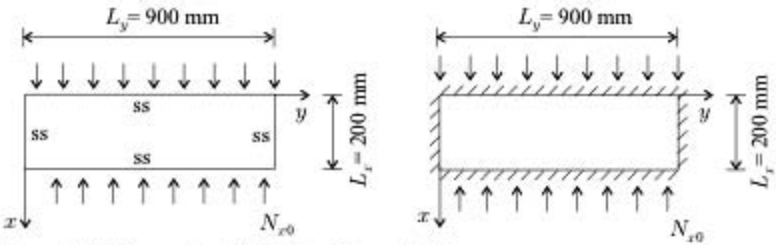

Figure 5.13: The sandwich plates in Example 5.2.

Solution. The plate may be treated as "long" (Example 5.1, page 180). The buckling loads of the corresponding beam are (Eqs. 7.175 and 6.337)

$$\widehat{N}_{cr} = \left(\frac{L^2}{\pi^2 EI} + \frac{1}{\widehat{S}} \right)^{-1} \quad \text{(ss)} \tag{5.82}$$

$$\widehat{N}_{cr} = \left(\frac{4L^2}{\pi^2 EI} + \frac{1}{\widehat{S}} \right)^{-1} \quad \text{(built-in).} \tag{5.83}$$

The buckling loads of the plate are obtained by replacing EI, $\widehat{S}$ by D_{11}, $\widetilde{S}_{11}$ (see page 186) as follows:

$$N_{x,\,cr} = \left(\frac{L_x^2}{\pi^2 D_{11}} + \frac{1}{\widetilde{S}_{11}} \right)^{-1} \quad \text{(ss)} \tag{5.84}$$

$$N_{x,\,cr} = \left(\frac{4L_x^2}{\pi^2 D_{11}} + \frac{1}{\widetilde{S}_{11}} \right)^{-1} \quad \text{(built-in).} \tag{5.85}$$

With the values of $D_{11} = 52.16\,\text{kN·m}$ and $\widetilde{S}_{11} = 18\,615\,\frac{\text{kN}}{\text{m}}$, (see Eqs. 5.53 and 5.54) and $L_x = 0.2\,\text{m}$, the buckling loads are

$$N_{x,\,cr} = \left(\frac{1}{12\,870} + \frac{1}{18\,615} \right)^{-1} = 7\,609\,\text{kN/m} \quad \text{(ss)} \tag{5.86}$$

$$N_{x,\,cr} = \left(\frac{1}{51\,481} + \frac{1}{18\,615} \right)^{-1} = 13\,672\,\text{kN/m} \quad \text{(built-in).} \tag{5.87}$$

5.3.2 Simply Supported Plates – Orthotropic and Symmetrical Layup

We consider a rectangular sandwich plate with dimensions L_x and L_y (Fig. 5.14). The layup of the plate is orthotropic (page 176) and symmetrical with respect to the plate's midplane. All four edges of the plate are simply supported. The sandwich plate is subjected to uniformly distributed compressive loads N_{x0} and N_{y0} along the edges. These loads are increased proportionally, that is, the loads are λN_{x0}, λN_{y0}, where λ is the load parameter. For a buckled plate the load parameter is denoted by λ_{cr}.

The expression for the strain energy is given by Eq. (5.64).

For a plate subjected to in-plane loads only, the potential of the external forces is (Eq. 4.108)

$$\Omega = \frac{1}{2} \int_0^{L_x} \int_0^{L_y} N_x \left(\frac{\partial w^o}{\partial x} \right)^2 + N_y \left(\frac{\partial w^o}{\partial y} \right)^2 dy dx, \tag{5.88}$$

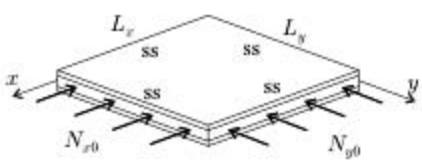

Figure 5.14: Rectangular sandwich plate subjected to biaxial compressive edge loads.

where N_x, N_y are the in-plane tensile forces related to the in-plane compressive forces λN_{x0}, λN_{y0} by

$$N_x = -\lambda N_{x0} \qquad N_y = -\lambda N_{y0}. \tag{5.89}$$

The deflection is assumed to be of the form given in Eq. (5.71). By substituting Eqs. (5.71), (5.64), (5.88), and (5.89) into Eqs. (5.72) and by performing the differentiation, after algebraic manipulations we obtain

$$\frac{L_x L_y}{4}\left(\begin{bmatrix} F_{33} & F_{34} & F_{35} \\ F_{34} & F_{44} & F_{45} \\ F_{35} & F_{45} & F_{55} \end{bmatrix} - \lambda \begin{bmatrix} N_{x0}\left(\frac{i\pi}{L_x}\right)^2 + N_{y0}\left(\frac{j\pi}{L_y}\right)^2 & 0 & 0 \\ 0 & 0 & 0 \\ 0 & 0 & 0 \end{bmatrix}\right) \times \begin{Bmatrix} w_{ij} \\ (\gamma_{xz})_{ij} \\ (\gamma_{yz})_{ij} \end{Bmatrix} = \begin{Bmatrix} 0 \\ 0 \\ 0 \end{Bmatrix}, \tag{5.90}$$

where $(\gamma_{xz})_{ij}$ and $(\gamma_{yz})_{ij}$ are defined by Eq. (5.74) and F_{ij} are given in Table 5.3 (page 184). When the load set is under the critical value, the deflection of the plate is zero. When the plate is not buckled, the deflection of the plate is zero, whereas for a buckled plate it is nonzero. The values of λ for the buckled plate (denoted by λ_{cr}) are the eigenvalues of Eq. (5.90) and are obtained by setting the determinant of the coefficient matrix to zero. This gives

$$(\lambda_{ij})_{cr} = \frac{1}{N_{x0}\left(\frac{i\pi}{L_x}\right)^2 + N_{y0}\left(\frac{j\pi}{L_y}\right)^2} \frac{\begin{vmatrix} F_{33} & F_{34} & F_{35} \\ F_{34} & F_{44} & F_{45} \\ F_{35} & F_{45} & F_{55} \end{vmatrix}}{\begin{vmatrix} F_{44} & F_{45} \\ F_{45} & F_{55} \end{vmatrix}}, \tag{5.91}$$

where $|\ \ |$ denotes the determinant. The values of $(\lambda_{ij})_{cr}$ are calculated for different sets of i and j, $(i, j = 1, 2, \ldots)$. The lowest resulting value of $(\lambda_{ij})_{cr}$ is the value of interest.

When the sandwich plate is isotropic, we obtain $(\lambda_{ij})_{cr}$ by replacing D_{11}, D_{12}, D_{66} in Table 5.3 by D^{iso}, $\nu^{iso}D^{iso}$, and $(1-\nu^{iso})D^{iso}/2$ (see Table 5.2, page 178) and $\tilde{S}_{11}$, $\tilde{S}_{22}$ by $\tilde{S}$ (see Eq. 5.39). With these substitutions Eq. (5.91) simplifies to

$$(\lambda_{ij})_{cr}^{iso} = \frac{\left(\frac{i}{L_x}\right)^2 + \left(\frac{j}{L_y}\right)^2}{N_{x0}\left(\frac{i}{L_x}\right)^2 + N_{y0}\left(\frac{j}{L_y}\right)^2}\left(N_{D,cr}^{-1} + \tilde{S}^{-1}\right)^{-1}, \tag{5.92}$$

where $N_{D,cr}$ is defined as

$$N_{D,cr} = \pi^2 D^{iso}\left[\left(\frac{i}{L_x}\right)^2 + \left(\frac{j}{L_y}\right)^2\right]. \tag{5.93}$$

5.3 Example. *A 0.9-m-long and 0.2-m-wide rectangular sandwich plate is made of a 0.02-m-thick core covered on both sides by graphite epoxy facesheets. The*

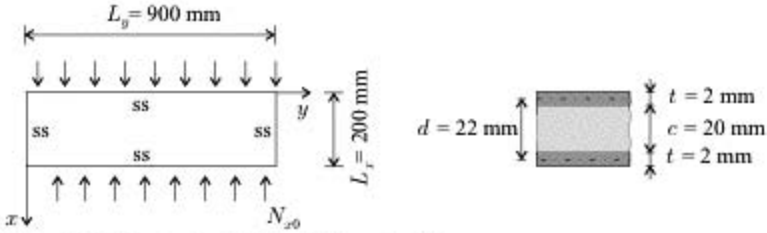

Figure 5.15: The sandwich plate in Example 5.3.

material properties are given in Table 3.6 (page 81). The layup of each facesheet is $[\pm 45_2^t/0_{12}/\pm 45_2^t]$*, and the thickness of each facesheet is* $0.002\,m$*. The 0-degree plies are parallel to the short edge of the plate. The plate, simply supported along all four edges (Fig. 5.15), is subjected to uniform compressive loads along the long edges. Calculate the buckling load. The core is isotropic (*$E_c = 2 \times 10^6\ kN/m^2$, $\nu_c = 0.3$*).*

Solution. We set $N_{y0} = 0$ in Eq. (5.91) and write

$$N_{x0}\,(\lambda_{ij})_{cr} = \frac{1}{\left(\frac{i\pi}{L_x}\right)^2} \frac{\begin{vmatrix} F_{33} & F_{34} & F_{35} \\ F_{34} & F_{44} & F_{45} \\ F_{35} & F_{45} & F_{55} \end{vmatrix}}{\begin{vmatrix} F_{44} & F_{45} \\ F_{45} & F_{55} \end{vmatrix}}. \tag{5.94}$$

The parameters F_{ij} are given in Table 5.3 (page 184) as follows:

$$\begin{aligned}
F_{33} &= D_{11}\left(\frac{i\pi}{L_x}\right)^4 + 2\,(D_{12} + 2D_{66})\left(\frac{i\pi}{L_x}\right)^2\left(\frac{j\pi}{L_y}\right)^2 + D_{22}\left(\frac{j\pi}{L_y}\right)^4 \\
F_{34} &= -D_{11}\left(\frac{i\pi}{L_x}\right)^3 - (D_{12} + 2D_{66})\frac{i\pi}{L_x}\left(\frac{j\pi}{L_y}\right)^2 \\
F_{35} &= -D_{22}\left(\frac{j\pi}{L_y}\right)^3 - (D_{12} + 2D_{66})\left(\frac{i\pi}{L_x}\right)^2\frac{j\pi}{L_y} \\
F_{44} &= D_{11}\left(\frac{i\pi}{L_x}\right)^2 + D_{66}\left(\frac{j\pi}{L_y}\right)^2 + \widetilde{S}_{11} \\
F_{45} &= (D_{12} + 2D_{66})\left(\frac{i\pi}{L_x}\right)\left(\frac{j\pi}{L_y}\right) \\
F_{55} &= D_{22}\left(\frac{j\pi}{L_y}\right)^2 + D_{66}\left(\frac{i\pi}{L_x}\right)^2 + \widetilde{S}_{22}.
\end{aligned} \tag{5.95}$$

The elements of the stiffness matrices are (Eqs. 5.53 and 5.54)

$$\begin{aligned}
&D_{11} = 52.16\,\text{kN}\cdot\text{m} \qquad D_{22} = 11.71\,\text{kN}\cdot\text{m} \qquad D_{12} = 7.96\,\text{kN}\cdot\text{m} \\
&D_{66} = 8.76\,\text{kN}\cdot\text{m} \qquad \widetilde{S}_{11} = 18\,615\frac{\text{kN}}{\text{m}} \qquad \widetilde{S}_{22} = 18\,615\frac{\text{kN}}{\text{m}}.
\end{aligned}$$

By substituting these stiffnesses and $L_x = 0.2\,\text{m}$, $L_y = 0.9\,\text{m}$ into Eq. (5.94), we obtain the following values of N_{x0}, $(\lambda_{ij})_{cr}$:

$i \setminus j$	1	2	3
1	7 965	9 070	11 041
2	13 875	14 491	15 544
3	16 195	16 668	17 470.

(5.96)

The smallest value is $N_{x0}\,(\lambda_{cr})_{ij} = 7\,965\,\text{kN/m}$, which corresponds to $i = j = 1$, Thus, the buckling load is

$$N_{x,cr} = (\lambda_{cr})_{11}\, N_{x0} = 7\,965\,\text{kN/m}. \tag{5.97}$$

In Example 5.2 we treated this sandwich as a long plate and obtained the buckling load $N_{xcr} = 7\,609\,\text{kN/m}$ (Eq. 5.86). This is within 5 percent of the value given by Eq. (5.97).

5.3.3 Face Wrinkling

We consider a sandwich plate. The top and bottom facesheets are identical, and each facesheet's layup is symmetrical with respect to the facesheet's midplane. The sandwich plate is subjected to in-plane forces N_x, N_y, N_{xy} (Fig. 5.16, left). Since the in-plane stiffnesses of the core are taken to be negligible, the in-plane stresses in the core may be neglected with respect to the in-plane stresses in the facesheets. Correspondingly, the in-plane forces (per unit length) in the facesheets are

$$N_x^{\text{f}} = \frac{N_x}{2} \qquad N_y^{\text{f}} = \frac{N_y}{2} \qquad N_{xy}^{\text{f}} = \frac{N_{xy}}{2} \qquad \text{f} = \text{t, b.} \tag{5.98}$$

The superscript f denotes either the top or the bottom facesheet. Under these in-plane forces the facesheets may become wavy (Fig. 5.16, right). These waves are precursors of local buckling, and the loadset at which these waves first occur is taken as the buckling loads. The waves may propagate in two directions, although generally the waves in one direction dominate. In our analysis we consider only waves in one direction.

The wavelength $2l$ depends on the material and on the geometry of the sandwich plate. Here, we consider two cases: (i) the wavelength is "short," such that

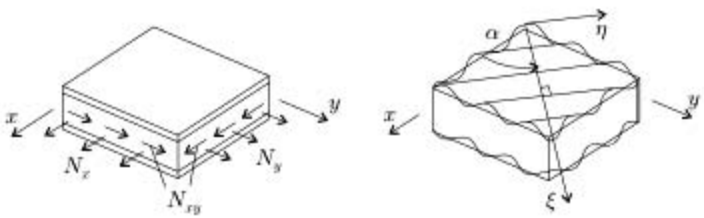

Figure 5.16: Face wrinkling of sandwich plates.

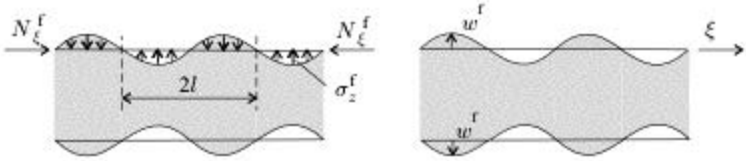

Figure 5.17: Forces and displacements of the buckled facesheets.

$l/h \ll 1$, and (ii) the wavelength is "long" such that $l/h \gg 1$ (h is the thickness of the plate as shown in Fig. 5.2).

The loads that contribute to the waviness of the facesheets are the in-plane load perpendicular to the wave N_ξ^f and the normal load σ_z^f (corresponding to the stress σ_z) exerted on the facesheet by the deformed core (Fig. 5.17, left). Under these loads the equilibrium equation of the facesheet is[1]

$$\Psi_\xi \frac{\partial^4 w^f}{\partial \xi^4} + N_\xi^f \frac{\partial^2 w^f}{\partial \xi^2} = \sigma_z^f, \tag{5.99}$$

where Ψ_ξ is the bending stiffness of the facesheet in the ξ direction – that is, the 11 element of the matrix $[D]$ in the ξ–η coordinate system. Transformation of the matrix $[D]$ follows the transformation rule of the matrix $[Q]$ given by Eq. (2.195). Thus, we have

$$\begin{aligned}\Psi_\xi = \left(D_{11}^f\right)_{\xi-\eta} = D_{11}^f \cos^4\alpha + D_{22}^f \sin^4\alpha + \left(2D_{12}^f + 4D_{66}^f\right)\cos^2\alpha \sin^2\alpha \\ +4\cos^3\alpha \sin\alpha D_{16}^f + 4\cos\alpha \sin^3\alpha D_{26}^f \qquad f = t, b.\end{aligned} \tag{5.100}$$

where α is the angle between the x- and ξ-axes and D_{ij}^f are the elements of the bending stiffness matrix of the facesheets in the x–y coordinate system.

The parameter w^f is the out-of-plane displacement (deflection) of the facesheet (Fig. 5.17, right),

$$w^f = w_0 \sin\frac{\pi\xi}{l}, \tag{5.101}$$

where w_0 is the amplitude of the deflection and l is the half buckling wavelength.

The parameter N_ξ^f is the in-plane force in the facesheet in the ξ direction and is obtained from the in-plane forces N_x^f, N_y^f, and N_{xy}^f by transformation. By using the stress transformation in Eq. (2.182), we can define N_ξ^f by the following equation:

$$N_\xi^f = -\left(N_x^f \cos^2\alpha + N_y^f \sin^2\alpha + 2N_{xy}^f \cos\alpha \sin\alpha\right) \qquad f = t, b. \tag{5.102}$$

We are interested in the value of N_ξ^f at which the waviness first arises.

Isotropic core – composite facesheets. When the core is isotropic, the out-of-plane stress in the core σ_z varies across the thickness as illustrated in Figure 5.18 (left). When the wavelength is small, the stress σ_z varies, as illustrated in Figure 5.18 (middle). Since the stresses vanish away from the facesheets, the problem may be

[1] S. P. Timoshenko and J. Gere, *Theory of Elastic Stability*. 2nd edition. McGraw-Hill, New York, 1961, p. 2.

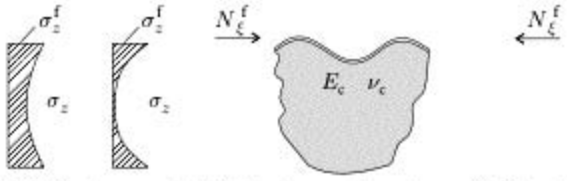

Figure 5.18: The stress σ_z distribution in an isotropic core (left) and in an isotropic core with short wavelength (middle); buckling of a plate on an elastic foundation (right).

treated as a plate on an infinite elastic foundation (Fig. 5.18, right). Then, the stress at the core facesheet interface σ_z^f is[2]

$$\sigma_z^f = -\frac{a}{l} w_0 \sin\frac{\pi\xi}{l} \qquad \text{where} \qquad a = \frac{2\pi E_c}{(3-\nu_c)(1+\nu_c)}, \tag{5.103}$$

where E_c and ν_c are the Young modulus and Poisson's ratio of the isotropic core.

Equations (5.99), (5.101), and (5.103) yield

$$\Psi_\xi w_0 \frac{\pi^4}{l^4} \sin\frac{\pi\xi}{l} - N_\xi^f w_0 \frac{\pi^2}{l^2} \sin\frac{\pi\xi}{l} = -\frac{a}{l} w_0 \sin\frac{\pi\xi}{l}. \tag{5.104}$$

When the facesheet becomes wavy, w_0 is not zero. The values of N_ξ^f corresponding to $w_0 \neq 0$ are the buckling loads $(N_\xi^f)_{cr}$. These buckling loads are given by the nontrivial solution of Eq. (5.104) and are

$$\left(N_\xi^f\right)_{cr} = \Psi_\xi \frac{\pi^2}{l^2} + \frac{a}{l}\frac{l^2}{\pi^2} \qquad \begin{matrix}\text{isotropic core}\\ \text{composite facesheets}\\ \text{short wave.}\end{matrix} \tag{5.105}$$

When the wavelength is long, the solution is obtained by assuming that the stress distribution σ_z is uniform (Fig. 5.19, middle) and σ_z^f is approximated as

$$\sigma_z^f = -\sigma_z = -E_c\epsilon_z = -w^f \frac{E_c}{c/2}, \tag{5.106}$$

where $\epsilon_z = w^f/(c/2)$ (Fig. 5.19, right). Substitution of Eqs. (5.101) and (5.106) into Eq. (5.99) gives

$$\Psi_\xi w_0 \frac{\pi^4}{l^4} \sin\frac{\pi\xi}{l} - N_\xi^f w_0 \frac{\pi^2}{l^2} \sin\frac{\pi\xi}{l} = -\frac{E_c}{c/2} w_0 \sin\frac{\pi\xi}{l}. \tag{5.107}$$

The nontrivial solution is

$$\left(N_\xi^f\right)_{cr} = \Psi_\xi \frac{\pi^2}{l^2} + \frac{E_c}{c/2}\frac{l^2}{\pi^2} \qquad \begin{matrix}\text{isotropic core}\\ \text{composite facesheets}\\ \text{long wave.}\end{matrix} \tag{5.108}$$

[2] H. G. Allen, *Analysis and Design of Structural Sandwich Panels*. Pergamon Press, Oxford, 1969, p. 158.

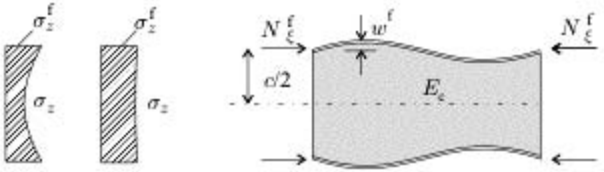

Figure 5.19: The stress σ_z distribution in an isotropic core (left); in an isotropic core with long wavelength (middle); buckled shape (right).

We are interested in the lowest value of $(N_\xi^f)_{cr}$. This value is obtained by setting the derivative of $(N_\xi^f)_{cr}$ with respect to l equal to zero as follows:

$$\frac{d\,(N_\xi^f)_{cr}}{dl} = 0. \tag{5.109}$$

Solution of this equation results in the half-wavelength l_{cr} corresponding to the lowest buckling load. Substitution of l_{cr} into the expressions for $(N_\xi^f)_{cr}$ gives $(N_\xi^f)_{cr,min}$. The results are summarized in the top half of Table 5.4.

The value of $(N_\xi^f)_{cr,min}$ depends on the direction α in which the wave propagates because Ψ_ξ depends on α (Eq. 5.100). The wave direction is not known a priori and must be determined. This is accomplished by observing that N_ξ^f is also a function of α (Eq. 5.102). The wave will first appear in the direction in which the ratio $(N_\xi^f)_{cr,min}/N_\xi^f$ is the smallest. This ratio is calculated for different angles, and the angle that results in the smallest ratio is the desired α.

Honeycomb core – composite facesheets. When the sandwich plate consists of a honeycomb core with composite facesheets, the stress at the core facesheet interface may be approximated by Eq. (5.106) for both short and long wavelengths. The buckling loads are identical to those given by Eq. (5.108) and are

$$(N_\xi^f)_{cr} = \Psi_\xi \frac{\pi^2}{l^2} + \frac{E_c}{c/2}\frac{l^2}{\pi^2} \qquad \begin{matrix}\text{honeycomb core}\\ \text{composite facesheets}\\ \text{short or long waves,}\end{matrix} \tag{5.110}$$

Table 5.4. Face wrinkling of sandwich plates with either a honeycomb or an isotropic core. The constant a is given by Eq. (5.103) and $G_c = \frac{E_z}{2(1+\nu_0)}$.

	Isotropic core		Honeycomb core
	Short wave	Long wave	Short or long wave
Composite facesheets	$(N_\xi^f)_{cr,min} = 1.5\sqrt[3]{\frac{2\Psi_\xi a^2}{\pi^2}}$ $l_{cr} = \sqrt[3]{2\frac{\pi^4\Psi_\xi}{a}}$		$(N_\xi^f)_{cr,min} = 2\sqrt{\Psi_\xi \frac{E_c}{c/2}}$ $l_{cr} = \pi\sqrt[4]{\frac{\Psi_\xi c/2}{E_c}}$
Isotropic facesheets	$(N_\xi^f)_{cr,min} = 1.5t\sqrt[3]{\frac{4E_f E_c G_c}{3(1-\nu_f^2)(3-\nu_c)^2(1+\nu_c)}}$ $\approx 0.79t\sqrt[3]{E_f E_c G_c}$ $l_{cr} = \sqrt[3]{\frac{\pi^4 E_f t^3}{6(1-\nu_f^2)a}}$		$(N_\xi^f)_{cr,min} = t\sqrt{\frac{\frac{2}{3}\frac{tE_f E_c}{c(1-\nu_f^2)}}}$ $l_{cr} = \pi\sqrt[4]{\frac{E_f}{24E_c(1-\nu_f^2)}t^3 c}$

where E_c is the Young modulus of the core perpendicular to the plane of the sandwich plate.

The lowest value of the buckling load and the direction α in which the wave propagates is determined as previously above for plates with isotropic core and composite facesheets.

Isotropic core – isotropic facesheets. We now consider sandwich plates with isotropic core and isotropic facesheets. The bending stiffness of an isotropic facesheet is (see Eqs. 3.42 and 5.100)

$$\Psi_\xi = D^{\text{iso}} = \frac{E_f t^3}{12\left(1-\nu_f^2\right)}, \tag{5.111}$$

where t is the thickness of the facesheet and the subscript f denotes the facesheet. When both the core and the facesheets are isotropic and the facesheets buckle with short waves, the lowest value of the buckling load is obtained by substituting Eq. (5.111) into Eq. (5.105) and by performing the differentiation indicated in Eq. (5.109). The result is

$$\left(N_\xi^f\right)_{\text{cr,min}} = t\left[1.5\sqrt[3]{\frac{4E_fE_cG_c}{3\left(1-\nu_f^2\right)(3-\nu_c)^2(1+\nu_c)}}\right] \quad \begin{array}{c}\text{isotropic core}\\ \text{isotropic facesheets}\\ \text{short wave.}\end{array} \tag{5.112}$$

where G_c is the shear modulus of the core ($G_c = E_c/2(1+\nu_c)$), f and c refer to the facesheets and the core. By the definition of the in-plane force (Eq.5.7) the term in the bracket is the critical stress.

By neglecting the Poisson ratios ($\nu_c = \nu_f = 0$), Eq. (5.112) reduces to

$$\left(N_\xi^f\right)_{\text{cr,min}} = t\left[0.79\sqrt[3]{E_fE_cG_c}\right] \quad \begin{array}{c}\text{isotropic core}\\ \text{isotropic facesheets}\\ \text{short wave.}\end{array} \tag{5.113}$$

Hoff and Mautner[3] obtained this expression with the value of the constant 0.91 instead of 0.79. However, for practical use they recommended the value 0.5.

When both the core and the facesheets are isotropic and the facesheets buckle with long waves, Eqs. (5.108), (5.111), and (5.109) give

$$\left(N_\xi^f\right)_{\text{cr,min}} = t\left[\sqrt{\frac{2}{3}\frac{E_fE_c}{c\left(1-\nu_f^2\right)}}\right] \quad \begin{array}{c}\text{isotropic core}\\ \text{isotropic facesheets}\\ \text{long wave.}\end{array} \tag{5.114}$$

For an isotropic facesheet the bending stiffness does not depend on the direction. Consequently, buckling waves occur in the direction in which the compressive stress is maximum.

[3] N. J. Hoff and S. E. Mautner, Buckling of Sandwich Type Panels. *Journal of the Aeronautical Sciences*, Vol. 12, 285–297, 1945. See also in J. R Vinson, *Sandwich Structures of Isotropic and Composite Materials*. Technomic, Lancaster, Pennsylvania, 1999, p. 239.

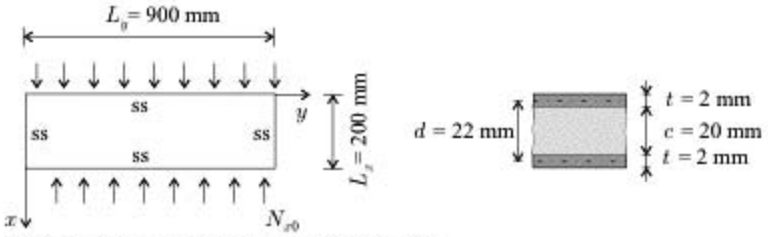

Figure 5.20: The sandwich plate in Example 5.4.

Honeycomb core – isotropic facesheets. Lastly, we consider a sandwich plate with honeycomb core and isotropic facesheets. The half wavelength l_{cr} may be short or long. In this case Eqs. (5.110), (5.111), and (5.109) yield

$$\left(N_\xi^f\right)_{cr,\min} = t\left[\sqrt{\frac{2}{3}\frac{E_f E_c}{c\left(1-\nu_f^2\right)}}\right] \qquad \begin{array}{c}\text{honeycomb core}\\ \text{isotropic facesheets}\\ \text{short or long wave.}\end{array} \tag{5.115}$$

This equation is identical to that given by Heath.[4]

The lowest buckling loads and the half wavelengths corresponding to these buckling loads are summarized in Table 5.4.

These expressions take into account face wrinkling in one direction only. They are accurate when only uniaxial load is applied to an orthotropic plate in one of the orthotropy directions. In case of biaxial loading these expressions may overestimate the buckling load. For most practical composite sandwich plates the error in the buckling loads given by these expressions is less than 30 percent.

5.4 Example. *A 0.2-m-long and 0.9-m-wide rectangular sandwich plate is made of a 0.02-m-thick core covered on both sides by graphite epoxy facesheets. The material properties are given in Table 3.6 (page 81). The layup of each facesheet is* $[\pm 45_2^f/0_{12}/\pm 45_2^f]$*, and the thickness of each facesheet is 0.002 m. The 0-degree plies are parallel to the short edge of the plate. The plate is simply supported along all four edges (Fig. 5.20). The plate is subjected to unidirectional in-plane loads* N_{x0}*. Estimate the load at which the facesheet wrinkles. The core is isotropic (*$E_c = 2 \times 10^6$ *kN/m*^{2}*,* $\nu_c = 0.3$*).*

Solution. Let us first assume that the facesheet wrinkles parallel to the y-axis with long waves ($\alpha = 0$, Fig. 5.16). In this direction Ψ_ξ is (Eq. 5.100)

$$\Psi_\xi = D_{11}^f = D_{11} = 45.30\ \text{N}\cdot\text{m}. \tag{5.116}$$

[4] W. G. Heath, Sandwich Construction, Part 2: The Optimum Design of Flat Sandwich Panels. *Aircraft Engineering*, Vol. 32, 230–235, 1960. See also in J. R Vinson, *Sandwich Structures of Isotropic and Composite Materials*. Technomic, Lancaster, Pennsylvania, 1999, p. 239.

The value of D_{11}^{f} is given in Table 3.7 (page 84). The lowest buckling load and the corresponding half wavelength are (Table 5.4, page 193)

$$(N_{\xi}^{f})_{cr,min} = 2\sqrt{\Psi_{\xi}\frac{E_c}{c/2}} = 19\,036\ \frac{kN}{m} \tag{5.117}$$

$$l_{cr} = \pi\sqrt[4]{\frac{\Psi_{\xi}c/2}{E_c}} = 0.0069\ m = 6.9\ mm. \tag{5.118}$$

The assumption that the wave is long is valid when l_{cr} is large compared with the core thickness. Here, l_{cr} is only about a third of the core thickness and, therefore, the long-wave approximation is invalid.

Let us now assume that the wave is short. With this assumption we have (Table 5.4, page 193)

$$(N_{\xi}^{f})_{cr,min} = 1.5\sqrt[3]{\frac{2\Psi_{\xi}a^2}{\pi^2}} = 34\,116\ \frac{kN}{m} \tag{5.119}$$

$$l_{cr} = \sqrt[3]{2\frac{\pi^4\Psi_{\xi}}{a}} = 0.0063\ m = 6.3\ mm, \tag{5.120}$$

where (Eq. 5.103)

$$a = \frac{2\pi E_c}{(3-\nu_c)(1+\nu_c)} = 35.80\times10^9\frac{N}{m^2}. \tag{5.121}$$

The wave may be assumed to be short when l_{cr} is significantly smaller than the core thickness c. Here, the ratio l_{cr}/c is about one-third. Thus, the short wave approximation is unreasonable.

In this problem, the wave cannot be treated as either long or short. As a conservative estimate we take the lower of the two buckling loads given by the long- and short-wave approximations. Thus, the lowest buckling load is (see Eq. 5.98)

$$N_{xcr} = 2\,(N_{\xi}^{f})_{cr,min} = 2\times19\,036 = 38\,072\ \frac{kN}{m}. \tag{5.122}$$

5.4 Free Vibration of Rectangular Sandwich Plates

In this section we obtain the natural frequencies f and, hence, the periods of vibration ($T = 1/f$) and the circular frequencies ($\omega = 2\pi f$) of sandwich plates. In the analyses that follows we assume that the plate is freely vibrating and is undamped.

5.4.1 Long Plates

We consider a long rectangular sandwich plate whose length is large compared with its width ($L_y \gg L_x$). The edges may be built-in, simply supported, or free, as illustrated in Figure 5.21.

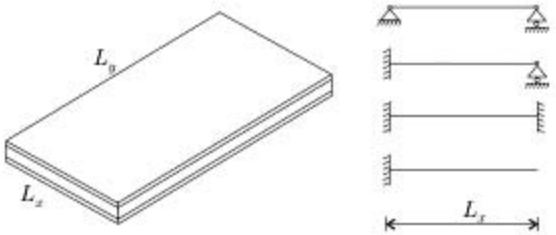

Figure 5.21: The different types of supports along the long edges of long sandwich plates undergoing free undamped vibration.

The deflected surface of the sandwich plate may be assumed to be cylindrical at a considerable distance from the short edges (Fig. 4.4). The equilibrium equations are Eqs. (4.191)–(4.193),

$$\frac{dV_x}{dx} + \rho (2\pi f)^2 w^o = 0 \tag{5.123}$$

$$\frac{dM_x}{dx} - V_x = 0, \tag{5.124}$$

where w^o is the deflection and ρ is the mass per unit area of the sandwich plate.

We now consider a sandwich plate that is symmetrical with respect to the midplane. The bending moment and the transverse shear force acting on the sandwich plate are (Eq. 5.44)

$$M_x = -D_{11}\frac{\partial \chi_{xz}}{\partial x} \qquad V_x = \widetilde{S}_{11}\gamma_{xz}. \tag{5.125}$$

Equations (5.123), (5.124), and (5.125), together with Eq. (5.2), give
sandwich plate, symmetrical layup:

$$-D_{11}\frac{d^3\chi_{xz}}{dx^3} + \rho (2\pi f)^2 w^o = 0 \tag{5.126}$$

$$D_{11}\frac{d^2\chi_{xz}}{dx^2} + \widetilde{S}_{11}\left(\frac{dw^o}{dx} - \chi_{xz}\right) = 0. \tag{5.127}$$

For a vibrating sandwich beam the corresponding equations are (see Eqs. 7.178–7.180, $\omega = 2\pi f$)
isotropic sandwich beam:

$$-\widehat{EI}\frac{d^3\chi}{dx^3} + \rho' (2\pi f)^2 w = 0 \tag{5.128}$$

$$\widehat{EI}\frac{d^2\chi}{dx^2} + \widehat{S}\left(\frac{dw}{dx} - \chi\right) = 0, \tag{5.129}$$

where $\widehat{EI}$ and $\widehat{S}$ are the bending and shear stiffnesses of the sandwich beam and ρ' is the mass per unit length.

The preceding set of equations describing the vibration of long sandwich plates (symmetrical layup) and isotropic sandwich beams are identical when D_{11}, $\widetilde{S}_{11}$, and ρ are replaced, respectively, by $\widehat{EI}$, $\widehat{S}$, and ρ'. Therefore, the natural

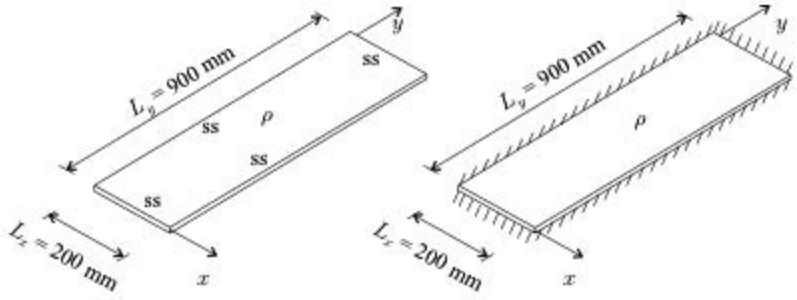

Figure 5.22: The sandwich plates in Example 5.5.

frequencies of a long sandwich plate (symmetrical layup) may be obtained by substituting the values of D_{11}, $\widetilde{S}_{11}$, and ρ for $\widehat{EI}$, $\widehat{S}$, ρ' in the expression given in Section 7.5 for the natural frequencies of the corresponding isotropic sandwich beam.

The natural frequencies of a long unsymmetrical sandwich plate may be obtained by substituting the values of Ψ (Eq.4.52), $\widetilde{S}_{11}$, and ρ for $\widehat{EI}$, $\widehat{S}$, ρ' in the expression for the natural frequencies of the corresponding isotropic sandwich beam.

5.5 Example. *A 0.9-m-long and 0.2-m-wide rectangular sandwich plate is made of a 0.02-m-thick core covered on both sides by graphite epoxy facesheets. The material properties are given in Table 3.6 (page 81). The layup of each facesheet is* $[\pm 45_2^{\mathrm{t}}/0_{12}/\pm 45_2^{\mathrm{t}}]$, *and the thickness of each facesheet is* 0.002 *m. The 0-degree plies are parallel to the short edge of the plate. The plate is either simply supported or built-in along all four edges (Fig. 5.22). A uniform mass is over the plate such that for the combined mass-plate system* $\rho = 200\ kg/m^2$. *Calculate the circular and the natural frequencies. The core is isotropic (*$E_c = 2 \times 10^6\ kN/m^2$, $\nu_c = 0.3$*).*

Solution. The plate may be treated as "long" (Example 5.1, page 180). The circular frequencies of the corresponding beam are (Eq. 7.243, Eq. 6.398, and Table 6.13, page 308)

$$\omega_i = \sqrt{\left(\frac{\rho'}{EI}\frac{L^4}{\mu_{Bi}^4} + \frac{\rho'}{\widehat{S}_{zz}}\frac{L^2}{\mu_{Si}^2}\right)^{-1}}, \tag{5.130}$$

where

$$\mu_{Bi} = \pi,\ 2\pi,\ 3\pi, \ldots \qquad \text{(ss)} \tag{5.131}$$

$$\mu_{Bi} = 4.730,\ 7.853,\ 10.996, \ldots \qquad \text{(built-in)} \tag{5.132}$$

and

$$\mu_{Si} = \pi,\ 2\pi,\ 3\pi, \ldots \qquad \text{(ss or built-in).} \tag{5.133}$$

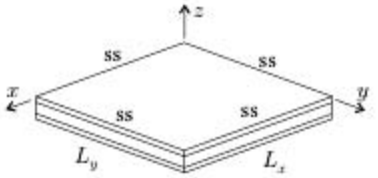

Figure 5.23: Rectangular sandwich plate with simply supported edges.

The circular frequencies of the plate are obtained by replacing EI, $\widehat{S}$, ρ' by D_{11}, $\widetilde{S}_{11}$, ρ (see page 198) as follows:

$$\omega = \sqrt{\left(\frac{\rho}{D_{11}}\frac{L_x^4}{\mu_{Bi}^4} + \frac{\rho}{\widetilde{S}_{11}}\frac{L_x^2}{\mu_{Si}^2}\right)^{-1}}. \tag{5.134}$$

With the values of $D_{11} = 52.16\ \text{kN}\cdot\text{m}$ and $\widetilde{S}_{11} = 18\,615\frac{\text{kN}}{\text{m}}$, (see Eqs. 5.53 and 5.54) and with $L_x = 0.2$ m, the first three modes of the circular frequencies of the plate are

$$\omega_1 = 3\,064 \quad \omega_2 = 8\,214 \quad \omega_3 = 13\,344\ 1/\text{s} \quad \text{(ss)} \tag{5.135}$$

$$\omega_1 = 4\,233 \quad \omega_2 = 8\,945 \quad \omega_3 = 13\,791\ 1/\text{s} \quad \text{(built-in)}. \tag{5.136}$$

The corresponding natural frequencies are ($f = \omega/2\pi$)

$$f_1 = 488 \quad f_2 = 1\,307 \quad f_3 = 2\,124\ \text{Hz} \quad \text{(ss)} \tag{5.137}$$

$$f_1 = 674 \quad f_2 = 1\,424 \quad f_3 = 2\,195\ \text{Hz} \quad \text{(built-in)}. \tag{5.138}$$

5.4.2 Simply Supported Plates – Orthotropic and Symmetrical Layup

A simply supported rectangular sandwich plate with dimensions L_x and L_y is considered (Fig. 5.23). The layup of the plate is orthotropic (page 176) and symmetrical with respect to the plate's midplane. The plate is undergoing free undamped vibration. The deflection of the plate is (Eq. 4.189)

$$w^o = \overline{w}^o \sin(2\pi f t). \tag{5.139}$$

Analogously, we express the rotations of the normals as

$$\chi_{xz} = \overline{\chi}_{xz} \sin(2\pi f t) \tag{5.140}$$

$$\chi_{yz} = \overline{\chi}_{yz} \sin(2\pi f t), \tag{5.141}$$

where $\overline{w}^o$, $\overline{\chi}_{xz}$, and $\overline{\chi}_{yz}$ are as yet unknown functions of x and y. These functions must be chosen such that $\overline{w}^o$, $\overline{\chi}_{xz}$, and $\overline{\chi}_{yz}$ satisfy the boundary conditions given in Section 5.2.2 (Eqs. 5.66–5.70). To determine these functions we introduce Eqs. (5.139)–(5.141) into the expression for the strain energy given by Eq. (5.64). This results in

$$U = \overline{U} \sin^2(2\pi f t), \tag{5.142}$$

where $\overline{U}$ is defined as

$$\overline{U} = \frac{1}{2}\int_0^{L_x}\int_0^{L_y}\left[\left(\frac{\partial \overline{\chi}_{xz}}{\partial x}\right)^2 D_{11} + \left(\frac{\partial \overline{\chi}_{yz}}{\partial y}\right)^2 D_{22} + 2\frac{\partial \overline{\chi}_{xz}}{\partial x}\frac{\partial \overline{\chi}_{yz}}{\partial y} D_{12} + \left(\frac{\partial \overline{\chi}_{xz}}{\partial y} + \frac{\partial \overline{\chi}_{yz}}{\partial x}\right)^2 D_{66} + \left(\frac{\partial \overline{w}^o}{\partial x} - \overline{\chi}_{xz}\right)^2 \widetilde{S}_{11} + \left(\frac{\partial \overline{w}^o}{\partial y} - \overline{\chi}_{yz}\right)^2 \widetilde{S}_{22}\right] dxdy. \tag{5.143}$$

Following the steps used in the analysis of free vibration of thin plates (Section 4.4.2), we arrive at the following expression for the natural frequency:

$$(2\pi f)^2 = \frac{\overline{U}}{\frac{1}{2}\rho \int_0^{L_x}\int_0^{L_y} \rho \overline{w}^{o2} dydx}. \tag{5.144}$$

We adopt the following expressions for $\overline{w}^o$, $\overline{\chi}_{xz}$, $\overline{\chi}_{yz}$:

$$\begin{aligned}
\overline{w}^o &= \sum_{i=1}^{I}\sum_{j=1}^{J} w_{ij} \sin\frac{i\pi x}{L_x}\sin\frac{j\pi y}{L_y} \\
\overline{\chi}_{xz} &= \sum_{i=1}^{I}\sum_{j=1}^{J} (\chi_{xz})_{ij} \cos\frac{i\pi x}{L_x}\sin\frac{j\pi y}{L_y} \\
\overline{\chi}_{yz} &= \sum_{i=1}^{I}\sum_{j=1}^{J} (\chi_{yz})_{ij} \sin\frac{i\pi x}{L_x}\cos\frac{j\pi y}{L_y}.
\end{aligned} \tag{5.145}$$

With these expressions the deflections and the rotations given by Eqs. (5.139)–(5.141) satisfy the boundary given by Eqs. (5.66)–(5.70). The unknown coefficients w_{ij}, $(\chi_{xz})_{ij}$, $(\chi_{yz})_{ij}$ are determined from the conditions (Eq. 4.217)

$$\frac{\partial f}{\partial (\chi_{xz})_{ij}} = 0 \qquad \frac{\partial f}{\partial (\chi_{yz})_{ij}} = 0 \qquad \frac{\partial f}{\partial w_{ij}} = 0. \tag{5.146}$$

After algebraic manipulations we obtain

$$\left(\frac{L_x L_y}{4}\begin{bmatrix} F_{33} & F_{34} & F_{35} \\ F_{34} & F_{44} & F_{45} \\ F_{35} & F_{45} & F_{55}\end{bmatrix} - \lambda\begin{bmatrix}1&0&0\\0&0&0\\0&0&0\end{bmatrix}\right)\begin{Bmatrix} w_{ij} \\ (\gamma_{xz})_{ij} \\ (\gamma_{yz})_{ij}\end{Bmatrix} = \begin{Bmatrix}0\\0\\0\end{Bmatrix}, \tag{5.147}$$

where $(\gamma_{xz})_{ij}$ and $(\gamma_{yz})_{ij}$ are defined by Eq. (5.74), F_{ij} are given in Table 5.3 (page 184), and λ is defined as

$$\lambda = \frac{1}{4}(2\pi f)^2 \rho L_x L_y. \tag{5.148}$$

In the case of free vibration the deflection is nonzero. For nonzero deflections, Eq. (5.147) is satisfied when the determinant of the matrix in the parentheses is zero. At this condition λ signifies the eigenvalues of Eq. (5.147), and we obtain

$$\lambda_{ij} = \frac{\begin{vmatrix} F_{33} & F_{34} & F_{35} \\ F_{34} & F_{44} & F_{45} \\ F_{35} & F_{45} & F_{55} \end{vmatrix}}{\begin{vmatrix} F_{44} & F_{45} \\ F_{45} & F_{55} \end{vmatrix}} \frac{L_x L_y}{4}. \tag{5.149}$$

The values of λ_{ij} are calculated for different sets of i and j, $(i, j = 1, 2, \ldots)$, of which the lowest value is of interest.

The natural frequencies are calculated from Eq. (5.148):

$$f_{ij} = \frac{1}{\pi}\sqrt{\frac{\lambda_{ij}}{\rho L_x L_y}}. \tag{5.150}$$

When the sandwich plate is isotropic, we obtain λ_{ij} by replacing D_{11}, D_{12}, D_{66} in Table 5.3 (page 184) by D^{iso}, $\nu^{\text{iso}} D^{\text{iso}}$, and $\left(1 - \nu^{\text{iso}}\right) D^{\text{iso}}/2$ (see Table 5.2, page 178) and $\widetilde{S}_{11}$, $\widetilde{S}_{22}$ by $\widetilde{S}$ (see Eq. 5.39). With these substitutions Eq. (5.149) simplifies to

$$\lambda_{ij} = \frac{L_x L_y}{4}\pi^2 \left[\left(\frac{i}{L_x}\right)^2 + \left(\frac{j}{L_y}\right)^2\right] \left(N_{D,ij}^{-1} + \widetilde{S}^{-1}\right)^{-1}, \tag{5.151}$$

where $N_{D,ij}$ is defined as

$$N_{D,ij} = \pi^2 D^{\text{iso}} \left[\left(\frac{i}{L_x}\right)^2 + \left(\frac{j}{L_y}\right)^2\right]. \tag{5.152}$$

5.6 Example. *A 0.9-m-long and 0.2-m-wide rectangular sandwich plate is made of a 0.02-m-thick core covered on both sides by graphite epoxy facesheets. The material properties are given in Table 3.6 (page 81). The layup of each facesheet is* $[\pm 45_2^{\text{f}}/0_{12}/\pm 45_2^{\text{f}}]$*, and the thickness of each facesheet is 0.002 m. The 0-degree*

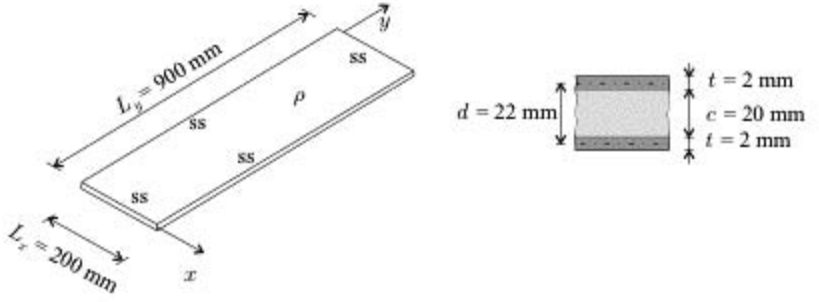

Figure 5.24: The sandwich plate in Example 5.6.

plies are parallel to the short edge of the plate. The plate is simply supported along all four edges (Fig. 5.24). A uniform mass is over the plate such that for the combined mass-plate system $\rho = 200\,kg/m^2$. Calculate the circular and the natural frequencies. The core is isotropic ($E_c = 2 \times 10^6\,kN/m^2$, $\nu_c = 0.3$).

Solution. The eigenvalues λ_{ij} are (Eq. 5.149)

$$\lambda_{ij} = \frac{\begin{vmatrix} F_{33} & F_{34} & F_{35} \\ F_{34} & F_{44} & F_{45} \\ F_{35} & F_{45} & F_{55} \end{vmatrix}}{\begin{vmatrix} F_{44} & F_{45} \\ F_{45} & F_{55} \end{vmatrix}} \frac{L_x L_y}{4}. \tag{5.153}$$

The parameters F_{ij} are given by Eq. (5.95). The elements of the stiffness matrices are (Eqs. 5.53 and 5.54)

$$D_{11} = 52.16\,\text{kN}\cdot\text{m} \qquad D_{22} = 11.71\,\text{kN}\cdot\text{m} \qquad D_{12} = 7.96\,\text{kN}\cdot\text{m}$$

$$D_{66} = 8.76\,\text{kN}\cdot\text{m} \qquad \widetilde{S}_{11} = 18\,615\frac{\text{kN}}{\text{m}} \qquad \widetilde{S}_{22} = 18\,615\frac{\text{kN}}{\text{m}},$$

and $L_x = 0.2\,\text{m}$, $L_y = 0.9\,\text{m}$. With these values, Eqs. (5.95) and (5.153) give the following values of $(\lambda_{cr})_{ij} \times 10^{-9}$:

$i \setminus j$	1	2	3
1	0.0884	0.1007	0.1226
2	0.6162	0.6436	0.6904
3	1.6183	1.6656	1.7458

(5.154)

The natural frequencies are (Eq. 5.150)

$$f_{ij} = \frac{1}{\pi}\sqrt{\frac{\lambda_{ij}}{\rho L_x L_y}}. \tag{5.155}$$

This yields the following values of f_{ij} (Hz):

$i \setminus j$	1	2	3
1	499	532	587
2	1 317	1 346	1 394
3	2 134	2 165	2 217

(5.156)

By treating the plate as long, in Example 5.5 (page 198) we obtained the following values for the first three natural frequencies: 488; 1 307; and 2 124 Hz (Eq. 5.137). These natural frequencies are within 3 percent of the values given above.

Beams

The response of composite beams to loading is more complex than that of isotropic beams, and the analyses of composite beams must take these complexities into account. This requires analyses that are, by necessity, more involved than for isotropic beams but which, nonetheless, result in expressions readily amenable to numerical computations.

In this chapter we treat rectangular solid cross sections as well as thin-walled beams that undergo small deformations and in which the material behaves in a linearly elastic manner. We neglect shear deformations and adopt the Bernoulli–Navier hypothesis, according to which the originally plane cross sections of a beam undergoing bending remain plane and perpendicular to the axis of the beam.

Axial, transverse, and torque loads may be applied to the beam (Fig. 6.1), resulting in the following *internal forces*: normal force $\widehat{N}$; bending moments $\widehat{M}_y$, $\widehat{M}_z$; torque $\widehat{T}$; and the transverse shear forces $\widehat{V}_z$, $\widehat{V}_y$ (Fig. 6.2).

6.1 Governing Equations

The response of a beam to the applied forces is described by the strain–displacement, force–strain, and equilibrium equations. These equations are given in this section for conditions in which there is no restrained warping. The effect of restrained warping is discussed in Sections 6.5.5, 6.5.6, and 6.6.4.

Here, as well as in the following analyses, we employ an x–y–z coordinate system with the origin at the centroid. The centroid is defined such that an axial load acting at the centroid does not change the curvature of the axis passing through the centroid. As a consequence of this definition, a bending moment acting on the beam does not introduce an axial strain along this axis. Unlike for isotropic beams, for composite beams the centroid does not necessarily coincide with the center of gravity of the cross section.

There are four independent displacements (Fig. 6.3): the axial displacement u, the transverse displacements v and w in the y and z directions, respectively, and the twist of the cross section ψ. The corresponding axial strain ϵ_x^o, curvatures $1/\rho_y$

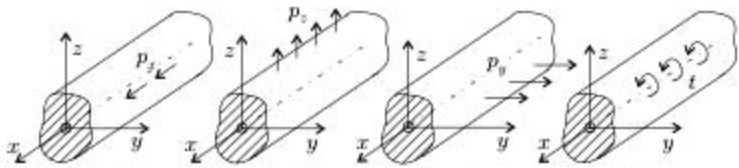

Figure 6.1: Axial, transverse, and torque loads acting on a section of a beam.

and $1/\rho_z$ in the x–z and x–y planes,[1] and the rate of twist ϑ are defined through the strain–displacement relationships

$$\epsilon_x^o = \frac{\partial u}{\partial x} \qquad \frac{1}{\rho_z} = -\frac{\partial^2 v}{\partial x^2} \qquad \frac{1}{\rho_y} = -\frac{\partial^2 w}{\partial x^2} \qquad \vartheta = \frac{\partial \psi}{\partial x}. \tag{6.1}$$

The generalized force–strain relationship is defined as

$$\begin{Bmatrix} \widehat{N} \\ \widehat{M}_y \\ \widehat{M}_z \\ \widehat{T} \end{Bmatrix} = \begin{bmatrix} P_{11} & P_{12} & P_{13} & P_{14} \\ P_{12} & P_{22} & P_{23} & P_{24} \\ P_{13} & P_{23} & P_{33} & P_{34} \\ P_{14} & P_{24} & P_{34} & P_{44} \end{bmatrix} \begin{Bmatrix} \epsilon_x^o \\ \frac{1}{\rho_y} \\ \frac{1}{\rho_z} \\ \vartheta \end{Bmatrix}, \tag{6.2}$$

where P_{ij} are the elements of the stiffness matrix.

The equilibrium equations for a straight beam subjected to the loads shown in Figure 6.1 are[2]

$$\begin{aligned} \frac{\partial \widehat{N}}{\partial x} &= -p_x & \frac{\partial \widehat{T}}{\partial x} &= -t \\ \frac{\partial \widehat{V}_y}{\partial x} &= -p_y & \frac{\partial \widehat{V}_z}{\partial x} &= -p_z \\ \frac{\partial \widehat{M}_y}{\partial x} &= \widehat{V}_z & \frac{\partial \widehat{M}_z}{\partial x} &= \widehat{V}_y. \end{aligned} \tag{6.3}$$

The preceding three sets of equations, (together with the appropriate boundary conditions) completely describe the displacements of, and the forces in, a composite beam.

The internal forces $\widehat{N}$, $\widehat{M}_y$, $\widehat{M}_z$, $\widehat{V}_y$, $\widehat{V}_z$, and $\widehat{T}$ are determined by the simultaneous solution of Eqs. (6.1)–(6.3) together with the appropriate boundary conditions given below. When a beam is statically determinate, the internal forces can be obtained from the equilibrium equations. When a composite beam is statically indeterminate, the internal forces can be obtained with the use of replacement stiffnesses in the relevant isotropic beam expressions provided that either the beam is orthotropic or the cross section is symmetrical and the load is applied in the plane of symmetry. The concepts of orthotropic beam and replacement stiffnesses are discussed in Section 6.1.2.

[1] T. H. G. Megson, *Aircraft Structures for Engineering Students*. 3rd edition. Halsted Press, John Wiley & Sons, New York, 1999, p. 284.

[2] B. K. Donaldson, *Analysis of Aircraft Structures. An Introduction*. McGraw-Hill, New York, 1993, pp. 277–278.

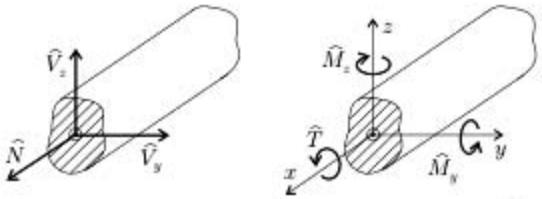

Figure 6.2: The normal force $\widehat{N}$; the bending moments $\widehat{M}_y$, $\widehat{M}_z$; the torque $\widehat{T}$; and the transverse shear forces $\widehat{V}_y$, $\widehat{V}_z$ inside a beam.

6.1.1 Boundary Conditions

At a built-in end, the in-plane displacements and the slopes are zero. At a simply supported end, the in-plane displacements and the moments are zero. At a free end, the moments and the transverse shear forces are zero.

When the end of the beam is restrained axially, the axial displacement is zero. When the end is not restrained axially, the axial force is zero.

When the end may rotate, the torque is zero. When the end is rotationally restrained, the twist is zero.

The preceding boundary conditions are summarized in Table 6.1.

6.1.2 Stiffness Matrix

The stiffness matrix depends on the geometry of the cross section and on the type of material used in the construction of the beam. The geometry (i.e., the shape) of the cross section changes when the beam is loaded. We neglect the effects of this change in shape on the stiffness and evaluate the stiffness matrix for the cross section of the unloaded beam.

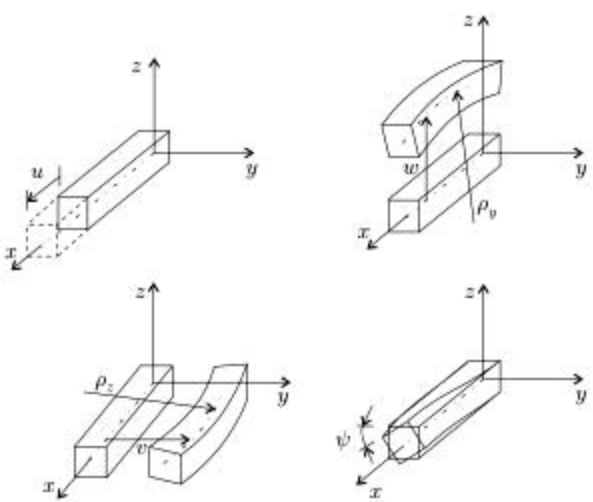

Figure 6.3: Displacements of a beam.

Table 6.1. Boundary conditions for beams.

	x–z plane		*x–y* plane	
Built-in	$w = 0$	$\frac{\partial w}{\partial x} = 0$	$v = 0$	$\frac{\partial v}{\partial x} = 0$
Simply supported	$w = 0$	$\widehat{M}_y = 0$	$v = 0$	$\widehat{M}_z = 0$
Free	$\widehat{V}_z = 0$	$\widehat{M}_y = 0$	$\widehat{V}_y = 0$	$\widehat{M}_z = 0$
Axially restrained	$u = 0$			
unrestrained	$\widehat{N} = 0$			
Rotationally restrained	$\psi = 0$			
unrestrained	$\widehat{T} = 0$			

For a beam made of an isotropic material ("isotropic beam") the force–strain relationships are[3]

$$\begin{Bmatrix} \widehat{N} \\ \widehat{M}_y \\ \widehat{M}_z \\ \widehat{T} \end{Bmatrix} = \begin{bmatrix} (EA) & 0 & 0 & 0 \\ 0 & (EI_{yy}) & (EI_{yz}) & 0 \\ 0 & (EI_{yz}) & (EI_{zz}) & 0 \\ 0 & 0 & 0 & (GI_t) \end{bmatrix} \begin{Bmatrix} \epsilon_x^0 \\ \frac{1}{\rho_y} \\ \frac{1}{\rho_z} \\ \vartheta \end{Bmatrix} \qquad \text{isotropic.} \tag{6.4}$$

The terms in parentheses are the tensile EA, bending EI_{yy}, EI_{zz}, $EI_{yz}\,(= EI_{zy})$, and torsional GI_t stiffnesses.

We observe that for an isotropic beam there is no coupling between tension (or compression), bending, and torsion. On the other hand, for a beam made of composite materials, in general, none of the elements of the stiffness matrix is zero, and there is coupling between tension, bending, and torsion. Accordingly, tension may cause bending and torsion, torsion may cause tension and bending, and bending may cause tension and torsion (see Eq. 6.2). The displacements resulting from these couplings are often unexpected and are most of the time undesirable. Fortunately for the designer, some of the couplings and the corresponding displacements are not present when either the beam's cross section is symmetrical or when the beam is orthotropic.

Symmetrical cross-section beams. First, we consider an isotropic beam whose cross section is symmetrical about the z-axis. An axial load $\widehat{N}$ and a bending moment $\widehat{M}_y$ (acting in the x–z symmetry plane) are applied to the beam. For this beam the force–strain relationships (Eq. 6.4) reduce to

$$\begin{Bmatrix} \widehat{N} \\ \widehat{M}_y \end{Bmatrix} = \begin{bmatrix} (EA) & 0 \\ 0 & (EI_{yy}) \end{bmatrix} \begin{Bmatrix} \epsilon_x^0 \\ \frac{1}{\rho_y} \end{Bmatrix} \qquad \begin{matrix} \text{isotropic} \\ \text{symmetrical cross section.} \end{matrix} \tag{6.5}$$

Next, we consider a composite beam whose cross section is symmetrical about the z-axis (Fig. 6.4). As a result of the symmetry, an axial load $\widehat{N}$ acting at the centroid does not introduce either bending or twisting of the beam, whereas a

[3] T. H. G. Megson, *Aircraft Structures for Engineering Students*. 3rd edition. Halsted Press, John Wiley & Sons, New York, 1999, pp. 56 and 285.

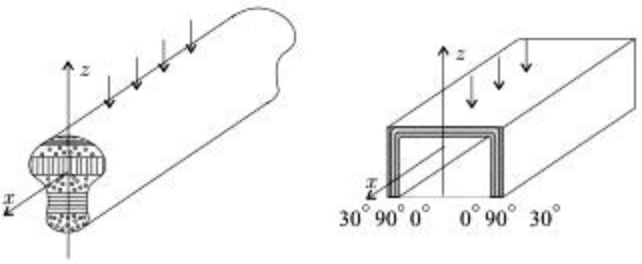

Figure 6.4: Illustrations of composite beams with symmetrical cross sections subjected to a transverse load in the x–z symmetry plane.

moment $\widehat{M}_y$ acting in the x–z symmetry plane introduces only bending in this plane. We designate the elements of the stiffness matrix by $\widehat{EA}$ and $\widehat{EI}_{yy}$ and write the stress–strain relationships as

$$\begin{Bmatrix} \widehat{N} \\ \widehat{M}_y \end{Bmatrix} = \begin{bmatrix} \widehat{EA} & 0 \\ 0 & \widehat{EI}_{yy} \end{bmatrix} \begin{Bmatrix} \epsilon_x^0 \\ \frac{1}{\rho_y} \end{Bmatrix} \qquad \begin{matrix} \text{composite} \\ \text{symmetrical cross section.} \end{matrix} \tag{6.6}$$

Orthotropic beams. A beam is orthotropic when its wall is made of an orthotropic laminate and one of the orthotropy axes is aligned with the axis of the beam. A laminate is orthotropic when every layer is made of either an isotropic material or a fiber-reinforced composite (page 75). In the latter case, a layer may consist of plies made either of woven fabric or of unidirectional fibers (Fig. 6.5). Woven fabric plies must be arranged such that one of the ply symmetry axes is aligned with the longitudinal x-axis of the beam. Unidirectional plies must be

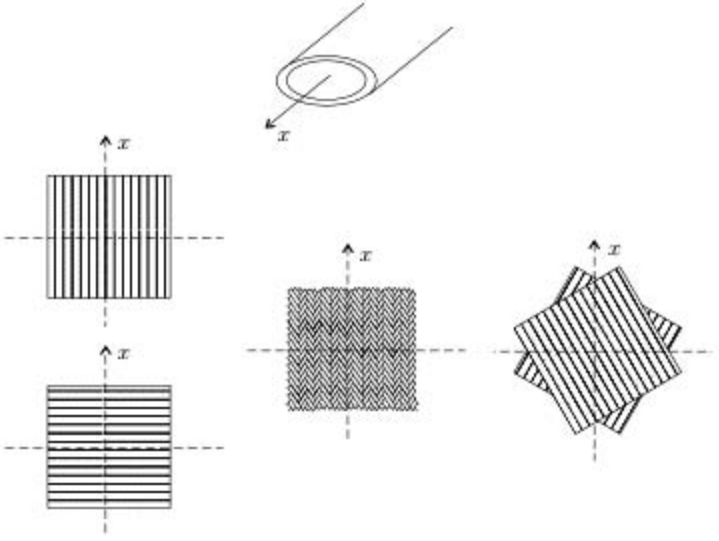

Figure 6.5: Layups that result in no coupling between tension, bending, and torsion. Unidirectional ply (left); woven fabric (middle); two-ply layer (right). For each configuration, one of the symmetry axes must be parallel to the beam's longitudinal x-axis.

mounted so that all the fibers are either parallel or perpendicular to the longitudinal x-axis or one of the symmetry axes of two adjacent unidirectional plies (treated as a single layer) must be parallel to the beam's longitudinal axis.

It is shown subsequently (Section 6.3.3) that for an orthotropic beam $P_{12} = P_{13} = P_{14} = P_{24} = P_{34} = 0$, and the force–strain relationship is

$$\begin{Bmatrix} \widehat{N} \\ \widehat{M}_y \\ \widehat{M}_z \\ \widehat{T} \end{Bmatrix} = \underbrace{\begin{bmatrix} P_{11} & 0 & 0 & 0 \\ 0 & P_{22} & P_{23} & 0 \\ 0 & P_{23} & P_{33} & 0 \\ 0 & 0 & 0 & P_{44} \end{bmatrix}}_{[P]} \begin{Bmatrix} \epsilon_x^0 \\ \frac{1}{\rho_y} \\ \frac{1}{\rho_z} \\ \vartheta \end{Bmatrix} \qquad \text{orthotropic.} \tag{6.7}$$

From the preceding equation we see that there is no tension–bending–torsion coupling in an orthotropic beam.

We designate the elements of the stiffness matrix by $\widehat{EA}$, $\widehat{EI}$, $\widehat{GI}_t$ and write

$$[P] = \begin{bmatrix} \widehat{EA} & 0 & 0 & 0 \\ 0 & \widehat{EI}_{yy} & \widehat{EI}_{yz} & 0 \\ 0 & \widehat{EI}_{yz} & \widehat{EI}_{zz} & 0 \\ 0 & 0 & 0 & \widehat{GI}_t \end{bmatrix} \qquad \text{orthotropic.} \tag{6.8}$$

Principal direction. For isotropic beams, there is a coordinate system y'–z' (Fig. 6.6) in which the moment of inertia $I_{y'z'}$ is zero ($I_{y'z'} = 0$). The angle between the y'-axis of this coordinate system and the y-axis is[4]

$$\tan 2\varphi = -\frac{2I_{yz}}{I_{yy} - I_{zz}} = -\frac{2EI_{yz}}{EI_{yy} - EI_{zz}}. \tag{6.9}$$

The relationships between the moments of inertia in the y–z and y'–z' coordinate systems are

$$I_{y'y'} = \frac{I_{yy} + I_{zz}}{2} + \sqrt{\left(\frac{I_{yy} - I_{zz}}{2}\right)^2 + I_{yz}^2} \tag{6.10}$$

$$I_{z'z'} = \frac{I_{yy} + I_{zz}}{2} - \sqrt{\left(\frac{I_{yy} - I_{zz}}{2}\right)^2 + I_{yz}^2} \tag{6.11}$$

$$I_{y'z'} = 0. \tag{6.12}$$

The directions y' and z' are called principal directions.

As in Eq. (6.9), for an orthotropic beam we write the angle between y' and y as

$$\tan 2\varphi = -\frac{2\widehat{EI}_{yz}}{\widehat{EI}_{yy} - \widehat{EI}_{zz}}. \tag{6.13}$$

[4] E. P. Popov, *Engineering Mechanics of Solids*. Prentice-Hall, Englewood Cliffs, New Jersey, 1990, p. 342.

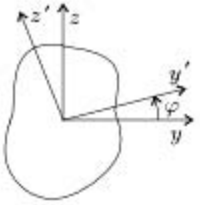

Figure 6.6: The y', z' coordinate system in which $I_{y'z'}$ is zero.

By referring to Eqs. (6.10)–(6.12), we express the bending stiffnesses in the y'–z' coordinate system in the forms

$$\widehat{EI}_{y'y'} = \frac{\widehat{EI}_{yy} + \widehat{EI}_{zz}}{2} + \sqrt{\left(\frac{\widehat{EI}_{yy} - \widehat{EI}_{zz}}{2}\right)^2 + \widehat{EI}_{yz}^2} \tag{6.14}$$

$$\widehat{EI}_{z'z'} = \frac{\widehat{EI}_{yy} + \widehat{EI}_{zz}}{2} - \sqrt{\left(\frac{\widehat{EI}_{yy} - \widehat{EI}_{zz}}{2}\right)^2 + \widehat{EI}_{yz}^2} \tag{6.15}$$

$$\widehat{EI}_{y'z'} = 0. \tag{6.16}$$

6.1.3 Compliance Matrix

With respect to the x–y–z coordinate system attached to the centroid, the strain–force relationships are defined as

$$\begin{Bmatrix} \epsilon_x^o \\ \frac{1}{\rho_y} \\ \frac{1}{\rho_z} \\ \vartheta \end{Bmatrix} = \begin{bmatrix} W_{11} & 0 & 0 & W_{14} \\ 0 & W_{22} & W_{23} & W_{24} \\ 0 & W_{23} & W_{33} & W_{34} \\ W_{14} & W_{24} & W_{34} & W_{44} \end{bmatrix} \begin{Bmatrix} \widehat{N} \\ \widehat{M}_y \\ \widehat{M}_z \\ \widehat{T} \end{Bmatrix}. \tag{6.17}$$

The W_{21} and W_{31} terms are zero because an axial force applied at the centroid does not cause bending, whereas W_{12} and W_{13} are zero because the compliance matrix is symmetrical. The compliance matrix $[W]$ is the inverse of the stiffness matrix

$$\begin{bmatrix} W_{11} & 0 & 0 & W_{14} \\ 0 & W_{22} & W_{23} & W_{24} \\ 0 & W_{23} & W_{33} & W_{34} \\ W_{14} & W_{24} & W_{34} & W_{44} \end{bmatrix} = \begin{bmatrix} P_{11} & P_{12} & P_{13} & P_{14} \\ P_{12} & P_{22} & P_{23} & P_{24} \\ P_{13} & P_{23} & P_{33} & P_{34} \\ P_{14} & P_{24} & P_{34} & P_{44} \end{bmatrix}^{-1}. \tag{6.18}$$

We obtain the compliance matrix of an orthotropic beam by substituting the elements of the matrix $[P]$ given in Eq. (6.8) into this expression. The

result is

$$[W] = \begin{bmatrix} \frac{1}{\widehat{EA}} & 0 & 0 & 0 \\ 0 & \frac{\widehat{EI}_{zz}}{\widehat{EI}_{yy}\widehat{EI}_{zz} - (\widehat{EI}_{yz})^2} & \frac{-\widehat{EI}_{yz}}{\widehat{EI}_{yy}\widehat{EI}_{zz} - (\widehat{EI}_{yz})^2} & 0 \\ 0 & \frac{-\widehat{EI}_{yz}}{\widehat{EI}_{yy}\widehat{EI}_{zz} - (\widehat{EI}_{yz})^2} & \frac{\widehat{EI}_{yy}}{\widehat{EI}_{yy}\widehat{EI}_{zz} - (\widehat{EI}_{yz})^2} & 0 \\ 0 & 0 & 0 & \frac{1}{\widehat{GI}_t} \end{bmatrix} \quad \text{orthotropic.} \tag{6.19}$$

6.1.4 Replacement Stiffnesses

The parameters $\widehat{EA}$, $\widehat{EI}$, $\widehat{GI}_t$ are referred to as replacement stiffnesses. By comparing Eq. (6.5) with Eq. (6.6) and Eqs. (6.4) with Eqs. (6.7) and (6.8), we note the similarity in the force–strain relationships of isotropic and composite beams. Therefore, the strains (and consequently the displacements) of an orthotropic beam and of a composite beam with symmetrical cross section can be obtained by replacing EA, EI, GI_t by $\widehat{EA}$, $\widehat{EI}$, $\widehat{GI}_t$ in the corresponding isotropic beam solution. For an orthotropic beam, the necessary substitutions are

Isotropic beam		Orthotropic beam
EA	$\Longrightarrow$	$\widehat{EA}$
$EI_{yy}, EI_{zz}, EI_{yz}$	$\Longrightarrow$	$\widehat{EI}_{yy}, \widehat{EI}_{zz}, \widehat{EI}_{yz}$
GI_t	$\Longrightarrow$	$\widehat{GI}_t$

For a composite beam with symmetrical cross section and loaded in the symmetry plane the following substitutions apply:

Isotropic beam symmetrical cross section		Composite beam symmetrical cross section
EA, EI_{yy}	$\Longrightarrow$	$\widehat{EA}, \widehat{EI}_{yy}$

As the preceding discussion indicates, the displacements of orthotropic beams and of composite beams with symmetrical cross section are similar to the displacements of isotropic beams. However, the stresses are markedly different in isotropic and in composite beams. In an isotropic beam subjected to an axial load and pure bending, there is only axial stress. In a composite beam subjected to an axial load and pure bending, in addition to the axial stress, there are also transverse normal and shear stresses. Furthermore, in an isotropic beam subjected to pure torque, there is only shear stress, whereas in a composite beam there are also axial and transverse normal stresses.

In this chapter the stresses are calculated by the laminate plate theory, which does not take into account the interlaminar stresses near free edges (page 166).

6.2 Rectangular, Solid Beams Subjected to Axial Load and Bending

We consider rectangular laminated beams having solid cross sections with an axial force $\widehat{N}$ acting at the centroid and a pure bending moment $\widehat{M}_y$ acting in the

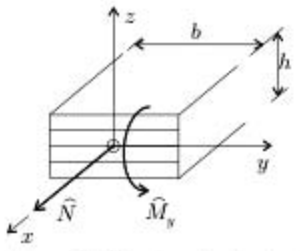

Figure 6.7: Rectangular laminated beam.

x–z plane (Fig. 6.7). In this section, we develop expressions for calculating the displacements and the stresses.

We treat the beam as a narrow plate and build the analysis on the results of laminate plate theory presented in Chapter 3. By convention, for plates along an edge parallel to the y-axis, the in-plane force per unit length is N_x, and the moment per unit length is M_x (Fig. 6.8). For beams, the total force $\widehat{N}$ along an edge parallel to y and the total moment in the x–z plane $\widehat{M}_y$ are specified. The total axial force in the beam $\widehat{N}$ corresponds to bN_x in the plate, and the total moment in the beam $\widehat{M}_y$ corresponds to bM_x in the plate (where b is the width). Thus, we can apply the laminate plate theory expressions to beams by making the following substitutions:

$$N_x = \frac{\widehat{N}}{b} \qquad M_x = \frac{\widehat{M}_y}{b}. \tag{6.20}$$

6.2.1 Displacements – Symmetrical Layup

The layup of the beam is symmetrical. As noted in the preceding section, we analyze this beam by the laminate plate theory, according to which the midplane strain and curvature of the plate are (Eqs. 3.31 and 3.32)

$$\epsilon_x^o = a_{11} N_x \qquad \kappa_x = d_{11} M_x \qquad \text{plate.} \tag{6.21}$$

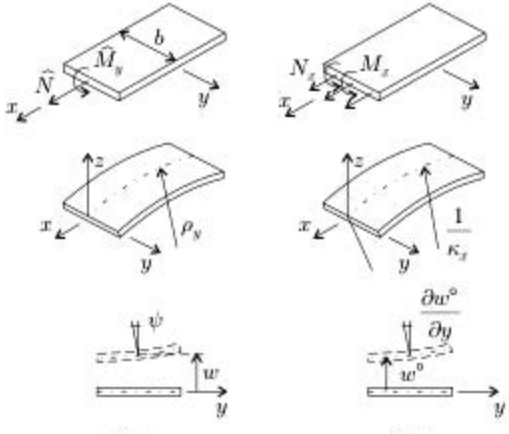

Beam Plate

Figure 6.8: Internal forces and curvatures in a beam and in the corresponding plate.

where a_{11} and d_{11} are the elements of the compliance matrices (Eqs. 3.29 and 3.30). We observe that the curvature of the plate in the x–z plane κ_x corresponds to the curvature of the beam $1/\rho_y$ (Fig. 6.8). If we replace κ_x with $1/\rho_y$, for a beam Eqs. (6.20) and (6.21) yield

$$\epsilon_x^o = \underbrace{\left(\frac{a_{11}}{b}\right)}_{W_{11}} \widehat{N} \qquad \frac{1}{\rho_y} = \underbrace{\left(\frac{d_{11}}{b}\right)}_{W_{22}} \widehat{M}_y \qquad \begin{matrix}\text{composite}\\ \text{beam.}\end{matrix} \tag{6.22}$$

By comparing this equation with Eq. (6.17), we see that the terms in parentheses are the W_{11} and W_{22} elements of the compliance matrix.

For a beam made of an isotropic material, the strain and curvature are (Eq. 6.5)

$$\epsilon_x^o = \frac{1}{EA}\widehat{N} \qquad \frac{1}{\rho_y} = \frac{1}{EI}\widehat{M}_y \qquad \begin{matrix}\text{isotropic}\\ \text{beam.}\end{matrix} \tag{6.23}$$

It follows from Eqs. (6.22) and (6.23) that the axial strain and the curvature of the axis (and consequently the displacements u and w) of a composite beam (symmetrical layup) can be calculated by replacing EA and EI by $\frac{b}{a_{11}}$ and $\frac{b}{d_{11}}$ in the relevant expressions for the corresponding isotropic beam.

An isotropic beam subjected to an axial force $\widehat{N}$ and a bending moment $\widehat{M}_y$ only bends in the x–z plane. On the other hand, under these loads the cross sections of a composite beam may also twist. To determine the amount of this twist we refer to the twisting of a plate. The out-of-plane curvature of a plate (symmetrical layup) is (Eq. 3.32)

$$\kappa_{xy} = d_{16} M_x \qquad \text{plate,} \tag{6.24}$$

where κ_{xy} is defined in Eq. (3.8) and is repeated below

$$\kappa_{xy} = -\frac{2\partial^2 w^o}{\partial x \partial y} = -2\frac{\partial \frac{\partial w^o}{\partial y}}{\partial x}, \tag{6.25}$$

where w^o is the deflection of the midplane. The expression $\partial w^o/\partial y$ in the plate corresponds to ψ in the beam (Fig. 6.8). Thus, we have

$$\kappa_{xy} = -2\frac{\partial \psi}{\partial x}. \tag{6.26}$$

Equations (6.1) and (6.26) give the rate of twist of the beam as follows:

$$\vartheta = -\frac{1}{2}\kappa_{xy}. \tag{6.27}$$

By combining Eqs. (6.20), (6.24), and (6.27), we obtain the rate of twist of a beam as follows:

$$\vartheta = \underbrace{\left(-\frac{1}{2}\frac{d_{16}}{b}\right)}_{W_{24}} \widehat{M}_y \qquad \begin{matrix}\text{composite}\\ \text{beam.}\end{matrix} \tag{6.28}$$

When only $\widehat{N}$ and $\widehat{M}_y$ act, the relevant elements of the compliance matrix are W_{11}, W_{22}, W_{23}, W_{14}, W_{24} (Eq. 6.17). The elements W_{11}, W_{22}, and W_{24} are given

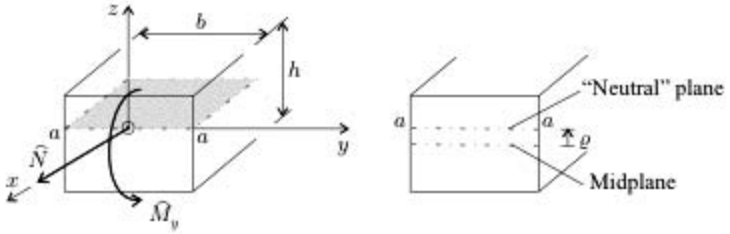

Figure 6.9: Unsymmetrical solid rectangular beam.

by Eqs. (6.22) and (6.28). Elements W_{14} and W_{23} are zero because the layup is symmetrical.

When the beam is orthotropic, d_{16} is zero (Eq. 3.37), and the rate of twist is zero ($\vartheta = 0$) when the beam is subjected to an $\hat{M}_y$ bending moment.

6.2.2 Displacements – Unsymmetrical Layup

The layup of the laminated beam is unsymmetrical. The centroid is located at the a–a plane at a distance ϱ from an arbitrary reference plane. This reference plane may be chosen as the midplane (Fig. 6.9). The location of this a–a plane is such that an axial load does not cause a change in the curvature $1/\rho_y$, and a bending moment does not cause axial strain ϵ_x^o. Thus, the a–a plane is analogous to the neutral plane (which, for beams made of isotropic materials, passes through the center of gravity).

We now consider a laminated plate (unsymmetrical layup) on which an axial force N_x and a moment M_x (per unit length) act in the a–a plane. For this plate, the following relationships hold in the a–a plane (Eq. 3.22):

$$\epsilon_x^o = \alpha_{11}^\varrho N_x + \beta_{11}^\varrho M_x \qquad \kappa_x = \beta_{11}^\varrho N_x + \delta_{11}^\varrho M_x \qquad \text{plate,} \tag{6.29}$$

where α_{11}^ϱ, β_{11}^ϱ, and δ_{11}^ϱ are evaluated at the a–a "neutral" plane. According to the aforementioned definition of the "neutral" plane, ϵ_x^o depends only on N_x, and κ_x depends only on M_x. Therefore, β_{11}^ϱ must be equal to zero. Thus, we write (see Eq. 3.48)

$$\beta_{11}^\varrho = \beta_{11} + \varrho\delta_{11} = 0, \tag{6.30}$$

where β_{11} and δ_{11} are evaluated at the arbitrarily chosen reference plane that here we have taken to be the midplane. The consequence of $\beta_{11}^\varrho = 0$ is twofold. The first consequence is that the distance ϱ is

$$\varrho = -\frac{\beta_{11}}{\delta_{11}}. \tag{6.31}$$

The second consequence is that Eq. (6.29) reduces to

$$\epsilon_x^o = \alpha_{11}^\varrho N_x \qquad \kappa_x = \delta_{11}^\varrho M_x \qquad \text{plate.} \tag{6.32}$$

We note again that the curvature of the plate κ_x corresponds to the curvature of the beam $1/\rho_y$. Then, for a beam, Eqs. (6.20) and (6.32) yield

$$\epsilon_x^o = \underbrace{\left(\frac{\alpha_{11}^o}{b}\right)}_{W_{11}} \widehat{N} \qquad \frac{1}{\rho_y} = \underbrace{\left(\frac{\delta_{11}^o}{b}\right)}_{W_{22}} \widehat{M}_y \qquad \begin{matrix}\text{composite}\\ \text{beam.}\end{matrix} \tag{6.33}$$

By comparing this equation with Eq. (6.17), we see that the terms in parentheses are the W_{11} and W_{22} elements of the compliance matrix.

It follows from Eqs. (6.33) and (6.23) that the axial strain and curvature of the axis (and consequently the displacements u and w) of a composite beam (unsymmetrical layup) can be calculated by replacing EA and EI by $\frac{b}{\alpha_{11}^o}$ and $\frac{b}{\delta_{11}^o}$ in the relevant expressions for the corresponding isotropic beam.

When an isotropic beam is subjected to an axial force $\widehat{N}$ and to a bending moment $\widehat{M}_y$, it will only bend in the x–z plane. The cross section of a composite beam subjected to $\widehat{N}$ and $\widehat{M}_y$ may also twist. To determine the rate of twist of a composite beam, we again refer to a laminated plate. The out-of-plane curvature of a laminated plate (unsymmetrical layup) is (see Eq. 3.22)

$$\kappa_{xy} = \beta_{16}^o N_x + \delta_{16}^o M_x \qquad \text{plate,} \tag{6.34}$$

where β_{16}^o, and δ_{16}^o are evaluated at the a–a "neutral" plane. From Eq. (3.48) we have

$$\beta_{16}^o = \beta_{16} + \varrho\delta_{16} \qquad \delta_{16}^o = \delta_{16}. \tag{6.35}$$

From Eqs. (6.20), (6.27), and (6.34) we obtain the rate of twist of the beam:

$$\vartheta = \underbrace{\left(-\frac{1}{2}\frac{\beta_{16}^o}{b}\right)}_{W_{14}} \widehat{N} + \underbrace{\left(-\frac{1}{2}\frac{\delta_{16}^o}{b}\right)}_{W_{24}} \widehat{M}_y \qquad \begin{matrix}\text{composite}\\ \text{beam.}\end{matrix} \tag{6.36}$$

By comparing this equation with Eq. (6.17), we see that the terms in the parentheses are the W_{14} and W_{24} elements of the compliance matrix.

When only $\widehat{N}$ and $\widehat{M}_y$ act, the relevant elements of the compliance matrix are W_{11}, W_{22}, W_{23}, W_{14}, W_{24} (Eq. 6.17). Elements W_{11}, W_{22}, W_{14}, and W_{24} are given by Eqs. (6.33) and (6.36), and W_{23} is zero.

When the beam is orthotropic and one of the orthotropy axes is aligned with the beam's axis, δ_{16} and β_{16} are zero (Eq. 3.37). Therefore, (see Eqs. 6.35 and 6.36), the rate of twist is zero ($\vartheta = 0$) when an orthotropic beam is subjected to an axial force $\widehat{N}$ and a bending moment $\widehat{M}_y$.

6.2.3 Stresses and Strains

The stresses and strains are given in this section for a rectangular thin beam whose thickness h is small compared with its width b (Fig. 6.9). We consider only regions away from the edges and employ the laminate plate theory expressions.

Symmetrical layup. At the neutral plane (which for a symmetrical laminate coincides with the midplane), the strains and curvatures are (see Eqs. 3.31, 3.32, and 6.20)

$$\begin{Bmatrix} \epsilon_x^o \\ \epsilon_y^o \\ \gamma_{xy}^o \end{Bmatrix} = \begin{bmatrix} a_{11} \\ a_{12} \\ a_{16} \end{bmatrix} \left\{ \frac{\hat{N}}{b} \right\} \qquad \begin{Bmatrix} \kappa_x \\ \kappa_y \\ \kappa_{xy} \end{Bmatrix} = \begin{bmatrix} d_{11} \\ d_{12} \\ d_{16} \end{bmatrix} \left\{ \frac{\hat{M}_y}{b} \right\}. \tag{6.37}$$

In a ply at a distance z from the midplane, the strains are (see Eq. 3.7)

$$\begin{Bmatrix} \epsilon_x \\ \epsilon_y \\ \gamma_{xy} \end{Bmatrix} = \begin{Bmatrix} \epsilon_x^o \\ \epsilon_y^o \\ \gamma_{xy}^o \end{Bmatrix} + z \begin{Bmatrix} \kappa_x \\ \kappa_y \\ \kappa_{xy} \end{Bmatrix}. \tag{6.38}$$

The ply stresses are given by (Eq. 3.11)

$$\begin{Bmatrix} \sigma_x \\ \sigma_y \\ \tau_{xy} \end{Bmatrix} = \begin{bmatrix} \overline{Q}_{11} & \overline{Q}_{12} & \overline{Q}_{16} \\ \overline{Q}_{21} & \overline{Q}_{22} & \overline{Q}_{26} \\ \overline{Q}_{61} & \overline{Q}_{62} & \overline{Q}_{66} \end{bmatrix} \begin{Bmatrix} \epsilon_x \\ \epsilon_y \\ \gamma_{xy} \end{Bmatrix}. \tag{6.39}$$

Unsymmetrical layup. The strains and curvatures of the axis passing through the centroid (which is in the "neutral" plane) are (see Eqs. 3.22 and 6.20)

$$\begin{Bmatrix} \epsilon_x^o \\ \epsilon_y^o \\ \gamma_{xy}^o \\ \kappa_x \\ \kappa_y \\ \kappa_{xy} \end{Bmatrix} = \begin{bmatrix} \alpha_{11}^o & 0 \\ \alpha_{12}^o & \beta_{21}^o \\ \alpha_{16}^o & \beta_{61}^o \\ 0 & \delta_{11}^o \\ \beta_{12}^o & \delta_{12}^o \\ \beta_{16}^o & \delta_{16}^o \end{bmatrix} \begin{Bmatrix} \frac{\hat{N}}{b} \\ \frac{\hat{M}_y}{b} \end{Bmatrix}, \tag{6.40}$$

where α^o and β^o are evaluated at the "neutral" plane (Fig. 6.9). The location of the "neutral" plane is given by Eq. (6.31).

In a ply at a distance z from the "neutral" plane, the strains and stresses are given by Eqs. (6.38) and (6.39).

6.1 Example. *An $L = 0.2$-m-long and $b = 0.02$-m-wide beam, with the cross section shown in Fig. 6.10, is made of graphite epoxy. The material properties are given in Table 3.6 (page 81). The layup is $[\pm 45_2^t/0_{12}/\pm 45_2^t]$. The beam, simply supported at each end, is loaded uniformly ($p = 1\,000$ N/m). Calculate the maximum bending moment, the maximum deflection, and the ply stresses and strains.*

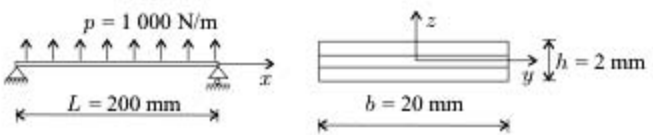

Figure 6.10: The beam in Example 6.1.

Solution. The maximum bending moment at the middle of the beam is (Table 7.3, page 332)

$$\widehat{M}_y = \frac{pL^2}{8} = 5\ \mathrm{N\cdot m}. \tag{6.41}$$

The maximum deflection of the corresponding isotropic beam is (Table 7.3)

$$\widetilde{w} = \frac{5}{384}\frac{pL^4}{EI}. \tag{6.42}$$

The maximum deflection of the composite beam is obtained by replacing EI by $\frac{b}{d_{11}}$ (see page 212)

$$\widetilde{w} = \frac{5}{384}\frac{pL^4}{\frac{b}{d_{11}}}. \tag{6.43}$$

With the value of $d_{11} = 33.10 \times 10^{-3}\ \frac{1}{\mathrm{N\cdot m}}$ (Table 3.8, page 85), the maximum deflection is

$$\widetilde{w} = 0.0345\ \mathrm{m} = 34.5\ \mathrm{mm}. \tag{6.44}$$

The axial force is zero ($\widehat{N} = 0$). Thus, with the compliance matrices given in Table 3.8, the midplane strains and curvatures are (see Eqs. 6.37 and 6.41)

$$\begin{Bmatrix} \epsilon_x^o \\ \epsilon_y^o \\ \gamma_{xy}^o \end{Bmatrix} = \begin{Bmatrix} a_{11} \\ a_{12} \\ a_{16} \end{Bmatrix} \left\{\frac{\widehat{N}}{b}\right\} = \begin{Bmatrix} 0 \\ 0 \\ 0 \end{Bmatrix} \tag{6.45}$$

$$\begin{Bmatrix} \kappa_x \\ \kappa_y \\ \kappa_{xy} \end{Bmatrix} = \begin{Bmatrix} d_{11} \\ d_{12} \\ d_{16} \end{Bmatrix} \left\{\frac{\widehat{M}_y}{b}\right\} = \begin{Bmatrix} 33.10 \\ -25.59 \\ 0 \end{Bmatrix} 10^{-3} \left\{\frac{5}{0.02}\right\} = \begin{Bmatrix} 8.28 \\ -6.40 \\ 0 \end{Bmatrix} \frac{1}{\mathrm{m}}, \tag{6.46}$$

where κ_x and κ_y are illustrated in Figure 6.11. In a ply, at a distance z from the midplane, the strains are given by Eq. (6.38) as follows:

$$\begin{Bmatrix} \epsilon_x \\ \epsilon_y \\ \gamma_{xy} \end{Bmatrix} = z \begin{Bmatrix} \kappa_x \\ \kappa_y \\ \kappa_{xy} \end{Bmatrix} = z \begin{Bmatrix} 8.27 \\ -6.40 \\ 0 \end{Bmatrix}. \tag{6.47}$$

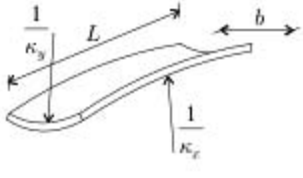

Figure 6.11: Illustration of the curvatures of the beam in Example 6.1.

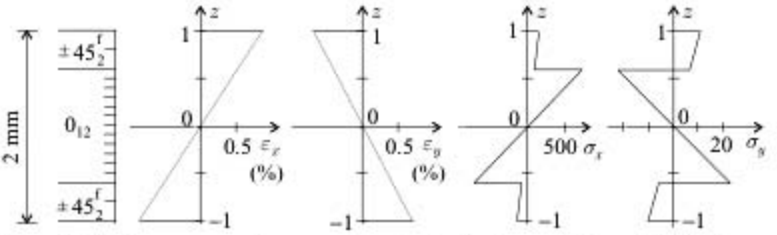

Figure 6.12: The nonzero stresses and strains in the beam in Example 6.1. The unit of σ is 10^6 N/m^2.

The stresses in the kth ply are (Eq. 6.39)

$$\begin{Bmatrix} \sigma_x \\ \sigma_y \\ \tau_{xy} \end{Bmatrix}_k = \begin{bmatrix} \overline{Q}_{11} & \overline{Q}_{12} & \overline{Q}_{16} \\ \overline{Q}_{21} & \overline{Q}_{22} & \overline{Q}_{26} \\ \overline{Q}_{61} & \overline{Q}_{62} & \overline{Q}_{66} \end{bmatrix}_k \begin{Bmatrix} \epsilon_x \\ \epsilon_y \\ \gamma_{xy} \end{Bmatrix}_k . \tag{6.48}$$

The elements of the $[\overline{Q}]$ matrix of the 0-degree ply are given by Eq. (3.65) and of the woven fabric by Eq. (3.66). The stresses are calculated with these values of the $[\overline{Q}]$ matrices and with the strains given in Eq. (6.47). The results are shown in Figure 6.12. We note again that these stresses are valid only in regions away from the edges.

6.3 Thin-Walled, Open-Section Orthotropic or Symmetrical Cross-Section Beams Subjected to Axial Load and Bending

In this section we present the deflections of, and stresses and strains in, thin-walled, open-section beams. The method is first illustrated via orthotropic T-beams with symmetrical cross section and via orthotropic L-beams. The analysis is then extended to orthotropic beams with arbitrary cross section and to nonorthotropic beams with symmetrical cross section.

6.3.1 Displacements of T-Beams

We consider a T-beam whose cross section is symmetrical with respect to the z-axis (Fig. 6.13). The layup of both the flange and the web is orthotropic and

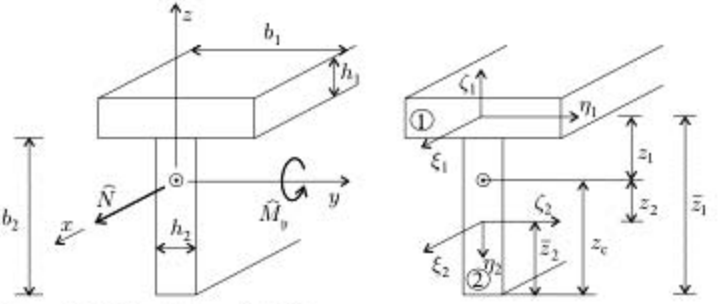

Figure 6.13: Illustration of the T-beam.

symmetrical. An axial force $\widehat{N}$ and a bending moment $\widehat{M}_y$ act at the centroid of the beam. The origin of the x–y–z coordinate system is attached to this centroid. In addition we use the ξ_1–η_1–ζ_1 and ξ_2–η_2–ζ_2 coordinate systems attached to the midpoints of the flange and the web, respectively. The flange and the web are designated by the subscripts 1 and 2.

In the following we derive the replacement stiffnesses. The displacements of a T-beam are obtained by substituting these replacement stiffnesses into the expressions for the displacements of the corresponding isotropic beam. Because the cross section is symmetrical with respect to the z-axis and the loads act in the x–z plane, the beam bends only about the y-axis. Consequently, only $\widehat{EA}$ and $\widehat{EI}_{yy}$ are of interest.

The calculation proceeds in four steps. In Step 1 we deform the axis of the beam and calculate the strains in, and the curvatures of, each wall segment; in Step 2 we calculate the forces and moments in each wall segment; in Step 3 we calculate the resultant forces and moments acting on the beam; in Step 4 we determine the replacement stiffnesses.

We treat both the flange and the web as thin plates and analyze them by the laminate plate theory.

Tensile stiffness $\widehat{EA}$ and centroid.

Step 1. The axis of the beam (passing through the centroid) is elongated, and the strain of the axis is denoted by ϵ_x^o. The beam does not bend, and the axial strains are the same across the cross section,

$$\epsilon_{\xi 1}^o = \epsilon_{\xi 2}^o = \epsilon_x^o, \tag{6.49}$$

where $\epsilon_{\xi 1}^o$ and $\epsilon_{\xi 2}^o$ are the axial strains in the midplanes of the flange and the web, respectively.

Step 2. The axial strains result in distributed axial forces (per unit length) $N_{\xi 1}$, $N_{\xi 2}$ in the midplanes of the flange and the web (Fig. 6.14, left). These forces are (see Eq. 3.31)

$$N_{\xi 1} = \frac{1}{(a_{11})_1}\epsilon_{\xi 1}^o \qquad N_{\xi 2} = \frac{1}{(a_{11})_2}\epsilon_{\xi 2}^o, \tag{6.50}$$

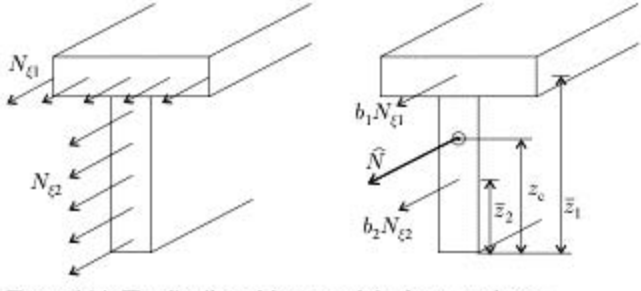

Figure 6.14: The distributed forces and the force resultants.

where $(a_{11})_1$ and $(a_{11})_2$ are evaluated in the ξ–η–ζ coordinate system at the midplanes of the flange and the web.

Step 3. The total forces acting in the flange and in the web are $b_1 N_{\xi 1}$ and $b_2 N_{\xi 2}$, respectively, and the total force acting on the beam is (Fig. 6.14, right)

$$\widehat{N} = b_1 N_{\xi 1} + b_2 N_{\xi 2}. \tag{6.51}$$

Step 4. Equations (6.49)–(6.51) give

$$\widehat{N} = \underbrace{\left(\frac{b_1}{(a_{11})_1} + \frac{b_2}{(a_{11})_2} \right)}_{\widehat{EA}} \epsilon_x^0. \tag{6.52}$$

The term indicated by the bracket is the replacement tensile stiffness $\widehat{EA}$.

The coordinate of the centroid z_c is calculated by a moment balance about the bottom edge of the web (Fig. 6.14, right) as follows:

$$z_c \widehat{N} = \bar{z}_1 b_1 N_{\xi 1} + \bar{z}_2 b_2 N_{\xi 2}. \tag{6.53}$$

The distances $\bar{z}_1$ and $\bar{z}_2$ are shown in Figure 6.14. By combining this equation with Eqs. (6.49)–(6.52), we obtain the position of the centroid:

$$z_c = \frac{\bar{z}_1 \frac{b_1}{(a_{11})_1} + \bar{z}_2 \frac{b_2}{(a_{11})_2}}{\frac{b_1}{(a_{11})_1} + \frac{b_2}{(a_{11})_2}}. \tag{6.54}$$

The coordinates of the centers of the flange and the web with respect to the centroid are (Fig. 6.13)

$$z_1 = \bar{z}_1 - z_c \qquad z_2 = \bar{z}_2 - z_c. \tag{6.55}$$

Depending on where the centroid is located, z_2 is either positive or negative. In Figure 6.13, z_2 is negative.

Bending stiffness $\widehat{EI}_{yy}$. The beam is bent about the y-axis passing through the centroid (Fig. 6.15). The radius of curvature of the beam is denoted by ρ_y.

Step 1. The strain varies linearly with z as follows:

$$\epsilon_x = \frac{1}{\rho_y} z. \tag{6.56}$$

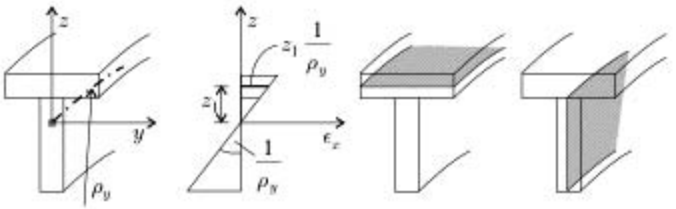

Figure 6.15: The radius of curvature ρ_y, the strain distribution, and the deformed shapes of the midplanes of the flange and the web.

At the midplane of the flange $z = z_1$ and the strain is

$$\epsilon^o_{\xi 1} = \frac{1}{\rho_y} z_1. \tag{6.57}$$

The curvature of the midplane of the flange about the y-axis (by definition) is

$$\kappa_{\xi 1} = \frac{1}{\rho_y}. \tag{6.58}$$

In the midplane of the web, the strain $\epsilon^o_{\xi 2}$ is

$$\epsilon^o_{\xi 2} = \frac{1}{\rho_y} z. \tag{6.59}$$

The midplane of the web remains flat, and its curvature is zero (Fig. 6.15) as denoted by

$$\kappa_{\xi 2} = 0. \tag{6.60}$$

Step 2. The axial force $N_{\xi 1}$ and the bending moment $M_{\xi 1}$ (per unit length) acting on the flange are (Eqs. 3.31 and 3.32)

$$N_{\xi 1} = \frac{1}{(a_{11})_1} \epsilon^o_{\xi 1} \qquad M_{\xi 1} = \frac{1}{(d_{11})_1} \kappa_{\xi 1}. \tag{6.61}$$

The preceding force and moment are illustrated in Figure 6.16 (left). The terms $(a_{11})_1$ and $(d_{11})_1$ are evaluated in the ξ–η–ζ coordinate system at the midplane of the flange.

The layup of the web is symmetrical, and $\kappa_{\xi 2} = 0$. Consequently, $M_{\xi 2}$ is zero. Thus, the only force acting in the web is $N_{\xi 2}$ (Fig. 6.16, right), and this force is

$$N_{\xi 2} = \frac{1}{(a_{11})_2} \epsilon^o_{\xi 2}, \tag{6.62}$$

where $(a_{11})_2$ is evaluated in the ξ–η–ζ coordinate system at the midplane of the web.

Step 3. The resultant bending moment about the y-axis is (Fig. 6.16)

$$\widehat{M}_y = b_1 N_{\xi 1} z_1 + b_1 M_{\xi 1} + \int_{(b_2)} N_{\xi 2} z dz, \tag{6.63}$$

where b_1, b_2, and z are shown in Figure 6.13.

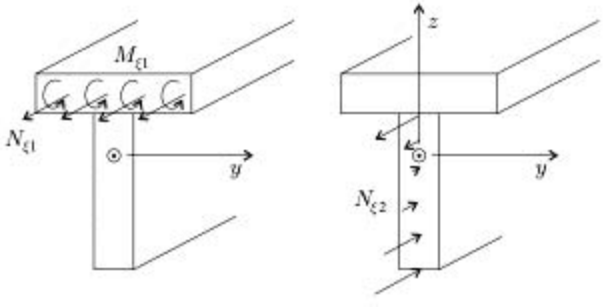

Figure 6.16: The distributed forces and moments (per unit length) in the flange and in the web of a T-beam bent about the y-axis.

Step 4. Equations (6.57)–(6.63) yield

$$\widehat{M}_y = \frac{1}{\rho_y}\underbrace{\left[z_1^2\frac{b_1}{(a_{11})_1} + \frac{b_1}{(d_{11})_1} + \frac{1}{(a_{11})_2}\left(\frac{b_2^3}{12} + z_2^2 b_2\right)\right]}_{\widehat{EI}_{yy}}. \tag{6.64}$$

The term indicated by the bracket is the replacement bending stiffness $\widehat{EI}_{yy}$.

6.3.2 Displacements of L-Beams

We consider an L-beam. The walls of the flanges are orthotropic, and one of the axes of orthotropy is aligned with the axis of the beam. The layups of the flanges need not be symmetrical with respect to the flanges' midplanes. The beam is subjected to an axial force $\widehat{N}$ and bending moments $\widehat{M}_y$ and $\widehat{M}_z$ acting at the centroid (Fig. 6.17).

We use an x–y–z coordinate system with its origin attached to the centroid of the beam and the ξ_1–η_1–ζ_1 and ξ_2–η_2–ζ_2 coordinate systems attached to the midpoints of the arbitrarily chosen reference planes in the horizontal and vertical flanges, respectively. The horizontal and vertical flanges are designated by the subscripts 1 and 2.

In this section the replacement stiffnesses are determined. The displacements are obtained by substituting these replacement stiffnesses into the expressions for the displacements of the corresponding isotropic beam. Because the cross section of the L-beam is unsymmetrical, all three bending stiffnesses $\widehat{EI}_{zz}$, $\widehat{EI}_{yy}$, and $\widehat{EI}_{yz}$ as well as the tensile stiffness $\widehat{EA}$ are needed to determine the displacements.

We treat the flanges as thin plates and employ the laminate plate theory equations. The calculation proceeds along the four steps used in the analysis of T-beams (page 218).

Tensile stiffness $\widehat{EA}$ and centroid. The tensile stiffness is obtained by considering the elongation of the beam while the axis of the beam remains straight.

Step 1. The axis of the beam (passing through the centroid) is elongated, and the strain of the axis is denoted by ϵ_x^o. In the absence of bending, the axial strains are

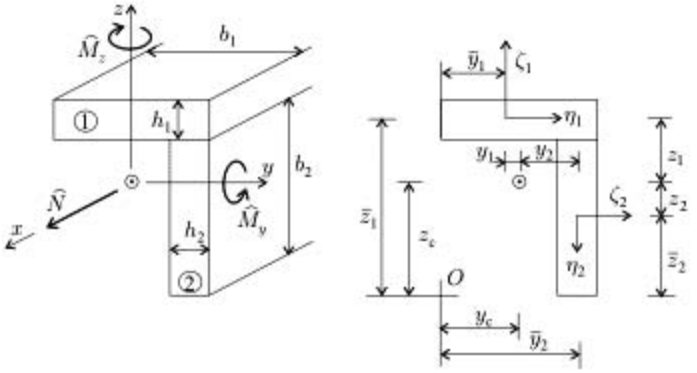

Figure 6.17: L-beam.

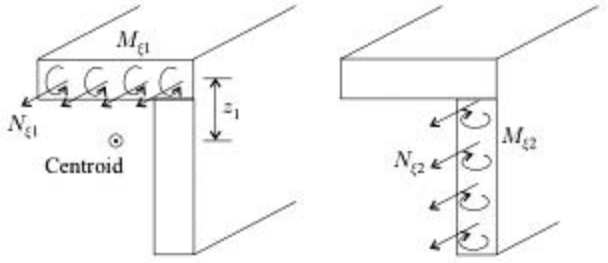

Figure 6.18: The distributed forces and moments acting in an L-beam with unsymmetrical layup when the axis of the beam is elongated.

the same across the cross section,

$$\epsilon^o_{\xi 1} = \epsilon^o_{\xi 2} = \epsilon^o_x, \tag{6.65}$$

where $\epsilon^o_{\xi 1}$ and $\epsilon^o_{\xi 2}$ are the axial strains of the reference planes of the two flanges, respectively. The locations of the reference planes may be chosen arbitrarily.

Step 2. The axial forces $N_{\xi 1}$, $N_{\xi 2}$ and the bending moments $M_{\xi 1}$, $M_{\xi 2}$ (per unit length) in the flanges (Fig. 6.18) are expressed in terms of the strains $\epsilon^o_{\xi 1}$, $\epsilon^o_{\xi 2}$. The derivation of these expressions is discussed subsequently on pages 227–228. Here we quote the results, which are

$$N_{\xi 1} = \frac{(\delta_{11})_1}{(D)_1}\epsilon^o_{\xi 1} \qquad N_{\xi 2} = \frac{(\delta_{11})_2}{(D)_2}\epsilon^o_{\xi 2} \tag{6.66}$$

$$M_{\xi 1} = -\frac{(\beta_{11})_1}{(D)_1}\epsilon^o_{\xi 1} \qquad M_{\xi 2} = -\frac{(\beta_{11})_2}{(D)_2}\epsilon^o_{\xi 2}, \tag{6.67}$$

where D is defined in Table 6.2, and δ_{11} and β_{11} are evaluated in the ξ–η–ζ coordinate system.

Table 6.2. The axial force and moments inside the wall ($N_\eta = N_{\xi\eta} = M_\eta = 0$). The elements of the compliance matrix δ_{11}, δ_{16}, δ_{66}, β_{11}, and β_{16} are evaluated in the wall's ξ–η–ζ coordinate system.

	Arbitrary cross section		Symmetrical cross section
	Orthotropic unsymmetrical layup	Orthotropic and symmetrical layup	Arbitrary layup
N_ξ	$\frac{\delta_{11}}{D}\epsilon^o_\xi - \frac{\beta_{11}}{D}\kappa_\xi$	$\frac{1}{a_{11}}\epsilon^o_\xi$	$\frac{\bar\delta_{11}}{D}\epsilon^o_\xi - \frac{\bar\beta_{11}}{D}\kappa_\xi$
M_ξ	$-\frac{\beta_{11}}{D}\epsilon^o_\xi + \frac{\alpha_{11}}{D}\kappa_\xi$	$\frac{1}{d_{11}}\kappa_\xi$	$-\frac{\bar\beta_{11}}{D}\epsilon^o_\xi + \frac{\bar\alpha_{11}}{D}\kappa_\xi$
$M_{\xi\eta}$	$=0$	0	$-\frac{\beta_{16}}{\delta_{66}}N_\xi - \frac{\delta_{16}}{\delta_{66}}M_\xi$
where	$\bar\alpha_{11} = \left(\alpha_{11} - \frac{\beta_{16}^2}{\delta_{66}}\right)$	$\bar\beta_{11} = \left(\beta_{11} - \frac{\beta_{16}\delta_{16}}{\delta_{66}}\right)$	$\bar\delta_{11} = \left(\delta_{11} - \frac{\delta_{16}^2}{\delta_{66}}\right)$
	$D = \alpha_{11}\delta_{11} - \beta_{11}^2$	$\overline{D} = \bar\alpha_{11}\bar\delta_{11} - \bar\beta_{11}^2$	

Step 3. The resultant axial force is (Fig. 6.18)

$$\widehat{N} = b_1 N_{\xi 1} + b_2 N_{\xi 2}, \tag{6.68}$$

where b_1 and b_2 are shown in Figure 6.17.

Step 4. Equations (6.65)–(6.68) give

$$\widehat{N} = \underbrace{\sum_{k=1}^{2} \frac{b_k (\delta_{11})_k}{(D)_k}}_{\widehat{EA}} \epsilon_x^o. \tag{6.69}$$

The term indicated by the bracket is the tensile stiffness $\widehat{EA}$. The terms $(D)_k$ and $(\delta_{11})_k$ are evaluated in the coordinate systems attached to the reference planes of the horizontal ($k = 1$) and vertical ($k = 2$) flanges, respectively.

The coordinates of the centroid z_c, y_c are calculated by moment equilibria about point O (Fig. 6.17). With the symbols defined in Figures 6.17 and 6.18, moment equilibria give

$$z_c \widehat{N} = \overline{z}_1 b_1 N_{\xi 1} + \overline{z}_2 b_2 N_{\xi 2} + b_1 M_{\xi 1} \tag{6.70}$$

$$y_c \widehat{N} = \overline{y}_1 b_1 N_{\xi 1} + \overline{y}_2 b_2 N_{\xi 2} + b_2 M_{\xi 2}. \tag{6.71}$$

By combining Eqs. (6.65)–(6.71), we obtain the coordinates of the centroid (Fig. 6.17):

$$z_c = \frac{b_1 \left(\overline{z}_1 \frac{(\delta_{11})_1}{(D)_1} - \frac{(\beta_{11})_1}{(D)_1} \right) + \frac{\overline{z}_2 b_2 (\delta_{11})_2}{(D)_2}}{\sum_{k=1}^{2} \frac{b_k (\delta_{11})_k}{(D)_k}} \tag{6.72}$$

$$y_c = \frac{\frac{\overline{y}_1 b_1 (\delta_{11})_1}{(D)_1} + b_2 \left(\overline{y}_2 \frac{(\delta_{11})_2}{(D)_2} - \frac{(\beta_{11})_2}{(D)_2} \right)}{\sum_{k=1}^{2} \frac{b_k (\delta_{11})_k}{(D)_k}}. \tag{6.73}$$

The coordinates of the centers of the flanges with respect to the centroid are (Fig. 6.17)

$$y_1 = \overline{y}_1 - y_c \qquad z_1 = \overline{z}_1 - z_c \tag{6.74}$$

$$y_2 = \overline{y}_2 - y_c \qquad z_2 = \overline{z}_2 - z_c. \tag{6.75}$$

The location of the centroid determines whether y_1, y_2, z_1, and z_2 are positive or negative. In Figure 6.17, y_2 and z_1 are positive and y_1 and z_2 are negative.

Bending stiffnesses $\widehat{EI}_{yy}$, $\widehat{EI}_{yz}$. To determine the bending stiffnesses $\widehat{EI}_{yy}$ and $\widehat{EI}_{yz}$ the beam is bent about the y-axis, which passes through the centroid. The radius of curvature is ρ_y (Fig. 6.19, left). This bending results in moments $\widehat{M}_y$ and $\widehat{M}_z$.

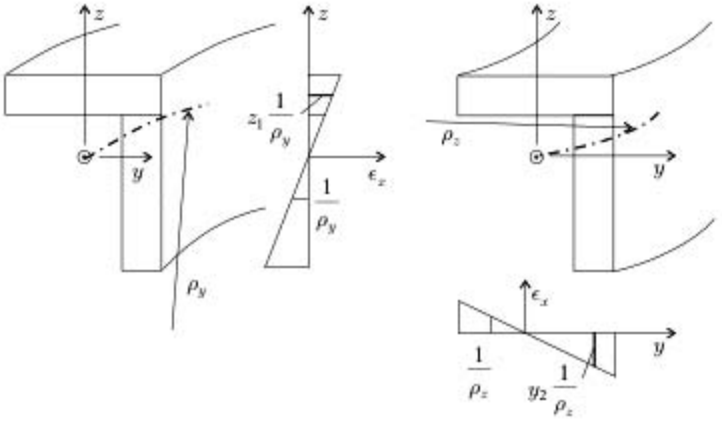

Figure 6.19: The radii of curvatures ρ_y and ρ_z and illustration of the axial strain distributions.

The bending stiffness $\widehat{EI}_{yy}$ is determined below.

Step 1. The strains and curvatures of the two flanges are identical to those of the T-beam (see Eqs. 6.57–6.60). Hence, we write

$$\epsilon^o_{\xi 1} = \frac{1}{\rho_y} z_1 \qquad \kappa_{\xi 1} = \frac{1}{\rho_y} \tag{6.76}$$

$$\epsilon^o_{\xi 2} = \frac{1}{\rho_y} z \qquad \kappa_{\xi 2} = 0. \tag{6.77}$$

Step 2. The axial forces $N_{\xi 1}$, $N_{\xi 2}$ and the bending moments $M_{\xi 1}$, $M_{\xi 2}$ in the flanges (Fig. 6.20) are expressed in terms of the strains $\epsilon^o_{\xi 1}$, $\epsilon^o_{\xi 2}$ and curvatures $\kappa_{\xi 1}$, $\kappa_{\xi 2}$. The derivation of these expressions is discussed subsequently on pages 227–228. Here we quote the results, which are

$$N_{\xi 1} = \frac{(\delta_{11})_1}{(D)_1}\epsilon^o_{\xi 1} - \frac{(\beta_{11})_1}{(D)_1}\kappa_{\xi 1} \qquad M_{\xi 1} = -\frac{(\beta_{11})_1}{(D)_1}\epsilon^o_{\xi 1} + \frac{(\alpha_{11})_1}{(D)_1}\kappa_{\xi 1} \tag{6.78}$$

$$N_{\xi 2} = \frac{(\delta_{11})_2}{(D)_2}\epsilon^o_{\xi 2} - \frac{(\beta_{11})_2}{(D)_2}\kappa_{\xi 2} \qquad M_{\xi 2} = -\frac{(\beta_{11})_2}{(D)_2}\epsilon^o_{\xi 2} + \frac{(\alpha_{11})_2}{(D)_2}\kappa_{\xi 2}. \tag{6.79}$$

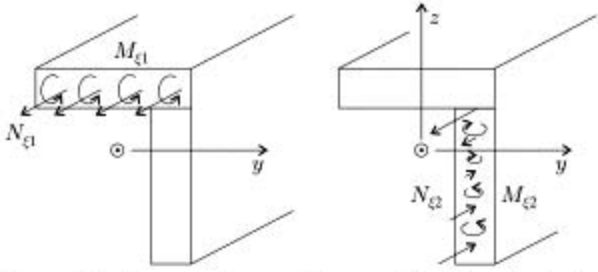

Figure 6.20: Forces and moments (per unit length) acting in the L-beam with unsymmetrical layup bent about the y-axis.

Step 3. The resulting bending moment $\widehat{M}_y$ about the y-axis is

$$\widehat{M}_y = b_1 N_{\xi 1} z_1 + b_1 M_{\xi 1} + \int_{(b_2)} N_{\xi 2} z dz. \tag{6.80}$$

Step 4. Equations (6.76)–(6.80) give

$$\widehat{M}_y = \frac{1}{\rho_y} \underbrace{\left[b_1 \left(\frac{(\delta_{11})_1}{(D)_1} z_1^2 - 2\frac{(\beta_{11})_1}{(D)_1} z_1 + \frac{(\alpha_{11})_1}{(D)_1} \right) + \frac{(\delta_{11})_2}{(D)_2} \left(\frac{b_2^3}{12} + z_2^2 b_2 \right) \right]}_{\widehat{EI}_{yy}}. \tag{6.81}$$

The term indicated by the bracket is the bending stiffness $\widehat{EI}_{yy}$.

The bending stiffness $\widehat{EI}_{yz}$ is determined below.

Steps 1 and 2. In the calculation of the bending moment $\widehat{M}_z$, the first two steps are identical to those given for the calculation of $\widehat{M}_y$.

Step 3. When the beam is bent about the y-axis, the resultant bending moment $\widehat{M}_z$ about the z-axis is (Figs. 6.20 and 6.17)

$$\widehat{M}_z = b_1 N_{\xi 1} y_1 + \int_{(b_2)} N_{\xi 2} y_2 dz + \int_{(b_2)} M_{\xi 2} dz. \tag{6.82}$$

Step 4. Equations (6.76)–(6.79) and (6.82) give

$$\widehat{M}_z = \frac{1}{\rho_y} \underbrace{\left[\left(\frac{(\delta_{11})_1}{(D)_1} z_1 - \frac{(\beta_{11})_1}{(D)_1} \right) b_1 y_1 + \left(\frac{(\delta_{11})_2}{(D)_2} y_2 - \frac{(\beta_{11})_2}{(D)_2} \right) z_2 b_2 \right]}_{\widehat{EI}_{yz}}. \tag{6.83}$$

The term indicated by the bracket is the bending stiffness $\widehat{EI}_{yz}$.

Bending stiffnesses $\widehat{EI}_{zz}$, $\widehat{EI}_{zy}$. To determine the bending stiffnesses $\widehat{EI}_{zz}$ and $\widehat{EI}_{zy}$, the beam is bent about the z-axis with a radius of curvature ρ_z (Fig. 6.19, right). Expressions for these bending moments can be derived in the same way as Eqs. (6.81) and (6.83). The results are

$$\widehat{M}_z = \frac{1}{\rho_z} \underbrace{\left[b_2 \left(\frac{(\delta_{11})_2}{(D)_2} y_2^2 - 2\frac{(\beta_{11})_2}{(D)_2} y_2 + \frac{(\alpha_{11})_2}{(D)_2} \right) + \frac{(\delta_{11})_1}{(D)_1} \left(\frac{b_1^3}{12} + y_1^2 b_1 \right) \right]}_{\widehat{EI}_{zz}} \tag{6.84}$$

$$\widehat{M}_y = \frac{1}{\rho_z} \underbrace{\left[\left(\frac{(\delta_{11})_1}{(D)_1} z_1 - \frac{(\beta_{11})_1}{(D)_1} \right) b_1 y_1 + \left(\frac{(\delta_{11})_2}{(D)_2} y_2 - \frac{(\beta_{11})_2}{(D)_2} \right) z_2 b_2 \right]}_{\widehat{EI}_{zy}}. \tag{6.85}$$

The terms indicated by the brackets are the bending stiffnesses $\widehat{EI}_{zz}$ and $\widehat{EI}_{zy}$ $(= \widehat{EI}_{yz})$.

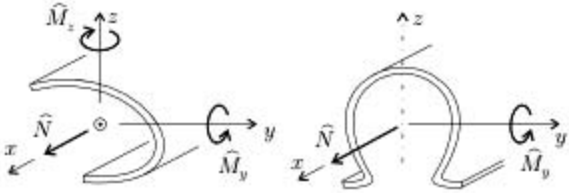

Figure 6.21: Illustration of thin-walled, open-section beams with symmetrical and unsymmetrical cross sections.

6.3.3 Displacements of Arbitrary Cross-Section Beams

In this section we treat thin-walled, open-section beams. The beams are subjected to an axial force $\widehat{N}$ and to bending moments $\widehat{M}_y$, $\widehat{M}_z$ acting at the centroid (Fig. 6.21).

Three types of beams are considered:

1. The layup of the wall is orthotropic but unsymmetrical; the beam's cross section is arbitrary.[5]
2. The layup of the wall is orthotropic and symmetrical; the beam's cross section is arbitrary.
3. The layup of the wall is arbitrary; the cross section is symmetrical with respect to the z-axis, and the loads $\widehat{N}$ and $\widehat{M}_z$ are applied in the x–z symmetry plane (Fig. 6.21, right).

There are no tension–bending–torsion couplings in any of the preceding three types of beams. In the first two types of beams these couplings are not present because the beam is orthotropic (page 207); in the third type of beam couplings are not present because the cross section is symmetrical and the loads act in the symmetry plane.

In the following we derive the replacement stiffnesses. The displacements are then obtained by substituting these replacement stiffnesses into the expressions for the displacements of the corresponding isotropic beam.

We perform the analysis for beams of the first type, that is, the layup is orthotropic but is not necessarily symmetrical and the cross section is arbitrary. We then generalize the results to the other two types of beams in the list above.

We employ three coordinate systems (Fig. 6.22). For the beam we use the x–y–z coordinate system with the origin at the centroid and the $\overline{x}$–$\overline{y}$–$\overline{z}$ coordinate system with the origin at an arbitrarily chosen point. We also define a ξ–η–ζ coordinate system with the origin at the reference plane of the wall. At each point in the wall ξ is parallel to the x coordinate, η is tangential to the circumference of the wall, and ζ is perpendicular to the circumference.

The calculation proceeds in four steps. In Step 1 we deform the axis of the beam (axial strain ϵ_x^o and curvatures $1/\rho_y$ and $1/\rho_z$) and calculate the strains in,

[5] J. C. Massa and E. J. Barbero, A Strength of Materials Formulation for Thin Walled Composite Beams with Torsion. *Journal of Composite Materials*, Vol. 32, 1560–1594, 1998.

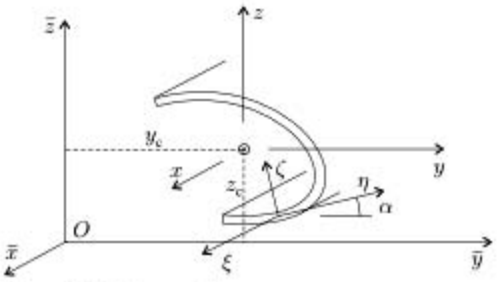

Figure 6.22: The coordinate systems.

and the curvatures of, the wall; in Step 2 we calculate the forces and moments in the wall; in Step 3 we calculate the resultant forces and moments acting on the beam; in Step 4 we determine the stiffnesses.

Step 1. The Bernoulli–Navier hypothesis states that the axial strain varies linearly with the curvatures of the beam. Thus, the axial strain ϵ_ξ^o at a point on the arbitrarily chosen reference surface of the wall is related to the axial strain ϵ_x^o and curvatures $1/\rho_y$ and $1/\rho_z$ of the beam by

$$\epsilon_\xi^o = \epsilon_x^o + z\frac{1}{\rho_y} + y\frac{1}{\rho_z}, \tag{6.86}$$

where z and y are the coordinates of the point on the wall's reference surface. From geometry, it can be shown that the wall's curvature κ_ξ in the ξ–ζ plane is, (Fig. 6.23)

$$\kappa_\xi = \frac{1}{\rho_y}\cos\alpha - \frac{1}{\rho_z}\sin\alpha, \tag{6.87}$$

where α is the angle between the η- and y-coordinate axes (Fig. 6.23).

Step 2. In this step we express the axial force N_ξ and bending moments M_ξ and $M_{\xi\eta}$ in terms of ϵ_ξ^o and κ_ξ. To derive the necessary expressions we observe that along the free longitudinal edges of the beam the in-plane forces and moments (per unit length) are zero: $N_\eta = N_{\xi\eta} = M_\eta = 0$ (Fig. 6.24). Since the dimensions of

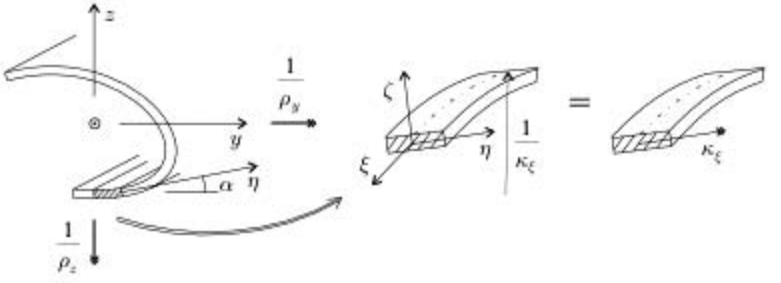

Figure 6.23: Curvatures of the beam (left) and the curvature of the wall (middle) and its vector representation (right).

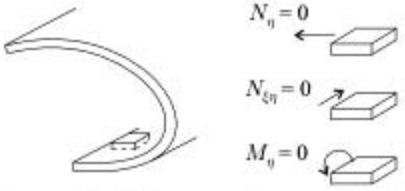

Figure 6.24: The forces and moments along the longitudinal edge of an open-section, thin-walled beam.

the cross section are small compared with the beam's length, these in-plane forces and moments are approximately zero inside the wall:

$$N_\eta = N_{\xi\eta} = M_\eta = 0. \tag{6.88}$$

We apply only axial strain and curvatures to the beam, but no twist. Therefore, the twist of the wall is zero:

$$\kappa_{\xi\eta} = 0. \tag{6.89}$$

We now recall the strain–force relationships given by Eq. (3.22) with the compliance matrix for an orthotropic material given by Eq. (3.37). To apply the relationships to the wall we replace x by ξ and y by η. The resulting generalized strain–force relationships are (orthotropic):

$$\begin{Bmatrix} \epsilon_\xi^o \\ \epsilon_\eta^o \\ \gamma_{\xi\eta}^o \\ \kappa_\xi \\ \kappa_\eta \\ \kappa_{\xi\eta} \end{Bmatrix} = \begin{bmatrix} \alpha_{11} & \alpha_{12} & 0 & \beta_{11} & \beta_{12} & 0 \\ \alpha_{12} & \alpha_{22} & 0 & \beta_{21} & \beta_{22} & 0 \\ 0 & 0 & \alpha_{66} & 0 & 0 & \beta_{66} \\ \beta_{11} & \beta_{21} & 0 & \delta_{11} & \delta_{12} & 0 \\ \beta_{12} & \beta_{22} & 0 & \delta_{12} & \delta_{22} & 0 \\ 0 & 0 & \beta_{66} & 0 & 0 & \delta_{66} \end{bmatrix} \begin{Bmatrix} N_\xi \\ N_\eta \\ N_{\xi\eta} \\ M_\xi \\ M_\eta \\ M_{\xi\eta} \end{Bmatrix}. \tag{6.90}$$

Substitution of Eqs. (6.88) and (6.89) into Eq. (6.90) yields

$$\begin{Bmatrix} \epsilon_\xi^o \\ \kappa_\xi \end{Bmatrix} = \begin{bmatrix} \alpha_{11} & \beta_{11} \\ \beta_{11} & \delta_{11} \end{bmatrix} \begin{Bmatrix} N_\xi \\ M_\xi \end{Bmatrix} + \begin{bmatrix} 0 \\ 0 \end{bmatrix} M_{\xi\eta} \tag{6.91}$$

$$\kappa_{\xi\eta} = 0 = 0 \times N_\xi + 0 \times M_\xi + \delta_{66} M_{\xi\eta}. \tag{6.92}$$

From these equations we can obtain N_ξ, M_ξ, and $M_{\xi\eta}$ in terms of ϵ_ξ^o and κ_ξ. The resulting expressions are listed in the left column of Table 6.2 (page 222).

Step 3. The resultant force and moments in the beam are (Fig. 6.25)

$$\widehat{N} = \int_{(S)} N_\xi d\eta \tag{6.93}$$

$$\widehat{M}_y = \int_{(S)} M_\xi \cos\alpha_k d\eta + \int_{(S)} z N_\xi d\eta \tag{6.94}$$

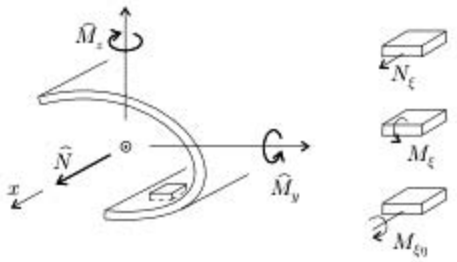

Figure 6.25: The forces and moments acting on the beam and the forces and moments (per unit length) acting inside the wall.

$$\widehat{M}_z = \int_{(S)} -M_\xi \sin\alpha_k d\eta + \int_{(S)} yN_\xi d\eta \tag{6.95}$$

$$\widehat{T} = \int_{(S)} 2M_{\xi\eta} d\eta = 0, \tag{6.96}$$

where S is the length of the circumference. The torque resultant $\widehat{T}$ is zero because, for orthotropic beams, $M_{\xi\eta}$ is zero (Eq. 6.92).

Since $\widehat{T}$ is zero for orthotropic beams, P_{14}, P_{24}, and P_{34} are zero (see Eq. 6.2). Consequently, there is no tension–bending–torsion coupling in orthotropic beams.

Step 4. We axially elongate the beam such that $1/\rho_y$ and $1/\rho_z$ remain zero. Thus, from Eqs. (6.86) and (6.87) we have

$$\epsilon_\xi^o = \epsilon_x^o \qquad \kappa_\xi = 0. \tag{6.97}$$

For a beam with orthotropic and unsymmetrical layup (arbitrary cross section) Eqs. (6.93) and (6.97), together with the expression for N_ξ in Table 6.2, left column, yield

$$\widehat{N} = \underbrace{\int_{(S)} \frac{\delta_{11}}{D} d\eta}_{\widehat{EA}} \epsilon_x^o. \tag{6.98}$$

The coordinates of the centroid are obtained by taking a moment about point O shown in Figure 6.22:

$$\widehat{N} y_c = \int_{(S)} N_\xi \bar{y} d\eta - \int_{(S)} M_\xi \sin\alpha_k d\eta \tag{6.99}$$

$$\widehat{N} z_c = \int_{(S)} N_\xi \bar{z} d\eta + \int_{(S)} M_\xi \cos\alpha_k d\eta, \tag{6.100}$$

where $\overline{y}$ and $\overline{z}$ are the coordinates of a point on the wall's reference surface in the $\overline{x}, \overline{y}, \overline{z}$ coordinate system. By setting $1/\rho_y = 1/\rho_z = 0$ and by using Eqs. (6.86), (6.98), and the expression for N_ξ in Table 6.2 (page 222), left column, we obtain the coordinates of the centroid as follows:

$$y_c = \frac{\int\limits_{(S)} \left(\overline{y}_k \frac{\delta_{11}}{D} + \frac{\beta_{11}}{D} \sin\alpha\right) d\eta}{\int\limits_{(S)} \frac{\delta_{11}}{D} d\eta} \qquad z_c = \frac{\int\limits_{(S)} \left(\overline{z}_k \frac{\delta_{11}}{D} - \frac{\beta_{11}}{D} \cos\alpha\right) d\eta}{\int\limits_{(S)} \frac{\delta_{11}}{D} d\eta}. \tag{6.101}$$

Next we determine the bending stiffnesses. First, we set ϵ_x^o equal to zero in Eqs. (6.86) and (6.87). Then, Eqs. (6.86), (6.87), (6.94), and (6.95) together with the expressions in Table 6.2 give the following resultant moments of a beam with orthotropic and unsymmetrical layup (arbitrary cross section):

$$\widehat{M}_y = \underbrace{\int\limits_{(S)} \left[\frac{\delta_{11}}{D} z^2 - \frac{2\beta_{11}}{D} z\cos\alpha_k + \frac{\alpha_{11}}{D} \cos^2\alpha\right] d\eta}_{\widehat{EI}_{yy}} \frac{1}{\rho_y}$$

$$+ \underbrace{\int\limits_{(S)} \left[\frac{\delta_{11}}{(D)} yz + \frac{\beta_{11}}{D} (z\sin\alpha - y\cos\alpha) - \frac{\alpha_{11}}{D} \cos\alpha\sin\alpha\right] d\eta}_{\widehat{EI}_{yz}} \frac{1}{\rho_z} \tag{6.102}$$

$$\widehat{M}_z = \underbrace{\int\limits_{(S)} \left[\frac{\delta_{11}}{(D)} yz + \frac{\beta_{11}}{D} (z\sin\alpha - y\cos\alpha) - \frac{\alpha_{11}}{D} \cos\alpha\sin\alpha\right] d\eta}_{\widehat{EI}_{yz}} \frac{1}{\rho_y}$$

$$+ \underbrace{\int\limits_{(S)} \left[\frac{\delta_{11}}{D} y^2 + \frac{2\beta_{11}}{D} y\sin\alpha + \frac{\alpha_{11}}{D} \sin^2\alpha\right] d\eta}_{\widehat{EI}_{zz}} \frac{1}{\rho_z}. \tag{6.103}$$

The tensile stiffnesses, the coordinates of the centroid, and the bending stiffnesses of beams with orthotropic and symmetrical layup (arbitrary cross section) and with arbitrary layup (symmetrical cross section) are obtained similarly. The main difference is in Step 2, where the appropriate stress–strain relationships must be used instead of Eq. (6.90). The results are given in Tables 6.3–6.5.

Choice of the reference surface. The expressions of the replacement stiffnesses simplify when the properties are not evaluated at an arbitrary reference surface but at a "neutral" surface, where β_{11} (orthotropic layup – arbitrary cross section) or $\overline{\beta}_{11}$ (arbitrary layup – symmetrical cross section) is zero. The surface is "neutral" in the sense that a bending moment M_ξ does not cause axial strain ϵ_ξ in this surface. (However, it is not a real neutral surface because, unlike in an isotropic beam, in this reference surface the strain perpendicular to the beam's axis ϵ_η is not zero.)

Table 6.3. The tensile and bending stiffnesses and the coordinates of the centroid of open- and closed-section beams with curved walls. The cross section is arbitrary, and the layup of the wall is orthotropic and symmetrical; a_{11} and d_{11} are evaluated at the midsurface.

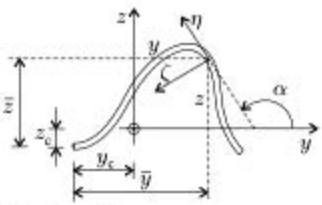

arbitrary cross section
orthotropic
symmetrical layup

Tensile stiffness

$$\widehat{EA} = \int_{(S)} \frac{1}{a_{11}} d\eta$$

Coordinates of the centroid

$$y_c = \frac{\int_{(S)} \bar{y} \frac{1}{a_{11}} d\eta}{\int_{(S)} \frac{1}{a_{11}} d\eta} \qquad z_c = \frac{\int_{(S)} \bar{z} \frac{1}{a_{11}} d\eta}{\int_{(S)} \frac{1}{a_{11}} d\eta}$$

Bending stiffnesses

$$\widehat{EI}_{yy} = \int_{(S)} \left(\frac{1}{a_{11}} z^2 + \frac{1}{d_{11}} \cos^2\alpha \right) d\eta$$

$$\widehat{EI}_{zz} = \int_{(S)} \left(\frac{1}{a_{11}} y^2 + \frac{1}{d_{11}} \sin^2\alpha \right) d\eta$$

$$\widehat{EI}_{yz} = \int_{(S)} \left(\frac{1}{a_{11}} yz + \frac{1}{d_{11}} \sin\alpha \cos\alpha \right) d\eta$$

The 11 component of the compliance matrix corresponding to the "neutral" surface is (Eq. 3.48)

$$\beta_{11}^{\varrho} = \beta_{11} + \varrho \delta_{11}, \tag{6.104}$$

where β_{11} and δ_{11} are the components of the compliance matrices in the arbitrarily chosen reference surface and ϱ is the location of the "neutral" surface (Fig. 6.26). At the "neutral" surface $\beta_{11}^{\varrho} = 0$, and the preceding equation yields

$$\tilde{\varrho} = -\frac{\beta_{11}}{\delta_{11}} \qquad \begin{matrix} \text{orthotropic layup} \\ \text{arbitrary cross section.} \end{matrix} \tag{6.105}$$

This equation applies to orthotropic beams with symmetrical as well as unsymmetrical cross sections.

For beams with arbitrary layup (symmetrical cross section), Eq. (3.48) and the expression for $\bar{\beta}_{11}$ in Table 6.2 (page 222) yield

$$\bar{\beta}_{11}^{\varrho} = \left(\beta_{11}^{\varrho} + \varrho \delta_{11}\right) - \frac{\left(\beta_{16} + \varrho \delta_{16}\right) \delta_{16}}{\delta_{66}} = \bar{\beta}_{11} + \varrho \bar{\delta}_{11}. \tag{6.106}$$

Table 6.4. The tensile and bending stiffnesses and the coordinates of the centroid of open- and closed-section beams with curved walls. The cross section is arbitrary, and the layup of the wall is orthotropic and unsymmetrical; δ_{11}, β_{11}, and α_{11} are evaluated in the wall's ξ–η–ζ coordinate system; D is defined in Table 6.2 and $\widehat{\delta}_{11}$ and $\widehat{D}$ are defined by Eq. (6.157).

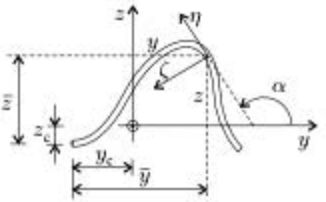

arbitrary cross section
orthotropic
unsymmetrical layup

Tensile stiffness

Open section: $\widehat{EA} = \int_{(S)} \frac{\delta_{11}}{D}\, d\eta$ Closed section: $\widehat{EA} = \int_{(S)} \frac{\widehat{\delta}_{11}}{\widehat{D}}\, d\eta$

Coordinates of the centroid

$$y_c = \frac{\int_{(S)} \left(\bar{z}_k \frac{\delta_{11}}{D} + \frac{\beta_{11}}{D} \sin\alpha \right) d\eta}{\int_{(S)} \frac{\delta_{11}}{D}\, d\eta} \qquad z_c = \frac{\int_{(S)} \left(z_k \frac{\delta_{11}}{D} - \frac{\beta_{11}}{D} \cos\alpha \right) d\eta}{\int_{(S)} \frac{\delta_{11}}{D}\, d\eta}$$

Bending stiffnesses

$$\widehat{EI}_{yy} = \int_{(S)} \left(\frac{\delta_{11}}{D} z^2 - \frac{2\beta_{11}}{D} z \cos\alpha_k + \frac{\alpha_{11}}{D} \cos^2\alpha \right) d\eta$$

$$\widehat{EI}_{zz} = \int_{(S)} \left(\frac{\delta_{11}}{D} y^2 + \frac{2\beta_{11}}{D} y \sin\alpha + \frac{\alpha_{11}}{D} \sin^2\alpha \right) d\eta$$

$$\widehat{EI}_{yz} = \int_{(S)} \left(\frac{\delta_{11}}{(D)} yz + \frac{\beta_{11}}{D} (z \sin\alpha - y \cos\alpha) - \frac{\alpha_{11}}{D} \cos\alpha \sin\alpha \right) d\eta$$

Table 6.5. The tensile and bending stiffnesses and the coordinates of the centroid of open-section beams with symmetrical cross section. The layup of the wall is unsymmetrical and nonorthotropic; $\overline{D}$, $\overline{\delta}_{11}$, and $\overline{\beta}_{11}$ are defined in Table 6.2. The elements of the compliance matrix are evaluated in the wall's ξ–η–ζ coordinate system.

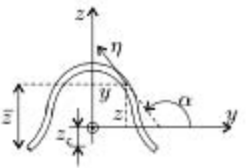

symmetrical cross section
nonorthotropic
unsymmetrical layup

Tensile stiffness

$$\widehat{EA} = \int_{(S)} \frac{\bar{\delta}_{11}}{D}\, d\eta$$

Coordinates of the centroid

$$y_c = 0 \qquad z_c = \frac{\int_{(S)} \left(\bar{z}_k \frac{\bar{\delta}_{11}}{D} - \frac{\bar{\beta}_{11}}{D} \cos\alpha \right) d\eta}{\int_{(S)} \frac{\bar{\delta}_{11}}{D}\, d\eta}$$

Bending stiffness

$$\widehat{EI}_{yy} = \int_{(S)} \left(\frac{\bar{\delta}_{11}}{D} z^2 - \frac{2\bar{\beta}_{11}}{D} z \cos\alpha_k + \frac{\bar{\alpha}_{11}}{D} \cos^2\alpha \right) d\eta$$

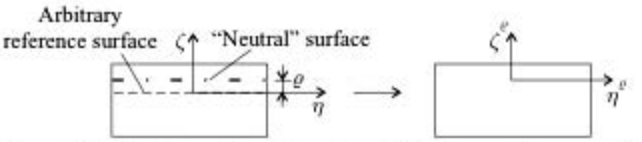

Figure 6.26: The "neutral" surface where $\widetilde{\beta}^{\varrho}_{11}$ (orthotropic layup – arbitrary cross section) or $\overline{\beta}^{\varrho}_{11}$ (arbitrary layup – symmetrical cross section) is zero.

From the condition $\overline{\beta}^{\varrho}_{11} = 0$ we obtain the location of the "neutral" surface of the wall as follows:

$$\overline{\varrho} = -\frac{\overline{\beta}_{11}}{\overline{\delta}_{11}} \qquad \begin{matrix} \text{arbitrary layup} \\ \text{symmetrical cross section.} \end{matrix} \tag{6.107}$$

For selected cross sections the replacement stiffnesses and the location of the centroid are given in Tables A.1–A.4.

Segmented wall. The beam's wall may consist of several flat wall segments (Fig. 6.27). The thickness of each wall segment is small compared with the width of the segment. The wall segments are designated by the subscript k ($k = 1, 2, \ldots, K$, where K is the total number of wall segments). The layup of each wall segment may be symmetrical or unsymmetrical with respect to the wall segment's midsurface.

When the wall consists of segments and each segment is flat, the integrals in Tables 6.3–6.5 may be replaced by summations

$$\int_{(S)} (\ )d\eta = \sum_{k=1}^{K} \int_{-b_k/2}^{b_k/2} (\ )d\eta, \tag{6.108}$$

where b_k is the width of the kth wall segment. For each wall segment we define a ξ–η–ζ coordinate system, where ξ is parallel to the x coordinate, η is along the circumference of the wall, and ζ is perpendicular to the wall (Fig. 6.27). The origin of this coordinate system may be at an arbitrarily chosen reference surface but must be at the middle of the width of the wall segment. By performing the integrations in Tables 6.3–6.5 we obtain the expressions given in Tables 6.6–6.8.

6.3.4 Stresses and Strains

In a thin-walled isotropic beam subjected to an axial load and to bending in the x–z plane there is only axial stress σ_x. In a thin-walled composite beam, in addition to the axial stress σ_ξ, transverse normal σ_η and shear $\tau_{\xi\eta}$ stresses are also present.

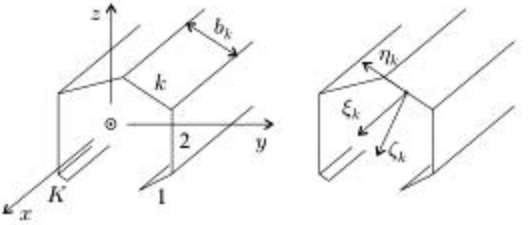

Figure 6.27: Thin-walled, open-section beams with segmented wall.

Table 6.6. The tensile and bending stiffnesses and the coordinates of the centroid of open- and closed-section beams with flat walls. The cross section is arbitrary, and the layup of each wall segment is orthotropic and symmetrical; a_{11} and d_{11} are evaluated at the wall's midplanes.

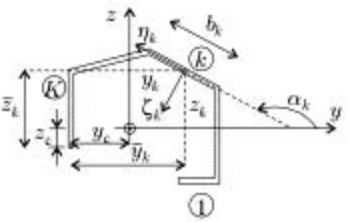

arbitrary cross section
orthotropic
symmetrical layup

Tensile stiffness

$$\widehat{EA} = \sum_{k=1}^{K} \frac{b_k}{(a_{11})_k}$$

Coordinates of the centroid

$$y_c = \frac{\sum_{k=1}^{K} \bar{y}_k \frac{b_k}{(a_{11})_k}}{\sum_{k=1}^{K} \frac{b_k}{(a_{11})_k}} \qquad z_c = \frac{\sum_{k=1}^{K} \bar{z}_k \frac{b_k}{(a_{11})_k}}{\sum_{k=1}^{K} \frac{b_k}{(a_{11})_k}}$$

Bending stiffnesses

$$\widehat{EI}_{yy} = \sum_{k=1}^{K} \left[\frac{1}{(a_{11})_k} \left(b_k z_k^2 + \frac{b_k^3 \sin^2 \alpha_k}{12} \right) + \frac{b_k}{(d_{11})_k} \cos^2 \alpha_k \right]$$

$$\widehat{EI}_{zz} = \sum_{k=1}^{K} \left[\frac{1}{(a_{11})_k} \left(b_k y_k^2 + \frac{b_k^3 \cos^2 \alpha_k}{12} \right) + \frac{b_k}{(d_{11})_k} \sin^2 \alpha_k \right]$$

$$\widehat{EI}_{yz} = \sum_{k=1}^{K} \frac{1}{(a_{11})_k} \left(b_k y_k z_k + \frac{b_k^3 \cos \alpha_k \sin \alpha_k}{12} \right) - \frac{b_k}{(d_{11})_k} \cos \alpha_k \sin \alpha_k$$

These stresses are illustrated in Fig. 6.28. However, the shear flow, defined as the integral of the shear stress across the thickness, is zero,

$$q = \int_{(h)} \tau_{\xi\eta} d\zeta = 0, \tag{6.109}$$

where h is the thickness of the wall. In the following subsections, we present analyses for calculating the three stress components $\sigma_\xi, \sigma_\eta, \tau_{\xi\eta}$ inside composite beams.

Orthotropic layup (arbitrary cross section). When the layup of the wall is orthotropic, the axial strain and the curvatures of the beam's axis passing through the centroid are (Eqs. 6.17 and 6.19)

$$\epsilon_x^0 = \frac{\hat{N}}{\widehat{EA}} \tag{6.110}$$

$$\frac{1}{\rho_y} = \frac{\widehat{EI}_{zz}\hat{M}_y - \widehat{EI}_{yz}\hat{M}_z}{\widehat{EI}_{yy}\widehat{EI}_{zz} - (\widehat{EI}_{yz})^2} \tag{6.111}$$

$$\frac{1}{\rho_z} = \frac{-\widehat{EI}_{yz}\hat{M}_y + \widehat{EI}_{yy}\hat{M}_z}{\widehat{EI}_{yy}\widehat{EI}_{zz} - (\widehat{EI}_{yz})^2}. \tag{6.112}$$

Table 6.7. The tensile and bending stiffnesses and the coordinates of the centroid of open- and closed-section beams with flat walls. The cross section is arbitrary, and the layup of each wall segment is orthotropic and unsymmetrical; δ_{11}, β_{11}, and α_{11} are evaluated in the wall's ξ–η–ζ coordinate system; D is defined in Table 6.2. The parameters $\widehat{\delta}_{11}$ and $\widehat{D}$ are defined by Eq. (6.157).

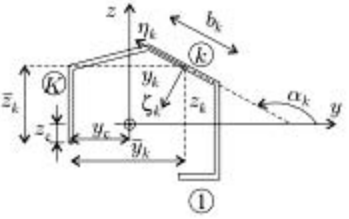

arbitrary cross section
orthotropic
unsymmetrical layup

Tensile stiffness

Open section: $\widehat{EA} = \sum_{k=1}^{K} \frac{(\delta_{11})_k b_k}{(D)_k}$ Closed section: $\widehat{EA} = \sum_{k=1}^{K} \frac{(\bar{\delta}_{11})_k b_k}{(\bar{D})_k}$

Coordinates of the centroid

$$y_c = \frac{\sum_{k=1}^{K} b_k \left(\bar{y}_k \frac{(\delta_{11})_k}{(D)_k} + \frac{(\beta_{11})_k}{(D)_k} \sin\alpha_k \right)}{\sum_{k=1}^{K} \frac{b_k (\delta_{11})_k}{(D)_k}} \qquad z_c = \frac{\sum_{k=1}^{K} b_k \left(\bar{z}_k \frac{(\delta_{11})_k}{(D)_k} - \frac{(\beta_{11})_k}{(D)_k} \cos\alpha_k \right)}{\sum_{k=1}^{K} \frac{b_k (\delta_{11})_k}{(D)_k}}$$

Bending stiffnesses

$$\widehat{EI}_{yy} = \sum_{k=1}^{K} \frac{(\delta_{11})_k}{(D)_k} \left(b_k z_k^2 + \frac{b_k^3 \sin^2\alpha_k}{12} \right) - \frac{2(\beta_{11})_k}{(D)_k} b_k z_k \cos\alpha_k + \frac{(\alpha_{11})_k}{(D)_k} b_k \cos^2\alpha_k$$

$$\widehat{EI}_{zz} = \sum_{k=1}^{K} \frac{(\delta_{11})_k}{(D)_k} \left(b_k y_k^2 + \frac{b_k^3 \cos^2\alpha_k}{12} \right) + \frac{2(\beta_{11})_k}{(D)_k} b_k y_k \sin\alpha_k + \frac{(\alpha_{11})_k}{(D)_k} b_k \sin^2\alpha_k$$

$$\widehat{EI}_{yz} = \sum_{k=1}^{K} \frac{(\delta_{11})_k}{(D)_k} \left(b_k y_k z_k + \frac{b_k^3 \cos\alpha_k \sin\alpha_k}{12} \right) + \frac{(\beta_{11})_k}{(D)_k} b_k (z_k \sin\alpha_k - y_k \cos\alpha_k) - \frac{(\alpha_{11})_k}{(D)_k} b_k \cos\alpha_k \sin\alpha_k$$

At an arbitrary point on the reference surface of the wall, the axial strain ϵ_ξ^o and curvature κ_ξ are related to the strain and curvatures of the beam by Eqs. (6.86) and (6.87).

$$\epsilon_\xi^o = \epsilon_x^o + y\frac{1}{\rho_z} + z\frac{1}{\rho_y} \tag{6.113}$$

$$\kappa_\xi = -\frac{1}{\rho_z}\sin\alpha + \frac{1}{\rho_y}\cos\alpha, \tag{6.114}$$

where α is the angle between the tangent of the wall (coordinate η) and the y-axis (Fig. 6.22).

The layup of the wall is orthotropic, and hence the following forces and moments are zero (see Eqs. 6.88 and 6.92):

$$N_\eta = N_{\xi\eta} = M_\eta = M_{\xi\eta} = 0. \tag{6.115}$$

Table 6.8. The tensile and bending stiffnesses and the coordinates of the centroid of open-section beams with symmetrical cross section. The layup of each wall segment is nonorthotropic and unsymmetrical; $\overline{D}$, $\overline{\delta}_{11}$, and $\overline{\beta}_{11}$ are defined in Table 6.2. The elements of the compliance matrix are evaluated in the wall's ξ–η–ζ coordinate system.

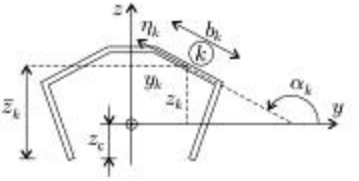

symmetrical cross section
nonorthotropic
unsymmetrical layup

Tensile stiffness

$$\widehat{EA} = \sum_{k=1}^{K} \frac{(\overline{\delta}_{11})_k b_k}{(\overline{D})_k}$$

Coordinates of the centroid

$$y_c = 0 \qquad z_c = \frac{\sum_{k=1}^{K} b_k \left(\overline{z}_k \frac{(\overline{\delta}_{11})_k}{(\overline{D})_k} - \frac{(\overline{\beta}_{11})_k}{(\overline{D})_k} \cos\alpha_k \right)}{\sum_{k=1}^{K} \frac{b_k (\overline{\delta}_{11})_k}{(\overline{D})_k}}$$

Bending stiffness

$$\widehat{EI}_{yy} = \sum_{k=1}^{K} \frac{(\overline{\delta}_{11})_k}{(\overline{D})_k} \left(b_k z_k^2 + \frac{b_k^3 \sin^2\alpha_k}{12} \right) - \frac{2(\overline{\beta}_{11})_k}{(\overline{D})_k} b_k z_k \cos\alpha_k + \frac{(\overline{\alpha}_{11})_k}{(\overline{D})_k} b_k \cos^2\alpha_k$$

The axial force N_ξ and the moment M_ξ (per unit length) in the wall are (Table 6.2, page 222)

$$N_\xi = \frac{\delta_{11}}{D} \epsilon_\xi^o - \frac{\beta_{11}}{D} \kappa_\xi \tag{6.116}$$

$$M_\xi = -\frac{\beta_{11}}{D} \epsilon_\xi^o + \frac{\alpha_{11}}{D} \kappa_\xi. \tag{6.117}$$

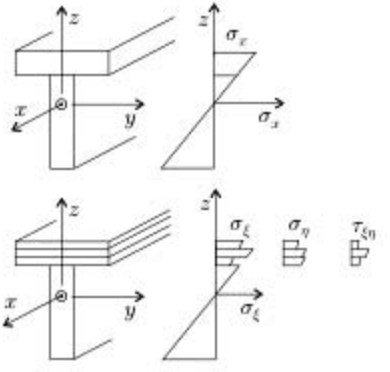

Figure 6.28: Illustration of the stresses in an isotropic (top) and a composite (bottom) T-beam subjected to bending in the x–z plane.

Equations (6.110) and (6.113)–(6.117) yield

$$N_\xi = \frac{1}{\rho_y}\left(z\frac{\delta_{11}}{D} - \cos\alpha\frac{\beta_{11}}{D}\right) + \frac{1}{\rho_z}\left(y\frac{\delta_{11}}{D} + \sin\alpha\frac{\beta_{11}}{D}\right) + \frac{\widehat{N}}{\widehat{EA}}\frac{\delta_{11}}{D} \tag{6.118}$$

$$M_\xi = \frac{1}{\rho_y}\left(-z\frac{\beta_{11}}{D} + \cos\alpha\frac{\alpha_{11}}{D}\right) - \frac{1}{\rho_z}\left(y\frac{\beta_{11}}{D} + \sin\alpha\frac{\alpha_{11}}{D}\right) - \frac{\widehat{N}}{\widehat{EA}}\frac{\beta_{11}}{D}, \tag{6.119}$$

where $1/\rho_y$ and $1/\rho_z$ are given by Eqs. (6.111) and (6.112). The strain–force relationships are (see Eq. 6.90)

$$\begin{Bmatrix} \epsilon_\xi^o \\ \epsilon_\eta^o \\ \gamma_{\xi\eta}^o \\ \kappa_\xi \\ \kappa_\eta \\ \kappa_{\xi\eta} \end{Bmatrix} = \begin{bmatrix} \alpha_{11} & \beta_{11} \\ \alpha_{12} & \beta_{21} \\ 0 & 0 \\ \beta_{11} & \delta_{11} \\ \beta_{12} & \delta_{12} \\ 0 & 0 \end{bmatrix} \begin{Bmatrix} N_\xi \\ M_\xi \end{Bmatrix}. \tag{6.120}$$

By applying the results of the laminate plate theory (see Eq. 3.7), we obtain the following expression for the strains in each ply:

$$\begin{Bmatrix} \epsilon_\xi \\ \epsilon_\eta \\ \gamma_{\xi\eta} \end{Bmatrix} = \begin{Bmatrix} \epsilon_\xi^o \\ \epsilon_\eta^o \\ \gamma_{\xi\eta}^o \end{Bmatrix} + \zeta \begin{Bmatrix} \kappa_\xi \\ \kappa_\eta \\ \kappa_{\xi\eta} \end{Bmatrix}. \tag{6.121}$$

The stresses from Eq. (3.11) are (orthotropic laminate, $\overline{Q}_{16} = \overline{Q}_{26} = 0$)

$$\begin{Bmatrix} \sigma_\xi \\ \sigma_\eta \\ \tau_{\xi\eta} \end{Bmatrix} = \begin{bmatrix} \overline{Q}_{11} & \overline{Q}_{12} & 0 \\ \overline{Q}_{21} & \overline{Q}_{22} & 0 \\ 0 & 0 & \overline{Q}_{66} \end{bmatrix} \begin{Bmatrix} \epsilon_\xi \\ \epsilon_\eta \\ \gamma_{\xi\eta} \end{Bmatrix}. \tag{6.122}$$

Equation (6.120) shows that $\gamma_{\xi\eta}^o$ and $\kappa_{\xi\eta}$ are zero. Consequently, $\gamma_{\xi\eta}$ (Eq. 6.121) is also zero, and the ply shear stress $\tau_{\xi\eta}$ (Eq. 6.122) is zero.

Orthotropic and symmetrical layup (arbitrary cross section). The layup of the wall is orthotropic and symmetrical. For orthotropic layup, the following forces and moments are zero (Eqs. 6.88 and 6.92):

$$N_\eta = N_{\xi\eta} = M_\eta = M_{\xi\eta} = 0. \tag{6.123}$$

The axial force N_ξ and the moment M_ξ (per unit length) in the wall are (see Table 6.2, page 222)

$$N_\xi = \frac{1}{a_{11}}\epsilon_\xi^o \qquad M_\xi = \frac{1}{d_{11}}\kappa_\xi. \tag{6.124}$$

Equations (6.110), (6.113), (6.114), and (6.124) yield

$$N_\xi = \frac{1}{\rho_y} z \frac{1}{a_{11}} + \frac{1}{\rho_z} y \frac{1}{a_{11}} + \frac{\widehat{N}}{\widehat{EA}} \frac{1}{a_{11}} \tag{6.125}$$

$$M_\xi = \frac{1}{\rho_y} \cos\alpha \frac{1}{d_{11}} - \frac{1}{\rho_z} \sin\alpha \frac{1}{d_{11}}. \tag{6.126}$$

For orthotropic and symmetrical layup the elements of the $[\alpha]$ and $[\delta]$ matrices are $\alpha_{ij} = a_{ij}, \delta_{ij} = d_{ij}$, whereas $\beta_{ij} = 0$. Thus, the strain–force relationships (Eqs. 6.90 and 3.28) give

$$\begin{Bmatrix} \epsilon_\xi^o \\ \epsilon_\eta^o \\ \gamma_{\xi\eta}^o \\ \kappa_\xi \\ \kappa_\eta \\ \kappa_{\xi\eta} \end{Bmatrix} = \begin{bmatrix} a_{11} & 0 \\ a_{12} & 0 \\ 0 & 0 \\ 0 & d_{11} \\ 0 & d_{12} \\ 0 & 0 \end{bmatrix} \begin{Bmatrix} N_\xi \\ M_\xi \end{Bmatrix}. \tag{6.127}$$

The ply strains and stresses are given by Eqs. (6.121) and (6.122).

Arbitrary layup (symmetrical cross section). The layup of the wall is arbitrary, and the cross section is symmetrical about the z-axis. The loads are applied in the x–z symmetry plane. Such a beam bends only about the y-axis. Correspondingly, $1/\rho_z$ is zero and we have (Eq. 6.6)

$$\epsilon_x^o = \frac{\widehat{N}}{\widehat{EA}} \qquad \frac{1}{\rho_y} = \frac{\widehat{M}_y}{\widehat{EI}_{yy}} \qquad \frac{1}{\rho_z} = 0. \tag{6.128}$$

With these substitutions, Eqs. (6.113) and (6.114) simplify to

$$\epsilon_\xi^o = \epsilon_x^o + z\frac{1}{\rho_y} \qquad \kappa_\xi = \frac{1}{\rho_y}\cos\alpha. \tag{6.129}$$

In the walls of an open cross-section beam, the following forces and moment are zero (see Eq. 6.88):

$$N_\eta = N_{\xi\eta} = M_\eta = 0. \tag{6.130}$$

The axial force N_ξ and the moments M_ξ and $M_{\xi\eta}$ (per unit length) inside the wall are (Table 6.2, page 222)

$$N_\xi = \frac{\overline{\delta}_{11}}{\overline{\overline{D}}}\epsilon_\xi^o - \frac{\overline{\beta}_{11}}{\overline{\overline{D}}}\kappa_\xi \tag{6.131}$$

$$M_\xi = -\frac{\overline{\beta}_{11}}{\overline{\overline{D}}}\epsilon_\xi^o + \frac{\overline{\alpha}_{11}}{\overline{\overline{D}}}\kappa_\xi \tag{6.132}$$

$$M_{\xi\eta} = -\frac{\beta_{16}}{\delta_{66}}N_\xi - \frac{\delta_{16}}{\delta_{66}}M_\xi. \tag{6.133}$$

Equations (6.128)–(6.133) may be rearranged to yield the axial force N_ξ and the moment M_ξ (per unit length) in terms of applied force and moment:

$$N_\xi = \frac{\widehat{M}_y}{\widehat{EI}_{yy}}\left(z\frac{\overline{\delta}_{11}}{\overline{\overline{D}}} - \cos\alpha\frac{\overline{\beta}_{11}}{\overline{\overline{D}}}\right) + \frac{\widehat{N}}{\widehat{EA}}\frac{\overline{\delta}_{11}}{\overline{\overline{D}}} \tag{6.134}$$

$$M_\xi = \frac{\widehat{M}_y}{\widehat{EI}_{yy}}\left(-z\frac{\overline{\beta}_{11}}{\overline{\overline{D}}} + \cos\alpha\frac{\overline{\alpha}_{11}}{\overline{\overline{D}}}\right) - \frac{\widehat{N}}{\widehat{EA}}\frac{\overline{\beta}_{11}}{\overline{\overline{D}}}. \tag{6.135}$$

The strain–force relationships in the x, y, z coordinate system are given by Eq. (3.22). We apply this equation in the ξ, η, ζ coordinate system with $N_\eta = N_{\xi\eta} = M_\eta = 0$. Thus, we write

$$\begin{Bmatrix} \epsilon_\xi^o \\ \epsilon_\eta^o \\ \gamma_{\xi\eta}^o \\ \kappa_\xi \\ \kappa_\eta \\ \kappa_{\xi\eta} \end{Bmatrix} = \begin{bmatrix} \alpha_{11} & \beta_{11} & \beta_{16} \\ \alpha_{12} & \beta_{21} & \beta_{26} \\ \alpha_{16} & \beta_{61} & \beta_{66} \\ \beta_{11} & \delta_{11} & \delta_{16} \\ \beta_{12} & \delta_{12} & \delta_{26} \\ \beta_{16} & \delta_{16} & \delta_{66} \end{bmatrix} \begin{Bmatrix} N_\xi \\ M_\xi \\ M_{\xi\eta} \end{Bmatrix}. \tag{6.136}$$

The ply strains are calculated by Eqs. (6.121). The ply stresses are (Eq. 3.11)

$$\begin{Bmatrix} \sigma_\xi \\ \sigma_\eta \\ \tau_{\xi\eta} \end{Bmatrix} = \begin{bmatrix} \overline{Q}_{11} & \overline{Q}_{12} & \overline{Q}_{16} \\ \overline{Q}_{21} & \overline{Q}_{22} & \overline{Q}_{26} \\ \overline{Q}_{61} & \overline{Q}_{62} & \overline{Q}_{66} \end{bmatrix} \begin{Bmatrix} \epsilon_\xi \\ \epsilon_\eta \\ \gamma_{\xi\eta} \end{Bmatrix}. \tag{6.137}$$

The elements of matrix $[\overline{Q}]$ are evaluated in the ξ, η, ζ coordinate system.

6.2 Example. *An $L = 0.6$-m-long T-section beam with the cross section shown in Figure 6.29 is made of graphite epoxy. The material properties are given in Table 3.6 (page 81). The layup is $[\pm 45_2^f/0_{12}/\pm 45_2^f]$. The beam is built-in at both ends. The beam is subjected to a uniformly distributed load ($p = -1\,500$ N/m) acting in the plane of symmetry. Calculate the maximum deflection and the ply stresses and strains.*

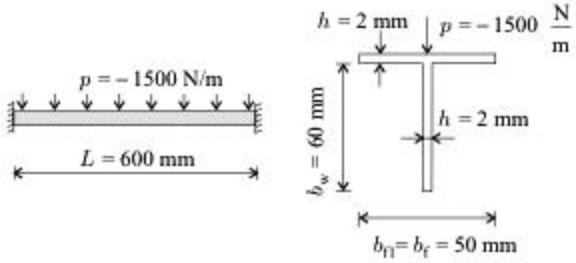

Figure 6.29: The T-beam in Example 6.2.

Solution. From Table A.2, with b_{f2} set equal to zero, the tensile stiffness and the location of the centroid are

$$\begin{aligned} \widehat{EA} &= \frac{b_{f1}}{(\alpha_{11})_{f1}} + \frac{b_w}{(a_{11})_w} = 21.22 \times 10^6 \text{ N} \\ z_c &= \frac{1}{\widehat{EA}} \left(\frac{b_{f1}}{(\alpha_{11})_{f1}} d + \frac{b_w}{(a_{11})_w} \frac{b_w}{2} \right) = 0.0441 \text{ m}. \end{aligned} \tag{6.138}$$

For symmetrical layup (which is the case here), α_{11} is replaced by a_{11}. The element a_{11} for both the web and the flange is $(a_{11})_w = (a_{11})_{f1} = 5.18 \times 10^{-9} \frac{\text{m}}{\text{N}}$ (Table 3.8, page 85). The dimensions $b_{f1} = b_f = 0.05$ m, $b_w = 0.06$ m, and $d = 0.061$ m are shown in Figures 6.29 and 6.30. Setting b_{f2} equal to zero in the expression given in Table A.2 results in the following bending stiffness:

$$\widehat{EI}_{yy} = \frac{b_{f1}}{(\alpha_{11})_{f1}} (d - z_c)^2 + \frac{b_{f1}}{(\delta_{11})_{f1}} + \frac{1}{(a_{11})_w} \left(\frac{b_{w1}^3 + b_{w2}^3}{3} \right). \tag{6.139}$$

For symmetrical layup (which is the case here) δ_{11} is replaced by d_{11}. The element d_{11} for both the web and the flange is $(d_{11})_w = (d_{11})_{f1} = 33.10 \times 10^{-3} \frac{1}{\text{N} \cdot \text{m}}$ (Table 3.8, page 85). Equation (6.139), with $b_{w2} = z_c = 0.0441$ m and $b_{w1} = b_w - z_c = 0.0159$ m, yields

$$\widehat{EI}_{yy} = 8\,530 \text{ N} \cdot \text{m}^2. \tag{6.140}$$

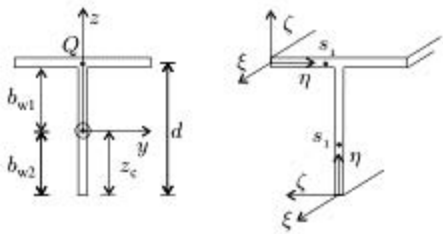

Figure 6.30: The cross section of the beam in Example 6.2.

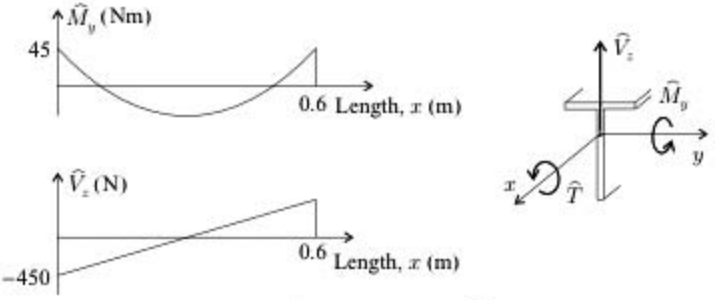

Figure 6.31: Bending moment $\widehat{M}_y$ and shear force $\widehat{V}_z$ for the beam in Example 6.2.

The distributed load is $p = -1\,500$ N/m. The corresponding bending moment $\widehat{M}_y$ and shear force $\widehat{V}_z$ diagrams are given in Fig. 6.31. The maximum values are

$$\widehat{M}_y^{\max} = -\frac{pL^2}{12} = 45\,\mathrm{N\cdot m} \tag{6.141}$$

$$\widehat{V}_z^{\max} = \frac{pL}{2} = -450\,\mathrm{N}.$$

The maximum deflection is (Table 7.3, page 332)

$$\widetilde{w} = \frac{1}{384}\frac{pL^4}{\widehat{E}\widehat{I}_{yy}} = -0.0593 \times 10^{-3}\,\mathrm{m} = -0.0593\,\mathrm{mm}. \tag{6.142}$$

The axial force N_ξ and the moment M_ξ (per unit length) in the wall are (see Eqs. 6.125, 6.126, 6.111, and 6.112)

$$\begin{aligned} N_\xi &= \frac{\widehat{M}_y}{\widehat{E}\widehat{I}_{yy}} z \frac{1}{a_{11}} \\ M_\xi &= \frac{\widehat{M}_y}{\widehat{E}\widehat{I}_{yy}} \cos\alpha \frac{1}{d_{11}}, \end{aligned} \tag{6.143}$$

where z is shown in Figure 6.30 and $\cos\ \alpha$ is zero for the web and $+1$ for the flange. For completeness we also calculate the shear flow, which will be discussed in Section 6.7. The shear flow is (Eq. 6.282)

$$q^{\mathrm{op}}(s_1) = N_{\xi\eta} = -\frac{\widehat{V}_z}{\widehat{E}\widehat{I}_{yy}} \int_0^{s_1} \left(z \frac{1}{a_{11}} \right) d\eta. \tag{6.144}$$

The η coordinate is shown in Figure 6.30. We next determine the forces at point Q, which is at the intersection of the flange and the web ($z = d - z_c$) at the built-in end ($x = 0$, $\widehat{M}_y = \widehat{M}_y^{\max}$, and $\widehat{V}_z = \widehat{V}_z^{\max}$). At point Q the forces and moments are

$$N_\xi = \frac{\widehat{M}_y^{\max}}{\widehat{E}\widehat{I}_{yy}}(d - z_c)\frac{1}{a_{11}} = 17\,209\,\frac{\mathrm{N}}{\mathrm{m}} \qquad M_\xi = \frac{\widehat{M}_y^{\max}}{\widehat{E}\widehat{I}_{yy}}\frac{1}{d_{11}} = 0.1594\,\frac{\mathrm{N\cdot m}}{\mathrm{m}}$$

$$q^{\mathrm{op}} = N_{\xi\eta} = \mp\frac{\widehat{V}_z^{\max}}{\widehat{E}\widehat{I}_{yy}}\frac{b_f}{2}(d - z_c)\frac{1}{a_{11}} = \pm 2\,151\,\frac{\mathrm{N}}{\mathrm{m}}. \tag{6.145}$$

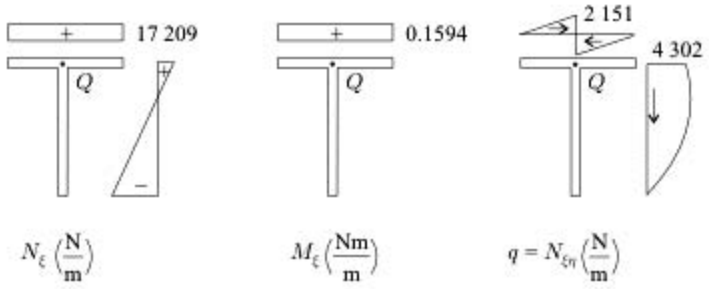

Figure 6.32: The axial force N_ξ, the moment M_ξ, and the shear force $N_{\xi\eta}$ in the flange and the web at the built-in end of the beam in Example 6.2.

The plus and minus values of the shear flow refer to the left and right of Q (Fig. 6.32). We also calculated these forces and moments around the entire cross section at $x = 0$. The results are shown in Figure 6.32.

The relevant elements of the compliance matrices are (Table 3.8, page 85)

$$a_{11} = 5.18 \times 10^{-9}\,\frac{\text{m}}{\text{N}} \qquad a_{12} = -3.52 \times 10^{-9}\,\frac{\text{m}}{\text{N}} \qquad a_{66} = 27.77 \times 10^{-9}\,\frac{\text{m}}{\text{N}}$$

$$d_{11} = 33.10 \times 10^{-3}\,\frac{1}{\text{N}\cdot\text{m}} \qquad d_{12} = -25.59 \times 10^{-3}\,\frac{1}{\text{N}\cdot\text{m}} \qquad d_{66} = 48.51 \times 10^{-3}\,\frac{1}{\text{N}\cdot\text{m}}.$$

At point Q the strains are calculated by the strain–force relationships (see Eq. 6.90 with α replaced by a, δ replaced by d, and β is zero)

$$\begin{Bmatrix} \epsilon_\xi^o \\ \epsilon_\eta^o \\ \gamma_{\xi\eta}^o \\ \kappa_\xi \\ \kappa_\eta \\ \kappa_{\xi\eta} \end{Bmatrix} = \begin{bmatrix} a_{11} & 0 & 0 \\ a_{12} & 0 & 0 \\ 0 & a_{66} & 0 \\ 0 & 0 & d_{11} \\ 0 & 0 & d_{12} \\ 0 & 0 & 0 \end{bmatrix} \begin{Bmatrix} N_\xi \\ N_{\xi\eta} \\ M_\xi \end{Bmatrix} = \begin{Bmatrix} 0.000\,0892 \\ -0.000\,0606 \\ -0.000\,0597 \\ 0.005\,28 \\ -0.004\,08 \\ 0 \end{Bmatrix}, \tag{6.146}$$

where κ_ξ, κ_η, and $\kappa_{\xi\eta}$ are in 1/m. With the preceding strains, the ply stresses are calculated by Eqs. (6.121) and (6.122). The results are given in Figure 6.33.

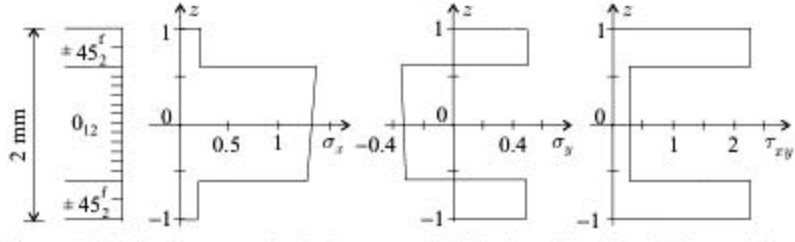

Figure 6.33: The ply stresses in the beam at the built-in end just left of the vertical symmetry axis of the flange in Example 6.2. The unit of the stresses is 10^6 N/m^2. (Just to the right of the symmetry axis, τ_{xy} is negative.)

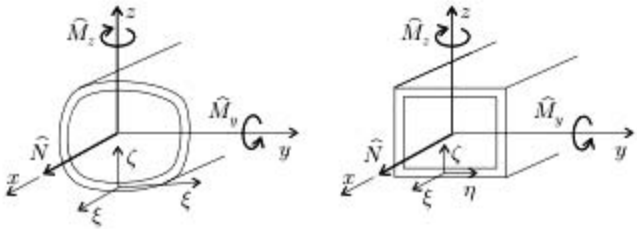

Figure 6.34: Thin-walled, closed section beams with curved and straight wall segments subjected to axial load and bending moments.

6.4 Thin-Walled, Closed-Section Orthotropic Beams Subjected to Axial Load and Bending

In this section we treat thin-walled, closed-section beams subjected to axial load and bending. The beam may consist of flat and curved walls (Fig. 6.34). The beams are subjected to an axial force $\widehat{N}$ and to bending moments $\widehat{M}_y$, $\widehat{M}_z$.

Two types of beams are considered:

1. The layup of the wall is orthotropic and symmetrical; the beam's cross section is arbitrary.
2. The layup of the wall is orthotropic but unsymmetrical; the beam's cross section is arbitrary.

There are no tension–bending–torsion couplings in either of the latter types of beams because the beam is orthotropic (page 207).

We define a ξ–η–ζ coordinate system along the wall. At each point ξ is parallel to the x coordinate, η is along the circumference of the wall, and ζ is perpendicular to the wall (Fig. 6.34). The origin of this coordinate system is in an arbitrarily chosen reference surface.

Displacements – symmetrical layup. The layup of the wall is orthotropic and symmetrical. Under the action of the applied loads $\widehat{N}$, $\widehat{M}_y$, and $\widehat{M}_z$, the shape of the cross section changes. To examine the change in shape we first look at an isotropic beam. The changed shape of the cross section of a solid isotropic beam is shown in Figure 6.35. The changed shape of a thin-walled isotropic beam is the same as that of a solid beam with the same initial cross section. There is only axial stress in the beam, and therefore, the cross-sectional shape would not be altered if the beam were cut.

A thin-walled composite beam with orthotropic and symmetrical layup behaves similarly to an isotropic beam, namely, under the actions of an axial load and bending the change in shape of the cross section of a closed-section beam is nearly the same as the change in shape of the cross section of an open-section beam (Fig. 6.36, middle). This implies that closed-section beams respond to the applied loads in much the same way as open-section beams. Therefore, we may treat thin-walled, closed-section beams with orthotropic and symmetrical layup

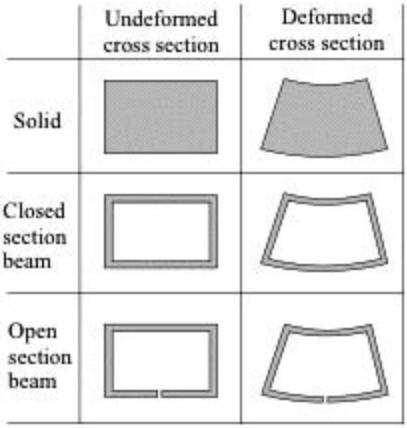

Figure 6.35: The changes of the cross sections of solid and thin-walled open- and closed-section isotropic beams subjected to axial load and bending.

in the same way as we treat open-section beams and calculate the displacements with the replacement stiffnesses given in Table 6.3 (page 231).

Displacements – unsymmetrical layup. The layup of the wall is orthotropic but unsymmetrical. When such a beam is subjected to loads $\widehat{N}$, $\widehat{M}_y$, and $\widehat{M}_z$, the shape of the cross sections changes significantly, as shown in Figure 6.36. In this case we can no longer approximate closed-section beams as open-section beams. An open-section beam would "open up" under the axial load and bending, as shown in Figure 6.36 (right). Similarly, if a closed section beam were cut, the two cut edges would move relative to each other, as shown in Figure 6.37. In a closed-section beam these displacements are prevented by a shear force $N_{\xi\eta}$, a bending moment M_η, a normal force N_η, and a transverse shear force V_η acting along the cut. Since the walls are orthotropic, (a) the beam does not twist ($\kappa_{\xi\eta} = 0$), and (b) the two "cut" edges do not move relative to each other in the axial direction. In the absence of these motions no shear force arises along the cut ($N_{\xi\eta} = 0$). The forces N_η and V_η are generally small and can be neglected ($N_\eta = 0$, $V_\eta = 0$). Thus,

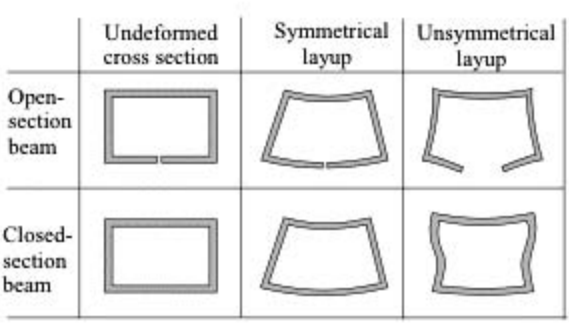

Figure 6.36: The changes of the cross sections of thin-walled open- and closed-section composite beams subjected to axial load and bending.

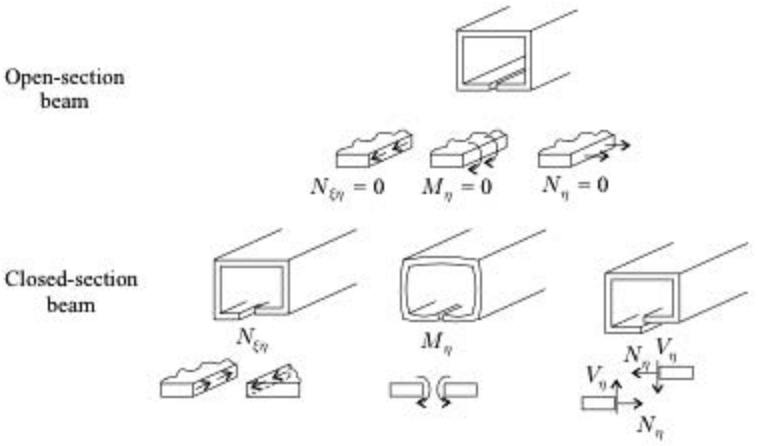

Figure 6.37: The forces along the lengthwise edges of an open-section beam (top) and along the cut of a closed-section beam (bottom).

in the case of orthotropic walls we have

$$\begin{aligned} N_\eta &= N_{\xi\eta} = 0 \\ \kappa_{\xi\eta} &= 0 \qquad\qquad \text{closed-section.} \\ V_\eta &= 0 \end{aligned} \tag{6.147}$$

There is a bending moment M_η along the cut that prevents rotation of the edges relative to each other. The slope of the wall must be the same to the left and to the right of the cut (Figure 6.38)

$$\left.\frac{\partial w^o}{\partial \eta}\right|_{\text{right}} = \left.\frac{\partial w^o}{\partial \eta}\right|_{\text{left}}, \tag{6.148}$$

where w^o is the displacement of the wall perpendicular to its reference surface. The change in curvature of the wall is

$$\kappa_\eta = -\frac{\partial^2 w^o}{\partial \eta^2}. \tag{6.149}$$

By integrating this equation from an arbitrary point $\eta = 0$ to s_1, we have

$$\int_0^{s_1} \kappa_\eta d\eta = -\left[\frac{\partial w^o}{\partial \eta}\right]_0^{s_1}. \tag{6.150}$$

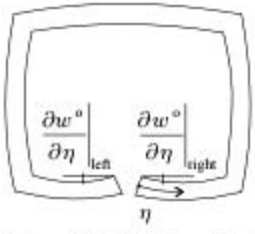

Figure 6.38: Relative rotation of the cut edges.

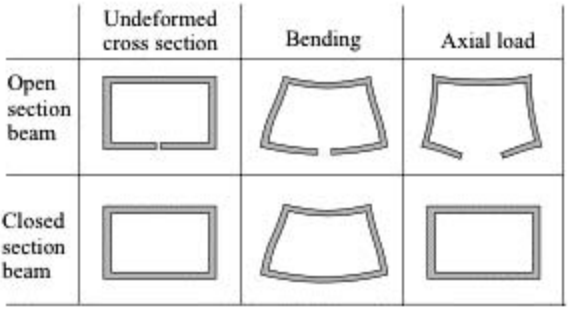

Figure 6.39: The changes of the cross sections of thin-walled open- and closed-section beams subjected to axial load and bending. Each wall has the same othotropic unsymmetrical layup.

By performing the integration along the entire circumference ($s_1 = S$), we obtain (see Eq. 6.148)

$$\int_0^S \kappa_\eta d\eta = \oint \kappa_\eta d\eta = -\left.\frac{\partial w^o}{\partial \eta}\right|_{\text{right}} + \left.\frac{\partial w^o}{\partial \eta}\right|_{\text{left}} = 0. \tag{6.151}$$

This compatibility condition must be enforced for closed-section beams. An analysis that takes this condition into account is presented in Section 6.6. This exact analysis is complex. In the next paragraph we present a simpler way to determine the replacement stiffnesses when the layup is the same around the circumference.

To establish the bending replacement stiffnesses, we observe that bending the cross-sectional shape of a closed cross-section beam with uniform layup around the circumference is similar to the shape of an open-section beam (Fig. 6.39). In this case the replacement stiffnesses $\widehat{EI}_{yy}$, $\widehat{EI}_{zz}$, and $\widehat{EI}_{yz}$ may be approximated by the expressions obtained for open-section beams (Tables 6.4 and 6.7, pages 232 and 235).

To establish the tensile replacement stiffness, we observe that the beam with uniform layup does not deform under tension (Fig. 6.39). In this case the change in curvature is zero along the circumference

$$\kappa_\eta \approx 0 \qquad \begin{matrix}\text{closed-section} \\ \text{in tension.}\end{matrix} \tag{6.152}$$

By substituting Eqs. (6.147) and (6.152) into Eq. (6.90), after algebraic manipulations, we obtain

$$N_\xi = \left(\frac{\widehat{\delta}_{11}}{\widehat{D}}\right)\epsilon_\xi^o - \left(\frac{\widehat{\beta}_{11}}{\widehat{D}}\right)\kappa_\xi \tag{6.153}$$

$$M_\xi = -\left(\frac{\widehat{\beta}_{11}}{\widehat{D}}\right)\epsilon_\xi^o + \left(\frac{\widehat{\alpha}_{11}}{\widehat{D}}\right)\kappa_\xi \tag{6.154}$$

$$M_\eta = -\frac{\beta_{12}}{\delta_{22}}N_\xi - \frac{\delta_{12}}{\delta_{22}}M_\xi, \tag{6.155}$$

where $\widehat{\alpha}_{11}$, $\widehat{\beta}_{11}$, $\widehat{\delta}_{11}$, and $\widehat{D}$ are defined as

$$\widehat{\alpha}_{11} = \left(\alpha_{11} - \frac{\beta_{12}^2}{\delta_{22}}\right) \qquad \widehat{\beta}_{11} = \left(\beta_{11} - \frac{\beta_{12}\delta_{12}}{\delta_{22}}\right) \tag{6.156}$$

$$\widehat{\delta}_{11} = \left(\delta_{11} - \frac{\delta_{12}^2}{\delta_{22}}\right) \qquad \widehat{D} = \widehat{\alpha}_{11}\widehat{\delta}_{11} - \widehat{\beta}_{11}^2. \tag{6.157}$$

By comparing Eq. (6.153) with the expression for N_ξ given for open-section beams in Table 6.2 (page 222), we see that they differ only by the terms in the brackets. Therefore, the tensile stiffness $\widehat{EA}$ of thin-walled closed-section beams (orthotropic but unsymmetrical layup) may be calculated from the expressions of open-section beams (Tables 6.4 and 6.7, pages 232 and 235) by replacing δ_{11}, D by $\widehat{\delta}_{11}$, $\widehat{D}$.

The W_{11}, W_{22}, $W_{23}(= W_{32})$, W_{33} elements of the compliance matrix are then determined by substituting the replacement stiffnesses (given in Tables 6.4 and 6.7) into Eq. (6.19).

The expressions for $\widehat{EA}$, $\widehat{EI}_{yy}$, $\widehat{EI}_{zz}$, and $\widehat{EI}_{yz}$ in Tables 6.4 and 6.7 are also reasonable approximations when the layup is not uniform but the wall is "thin."

Stresses and strains. As with displacements, the stresses and strains in closed-section beams with orthotropic and symmetrical layup can be calculated by the same expressions used for the stresses and strains in open-section beams (see Section 6.3.4, orthotropic and symmetrical layup).

When a closed-section beam with orthotropic but unsymmetrical layup is in bending, the stresses and strains can be calculated by the same expressions used for the stresses and strains in open-section beams (see Section 6.3.4, orthotropic layup, arbitrary cross section).

When a closed-section beam with orthotropic but unsymmetrical layup is in tension, we determine the stresses and strains as follows. At an arbitrary point on the reference surface of the wall the axial strain is related to the strain of the beam's axis by (Eq. 6.113) as follows:

$$\epsilon_\xi^o = \epsilon_x^o. \tag{6.158}$$

When the layup of the wall is orthotropic, $N_\eta = N_{\xi\eta} = M_{\xi\eta} = 0$, and the axial force and the moment (per unit length) in the wall are given by Eqs. (6.153) and (6.154). Thus, we have

$$N_\xi = \frac{\widehat{N}}{\widehat{EA}}\frac{\widehat{\delta}_{11}}{\widehat{D}} \qquad M_\xi = -\frac{\widehat{N}}{\widehat{EA}}\frac{\widehat{\beta}_{11}}{\widehat{D}}. \tag{6.159}$$

The strain–force relationships (see Eq. 6.90) give the strains

$$\begin{Bmatrix} \epsilon_\xi^o \\ \epsilon_\eta^o \\ \gamma_{\xi\eta}^o \\ \kappa_\xi \\ \kappa_\eta \\ \kappa_{\xi\eta} \end{Bmatrix} = \begin{bmatrix} \alpha_{11} & \beta_{11} & \beta_{12} \\ \alpha_{12} & \beta_{21} & \beta_{22} \\ 0 & 0 & 0 \\ \beta_{11} & \delta_{11} & \delta_{12} \\ \beta_{12} & \delta_{12} & \delta_{22} \\ 0 & 0 & 0 \end{bmatrix} \begin{Bmatrix} N_\xi \\ M_\xi \\ M_\eta \end{Bmatrix}, \tag{6.160}$$

where M_η is given by Eq. (6.155).

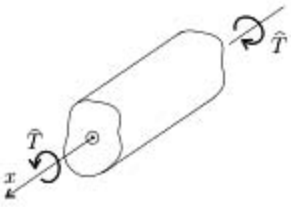

Figure 6.40: Beam subjected to torque $\hat{T}$.

The strains and stresses inside the wall (orthotropic, unsymmetrical layup) are calculated by Eqs. (6.121) and (6.137).

6.5 Torsion of Thin-Walled Beams

We consider thin-walled, open- and closed-section beams subjected to pure torque (Fig. 6.40). Because of the torque, the beam twists about an axis that passes through the center of twist. When the beam is isotropic, the twist axis remains straight. For a composite beam the twist axis becomes curved, except when the beam is orthotropic.

The stresses differ in thin-walled isotropic and composite beams. Under the action of pure torque there are only shear stresses inside the wall of an isotropic beam, whereas there are also normal stresses inside the wall of a composite beam.

Under the action of the torque, each cross section rotates (twists) as a rigid body in its own plane about the center of twist. In addition, the cross sections suffer warping displacements normal to their (cross-sectional) planes. We are interested in the twist, the warping displacements, and the stresses inside the walls.

Stiffness and rate of twist. Under the action of pure torsion (no axial constraint), the rate of twist of an isotropic beam is (Eq. 6.4)

$$\vartheta = \frac{\hat{T}}{GI_t} \qquad \text{isotropic.} \tag{6.161}$$

Similarly, for a composite beam we write

$$\vartheta = \frac{\hat{T}}{\widehat{GI}_t} \qquad \text{composite.} \tag{6.162}$$

With these definitions the rate of twist of composite beams can be obtained by replacing the stiffnesses GI_t by $\widehat{GI}_t$ in the expressions for the torsion of isotropic beams. In the following we obtain expressions for $\widehat{GI}_t$.

6.5.1 Thin Rectangular Cross Section

We consider a solid, rectangular, thin beam (Fig. 6.41). The layup of the beam is arbitrary. The width of the beam b is large compared with its thickness h ($b >> h$). The applied torque gives rise to shear stresses in the beam that may be represented by a resultant shear flow q, the unit of which is force per length. This induced shear

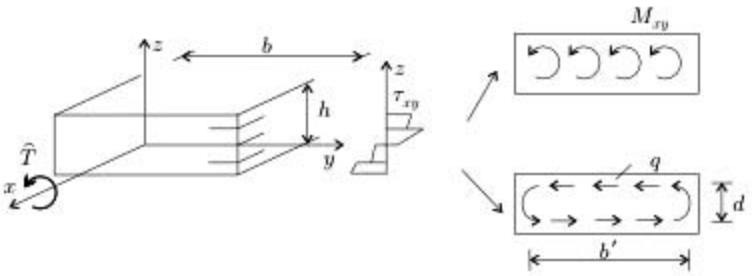

Figure 6.41: The shear stress distribution, the twist moment, and the shear flow in a solid thin beam under torsion.

equilibrates the applied torque (Fig. 6.41),

$$\widehat{T} = (qd)b' + (qb')d, \tag{6.163}$$

where d and b' are the length and width of the path of the resultant shear flow. The latter is taken to be approximately equal to the width of the beam ($b' \approx b$). The twist moment M_{xy} (per unit length) in the cross section is

$$M_{xy} = -qd. \tag{6.164}$$

Equations (6.163) and (6.164), with the approximation $b' = b$, yield

$$\widehat{T} = -2bM_{xy}. \tag{6.165}$$

When the beam is treated as a plate, the out-of-plane curvature κ_{xy} is (see Eqs. 3.22)

$$\kappa_{xy} = \delta_{66} M_{xy}. \tag{6.166}$$

The rate of twist ϑ is (Eq. 6.27)

$$\vartheta = \frac{\partial \psi}{\partial x} = -\frac{1}{2}\kappa_{xy}. \tag{6.167}$$

By combining Eqs. (6.166), (6.167), and (6.165), we obtain the rate of twist

$$\vartheta = \frac{\delta_{66}}{4b}\widehat{T}, \tag{6.168}$$

where δ_{66} is evaluated at an arbitrarily chosen reference plane. By comparing Eqs. (6.162) and (6.168), we see that the torsional stiffness of a flat thin-walled beam is

$$\widehat{GI}_t = \frac{4b}{\delta_{66}}. \tag{6.169}$$

For a thin-walled isotropic beam, $\delta_{66} = d_{66} = 12/Gh^3$ (Eq. 3.43), and the torsional stiffness in Eq. (6.169) becomes $\widehat{GI}_t = GI_t = G\frac{bh^3}{3}$.

When the wall is not flat but is curved, the torsional stiffness may be approximated by

$$\widehat{GI}_t = 4 \int_0^S \frac{1}{\delta_{66}} d\eta, \tag{6.170}$$

where η is the coordinate along the circumference of the wall and S is the length of the entire circumference.

Although the beam is subjected to pure torque, there are axial ϵ_x^o and shear strains γ_{xy}^o, and there is a change in the curvature κ_x given by (see Eq. 3.22)

$$\begin{Bmatrix} \epsilon_x^o \\ \gamma_{xy}^o \\ \kappa_x \end{Bmatrix} = \begin{bmatrix} \beta_{16} \\ \beta_{66} \\ \delta_{16} \end{bmatrix} M_{xy}. \tag{6.171}$$

This equation together with Eq. (6.165) yields

$$\begin{Bmatrix} \epsilon_x^o \\ \gamma_{xy}^o \\ \kappa_x \end{Bmatrix} = - \begin{bmatrix} \beta_{16} \\ \beta_{66} \\ \delta_{16} \end{bmatrix} \frac{\widehat{T}}{2b}. \tag{6.172}$$

To determine W_{14}, W_{24}, and W_{44} elements of the compliance matrix, we rearrange Eqs. (6.168) and (6.172) in the form

$$\begin{Bmatrix} \epsilon_x^o \\ \kappa_x = 1/\rho_y \\ \vartheta \end{Bmatrix} = \begin{Bmatrix} -\frac{1}{2b}\beta_{16} \\ -\frac{1}{2b}\delta_{16} \\ \frac{\delta_{66}}{4b} \end{Bmatrix} \widehat{T}. \tag{6.173}$$

By comparing this equation with Eq. (6.17), we see that the terms in brackets are the $W_{14}(= -\beta_{16}/2b)$, $W_{24}(= -\delta_{16}/2b)$, and $W_{44}(= \delta_{66}/4b)$ elements of the compliance matrix.

When the layup is symmetrical, β_{66} is zero and there is no shear strain. When the layup is orthotropic, β_{16} and δ_{16} are zero, and there is neither axial strain nor a change in curvature. When the layup is both orthotropic and symmetrical, there are neither axial nor shear strains and there is no change in curvature.

6.5.2 Open-Section Orthotropic Beams

The wall of an open-section beam may be considered to consist of thin wall segments (Fig. 6.27). The torsional stiffness of a thin-walled, open-section isotropic beam may be approximated by

$$GI_t = (GI_t)_1 + (GI_t)_2 + \ldots + (GI_t)_K, \tag{6.174}$$

where the subscript refers to the kth segment. Similarly, we approximate the torsional stiffness of a composite beam with orthotropic walls by

$$\widehat{GI}_t = (\widehat{GI}_t)_1 + (\widehat{GI}_t)_2 + \ldots + (\widehat{GI}_t)_K \tag{6.175}$$

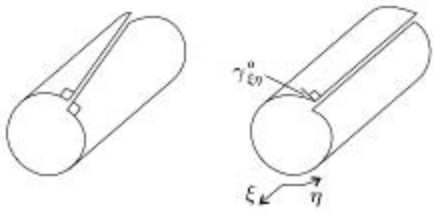

Figure 6.42: Warping of an open-section composite beam due to torsion and due to shear strain.

For flat and curved segments, $(\widehat{GI}_t)_k$ are given by Eqs. (6.169) and (6.170).

The rate of twist is calculated by

$$\vartheta = \frac{\widehat{T}}{\widehat{GI}_t}. \tag{6.176}$$

Stresses and strains. In each wall segment we employ a ξ–η–ζ coordinate system. The origin of each coordinate system is at the wall segment's reference surface. The out-of-plane curvature of each wall segment is obtained from Eq. (6.167) by replacing x and y by ξ and η as follows:

$$\kappa_{\xi\eta} = -2\vartheta. \tag{6.177}$$

We consider only $M_{\xi\eta}$ resulting from the torque. Thus we have (see Eq. 6.90)

$$\gamma^o_{\xi\eta} = \beta_{66} M_{\xi\eta} \qquad \kappa_{\xi\eta} = \delta_{66} M_{\xi\eta} \tag{6.178}$$

$$\epsilon^o_\xi = \epsilon^o_\eta = \kappa_\xi = \kappa_\eta = 0. \tag{6.179}$$

Equations (6.178) and (6.177) give

$$M_{\xi\eta} = \frac{1}{\delta_{66}}\kappa_{\xi\eta} = -\frac{2}{\delta_{66}}\vartheta. \tag{6.180}$$

Equations (6.121) and (6.122) together with Eq. (6.179) yield the strains and stresses

$$\begin{Bmatrix} \epsilon_\xi \\ \epsilon_\eta \\ \gamma_{\xi\eta} \end{Bmatrix} = \begin{Bmatrix} 0 \\ 0 \\ \gamma^o_{\xi\eta} \end{Bmatrix} + \zeta \begin{Bmatrix} 0 \\ 0 \\ \kappa_{\xi\eta} \end{Bmatrix} \tag{6.181}$$

$$\begin{Bmatrix} \sigma_\xi \\ \sigma_\eta \\ \tau_{\xi\eta} \end{Bmatrix} = \begin{bmatrix} 0 \\ 0 \\ \overline{Q}_{66} \end{bmatrix} \gamma_{\xi\eta}. \tag{6.182}$$

Warping. A thin-walled, open-section beam warps when subjected to a pure torque. Under torsion the wall of a beam (no shear deformation) warps, as shown in Figure 6.42, (left). The axial displacement u relative to an arbitrarily chosen reference point ($\eta = 0$) is[6]

$$u(s_1) - u(0) = -2A_{s_1}\vartheta, \tag{6.183}$$

[6] T. H. G. Megson, *Aircraft Structures for Engineering Students*. 3rd edition. Halsted Press, John Wiley & Sons, New York, 1999, p. 318.

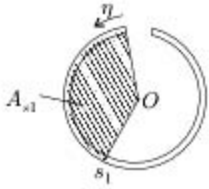

Figure 6.43: The swept area.

where ϑ is the rate of twist, and A_{s_1} is the swept area from $\eta = 0$ to $\eta = s_1$ (Fig. 6.43) about the center of twist (point O). For thin-walled beams the center of twist and the shear center coincide. The shear center is defined such that a transverse load acting at the shear center of an orthotropic beam does not cause twist (see Section 6.7.3).

When there is no shear strain the angle between the circumferential and the longitudinal edges remains 90 degrees (Fig. 6.42). For a composite beam the shear strain is zero when β_{66} is zero (see Eq. 6.178). When β_{66} is not zero the originally 90-degree angle between the circumferential and the longitudinal edges becomes $90^\circ + \gamma^\circ_{\xi\eta}$. This change in angle introduces the additional axial displacement along the circumference

$$u(s_1) - u(0) = \int_0^{s_1} \gamma^\circ_{\xi\eta} d\eta. \tag{6.184}$$

The total relative axial displacement (warping) is (see Eqs. 6.183 and 6.184)

$$\Delta u = u(s_1) - u(0) = -2A_{s_1}\vartheta + \int_0^{s_1} \gamma^\circ_{\xi\eta} d\eta. \tag{6.185}$$

For a thin-walled, open-section beam with orthotropic layup $\gamma^\circ_{\xi\eta}$ is given by Eq. (6.178).

When the layup of each wall segment is symmetrical, $\gamma^\circ_{\xi\eta}$ is zero, and such composite beams warp similarly to that of isotropic beams.

6.5.3 Closed-Section Orthotropic Beams – Single Cell

For a thin-walled, closed-section beam, the points $\eta = 0$ and $\eta = S$ coincide (Fig. 6.44), and thus the warping is

$$\Delta u = u(0) - u(S) = 0, \tag{6.186}$$

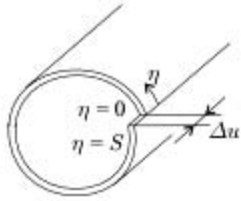

Figure 6.44: The relative displacement at the "cut" of a closed-section beam subjected to pure torque.

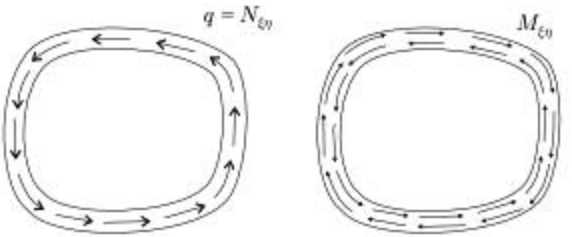

Figure 6.45: The torque carried by $N_{\xi\eta}$ and by $M_{\xi\eta}$.

where S is the length of the circumference. By employing Eq. (6.185), we write

$$\Delta u = -2A\vartheta + \int_0^S \gamma^{\circ}_{\xi\eta} d\eta = -2A\vartheta + \oint \gamma^{\circ}_{\xi\eta} d\eta = 0, \tag{6.187}$$

where A is the enclosed area and $\gamma^{\circ}_{\xi\eta}$ is the shear strain. From this equation the rate of twist is

$$\vartheta = \frac{1}{2A} \oint \gamma^{\circ}_{\xi\eta} d\eta. \tag{6.188}$$

In thin-walled, closed-section beams the torque due to the induced twist moment $M_{\xi\eta}$ is small compared with the torque due to the induced shear force $N_{\xi\eta}$ (Fig. 6.45). In the following we neglect the twist moment $M_{\xi\eta}$.

We introduce the shear flow q defined as the integral of the shear stress across the thickness

$$q = \int_{(h)} \tau_{\xi\eta} d\zeta \equiv N_{\xi\eta}, \tag{6.189}$$

where h is the thickness of the wall. The torque produced by q (or $N_{\xi\eta}$) is (Fig. 6.46)

$$\widehat{T} = \oint qp d\eta = 2Aq, \tag{6.190}$$

where p is the distance between an arbitrary point and the tangent to the wall. Accordingly, the shear flow is

$$q = \frac{\widehat{T}}{2A}. \tag{6.191}$$

Equation (6.191) is the same as the Bredt–Batho formula[7] developed for thin-walled, closed-section isotropic beams.

Equation (6.90) yields

$$\gamma^{\circ}_{\xi\eta} = \alpha_{66} N_{\xi\eta} + \beta_{66} M_{\xi\eta}. \tag{6.192}$$

To simplify this expression we select a reference surface at which β_{66} (denoted by β^{v}_{66}) is zero. The 66 component of the compliance matrix corresponding to this

[7] T. H. G. Megson, *Aircraft Structures for Engineering Students*. 3rd edition. Halsted Press, John Wiley & Sons, New York, 1999, p. 307.

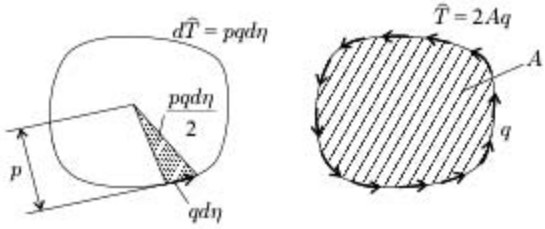

Figure 6.46: The torque carried by the shear flow q.

surface, which we refer to as the "torque neutral" surface, is (Eq. 3.48)

$$\beta_{66}^{\nu} = \beta_{66} + \nu\delta_{66}, \tag{6.193}$$

where β_{66} and δ_{66} are the components of the compliance matrices in the arbitrarily chosen reference surface, and ν is the location of the "torque neutral" surface (Fig. 6.47). For $\beta_{66}^{\nu} = 0$, Eq. (6.193) yields

$$\nu = -\frac{\beta_{66}}{\delta_{66}}. \tag{6.194}$$

By applying Eq. (6.192) at the "torque neutral" surface, we have

$$\gamma_{\xi\eta}^{o} = \alpha_{66}^{\nu} N_{\xi\eta} = \alpha_{66}^{\nu} q, \tag{6.195}$$

where the superscript ν refers to the "torque neutral" surface (Eq. 6.194), and α_{66}^{ν} is given by Eqs. (3.48) and (6.194) as follows:

$$\alpha_{66}^{\nu} = \alpha_{66} + 2\nu\beta_{66} + \nu^2\delta_{66} = \alpha_{66} - \frac{\beta_{66}^2}{\delta_{66}}. \tag{6.196}$$

By combining Eqs. (6.188)–(6.195), we obtain

$$\vartheta = \widehat{T}\frac{1}{4A^2}\oint \alpha_{66}^{\nu} d\eta. \tag{6.197}$$

With reference to Eq. (6.162), we see that the replacement torsional stiffness $\widehat{GI}_t$ is

$$\widehat{GI}_t = \frac{4A^2}{\oint \alpha_{66}^{\nu} d\eta}. \tag{6.198}$$

When the wall's layup is symmetrical, $\alpha_{66}^{\nu} = a_{66}$. For a thin-walled isotropic beam, $\alpha_{66}^{\nu} = a_{66} = 1/Gh$ (Eq. 3.43), and the torsional stiffness (Eq. 6.198) becomes $\widehat{GI}_t = GI_t = G\frac{4A^2}{\oint(1/h)d\eta}$.

The W_{44} element of the compliance matrix is $W_{44} = 1/\widehat{GI}_t$.

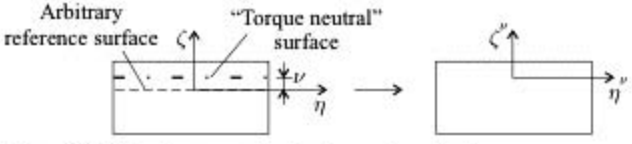

Figure 6.47: The torque neutral surface where $\widetilde{\beta}_{66}^{\nu}$ is zero.

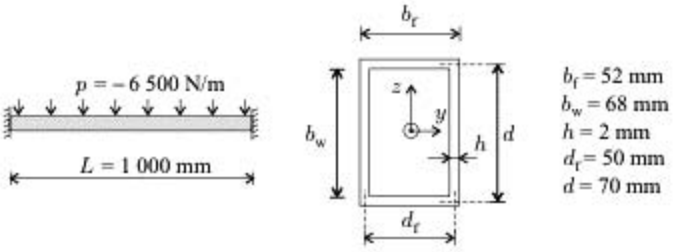

Figure 6.48: The beam in Example. 6.3.

Stresses and strain. The strains and curvature in each ply at the "torque neutral" surface are given by (see Eq. 6.90)

$$\begin{Bmatrix} \epsilon_\xi^o \\ \epsilon_\eta^o \\ \gamma_{\xi\eta}^o \\ \kappa_\xi \\ \kappa_\eta \\ \kappa_{\xi\eta} \end{Bmatrix} = \begin{bmatrix} 0 \\ 0 \\ \alpha_{66}^v \\ 0 \\ 0 \\ 0 \end{bmatrix} N_{\xi\eta}, \tag{6.199}$$

where $N_{\xi\eta} \equiv q$ is the shear flow calculated by Eq. (6.191).

With the preceding strains and curvatures, the stresses are calculated by Eqs. (6.181) and (6.182).

6.3 Example. *An $L = 1.0$-m-long box beam, with the cross section shown in Figure 6.48, is made of graphite epoxy. The material properties are given in Table 3.6 (page 81). The layup is $[\pm 45_2^t/0_{12}/\pm 45_2^t]$. The beam, built-in at each end, is subjected to a uniformly distributed load ($p = -6\,500$ N/m) acting at the midplane of the left web (Fig. 6.49). By neglecting the effects of axial restraint, calculate the maximum deflection and the maximum twist.*

Solution. The cross section is doubly symmetrical, and both the centroid and the shear center (see Section 6.7.3) coincide with the center of the cross section. The

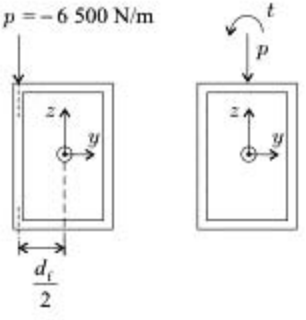

Figure 6.49: Loading on the box beam in Example 6.3 (left), and the loading with respect to the shear center (right).

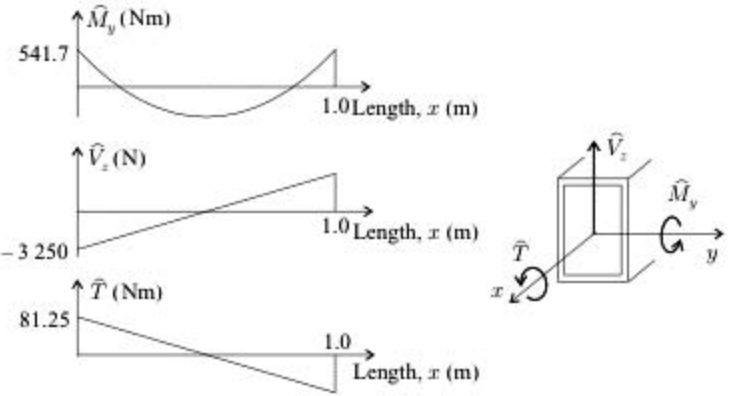

Figure 6.50: The bending moment $\widehat{M}_y$, shear force $\widehat{V}_z$, and torque $\widehat{T}$ diagrams for the beam in Example 6.3.

loads with respect to the shear center are (Fig. 6.49)

$$\begin{aligned} p &= -6\,500\,\frac{\mathrm{N}}{\mathrm{m}} && \text{(distributed load)} \\ t &= -p \times \frac{d_{\mathrm{f}}}{2} = 162.5\,\frac{\mathrm{N\cdot m}}{\mathrm{m}} && \text{(distributed torque).} \end{aligned} \tag{6.200}$$

The corresponding bending moment $\widehat{M}_y$, shear force $\widehat{V}_z$, and torque $\widehat{T}$ diagrams are shown in Figure 6.50. The maximum values are

$$\begin{aligned} \widehat{M}_y^{\max} &= -\frac{pL^2}{12} = 541.7\ \mathrm{N\cdot m} \\ \widehat{V}_z^{\max} &= \frac{pL}{2} = -3\,250\ \mathrm{N} \\ \widehat{T}^{\max} &= \frac{tL}{2} = 81.25\ \mathrm{N\cdot m}. \end{aligned} \tag{6.201}$$

The compliance matrices for the flange and the web are the same, and their relevant elements are (Table 3.8, page 85)

$$a_{11} = 5.18 \times 10^{-9}\,\frac{\mathrm{m}}{\mathrm{N}} \qquad a_{66} = 27.77 \times 10^{-9}\,\frac{\mathrm{m}}{\mathrm{N}} \qquad d_{11} = 33.10 \times 10^{-3}\,\frac{1}{\mathrm{N\cdot m}}.$$

The dimensions are (Fig. 6.48) $b_{\mathrm{f}} = 0.052\,\mathrm{m}$, $b_{\mathrm{w}} = 0.068\,\mathrm{m}$, $d = 0.07\,\mathrm{m}$, $d_{\mathrm{f}} = 0.05\,\mathrm{m}$.

From Table A.1 the bending stiffnesses are

$$\begin{aligned} \widehat{EI}_{yy} &= \frac{b_{\mathrm{f}}}{(a_{11})_{\mathrm{f}}}\frac{d^2}{2} + \frac{2b_{\mathrm{f}}}{(d_{11})_{\mathrm{f}}} + \frac{2b_{\mathrm{w}}^3}{12(a_{11})_{\mathrm{w}}} = 34\,692\ \mathrm{N\cdot m^2} \\ \widehat{EI}_{zz} &= \frac{b_{\mathrm{w}}}{(a_{11})_{\mathrm{w}}}\frac{d_{\mathrm{f}}^2}{2} + \frac{2b_{\mathrm{w}}}{(d_{11})_{\mathrm{w}}} + \frac{2b_{\mathrm{f}}^3}{12(a_{11})_{\mathrm{f}}} = 20\,924\ \mathrm{N\cdot m^2}. \end{aligned} \tag{6.202}$$

The torsional stiffness $\widehat{GI}_{\mathrm{t}}$ is (Table A.6, with α_{66}^{v} replaced by a_{66})

$$\widehat{GI}_{\mathrm{t}} = \frac{2d_{\mathrm{f}}^2 d^2}{a_{66}(d_{\mathrm{f}} + d)} = 7\,352\ \mathrm{N\cdot m^2}. \tag{6.203}$$

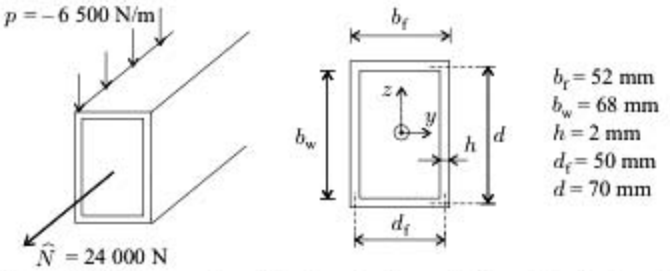

Figure 6.51: Cross section of the beam in Example 6.4 and the load applied on the beam.

The maximum deflection is (Table 7.3, page 332)

$$\widetilde{w} = \frac{1}{384}\frac{pL^4}{\widehat{E}\widehat{I}_{yy}} = -0.000\,488\,\text{m} = -0.488\,\text{mm}. \tag{6.204}$$

The maximum twist is at $x = L/2$ and is

$$\psi = \int_0^{L/2} \vartheta\, dx = \int_0^{L/2} \frac{\widehat{T}}{\widehat{G}\widehat{I}_t} dx. \tag{6.205}$$

The torque $\widehat{T}$ varies linearly with x, and the preceding integral yields

$$\psi = \frac{\widehat{T}^{\max} L}{4\widehat{G}\widehat{I}_t} = 0.002\,76\,\text{rad} = 0.158^\circ. \tag{6.206}$$

6.4 Example. *An $L = 1.0$-m-long box beam, with the cross section shown in Figure 6.51, is made of graphite epoxy. The material properties are given in Table 3.6 (page 81). The layup is $[\pm 45_5^t/0_{10}]$. The fabric is on the outside of the wall. The beam, built-in at each end, is subjected to a uniformly distributed load ($p = -6\,500$ N/m) acting along the midplane of the left web and to an axial load $\widehat{N} = 24\,000$ N. By neglecting the effects of axial restraint, calculate the maximum deflection and the maximum twist.*

Solution. The cross section is doubly symmetrical, and the centroid and the shear center (see Section 6.7.3) coincide with the center of the cross section. The loads with respect to the shear center and the corresponding bending moment $\widehat{M}_y$, shear force $\widehat{V}_z$, and torque $\widehat{T}$ are given in Example 6.3 (page 255).

The layup of each wall is orthotropic and unsymmetrical. The compliance matrices for the flange and the web are the same, and their relevant elements are (see Table 3.9, page 86).

$$\alpha_{11}^{MP} = 11.65 \times 10^{-9}\,\frac{\text{m}}{\text{N}} \qquad \alpha_{66}^{MP} = 43.70 \times 10^{-9}\,\frac{\text{m}}{\text{N}}$$

$$\beta_{11}^{MP} = -13.97 \times 10^{-6}\,\frac{1}{\text{N}} \qquad \beta_{12}^{MP} = 12.22 \times 10^{-6}\,\frac{1}{\text{N}} \qquad \beta_{66}^{MP} = 51.60 \times 10^{-6}\,\frac{1}{\text{N}}$$

$$\delta_{11}^{MP} = 34.94 \times 10^{-3}\,\frac{1}{\text{N}\cdot\text{m}} \qquad \delta_{12}^{MP} = -25.74\,\frac{1}{\text{N}\cdot\text{m}} \qquad \delta_{22}^{MP} = 98.83\,\frac{1}{\text{N}\cdot\text{m}},$$

$$\delta_{66}^{MP} = 131.11 \times 10^{-3}\,\frac{1}{\text{N}\cdot\text{m}}$$

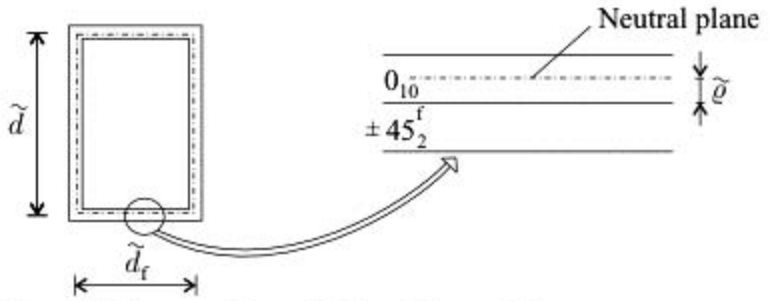

Figure 6.52: The neutral plane of the beam in Example 6.4.

where MP refers to the midplane of the wall. The dimensions of the beam are (Fig. 6.51) $b_f = 0.052$ m, $b_w = 0.068$ m, $d = 0.07$ m, and $d_f = 0.05$ m.

To evaluate the bending stiffnesses, we determine the position of the neutral plane (Eq. 6.105 and Fig. 6.52) as follows:

$$\tilde{\varrho} = -\frac{\beta_{11}^{MP}}{\delta_{11}^{MP}} = 0.0004 \text{ m} = 0.400 \text{ mm}. \tag{6.207}$$

At the $\tilde{\varrho}$ reference plane the compliances of the flanges and the webs are (Eq. 3.48)

$$\begin{aligned} \alpha_{11} &= \alpha_{11}^{MP} + 2\tilde{\varrho}\beta_{11}^{MP} + \tilde{\varrho}^2\delta_{11}^{MP} = 6.056 \times 10^{-9}\,\frac{\text{m}}{\text{N}} \\ \beta_{66} &= \beta_{66}^{MP} + \tilde{\varrho}\delta_{66}^{MP} = 104.04 \times 10^{-6}\,\frac{1}{\text{N}} \qquad \text{at } \tilde{\varrho} \\ \delta_{11} &= \delta_{11}^{MP} = 34.94 \times 10^{-3}\,\frac{1}{\text{N}\cdot\text{m}}. \end{aligned} \tag{6.208}$$

From Table A.3 the bending stiffnesses are

$$\widehat{EI}_{yy} = \frac{b_f}{(\alpha_{11})_f}\frac{\tilde{d}^2}{2} + \frac{2b_f}{(\delta_{11})_f} + \frac{2b_w^3}{12(\alpha_{11})_w} = 29\,214 \text{ N}\cdot\text{m}^2 \tag{6.209}$$

$$\widehat{EI}_{zz} = \frac{b_w}{(\alpha_{11})_w}\frac{\tilde{d}_f^2}{2} + \frac{2b_w}{(\delta_{11})_w} + \frac{2b_f^3}{12(\alpha_{11})_f} = 17\,463 \text{ N}\cdot\text{m}^2, \tag{6.210}$$

where the dimensions $\tilde{d}$ and $\tilde{d}_f$ are (Fig. 6.52) $\tilde{d} = d - 2\tilde{\varrho} = 0.0692$ m, $\tilde{d}_f = d_f - 2\tilde{\varrho} = 0.0492$ m.

The torsional stiffness $\widehat{GI}_t$ is given in Table A.6 with reference to the $\tilde{\varrho}$ neutral plane as

$$\widehat{GI}_t = \frac{2d_f^2 d^2}{\alpha_{66}^{\nu}(d_f + d)} = 8\,726 \text{ N}\cdot\text{m}^2, \tag{6.211}$$

where α_{66}^{ν} is (Eq. 6.196)

$$\alpha_{66}^{\nu} = \alpha_{66}^{MP} - \frac{(\beta_{66}^{MP})^2}{\delta_{66}^{MP}} = 23.40 \times 10^{-9}\frac{\text{m}}{\text{N}}. \tag{6.212}$$

The accuracy of $\widehat{GI}_t$, as calculated by Eq. (6.211), is improved when $\widehat{GI}_t$ is evaluated in reference to the "torque neutral" surface. Equation (6.194) gives $\nu = -\beta_{66}^{MP}/\delta_{66}^{MP} = -0.394$ mm. When d and d_f are replaced by $d - 2\nu = 0.0708$ and $d_f - 2\nu = 0.0508$ m, respectively, Eq. (6.211) results in $\widehat{GI}_t = 9\,087$ N $\cdot$ m^2.

Next, we calculate the tensile stiffness. From Eqs. (6.156) and (6.157), we have

$$\begin{aligned}\widehat{\beta}_{11}^{\mathrm{MP}} &= \left(\beta_{11}^{\mathrm{MP}} - \frac{\beta_{12}^{\mathrm{MP}}\delta_{12}^{\mathrm{MP}}}{\delta_{22}^{\mathrm{MP}}}\right) = -10.79 \times 10^{-6}\,\frac{1}{\mathrm{N}} \\ \widehat{\delta}_{11}^{\mathrm{MP}} &= \left(\delta_{11}^{\mathrm{MP}} - \frac{\left(\delta_{12}^{\mathrm{MP}}\right)^2}{\delta_{22}^{\mathrm{MP}}}\right) = 28.23 \times 10^{-3}\,\frac{1}{\mathrm{N\cdot m}}.\end{aligned} \tag{6.213}$$

The location of the reference surface is (Eq. A.3)

$$\widehat{\varrho} = -\frac{\widehat{\beta}_{11}^{\mathrm{MP}}}{\widehat{\delta}_{11}^{\mathrm{MP}}} = 0.000\,382\ \mathrm{m} = 0.382\ \mathrm{mm}. \tag{6.214}$$

At the $\widehat{\varrho}$ reference surface, the compliances of the flanges and the webs are (Eq. 3.48)

$$\begin{aligned}\alpha_{11} &= \alpha_{11}^{\mathrm{MP}} + 2\widehat{\varrho}\beta_{11}^{\mathrm{MP}} + \widehat{\varrho}^2\delta_{11}^{\mathrm{MP}} = 6.067 \times 10^{-9}\,\frac{\mathrm{m}}{\mathrm{N}} \\ \beta_{12} &= \beta_{12}^{\mathrm{MP}} + \widehat{\varrho}\delta_{12}^{\mathrm{MP}} = 2.380 \times 10^{-6}\,\frac{1}{\mathrm{N}} \\ \delta_{11} &= \delta_{11}^{\mathrm{MP}} = 34.94 \times 10^{-3}\,\frac{1}{\mathrm{N\cdot m}} \\ \delta_{12} &= \delta_{12}^{\mathrm{MP}} = -25.74 \times 10^{-3}\,\frac{1}{\mathrm{N\cdot m}} \\ \delta_{22} &= \delta_{22}^{\mathrm{MP}} = 98.83 \times 10^{-3}\,\frac{1}{\mathrm{N\cdot m}}.\end{aligned} \tag{6.215}$$

With these compliances from Eqs. (6.156) and (6.157), for both the flange and the web we have

$$\begin{aligned}\widehat{\alpha}_{11} &= \left(\alpha_{11} - \frac{(\beta_{12})^2}{\delta_{22}}\right) = 6.01 \times 10^{-9}\,\frac{\mathrm{m}}{\mathrm{N}} \\ \widehat{\delta}_{11} &= \left(\delta_{11} - \frac{(\delta_{12})^2}{\delta_{22}}\right) = 28.23 \times 10^{-3}\,\frac{1}{\mathrm{N\cdot m}}.\end{aligned} \tag{6.216}$$

From Table A.3 the tensile stiffness is

$$\widehat{EA} = \frac{2b_{\mathrm{f}}}{(\widehat{\alpha}_{11})_{\mathrm{f}}} + \frac{2b_{\mathrm{w}}}{(\widehat{\alpha}_{11})_{\mathrm{w}}} = 39.934 \times 10^{6}\ \mathrm{N}. \tag{6.217}$$

The maximum deflection is (Table 7.3, page 332)

$$\widetilde{w} = \frac{1}{384}\frac{pL^4}{\widehat{EI}_{yy}} = -0.000\,579\ \mathrm{m} = -0.579\ \mathrm{mm}. \tag{6.218}$$

The maximum twist is at $x = L/2$ and is

$$\psi = \int_0^{L/2} \vartheta\, dx = \int_0^{L/2} \frac{\widehat{T}}{\widehat{GI}_{\mathrm{t}}} dx. \tag{6.219}$$

Torque $\widehat{T}$ varies linearly with x, thus, the integral above yields

$$\psi = \frac{\widehat{T}^{\max} L}{4\widehat{GI}_{\mathrm{t}}} = 0.002\,33\ \mathrm{rad} = 0.133^{\circ}, \tag{6.220}$$

where $\widehat{T}^{\max} = 81.25 \frac{\text{N}\cdot\text{m}}{\text{m}}$ (Eq. 6.201). The elongation of the beam is

$$\Delta L = \int_0^L \varepsilon_x dx = \int_0^L \frac{\widehat{N}}{\widehat{EA}} dx = \frac{\widehat{N}L}{\widehat{EA}} = 0.000\,601\,\text{m} = 0.601\,\text{mm}. \quad (6.221)$$

6.5.4 Closed Section Orthotropic Beams – Multicell

For multicell composite beams the rate of twist and the shear flows are determined in the same way as for isotropic beams. Accordingly, for a beam consisting of L cells the torque is

$$\widehat{T} = \sum_{l=1}^{L} 2A_l q_l, \quad (6.222)$$

where A_l is the enclosed area of the lth cell and q_l is the shear flow in the lth cell (Fig. 6.53). The shear strain $\gamma^o_{\xi\eta}$ in each wall segment is calculated by (Eq. 6.195)

$$\gamma^o_{\xi\eta} = \alpha^v_{66} q, \quad (6.223)$$

where q is the shear flow in the wall segment. Then, the rate of twist of each cell is (Eq. 6.188)

$$\begin{aligned}
\vartheta_1 &= \frac{1}{2A_1} \oint_{\text{cell 1}} \alpha^v_{66} q d\eta \\
\vartheta_2 &= \frac{1}{2A_2} \oint_{\text{cell 2}} \alpha^v_{66} q d\eta \\
&\vdots \\
\vartheta_L &= \frac{1}{2A_L} \oint_{\text{cell } L} \alpha^v_{66} q d\eta.
\end{aligned} \quad (6.224)$$

For a wall that belongs to one cell only, q is equal to the shear flow of the appropriate cell ($q = q_l$). For a wall that belongs to two cells, the shear flow is the sum of the shear flows of the adjacent cells, as illustrated in Figure 6.53.

The rate of twist of each cell is the same

$$\vartheta = \vartheta_1 = \vartheta_2 = \ldots = \vartheta_L. \quad (6.225)$$

There are $L+1$ equations (Eqs. 6.224 and 6.222) that can be solved for the $L+1$ unknowns: q_l ($l = 1, 2, \ldots, L$) and ϑ.

The stresses in the walls are calculated as for a single-cell beam.

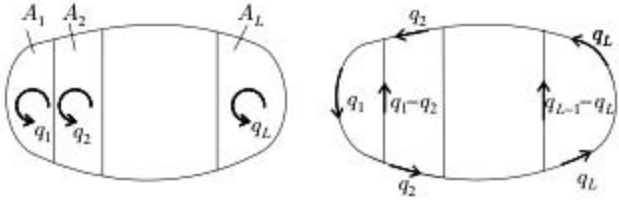

Figure 6.53: Shear flow in multicell beams.

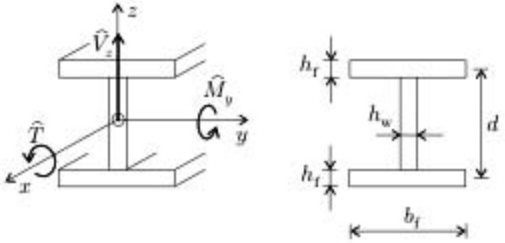

Figure 6.54: Thin-walled I-beam.

6.5.5 Restrained Warping – Open-Section Orthotropic Beams

When an isotropic beam is subjected to pure torsion and the cross sections of the beam are free to warp, the torque is (Eq. 6.161)

$$\widehat{T} = (GI_t)\,\vartheta. \tag{6.226}$$

When the beam is axially constrained at one of its cross sections (for example at a built-in end), then, at this cross section, warping cannot occur. The shorter the beam, the more important are the effects of restrained warping. Furthermore, the effects of restrained warping are more pronounced for thin-walled open-section beams than for thin-walled closed-section beams and for solid cross-section beams. Therefore, in this section, we consider only restrained warping of open-section beams.

We illustrate the analysis through the example of a symmetrical I-beam (Fig. 6.54).

Isotropic I beams. Under pure torque, in the absence of axial constraint, the shear stress distribution in an isotropic I-beam is as shown in Figure 6.55. When the beam is axially restrained, axial forces N_ξ (per unit length) are introduced in the wall (Fig. 6.56, bottom). These axial forces create a bending moment $\widehat{M}_f$[8]

$$\widehat{M}_f = -\frac{d^2 v_f}{dx^2} EI_f, \tag{6.227}$$

where I_f is the moment of inertia of the flange about the z-axis denoted by

$$I_f = \frac{h_f b_f^3}{12}, \tag{6.228}$$

b_f and h_f are the width and the thickness of the flanges (Fig. 6.54), respectively; v_f is the displacement of the flange due to the rotation about the x-axis (Fig. 6.57),

$$v_f = \psi \frac{d}{2}, \tag{6.229}$$

where d is the distance between the midplanes of the flanges. We recall that

[8] T. H. G. Megson, *Aircraft Structures for Engineering Students*. 3rd edition. Halsted Press, John Wiley & Sons, New York, 1999, p. 467.

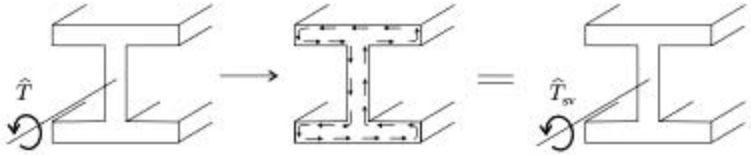

Figure 6.55: Isotropic I-beam under pure torque with no axial constraint.

$\vartheta = d\psi/dx$ (Eq. 6.1). Thus, we have

$$\frac{dv_f}{dx} = \vartheta \frac{d}{2}. \tag{6.230}$$

The bending moment $\hat{M}_f$ may now be expressed as

$$\hat{M}_f = -\frac{d\vartheta}{dx} E \frac{h_f b_f^3}{12} \frac{d}{2}. \tag{6.231}$$

We now introduce the bimoment $\hat{M}_\omega$ defined for an I-beam as

$$\hat{M}_\omega = \hat{M}_f d. \tag{6.232}$$

The last two equations give

$$\hat{M}_\omega = -\frac{d\vartheta}{dx} \underbrace{\left(\frac{E h_f b_f^3}{24} d^2\right)}_{EI_\omega}. \tag{6.233}$$

The term indicated by the bracket is the warping stiffness EI_ω.

Owing to the axial constraint, the bending moment $\hat{M}_f$ varies along the x-axis of the beam. Correspondingly, there is a shear force in the flanges. The relationship between the flange shear force and the flange bending moment is

$$\hat{V}_f = \frac{d\hat{M}_f}{dx}. \tag{6.234}$$

The shear force results in a torque $\hat{T}_\omega$ (Fig. 6.56, bottom) defined by

$$\hat{T}_\omega = \hat{V}_f d. \tag{6.235}$$

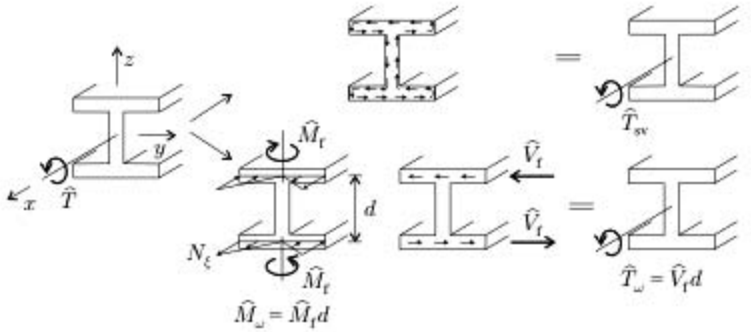

Figure 6.56: Isotropic I-beam under pure torque with axial constraint.

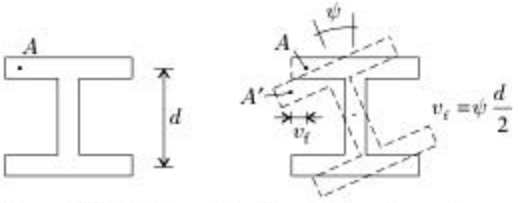

Figure 6.57: Rotation of an I-beam about the x-axis.

Equations (6.232), (6.234), and (6.235) give

$$\widehat{T}_\omega = \frac{d\widehat{M}_\omega}{dx}. \tag{6.236}$$

From Eqs. (6.236) and (6.233) we have

$$\widehat{T}_\omega = -EI_\omega \frac{d^2\vartheta}{dx^2}, \tag{6.237}$$

where the warping stiffness EI_ω is (see Eq. 6.233)

$$EI_\omega = \frac{Eht_f b_f^3}{24} d^2. \tag{6.238}$$

The total torque is

$$\widehat{T} = \underbrace{(GI_t)\,\vartheta}_{\widehat{T}_{sv}} + \underbrace{(EI_\omega)\left(-\frac{d^2\vartheta}{dx^2}\right)}_{\widehat{T}_\omega}, \tag{6.239}$$

where $\widehat{T}_{sv}$ and $\widehat{T}_\omega$ are referred to as the "Saint-Venant" and the "restrained-warping-induced" torques, respectively.

***Orthotropic* I-*beams*.** The expression for the torque of orthotropic beams is similar to the expression for isotropic I-beams (Eq. 6.239) as follows:

$$\widehat{T} = \underbrace{\widehat{GI}_t\vartheta}_{\widehat{T}_{sv}} + \underbrace{\widehat{EI}_\omega\left(-\frac{d^2\vartheta}{dx^2}\right)}_{\widehat{T}_\omega}. \tag{6.240}$$

The torsional stiffness $\widehat{GI}_t$ presented in Section 6.5.2 is unaffected by the axial constraint and is given by Eq. (6.175).

It remains to determine the warping stiffness $\widehat{EI}_\omega$. By referring to Eq. (6.238), we see that the warping stiffness of an isotropic I-beam is a function of the product of the flange's modulus E and thickness h ($\widehat{EI}_\omega \sim Eh$). This Eh is related to the axial force (per unit length) in the flange as follows:

$$N_\xi = h\sigma_\xi = Eh\epsilon_\xi^o. \tag{6.241}$$

For a beam with orthotropic layup, N_ξ is (see Table 6.2, page 222)

$$N_\xi = \frac{\delta_{11}}{D}\epsilon_\xi^o - \frac{\beta_{11}}{D}\kappa_\xi. \tag{6.242}$$

Table 6.9. Boundary conditions for beams in torsion.

Warping restrained	$\vartheta = 0$
unrestrained	$\widehat{M}_\omega = 0$
Rotationally restrained	$\psi = 0$
unrestrained	$\widehat{T} = 0$

This equation applies at a reference plane chosen arbitrarily. At the "neutral" plane (see Eq. 6.105) $\beta_{11} = 0$, and, hence (see Table 6.2, page 222), we have that $\delta_{11}/D = 1/\alpha_{11}^{\varrho}$, where the superscript ϱ indicates that α_{11}^{ϱ} is evaluated at the flange's "neutral" plane. With these substitutions the preceding equation becomes

$$N_\xi = \frac{1}{\alpha_{11}^{\varrho}} \epsilon_\xi^o. \tag{6.243}$$

By comparing Eqs. (6.243) and (6.241), we see that an orthotropic beam's tensile stiffness $1/\alpha_{11}^{\varrho}$ corresponds to an isotropic beam's tensile stiffness Eh. We use this correspondence and evaluate the warping stiffness of an orthotropic I-beam by replacing Eh by $1/\alpha_{11}^{\varrho}$ in Eq. (6.238). The result is

$$\widehat{EI}_\omega = \frac{\frac{1}{\alpha_{11}^{\varrho}} b_f^3}{24} d^2. \tag{6.244}$$

Orthotropic beam – arbitrary cross section. Equation (6.240) can also be used for thin-walled beams with other cross-sectional shapes by using the appropriate torsional and warping stiffnesses. The torsional stiffness $\widehat{GI}_t$ is given by Eqs. (6.170) and (6.175). The warping stiffness $\widehat{EI}_\omega$ of an orthotropic beam is obtained by replacing Eh by $1/\alpha_{11}^{\varrho}$ in the appropriate expressions[9] for the corresponding isotropic beam. The warping stiffnesses $\widehat{EI}_\omega$ of frequently used cross sections are included in Table A.5.

Boundary conditions. When the warping of the cross section at the end of a beam is restrained, the distortion is zero. When warping is not restrained, the bimoment is zero.

When the end may rotate, the torque is zero. When the end is rotationally restrained, the rate of twist is zero.

The preceding boundary conditions are summarized in Table 6.9.

6.5.6 Restrained Warping – Closed-Section Orthotropic Beams

Warping of closed-section beams is often negligible. Warping may become significant, though, when the shear stiffnesses of different wall segments are markedly different. This is illustrated in Figure 6.58.

[9] S. P. Timoshenko and J. Gere, *Theory of Elastic Stability*. 2nd edition. McGraw-Hill, New York, 1961, p. 530.

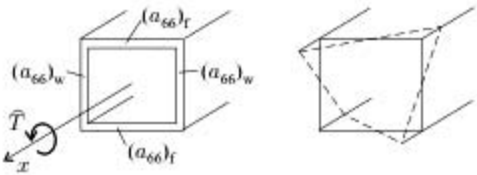

Figure 6.58: Warping of a box beam subjected to torsion when $(a_{66})_f \ll (a_{66})_w$.

6.6 Thin-Walled Beams with Arbitrary Layup Subjected to Axial Load, Bending, and Torsion

In this section we treat thin-walled, open- and closed-section beams. The beam's wall consists of flat segments (Fig. 6.59) designated by the subscript k ($k = 1, 2, \ldots,$ K, where K is the total number of wall segments). The cross section may be symmetrical or unsymmetrical, and the layup of the beam is arbitrary, that is, the layers are not necessarily orthotropic.

The beam is subjected to an axial force $\widehat{N}$, bending moments $\widehat{M}_y$, $\widehat{M}_z$, and torque $\widehat{T}$ acting at the centroid.

We employ two coordinate systems (Fig. 6.60) for the beam; the x–y–z coordinate system with its origin at the centroid and the $\overline{x}$–$\overline{y}$–$\overline{z}$ coordinate system with its origin at an arbitrarily chosen point. The location of the centroid with respect to the origin of the $\overline{x}$–$\overline{y}$–$\overline{z}$ coordinate system is given in Section 6.6.3.

The displacements of the longitudinal axis, passing through the centroid, are u, v, w, ψ (Fig. 6.3), where u is the axial displacement, v and w are the transverse displacements in the y and z directions, and ψ is the twist of the cross section. In the x–y–z coordinate system the relationships between these displacements, the axial strain ϵ_x^o, the curvatures $1/\rho_y$, $1/\rho_z$ of the x-axis, and the rate of twist ϑ (Eq. 6.1) are

$$\frac{\partial u}{\partial x} = \epsilon_x^o \qquad \frac{\partial^2 v}{\partial x^2} = -\frac{1}{\rho_z} \qquad \frac{\partial^2 w}{\partial x^2} = -\frac{1}{\rho_y} \qquad \frac{\partial \psi}{\partial x} = \vartheta. \tag{6.245}$$

In the $\overline{x}$–$\overline{y}$–$\overline{z}$ coordinate system these relationships become

$$\frac{\partial \overline{u}}{\partial \overline{x}} = \epsilon_{\overline{x}}^o \qquad \frac{\partial^2 \overline{v}}{\partial \overline{x}^2} = -\frac{1}{\rho_{\overline{z}}} \qquad \frac{\partial^2 \overline{w}}{\partial \overline{x}^2} = -\frac{1}{\rho_{\overline{y}}} \qquad \frac{\partial \overline{\psi}}{\partial \overline{x}} = \overline{\vartheta}, \tag{6.246}$$

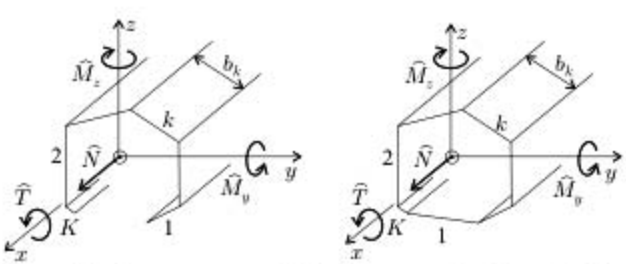

Figure 6.59: Forces on open and closed cross-section, thin-walled beams with flat wall segments.

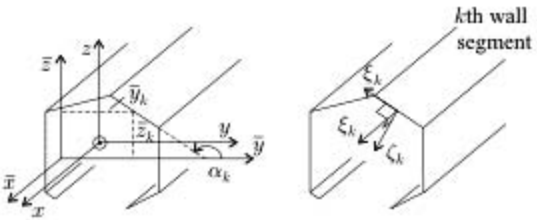

Figure 6.60: The coordinate systems employed in the analysis of thin-walled beams with arbitrary layup.

where $\epsilon_{\bar{x}}^{o}$, $1/\rho_{\bar{y}}$, $1/\rho_{\bar{z}}$ are the axial strain and the curvatures of the longitudinal axis passing through the origin of the $\bar{x}$–$\bar{y}$–$\bar{z}$ coordinate system, and $\bar{u}$, $\bar{v}$, $\bar{w}$, and $\bar{\psi}$ are the displacements of the $\bar{x}$-axis.

The force, moment, and torque resultants at the origin of the bar coordinate system $\widehat{N}_{\bar{x}}$, $\widehat{M}_{\bar{y}}$, $\widehat{M}_{\bar{z}}$, $\widehat{T}_{\bar{x}}$ are related to the force applied at the centroid by the expressions,

$$\widehat{N}_{\bar{x}} = \widehat{N} \qquad \widehat{M}_{\bar{y}} = \widehat{M}_y + z_c\widehat{N} \qquad \widehat{M}_{\bar{z}} = \widehat{M}_z + y_c\widehat{N} \qquad \widehat{T}_{\bar{x}} = \widehat{T}, \tag{6.247}$$

where z_c and y_c are the coordinates of the centroid in the bar coordinate system (Fig. 6.61). For both open- and closed-section beams the force–strain and strain–force relationships in the x–y–z coordinate system are (Eqs. 6.2 and 6.17)

$$\begin{Bmatrix} \widehat{N}_x \\ \widehat{M}_y \\ \widehat{M}_z \\ \widehat{T} \end{Bmatrix} = \begin{bmatrix} P_{11} & P_{12} & P_{13} & P_{14} \\ P_{12} & P_{22} & P_{23} & P_{24} \\ P_{13} & P_{23} & P_{33} & P_{34} \\ P_{14} & P_{24} & P_{34} & P_{44} \end{bmatrix} \begin{Bmatrix} \epsilon_x^o \\ \frac{1}{\rho_y} \\ \frac{1}{\rho_z} \\ \vartheta \end{Bmatrix} \tag{6.248}$$

$$\begin{Bmatrix} \epsilon_x^o \\ \frac{1}{\rho_y} \\ \frac{1}{\rho_z} \\ \vartheta \end{Bmatrix} = \begin{bmatrix} W_{11} & 0 & 0 & W_{14} \\ 0 & W_{22} & W_{23} & W_{24} \\ 0 & W_{23} & W_{33} & W_{34} \\ W_{14} & W_{24} & W_{34} & W_{44} \end{bmatrix} \begin{Bmatrix} \widehat{N}_x \\ \widehat{M}_y \\ \widehat{M}_z \\ \widehat{T} \end{Bmatrix}. \tag{6.249}$$

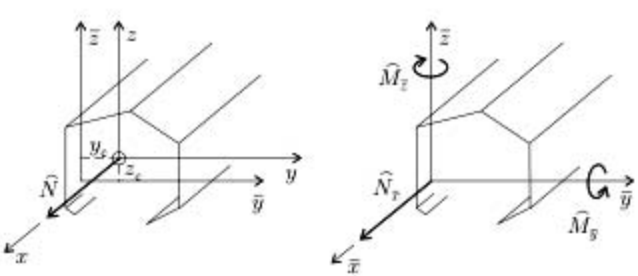

Figure 6.61: Beam subjected to an axial force at the centroid and the resultant axial force and moments in the $\bar{x}$–$\bar{y}$–$\bar{z}$ coordinate system.

In the bar coordinate system these relationships are written as

$$\begin{Bmatrix} \widehat{N}_{\overline{x}} \\ \widehat{M}_{\overline{y}} \\ \widehat{M}_{\overline{z}} \\ \widehat{T}_{\overline{x}} \end{Bmatrix} = \begin{bmatrix} \overline{P}_{11} & \overline{P}_{12} & \overline{P}_{13} & \overline{P}_{14} \\ \overline{P}_{12} & \overline{P}_{22} & \overline{P}_{23} & \overline{P}_{24} \\ \overline{P}_{13} & \overline{P}_{23} & \overline{P}_{33} & \overline{P}_{34} \\ \overline{P}_{14} & \overline{P}_{24} & \overline{P}_{34} & \overline{P}_{44} \end{bmatrix} \begin{Bmatrix} \epsilon^0_{\overline{x}} \\ \frac{1}{\rho_{\overline{y}}} \\ \frac{1}{\rho_{\overline{z}}} \\ \vartheta \end{Bmatrix} \tag{6.250}$$

$$\begin{Bmatrix} \epsilon^0_{\overline{x}} \\ \frac{1}{\rho_{\overline{y}}} \\ \frac{1}{\rho_{\overline{z}}} \\ \vartheta \end{Bmatrix} = \begin{bmatrix} \overline{W}_{11} & \overline{W}_{12} & \overline{W}_{13} & \overline{W}_{14} \\ \overline{W}_{12} & \overline{W}_{22} & \overline{W}_{23} & \overline{W}_{24} \\ \overline{W}_{13} & \overline{W}_{23} & \overline{W}_{33} & \overline{W}_{34} \\ \overline{W}_{14} & \overline{W}_{24} & \overline{W}_{34} & \overline{W}_{44} \end{bmatrix} \begin{Bmatrix} \widehat{N}_{\overline{x}} \\ \widehat{M}_{\overline{y}} \\ \widehat{M}_{\overline{z}} \\ \widehat{T}_{\overline{x}} \end{Bmatrix}, \tag{6.251}$$

where $[P]$, $[\overline{P}]$, $[W]$, and $[\overline{W}]$ are the stiffness and compliance matrices in the centroid x–y–z and bar $\overline{x}$–$\overline{y}$–$\overline{z}$ coordinate systems. These matrices are obtained by reasoning similar to that used in the derivations of the stiffness and compliance matrices of orthotropic beams (Sections 6.3.3 and 6.4). For beams with arbitrary layup the algebraic steps are long and laborious[10] and their presentation is beyond the scope of this book. The results are summarized in Table 6.10.

The compliances $\alpha_{ij}, \beta_{ij}, \delta_{ij}$, which appear in Table 6.10, are evaluated in the local ξ–η–ζ coordinate system. For the kth segment we employ the ξ_k–η_k–ζ_k coordinate system with the origin at the midpoint of the reference plane of the kth segment, where ξ is parallel to the x coordinate, η is along the circumference of the wall, and ζ is perpendicular to the circumference; $\overline{y}_k$ and $\overline{z}_k$ are the coordinates of the ξ_k–η_k–ζ_k coordinate system's origin, which is at the midpoint of the reference plane (Fig. 6.60). For closed-section beams, η_k points in the counterclockwise direction (Fig. 6.62), α_k is the angle between the η_k and $\overline{y}$ coordinate axes, and b_k is the width of the wall segment (Fig. 6.59).

We observe that for orthotropic beams the expressions in Table 6.10 yield the stiffness matrix given in Eq. (6.7).

6.6.1 Displacements of Open- and Closed-Section Beams

In the analysis we must take into account that thin-walled beams with arbitrary layup respond to loads differently than beams with orthotropic layup. For example, an orthotropic beam subjected to an axial load deforms, as shown in Figure 6.63 (left). A thin-walled beam with arbitrary layup deforms as shown in Figure 6.63 (right). Thus, the cross sections of beams with arbitrary layup do not remain plane, and the Bernoulli–Navier hypothesis is inapplicable. Nonetheless, in a long body, such as a beam, the strains may be considered to be constant in the axial direction, and we may apply the plane–strain condition (Section 2.4) in the analysis.

The displacements are then calculated with this approximation from the governing equations together with the force–strain relationship given in Table 6.10.

[10] L. P. Kollár and A. Pluzsik, Analysis of Thin Walled Composite Beams with Arbitrary Layup, *Journal of Reinforced Plastics and Composites*, Vol. 21, 1423–1465, 2002.

Table 6.10. Stiffness and compliance matrices in the bar ($[\overline{P}]$, $[\overline{W}]$) and centroid ($[P]$, $[W]$) coordinate systems of open- and closed-section beams with arbitrary layup. The elements α_{ij}, β_{ij}, δ_{ij} are evaluated at the ξ_k–η_k–ζ_k coordinate system of each wall segment. The enclosed area of closed-section beams is denoted by A. The superscript T denotes transpose.

Bar coordinate system: $[\overline{W}] = [\overline{P}]^{-1}$

Open-section beam: $[\overline{P}] = \sum_{k=1}^{K} [R_k]^T [\omega_k]^{-1} [R_k]$

Closed-section beam: $[\overline{P}] = \sum_{k=1}^{K} ([R_k]^T [\omega_k]^{-1} [R_k]) + [L]^T [F]^{-1} [L]$

Centroid coordinate system: $[W] = [R_b]^T [\overline{W}] [R_b]$ $\quad [P] = [W]^{-1}$

$$[R_k] = \begin{bmatrix} 1 & \bar{z}_k & \bar{y}_k & 0 \\ 0 & \cos\alpha_k & -\sin\alpha_k & 0 \\ 0 & \sin\alpha_k & \cos\alpha_k & 0 \\ 0 & 0 & 0 & 1 \end{bmatrix} \qquad \begin{bmatrix} \tilde{A}_{11} & \tilde{A}_{12} & \tilde{A}_{13} \\ \tilde{A}_{12} & \tilde{A}_{22} & \tilde{A}_{23} \\ \tilde{A}_{13} & \tilde{A}_{23} & \tilde{A}_{33} \end{bmatrix}_k = \begin{bmatrix} \alpha_{11} & \beta_{11} & \beta_{16} \\ \beta_{11} & \delta_{11} & \delta_{16} \\ \beta_{16} & \delta_{16} & \delta_{66} \end{bmatrix}_k^{-1}$$

$$[\omega_k] = \frac{1}{b_k} \begin{bmatrix} \alpha_{11} & \beta_{11} & 0 & -\frac{1}{2}\beta_{16} \\ \beta_{11} & \delta_{11} & 0 & -\frac{1}{2}\delta_{16} \\ 0 & 0 & \frac{12}{(\tilde{A}_{11})_k b_k^2} & 0 \\ -\frac{1}{2}\beta_{16} & -\frac{1}{2}\delta_{16} & 0 & \frac{1}{4}\delta_{66} \end{bmatrix} \qquad [R_b] = \begin{bmatrix} 1 & 0 & 0 & 0 \\ z_c & 1 & 0 & 0 \\ y_c & 0 & 1 & 0 \\ 0 & 0 & 0 & 1 \end{bmatrix}$$

$$[I] = \sum_{k=1}^{K} \begin{bmatrix} \alpha_{16} & \beta_{61} & 0 & -\frac{1}{2}\beta_{66} \\ \beta_{12} & \delta_{12} & 0 & -\frac{1}{2}\delta_{26} \end{bmatrix}_k [\omega_k]^{-1} [R_k] \qquad [L] = \begin{bmatrix} 0 & 0 & 0 & 2A \\ 0 & 0 & 0 & 0 \end{bmatrix} - [I]$$

$$[F] = \sum_{k=1}^{K} \left(b_k \begin{bmatrix} \alpha_{66} & \beta_{62} \\ \beta_{62} & \delta_{22} \end{bmatrix}_k - \begin{bmatrix} \alpha_{16} & \beta_{61} & 0 & -\frac{1}{2}\beta_{66} \\ \beta_{12} & \delta_{12} & 0 & -\frac{1}{2}\delta_{26} \end{bmatrix}_k [\omega_k]^{-1} \begin{bmatrix} \alpha_{16} & \beta_{12} \\ \beta_{61} & \delta_{12} \\ 0 & 0 \\ -\frac{1}{2}\beta_{66} & -\frac{1}{2}\delta_{26} \end{bmatrix}_k \right)$$

$$[R_0] = \begin{bmatrix} 1 & 0 & \eta & 0 \\ 0 & 1 & 0 & 0 \\ 0 & 0 & 0 & -2 \end{bmatrix} \qquad [\tilde{\mu}_k] = \begin{bmatrix} \alpha_{11} & \beta_{11} & \beta_{16} \\ \beta_{11} & \delta_{11} & \delta_{16} \\ \beta_{16} & \delta_{16} & \delta_{66} \end{bmatrix}_k \qquad [\tilde{\nu}_k] = \begin{bmatrix} \alpha_{16} & \beta_{12} \\ \beta_{61} & \delta_{12} \\ \beta_{66} & \delta_{26} \end{bmatrix}_k$$

6.6.2 Stresses and Strains in Open- and Closed-Section Beams

We describe the stresses and strains inside the wall with reference to each wall segment's ξ_k–η_k–ζ_k coordinate system (Fig. 6.60). The forces and moments inside the wall are shown in Figure 6.64.

By applying the results of the laminate plate theory, the strains and stresses in the kth wall segment are obtained by replacing x by ξ, y by η, and z by ζ in

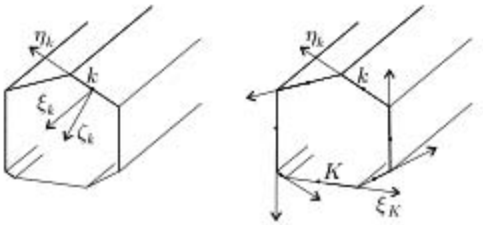

Figure 6.62: The local coordinate system attached to the kth wall segment (left) and the directions of the η coordinates (right) in a closed-section beam.

Eqs. (3.7) and (3.11) as follows:

$$\begin{Bmatrix} \epsilon_\xi \\ \epsilon_\eta \\ \gamma_{\xi\eta} \end{Bmatrix}_k = \begin{Bmatrix} \epsilon^o_\xi \\ \epsilon^o_\eta \\ \gamma^o_{\xi\eta} \end{Bmatrix}_k + \zeta \begin{Bmatrix} \kappa_\xi \\ \kappa_\eta \\ \kappa_{\xi\eta} \end{Bmatrix}_k \tag{6.252}$$

$$\begin{Bmatrix} \sigma_\xi \\ \sigma_\eta \\ \tau_{\xi\eta} \end{Bmatrix}_k = \begin{bmatrix} \overline{Q}_{11} & \overline{Q}_{12} & \overline{Q}_{16} \\ \overline{Q}_{21} & \overline{Q}_{22} & \overline{Q}_{26} \\ \overline{Q}_{16} & \overline{Q}_{26} & \overline{Q}_{66} \end{bmatrix}_k \begin{Bmatrix} \epsilon_\xi \\ \epsilon_\eta \\ \gamma_{\xi\eta} \end{Bmatrix}_k , \tag{6.253}$$

where $[\overline{Q}]_k$ is evaluated in the kth wall segment's ξ_k–η_k–ζ_k coordinate system.

In the kth segment's reference plane the strains and curvatures are calculated from the strain–force relationships (Eq. 3.22), which, for convenience, are reproduced as follows:

$$\begin{Bmatrix} \epsilon^o_\xi \\ \epsilon^o_\eta \\ \gamma^o_{\xi\eta} \\ \kappa_\xi \\ \kappa_\eta \\ \kappa_{\xi\eta} \end{Bmatrix}_k = \begin{bmatrix} \alpha_{11} & \alpha_{12} & \alpha_{16} & \beta_{11} & \beta_{12} & \beta_{16} \\ \alpha_{12} & \alpha_{22} & \alpha_{26} & \beta_{21} & \beta_{22} & \beta_{26} \\ \alpha_{16} & \alpha_{26} & \alpha_{66} & \beta_{61} & \beta_{62} & \beta_{66} \\ \beta_{11} & \beta_{21} & \beta_{61} & \delta_{11} & \delta_{12} & \delta_{16} \\ \beta_{12} & \beta_{22} & \beta_{62} & \delta_{12} & \delta_{22} & \delta_{26} \\ \beta_{16} & \beta_{26} & \beta_{66} & \delta_{16} & \delta_{26} & \delta_{66} \end{bmatrix}_k \begin{Bmatrix} N_\xi \\ N_\eta \\ N_{\xi\eta} \\ M_\xi \\ M_\eta \\ M_{\xi\eta} \end{Bmatrix}_k , \tag{6.254}$$

where the k subscript refers to the kth segment and α_{ij}, β_{ij}, δ_{ij} are evaluated in the kth wall segment's ξ_k–η_k–ζ_k coordinate system. The preceding expressions apply both to open- and closed-section beams. The difference in the two types of beams is in the expressions used to calculate the forces and moment (per unit length)

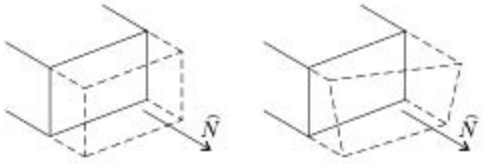

Figure 6.63: Displacements of an orthotropic beam (left) and a beam with arbitrary layup (right) under tension.

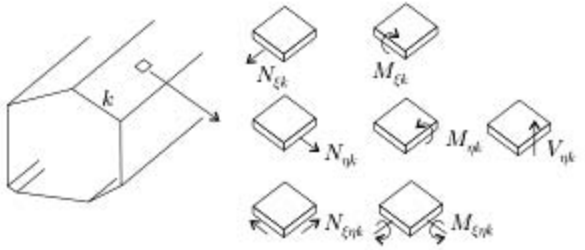

Figure 6.64: The forces and moments (per unit length) acting in the kth wall of an open- or closed-section beam.

inside the wall. The relevant expressions, derived by Pluzsik and Kollár,[11] are summarized in the remainder of this section.

Open-section beam. Along the free longitudinal edges of the beam, the in-plane forces and moments (per unit length) are zero: $N_\eta = N_{\xi\eta} = M_\eta = 0$ (Fig. 6.24). Since the dimensions of the cross section are small compared with the beam's length, these in-plane forces and moments are approximately zero inside the wall:

$$N_\eta = N_{\xi\eta} = M_\eta = 0. \tag{6.255}$$

The expressions for N_ξ, M_ξ, $M_{\xi\eta}$ are

$$\begin{Bmatrix} N_\xi \\ M_\xi \\ M_{\xi\eta} \end{Bmatrix}_k = [\widetilde{\mu}_k]^{-1}[R_\eta][R_k][\overline{W}] \begin{Bmatrix} \widehat{N}_{\overline{x}} \\ \widehat{M}_{\overline{y}} \\ \widehat{M}_{\overline{z}} \\ \widehat{T}_{\overline{x}} \end{Bmatrix}, \tag{6.256}$$

where $[\widetilde{\mu}_k]$, $[R_\eta]$, and $[R_k]$ are defined in Table 6.10.

Closed-section beam. In a closed-section beam, N_η is negligible; thus,

$$N_{\eta k} = 0. \tag{6.257}$$

The remaining forces and moments are

$$\begin{Bmatrix} N_{\xi\eta} \\ M_\eta \end{Bmatrix}_k = [F]^{-1}[L] \begin{Bmatrix} \epsilon^0_{\overline{x}} \\ \frac{1}{\rho_{\overline{y}}} \\ \frac{1}{\rho_{\overline{z}}} \\ \vartheta \end{Bmatrix} = [F]^{-1}[L][\overline{W}] \begin{Bmatrix} \widehat{N}_{\overline{x}} \\ \widehat{M}_{\overline{y}} \\ \widehat{M}_{\overline{z}} \\ \widehat{T}_{\overline{x}} \end{Bmatrix} \tag{6.258}$$

$$\begin{Bmatrix} N_\xi \\ M_\xi \\ M_{\xi\eta} \end{Bmatrix}_k = [\widetilde{\mu}_k]^{-1}([R_\eta][R_k] - [\widetilde{\nu}_k][F]^{-1}[L])[\overline{W}] \begin{Bmatrix} \widehat{N}_{\overline{x}} \\ \widehat{M}_{\overline{y}} \\ \widehat{M}_{\overline{z}} \\ \widehat{T}_{\overline{x}} \end{Bmatrix}, \tag{6.259}$$

where $[\widetilde{\mu}_k]$, $[R_\eta]$, $[R_k]$, $[\widetilde{\nu}_k]$, $[F]$, and $[L]$ are defined in Table 6.10.

[11] Ibid.

6.6.3 Centroid

The centroid is located such that the beam's axis remains straight when an axial force $\widehat{N}$ is applied at the centroid. Although this axis remains straight, the beam may twist about the axis of twist, which does not necessarily coincide with the axis passing through the centroid.

From Eqs. (6.251) and (6.247), the curvatures of the axis, passing through the origin of the bar coordinate system, are

$$\begin{Bmatrix} \frac{1}{\rho_{\bar{y}}} \\ \frac{1}{\rho_{\bar{z}}} \end{Bmatrix} = \begin{bmatrix} \overline{W}_{12} & \overline{W}_{22} & \overline{W}_{23} \\ \overline{W}_{13} & \overline{W}_{23} & \overline{W}_{33} \end{bmatrix} \begin{Bmatrix} 1 \\ z_c \\ y_c \end{Bmatrix} \widehat{N}_{\bar{x}}. \tag{6.260}$$

Since $\widehat{N}_{\bar{x}}$ is applied at the centroid, the curvatures of the axis passing through the centroid are zero ($1/\rho_y = 1/\rho_z = 0$). Furthermore, the curvatures of the axis passing through the centroid are the same as the curvatures of the axis passing through the origin of the bar coordinate system. Thus we have

$$\frac{1}{\rho_y} = \frac{1}{\rho_z} = \frac{1}{\rho_{\bar{y}}} = \frac{1}{\rho_{\bar{z}}} = 0. \tag{6.261}$$

Equations (6.260) and (6.261) yield the coordinates z_c, y_c of the centroid with respect to the origin of the bar coordinate system as follows:

$$\begin{Bmatrix} z_c \\ y_c \end{Bmatrix} = -\begin{bmatrix} \overline{W}_{22} & \overline{W}_{23} \\ \overline{W}_{23} & \overline{W}_{33} \end{bmatrix}^{-1} \begin{bmatrix} \overline{W}_{12} \\ \overline{W}_{13} \end{bmatrix}. \tag{6.262}$$

6.6.4 Restrained Warping

When restrained warping is taken into account and the layup of each wall is balanced, the force–strain relationships may be approximated by[12]

$$\begin{Bmatrix} \widehat{N}_x \\ \widehat{M}_y \\ \widehat{M}_z \\ \widehat{T}_{sv} \\ \widehat{T}_\omega \end{Bmatrix} = \begin{bmatrix} P_{11} & P_{12} & P_{13} & P_{14} & 0 \\ P_{12} & P_{22} & P_{23} & P_{24} & 0 \\ P_{13} & P_{23} & P_{33} & P_{34} & 0 \\ P_{14} & P_{24} & P_{34} & P_{44} & 0 \\ 0 & 0 & 0 & 0 & \widehat{EI}_\omega \end{bmatrix} \begin{Bmatrix} \epsilon_x^o \\ \frac{1}{\rho_y} \\ \frac{1}{\rho_z} \\ \vartheta \\ -\dfrac{d^2\vartheta}{dx^2} \end{Bmatrix}, \tag{6.263}$$

where $\widehat{EI}_\omega$ is to be calculated as for orthotropic beams. The effects of restrained warping on the displacements and stresses of beams with unbalanced layup are discussed by Bould and Tzeng.[13]

[12] A. Pluzsik and L. P. Kollár, Effect of Shear Deformation and Restrained Warping on the Displacements of Composite Beams, *Journal of Reinforced Plastics and Composites*, Vol. 21, 2002 (in press).

[13] N. R. Bould and L. Tzeng, A Vlasov Theory for Fiber-Reinforced Beams with Thin-Walled Cross-Sections. *International Journal of Solids and Structures*, Vol. 20, 277–297, 1984.

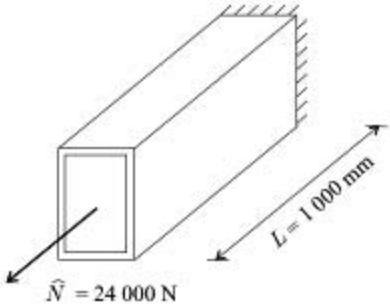

Figure 6.65: The box beam in Example 6.5.

6.5 Example. *An $L = 1$-m-long box-beam, with the cross section shown in Fig. 6.65, is made of graphite epoxy unidirectional plies. The material properties are given in Table 3.6 (page 81). The layup is $[0_{10}/45_{10}]$, with the 0-degree ply on the outside of the wall. The beam, built-in at one end and free at the other end, is subjected to an axial load of 24 000 N. By neglecting the effects of axial restraint, find the position of the centroid and calculate the maximum axial displacement and the maximum twist.*

Solution. The analysis follows the steps in Table 6.10 (page 268). From Table 6.10 we have

$$[R_k] = \begin{bmatrix} 1 & \bar{z}_k & \bar{y}_k & 0 \\ 0 & \cos\alpha_k & -\sin\alpha_k & 0 \\ 0 & \sin\alpha_k & \cos\alpha_k & 0 \\ 0 & 0 & 0 & 1 \end{bmatrix}, \tag{6.264}$$

where $\bar{y}_k$ and $\bar{z}_k$ are the coordinates of the midpoints of the wall segments, and α_k is the angle between η and the y coordinates at which η is tangent to the wall segment (Fig. 6.60). The values of these parameters for each flange and web are shown in Figure 6.66. With these values $[R_k]$ are

$$[R_1] = \begin{bmatrix} 1 & -0.035 & 0 & 0 \\ 0 & 1 & 0 & 0 \\ 0 & 0 & 1 & 0 \\ 0 & 0 & 0 & 1 \end{bmatrix} \quad [R_2] = \begin{bmatrix} 1 & 0 & 0.025 & 0 \\ 0 & 0 & -1 & 0 \\ 0 & 1 & 0 & 0 \\ 0 & 0 & 0 & 1 \end{bmatrix}$$

$$[R_3] = \begin{bmatrix} 1 & 0.035 & 0 & 0 \\ 0 & -1 & 0 & 0 \\ 0 & 0 & -1 & 0 \\ 0 & 0 & 0 & 1 \end{bmatrix} \quad [R_4] = \begin{bmatrix} 1 & 0 & -0.025 & 0 \\ 0 & 0 & 1 & 0 \\ 0 & -1 & 0 & 0 \\ 0 & 0 & 0 & 1 \end{bmatrix}.$$

The $[\widetilde{A}]$ matrix for each web and each flange is

$$\begin{bmatrix} \widetilde{A}_{11} & \widetilde{A}_{12} & \widetilde{A}_{13} \\ \widetilde{A}_{12} & \widetilde{A}_{22} & \widetilde{A}_{23} \\ \widetilde{A}_{13} & \widetilde{A}_{23} & \widetilde{A}_{33} \end{bmatrix}_k = \begin{bmatrix} \alpha_{11} & \beta_{11} & \beta_{16} \\ \beta_{11} & \delta_{11} & \delta_{16} \\ \beta_{16} & \delta_{16} & \delta_{66} \end{bmatrix}_k^{-1}. \tag{6.265}$$

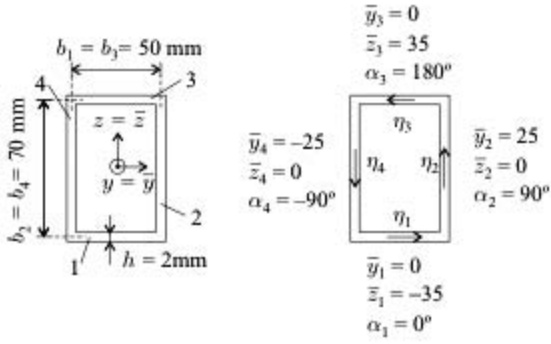

Figure 6.66: Parameters of the walls of the beam in Example 6.5.

With the elements of the compliance matrix in Eq. (3.56), $\tilde{A}_{11}$ for the flanges ($k = 1, 3$) and for the webs ($k = 2, 4$) are

$$(\tilde{A}_{11})_1 = (\tilde{A}_{11})_2 = (\tilde{A}_{11})_3 = (\tilde{A}_{11})_4 = 1.615 \times 10^8. \tag{6.266}$$

The distances between the midplanes of the corresponding wall segments are $b_1 = b_3 = 0.050$ m, $b_2 = b_4 = 0.070$ m (Fig. 6.66). The elements of $[\omega_k]$ are

$$[\omega_1] = [\omega_3] = \begin{bmatrix} 0.2688 & 341.4 & 0 & 110.6 \\ 341.4 & 806\,350 & 0 & 214\,130 \\ 0 & 0 & 594 & 0 \\ 110.6 & 214\,130 & 0 & 974\,290 \end{bmatrix} 10^{-6}$$

$$[\omega_2] = [\omega_4] = \begin{bmatrix} 0.1920 & 243.8 & 0 & 78.98 \\ 243.8 & 575\,970 & 0 & 152\,950 \\ 0 & 0 & 216.62 & 0 \\ 78.98 & 152\,950 & 0 & 695\,920 \end{bmatrix} \times 10^{-6}.$$

The $[I]$, $[L]$, and $[F]$ matrices are

$$\begin{aligned} [I] &= \begin{bmatrix} -107.82 & 0 & 0 & 0.080\,61 \\ -24.10 & 0 & 0 & 0.187\,36 \end{bmatrix} \times 10^{-3} \\ [L] &= \begin{bmatrix} 0.107\,8 & 0 & 0 & 0.006\,919 \\ 24.10 & 0 & 0 & -0.187\,36 \end{bmatrix} \times 10^{3} \\ [F] &= \begin{bmatrix} 0.013\,39 & -6.474 \\ -6.474 & 22\,150 \end{bmatrix} \times 10^{-6}. \end{aligned} \tag{6.267}$$

The stiffness matrix of the beam is

$$\begin{aligned} [\overline{P}] &= ([R_1]^T[\omega_1]^{-1}[R_1] + [R_2]^T[\omega_2]^{-1}[R_2] + [R_3]^T[\omega_3]^{-1}[R_3] + [L]^T[F]^{-1}[L]) \\ &= \begin{bmatrix} 39.93 & 0 & 0 & 0.067\,53 \\ 0 & 0.029\,49 & 0 & 0 \\ 0 & 0 & 0.017\,98 & 0 \\ 0.067\,53 & 0 & 0 & 0.004\,105 \end{bmatrix} \times 10^6, \end{aligned} \tag{6.268}$$

where $\overline{P}_{11}$ is in N; $\overline{P}_{22}$, $\overline{P}_{33}$, and $\overline{P}_{44}$ are in N · m^2; and $\overline{P}_{14}$ is in N · m. The compliance matrix is

$$[\overline{W}] = [\overline{P}]^{-1} = \begin{bmatrix} 0.025\,76 & 0 & 0 & -0.423\,7 \\ 0 & 33.91 & 0 & 0 \\ 0 & 0 & 55.63 & 0 \\ -0.423\,7 & 0 & 0 & 250.56 \end{bmatrix} \times 10^{-6}, \tag{6.269}$$

where $\overline{W}_{11}$ is in $\frac{1}{\text{N}}$; $\overline{W}_{22}$, $\overline{W}_{33}$, and $\overline{W}_{44}$ are in $\frac{1}{\text{N}\cdot\text{m}^2}$; $\overline{W}_{14}$ is in $\frac{1}{\text{N}\cdot\text{m}}$.

The location of the centroid is given by Eq. (6.262). With the preceding elements of the compliance matrix, we have

$$\begin{Bmatrix} z_c \\ y_c \end{Bmatrix} = -\begin{bmatrix} \overline{W}_{22} & \overline{W}_{23} \\ \overline{W}_{23} & \overline{W}_{33} \end{bmatrix}^{-1} \begin{bmatrix} \overline{W}_{12} \\ \overline{W}_{13} \end{bmatrix} = \begin{Bmatrix} 0 \\ 0 \end{Bmatrix}. \tag{6.270}$$

The forces acting at the centroid are

$$\begin{Bmatrix} \widehat{N} \\ \widehat{M}_y \\ \widehat{M}_z \\ \widehat{T} \end{Bmatrix} = \begin{Bmatrix} 24\,000 \\ 0 \\ 0 \\ 0 \end{Bmatrix}. \tag{6.271}$$

The strains, which are uniform along the cantilever, are (Eq. 6.249)

$$\begin{Bmatrix} \epsilon_x^0 \\ \frac{1}{\rho_y} \\ \frac{1}{\rho_z} \\ \vartheta \end{Bmatrix} = 10^{-7} \times \begin{bmatrix} 0.2576 & 0 & 0 & -0.0042 \\ 0 & 0.0004 & 0 & 0 \\ 0 & 0 & 0.0006 & 0 \\ -0.0042 & 0 & 0 & 0.0025 \end{bmatrix} \begin{Bmatrix} 24\,000 \\ 0 \\ 0 \\ 0 \end{Bmatrix}$$

$$= \begin{Bmatrix} 0.6182 \times 10^{-3} \\ 0 \\ 0 \\ -0.010\,17 \end{Bmatrix}. \tag{6.272}$$

The unit of ϑ is 1/m. The axial displacement and the twist of the free end are

$$\begin{aligned} u &= \epsilon_x^0 \times L = 0.6182 \times 10^{-3} \times 1 = 0.000\,618\ \text{m} = 0.618\ \text{mm} \\ \psi &= \vartheta \times L = -0.010\,17 \times 1 = -0.010\,17\ \text{rad} = -0.58^\circ. \end{aligned} \tag{6.273}$$

In comparison, u and ψ calculated by the finite element method are

$$u = 0.616\ \text{mm} \qquad \psi = -0.57^\circ. \tag{6.274}$$

6.7 Transversely Loaded Thin-Walled Beams

We consider a transversely loaded beam (Fig. 6.67). The applied transverse load, with components p_y and p_z, produces bending moments $\widehat{M}_y$, $\widehat{M}_z$, a torque $\widehat{T}$, and transverse shear forces $\widehat{V}_y$, $\widehat{V}_z$. The bending moments $\widehat{M}_y$, $\widehat{M}_z$ give rise to an axial

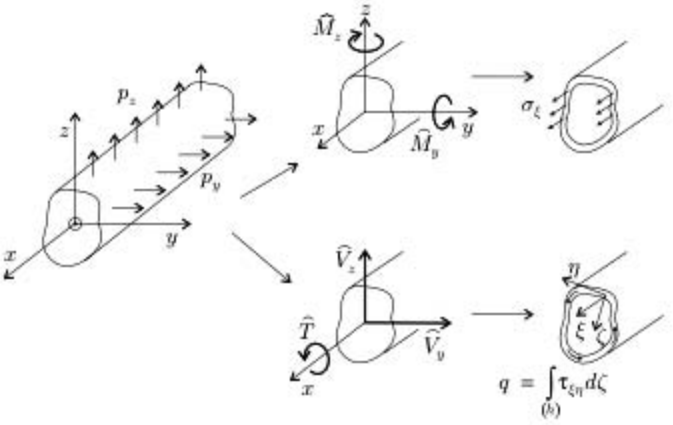

Figure 6.67: Internal forces and stresses acting on the cross section of a transversely loaded thin-walled beam. The ξ–η–ζ coordinate system is shown in Figure 6.60.

stress σ_ξ, and the internal forces $\widehat{V}_y$, $\widehat{V}_z$, and $\widehat{T}$ give rise to shear stress $\tau_{\xi\eta}$ in the wall. It is customary to represent the shear stress by the shear flow q defined as (Eq. 6.189),

$$q \equiv \int_{(h)} \tau_{\xi\eta} d\zeta = N_{\xi\eta}, \tag{6.275}$$

where h is the thickness of the wall.

The load p_z applied along a line A–A may be replaced by an equivalent load system consisting of a load p_z applied along line B–B and a torque load $t = -p_z d$, where d is the horizontal distance between points A and B (Fig. 6.68). The load p_z results in a shear flow q^V while the torque load introduces a shear flow q^T. The total shear flow is

$$q = q^T + q^V. \tag{6.276}$$

Both shear flows q^T and q^V as well as the axial stress σ_ξ cause twisting of the beam, represented by the rate of twist ϑ as follows:

$$\vartheta \Longrightarrow \underset{\sigma_\xi}{\text{due to}} + \underset{q^T}{\text{due to}} + \underset{q^V}{\text{due to}} \qquad \underset{\text{line } A\text{–}A}{p_z \text{ along an arbitrary}}$$

There is a special location of the line B–B referred to as the shear center.[14] When the load is applied at this location (i.e., at the shear center), the shear flow q^V does not cause twisting of the beam, and the rate of twist depends only on σ_ξ and q^T:

$$\vartheta \Longrightarrow \underset{\sigma_\xi}{\text{due to}} + \underset{q^T}{\text{due to}} \qquad \underset{\text{shear center.}}{p_z \text{ at the}}$$

[14] E. H. Mansfield and A. J. Sobey, The Fiber Composite Helicopter Blade – Part 1: Stiffness Properties – Part 2: Prospects for Aeroelastic Tailoring. *Aeronautical Quarterly*, Vol. 30, 413–449, 1979.

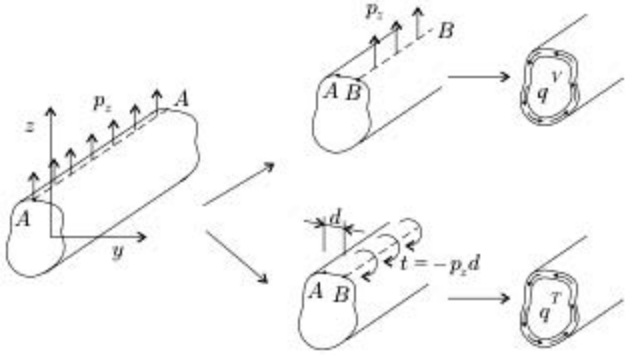

Figure 6.68: Shear flow in a transversely loaded thin-walled beam.

For a beam with arbitrary layup the axial stress σ_ξ introduces a twist even when the load is applied at the shear center. However, σ_ξ does not introduce a twist in orthotropic beams. Therefore, when the beam is orthotropic *and* the load acts at the shear center, the rate of twist depends only on the shear flow due to the torque:

$$\vartheta \Longrightarrow \text{due to } q^T \qquad \begin{matrix} \text{orthotropic} \\ p_z \text{ at the shear center.} \end{matrix}$$

In summary, when the transverse load acts at the shear center, an orthotropic beam does not twist, whereas a beam with arbitrary layup does twist.

The transverse load p_z causes transverse shear forces $\widehat{V}_y$, $\widehat{V}_z$, bending moments $\widehat{M}_y$, $\widehat{M}_z$, and torque $\widehat{T}$ (Fig. 6.67). The displacements caused by the shear forces $\widehat{V}_y$, $\widehat{V}_z$ are neglected. The displacements due to the bending moments $\widehat{M}_y$ and $\widehat{M}_z$ and the torque $\widehat{T}$ are determined by the analyses presented in Sections 6.3–6.6.

The normal stresses are determined by the analyses presented in Sections 6.3.4, 6.4, and 6.6.2.

The shear stresses in the wall induced by the bending moments $\widehat{M}_y$ and $\widehat{M}_z$ and the torque $\widehat{T}$ are determined by the analyses presented in Sections 6.5 and 6.6. The shear stresses in the wall due to the shear forces $\widehat{V}_y$, $\widehat{V}_z$ are discussed next. The total stresses are obtained by superimposing the stresses caused by bending, torsion, and shear.

6.7.1 Beams with Orthotropic Layup or with Symmetrical Cross Section

We consider beams that have either orthotropic layup (page 207) or have symmetrical cross section with the loads applied in the symmetry plane (Fig. 6.4).

In the following we calculate the shear flow in open- and closed-section beams when the shear forces $\widehat{V}_z$ and $\widehat{V}_y$ act at the shear center (Fig. 6.69).

Open-section beams. There is no load applied in the axial direction. Equilibrium of an element in the axial $\xi \equiv x$ direction gives (Fig. 6.70)

$$\frac{\partial q^{\text{op}}}{\partial \eta} + \frac{\partial N_\xi}{\partial \xi} = 0, \tag{6.277}$$

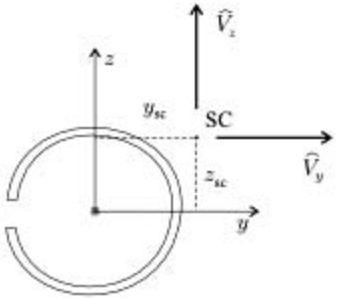

Figure 6.69: Beam subjected to shear forces at the shear center.

where q^{op} is the shear flow and N_ξ is the axial force (per unit length) at an arbitrarily chosen reference surface. Integration of this expression yields

$$q^{op}(s_1) = -\int_0^{s_1} \frac{\partial N_\xi}{\partial \xi} d\eta, \tag{6.278}$$

where η is the coordinate along the wall and s_1 is the distance from the free edge to the point of interest.

For an orthotropic wall segment (unsymmetrical layup) N_ξ is obtained by combining Eqs. (6.118), (6.111), and (6.112) as follows:

$$\begin{aligned} N_\xi = {} & \frac{\widehat{EI}_{zz}\widehat{M}_y - \widehat{EI}_{yz}\widehat{M}_z}{\widehat{EI}_{yy}\widehat{EI}_{zz} - (\widehat{EI}_{yz})^2}\left(z\frac{\delta_{11}}{D} - \cos\alpha\frac{\beta_{11}}{D}\right) \\ & + \frac{-\widehat{EI}_{yz}\widehat{M}_y + \widehat{EI}_{yy}\widehat{M}_z}{\widehat{EI}_{yy}\widehat{EI}_{zz} - (\widehat{EI}_{yz})^2}\left(y\frac{\delta_{11}}{D} + \sin\alpha\frac{\beta_{11}}{D}\right) + \frac{\widehat{N}}{\widehat{EA}}\frac{\delta_{11}}{D}. \end{aligned} \tag{6.279}$$

The relationship between the shear forces and the bending moments are (Eq. 6.3)

$$\widehat{V}_z = \frac{\partial \widehat{M}_y}{\partial x} \qquad \widehat{V}_y = \frac{\partial \widehat{M}_z}{\partial x}. \tag{6.280}$$

By combining Eqs. (6.278)–(6.280), and by noting that for a transversely loaded beam the normal force $\widehat{N}$ is zero, we obtain the following expression for the shear flow:

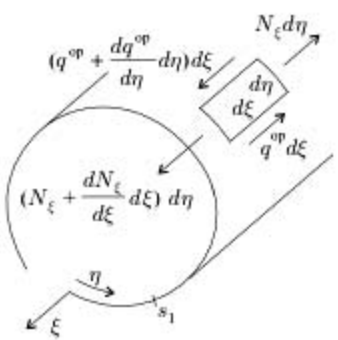

Figure 6.70: Forces on an element of a transversely loaded, thin-walled open-section beam.

orthotropic and unsymmetrical layup, arbitrary cross section:

$$q^{\text{op}}(s_1) = -\frac{\widehat{EI}_{zz}\widehat{V}_z - \widehat{EI}_{yz}\widehat{V}_y}{\widehat{EI}_{yy}\widehat{EI}_{zz} - (\widehat{EI}_{yz})^2}\int_0^{s_1}\left(z\frac{\delta_{11}}{D} - \cos\alpha\frac{\beta_{11}}{D}\right)d\eta$$
$$-\frac{-\widehat{EI}_{yz}\widehat{V}_z + \widehat{EI}_{yy}\widehat{V}_y}{\widehat{EI}_{yy}\widehat{EI}_{zz} - (\widehat{EI}_{yz})^2}\int_0^{s_1}\left(y\frac{\delta_{11}}{D} + \sin\alpha\frac{\beta_{11}}{D}\right)d\eta. \tag{6.281}$$

We emphasize that $\widehat{V}_z$ and $\widehat{V}_y$ act at the shear center and $\widehat{EI}_{yy}$, $\widehat{EI}_{yz}$, $\widehat{EI}_{zz}$, are the bending stiffnesses in the y–z coordinate system attached to the centroid of the cross section.

When the layup of each wall segment is orthotropic and symmetrical, the expression for the shear flow is obtained from Eqs. (6.278), (6.280), (6.111), (6.112), and (6.125)

orthotropic and symmetrical layup, arbitrary cross section:

$$q^{\text{op}}(s_1) = -\frac{\widehat{EI}_{zz}\widehat{V}_z - \widehat{EI}_{yz}\widehat{V}_y}{\widehat{EI}_{yy}\widehat{EI}_{zz} - (\widehat{EI}_{yz})^2}\int_0^{s_1}\left(z\frac{1}{a_{11}}\right)d\eta$$
$$-\frac{-\widehat{EI}_{yz}\widehat{V}_z + \widehat{EI}_{yy}\widehat{V}_y}{\widehat{EI}_{yy}\widehat{EI}_{zz} - (\widehat{EI}_{yz})^2}\int_0^{s_1}\left(y\frac{1}{a_{11}}\right)d\eta. \tag{6.282}$$

When the beam's cross section is symmetrical, the shear center is in the x–z symmetry plane. When the transverse load acts in this symmetry plane, the force is given by Eq. (6.131), (nonorthotropic, unsymmetrical layup). This equation, in combination with Eqs. (6.278), (6.280), and (6.111), yields

arbitrary layup, symmetrical cross section:

$$q^{\text{op}}(s_1) = -\frac{\widehat{V}_z}{\widehat{EI}_{yy}}\int_0^{s_1}\left(z\frac{\overline{\delta}_{11}}{\overline{D}} - \cos\alpha\frac{\overline{\beta}_{11}}{\overline{D}}\right)d\eta. \tag{6.283}$$

For an isotropic beam $1/a_{11} = Eh$ (Eq. 3.43), and the expression for the shear flow (Eq. 6.282) becomes

isotropic beam:

$$q^{\text{op}}(s_1) = -\frac{I_{zz}\widehat{V}_z - I_{yz}\widehat{V}_y}{I_{yy}I_{zz} - (I_{yz})^2}\int_0^{s_1}(zh)\,d\eta - \frac{-I_{yz}\widehat{V}_z + I_{yy}\widehat{V}_y}{I_{yy}I_{zz} - (I_{yz})^2}\int_0^{s_1}(yh)\,d\eta. \tag{6.284}$$

Illustration of the shear flow in an open-section beam is given in Example 6.2 (page 239).

Closed-section beams – single cell. In a single-cell, closed-section beam, the shear flow may be expressed in two parts. The first part is the shear flow (denoted by q^{op}) that would exist if the beam were cut longitudinally and the beam were open. The second is a constant shear flow q^{c} induced by the forces acting along

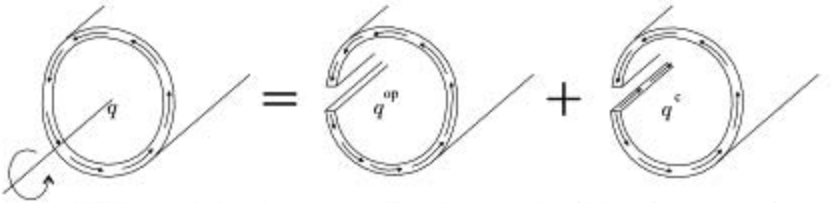

Figure 6.71: Superposition of the open cell and constant shear flows in a transversely loaded, single-cell closed-section beam.

the "cut" edges (Fig. 6.71) (q^c depends on the location of the cut). Thus, we write the shear flow in the closed single-cell beam as

$$q = q^{op} + q^c. \tag{6.285}$$

The shear flow q^{op} is calculated by Eqs. (6.278)–(6.283). The constant shear flow q^c is determined as follows. When the shear forces $\widehat{V}_y$ and $\widehat{V}_z$ act at the shear center (which is the case here), the beam does not twist. Hence, from Eq. (6.188) we have

$$\vartheta = \frac{1}{2A}\oint \gamma^o_{\xi\eta} d\eta = 0. \tag{6.286}$$

The shear strain $\gamma^o_{\xi\eta}$ in each wall segment is calculated at the "torque neutral" surface. From Eq. (6.195) we have

$$\gamma^o_{\xi\eta} = \alpha^v_{66} q. \tag{6.287}$$

From Eqs. (6.285)–(6.287) we obtain

$$\vartheta = \frac{1}{2A}\oint \alpha^v_{66} q^{op} d\eta + \frac{1}{2A} q^c \oint \alpha^v_{66} d\eta = 0. \tag{6.288}$$

From this equation we have

$$q^c = -\frac{\oint \alpha^v_{66} q^{op} d\eta}{\oint \alpha^v_{66} d\eta}. \tag{6.289}$$

Closed-section beams – multicell. To calculate the shear flow in a multicell beam (Fig. 6.72), we "cut" longitudinally each cell, thereby producing an open-section beam. The shear flow q^{op} in this open-section beam is calculated by the analysis given by Eqs. (6.278)–(6.283).

In each cell there is a constant shear flow q_i^c induced by the forces acting along the edges of the cut. In a beam with L cells there are L constant shear flows. The shear flow is the sum of the open-section and the constant shear flows. For a wall that belongs to one cell only, q is the sum of the open-cell shear flow and the constant shear flow in the appropriate cell ($q = q^{op} + q_i^c$). For a wall adjoining two cells, the shear flow is the sum of the constant shear flows of the adjacent cells and the open-section beam shear flow, as illustrated in Fig. 6.72.

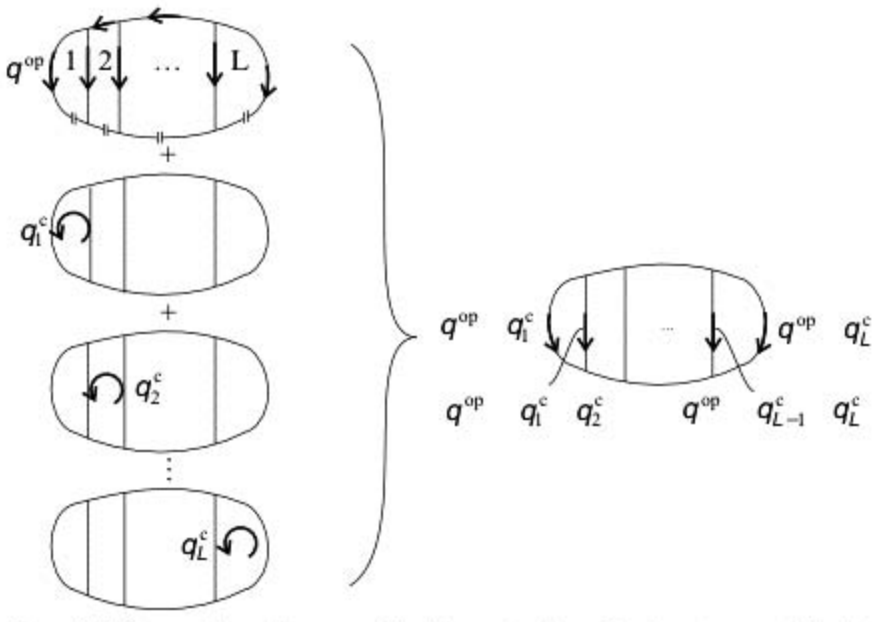

Figure 6.72: Superposition of the open cell and the constant shear flows in a transversely loaded, multicell, closed-section beam.

When the shear forces $\widehat{V}_y$ and $\widehat{V}_z$ act at the shear center (which is the case here), the beam does not twist ($\vartheta = 0$). Hence, for each cell we write (Eq. 6.188)

$$\vartheta = \frac{1}{2A_l} \oint_{\text{cell } l} \gamma^o_{\xi\eta} d\eta = 0 \qquad l = 1, 2, \ldots, L. \tag{6.290}$$

The shear strain $\gamma^o_{\xi\eta}$ at the "torque neutral" surface in each wall segment is (Eq. 6.195)

$$\gamma^o_{\xi\eta} = \alpha^v_{66} q, \tag{6.291}$$

where q is the shear flow in the wall segment (Eq. 6.285).

By combining Eqs. (6.290) and (6.291), we obtain

$$\frac{1}{2A_l} \oint_{\text{cell } l} \alpha^v_{66} q d\eta = 0 \qquad l = 1, 2, \ldots, L. \tag{6.292}$$

Equation (6.292) represents L equations, which can be solved for the L unknowns: $q_1^c, q_2^c, \ldots, q_L^c$.

The stresses in the walls are calculated the same way as for a single-cell beam.

6.7.2 Beams with Arbitrary Layup

In this section we determine the shear flows (caused by the shear forces $\widehat{V}_z$ and $\widehat{V}_y$ acting at the shear center) in beams consisting of wall segments with arbitrary layup. No load is applied in the axial direction. Equilibrium in the ξ direction gives

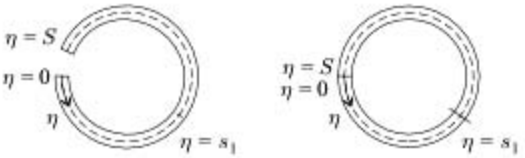

Figure 6.73: Coordinate η along the circumference of an open- and a closed-section beam.

(Eq. 6.277, see Fig. 6.70)

$$\frac{\partial q}{\partial \eta} + \frac{\partial N_\xi}{\partial \xi} = 0. \tag{6.293}$$

To determine the shear flow q, the derivative of the axial force (per unit length) $\partial N_\xi / \partial \xi$ must be known.

Open-section beams. In an open-section beam the shear flow is (Eq. 6.278)

$$q^{\text{op}}(s_1) = -\int_0^{s_1} \frac{\partial N_\xi}{\partial \xi} d\eta, \tag{6.294}$$

where η is the coordinate along the circumference (Fig. 6.73, left). The term $\partial N_\xi / \partial \xi$ is evaluated as follows. By differentiating both sides of Eq. (6.256) with respect to ξ, we have

$$\begin{Bmatrix} \frac{\partial N_\xi}{\partial \xi} \\ \frac{\partial M_\xi}{\partial \xi} \\ \frac{\partial M_{\xi\eta}}{\partial \xi} \end{Bmatrix}_k = [\tilde{\mu}_k]^{-1} [R_\eta] [R_k] [\overline{W}] \begin{Bmatrix} \frac{\partial \widehat{N}_{\bar{x}}}{\partial \xi} \\ \frac{\partial \widehat{M}_{\bar{y}}}{\partial \xi} \\ \frac{\partial \widehat{M}_{\bar{z}}}{\partial \xi} \\ \frac{\partial \widehat{T}_{\bar{x}}}{\partial \xi} \end{Bmatrix}. \tag{6.295}$$

There is no applied load in the axial direction ($\widehat{N}_{\bar{x}} = 0$), and $\partial \widehat{N}_{\bar{x}} / \partial \xi$ is zero. In addition, (see Eq. 6.247) we have

$$\widehat{M}_{\bar{y}} = \widehat{M}_y \qquad \widehat{M}_{\bar{z}} = \widehat{M}_z. \tag{6.296}$$

The shear forces are (Eq. 6.3, $\xi \equiv x$)

$$\widehat{V}_z = \frac{\partial \widehat{M}_{\bar{y}}}{\partial \xi} \qquad \widehat{V}_y = \frac{\partial \widehat{M}_{\bar{z}}}{\partial \xi}. \tag{6.297}$$

The transverse load acts at the shear center. Hence, the torque load t is zero, and we have (see Eq. 6.3)

$$\frac{\partial \widehat{T}}{\partial \xi} = -t = 0. \tag{6.298}$$

Substitution of Eqs. (6.297), (6.298) and $\partial \widehat{N}_{\bar{x}} / \partial \xi = 0$ into Eq. (6.295) gives

$$\begin{Bmatrix} \frac{\partial N_\xi}{\partial \xi} \\ \frac{\partial M_\xi}{\partial \xi} \\ \frac{\partial M_{\xi\eta}}{\partial \xi} \end{Bmatrix}_k = [\tilde{\mu}_k]^{-1} [R_\eta] [R_k] [\overline{W}] \begin{Bmatrix} 0 \\ \widehat{V}_z \\ \widehat{V}_y \\ 0 \end{Bmatrix}. \tag{6.299}$$

We are interested only in $\partial N_\xi/\partial\xi$ given by this equation since this is used in Eq. (6.294) to determine the shear flow.

Closed-section beams. In a closed-section beam the shear flow is obtained by integration of Eq. (6.293),

$$q = \underbrace{-\int_0^{s_1} \frac{\partial N_\xi}{\partial \xi} d\eta}_{q^{op}} + q^c, \tag{6.300}$$

where q^{op} is defined as

$$q^{op} = -\int_0^{s_1} \frac{\partial N_\xi}{\partial \xi} d\eta, \tag{6.301}$$

η is the coordinate along the circumference (Fig. 6.73, right) and q^c is a constant shear flow. The term $\partial N_\xi/\partial\xi$ is obtained by differentiating both sides of Eq. (6.259) as follows:

$$\begin{Bmatrix} \frac{\partial N_\xi}{\partial \xi} \\ \frac{\partial M_\xi}{\partial \xi} \\ \frac{\partial M_{\xi\eta}}{\partial \xi} \end{Bmatrix}_k = [\widetilde{\mu}_k]^{-1}([R_\eta][R_k] - [\widetilde{\nu}_k][F]^{-1}[L])[\overline{W}] \begin{Bmatrix} \frac{\partial \widehat{N}_{\overline{x}}}{\partial \xi} \\ \frac{\partial \widehat{M}_{\overline{y}}}{\partial \xi} \\ \frac{\partial \widehat{M}_{\overline{z}}}{\partial \xi} \\ \frac{\partial \widehat{T}_{\overline{x}}}{\partial \xi} \end{Bmatrix}. \tag{6.302}$$

Since there is no applied load in the axial direction, $\partial \widehat{N}_{\overline{x}}/\partial\xi$ is zero. Furthermore, the transverse load acts at the shear center. Hence, the torque load t is zero and, consequently, $\partial \widehat{T}/\partial\xi$ is zero (see Eq. 6.3). When Eq. (6.297) is used, the preceding equation (Eq. 6.302) results in

$$\begin{Bmatrix} \frac{\partial N_\xi}{\partial \xi} \\ \frac{\partial M_\xi}{\partial \xi} \\ \frac{\partial M_{\xi\eta}}{\partial \xi} \end{Bmatrix}_k = [\widetilde{\mu}_k]^{-1}([R_\eta][R_k] - [\widetilde{\nu}_k][F]^{-1}[L])[\overline{W}] \begin{Bmatrix} 0 \\ \widehat{V}_z \\ \widehat{V}_y \\ 0 \end{Bmatrix}, \tag{6.303}$$

where $\widehat{V}_y$ and $\widehat{V}_z$ are the shear forces (Fig. 6.2). The term $\partial N_\xi/\partial\xi$ given by this expression is used to calculate q^{op} (Eq. 6.301).

The constant shear flow is denoted by q^c. We note that the rate of twist ϑ in the x–y–z coordinate system is the same as the rate of twist $\overline{\vartheta}$ in the $\overline{x}$–$\overline{y}$–$\overline{z}$ coordinate system. Thus, from Eq. (6.187) we have

$$-2A\overline{\vartheta} + \oint \gamma^o_{\xi\eta} d\eta = 0. \tag{6.304}$$

Equation (6.151) gives

$$\oint \kappa_\eta d\eta = 0. \tag{6.305}$$

By introducing Eq. (6.254) into these equations, and by noting that $N_{\xi\eta} = q$, and $N_\eta = 0$, we obtain

$$0 = \begin{Bmatrix} -2A\bar{\vartheta} \\ 0 \end{Bmatrix} + \oint \begin{bmatrix} \alpha_{16} & \beta_{16} & \beta_{66} \\ \beta_{12} & \delta_{12} & \delta_{26} \end{bmatrix} \begin{Bmatrix} N_\xi \\ M_\xi \\ M_{\xi\eta} \end{Bmatrix} d\eta + \oint \begin{bmatrix} \alpha_{66} & \beta_{26} \\ \beta_{26} & \delta_{22} \end{bmatrix} \begin{Bmatrix} q \\ M_\eta \end{Bmatrix} d\eta, \tag{6.306}$$

where $q = q^{\mathrm{op}} + q^{\mathrm{c}}$. The terms N_ξ, M_ξ, and $M_{\xi\eta}$ are evaluated by Eq. (6.259), and q^{op} by Eqs. (6.301) and (6.303). To determine M_η and q^{c}, we observe that these result from the bending moments $\widehat{M}_{\bar{z}}$, $\widehat{M}_{\bar{y}}$ and the shear forces $\widehat{V}_y$, $\widehat{V}_z$. Thus, we write

$$\begin{aligned} M_\eta &= M'_\eta + M''_\eta \\ q &= \underbrace{q^{\mathrm{c}\prime}}_{\substack{\text{due to} \\ \widehat{M}_{\bar{z}},\, \widehat{M}_{\bar{y}}}} + \underbrace{q^{\mathrm{op}} + q^{\mathrm{c}\prime\prime}}_{\substack{\text{due to} \\ \widehat{V}_y,\, \widehat{V}_z}}, \end{aligned} \tag{6.307}$$

where M'_η and $q^{\mathrm{c}\prime}$ are calculated by Eq. (6.258).

The terms $\widehat{V}_y$ and $\widehat{V}_z$ introduce only M''_η, q^{op}, and $q^{\mathrm{c}\prime\prime}$. Thus, when these shear forces are considered, we have $M_\eta = M''_\eta$, $q = q^{\mathrm{op}} + q^{\mathrm{c}} = q^{\mathrm{op}} + q^{\mathrm{c}\prime\prime}$, and $N_\xi = M_\xi = M_{\xi\eta} = 0$. The shear forces act at the shear center and hence the cross section does not twist ($\bar{\vartheta} = 0$). Accordingly, (Eq. 6.306) becomes

$$0 = \oint \begin{Bmatrix} \alpha_{66} \\ \beta_{26} \end{Bmatrix} q^{\mathrm{op}} d\eta + \oint \begin{bmatrix} \alpha_{66} & \beta_{26} \\ \beta_{26} & \delta_{22} \end{bmatrix} d\eta \begin{Bmatrix} q^{\mathrm{c}\prime\prime} \\ M''_\eta \end{Bmatrix}. \tag{6.308}$$

These equations are to be solved for $q^{\mathrm{c}\prime\prime}$ and M''_η as follows:

$$\begin{Bmatrix} q^{\mathrm{c}\prime\prime} \\ M''_\eta \end{Bmatrix} = -\left\{ \oint \begin{bmatrix} \alpha_{66} & \beta_{26} \\ \beta_{26} & \delta_{22} \end{bmatrix} d\eta \right\}^{-1} \oint \begin{Bmatrix} \alpha_{66} \\ \beta_{26} \end{Bmatrix} q^{\mathrm{op}} d\eta. \tag{6.309}$$

6.7.3 Shear Center

By definition, shear forces acting at the shear center do not cause twist. We designate the location of the shear center by the distances z_{sc} and y_{sc} from the centroid (Fig. 6.74). To determine these distances, we apply a force $\widehat{V}_y$ acting at the shear center and calculate the corresponding shear flow q. The torque of the external force about the centroid is equal to the torque produced by the internal shear flow (Fig. 6.75) as follows:

$$-\widehat{V}_y z_{\mathrm{sc}} = \int_{(S)} qp\, d\eta. \tag{6.310}$$

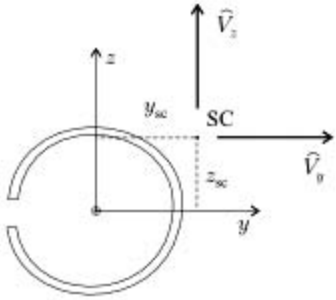

Figure 6.74: Shear center.

Hence, the z coordinate of the shear center is

$$z_{sc} = -\frac{\int_{(S)} qpd\eta}{\hat{V}_y}, \tag{6.311}$$

where q is the shear flow due to $\hat{V}_y$.

The distance y_{sc} is determined by applying a force $\hat{V}_z$ at the shear center (Fig. 6.74). By an argument similar to that leading to the preceding equation, we have

$$y_{sc} = \frac{\int_{(S)} qpd\eta}{\hat{V}_z}, \tag{6.312}$$

where q is the shear flow due to $\hat{V}_z$.

For beams with arbitrary layup, the shear flow is determined by the equations given in Section 6.7.2. For orthotropic beams the shear flows are determined by the equations given in Section 6.7.1.

Approximate calculation of the shear center. Approximate expressions for the location of the shear center of open-section orthotropic beams can be obtained as follows. The major contributor to the shear flow is the normal axial stress N_ξ caused by bending. In a thin-walled composite segment N_ξ may be approximated by Eq. (6.243) and in an isotropic beam by Eq. (6.241). By comparing these equations we see that the composite beam's tensile stiffness $1/\alpha_{11}^o$ corresponds to the isotropic beam's tensile stiffness Eh. Thus, the location of the shear center of an open-section orthotropic beam may be approximated by replacing Eh by $1/\alpha_{11}^o$ in the expression[15] for the location of the shear center of the corresponding isotropic beam. The coordinates of shear centers of frequently used cross sections are given in Table A.5.

6.6 Example. *An $L = 0.6$-m-long C-section beam, with the cross section shown in Figure 6.76, is made of graphite epoxy. The material properties are given in Table 3.6 (page 81). The layup is $[\pm 45_2^t/0_{12}/\pm 45_2^t]$. The beam is built-in at both ends. The beam is subjected to a uniformly distributed load ($p = -1\,500$ N/m) acting along*

[15] S. P. Timoshenko and J. Gere, *Theory of Elastic Stability*. 2nd edition. McGraw-Hill, New York, 1961, p. 530.

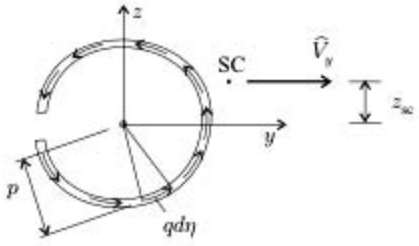

Figure 6.75: The shear force $\widehat{V}_y$ and the corresponding shear flow.

the centerline of the flange (Fig. 6.77). By neglecting the effects of axial restraint, find the position of the shear center and calculate the maximum deflection, the maximum twist, and the ply stresses and strains.

Solution. From Table A.1 the tensile stiffness and the location of the centroid are

$$\begin{aligned} \widehat{EA} &= \frac{2b_f}{(a_{11})_f} + \frac{b_w}{(a_{11})_w} = 30.87 \times 10^6 \text{ N} \\ y_c &= \frac{1}{\widehat{EA}}\left(\frac{2b_f}{(a_{11})_f}\frac{b_f}{2} + \frac{b_w}{(a_{11})_w} d_f\right) = 0.0340 \text{ m}, \end{aligned} \tag{6.313}$$

where a_{11} for both the web and the flange is $(a_{11})_w = (a_{11})_f = 5.18 \times 10^{-9}$ m/N (Table 3.8, page 85). The dimensions $b_f = 0.05$ m, $b_w = 0.06$ m, $d_f = 0.049$ m, and $d = 0.062$ m are shown in Fig.6.76. The bending stiffnesses are (Table A.1)

$$\begin{aligned} \widehat{EI}_{yy} &= \frac{b_f}{(a_{11})_f}\frac{d^2}{2} + \frac{2b_f}{(d_{11})_f} + \frac{b_w^3}{12(a_{11})_w} \\ \widehat{EI}_{zz} &= \frac{b_w}{(a_{11})_w}(d_f - y_c)^2 + \frac{b_w}{(d_{11})_w} + \frac{2}{(a_{11})_f}\left(\frac{y_c^3}{3} + \frac{(b_f - y_c)^3}{3}\right), \end{aligned} \tag{6.314}$$

where d_{11} for both the web and the flange is $(d_{11})_w = (d_{11})_f = 33.10 \times 10^{-3} \frac{1}{\text{N} \cdot \text{m}}$ (Table 3.8, page 85). Equation (6.314) yields

$$\widehat{EI}_{yy} = 22\,015 \text{ N} \cdot \text{m}^2 \qquad \widehat{EI}_{zz} = 8\,188 \text{ N} \cdot \text{m}^2. \tag{6.315}$$

The torsional stiffness and the location of the shear center are given in Table A.5. For symmetrical layup (which is the case here), δ is replaced by d

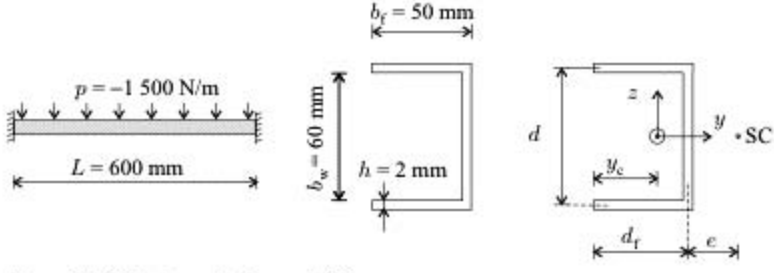

Figure 6.76: The beam in Example 6.6.

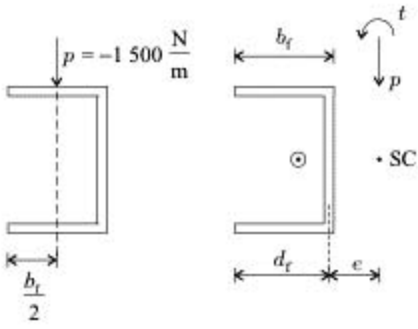

Figure 6.77: Loading on the C-section beam in Example 6.6 (left) and loading with respect to the shear center (right).

and α by a, and we write

$$\widehat{GI}_t = 4\left(\frac{2b_f}{(d_{66})_f} + \frac{b_w}{(d_{66})_w}\right) = 13.19\ \mathrm{N\cdot m^2} \tag{6.316}$$

$$e = \frac{\dfrac{3b_f^2}{(a_{11})_f}}{\dfrac{6b_f}{(a_{11})_f} + \dfrac{d}{(a_{11})_w}} = 0.0207\ \mathrm{m}, \tag{6.317}$$

where for both the web and the flange d_{66} is $(d_{66})_w = (d_{66})_f = 48.51 \times 10^{-3}\frac{1}{\mathrm{N\cdot m}}$ (Table 3.8, page 85).

The loads with respect to the shear center are (Fig. 6.77, $d_f + e - \frac{b_f}{2} = 0.0447\ \mathrm{m}$)

$$\begin{aligned} p &= -1\,500\ \frac{\mathrm{N}}{\mathrm{m}} && \text{(distributed load)} \\ t &= -p \times \left(d_f + e - \frac{b_f}{2}\right) = 67.08\ \frac{\mathrm{N\cdot m}}{\mathrm{m}} && \text{(distributed torque).} \end{aligned} \tag{6.318}$$

The corresponding bending moment $\widehat{M}_y$, shear force $\widehat{V}_z$, and torque $\widehat{T}$ diagrams are given in Figure 6.78. The maximum values are

$$\begin{aligned} \widehat{M}_y^{\max} &= -\frac{pL^2}{12} = 45\ \mathrm{N\cdot m} \\ \widehat{V}_z^{\max} &= \frac{pL}{2} = -450\ \mathrm{N} \\ \widehat{T}^{\max} &= \frac{tL}{2} = 20.12\ \mathrm{N\cdot m}. \end{aligned} \tag{6.319}$$

The maximum deflection is (Table 7.3, page 332)

$$\widetilde{w} = \frac{1}{384}\frac{pL^4}{\widehat{EI}_{yy}} = -0.023 \times 10^{-3}\ \mathrm{m} = -0.0230\ \mathrm{mm}. \tag{6.320}$$

The maximum twist is at $x = L/2$ and is

$$\psi = \int_0^{L/2} \vartheta\, dx = \int_0^{L/2} \frac{\widehat{T}}{\widehat{GI}_t} dx, \tag{6.321}$$

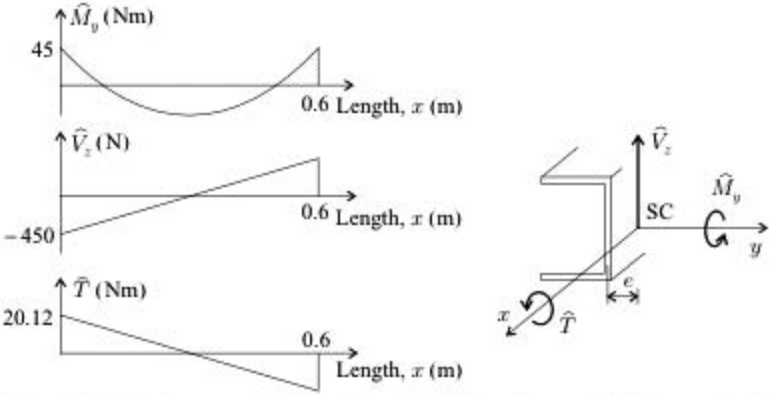

Figure 6.78: Bending moment $\widehat{M}_y$, shear force $\widehat{V}_z$, and torque $\widehat{T}$ diagrams for the beam in Example. 6.6.

where $\widehat{T}$ varies linearly with x (Fig. 6.78). Thus, the preceding integral yields

$$\psi = \frac{\widehat{T}^{\max} L}{4\widehat{G}\widehat{I}_t} = 0.2288 \text{ rad} = 13.1^\circ. \tag{6.322}$$

When restrained warping is taken into account, ψ is 0.217° (Example 6.7, Eq. 6.324). This demonstrates that restrained warping must be considered when calculating the rotation of open-section beams.

6.7 Example. *An $L = 0.6$-m-long C-section beam, with the cross section shown in Figure 6.79, is made of graphite epoxy. The material properties are given in Table 3.6 (page 81). The layup is $[\pm 45_2^f/0_{12}/\pm 45_2^f]$. The beam is built-in at both ends. The beam is subjected to a uniformly distributed load ($p = -1\,500$ N/m) acting along the centerline of the flange. By taking axial restraint into account, calculate the maximum deflection and the maximum twist.*

Solution. The bending moment $\widehat{M}_y$, shear force $\widehat{V}_z$, torque $\widehat{T}$, and the maximum deflection are identical to those given in Example 6.6. The twist is calculated as follows. The warping stiffness is given in Table A.5 (page 457). We replace α by a,

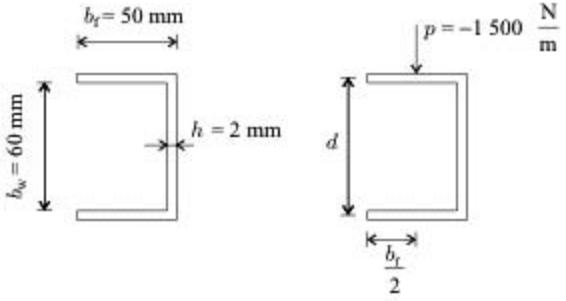

Figure 6.79: The cross section of the beam in Example 6.7 and the loading on the beam.

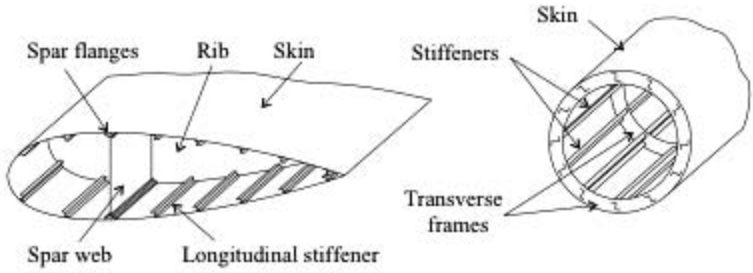

Figure 6.80: Illustration of stiffened structures.

and write

$$\widehat{EI}_\omega = \frac{b_f^3 d^2}{12} \frac{\frac{1}{(a_{11})_f}}{\frac{6b_f}{(a_{11})_f} + \frac{d}{(a_{11})_w}} \frac{\frac{3b_f}{(a_{11})_f} + \frac{2d}{(a_{11})_w}}{} = 5.847\ \mathrm{N \cdot m^4}, \tag{6.323}$$

where the dimensions $b_f = 0.05$ m and $d = 0.062$ m are shown in Figure 6.79, and a_{11} for both the web and the flange is $(a_{11})_w = (a_{11})_f = 5.18 \times 10^{-9}\ \frac{\mathrm{m}}{\mathrm{N}}$ (Table 3.8, page 85).

The maximum twist is at $x = L/2$ and is[16]

$$\psi = \frac{tL}{2\widehat{EI}_\omega \beta^3} \left[\frac{\beta L}{4} - \tanh\left(\frac{\beta L}{4}\right) \right] = 0.003\,79\ \mathrm{rad} = 0.217^\circ. \tag{6.324}$$

where t is the distributed torque load ($t = 67.08\ \frac{\mathrm{N \cdot m}}{\mathrm{m}}$, Eq. 6.318), and β is

$$\beta = \sqrt{\frac{\widehat{GI}_t}{\widehat{EI}_\omega}} = 1.502, \tag{6.325}$$

where $\widehat{GI}_t = 13.19\ \mathrm{N \cdot m^2}$ is given by Eq. (6.316). If we disregard restrained warping, the maximum twist is $\psi = 13.1^\circ$ (Eq. 6.322). By comparing this value with the value given above in Eq. (6.324), we see that restrained warping significantly reduces the twist.

6.8 Stiffened Thin-Walled Beams

Thin-walled structures are often reinforced with longitudinal stiffeners and transverse frames. Illustrations of such reinforced (semimonocoque) structures are airplane wings and fuselages (Fig. 6.80). In many applications such structures may be treated as reinforced thin-walled beams. Then, to simplify the analysis, the beam is idealized by representing the stiffeners as concentrated areas, sometimes called flanges or booms (Fig. 6.81). It is assumed that the flange carries all the bending load, and the web between the flanges carries the shear load. In the following we analyze stiffened beams in which the web is orthotropic.

[16] W. C. Young and R. G. Budynas, *Roark's Formulas for Stresses and Strains*. 7th edition. McGraw-Hill, New York, 2002, p. 425.



Figure 6.81: An actual and the idealized stiffened thin-walled beam.

The tensile stiffness of the beam is

$$\widehat{EA} = \sum_{m=1}^{M} \widehat{EA}_m, \tag{6.326}$$

where $\widehat{EA}_m$ is the tensile stiffness of the mth flange, and M is the total number of flanges (Fig. 6.82). The coordinates of the centroid are

$$y_c = \frac{\sum_{m=1}^{M} \bar{y}_m \widehat{EA}_m}{\widehat{EA}} \qquad z_c = \frac{\sum_{m=1}^{M} \bar{z}_m \widehat{EA}_m}{\widehat{EA}}, \tag{6.327}$$

where $\bar{z}_m$ and $\bar{y}_m$ are the coordinates of the mth flange in the $\bar{y}$–$\bar{z}$ arbitrarily chosen coordinate system.

The bending stiffnesses are

$$\widehat{EI}_{zz} = \sum_{m=1}^{M} y_m^2 \widehat{EA}_m \tag{6.328}$$

$$\widehat{EI}_{yy} = \sum_{m=1}^{M} z_m^2 \widehat{EA}_m \tag{6.329}$$

$$\widehat{EI}_{yz} = \sum_{m=1}^{M} y_m z_m \widehat{EA}_m, \tag{6.330}$$

where z_m and y_m are coordinates of the mth flange in the coordinate system attached to the centroid. The displacements and the radii of curvatures of semi-monocoque beams can be obtained by replacing EA and EI by the preceding replacement stiffnesses in the expressions describing the deflections of the corresponding isotropic beam.

The normal force carried by the mth flange is

$$\widehat{N}_{xm} = \left(\frac{1}{\rho_y} z_m + \frac{1}{\rho_z} y_m + \epsilon_x^o \right) \widehat{EA}_m, \tag{6.331}$$

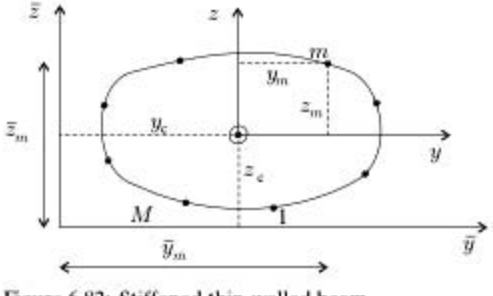

Figure 6.82: Stiffened thin-walled beam.

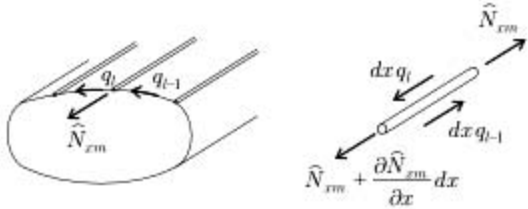

Figure 6.83: Equilibrium of a flange of a stiffened thin-walled beam.

where ρ_y, ρ_z are the radii of curvatures of the axis passing through the centroid and ϵ_x^o is the elongation of the longitudinal axis through the centroid (Eqs. 6.17 and 6.19).

The shear flows in reinforced (semimonocoque) and unreinforced (monocoque) beams are different. In reinforced walls the shear flow is calculated on the basis of the preceding stated approximation, namely, that the flanges carry all the bending load and the walls the shear load. Force balance in the direction of the flange results in (Fig. 6.83)

$$q_l - q_{l-1} = -\frac{\partial \widehat{N}_{xm}}{\partial x}, \tag{6.332}$$

where q_l and q_{l-1} are the shear flows in two adjacent walls, and $\widehat{N}_{xm}$ is the axial force in the mth flange. By utilizing the expression given for $\widehat{N}_{xm}$ in Eq. (6.331) and employing Eqs. (6.17) and (6.19), we obtain the change in shear flow induced by a flange as follows:

$$\begin{aligned} q_l - q_{l-1} = &-\frac{\widehat{EI}_{zz}\widehat{V}_z - \widehat{EI}_{yz}\widehat{V}_y}{\widehat{EI}_{yy}\widehat{EI}_{zz} - (\widehat{EI}_{yz})^2} z_m \widehat{EA}_m \\ &-\frac{-\widehat{EI}_{yz}\widehat{V}_z + \widehat{EI}_{yy}\widehat{V}_y}{\widehat{EI}_{yy}\widehat{EI}_{zz} - (\widehat{EI}_{yz})^2} y_m \widehat{EA}_m. \end{aligned} \tag{6.333}$$

Torsion. In the absence of axial constraint there are no axial forces either in open- or in closed-section semimonocoque beams subjected to pure torque. Therefore, the presence of booms does not affect the shear flow, and the analyses given in Section 6.5 for the torsion of unreinforced (monocoque) thin-walled beams apply to reinforced (semimonocoque) thin-walled beams.

6.9 Buckling of Beams

In this section we address the buckling loads of orthotropic composite beams. The buckling loads of such beams are calculated from the equilibrium equations (which include the changes in geometry during buckling) and the strain–displacement and the force–strain relationships. The first two of these are identical for isotropic and orthotropic beams. However, the force–strain relationships of isotropic and orthotropic beams are different. The force–strain relationships for an isotropic beam are obtained by combining Eqs. (6.4) and (6.239)

isotropic:

$$\begin{Bmatrix} \widehat{N} \\ \widehat{M}_y \\ \widehat{M}_z \\ \widehat{T}_{sv} \\ \widehat{T}_{\omega} \end{Bmatrix} = \begin{bmatrix} EA & 0 & 0 & 0 & 0 \\ 0 & EI_{yy} & EI_{yz} & 0 & 0 \\ 0 & EI_{yz} & EI_{zz} & 0 & 0 \\ 0 & 0 & 0 & GI_t & 0 \\ 0 & 0 & 0 & 0 & EI_{\omega} \end{bmatrix} \begin{Bmatrix} \epsilon_x^o \\ \frac{1}{\rho_y} \\ \frac{1}{\rho_z} \\ \vartheta \\ -\frac{\partial^2 \vartheta}{\partial x^2} \end{Bmatrix}. \tag{6.334}$$

We express the force–strain relationships of orthotropic beams as (Eqs. 6.7, 6.8, and 6.240)

orthotropic:

$$\begin{Bmatrix} \widehat{N} \\ \widehat{M}_y \\ \widehat{M}_z \\ \widehat{T}_{sv} \\ \widehat{T}_{\omega} \end{Bmatrix} = \begin{bmatrix} \widehat{EA} & 0 & 0 & 0 & 0 \\ 0 & \widehat{EI}_{yy} & \widehat{EI}_{yz} & 0 & 0 \\ 0 & \widehat{EI}_{yz} & \widehat{EI}_{zz} & 0 & 0 \\ 0 & 0 & 0 & \widehat{GI}_t & 0 \\ 0 & 0 & 0 & 0 & \widehat{EI}_{\omega} \end{bmatrix} \begin{Bmatrix} \epsilon_x^o \\ \frac{1}{\rho_y} \\ \frac{1}{\rho_z} \\ \vartheta \\ -\frac{\partial^2 \vartheta}{\partial x^2} \end{Bmatrix}. \tag{6.335}$$

The equations governing the buckling loads of isotropic and orthotropic beams differ only in their stiffness matrices. Therefore, the buckling load of an orthotropic beam can be obtained by replacing the isotropic stiffnesses with the replacement stiffnesses in the expression of the buckling load of the corresponding isotropic beam as follows:

$$\begin{aligned} &\text{Isotropic beams} \qquad \text{Orthotropic beams} \\ &EA \Longrightarrow \widehat{EA} \\ &EI_{yy},\ EI_{zz},\ EI_{yz} \Longrightarrow \widehat{EI}_{yy},\ \widehat{EI}_{zz},\ \widehat{EI}_{yz} \\ &GI_t,\ EI_{\omega} \Longrightarrow \widehat{GI}_t,\ \widehat{EI}_{\omega}. \end{aligned} \tag{6.336}$$

The stiffnesses of selected orthotropic beams are given in Tables A.1–A.5. The warping stiffness $\widehat{EI}_{\omega}$ is given only for open-section beams because, generally, it can be neglected for closed-section beams.

As examples, in the following we present the buckling loads of beams subjected to axial loads, bending moments, and transverse loads.

6.9.1 Beams Subjected to Axial Load (Flexural–Torsional Buckling)

We now consider orthotropic beams subjected to an axial load. Under this load the beam may undergo flexural and torsional buckling.

Doubly symmetrical cross section. We consider orthotropic beams with cross sections symmetrical with respect to both the y- and the z-axes ($\widehat{EI}_{yz} = 0$). When the cross section of the beam has two axes of symmetry (doubly symmetrical cross section), it may buckle (a) in one of the planes of symmetry, (b) in the other plane of symmetry, and (c) torsionally (Fig. 6.84).

Buckling loads of doubly symmetrical cross-section isotropic beams are given by Timoshenko and Gere.[17] By exchanging the isotropic stiffnesses in the

[17] S. P. Timoshenko and J. Gere, *Theory of Elastic Stability*. 2nd edition. McGraw-Hill, New York, 1961, pp. 49 and 229.

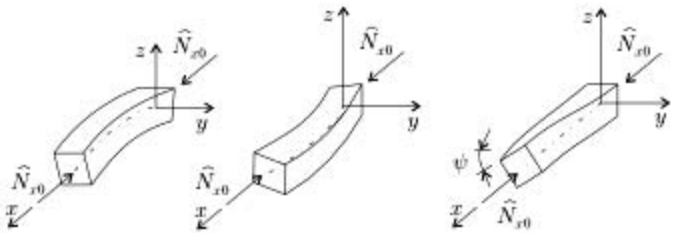

Figure 6.84: Illustrations of buckling in the x–z and x–y planes and of torsional buckling.

Timoshenko and Gere expressions with the replacement stiffnesses (see Eq. 6.336), the buckling loads of orthotropic beams are

$$\begin{aligned}
\widehat{N}^{\mathrm{B}}_{\mathrm{cr}y} &= \frac{\pi^2 \widehat{EI}_{yy}}{(kL)^2} && \text{buckling in the } x\text{–}z \text{ plane} \\
\widehat{N}^{\mathrm{B}}_{\mathrm{cr}z} &= \frac{\pi^2 \widehat{EI}_{zz}}{(kL)^2} && \text{buckling in the } x\text{–}y \text{ plane} \\
\widehat{N}^{\mathrm{B}}_{\mathrm{cr}\psi} &= \widehat{N}^{\mathrm{B}}_{\mathrm{cr}\omega} + \frac{1}{i_\omega^2}\widehat{GI}_{\mathrm{t}} && \text{torsional buckling,}
\end{aligned} \tag{6.337}$$

where $\widehat{N}^{\mathrm{B}}_{\mathrm{cr}\omega}$ is

$$\widehat{N}^{\mathrm{B}}_{\mathrm{cr}\omega} = \frac{1}{i_\omega^2}\frac{\pi^2 \widehat{EI}_\omega}{(kL)^2}, \tag{6.338}$$

L is the length of the beam, i_ω is the polar radius of gyration of the cross section about the shear center, which, for an isotropic beam,[18] is

$$i_\omega^2 = z_{\mathrm{sc}}^2 + y_{\mathrm{sc}}^2 + \frac{I_{zz} + I_{yy}}{A}, \tag{6.339}$$

where y_{sc} and z_{sc} are the coordinates of the shear center with respect to the centroid. For an orthotropic composite beam we define i_ω as

$$i_\omega^2 = z_{\mathrm{sc}}^2 + y_{\mathrm{sc}}^2 + \frac{\widehat{EI}_{zz} + \widehat{EI}_{yy}}{\widehat{EA}}. \tag{6.340}$$

The effective length factor k is given in Table 6.11 for different end conditions.

For long beams ($\widehat{GI}_{\mathrm{t}} \gg \widehat{EI}_\omega/L^2$) the torsional buckling load simplifies to

$$\widehat{N}^{\mathrm{B}}_{\mathrm{cr}\psi} = \frac{1}{i_\omega^2}\widehat{GI}_{\mathrm{t}} \qquad \begin{array}{c}\text{torsional buckling} \\ \text{long beam.}\end{array} \tag{6.341}$$

For short beams ($\widehat{GI}_{\mathrm{t}} \ll \widehat{EI}_\omega/L^2$) the torsional buckling load is

$$\widehat{N}^{\mathrm{B}}_{\mathrm{cr}\psi} = \widehat{N}^{\mathrm{B}}_{\mathrm{cr}\omega} = \frac{1}{i_\omega^2}\frac{\pi^2 \widehat{EI}_\omega}{(kL)^2} \qquad \begin{array}{c}\text{torsional buckling} \\ \text{short beam.}\end{array} \tag{6.342}$$

[18] Ibid., p. 233.

Table 6.11. The factor k in Eqs. (6.337) and (6.338). The simple supports in cases (a) and (b) restrain the rotation about the x-axis, but the cross section is free to warp and free to rotate about the y- and z-axes

Geometry, loading	k
(a) 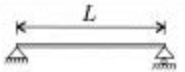	$k = 1$
(b) 	$k = 0.7$
(c) 	$k = 0.5$
(d) 	$k = 2$

Symmetrical cross section. We consider orthotropic beams with cross sections symmetrical with respect to the z-axis ($\widehat{EI}_{yz} = 0$). When the cross section of the beam has one axis of symmetry, it may undergo (a) buckling in the plane of symmetry (x–z plane), or (b) combined flexural–torsional buckling. The buckling load corresponding to buckling in the x–z plane is[19]

$$\widehat{N}_{\mathrm{cr1}} = \widehat{N}^{\mathrm{B}}_{\mathrm{cry}} \qquad \text{buckling in the } x\text{–}z \text{ plane.} \tag{6.343}$$

The buckling loads $\widehat{N}_{\mathrm{cr2}}$ and $\widehat{N}_{\mathrm{cr3}}$, corresponding to flexural–torsional buckling, are the roots of the following equation:

$$\left| \begin{bmatrix} \widehat{N}^{\mathrm{B}}_{\mathrm{crz}} & \\ & \widehat{N}^{\mathrm{B}}_{\mathrm{cr}\psi} i_\omega^2 \end{bmatrix} - \widehat{N}_{\mathrm{cr}} \begin{bmatrix} 1 & z_{\mathrm{sc}} \\ z_{\mathrm{sc}} & i_\omega^2 \end{bmatrix} \right| = 0, \tag{6.344}$$

where $|\ \ |$ denotes the determinant. This equation can be written in the form

$$\widehat{N}^2_{\mathrm{cr}}(i_\omega^2 - z_{\mathrm{sc}}^2) - \widehat{N}_{\mathrm{cr}}(\widehat{N}^{\mathrm{B}}_{\mathrm{crz}} + \widehat{N}^{\mathrm{B}}_{\mathrm{cr}\psi}) i_\omega^2 + \widehat{N}^{\mathrm{B}}_{\mathrm{crz}} \widehat{N}^{\mathrm{B}}_{\mathrm{cr}\psi} i_\omega^2 = 0, \tag{6.345}$$

where $\widehat{N}^{\mathrm{B}}_{\mathrm{cry}}$, $\widehat{N}^{\mathrm{B}}_{\mathrm{crz}}$, and $\widehat{N}^{\mathrm{B}}_{\mathrm{cr}\psi}$ are given by Eq. (6.337), and the effective length factor k is given in Table 6.11.

Equation (6.343) yields the value of $\widehat{N}_{\mathrm{cr1}}$, and Eq. (6.345) yields two values of $\widehat{N}_{\mathrm{cr}}$ denoted by $\widehat{N}_{\mathrm{cr2}}$ and $\widehat{N}_{\mathrm{cr3}}$. The buckling load of interest is the lowest of these three values. We note that the $\widehat{N}_{\mathrm{cr2}}$ and $\widehat{N}_{\mathrm{cr3}}$ values resulting from Eq. (6.345) are approximate when one end of the beam is fixed and the other end is simply supported (case b in Table 6.11).

[19] Ibid., p. 235.

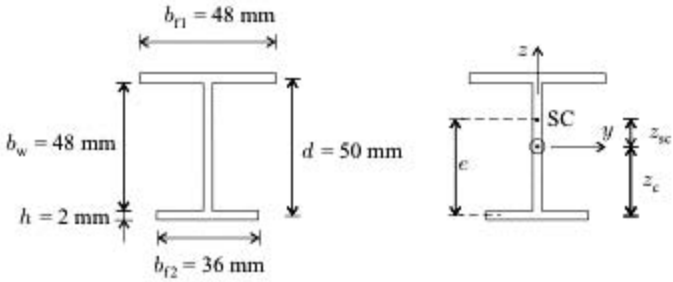

Figure 6.85: The cross section of the beam in Example 6.8 and the loading on the beam.

Unsymmetrical cross sections. When the cross section is unsymmetrical, an orthotropic beam undergoes combined flexural–torsional buckling, and the buckling loads $\widehat{N}_{cr}$ are given by the solution of the following (third-order) equation[20]:

$$\left| \begin{bmatrix} \widehat{N}^{B}_{crz} & 0 & 0 \\ 0 & \widehat{N}^{B}_{cry} & 0 \\ 0 & 0 & \widehat{N}^{B}_{cr\psi} i_\omega^2 \end{bmatrix} - \widehat{N}_{cr} \begin{bmatrix} 1 & 0 & z_{sc} \\ 0 & 1 & -y_{sc} \\ z_{sc} & -y_{sc} & i_\omega^2 \end{bmatrix} \right| = 0. \tag{6.346}$$

In the preceding equation the coordinate directions y and z must be in the principal directions (page 208) such that $\widehat{EI}_{yz}$ is zero ($\widehat{EI}_{yz} = 0$); $|\ \ |$ denotes the determinant. The terms $\widehat{N}^{B}_{cry}$, $\widehat{N}^{B}_{crz}$, and $\widehat{N}^{B}_{cr\psi}$ are given by Eq. (6.337), and the constant k is given in Table 6.11. The solution of Eq. (6.346) results in three values of $\widehat{N}_{cr}$, of which the lowest value is of interest. The resulting $\widehat{N}_{cr}$ is approximate when one end of the beam is fixed and the other end is simply supported (case b in Table 6.11).

6.8 Example. *An $L = 0.5$-m-long I-section beam, with the cross section shown in Figure 6.85, is made of graphite epoxy unidirectional plies. The material properties are given in Table 3.6 (page 81). The layup is $[0_{20}]$. The beam is simply supported at each end. Determine the buckling load when the beam is subjected to an axial load.*

Solution. The compliance matrices for the flange and the web are the same, and their relevant elements are (Table 3.8, page 85)

$$a_{11} = 3.38 \times 10^{-9} \frac{\text{m}}{\text{N}}$$

$$d_{11} = 10.14 \times 10^{-3} \frac{1}{\text{N} \cdot \text{m}} \qquad d_{66} = 329.67 \times 10^{-3} \frac{1}{\text{N} \cdot \text{m}}.$$

The dimensions of the cross section are $b_{f1} = 0.048\,\text{m}$, $b_{f2} = 0.036\,\text{m}$, $b_w = 0.048\,\text{m}$, $d = 0.050\,\text{m}$, $h = 0.002\,\text{m}$ (Fig. 6.85).

The tensile stiffness, the location of the centroid, and the bending stiffnesses are given in Table A.2. For symmetrical layup $(\delta_{11})_f$ and $(\delta_{11})_w$ are replaced by d_{11}

[20] Ibid., p. 233.

and $(\alpha_{11})_f$ and $(\alpha_{11})_w$ by a_{11}, and from Table A.2 we have

$$\widehat{EA} = \frac{b_{f1}}{a_{11}} + \frac{b_{f2}}{a_{11}} + \frac{b_w}{a_{11}} = 39.07 \times 10^6 \text{ N}$$

$$z_c = \frac{1}{\widehat{EA}}\left(\frac{b_{f1}}{a_{11}}d + \frac{b_w}{a_{11}}\frac{d}{2}\right) = 0.027\,27 \text{ m}$$

$$\widehat{EI}_{zz} = \frac{b_w}{d_{11}} + \frac{1}{a_{11}}\frac{b_{f1}^3}{12} + \frac{1}{a_{11}}\frac{b_{f2}^3}{12} = 3\,884 \text{ N} \cdot \text{m}^2 \tag{6.347}$$

$$\widehat{EI}_{yy} = \frac{b_{f1}}{a_{11}}(d - z_c)^2 + \frac{b_{f2}}{a_{11}}z_c^2 + \frac{b_{f1}}{d_{11}} + \frac{b_{f2}}{d_{11}} + \frac{1}{a_{11}}\left(\frac{b_{w1}^3 + b_{w2}^3}{3}\right) = 18\,074 \text{ N} \cdot \text{m}^2,$$

where b_{w1} and b_{w2} are calculated with the preceding value of z_c (see Table A.2) as follows:

$$b_{w1} = z_c - \frac{h}{2} = 0.026\,27 \text{ m} \qquad b_{w2} = b_w - b_{w1} = 0.021\,73 \text{ m}.$$

The torsional stiffness, the location of the shear center, and the warping stiffness are given in Table A.5. For symmetrical layup $(\delta_{66})_f$ and $(\delta_{66})_w$ are replaced by d_{66} and $(\alpha_{11})_f$ and $(\alpha_{11})_w$ by a_{11} (Table 3.8, page 85), and we write

$$\widehat{GI}_t = 4\left(\frac{b_{f1}}{d_{66}} + \frac{b_{f2}}{d_{66}} + \frac{d}{d_{66}}\right) = 1.602 \text{ N} \cdot \text{m}^2$$

$$e = d\frac{\frac{b_{f1}^3}{a_{11}}}{\frac{b_{f1}^3}{a_{11}} + \frac{b_{f2}^3}{a_{11}}} = 0.035\,17 \text{ m} \tag{6.348}$$

$$\widehat{EI}_\omega = \frac{\frac{b_{f2}^3}{a_{11}}}{12}ed = 2.024 \text{ N} \cdot \text{m}^4.$$

The cross section is symmetrical with respect to the z-axis, and the coordinates of the shear center with respect to the centroid are (Fig. 6.85)

$$y_{sc} = 0 \qquad z_{sc} = e - z_c = 0.000\,789 \text{ m}. \tag{6.349}$$

The polar radius of gyration about the shear center i_ω is (Eq. 6.340)

$$i_\omega = \sqrt{z_{sc}^2 + y_{sc}^2 + \frac{\widehat{EI}_{zz} + \widehat{EI}_{yy}}{\widehat{EA}}} = 0.024\,99 \text{ m}. \tag{6.350}$$

For a simply supported beam ($k = 1$, Table 6.11, page 293), Eq. (6.337) gives

$$\widehat{N}_{cry}^B = \frac{\pi^2 \widehat{EI}_{yy}}{L^2} = 713.55 \text{ kN} \qquad x\text{–}z \text{ plane}$$

$$\widehat{N}_{crz}^B = \frac{\pi^2 \widehat{EI}_{zz}}{L^2} = 153.32 \text{ kN} \qquad x\text{–}y \text{ plane} \tag{6.351}$$

$$\widehat{N}_{cr\psi}^B = \widehat{N}_{cr\omega}^B + \frac{1}{i_\omega^2}\widehat{GI}_t = 130.53 \text{ kN} \qquad \text{torsion},$$

where (Eq. 6.338)

$$\widehat{N}_{cr\omega}^B = \frac{1}{i_\omega^2}\frac{\pi^2 \widehat{EI}_\omega}{(kL)^2} = 127.96 \text{ kN}. \tag{6.352}$$

The buckling load $\widehat{N}_{cr1}$ is (Eq. 6.343),

$$\widehat{N}_{cr1} = \widehat{N}^{B}_{cry} = 713.55 \text{ kN} \qquad \text{buckling in the } x\text{–}z \text{ plane,} \tag{6.353}$$

and $\widehat{N}_{cr2}$ and $\widehat{N}_{cr3}$ are the roots of Eq. (6.345) as follows:

$$\widehat{N}^{2}_{cr}\left(i^{2}_{\omega} - z^{2}_{sc}\right) - \widehat{N}_{cr}\left(\widehat{N}^{B}_{crz} + \widehat{N}^{B}_{cr\psi}\right) i^{2}_{\omega} + \widehat{N}^{B}_{crz}\widehat{N}^{B}_{cr\psi} i^{2}_{\omega} = 0. \tag{6.354}$$

Solution of this equation yields the flexural–torsional buckling loads

$$\widehat{N}_{cr2} = 208.88 \text{ kN} \qquad \widehat{N}_{cr3} = 106.43 \text{ kN}. \tag{6.355}$$

6.9.2 Lateral–Torsional Buckling of Orthotropic Beams with Symmetrical Cross Section

We consider orthotropic beams. The cross section of the beam is symmetrical with respect to the z-axis ($\widehat{EI}_{yz} = 0$). The beam is simply supported at each end. At the simple support the beam is restrained from rotating about the x-axis, but the cross section is free to rotate about the y- and z-axes and is free to warp.

The beam is subjected to two equal and opposite bending moments at the two ends of the beam (Fig. 6.86, top), a uniformly distributed load p in the plane of symmetry (Fig. 6.86, middle), or a concentrated force P in the plane of symmetry at the midspan of the beam (Fig. 6.86, bottom). The distance between the shear center and the point where the load acts is denoted by Δ.

At certain applied loads the beam buckles laterally while the cross sections of the beam rotate (Fig. 6.87). This phenomenon is called lateral buckling, or lateral–torsional buckling.

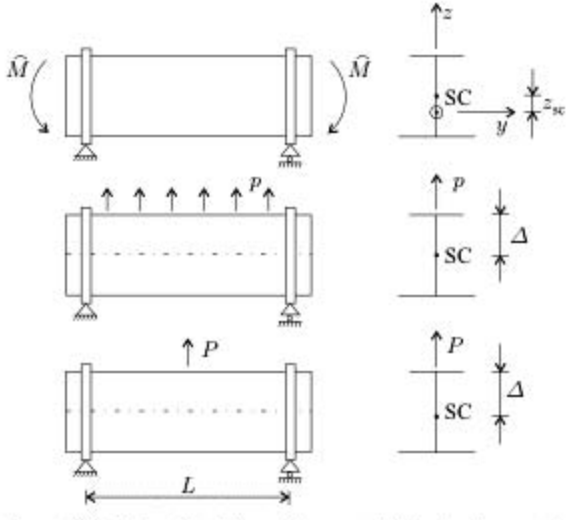

Figure 6.86: Lateral buckling of beams subjected to two equal and opposite bending moments at the two ends of the beam (top), a uniformly distributed load p in the plane of symmetry (middle), and a concentrated force P in the plane of symmetry at the midspan of the beam (bottom). The distance between the shear center and the point where the load acts is denoted by Δ.

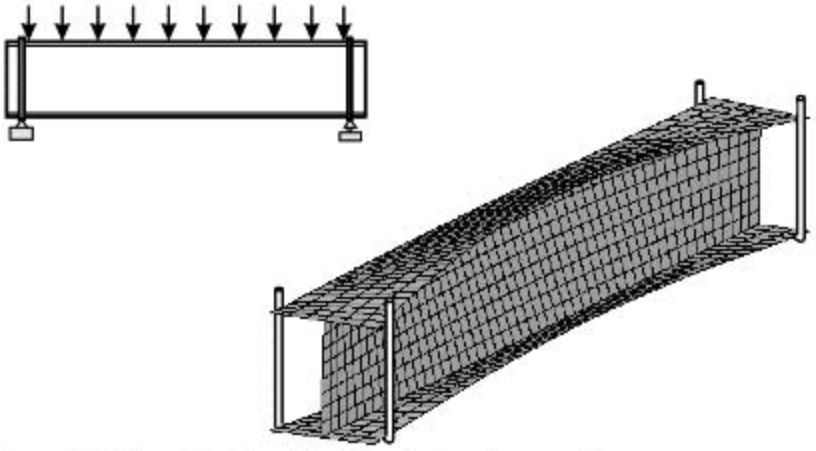

Figure 6.87: Illustration of lateral buckling of a simply supported beam.

Allen and Bulson[21] presented the following formula for the buckling load of an isotropic beam:

$$\widehat{Q}_{cr} = G_1 \frac{\pi^2}{L^2} \widehat{EI}_{zz} \left[G_2\Delta + G_3 \frac{\beta_1}{2} \pm \sqrt{\left(G_2\Delta + G_3 \frac{\beta_1}{2} \right)^2 + \frac{\widehat{EI}_\omega}{\widehat{EI}_{zz}} \left(1 + \frac{\widehat{GI}_t}{\widehat{EI}_\omega} \frac{L^2}{\pi^2} \right)} \right], \tag{6.356}$$

where $\widehat{Q}_{cr}$ is the critical value of the bending moment and is related to the applied loads, as shown in Table 6.12. The positive sign before the square root results in a positive load (which acts upward), whereas the negative sign results in a negative load (which acts downward); G_1–G_3 are constants. We recall Eqs. (6.337) and (6.338), which relate $\widehat{N}^{B}_{crz}$ and $\widehat{N}^{B}_{cr\psi}$ to the stiffnesses

$$\widehat{N}^{B}_{crz} = \frac{\pi^2 \widehat{EI}_{zz}}{(kL)^2} \tag{6.357}$$

$$\widehat{N}^{B}_{cr\psi} = \widehat{N}^{B}_{cr\omega} + \frac{1}{i_\omega^2} \widehat{GI}_t = \frac{1}{i_\omega^2} \frac{\pi^2 \widehat{EI}_\omega}{(kL)^2} + \frac{1}{i_\omega^2} \widehat{GI}_t, \tag{6.358}$$

where $k = 1$ for a simply supported beam. By combining and rearranging Eqs. (6.356)–(6.358), we obtain

$$\widehat{Q}_{cr} = F_1 \widehat{N}^{B}_{crz} \left(F_2\Delta + F_3\beta_1 \pm \sqrt{(F_2\Delta + F_3\beta_1)^2 + \frac{\widehat{N}^{B}_{cr\psi} i_\omega^2}{\widehat{N}^{B}_{crz}}} \right), \tag{6.359}$$

where F_1, F_2, F_3 are constants (their values are also listed in Table 6.12), and β_1 is a parameter that depends on the shape of the cross section[22]

$$\beta_1 = J_1 + J_2 - 2z_{sc}. \tag{6.360}$$

[21] H. G. Allen and P. S. Bulson, *Background to Buckling*. McGraw-Hill, London, 1980, p. 492.
[22] Ibid., p. 495.

Table 6.12. The buckling loads and the corresponding constants in Eq. (6.359).

		F_1	F_2	F_3
(a) Moment	$\hat{M}_{cr} = \hat{Q}_{cr}$	1	0	0.5
(b) Distributed load	$p_{cr} = \frac{8\hat{Q}_{cr}}{L^2}$	1.13	0.45	0.267
(c) Concentrated force	$P_{cr} = \frac{4\hat{Q}_{cr}}{L}$	1.35	0.55	0.212

For a beam made of isotropic material J_1 and J_2 are

$$J_1 = \frac{1}{I_{yy}} \int_{(A)} z^3 dA \qquad J_2 = \frac{1}{I_{yy}} \int_{(A)} zy^2 dA \tag{6.361}$$

For a thin-walled, open-section isotropic beam, J_1 and J_2 may be written as

$$\begin{aligned} J_1 &= \frac{1}{EI_{yy}} \int_{(S)} (Eh)\, z^3 d\eta \\ J_2 &= \frac{1}{EI_{yy}} \int_{(S)} (Eh)\, zy^2 d\eta \end{aligned} \qquad \text{isotropic,} \tag{6.362}$$

where h is the thickness of the wall and η is the coordinate along the circumference. For an orthotropic beam Eh is replaced by $1/\alpha^{\varphi}_{11}$ (Eqs. 6.243 and 6.241), and EI is replaced by $\widehat{EI}$ (α^{φ}_{11} is evaluated at the "neutral" plane; see Eq. 6.105). This gives

$$\begin{aligned} J_1 &= \frac{1}{\widehat{EI}_{yy}} \int_{(S)} \frac{1}{\alpha^{\varphi}_{11}} z^3 d\eta \\ J_2 &= \frac{1}{\widehat{EI}_{yy}} \int_{(S)} \frac{1}{\alpha^{\varphi}_{11}} zy^2 d\eta \end{aligned} \qquad \text{orthotropic.} \tag{6.363}$$

For orthotropic I-beams whose cross-section is symmetrical with respect the midplane of the web the preceding integrals give

$$\begin{aligned} J_1 &= \frac{1}{\widehat{EI}_{yy}} \left(\frac{1}{(\alpha^{\varphi}_{11})_{f1}} b_{f1} (d - z_c)^3 - \frac{1}{(\alpha^{\varphi}_{11})_{f2}} b_{f2} z_c^3 + \frac{1}{(a_{11})_w} \frac{b_{w1}^4 - b_{w2}^4}{4} \right) \\ J_2 &= \frac{1}{\widehat{EI}_{yy}} \left(\frac{1}{(\alpha^{\varphi}_{11})_{f1}} \frac{b_{f1}^3}{12} (d - z_c) - \frac{1}{(\alpha^{\varphi}_{11})_{f2}} \frac{b_{f2}^3}{12} z_c \right). \end{aligned} \tag{6.364}$$

The dimensions are defined in Table A.2 (page 455).

For doubly symmetrical isotropic and orthotropic beams, β_1 is zero.

Equation (6.359) is accurate for beams subjected to concentrated bending moments (Fig. 6.86, top). For simply supported beams subjected to a distributed load or to a concentrated force at the midspan, Eq. (6.359) gives the buckling load within about 5 percent.

6.9 Example. *An $L = 0.5$-m-long I-section beam, with the cross section shown in Figure 6.85, is made of graphite epoxy unidirectional plies. The material properties are given in Table 3.6 (page 81). The layup is* $[0_{20}]$. *The beam is simply supported at*

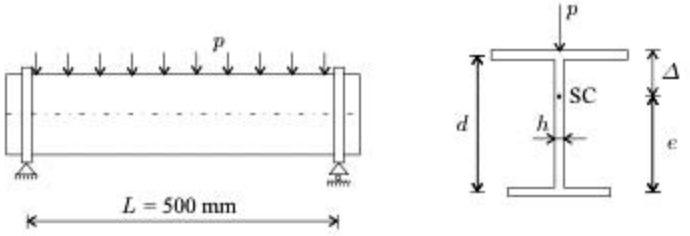

Figure 6.88: The beam in Example. 6.9.

each end. Determine the buckling load when the beam is subjected to a distributed load along the top flange (Fig. 6.88).

Solution. For a transversely loaded beam the buckling load is (Table 6.12)

$$p_{cr} = \frac{8\widehat{Q}_{cr}}{L^2}, \tag{6.365}$$

where $\widehat{Q}_{cr}$ is given by Eq.(6.359) as

$$\widehat{Q}_{cr} = F_1 \widehat{N}^{B}_{cr_z} \left(F_2\Delta + F_3\beta_1 - \sqrt{(F_2\Delta + F_3\beta_1)^2 + \frac{\widehat{N}^{B}_{cr_\psi} i_\omega^2}{\widehat{N}^{B}_{cr_z}}} \right). \tag{6.366}$$

The sign before the square root is negative because the load is downward. From Eq. (6.364) with α^{o}_{11} replaced by a_{11}, we have

$$\begin{aligned} J_1 &= \frac{1}{\widehat{E}I_{yy}} \left(\frac{1}{a_{11}} b_{f1} (d - z_c)^3 - \frac{1}{a_{11}} b_{f2} z_c^3 + \frac{1}{a_{11}} \frac{b_{w1}^4 - b_{w2}^4}{4} \right) \\ J_2 &= \frac{1}{\widehat{E}I_{yy}} \left(\frac{1}{a_{11}} \frac{b_{f1}^3}{12} (d - z_c) - \frac{1}{a_{11}} \frac{b_{f2}^3}{12} z_c \right). \end{aligned} \tag{6.367}$$

The parameters of interest in this problem are (see Example 6.8, page 294)

$$\begin{array}{lll} a_{11} = 3.38 \times 10^{-9} \dfrac{\text{m}}{\text{N}} & \widehat{E}I_{yy} = 18\,074\ \text{N}\cdot\text{m}^2 & h = 0.002\ \text{m} \\ b_{f1} = 0.048\ \text{m} & b_{f2} = 0.036\ \text{m} & d = 0.050\ \text{m} \\ b_{w2} = 0.021\,73\ \text{m} & b_{w1} = 0.026\,27\ \text{m} & z_c = 0.027\,27\ \text{m} \\ z_{sc} = 0.000\,789\ \text{m} & e = 0.035\,17\ \text{m} & i_\omega = 0.024\,99\ \text{m} \\ \widehat{N}^{B}_{cr_z} = 153.32\ \text{kN} & \widehat{N}^{B}_{cr_y} = 713.55\ \text{kN} & \widehat{N}^{B}_{cr_\psi} = 130.53\ \text{kN}. \end{array}$$

With the preceding parameters we obtain

$$J_1 = -0.003\,770\ \text{m} \qquad J_2 = 0.001\,694\ \text{m}, \tag{6.368}$$

and β_1 is (Eq. 6.360)

$$\beta_1 = J_1 + J_2 - 2z_{sc} = -0.017\,86 \text{ m}. \tag{6.369}$$

The beam is loaded on the top flange; hence, we have

$$\Delta = d - e + h/2 = 0.015\,84 \text{ m}. \tag{6.370}$$

The value of $\widehat{Q}_{cr}$ is calculated with the preceding parameters and with $F_1 = 1.13$, $F_2 = 0.45$, $F_3 = 0.267$ (Table 6.12, page 298). The result is

$$\widehat{Q}_{cr} = -3\,607 \text{ N} \cdot \text{m}. \tag{6.371}$$

Equations (6.365) and (6.371) give

$$p_{cr} = \frac{8\widehat{Q}_{cr}}{L^2} = -115\,407 \frac{\text{N}}{\text{m}}. \tag{6.372}$$

6.9.3 Local Buckling

In this section we consider local buckling of orthotropic thin-walled beams that arise due to axial compressive stresses introduced by axial forces and bending moments.

Local buckling analyses of beams are generally performed by modeling the wall segments as long plates and by assuming that edges common to two or more plates remain straight. Then the buckling load may be determined either by assuming that every wall segment buckles simultaneously while the continuity conditions at each intersection are satisfied,[23,24] or by considering the wall segments as individual plates rotationally restrained by the adjacent wall segments.[25–27] Here, we derive explicit expressions for the local buckling loads based on the latter method.

The procedure for calculating the load at which local buckling occurs is illustrated via the example of an axially loaded thin-walled, closed-section rectangular beam (Fig. 6.89). First, each wall segment is considered to be simply supported (Fig. 6.89, a) and the load $(N_{x,cr})^{ss}$ for each wall segment is calculated using the expression given in the first row of Table 4.11 (page 136). The axial strain at which the wall segment buckles is calculated by $(N_{x,cr})^{ss}a_{11}$ (Eq. 3.31), where a_{11} is the 11 element of the compliance matrix of the wall segment. The segment with the lowest

[23] D. J. Lee, The Local Buckling Coefficient for Orthotropic Structural Sections. *Aeronautical Journal*, Vol. 82, 313–320, 1978.

[24] A. Zureick and B. Shih, Local Buckling of Fiber-Reinforced Polymeric Structural Members Under Linearly-Varying Edge Loading – Part 1. Theoretical Formulation. *Composite Structures*, Vol. 41, 79–86, 1998.

[25] P. Qiao, J. F. Davalos, and J. Wang, Local Buckling of Composite FRP Shapes by Discrete Plate Analysis. *Journal of Structural Engineering*, Vol. 127, 245–255, 2001.

[26] E. J. Barbero and I. Raftoyiannis, Local Buckling of FRP Beams and Columns. *Journal of Materials in Civil Engineering*, Vol. 5, 339–355, 1993.

[27] J. P. H. Webber, P. T. Holt, and D. A. Lee, Instability of Carbon Fibre Reinforced Flanges of I Section Beams and Columns. *Composite Structures*, Vol. 4, 245–265, 1985.

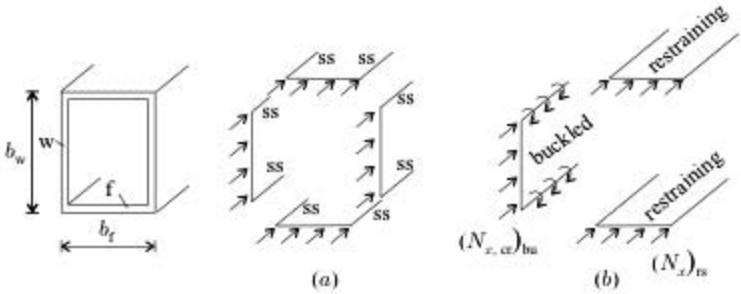

Figure 6.89: Local buckling of an axially loaded box beam.

critical strain is considered further because the wall segment (web or flange) in which the axial strain is the lowest is most susceptible to buckling. We calculate the buckling load of this segment by treating it as a plate rotationally restrained by the adjoining wall segment or segments (Fig. 6.89, b). The buckling load is calculated by the expression given in the fourth row of Table 4.11 (page 136).

The spring constant $\widetilde{k}$ depends on the adjacent (restraining) wall segment. To determine the spring constant, we recall Eq. (4.149)

$$\widetilde{k} = \frac{M_y}{\frac{\partial w}{\partial y}}, \tag{6.373}$$

where $\partial w/\partial y$ is the rotation of the edge.

A conservative estimate of $\widetilde{k}$ is obtained[28] when the deformed shape is cylindrical ("long-plate" approximation). For a long plate ($\kappa_x = \kappa_{xy} = 0$), the moment is (Eq. 4.3)

$$M_y = (D_{22})_{rs}\,\kappa_y, \tag{6.374}$$

where the subscript rs refers to the restraining segment (Fig. 6.90). The term $\kappa_y = -\partial^2 w^o/\partial y^2$ (Eq. 4.2), and we write

$$\int_0^{L_{rs}/2} (-\kappa_y)\,dy = \underbrace{\left.\frac{\partial w}{\partial y}\right|_{\text{at } L_{rs}/2}}_{0} - \left.\frac{\partial w}{\partial y}\right|_{\text{at } 0}, \tag{6.375}$$

where $\partial w/\partial y$ is zero at $L_{rs}/2$ (Fig. 6.90), and we have

$$\kappa_y \frac{L_{rs}}{2} = \left.\frac{\partial w}{\partial y}\right|_{\text{at } 0}. \tag{6.376}$$

Equations (6.373), (6.374), and (6.376) give

$$\widetilde{k} = \frac{2\,(D_{22})_{rs}}{L_{rs}}. \tag{6.377}$$

[28] F. Bleich, *Buckling of Metal Structures*. McGraw-Hill, New York, 1952, p. 339.

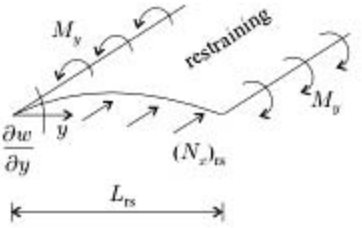

Figure 6.90: The restraining wall segment of the box beam.

The preceding expression is valid when no axial load acts. The effect of axial loading is taken into account by an amplification factor r defined as[29,30]

$$r = \frac{1}{1 - \frac{(N_x)_{rs}}{(N_{x,cr})^{ss}_{rs}}}, \tag{6.378}$$

where $(N_x)_{rs}$ is the applied axial load (Fig. 6.90) and $(N_{x,cr})^{ss}_{rs}$ is the buckling load of the simply supported restraining wall segment; r is unity when the axial load is zero and is infinity when the axial load is equal to the buckling load. Taking this amplification factor into account, the spring constant is

$$\tilde{k} = \frac{2(D_{22})_{rs}}{L_{rs}} \frac{1}{r}. \tag{6.379}$$

The axial strains of the restraining and the buckled wall segments are the same, and, consequently, $(N_x)_{rs}$ is (Fig. 6.89, b)

$$(N_x)_{rs} = (N_{x,cr})_{bu} \frac{(a_{11})_{bu}}{(a_{11})_{rs}}, \tag{6.380}$$

where the subscript bu refers to the wall segment that buckles and $(N_{x,cr})_{bu}$ is the buckling load of the rotationally restrained buckled wall segment. The value of $(N_{x,cr})_{bu}$ is not known a priori. We may approximate $(N_{x,cr})_{bu}$ by the buckling load $(N_{x,cr})^{ss}_{bu}$ of a simply supported wall. With this approximation, r becomes

$$r = \frac{1}{1 - \frac{(N_{x,cr})^{ss}_{bu}(a_{11})_{bu}}{(N_{x,cr})^{ss}_{rs}(a_{11})_{rs}}}. \tag{6.381}$$

If the webs and the flanges were simply supported, their buckling loads would be (Table 4.11, first row, page 136)

$$\begin{aligned}(N_{x,cr})^{ss}_{f} &= \frac{\pi^2}{b_f^2}\left[2\sqrt{(D_{11})_f(D_{22})_f} + 2((D_{12})_f + 2(D_{66})_f)\right] \\ (N_{x,cr})^{ss}_{w} &= \frac{\pi^2}{b_w^2}\left[2\sqrt{(D_{11})_w(D_{22})_w} + 2((D_{12})_w + 2(D_{66})_w)\right].\end{aligned} \tag{6.382}$$

[29] Ibid., pp. 331–339.

[30] S. P. Timoshenko and J. Gere, *Theory of Elastic Stability*. 2nd edition. McGraw-Hill, New York, 1961, pp. 15 and 424.

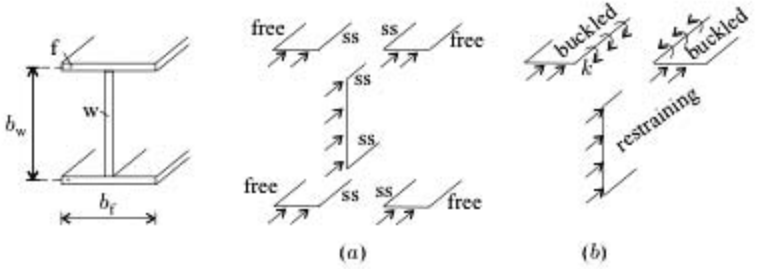

Figure 6.91: Local buckling of an axially loaded I-beam.

The flanges buckle first when $(N_{x,cr})_f^{ss}(a_{11})_f < (N_{x,cr})_w^{ss}(a_{11})_w$. In this case the web restrains the rotation of the flange, and the spring constant is

$$\widetilde{k} = \frac{2(D_{22})_w}{b_w}\left(1 - \frac{(N_{x,cr})_f^{ss}(a_{11})_f}{(N_{x,cr})_w^{ss}(a_{11})_w}\right). \tag{6.383}$$

The buckling load of the flange is then calculated with this spring constant by the expression in the fourth row of Table 4.11 (page 136).

The webs buckle first when $(N_{x,cr})_f^{ss}(a_{11})_f > (N_{x,cr})_w^{ss}(a_{11})_w$. In this case the flange restrains the rotation of the web, and the spring constant is

$$\widetilde{k} = \frac{2(D_{22})_f}{b_f}\left(1 - \frac{(N_{x,cr})_w^{ss}(a_{11})_w}{(N_{x,cr})_f^{ss}(a_{11})_f}\right). \tag{6.384}$$

The buckling load of the web is then calculated with this spring constant by the expression in the fourth row of Table 4.11.

I-beams. We now apply the preceeding procedure to I-beams (Fig. 6.91).

If the web and the flanges were simply supported, their buckling loads would be (Tables 4.9, and 4.11, first row, pages 125 and 136)

$$\begin{aligned}(N_{x,cr})_f^{ss} &= \frac{12(D_{66})_f}{(b_f/2)^2}\\ (N_{x,cr})_w^{ss} &= \frac{\pi^2}{b_w^2}(2\sqrt{(D_{11})_w(D_{22})_w} + 2((D_{12})_w + 2(D_{66})_w)).\end{aligned} \tag{6.385}$$

The flanges buckle first when $(N_{x,cr})_f^{ss}(a_{11})_f < (N_{x,cr})_w^{ss}(a_{11})_w$. In this case the web restrains the rotation of the flanges, and the spring constant is

$$\widetilde{k} = \frac{(D_{22})_w}{b_w}\left(1 - \frac{(N_{x,cr})_f^{ss}(a_{11})_f}{(N_{x,cr})_w^{ss}(a_{11})_w}\right). \tag{6.386}$$

The factor 2 is omitted because the web restrains two "half" flanges. The buckling load of the flanges is calculated with this spring constant by the expression in the sixth row of Table 4.11.

The web buckles first when $(N_{x,cr})_f^{ss}(a_{11})_f > (N_{x,cr})_w^{ss}(a_{11})_w$. In this case, as a conservative estimate, we take $\widetilde{k}$ to be zero ($\widetilde{k} = 0$). The buckling load is then calculated by the expression in the first row of Table 4.11. This expression is developed by replacing the rotationally restrained wall segments by simply supported

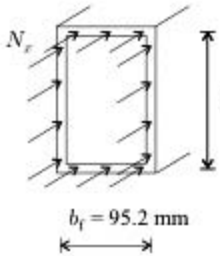

Figure 6.92: The cross section of the beam in Example 6.10.

wall segments. Expressions that do not include this simplification but take the rotational restraint into account are given by Kollár.[31]

6.10 Example. *The box-section beam shown in Figure 6.92 is subjected to axial compression. Determine the load that results in local buckling. The beam is orthotropic, and the bending stiffnesses of both the flange and the web are* $D_{11} = 444\ N \cdot m$, $D_{22} = 461\ N \cdot m$, $D_{12} = 103\ N \cdot m$, $D_{66} = 107\ N \cdot m$.

Solution. The widths of the flange and the web are $b_f = 0.0952$ m and $b_w = 0.1968$ m. With these values the buckling loads (with the flange and the web considered as simply supported plates) are (Eq. 6.382)

$$\begin{aligned}(N_{x,cr})_f^{ss} &= \frac{\pi^2}{b_f^2}[2\sqrt{D_{11}D_{22}} + 2(D_{12} + 2D_{66})] = 1\,674\,\frac{\text{kN}}{\text{m}} \\ (N_{x,cr})_w^{ss} &= \frac{\pi^2}{b_w^2}[2\sqrt{D_{11}D_{22}} + 2(D_{12} + 2D_{66})] = 392\,\frac{\text{kN}}{\text{m}}.\end{aligned} \tag{6.387}$$

The layups of the web and the flange are identical, $(a_{11})_f = (a_{11})_w$. Consequently, $(N_{x,cr})_f^{ss}(a_{11})_f > (N_{x,cr})_w^{ss}(a_{11})_w$, and the web buckles first. The web is restrained by the flanges (Fig. 6.92, right). The spring constant is (Eq. 6.383)

$$\widetilde{k} = \frac{2(D_{22})_f}{b_f}\left(1 - \frac{(N_{x,cr})_w^{ss}(a_{11})_w}{(N_{x,cr})_f^{ss}(a_{11})_f}\right) = 7\,414\ \text{N} \tag{6.388}$$

The parameter of restraint is (Table 4.11, page 136)

$$\zeta = \frac{(D_{22})_w}{\widetilde{k}b_w} = 0.316. \tag{6.389}$$

The buckling load of the web is calculated by the expression in Table 4.11 (page 136, fourth row) as follows:

$$(N_{x,cr})_w = \frac{\pi^2}{b_w^2}\left[2\sqrt{1 + 4.139\xi}\sqrt{(D_{11})_w(D_{22})_w} + (2 + 0.62\xi^2)((D_{12})_w + 2(D_{66})_w)\right],$$

where

$$\xi = \frac{1}{1 + 10\zeta} = 0.240. \tag{6.390}$$

[31] L. P. Kollár, Local Buckling of Composite (FRP) Beams. *Journal of Structural Engineering*, 2003.

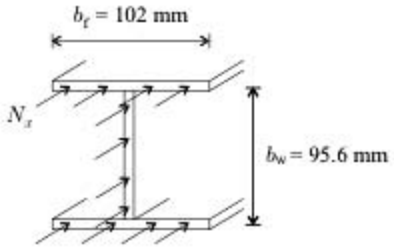

Figure 6.93: The cross section of the beam in Example. 6.11

With this value the buckling load of the web is

$$(N_{x,\mathrm{cr}})_w = 490\ \frac{\mathrm{kN}}{\mathrm{m}}. \tag{6.391}$$

This buckling load agrees closely with the result of a finite element analysis ($N_{x,\mathrm{cr}} = 501$ kN/m) and with the buckling load calculated by the numerical solution of the equations given by Lee[32] ($N_{x,\mathrm{cr}} = 519$ kN/m).

6.11 Example. *The I-section beam shown in Figure 6.93 is subjected to axial compression. Determine the load that results in local buckling. The beam is orthotropic and the bending stiffnesses of both the flange and the web are* $D_{11} = 698\ N \cdot m$, $D_{22} = 326\ N \cdot m$, $D_{12} = 127\ N \cdot m$, $D_{66} = 103\ N \cdot m$.

Solution. The width of the flange and the web are $b_f = 0.102$ m and $b_w = 0.0956$ m. When the flange is simply supported along one edge and free at the other edge and the web is simply supported at both edges, the buckling loads are (Eq. 6.385)

$$\begin{aligned}(N_{x,\mathrm{cr}})_f^{ss} &= \frac{12\,(D_{66})_f}{(b_f/2)^2} = 475\ \frac{\mathrm{kN}}{\mathrm{m}} \\ (N_{x,\mathrm{cr}})_w^{ss} &= \frac{\pi^2}{b_w^2}[2\sqrt{D_{11}D_{22}} + 2\,(D_{12} + 2D_{66})] = 1\,750\ \frac{\mathrm{kN}}{\mathrm{m}}.\end{aligned} \tag{6.392}$$

The layups of the web and the flange are identical, $(a_{11})_f = (a_{11})_w$. Consequently, $(N_{x,\mathrm{cr}})_f^{ss}\,(a_{11})_f < (N_{x,\mathrm{cr}})_w^{ss}(a_{11})_w$, and the flange buckles first. The flange is restrained by the web (Fig. 6.93, right). The spring constant is (Eq. 6.386)

$$\widetilde{k} = \frac{(D_{22})_w}{b_w}\left(1 - \frac{(N_{x,\mathrm{cr}})_f^{ss}\,(a_{11})_f}{(N_{x,\mathrm{cr}})_w^{ss}\,(a_{11})_w}\right) = 2\,484\ \mathrm{N}. \tag{6.393}$$

The parameters ν, K, ζ, and η are (Table 4.11, page 136)

$$\nu = \frac{D_{12}}{2D_{66} + D_{12}} = 0.381 \qquad K = \frac{2D_{66} + D_{12}}{\sqrt{D_{11}D_{22}}} = 0.698 \tag{6.394}$$

$$\zeta = \frac{(D_{22})_w}{\widetilde{k}\,(b_f/2)} = 2.57 \qquad \eta = \frac{1}{\sqrt{1 + (7.22 - 3.55\,\nu)\,\zeta}} = 0.249. \tag{6.395}$$

[32] D. J. Lee, The Local Buckling Coefficient for Orthotropic Structural Sections. *Aeronautical Journal*, Vol. 82, 313–320, 1978.

The buckling load of the flange is calculated by the expression in Table 4.11 (page 136, sixth row, $K < 1$) as follows:

$$(N_{x,\mathrm{cr}})_{\mathrm{f}} = \frac{\sqrt{(D_{11})_{\mathrm{f}}(D_{22})_{\mathrm{f}}}}{(b_{\mathrm{f}}/2)^2}\left\{K[\eta 15.1\sqrt{1-\nu}+(1-\eta)\,6\,(1-\nu)]+\frac{7\,(1-K)}{\sqrt{1+4.12\,\zeta}}\right\}$$
$$= 850\ \mathrm{kN/m}. \tag{6.396}$$

This buckling load agrees closely with the result of the finite element analysis of Qiao et al.[33] ($N_{x,\mathrm{cr}} = 824$ kN/m), with the buckling load calculated by the numerical solution of the equations given by Lee[34] ($N_{x,\mathrm{cr}} = 916$ kN/m), and with the data of Tomblin and Barbero,[35] who tested beams of different lengths. The buckling loads measured by Tomblin and Barbero are $P_{\mathrm{cr}} = 247, 224$, and 222 kN, which yield $N_{x,\mathrm{cr}} = 841, 763$, and 759 kN/m.

6.10 Free Vibration of Beams (Flexural–Torsional Vibration)

In this section we present the natural frequencies of orthotropic beams. These frequencies are determined from the equilibrium, strain–displacement, and force–strain relationships. The first two of these equations are identical for isotropic and orthotropic beams, whereas the force–strain relationships differ, the differences being in the stiffness matrices (see Eqs. 6.334 and 6.335). Therefore, as in the case of buckling loads, the natural frequencies of an orthotropic beam can be obtained by replacing the isotropic stiffnesses with the replacement stiffnesses (Eq. 6.336) in the expression of the corresponding isotropic beam.

In the next sections we present the circular frequencies ω of orthotropic beams with doubly symmetrical, symmetrical, and unsymmetrical cross sections. The natural frequencies and the period of vibration are related to ω as follows:

$$f = \frac{\omega}{2\pi} \qquad T = \frac{2\pi}{\omega}. \tag{6.397}$$

6.10.1 Doubly Symmetrical Cross Sections

The beam is orthotropic and its cross section has two axes of symmetry y and z. The mass is also symmetrical with respect to these axes, and, accordingly, the center of mass coincides with the origin of the y–z coordinate system.

A beam with two cross-sectional planes of symmetry may undergo flexural vibration in either of the two planes of symmetry and torsional vibration (Fig. 6.94).

[33] P. Qiao, J. F. Davalos, and J. Wang, Local Buckling of Composite FRP Shapes by Discrete Plate Analysis. *Journal of Structural Engineering*, Vol. 127, 245–255, 2001.

[34] D. J. Lee, The Local Buckling Coefficient for Orthotropic Structural Sections. *Aeronautical Journal*, Vol. 82, 313–320, 1978.

[35] J. Tomblin and E. J. Barbero, Local Buckling Experiments on FRP Columns. *Thin-Walled Structures*, Vol. 18, 97–116, 1994.

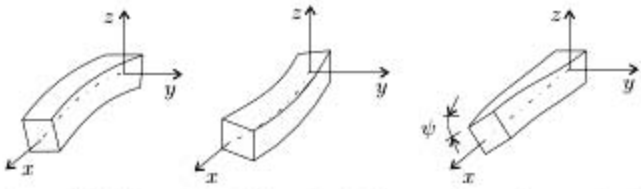

Figure 6.94: Illustration of vibration in the x–z and x–y planes and of torsional vibration.

Expressions for the circular frequencies corresponding to the flexural vibration of an isotropic beam are given by Weaver et al.[36] By replacing EI by $\widehat{EI}$ the circular frequencies of orthotropic beams are

$$\left(\omega_{yi}^{\mathrm{B}}\right)^2 = \frac{\widehat{EI}_{yy}}{\rho}\frac{\mu_{Bi}^4}{L^4} \qquad \text{vibration in the } x\text{–}z \text{ plane} \tag{6.398}$$

$$\left(\omega_{zi}^{\mathrm{B}}\right)^2 = \frac{\widehat{EI}_{zz}}{\rho}\frac{\mu_{Bi}^4}{L^4} \qquad \text{vibration in the } x\text{–}y \text{ plane.} \tag{6.399}$$

where L is the length of the beam, ρ is the mass per unit length, and μ_{Bi} for different end supports are given in Table 6.13. The subscript $i = 1, 2, \ldots$ indicates the first, second, and so forth, modes.

Expressions for the torsional circular frequencies $\omega_{\psi i}^{\mathrm{B}}$ of isotropic beams are also given by Weaver et al. With the replacement stiffnesses, the circular frequencies of long ($\widehat{GI}_{\mathrm{t}} \gg \widehat{EI}_{\omega}/L^2$) and short ($\widehat{GI}_{\mathrm{t}} \ll \widehat{EI}_{\omega}/L^2$) orthotropic beams are

$$\left(\omega_{\psi i}^{\mathrm{B}}\right)^2 = \frac{\widehat{GI}_{\mathrm{t}}}{\Theta}\frac{\mu_{Gi}^2}{L^2} \qquad \begin{array}{l}\text{torsional vibration}\\ \text{long beam}\end{array} \tag{6.400}$$

$$\left(\omega_{\psi i}^{\mathrm{B}}\right)^2 = \frac{\widehat{EI}_{\omega}}{\Theta}\frac{\mu_{Bi}^4}{L^4} \qquad \begin{array}{l}\text{torsional vibration}\\ \text{short beam.}\end{array} \tag{6.401}$$

where Θ is the polar moment of mass per unit length about the shear center[37],

$$\Theta = \int_{(A)} \rho_{\mathrm{comp}}(y^2 + z^2)\,dA, \tag{6.402}$$

ρ_{comp} is mass per unit volume, A is the area of the cross section, and μ_{Bi} and μ_{Gi} are given in Table 6.13 for different end supports.

We approximate the torsional circular frequencies of a beam of arbitrary length by

$$\left(\omega_{\psi i}^{\mathrm{B}}\right)^2 = \left(\omega_{\psi i}^{\mathrm{B}}\right)^2\Big|_{\mathrm{short}} + \left(\omega_{\psi i}^{\mathrm{B}}\right)^2\Big|_{\mathrm{long}} \qquad \text{torsional vibration.} \tag{6.403}$$

[36] W. Weaver, S. P. Timoshenko, and D. H. Young, *Vibration Problems in Engineering*. 5th edition. John Wiley & Sons, New York, 1990, pp. 422–432.

[37] Ibid., p. 476.

Table 6.13. The constants μ_{Bi} and μ_{Gi} in Eqs. (6.398), (6.399), (6.401), (6.406). The simple supports in cases (a) and (b) restrain the rotation about the x-axis, but the cross section is free to warp and free to rotate about the y- and z-axes.

Geometry		μ_B	μ_G
(a)	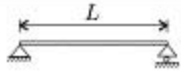	$\mu_{Bi} = i\pi$	$\mu_{Gi} = i\pi$
(b)		$\mu_{B1} = 3.927$ $\mu_{B2} = 7.069$ $\mu_{Bi} \approx (i + 0.25)\pi$	$\mu_{Gi} = i\pi$
(c)		$\mu_{B1} = 4.730$ $\mu_{B2} = 7.853$ $\mu_{Bi} \approx (i + 0.5)\pi$	$\mu_{Gi} = i\pi$
(d)		$\mu_{B1} = 1.875$ $\mu_{B2} = 4.694$ $\mu_{Bi} \approx (i - 0.5)\pi$	$\mu_{Gi} = (i - 0.5)\pi$
(e)		$\mu_{B1} = 4.730$ $\mu_{B2} = 7.853$ $\mu_{B3} = 10.996$ $\mu_{Bi} \approx (i + 0.5)\pi$	$\mu_{G1} = 6.283$ $\mu_{G2} = 8.987$ $\mu_{G3} = 12.566$ $\mu_{Gi} \approx (i + 1)\pi$

By using Eqs. (6.400) and (6.401), we have

$$\left(\omega^{\mathrm{B}}_{\psi i}\right)^2 = \frac{\widehat{EI}_\omega}{\Theta}\frac{\mu^4_{Bi}}{L^4} + \frac{\widehat{GI}_1}{\Theta}\frac{\mu^2_{Gi}}{L^2}. \tag{6.404}$$

We introduce the definition

$$\omega^{\mathrm{B}}_{\omega i} = \sqrt{\frac{\widehat{EI}_\omega}{\Theta}\frac{\mu^4_{Bi}}{L^4}}. \tag{6.405}$$

With this definition the circular frequency is

$$\left(\omega^{\mathrm{B}}_{\psi i}\right)^2 = \left(\omega^{\mathrm{B}}_{\omega i}\right)^2 + \frac{\widehat{GI}_1}{\Theta}\frac{\mu^2_{Gi}}{L^2} \qquad \begin{matrix}\text{torsional}\\ \text{vibration.}\end{matrix} \tag{6.406}$$

Equation (6.406) is exact for simply supported beams (case (a) in Table 6.13). For beams with the types of supports shown as cases (b), (c), and (e), the equation underestimates the circular frequencies (and overestimates the period of vibration) by less than 6 percent. For cantilever beams (case d), Eq. (6.406) may underestimate the circular frequencies (and overestimate the period of vibration) by up to 14 percent.

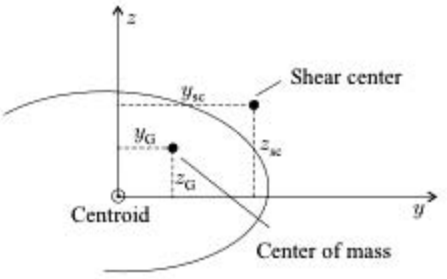

Figure 6.95: Coordinates of the center of mass and the shear center.

6.10.2 Beams with Symmetrical Cross Sections

We consider orthotropic beams with cross sections symmetrical with respect to the z-axis ($\widehat{EI}_{yz} = 0$). The mass is also symmetrical with respect to the z-axis, and, accordingly, the center of mass is on the z-axis. When the cross section of the beam has one axis of symmetry, it may undergo flexural vibration in the x–z plane as well as flexural–torsional vibration.

For such a beam there are three sets of circular frequencies. The first of these is[38]

$$\omega_1 = \omega_{yi}^{\mathrm{B}} \qquad \text{vibration in the } x\text{–}z \text{ plane.} \tag{6.407}$$

The second and third sets of circular frequencies, ω_2 and ω_3, corresponding to the flexural–torsional vibration, are the two roots of the following equation:

$$\left| \begin{bmatrix} \left(\omega_{zi}^{\mathrm{B}}\right)^2 & 0 \\ 0 & \left(\omega_{\psi i}^{\mathrm{B}}\right)^2 \frac{\Theta}{\rho} \end{bmatrix} - \omega^2 \begin{bmatrix} 1 & -(z_G - z_{sc}) \\ -(z_G - z_{sc}) & \frac{\Theta}{\rho} \end{bmatrix} \right| = 0, \tag{6.408}$$

where $|\ \ |$ denotes the determinant, ρ is the mass per unit length, z_{sc} is the coordinate of the shear center, z_G is the coordinate of the center of mass (Fig. 6.95), and Θ is the polar moment of mass per unit length about the shear center

$$\Theta = \int_A \rho_{\mathrm{comp}} \left[y^2 + (z - z_{sc})^2 \right] dA. \tag{6.409}$$

In these equations ω_{yi}^{B}, ω_{zi}^{B}, and $\omega_{\psi i}^{\mathrm{B}}$ are given by Eqs. (6.398), (6.399), and (6.406). Solution of Eq. (6.408) provides the exact values of ω_2 and ω_3 only for simply supported beams (case (a) in Table 6.13).

6.10.3 Beams with Unsymmetrical Cross Sections

The cross section of the beam is unsymmetrical and the layup is orthotropic. The beam undergoes combined flexural–torsional vibration, which is analogous to flexural–torsional buckling. Therefore, we extend Eq. (6.408) and write it in the

[38] Ibid., p. 477.

following form, which is analogous to Eq. (6.346):

$$\left|\begin{bmatrix} (\omega_{zi}^{B})^2 & 0 & 0 \\ 0 & (\omega_{yi}^{B})^2 & 0 \\ 0 & 0 & (\omega_{\psi i}^{B})^2 \frac{\Theta}{\rho} \end{bmatrix} - \omega^2 \begin{bmatrix} 1 & 0 & -(z_G - z_{sc}) \\ 0 & 1 & (y_G - y_{sc}) \\ -(z_G - z_{sc}) & (y_G - y_{sc}) & \frac{\Theta}{\rho} \end{bmatrix}\right| = 0, \tag{6.410}$$

where ω is the circular frequency, y_{sc} and z_{sc} are the coordinates of the shear center, ρ is the mass per unit length, y_G and z_G are the coordinates of the center of mass (Fig. 6.95), and Θ is the polar moment of mass per unit length about the shear center,

$$\Theta = \int_A \rho_{comp}\left[(y - y_{sc})^2 + (z - z_{sc})^2 \right] dA, \tag{6.411}$$

where ω_{yi}^{B}, ω_{zi}^{B} and $\omega_{\psi i}^{B}$ are given by Eqs. (6.398), (6.399), and (6.406). Equation (6.410) yields three sets of ω; the values are only exact for simply supported beams (case (a) in Table 6.13).

6.12 Example. *An $L = 0.5$-m-long I-section beam, with the cross section shown in Figure 6.96, is made of graphite epoxy unidirectional plies. The material properties are given in Table 3.6 (page 81). The density of the composite is 1.6 g/cm^3. The layup is $[0_{20}]$. The beam is simply supported at each end. Calculate the natural frequencies of the beam.*

Solution. The mass per unit length is

$$\rho = \rho_{comp} A = 1600 \frac{\text{kg}}{\text{m}^3} \times 0.264 \times 10^{-3}\,\text{m}^2 = 0.4224 \frac{\text{kg}}{\text{m}}, \tag{6.412}$$

where A is the area of the cross section $A = h(b_{f1} + b_{f2} + b_w) = 0.264 \times 10^{-3}\,\text{m}^2$ (Fig. 6.96). The location of the center of mass coincides with the centroid of the cross section

$$z_G = 0. \tag{6.413}$$

The polar moment of mass per unit length about the shear center is (Eq. 6.402)

$$\Theta = \int_{(A)} \rho_{comp}\left[y^2 + (z - z_{sc})^2 \right] dA = \rho_{comp}\left[I_p + (z_G - z_{sc})^2 A \right]$$
$$= 263.7 \times 10^{-6}\,\text{kg} \cdot \text{m}, \tag{6.414}$$

where $z_{sc} = 0.000\,789$ m (Eq. 6.349) and $I_p = I_{zz} + I_{yy}$ is the polar moment of inertia ($I_{zz} = 26.24 \times 10^{-9}\,\text{m}^4$, $I_{yy} = 122.12 \times 10^{-9}\,\text{m}^4$).

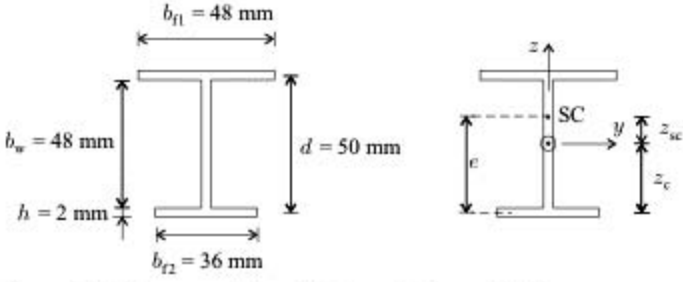

Figure 6.96: The cross section of the beam in Example 6.12.

With the preceding values of ρ and Θ, and with the parameters $\mu_{B1} = \mu_{G1} = \pi$ (Table 6.13, page 308), Eqs. (6.398), (6.399), (6.405), and (6.406) give

$$\omega_{y1}^{B} = \sqrt{\frac{\widehat{EI}_{yy}}{\rho}\frac{\mu_{B1}^4}{L^4}} = 8\,166\,\frac{1}{s}$$

$$\omega_{z1}^{B} = \sqrt{\frac{\widehat{EI}_{zz}}{\rho}\frac{\mu_{B1}^4}{L^4}} = 3\,785\,\frac{1}{s} \tag{6.415}$$

$$\omega_{\omega 1}^{B} = \sqrt{\frac{\widehat{EI}_{\omega}}{\Theta}\frac{\mu_{B1}^4}{L^4}} = 3\,458\,\frac{1}{s}$$

$$\omega_{\psi 1}^{B} = \sqrt{\left(\omega_{\omega 1}^{B}\right)^2 + \frac{\widehat{GI}_t}{\Theta}\frac{\mu_{G1}^2}{L^2}} = 3\,493\,\frac{1}{s}. \tag{6.416}$$

The circular frequency ω_1 is (Eq. 6.407)

$$\omega_1 = \omega_{y1}^{B} = 8\,166\,\frac{1}{s}, \tag{6.417}$$

and ω_2 and ω_3 are the roots of Eq. (6.408) as follows:

$$\left|\begin{bmatrix}\left(\omega_{z1}^{B}\right)^2 & 0\\ 0 & \left(\omega_{\psi 1}^{B}\right)^2\frac{\Theta}{\rho}\end{bmatrix} - \omega^2\begin{bmatrix}1 & (z_G - z_{sc})\\ (z_G - z_{sc}) & \frac{\Theta}{\rho}\end{bmatrix}\right| = 0 \tag{6.418}$$

$$\omega_2 = 6\,024\,\frac{1}{s} \qquad \omega_3 = 2\,838\,\frac{1}{s}. \tag{6.419}$$

The natural frequencies are $f = \omega/2\pi$

$$f_1 = 1\,300\ \text{Hz} \qquad f_2 = 959\ \text{Hz} \qquad f_3 = 452\ \text{Hz}. \tag{6.420}$$

6.11 Summary

In Table 6.14 we summarize the various beam problems considered in this chapter and the relevant section numbers.

Attention is called again to the important fact that the displacements, buckling loads, and natural frequencies of an orthotropic or symmetrical cross-section beam can be determined by simply replacing the isotropic stiffnesses with the appropriate replacement stiffnesses in the expressions for the corresponding isotropic beam. It is for this reason that, in this chapter, emphasis is given to the development of replacement stiffnesses.

For beams with arbitrary layup there is no direct analogy with isotropic beams. Therefore, each problem must be treated individually.

Table 6.14. Section numbers for solid cross section and for thin-walled unreinforced (monocoque) beams. Stiffened thin-walled (semimonocoque) beams are discussed in Section 6.8.

		Monocoque	
	Solid	Thin-walled open-section	Thin-walled closed-section
End loads ($\hat{N}$, $\hat{M}_y$, $\hat{M}_z$, $\hat{T}$)			
Orthotropic layup			
Axial and bending ($\hat{EA}$, $\hat{EI}$)	6.2	6.3	6.4
Torsion			
no restrained warping ($\hat{GI}_t$)	6.5.1	6.5.2	6.5.3, 6.5.4
with restrained warping ($\hat{EI}_\omega$)	–	6.5.5	–
Arbitrary layup			
Axial, bending, and torsion			
no restrained warping	6.2, 6.5.1	6.6.1, 6.6.2	6.6.1, 6.6.2
with restrained warping	–	6.6.4	–
Transverse loads			
Orthotropic layup		6.7.1, 6.7.3	
Arbitrary layup		6.7.2, 6.7.3	
Buckling			
Axially loaded (orthotropic layup or symmetrical cross section)		6.9.1	
Lateral buckling (symmetrical cross section)		6.9.2	
Local buckling		6.9.3	
Free vibration (orthotropic layup or symmetrical cross section)		6.10	

Beams with Shear Deformation

Frequently, beams undergoing small deformations may be analyzed by the Bernoulli–Navier hypothesis, namely, by the assumptions that planes of the cross section remain plane and perpendicular to the axis (Fig. 7.1, left).

In this chapter we treat beams for which the Bernoulli–Navier hypothesis is invalid. In the analysis we employ an x, y, z, coordinate system with the origin in the centroid. Furthermore, to simplify the notation, we use single subscripts y and z describing shear in the x–y and x–z planes.

In the x–z plane the deflection of the beam's axis w is related to the rotation of the cross section χ_z by

$$\frac{dw}{dx} = \chi_z \qquad \begin{matrix}\text{no shear deformation} \\ x\text{–}z \text{ plane.}\end{matrix} \tag{7.1}$$

For thick solid cross-section beams, sandwich beams, and thin-walled beams the first assumption (that planes of the cross section remain plane) is reasonable. The second assumption may no longer be valid because cross sections do not necessarily remain perpendicular to the axis (Fig. 7.1, right). In this case the deflection of the beam is

$$\frac{dw}{dx} = \chi_z + \gamma_z \qquad \begin{matrix}\text{with shear deformation} \\ x\text{–}z \text{ plane,}\end{matrix} \tag{7.2}$$

where γ_z is the transverse shear strain in the x–z plane. The theory, based on the assumption that cross sections remain plane but not perpendicular to the axis is frequently called first-order shear theory. A beam, in which shear deformation is taken into account is called a Timoshenko beam.

Similarly, in the x–y plane, we have

$$\frac{dv}{dx} = \chi_y + \gamma_y \qquad \begin{matrix}\text{with shear deformation} \\ x\text{–}y \text{ plane,}\end{matrix} \tag{7.3}$$

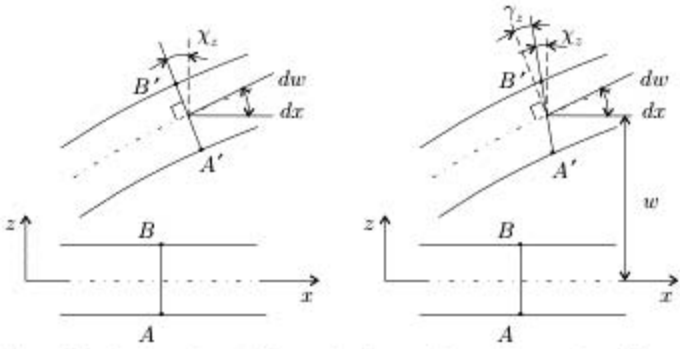

Figure 7.1: Deformation of a beam in the x–z plane without shear deformation (left) and with shear deformation (right).

The rotations of the cross sections χ_z, χ_y are caused by the bending moments $\widehat{M}_y$, $\widehat{M}_z$, and the transverse shear strains γ_z, γ_y are caused by the transverse shear forces $\widehat{V}_z$, $\widehat{V}_y$. The relationships between χ and $\widehat{M}$ and between γ and $\widehat{V}$ are presented in Section 7.1.2 for orthotropic beams.

In torsion, when shear deformation of the wall is neglected, the rate of twist ϑ^{B} is related to the twist of the cross section about the beam's axis ψ by (Fig. 7.2, left)

$$\frac{d\psi}{dx} = \vartheta^{\mathrm{B}} \qquad \text{no shear deformation.} \tag{7.4}$$

When shear deformation is not negligible, there is an additional rate of twist of the cross section ϑ^{S}, as shown in Figure 7.2, right. Thus, in the presence of shear deformation, the rate of twist of the beam is[1]

$$\frac{d\psi}{dx} = \vartheta^{\mathrm{B}} + \vartheta^{\mathrm{S}} \qquad \text{with shear deformation.} \tag{7.5}$$

For open-section beams, ϑ^{B} is the rate of twist due to warping when the shear strain γ is zero, and ϑ^{S} is the rate of twist due to the shear deformation when warping is zero (Fig. 7.2). For closed-section beams the interpretation of ϑ^{B} and ϑ^{S} is more complicated and is not given here.

7.1 Governing Equations

The response of a beam to the applied forces is described by the strain–displacement, force–strain, and equilibrium equations. These equations are given in this section for orthotropic beams, including the effect of restrained warping.

[1] X. Wu and C. T. Sun, Simplified Theory for Composite Thin-Walled Beams. *AIAA Journal*, Vol. 30, 2945–2951, 1992.

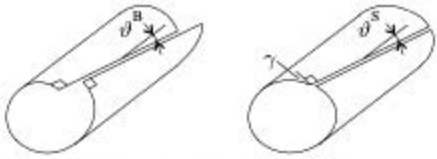

Figure 7.2: The rate of twist ϑ^{B} due to warping when the shear strain is zero (left) and the rate of twist ϑ^{S} due to shear deformation when warping is zero (right).

7.1.1 Strain–Displacement Relationships

There are seven independent displacements, of which the following four are identical to the displacements of beams without shear deformation (Fig. 6.3): the axial displacement u, the transverse displacements v and w in the y and z directions, respectively, and the twist of the cross section ψ. When the shear deformation is taken into account, there are three additional displacements, namely, the rotations of the cross section χ_z, χ_y in the x–z and x–y planes, respectively, and the rate of twist due to warping, ϑ^{B}, when the shear strain γ is zero. We define the following generalized strain components (hereafter referred to as strain):

$$\epsilon_x^o = \frac{\partial u}{\partial x} \qquad \frac{1}{\rho_z} = -\frac{\partial \chi_y}{\partial x} \qquad \frac{1}{\rho_y} = -\frac{\partial \chi_z}{\partial x} \qquad \Gamma = -\frac{\partial \vartheta^{\mathrm{B}}}{\partial x} \qquad \vartheta = \frac{d\psi}{dx} \tag{7.6}$$

We note that ρ_z and ρ_y are not the radii of curvatures of the beam's axis; they are the radii of curvatures only when shear deformation is neglected. Equations (7.2), (7.3), and (7.5) yield

$$\gamma_z = \frac{dw}{dx} - \chi_z \qquad \gamma_y = \frac{dv}{dx} - \chi_y \qquad \vartheta^{\mathrm{S}} = \frac{d\psi}{dx} - \vartheta^{\mathrm{B}}. \tag{7.7}$$

7.1.2 Force–Strain Relationships

The force–strain relationships are first presented in detail for an orthotropic I-beam with doubly symmetrical cross section subjected to bending moment $\widehat{M}_y$, shear force acting through the plane of symmetry $\widehat{V}_z$, and torque $\widehat{T}$ (Fig. 7.3). The relationships thus obtained are then generalized to beams with arbitrary cross sections.

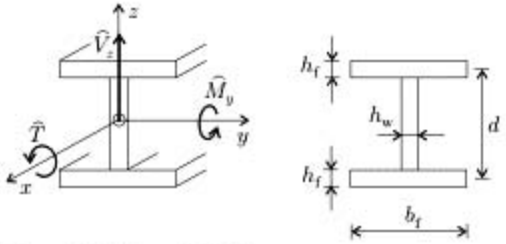

Figure 7.3: Thin-walled I-beam.

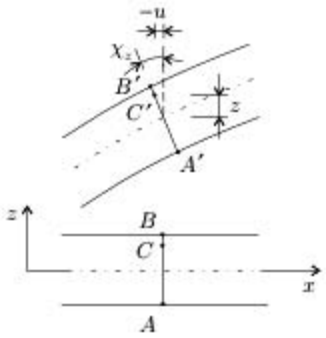

Figure 7.4: Displacement u of point C in the axial direction.

I-*beam.* In the absence of twist, the displacement u in the x direction at a point located at distance z from the centroid is (Fig. 7.4, $\chi_z \approx \tan \chi_z = -\frac{u}{z}$)

$$u = -z\chi_z, \tag{7.8}$$

where χ_z is the rotation of the cross section in the x–z plane.

The strain–displacement relationship (Eq. 2.2), together with Eq. (7.8), gives the axial strain

$$\epsilon_x = \frac{du}{dx} = -z\frac{d\chi_z}{dx}. \tag{7.9}$$

The bending moment about the y-axis is defined as

$$\widehat{M}_y = \int_A z\sigma_x dA. \tag{7.10}$$

For an isotropic material $\sigma_x = E\epsilon_x$, and we have

$$\widehat{M}_y = \int_A zE\left(-z\frac{d\chi_z}{dx}\right)dA = -E\underbrace{\int_A z^2 dA}_{I_{yy}}\frac{d\chi_z}{dx}. \tag{7.11}$$

Recalling the analyses in Sections 6.3 and 6.4, we replace EI by $\widehat{EI}$ for composite beams and write

$$\widehat{M}_y = \widehat{EI}_{yy}\underbrace{\left(-\frac{d\chi_z}{dx}\right)}_{1/\rho_y} \qquad \text{orthotropic beam.} \tag{7.12}$$

where $\widehat{EI}_{yy}$ is the replacement bending stiffness. Replacement bending stiffnesses for beams are given in Tables 6.3–6.8 (page 231) and A.1–A.4.

The shear strain varies linearly with the shear force. Thus, formalistically, we write

$$\widehat{V}_z = \widehat{S}_{zz}\gamma_z \qquad \text{orthotropic beam,} \tag{7.13}$$

where $\widehat{S}_{zz}$ is the shear stiffness.

Next, we consider an orthotropic beam subjected to a torque $\widehat{T}$ (Eq. 6.240):

$$\widehat{T} = \widehat{T}_{sv} + \widehat{T}_{\omega}. \tag{7.14}$$

The torque $\widehat{T}_{sv}$ (Saint-Venant torque, Fig. 6.56, top) is (Eq. 6.240)

$$\widehat{T}_{sv} = \widehat{GI}_t \vartheta \qquad \begin{matrix}\text{Saint-Venant} \\ \text{torque.}\end{matrix} \tag{7.15}$$

The torque $\widehat{T}_{\omega}$ (restrained-warping-induced torque, Fig 6.56, bottom) is derived below following the reasoning used for an I-beam without shear deformation (Section 6.5.5).

The displacement of the flange v_f is (Fig. 6.57)

$$v_f = \psi \frac{d}{2}, \tag{7.16}$$

where ψ is the twist of the cross section about the beam's axis and d is the distance between the midplanes of the flanges. The rate of twist is $\vartheta = d\psi/dx$ (Eq. 6.1), and we write

$$\frac{dv_f}{dx} = \frac{d}{2}\vartheta. \tag{7.17}$$

On the basis of Eq. (7.3), the first derivative of the displacement is written as

$$\frac{dv_f}{dx} = (\chi)_f + (\gamma)_f, \tag{7.18}$$

where $(\chi)_f$ is the rotation of the cross section of the flange about the z-axis (Fig. 7.3), and $(\gamma)_f$ is the shear strain in the flange.

We express the rate of twist in the form[2] (Eq. 7.5)

$$\vartheta = \vartheta^B + \vartheta^S. \tag{7.19}$$

The first term represents the rate of twist in the absence of shear deformation, and the second term is the rate of twist due to shear deformation. Equations (7.17)–(7.19) give

$$(\chi)_f = \frac{d}{2}\vartheta^B \qquad (\gamma)_f = \frac{d}{2}\vartheta^S. \tag{7.20}$$

Recalling Eq. (7.12), we write the bending moment $\widehat{M}_f$ for an orthotropic flange in the presence of shear deformation as

$$\widehat{M}_f = \widehat{EI}_f \left(-\frac{d(\chi)_f}{dx}\right) = -\widehat{EI}_f \frac{d}{2}\frac{d\vartheta^B}{dx}, \tag{7.21}$$

where the second equality is written by virtue of Eq. (7.20), and $\widehat{EI}_f$ is the bending stiffness of the flange about the z-axis.

For an I-beam the bimoment is (Eq. 6.232)

$$\widehat{M}_{\omega} = \widehat{M}_f d. \tag{7.22}$$

[2] X. Wu and C. T. Sun, Simplified Theory for Composite Thin-Walled Beams. *AIAA Journal*, Vol. 30, 2945–2951, 1992.

The last two equations give

$$\widehat{M}_\omega = \underbrace{\left(\frac{d^2}{2}\widehat{EI}_f\right)}_{\widehat{EI}_\omega}\underbrace{\left(-\frac{d\vartheta^B}{dx}\right)}_{\Gamma}, \tag{7.23}$$

where the term in the first parentheses $\widehat{EI}_\omega (= \frac{d^2}{2}\widehat{EI}_f)$ is the warping stiffness, which for an isotropic beam is given by Eq. (6.238) and for an orthotropic I-beam by Eq. (6.244).

The shear force in the flange is related to $\widehat{M}_f$ by

$$\widehat{V}_f = \frac{d\widehat{M}_f}{dx}. \tag{7.24}$$

By referring to Eq. (7.13), we write $\widehat{V}_f$ as

$$\widehat{V}_f = (\widehat{S}_{yy})_f(\gamma)_f, \tag{7.25}$$

where $(\widehat{S}_{yy})_f$ is the shear stiffness of the flange in the x–y plane. The warping-induced torque is (Eq. 6.235)

$$\widehat{T}_\omega = \widehat{V}_f d. \tag{7.26}$$

Equations (7.22), (7.24), and (7.26) result in

$$\widehat{T}_\omega = \frac{d\widehat{M}_\omega}{dx}. \tag{7.27}$$

From Eqs. (7.26), (7.25), and (7.20) we obtain

$$\widehat{T}_\omega = \underbrace{\left[(\widehat{S}_{yy})_f\frac{d^2}{2}\right]}_{\widehat{S}_{\omega\omega}}\vartheta^S \qquad \begin{array}{l}\text{restrained–warping-}\\ \text{induced torque,}\end{array} \tag{7.28}$$

where $\widehat{S}_{\omega\omega}$ is the rotational shear stiffness defined as

$$\widehat{S}_{\omega\omega} = (\widehat{S}_{yy})_f\frac{d^2}{2}. \tag{7.29}$$

Equations (7.12), (7.13), (7.15), (7.23), and (7.28) are the force–strain relationships for an orthotropic I-beam with doubly symmetrical cross section subjected to a bending moment $\widehat{M}_y$, a shear force acting in the plane of symmetry $\widehat{V}_z$, and a torque $\widehat{T}(= \widehat{T}_{sv} + \widehat{T}_\omega)$.

Arbitrary cross-section beams. We now consider orthotropic beams of arbitrary cross sections with internal forces $\widehat{N}$, $\widehat{M}_y$, $\widehat{M}_z$, $\widehat{V}_y$, $\widehat{V}_z$, and $\widehat{M}_\omega$, $\widehat{T}$.

The relationship between the axial force (acting at the centroid) and the axial strain is (Eqs. 6.7 and 6.8)

$$\widehat{N} = \widehat{EA}\epsilon_x^o. \tag{7.30}$$

The bending moments and bimoment for a (symmetrical) I-beam are (see Eqs. 7.12 and 7.23)

$$\begin{Bmatrix} \widehat{M}_z \\ \widehat{M}_y \\ \widehat{M}_\omega \end{Bmatrix} = \begin{bmatrix} \widehat{EI}_{zz} & 0 & 0 \\ 0 & \widehat{EI}_{yy} & 0 \\ 0 & 0 & \widehat{EI}_{\omega} \end{bmatrix} \begin{Bmatrix} -\frac{d\chi_z}{dx} \\ -\frac{d\chi_y}{dx} \\ -\frac{d\vartheta^{\mathrm{B}}}{dx} \end{Bmatrix}, \tag{7.31}$$

where the equation for $\widehat{M}_z$ is analogous to the equation for $\widehat{M}_y$. For an arbitrary cross-section orthotropic beam, the 12 and 21 elements are not zero. Hence, we write

$$\begin{Bmatrix} \widehat{M}_z \\ \widehat{M}_y \\ \widehat{M}_\omega \end{Bmatrix} = \begin{bmatrix} \widehat{EI}_{zz} & \widehat{EI}_{yz} & 0 \\ \widehat{EI}_{yz} & \widehat{EI}_{yy} & 0 \\ 0 & 0 & \widehat{EI}_{\omega} \end{bmatrix} \begin{Bmatrix} -\frac{d\chi_z}{dx} \\ -\frac{d\chi_y}{dx} \\ -\frac{d\vartheta^{\mathrm{B}}}{dx} \end{Bmatrix}. \tag{7.32}$$

By utilizing the definitions given in Eq. (7.6), these equations may be written as

$$\begin{Bmatrix} \widehat{M}_z \\ \widehat{M}_y \\ \widehat{M}_\omega \end{Bmatrix} = \begin{bmatrix} \widehat{EI}_{zz} & \widehat{EI}_{yz} & 0 \\ \widehat{EI}_{yz} & \widehat{EI}_{yy} & 0 \\ 0 & 0 & \widehat{EI}_{\omega} \end{bmatrix} \begin{Bmatrix} \frac{1}{\rho_z} \\ \frac{1}{\rho_y} \\ \Gamma \end{Bmatrix}. \tag{7.33}$$

The relationship between $\widehat{T}_{\mathrm{sv}}$ and the rate of twist ϑ is (Eq. 7.15)

$$\widehat{T}_{\mathrm{sv}} = \widehat{GI}_{\mathrm{t}}\vartheta. \tag{7.34}$$

The shear forces and the restrained-warping-induced torque for a (doubly symmetrical) I-beam is (see Eqs. 7.13 and 7.28)

$$\begin{Bmatrix} \widehat{V}_y \\ \widehat{V}_z \\ \widehat{T}_\omega \end{Bmatrix} = \begin{bmatrix} \widehat{S}_{yy} & 0 & 0 \\ 0 & \widehat{S}_{zz} & 0 \\ 0 & 0 & \widehat{S}_{\omega\omega} \end{bmatrix} \begin{Bmatrix} \gamma_y \\ \gamma_z \\ \vartheta^{\mathrm{S}} \end{Bmatrix}, \tag{7.35}$$

where the first equality is analogous to the second one. Shear is introduced by $\widehat{T}_\omega$ and by $\widehat{V}_y$ and $\widehat{V}_z$. Therefore, the force–strain relationships are coupled. We now extend the preceding equations to include these couplings and (for arbitrary cross-section beams) write the force–strain relationships as

$$\begin{Bmatrix} \widehat{V}_y \\ \widehat{V}_z \\ \widehat{T}_\omega \end{Bmatrix} = \begin{bmatrix} \widehat{S}_{yy} & \widehat{S}_{yz} & \widehat{S}_{y\omega} \\ \widehat{S}_{yz} & \widehat{S}_{zz} & \widehat{S}_{z\omega} \\ \widehat{S}_{y\omega} & \widehat{S}_{z\omega} & \widehat{S}_{\omega\omega} \end{bmatrix} \begin{Bmatrix} \gamma_y \\ \gamma_z \\ \vartheta^{\mathrm{S}} \end{Bmatrix} = \left[\widehat{S}_{ij}\right] \begin{Bmatrix} \gamma_y \\ \gamma_z \\ \vartheta^{\mathrm{S}} \end{Bmatrix}, \tag{7.36}$$

where $[\widehat{S}_{ij}]$ is the shear stiffness matrix of the beam. The inverse of Eq. (7.36) is

$$\begin{Bmatrix} \gamma_y \\ \gamma_z \\ \vartheta^S \end{Bmatrix} = [\widehat{s}_{ij}] \begin{Bmatrix} \widehat{V}_y \\ \widehat{V}_z \\ \widehat{T}_\omega \end{Bmatrix}, \tag{7.37}$$

where $[\widehat{s}_{ij}]$ is the shear compliance matrix

$$\begin{bmatrix} \widehat{S}_{yy} & \widehat{S}_{yz} & \widehat{S}_{y\omega} \\ \widehat{S}_{yz} & \widehat{S}_{zz} & \widehat{S}_{z\omega} \\ \widehat{S}_{y\omega} & \widehat{S}_{z\omega} & \widehat{S}_{\omega\omega} \end{bmatrix} = \begin{bmatrix} \widehat{s}_{yy} & \widehat{s}_{yz} & \widehat{s}_{y\omega} \\ \widehat{s}_{yz} & \widehat{s}_{zz} & \widehat{s}_{z\omega} \\ \widehat{s}_{y\omega} & \widehat{s}_{z\omega} & \widehat{s}_{\omega\omega} \end{bmatrix}^{-1}. \tag{7.38}$$

Equations (7.30), (7.33), (7.34), and (7.36) are the force–strain relationships for a beam with shear deformation. The way in which the elements of the stiffness and compliance matrices are determined is discussed in Section 7.2.

7.1.3 Equilibrium Equations

In the presence of shear deformation the equilibrium equations for a straight beam subjected to the loads shown in Figure 6.1 are identical to those of a beam without shear deformation (see Eq. 6.3):

$$\begin{aligned} \frac{\partial \widehat{N}}{\partial x} &= -p_x & \frac{\partial(\widehat{T}_{sv} + \widehat{T}_\omega)}{\partial x} &= -t \\ \frac{\partial \widehat{V}_y}{\partial x} &= -p_y & \frac{\partial \widehat{V}_z}{\partial x} &= -p_z \\ \frac{\partial \widehat{M}_y}{\partial x} &= \widehat{V}_z & \frac{\partial \widehat{M}_z}{\partial x} &= \widehat{V}_y. \end{aligned} \tag{7.39}$$

When the beam is axially constrained, we have the additional equation (Eq. 7.27) as follows:

$$\frac{d\widehat{M}_\omega}{dx} = \widehat{T}_\omega. \tag{7.40}$$

7.1.4 Summary of Equations

In summary, we have 23 unknowns: 7 generalized displacements (u, v, w, ψ, χ_z, χ_y, ϑ^B), 8 generalized strain components (ϵ_x^o, $1/\rho_z$, $1/\rho_y$, Γ, γ_y, γ_z, ϑ^S, ϑ), and 8 generalized internal forces ($\widehat{N}$, $\widehat{M}_z$, $\widehat{M}_y$, $\widehat{M}_\omega$, $\widehat{V}_y$, $\widehat{V}_z$, $\widehat{T}_\omega$, $\widehat{T}_{sv}$).

The equations that yield the solution are as follows:

	Number of equations	Equation number
strain–displacement	8	7.6, 7.7
force–strain	8	7.30, 7.33, 7.34, 7.36
equilibrium	7	7.39, 7.40

Table 7.1. Boundary conditions for beams with shear stiffnesses

	$x-z$ plane		$x-y$ plane	
Built-in	$w=0$	$\chi_z=0$	$v=0$	$\chi_y=0$
Simply supported	$w=0$	$\hat{M}_y=0$	$v=0$	$\hat{M}_z=0$
Free	$\hat{V}_z=0$	$\hat{M}_y=0$	$\hat{V}_y=0$	$\hat{M}_z=0$
Axially restrained	$u=0$			
unrestrained	$\hat{N}=0$			
Warping restrained	$\vartheta^{\mathrm{B}}=0$			
unrestrained	$\hat{M}_\omega=0$			
Rotationally restrained	$\psi=0$			
unrestrained	$\hat{T}=0$			

In general the strain–displacement, force–strain, and equilibrium equations must be solved simultaneously to determine the forces in the beam. The analysis becomes simpler when the beam is orthotropic. When the beam is orthotropic the internal forces can be determined by substituting the replacement stiffnesses into the corresponding isotropic beam expressions. The replacement stiffnesses are discussed in Section 7.2.

7.1.5 Boundary Conditions

At a built-in end the displacement and the rotations of the cross section are zero. At a simply supported end the displacement and the moment are zero. At a free end the moments and the shear force are zero.

When the end of the beam is restrained so that it cannot move axially, the axial displacement is zero. When the end is not restrained axially, the axial force is zero. When warping of the cross section is restrained, the distortion is zero. When warping is not restrained, the bimoment is zero.

When the end may rotate, the torque is zero. When the end is rotationally restrained, the rate of twist is zero.

The preceding boundary conditions are summarized in Table 7.1.

7.2 Stiffnesses and Compliances of Beams

The stiffnesses that characterize orthotropic beams with shear deformation are shown in Table 7.2. For thin-walled beams these stiffnesses are given in Sections 6.2–6.6 except for the shear stiffnesses derived below in Sections 7.2.1 and 7.2.2. The stiffnesses of sandwich beams are presented in Section 7.2.3.

The shear stiffness of thick solid-section beams are not discussed here; they are given by Whitney.[3]

[3] J. M. Whitney, *Structural Analysis of Laminated Anisotropic Plates*. Technomic, Lancaster, Pennsylvania, 1987, p. 270.

Table 7.2. Stiffnesses of orthotropic beams with shear deformation

Tensile stiffness	$\widehat{EA}$	Sections 6.2–6.4
Bending stiffnesses	$\widehat{EI}_{zz}$, $\widehat{EI}_{yy}$, $\widehat{EI}_{yz}$	Sections 6.2–6.4
Torsional stiffness	$\widehat{GI}_t$	Sections 6.5.1–6.6.2
Warping stiffness	$\widehat{EI}_\omega$	Section 6.6.4
Shear stiffnesses	$\widehat{S}_{yy}$, $\widehat{S}_{zz}$, $\widehat{S}_{\omega\omega}$, $\widehat{S}_{yz}$, $\widehat{S}_{y\omega}$, $\widehat{S}_{z\omega}$	Sections 7.2.1–7.2.3

7.2.1 Shear Stiffnesses and Compliances of Thin-Walled Open-Section Beams

To determine the shear stiffness and shear compliance matrices of thin-walled open-section beams we consider an element of length ΔL of a thin-walled open-section beam (Fig. 7.5). On the two faces of the element there are equal and opposite shear forces $\widehat{V}_y$, equal and opposite shear forces $\widehat{V}_z$, equal and opposite torques $\widehat{T}(= \widehat{T}_{sv} + \widehat{T}_\omega)$, and axial stresses σ_x, which are different at the two faces. We neglect the Saint-Venant torque; hence, $\widehat{T} = \widehat{T}_\omega$.

The shear stresses are represented by the shear flow q,

$$q = \widehat{V}_y q_y^* + \widehat{V}_z q_z^* + \widehat{T}_\omega q_\omega^*, \tag{7.41}$$

where q_y^* and q_z^* are shear flows (per unit force) and are calculated by setting either $\widehat{V}_y = 1$ and $\widehat{V}_z = 0$ or $\widehat{V}_y = 0$ and $\widehat{V}_z = 1$ in Eq. (6.281) and q_ω^* is the shear flow (per unit torque) introduced by a unit torque $\widehat{T}_\omega$; q_ω^* is evaluated by replacing Eh by $1/\alpha_{11}^\varrho$ (see page 264) in the expression of q_ω^* given[4] for the corresponding isotropic beams.

In the following we take into account only shear deformation caused by shear. Thus, the strain energy is (Eq. 2.200)

$$U = \frac{1}{2}\int\int\int (\tau_{\xi\eta}\gamma_{\xi\eta})\, d\zeta d\eta d\xi, \tag{7.42}$$

where ζ is the coordinate perpendicular to the wall, η is the coordinate along the circumference of the cross section, and $\xi = x$. We assume that the shear flow $q(= \int \tau_{\xi\eta} d\zeta)$ does not vary along the ΔL long element and the shear strain $\gamma_{\xi\eta}$ is uniform across the thickness of the wall. Thus, the strain energy is

$$U = \frac{1}{2}\int (\gamma_{\xi\eta}^\circ q)\, d\eta\, \Delta L, \tag{7.43}$$

where $\gamma_{\xi\eta}^\circ$ is the shear strain in the wall's reference surface and is related to the shear flow in the composite wall by $\gamma_{\xi\eta}^\circ = \alpha_{66}^v q$ (see Eq. 6.195), where α_{66}^v is given by $\alpha_{66}^v = \alpha_{66}^\varrho - \frac{(\beta_{66}^\varrho)^2}{\delta_{66}^\varrho}$ (see Eq. 6.196). The superscript ϱ indicates that the compliances

[4] T. H. G. Megson, *Aircraft Structures for Engineering Students*. 3rd edition. Halsted Press, John Wiley & Sons, New York, 1999, pp. 465–472.

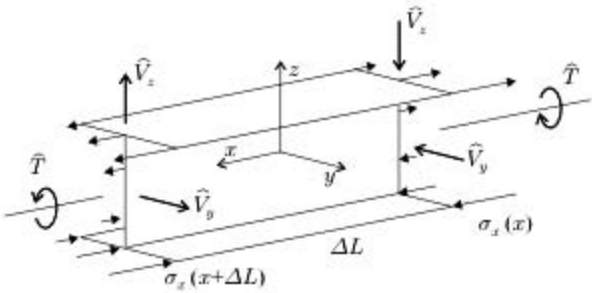

Figure 7.5: The loads applied to a thin-walled, open-section beam.

are evaluated in the ϱ reference plane defined in Figure 6.26. When this expression is used, Eq. (7.43) becomes

$$U = \frac{1}{2}\int \left(\alpha^{v}_{66} q^2\right) d\eta \Delta L. \tag{7.44}$$

The work done by the external forces due to shear deformation is

$$W = \underbrace{\frac{1}{2}\hat{V}_y \gamma_y \Delta L}_{\substack{\text{due to displacement} \\ \text{in the } y \text{ direction}}} + \underbrace{\frac{1}{2}\hat{V}_z \gamma_z \Delta L}_{\substack{\text{due to displacement} \\ \text{in the } z \text{ direction}}} + \underbrace{\frac{1}{2}\hat{T}_\omega \vartheta^S \Delta L}_{\substack{\text{due to the twist-} \\ \text{induced} \\ \text{displacement}}}$$

$$+ \underbrace{\frac{1}{2}\left(\int_{\text{at } x} \sigma_x u_x dA - \int_{\text{at } x+\Delta L} \sigma_x u_x dA\right)}_{\text{due to warping (neglected)}}. \tag{7.45}$$

We neglect the work done by the axial stresses on the shear–force-induced warping.

The law of conservation of energy gives

$$U = W. \tag{7.46}$$

By introducing Eqs. (7.44), (7.45), (7.37), and (7.41) into Eq. (7.46), and by performing the algebra, we obtain

$$\begin{aligned}
&\hat{V}_y^2 \tfrac{1}{2} \hat{s}_{yy} + \hat{V}_z^2 \tfrac{1}{2} \hat{s}_{zz} + \hat{T}_\omega^2 \tfrac{1}{2} \hat{s}_{\omega\omega} + \hat{V}_y \hat{V}_z \hat{s}_{yz} + \hat{V}_y \hat{T}_\omega \hat{s}_{y\omega} + \hat{V}_z \hat{T}_\omega \hat{s}_{z\omega} = \\
&\hat{V}_y^2 \tfrac{1}{2} \int_{(S)} \alpha^{v}_{66} (q_y^*)^2 d\eta + \hat{V}_z^2 \tfrac{1}{2} \int_{(S)} \alpha^{v}_{66} (q_z^*)^2 d\eta + \hat{T}_\omega^2 \tfrac{1}{2} \int_{(S)} \alpha^{v}_{66} (q_\omega^*)^2 d\eta \\
&+ \hat{V}_y \hat{V}_z \int_{(S)} \alpha^{v}_{66} q_y^* q_z^* d\eta + \hat{V}_y \hat{T}_\omega \int_{(S)} \alpha^{v}_{66} q_y^* q_\omega^* d\eta + \hat{V}_z \hat{T}_\omega \int_{(S)} \alpha^{v}_{66} q_z^* q_\omega^* d\eta,
\end{aligned} \tag{7.47}$$

where S indicates integration around the entire circumference. This equation is

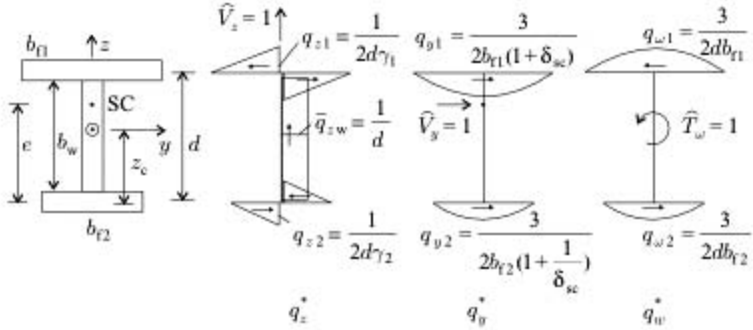

Figure 7.6: I-beam and the shear flows from unit shear forces in the z and y directions and from a unit torque.

valid for arbitrary values of $\hat{V}_y$, $\hat{V}_z$, and $\hat{T}_\omega$. Hence, the elements of the shear compliance matrix are

$$\hat{s}_{yy} = \int_{(S)} \alpha_{66}^v (q_y^*)^2 d\eta \qquad \hat{s}_{zz} = \int_{(S)} \alpha_{66}^v (q_z^*)^2 d\eta \qquad \hat{s}_{\omega\omega} = \int_{(S)} \alpha_{66}^v (q_\omega^*)^2 d\eta$$

$$\hat{s}_{z\omega} = \int_{(S)} \alpha_{66}^v q_z^* q_\omega^* d\eta \qquad \hat{s}_{y\omega} = \int_{(S)} \alpha_{66}^v q_y^* q_\omega^* d\eta \qquad \hat{s}_{yz} = \int_{(S)} \alpha_{66}^v q_z^* q_y^* d\eta. \tag{7.48}$$

The stiffness is given by Eq. (7.38).

I-beam. We consider an I-beam symmetrical about the z-axis (Fig. 7.6). The layup of the web is symmetrical, although the layups of the top and bottom flanges may be unsymmetrical. Unit forces $\hat{V}_z$ and $\hat{V}_y$ and a unit torque $\hat{T}_\omega$ are applied at the shear center.

The shear flows, resulting from unit shear forces $\hat{V}_z = 1$ and $\hat{V}_y = 1$ acting at the shear center and from a unit torque $\hat{T} = \hat{T}_\omega = 1$, are shown in Figure 7.6. Details of the calculations are not presented here. We merely note that the shear flow along the length of the web due to $\hat{V}_z$ is taken to be constant. We now define γ_1, γ_2, δ_c, and δ_{sc} as follows:

$$\gamma_1 = 1 + \frac{1}{3}\frac{(\alpha_{11})_{f1}}{(\alpha_{11})_w}\frac{d}{b_{f1}\left(1+\frac{1}{\delta_c}\right)} \qquad \delta_c = \frac{d - z_c}{z_c}$$

$$\gamma_2 = 1 + \frac{1}{3}\frac{(\alpha_{11})_{f2}}{(\alpha_{11})_w}\frac{d}{b_{f2}(1+\delta_c)} \qquad \delta_{sc} = \frac{d-e}{e}, \tag{7.49}$$

where e is the location of the shear center, z_c is the location of the centroid, d is the distance between the midplanes of the flanges, and b_{f1} and b_{f2} are the widths of the flanges (Fig. 7.6.)

To calculate $\hat{s}_{yy}$ we apply $\hat{V}_y$ and perform the integration indicated in Eq. (7.48) for the web and for the top and bottom flanges. When only $\hat{V}_y$ acts, there is no shear flow in the web (Fig. 7.6), and hence the integration needs to be performed

only for the two flanges as follows:

$$\widehat{s}_{yy} = \int_{(S)} \alpha_{66}^{v}(q_y^*)^2 d\eta = \int_0^{b_{f1}} \left\{ (\alpha_{66}^{v})_{f1} \left[\frac{3}{2b_{f1}(1+\delta_{sc})} 4\frac{\eta}{b_{f1}} \left(1 - \frac{\eta}{b_{f1}}\right) \right]^2 \right\} d\eta$$
$$+ \int_0^{b_{f2}} \left\{ (\alpha_{66}^{v})_{f2} \left[\frac{3}{2b_{f2}\left(1+\frac{1}{\delta_{sc}}\right)} 4\frac{\eta}{b_{f2}} \left(1 - \frac{\eta}{b_{f2}}\right) \right]^2 \right\} d\eta. \tag{7.50}$$

By performing the integrations, we obtain

$$\widehat{s}_{yy} = 1.2 \left[\frac{(\alpha_{66}^{v})_{f1}}{b_{f1}(1+\delta_{sc})^2} + \frac{(\alpha_{66}^{v})_{f2}}{b_{f2}\left(1+\frac{1}{\delta_{sc}}\right)^2} \right], \tag{7.51}$$

where the subscripts f1 and f2 refer to the top and bottom flanges. The other elements of the shear compliance matrix are calculated similarly from Eq. (7.48) with the shear flows shown in Figure 7.6. The results are

$$\widehat{s}_{zz} = \int_{(S)} \alpha_{66}^{v}(q_z^*)^2 d\eta = \frac{(\alpha_{66}^{v})_w}{d} + \frac{1}{12}\frac{(\alpha_{66}^{v})_{f1} b_{f1}}{d^2\gamma_1^2} + \frac{1}{12}\frac{(\alpha_{66}^{v})_{f2} b_{f2}}{d^2\gamma_2^2} \tag{7.52}$$

$$\widehat{s}_{\omega\omega} = \int_{(S)} \alpha_{66}^{v}(q_\omega^*)^2 d\eta = \frac{1.2}{d^2}\left(\frac{(\alpha_{66}^{v})_{f1}}{b_{f1}} + \frac{(\alpha_{66}^{v})_{f2}}{b_{f2}} \right) \tag{7.53}$$

$$\widehat{s}_{y\omega} = \int_{(S)} \alpha_{66}^{v} q_y^* q_\omega^* d\eta = \frac{1.2}{d}\left(-\frac{(\alpha_{66}^{v})_{f1}}{b_{f1}(1+\delta_{sc})} + \frac{(\alpha_{66}^{v})_{f2}}{b_{f2}\left(1+\frac{1}{\delta_{sc}}\right)} \right) \tag{7.54}$$

$$\widehat{s}_{yz} = \int_{(S)} \alpha_{66}^{v} q_y^* q_z^* d\eta = 0 \qquad \widehat{s}_{z\omega} = \int \alpha_{66}^{v} q_z^* q_\omega^* d\eta = 0. \tag{7.55}$$

The stiffness is given by Eq. (7.38).

Arbitrary cross-section beam. The shear compliances of selected thin-walled composite beams[5] are presented in Tables A.8 and A.9. The shear stiffness matrix is determined by Eq. (7.38).

7.2.2 Shear Stiffnesses and Compliances of Thin-Walled Closed-Section Beams

When there is no restrained warping ($\widehat{T}_\omega = 0$, and consequently $\vartheta^S = 0$, see Eq. 7.28), the shear-force–strain relationships (Eq. 7.36) become

$$\begin{Bmatrix} \widehat{V}_y \\ \widehat{V}_z \end{Bmatrix} = \begin{bmatrix} \widehat{S}_{yy} & \widehat{S}_{yz} \\ \widehat{S}_{yz} & \widehat{S}_{zz} \end{bmatrix} \begin{Bmatrix} \gamma_y \\ \gamma_z \end{Bmatrix}. \tag{7.56}$$

[5] L. P. Kollár, Flexural-Torsional Vibration of Open Section Composite Beams with Shear Deformation. *International Journal of Solids and Structures*, Vol. 38, 7543–7558, 2001.

The shear compliance matrix is (see Eq. 7.38)

$$\begin{bmatrix} \widehat{s}_{yy} & \widehat{s}_{yz} \\ \widehat{s}_{yz} & \widehat{s}_{zz} \end{bmatrix} = \begin{bmatrix} \widehat{S}_{yy} & \widehat{S}_{yz} \\ \widehat{S}_{yz} & \widehat{S}_{zz} \end{bmatrix}^{-1}. \tag{7.57}$$

The elements of the shear stiffness matrix of orthotropic thin-walled closed-section beams are obtained by reasoning similar to that used for open-section beams. Thus, from Eq. (7.48) we have

$$\widehat{s}_{yy} = \oint \alpha_{66}^{v} (q_y^*)^2 d\eta \qquad \widehat{s}_{zz} = \oint \alpha_{66}^{v} (q_z^*)^2 d\eta \qquad \widehat{s}_{yz} = \oint \alpha_{66}^{v} q_z^* q_y^* d\eta, \tag{7.58}$$

where q_y^* and q_z^* are shear flows (per unit force) calculated by setting either $\widehat{V}_y = 1$ and $\widehat{V}_z = 0$ or $\widehat{V}_y = 0$ and $\widehat{V}_z = 1$. These shear flows are calculated according to the analysis of thin-walled closed-section beams (Section 6.7). Shear compliances of rectangular and circular cross-section thin-walled beams are given in Table A.7.

The shear stiffness are given by Eq. (7.38).

7.2.3 Stiffnesses of Sandwich Beams

Like sandwich plates (page 169), sandwich beams consist of a foam or honeycomb core covered by facesheets (Fig. 7.7). The core acts much like the web in an I-beam; it separates the two facesheets, resulting in high bending stiffness.

In this section we consider orthotropic sandwich beams consisting of an orthotropic core and orthotropic facesheets (Fig. 7.7).

To determine the shear stiffness in the x–z plane, we apply a shear force $\widehat{V}_z$. For an orthotropic sandwich plate the relationships between the shear forces (per unit length) and the shear strains are (Eqs. 5.15, 5.34)

$$\begin{Bmatrix} V_x \\ V_y \end{Bmatrix} = \begin{bmatrix} \widetilde{S}_{11} & 0 \\ 0 & \widetilde{S}_{22} \end{bmatrix} \begin{Bmatrix} \gamma_{xz} \\ \gamma_{yz} \end{Bmatrix} \qquad \begin{matrix} \text{sandwich} \\ \text{plate.} \end{matrix} \tag{7.59}$$

The total shear force $\widehat{V}_z$ corresponds to bV_x in the plate (where b is the width), and $V_y = 0$ (only $\widehat{V}_z$ acts). Thus, we can apply the laminate plate theory expressions

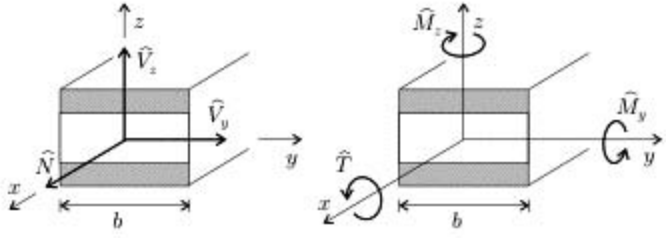

Figure 7.7: Sandwich beam.

to sandwich beams by making the following substitutions:

$$V_x = \frac{\widehat{V}_z}{b} \qquad V_y = 0, \tag{7.60}$$

where b is the width of the beam. The shear strain in the plate γ_{xz} corresponds to the transverse shear strain γ_z in the beam (Fig. 7.1). Thus, Eqs. (7.59) and (7.60) yield

$$\gamma_z = \left(\frac{1}{\widetilde{S}_{11}}\frac{1}{b}\right)\widehat{V}_z \qquad \begin{matrix}\text{sandwich}\\ \text{beam.}\end{matrix} \tag{7.61}$$

The term in parentheses is the shear compliance of a sandwich beam in the x–z plane (see Eq. 7.37)

$$\widehat{s}_{zz} = \frac{1}{\widetilde{S}_{11}b}. \tag{7.62}$$

To determine the bending stiffness in the x–z plane, we again refer to a sandwich plate for which Eqs. (5.11) and (5.12) yield

$$\begin{Bmatrix}\epsilon_x^o\\ \epsilon_y^o\\ \gamma_{xy}^o\end{Bmatrix} = [\alpha]\begin{Bmatrix}N_x\\ N_y\\ N_{xy}\end{Bmatrix} + [\beta]\begin{Bmatrix}M_x\\ M_y\\ M_{xy}\end{Bmatrix} \tag{7.63}$$

$$\begin{Bmatrix}-\frac{\partial\chi_{xz}}{\partial x}\\ -\frac{\partial\chi_{yz}}{\partial y}\\ -\frac{\partial\chi_{xz}}{\partial y}-\frac{\partial\chi_{yz}}{\partial x}\end{Bmatrix} = [\beta]^T\begin{Bmatrix}N_x\\ N_y\\ N_{xy}\end{Bmatrix} + [\delta]\begin{Bmatrix}M_x\\ M_y\\ M_{xy}\end{Bmatrix}, \tag{7.64}$$

where M_x, M_y, M_{xy}, N_x, N_y, N_{xy} are bending moments and in-plane forces per unit length and $[\delta]$, $[\beta]$, and $[\delta]$ are evaluated in the x, y, z coordinate system. We now apply only a bending moment $\widehat{M}_y$ to the sandwich beam (Fig. 7.7). The relationship between the bending moment in the plate M_x and the beam $\widehat{M}_y$ is (Eq. 6.20)

$$M_x = \frac{\widehat{M}_y}{b}. \tag{7.65}$$

Since only $\widehat{M}_y$ acts, we have

$$M_y = M_{xy} = N_x = N_y = N_{xy} = 0. \tag{7.66}$$

Equations (7.64), (7.65), and (7.66) yield ($\chi_{xz} = \chi_x$)

$$-\frac{\partial\chi_x}{\partial x} = \left(\frac{\delta_{11}}{b}\right)\widehat{M}_y. \tag{7.67}$$

We compare Eq. (7.67) with Eq. (7.32) and note that an orthotropic sandwich beam is symmetrical with respect to the z-axis and hence $\widehat{EI}_{yz}$ is zero. Thus, the bending stiffness in the x–z plane is

$$\widehat{EI}_{yy} = \frac{b}{\delta_{11}}. \tag{7.68}$$

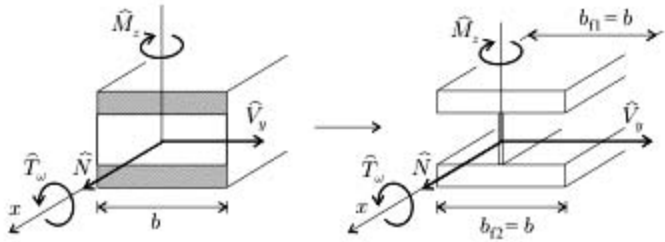

Figure 7.8: Sandwich beam and the equivalent I-beam.

The presence of the core has little effect (i) on the bending stiffnesses in the x–y plane, (ii) on the tensile stiffness, (iii) on the warping stiffness, and (iv) on every element but the $\widehat{s}_{zz}$ element of the shear compliance matrix. We utilize this observation and determine these properties by neglecting the core.

When the core is neglected, the sandwich beam behaves like an I-beam with a thin web (Fig. 7.8). We now use the expressions for an I-beam in Tables A.2, A.5, and A.8 and substitute b for both b_{f1} and b_{f2}, the superscripts t and b for subscripts f1 and f2, and set the terms referring to the web to zero. The resulting bending, tensile, and warping stiffnesses are

$$\widehat{EI}_{zz} = \frac{1}{\alpha_{11}^{t}}\frac{b^3}{12} + \frac{1}{\alpha_{11}^{b}}\frac{b^3}{12} \qquad \widehat{EA} = \frac{1}{\alpha_{11}^{t}}b + \frac{1}{\alpha_{11}^{b}}b \qquad \widehat{EI}_{\omega} = \frac{b^3\frac{1}{\alpha_{11}^{t}}}{12}ed, \tag{7.69}$$

where α_{11}^{t} and α_{11}^{b} are evaluated in the coordinate systems whose origins are at the "neutral" reference planes (which is at $\widetilde{\varrho}$, Eq. 6.105) in the top and bottom flanges, respectively. When the core thickness is so low as to prevent distortion of the cross section, the warping stiffness is lower than the value given in Eq. (7.69). A conservative estimate of the warping stiffness is its lower limit, which is $\widehat{EI}_{\omega} = 0$. The locations of the centroid z_c and the shear center e are (Fig. 7.9)

$$z_c = \frac{1}{\widehat{EA}}\left(\frac{1}{\alpha_{11}^{t}}bd\right) \qquad e = d\frac{\frac{1}{\alpha_{11}^{t}}}{\frac{1}{\alpha_{11}^{t}} + \frac{1}{\alpha_{11}^{b}}} = z_c. \tag{7.70}$$

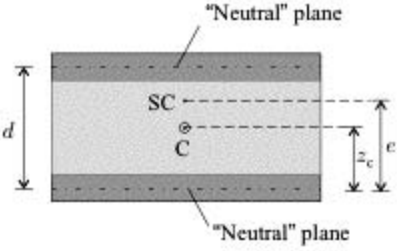

Figure 7.9: Location of the shear center and the centroid of a sandwich beam.

The shear compliances are

$$\widehat{s}_{yy} = \frac{1.2}{b}\left(\frac{\left(\alpha_{66}^{v}\right)^{t}}{(1+\delta_{sc})^{2}} + \frac{\left(\alpha_{66}^{v}\right)^{b}}{\left(1+\frac{1}{\delta_{sc}}\right)^{2}}\right) \tag{7.71}$$

$$\widehat{s}_{\omega\omega} = \frac{1.2}{d^2 b}\left(\left(\alpha_{66}^{v}\right)^{t} + \left(\alpha_{66}^{v}\right)^{b}\right) \tag{7.72}$$

$$\widehat{s}_{y\omega} = \frac{1.2}{db}\left(-\frac{\left(\alpha_{66}^{v}\right)^{t}}{1+\delta_{sc}} + \frac{\left(\alpha_{66}^{v}\right)^{b}}{1+\frac{1}{\delta_{sc}}}\right) \tag{7.73}$$

$$\widehat{s}_{yz} = 0 \qquad \widehat{s}_{z\omega} = 0, \tag{7.74}$$

where α_{66}^{v} is given by Eq. (6.196) and $\delta_{sc} = (d-e)/d$. The elements of the shear stiffness matrix are determined by substituting the elements of the shear compliance matrix into Eq. (7.38).

Next we present upper and lower bounds of the torsional stiffness of a sandwich beam. The upper bound is the torsional stiffness of a solid (not sandwich) beam with the same cross section as the sandwich beam (Eq. 6.169)

$$\widehat{GI}_t = \frac{4b}{\delta_{66}} \qquad \text{upper bound.} \tag{7.75}$$

The lower bound of the torsional stiffness corresponds to the torsional stiffness of a sandwich beam in which the shear stiffness of the core in the y–z plane is neglected. In this case we need to consider only the two facesheets. The torsional stiffnesses of the facesheets are (Eq. 6.169) $4b/\delta_{66}^{t}$ and $4b/\delta_{66}^{b}$, where superscripts t and b refer to the top and bottom facesheets. The torsional stiffness of the sandwich beam with two facesheets is

$$\widehat{GI}_t = \frac{4b}{\delta_{66}^{t}} + \frac{4b}{\delta_{66}^{b}} \qquad \text{lower bound.} \tag{7.76}$$

7.3 Transversely Loaded Beams

In this section we present the deflections of orthotropic beams, with cross sections symmetrical with respect to the x–z plane. A transverse load p_z (per unit length) acts in the plane of symmetry (Fig. 6.1). The relevant equilibrium equations are (Eq. 7.39)

$$\frac{d\widehat{V}_z}{dx} + p_z = 0 \tag{7.77}$$

$$\frac{d\widehat{M}_y}{dx} - \widehat{V}_z = 0, \tag{7.78}$$

where $\widehat{V}_z$ is the shear force, and $\widehat{M}_y$ is the bending moment in the x–z plane. For beams with symmetrical cross sections, $\widehat{EI}_{yz} = 0$, $\widehat{S}_{yz} = 0$, and $\widehat{S}_{z\omega} = 0$, and

Eqs. (7.32) and (7.36) give

$$\widehat{M}_y = -\widehat{EI}_{yy}\frac{d\chi_z}{dx} \qquad \widehat{V}_z = \widehat{S}_{zz}\gamma_z. \tag{7.79}$$

For simplicity, we introduce the following notations:

$$\begin{aligned} \widehat{M}_y &\equiv \widehat{M} & \widehat{V}_z &\equiv \widehat{V} \\ \widehat{EI}_{yy} &\equiv \widehat{EI} & \widehat{S}_{zz} &\equiv \widehat{S} \\ \chi_z &\equiv \chi & \gamma_z &\equiv \gamma \\ p_z &= p. \end{aligned} \tag{7.80}$$

With these notations we have

$$\widehat{M} = -\widehat{EI}\frac{d\chi}{dx} \qquad \widehat{V} = \widehat{S}\gamma. \tag{7.81}$$

Equations (7.78) and (7.81) yield

$$\gamma = -\frac{\widehat{EI}}{\widehat{S}}\frac{d^2\chi}{dx^2}. \tag{7.82}$$

By combining Eqs. (7.77), (7.78), (7.79) and by using Eq. (7.2), we obtain

$$-\widehat{EI}\frac{d^3\chi}{dx^3} + p = 0 \tag{7.83}$$

$$\widehat{EI}\frac{d^2\chi}{dx^2} + \widehat{S}\left(\frac{dw}{dx} - \chi\right) = 0. \tag{7.84}$$

Equations (7.83) and (7.84), together with the boundary conditions listed in Table 7.1 (page 321), provide the deflection w and the rotation of the cross section χ.

Known bending moment distribution. When the bending moment distribution along the beam is known, the deflection may be obtained by the following procedure. The deflection is due to both bending and shear deformation

$$w = w^{\mathrm{B}} + w^{\mathrm{S}}. \tag{7.85}$$

We recall that the deflection is related to the rotation of the cross section and to the shear strain by (Eq. 7.2)

$$\frac{dw}{dx} = \chi + \gamma. \tag{7.86}$$

We combine the two preceding equations and write

$$\frac{dw}{dx} = \frac{dw^{\mathrm{B}}}{dx} + \frac{dw^{\mathrm{S}}}{dx} = \chi + \gamma. \tag{7.87}$$

Thus, we have

$$\frac{dw^{\mathrm{B}}}{dx} = \chi \qquad \frac{dw^{\mathrm{S}}}{dx} = \gamma. \tag{7.88}$$

Substitution of the first of these expressions into Eq. (7.79) gives

$$\frac{d^2w^{\mathrm{B}}}{dx^2} = -\frac{\widehat{M}}{\widehat{EI}}. \tag{7.89}$$

From the second expression in Eq. (7.88) we obtain

$$w^S = \int \gamma dx. \tag{7.90}$$

By replacing γ with $\widehat{V}/\widehat{S}$ (Eq. 7.79) and by performing the integration, we have

$$w^S = \int \frac{\widehat{V}}{\widehat{S}} dx = C_0 + \frac{\widehat{M}}{\widehat{S}}, \tag{7.91}$$

where C_0 is an integration constant. The deflections w^B and w^S are now determined by the following steps:

1. For the known bending moment $\widehat{M}$, the deflection w^B is determined for a beam without shear deformation by using the expression for the corresponding isotropic beam and by replacing the isotropic bending stiffness EI by $\widehat{EI}$.
2. The deflection w^S is calculated by the expression

$$w^S = C_0 + \frac{\widehat{M}}{\widetilde{S}}. \tag{7.92}$$

The constant C_0 is determined from the boundary condition at the support where the deflection w is zero ($w^S = w^B = 0$). Thus, C_0 is

$$C_0 = -\left.\frac{\widehat{M}}{\widetilde{S}}\right|_{\text{where } w=0}. \tag{7.93}$$

3. The total deflection is

$$w = w^B + w^S. \tag{7.94}$$

Maximum deflections of selected beams are given in Table 7.3.

Sandwich beams with arbitrary layup. The preceding analysis for orthotropic beams can be extended to transversely loaded nonorthotropic sandwich beams provided that the beam is free to rotate about its axis. An important practical example is a beam built-in at one end and free at the other end (cantilever beam).

The internal forces arising from the applied loads are $\widehat{M}_y$ and $\widehat{V}_z$ (Fig. 7.10). For sandwich plates the relationships between the shear forces per unit length and the shear strains are (Eq. 5.15)

$$\begin{Bmatrix} V_x \\ V_y \end{Bmatrix} = \begin{bmatrix} \widetilde{S}_{11} & \widetilde{S}_{12} \\ \widetilde{S}_{12} & \widetilde{S}_{22} \end{bmatrix} \begin{Bmatrix} \gamma_{xz} \\ \gamma_{yz} \end{Bmatrix} \quad \begin{matrix} \text{sandwich} \\ \text{plate.} \end{matrix} \tag{7.95}$$

Equation (7.95) with $V_y = 0$ yields

$$V_x = \left(\frac{\widetilde{S}_{11}\widetilde{S}_{22} - \widetilde{S}_{12}^2}{\widetilde{S}_{22}} \right) \gamma_{xz}. \tag{7.96}$$

The shear forces in a sandwich beam are (Eq. 7.60)

$$V_x = \frac{\widehat{V}_z}{b} \qquad V_y = 0, \tag{7.97}$$

where b is the width of the beam.

Table 7.3. Bending moments and maximum deflections of beams with bending stiffness $\widehat{EI}$ and shear stiffness $\widehat{S}$

Geometry, loading, bending moment	Maximum deflection $\bar{w} = \bar{w}^B + \bar{w}^S$	$\frac{\bar{w}^B}{\bar{w}^S}$
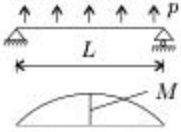	$\bar{w}^B = \frac{5}{384}\frac{pL^4}{\widehat{EI}}$ $\bar{w}^S = \frac{pL^2}{8\widehat{S}}$	$\frac{5}{48}\frac{L^2\widehat{S}}{\widehat{EI}}$
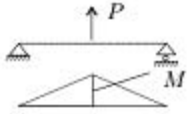	$\bar{w}^B = \frac{PL^3}{48\widehat{EI}}$ $\bar{w}^S = \frac{PL}{4\widehat{S}}$	$\frac{4}{48}\frac{L^2\widehat{S}}{\widehat{EI}}$
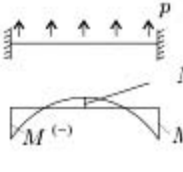	$\bar{w}^B = \frac{1}{384}\frac{pL^4}{\widehat{EI}}$ $\bar{w}^S = \frac{pL^2}{8\widehat{S}}$	$\frac{1}{48}\frac{L^2\widehat{S}}{\widehat{EI}}$
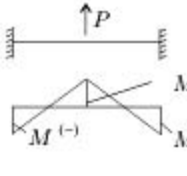	$\bar{w}^B = \frac{PL^3}{192\widehat{EI}}$ $\bar{w}^S = \frac{PL}{4\widehat{S}}$	$\frac{1}{48}\frac{L^2\widehat{S}}{\widehat{EI}}$
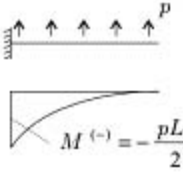	$\bar{w}^B = \frac{1}{8}\frac{pL^4}{\widehat{EI}}$ $\bar{w}^S = \frac{pL^2}{2\widehat{S}}$	$\frac{12}{48}\frac{L^2\widehat{S}}{\widehat{EI}}$
	$\bar{w}^B = \frac{PL^3}{3\widehat{EI}}$ $\bar{w}^S = \frac{PL}{\widehat{S}}$	$\frac{16}{48}\frac{L^2\widehat{S}}{\widehat{EI}}$

The shear strain in the plate γ_{xz} corresponds to the transverse shear strain γ_z in the beam, and $\widehat{V}_z = V_x b$. Thus, we have for a beam

$$\widehat{V}_z = \left(\frac{\widetilde{S}_{11}\widetilde{S}_{22} - \widetilde{S}_{12}^2}{\widetilde{S}_{22}} b\right)\gamma_z \qquad \begin{matrix}\text{sandwich}\\ \text{beam.}\end{matrix} \tag{7.98}$$

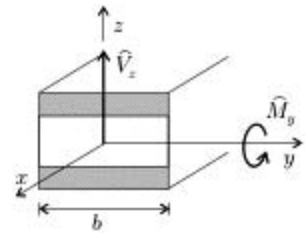

Figure 7.10: Sandwich beam subjected to bending and shear.

The term in parentheses is the shear stiffness (Eq. 7.81):

$$\widehat{S} = \frac{\widetilde{S}_{11}\widetilde{S}_{22} - \widetilde{S}_{12}^2}{\widetilde{S}_{22}} b. \tag{7.99}$$

where $\widetilde{S}_{11}$, $\widetilde{S}_{22}$ and $\widetilde{S}_{12}$ are given by Eq. (5.32).

To determine the bending stiffness in the x–z plane we again start the analysis with sandwich plates. From Eqs. (5.11) and (5.12), for a sandwich plate we have

$$\begin{Bmatrix} -\frac{\partial \chi_{xz}}{\partial x} \\ -\frac{\partial \chi_{yz}}{\partial y} \\ -\frac{\partial \chi_{xz}}{\partial y} - \frac{\partial \chi_{yz}}{\partial x} \end{Bmatrix} = [\delta] \begin{Bmatrix} M_x \\ M_y \\ M_{xy} \end{Bmatrix} + [\beta] \begin{Bmatrix} N_x \\ N_y \\ N_{xy} \end{Bmatrix} \tag{7.100}$$

$$\begin{Bmatrix} \epsilon_x^o \\ \epsilon_y^o \\ \gamma_{xy}^o \end{Bmatrix} = [\beta] \begin{Bmatrix} M_x \\ M_y \\ M_{xy} \end{Bmatrix} + [\alpha] \begin{Bmatrix} N_x \\ N_y \\ N_{xy} \end{Bmatrix}, \tag{7.101}$$

where M_x, M_y, M_{xy}, N_x, N_y, N_{xy} are moments and forces per unit length, and $[\delta]$, $[\beta]$ and $[\delta]$ are evaluated in the x, y, z coordinate system. We now apply a bending moment $\widehat{M}_y$ to the sandwich beam. The relationship between the bending moment in the sandwich plate M_x and the sandwich beam $\widehat{M}_y$ is (Eq. 6.20)

$$M_x = \frac{\widehat{M}_y}{b}. \tag{7.102}$$

Since only $\widehat{M}_y$ acts, we have

$$M_y = M_{xy} = N_x = N_y = N_{xy} = 0. \tag{7.103}$$

From Eqs. (7.100), (7.102), and (7.103), $\partial \chi_x / \partial x = (\partial \chi_{xz} / \partial x)$ is

$$-\frac{\partial \chi_x}{\partial x} = \left(\frac{\delta_{11}}{b}\right) \widehat{M}_y. \tag{7.104}$$

By comparing Eq. (7.104) with Eq. (7.81), we see that the term in parentheses is the inverse of the replacement bending stiffness:

$$\widehat{EI} = \frac{b}{\delta_{11}}. \tag{7.105}$$

The deflections in the x–z plane are calculated by the three steps described on page 331 with $\widehat{S}$ given by Eq. (7.99) and $\widehat{EI}$ by Eq. (7.105).

We note that a nonorthotropic sandwich beam under the action of a bending moment in the x–z plane may also bend in the x–y plane and may also twist.

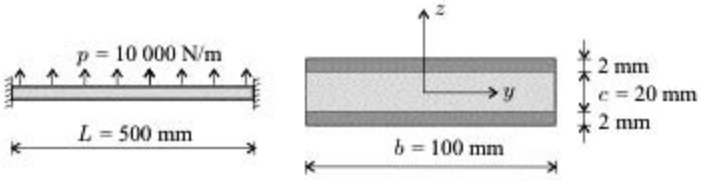

Figure 7.11: The sandwich beam in Example 7.1

7.1 Example. *An $L = 0.5$-m-long and $b = 0.01$-m-wide rectangular sandwich beam is made of a 0.02-m-thick core covered on both sides by graphite epoxy facesheets (Fig. 7.11). The material properties are given in Table 3.6 (page 81). The layup of each facesheet is $[\pm 45_2^{\mathrm{t}}/0_{12}/\pm 45_2^{\mathrm{t}}]$. The thickness of each facesheet is 0.002 m. The beam, built-in at both ends, is subjected to a uniformly distributed load $p =$ 10 000 N/m. Calculate the maximum deflection of the beam. The core is isotropic ($E_{\mathrm{c}} = 2 \times 10^6$ kN/m^2, $\nu_{\mathrm{c}} = 0.3$).*

Solution. The bending compliance matrix is (see Eq. 5.53)

$$[d] = \begin{bmatrix} 52.16 & 7.96 & 0 \\ 7.96 & 11.71 & 0 \\ 0 & 0 & 8.76 \end{bmatrix}^{-1} 10^{-3} = \begin{bmatrix} 21.39 & -14.55 & 0 \\ -14.55 & 95.31 & 0 \\ 0 & 0 & 114.21 \end{bmatrix} 10^{-6} \frac{1}{\mathrm{N \cdot m}}. \tag{7.106}$$

For symmetrical layup $[\delta] = [d]$, and the bending stiffness is (Eq. 7.68)

$$\widehat{EI}_{yy} = \frac{b}{\delta_{11}} = \frac{0.1}{21.39 \times 10^{-6}} = 4\,675\ \mathrm{N \cdot m^2}. \tag{7.107}$$

From Eq. (7.62), (with $\widetilde{S}_{11} = 18.615 \times 10^6 \frac{\mathrm{N}}{\mathrm{m}}$, Eq. 5.54) we have

$$\widehat{s}_{zz} = \frac{1}{\widetilde{S}_{11} b} = 537.17 \times 10^{-9} \frac{1}{\mathrm{N}}. \tag{7.108}$$

The beam is orthotropic, and $\widehat{s}_{yz} = \widehat{s}_{z\omega} = 0$ (Eq. 7.74). Thus, from Eqs. (7.38) and (7.108) we have

$$\widehat{S}_{zz} = \frac{1}{\widehat{s}_{zz}} = 1\,862 \times 10^3\ \mathrm{N}. \tag{7.109}$$

From Table 7.3, third row (page 332), with $\widehat{EI} = \widehat{EI}_{yy}$ and $\widehat{S} = \widehat{S}_{zz}$, the maximum deflection is

$$\widetilde{w} = \frac{1}{384} \frac{pL^4}{\widehat{EI}} + \frac{pL^2}{8\widehat{S}} = \underbrace{0.000\,348}_{\substack{\text{without shear} \\ \text{deformation}}} + 0.000\,168 = 0.000\,516\ \mathrm{m} = 0.52\ \mathrm{mm}.$$

7.4 Buckling of Beams

In this section we present the buckling loads of orthotropic beams subjected to either axial or transverse loads.

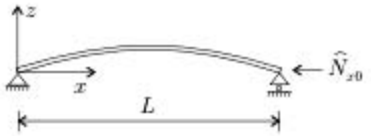

Figure 7.12: Buckling in the x–z plane.

7.4.1 Axially Loaded Beams with Doubly Symmetrical Cross Sections (Flexural and Torsional Buckling)

The beam is orthotropic and its cross section is symmetrical with respect to both the y- and the z-axes ($\widehat{EI}_{yz} = 0$). A compressive axial load $\widehat{N}_{x0}$ is applied at the centroid of the beam (Fig. 7.12). We wish to determine the axial load at which the beam buckles.

When the cross section of the beam has two axes of symmetry (doubly symmetrical cross section), it may buckle (a) in one of the planes of symmetry, (b) in the other plane of symmetry, (c) torsionally (Fig. 6.84). Accordingly, there are three sets of buckling loads

$$\widehat{N}_{cr1} = \widehat{N}_{cry} \qquad \widehat{N}_{cr2} = \widehat{N}_{crz} \qquad \widehat{N}_{cr3} = \widehat{N}_{cr\psi}, \tag{7.110}$$

where $\widehat{N}_{cry}$ and $\widehat{N}_{crz}$ correspond to buckling in the x–z and x–y planes and $\widehat{N}_{cr\psi}$ to torsional buckling (in which case the axis of the beam rotates but does not bend).

Buckling in the x–z plane. We consider a beam of length L that buckles in the x–z plane (Fig. 7.12). The equilibrium equations are identical to those of beams without shear deformation and are[6]

$$\frac{d\widehat{V}_z}{dx} - \widehat{N}_{x0}\frac{d^2w}{dx^2} = 0 \tag{7.111}$$

$$\frac{d\widehat{M}_y}{dx} - \widehat{V}_z = 0, \tag{7.112}$$

where w is the deflection of the beam's axis in the x–z symmetry plane, $\widehat{V}_z$ is the shear force, and $\widehat{M}_y$ is the bending moment. By substituting Eq. (7.79) into (7.111) and (7.112), and by using Eq. (7.2), we obtain the following equilibrium equations for a composite beam:

$$-\widehat{EI}_{yy}\frac{d^3\chi_z}{dx^3} - \widehat{N}_{x0}\frac{d^2w}{dx^2} = 0 \tag{7.113}$$

$$-\widehat{EI}_{yy}\frac{d^2\chi_z}{dx^2} - \widehat{S}_{zz}\left(\frac{dw}{dx} - \chi_z\right) = 0. \tag{7.114}$$

[6] S. P. Timoshenko and J. Gere, *Theory of Elastic Stability*. 2nd edition. McGraw-Hill, New York, 1961, p. 3.

With the notation $\widehat{EI}_{yy} \equiv \widehat{EI}, \widehat{S}_{zz} \equiv \widehat{S}, \chi_z \equiv \chi$, these equations may be rearranged to yield

$$-\widehat{EI}\frac{d^3\chi}{dx^3} - \widehat{N}_{x0}\left(\frac{d\chi}{dx} - \frac{\widehat{EI}}{\widehat{S}}\frac{d^3\chi}{dx^3}\right) = 0 \tag{7.115}$$

$$\frac{dw}{dx} = \chi - \frac{\widehat{EI}}{\widehat{S}}\frac{d^2\chi}{dx^2}. \tag{7.116}$$

Solution of the first of these equations is[7]

$$\chi = C_1 \sin\frac{\mu}{L}x + C_2 \cos\frac{\mu}{L}x + C_3. \tag{7.117}$$

We substitute this expression into Eq. (7.116) and integrate the equation. The result is

$$w = \left(-C_1 \cos\frac{\mu}{L}x + C_2 \sin\frac{\mu}{L}x\right)\frac{L}{\mu}\left(1 + \frac{\widehat{EI}}{\widehat{S}L^2}\mu^2\right) + C_3 x + C_4, \tag{7.118}$$

where C_1–C_4 are constants determined from the boundary conditions and μ is a parameter defined as

$$\mu = L\sqrt{\frac{1}{\widehat{EI}}\frac{1}{\frac{1}{\widehat{N}_{x0}} - \frac{1}{\widehat{S}}}}. \tag{7.119}$$

Equations (7.117)–(7.119) together with the boundary conditions are used to determine the buckling load. In the following we derive the buckling loads of beams built-in at both ends and of beams built-in at one end and simply supported at the other end.

Beams with both ends built in. When both ends of the beam are built-in, the displacement and the rotation of the cross section at each end are zero (Table 7.1, page 321) as follows:

$$w(L) = 0 \qquad \chi(L) = 0 \qquad w(0) = 0 \qquad \chi(0) = 0. \tag{7.120}$$

By substituting w and χ (given by Eqs. 7.117 and 7.118) into these boundary conditions, we obtain

$$\begin{bmatrix} -\Phi\cos\mu & \Phi\sin\mu & L & 1 \\ \sin\mu & \cos\mu & 1 & 0 \\ -\Phi & 0 & 0 & 1 \\ 0 & 1 & 1 & 0 \end{bmatrix}\begin{Bmatrix} C_1 \\ C_2 \\ C_3 \\ C_4 \end{Bmatrix} = \begin{Bmatrix} 0 \\ 0 \\ 0 \\ 0 \end{Bmatrix}, \tag{7.121}$$

where Φ is defined as

$$\Phi = \frac{L}{\mu}\left(1 + \frac{\widehat{EI}}{\widehat{S}L^2}\mu^2\right). \tag{7.122}$$

When the beam buckles, the deflection is nonzero and, hence, at least one of the constants C_1–C_4 must be nonzero. Thus, at buckling, Eq. (7.121) is satisfied

[7] E. Kreyszig, *Advanced Engineering Mathematics*. 7th edition. John Wiley & Sons, New York, 1993, pp. 136–138.

only when the determinant of the matrix is zero, which is a requirement that is met when

$$2\Phi(1-\cos\mu)-L\sin\mu=0. \tag{7.123}$$

This equation is satisfied when μ is

$$\mu=\mu_i=2i\pi, \tag{7.124}$$

where i is an integer ($i=1,2,3,\ldots$). With these values of μ_i, Eq. (7.119) gives the buckling loads ($\widehat{N}_{x0}=\widehat{N}_{cryi}$)

$$\frac{1}{\widehat{N}_{cryi}}=\frac{\left(\frac{L}{2i}\right)^2}{\pi^2\widehat{EI}}+\frac{1}{\widehat{S}}. \tag{7.125}$$

We are interested in the lowest value of the buckling load. For the built-in beam under consideration the lowest value of $\widehat{N}_{cryi}$ is obtained when $i=1$. This value is denoted by $\widehat{N}_{cry}$

$$\frac{1}{\widehat{N}_{cry}}=\frac{1}{\frac{\pi^2\widehat{EI}}{\left(\frac{L}{2}\right)^2}}+\frac{1}{\widehat{S}}. \tag{7.126}$$

The first term in this expression is the inverse of the buckling load of a beam without shear deformation (Eq. 6.337, Table 6.11, page 293):

$$\widehat{N}^{B}_{cry}=\frac{\pi^2\widehat{EI}}{\left(\frac{L}{2}\right)^2}. \tag{7.127}$$

We now can write Eq. (7.126) as

$$\widehat{N}_{cry}=\frac{1}{\frac{1}{\widehat{N}^{B}_{cy}}+\frac{1}{\widehat{S}}}. \tag{7.128}$$

This equation shows that the buckling load decreases with decreasing shear stiffness and, correspondingly, with increasing shear deformation.

Beams with one end built-in the other end simply supported. At the built-in end ($x=L$) the deflection w and the rotation χ are zero (Table 7.1, page 321); at the simply supported end ($x=0$), the deflection w and the first derivative of χ are zero

$$w(L)=0 \qquad \chi(L)=0 \qquad w(0)=0 \qquad \frac{d\chi(0)}{dx}=0. \tag{7.129}$$

By substituting w and χ (given by Eqs. 7.117 and 7.118) into these boundary conditions, we obtain

$$\begin{bmatrix} -\Phi\cos\mu & \Phi\sin\mu & L & 1\\ \sin\mu & \cos\mu & 1 & 0\\ -\Phi & 0 & 0 & 1\\ \mu & 0 & 0 & 0 \end{bmatrix}\begin{Bmatrix} C_1\\ C_2\\ C_3\\ C_4 \end{Bmatrix}=\begin{Bmatrix} 0\\ 0\\ 0\\ 0 \end{Bmatrix}. \tag{7.130}$$

where Φ is given by Eq. (7.122). When the beam buckles, the deflection is nonzero, and, hence, at least one of the constants C_1–C_4 must be nonzero. Thus, at buckling, Eq. (7.130) is satisfied only when the determinant of the matrix is zero. This requirement is met when

$$\left(1 + \frac{\widehat{EI}}{\widehat{S}L^2}\mu^2\right) \tan \mu = \mu. \tag{7.131}$$

The values of μ that satisfy this equation are denoted by μ_i ($i = 1, 2, \ldots$). The values of μ_i must be obtained numerically. The buckling loads $\widehat{N}_{\text{cry}i} (= \widehat{N}_{x0})$ are obtained from Eq. (7.119) and are expressed as

$$\frac{1}{\widehat{N}_{\text{cry}i}} = \frac{1}{\frac{\mu_i^2 \widehat{EI}}{L^2}} + \frac{1}{\widehat{S}}. \tag{7.132}$$

The lowest value of μ_i results in the buckling load. The lowest value of μ_i may be approximated by setting $(1 + \frac{\widehat{EI}}{\widehat{S}L^2}\mu^2)$ equal to unity in Eq. (7.131). With this approximation the lowest value of μ_i is $\mu_1 = \pi/0.70$, and the buckling load becomes

$$\frac{1}{\widehat{N}_{\text{cry}}} \simeq \frac{1}{\frac{\pi^2 \widehat{EI}}{(0.7L)^2}} + \frac{1}{\widehat{S}}. \tag{7.133}$$

This expression overestimates the buckling load by less than 6 percent.

The first term in the expression above is the inverse of the buckling load of a beam without shear deformation (see Eq. 6.337 and Table 6.11):

$$\widehat{N}^{\text{B}}_{\text{cry}} = \frac{\pi^2 \widehat{EI}}{(0.7L)^2}. \tag{7.134}$$

We now write

$$\widehat{N}_{\text{cry}} \simeq \frac{1}{\frac{1}{\widehat{N}^{\text{B}}_{\text{cry}}} + \frac{1}{\widehat{S}}}. \tag{7.135}$$

This equation shows that the buckling load decreases with decreasing shear stiffness and, correspondingly, with increasing shear deformation.

Different types of end supports. Equations (7.128) and (7.135) show that for beams with one end built-in and the other simply supported or with both ends built-in, the buckling load in the x–z plane may be written in the form ($\widehat{S} = \widehat{S}_{zz}$) as

$$\widehat{N}_{\text{cry}} = \left(\frac{1}{\widehat{N}^{\text{B}}_{\text{cry}}} + \frac{1}{\widehat{S}_{zz}}\right)^{-1}, \tag{7.136}$$

where $\widehat{N}^{\text{B}}_{\text{cry}}$ is the buckling load of the beam without shear deformation.

By analyses similar to those presented above, it can be shown that this expression is also applicable to beams with both ends simply supported or with one end built-in and the other end free. In applying Eq. (7.136), $\widehat{N}^{\text{B}}_{\text{cry}}$ is calculated by

Eq. (6.337) with the k values listed in Table 6.11 (page 293). Equation (7.136) is accurate for cases (a), (c), and (d) in Table 6.11 and may overestimate the buckling load by up to 6 percent for case (b).

Buckling in the x–y plane. We express the buckling load in the x–y plane similarly to the buckling load in the x–z plane as

$$\widehat{N}_{cry} = \left(\frac{1}{\widehat{N}^{B}_{cry}} + \frac{1}{\widehat{S}_{yy}} \right)^{-1}, \tag{7.137}$$

where $\widehat{N}^{B}_{cry}$ is the buckling load for the beam without shear deformation (see Eq. 6.337).

Torsional buckling. We consider a doubly symmetrical cross-section beam subjected to an axial load $\widehat{N}_{x0}$. Under this load the beam may rotate about the axis. For such a beam the equilibrium equation is[8]

$$\frac{d\widehat{T}}{dx} - \widehat{N}_{x0} i_{\omega}^2 \frac{d^2\psi}{dx^2} = 0, \tag{7.138}$$

where ψ is the twist of the cross section about the axis, $\widehat{T}$ is the torque, and i_{ω} is the polar radius of gyration defined by Eq. (6.340),

$$i_{\omega}^2 = z_{sc}^2 + y_{sc}^2 + \frac{\widehat{EI}_{zz} + \widehat{EI}_{yy}}{\widehat{EA}}, \tag{7.139}$$

and $\widehat{T}$ is given by Eq. (7.14) as

$$\widehat{T} = \widehat{T}_{sv} + \widehat{T}_{\omega}. \tag{7.140}$$

From Eq. (7.40) we have

$$\frac{d\widehat{M}_{\omega}}{dx} - \widehat{T}_{\omega} = 0. \tag{7.141}$$

The force–strain relationships for a beam with doubly symmetrical cross section are (Eqs. 7.32, 7.34, 7.36)

$$\widehat{M}_{\omega} = -\widehat{EI}_{\omega} \frac{d\vartheta^{B}}{dx} \qquad \widehat{T}_{sv} = \widehat{GI}_{t}\vartheta \qquad \widehat{T}_{\omega} = \widehat{S}_{\omega\omega}\vartheta^{S}, \tag{7.142}$$

where ϑ, and ϑ^{S} are (Eqs. 7.6 and 7.7)

$$\vartheta = \frac{d\psi}{dx} \qquad \vartheta^{S} = \frac{d\psi}{dx} - \vartheta^{B}. \tag{7.143}$$

Equations (7.138)–(7.143) may be combined to yield

$$\widehat{S}_{\omega\omega}\left(\frac{d^2\psi}{dx^2} - \frac{d\vartheta^{B}}{dx} \right) + \widehat{GI}_{t} \frac{d^2\psi}{dx^2} - \widehat{N}_{x0} i_{\omega}^2 \frac{d^2\psi}{dx^2} = 0 \tag{7.144}$$

$$-\widehat{EI}_{\omega} \frac{d^2\vartheta^{B}}{dx^2} - \widehat{S}_{\omega\omega}\left(\frac{d\psi}{dx} - \vartheta^{B} \right) = 0. \tag{7.145}$$

[8] S. P. Timoshenko and J. Gere, *Theory of Elastic Stability*. 2nd edition. New York, McGraw-Hill, 1961, p. 227, Eqs. (b) and (d).

After algebraic manipulations these equations become

torsional buckling:

$$-\widehat{EI}_\omega \frac{d^3\vartheta^B}{dx^3} - (\widehat{N}_{x0} i_\omega^2 - \widehat{GI}_t)\left(\frac{d\vartheta^B}{dx} - \frac{\widehat{EI}}{\widehat{S}_{\omega\omega}} \frac{d^3\vartheta^B}{dx^3}\right) = 0 \tag{7.146}$$

$$\frac{d\psi}{dx} = \vartheta^B - \frac{\widehat{EI}}{\widehat{S}_{\omega\omega}} \frac{d^2\vartheta^B}{dx^2}. \tag{7.147}$$

The corresponding equations for buckling in the x–z plane were derived previously (Eqs. 7.115 and 7.116) and, for convenience, are repeated below

in-plane buckling:

$$-\widehat{EI}\frac{d^3\chi}{dx^3} - \widehat{N}_{x0}\left(\frac{d\chi}{dx} - \frac{\widehat{EI}}{\widehat{S}} \frac{d^3\chi}{dx^3}\right) = 0 \tag{7.148}$$

$$\frac{dw}{dx} = \chi - \frac{\widehat{EI}}{\widehat{S}} \frac{d^2\chi}{dx^2}. \tag{7.149}$$

It is readily seen that these two equations are identical to Eqs. (7.146) and (7.147) when the following substitutions are made:

In-plane buckling		Torsional buckling
$\widehat{N}_{x0}$	$\Longrightarrow$	$\widehat{N}_{x0} i_\omega^2 - \widehat{GI}_t$
$\widehat{EI}$	$\Longrightarrow$	$\widehat{EI}_\omega$
$\widehat{S}$	$\Longrightarrow$	$\widehat{S}_{\omega\omega}$
w	$\Longrightarrow$	ψ
χ	$\Longrightarrow$	ϑ^B.

(7.150)

For in-plane buckling the load $\widehat{N}_{x0}$ at which the beam buckles is denoted by $\widehat{N}_{cry}$. For torsional buckling, the load at which the beam buckles is denoted by $\widehat{N}_{cr\psi}$. Thus, the solutions for buckling in the x–z plane (Eq. 7.136) are applicable to torsional buckling with the following substitutions:

In-plane buckling		Torsional buckling
$\widehat{N}_{cry}$	$\Longrightarrow$	$\widehat{N}_{cr\psi} i_\omega^2 - \widehat{GI}_t$
$\widehat{EI}$	$\Longrightarrow$	$\widehat{EI}_\omega$
$\widehat{S}$	$\Longrightarrow$	$\widehat{S}_{\omega\omega}$.

(7.151)

The parameters w and χ are not included here because they do not appear in the expression for the buckling load.

From Eqs. (7.136) and (6.337) we obtain

$$\frac{1}{\widehat{N}_{cry}} = \frac{1}{\frac{\pi^2 \widehat{EI}_{yy}}{(kL)^2}} + \frac{1}{\widehat{S}_{zz}}. \tag{7.152}$$

By replacing $\widehat{N}_{cry}$, $\widehat{EI}$, and $\widehat{S}_{zz}$ $(= \widehat{S})$ with the expressions in Eq. (7.151), we have

$$\frac{1}{\widehat{N}_{cr\psi} i_\omega^2 - \widehat{GI}_t} = \frac{1}{\frac{\pi^2 \widehat{EI}_\omega}{(kL)^2}} + \frac{1}{\widehat{S}_{\omega\omega}}, \tag{7.153}$$

where $\widehat{N}^{\mathrm{B}}_{\mathrm{cr}\omega}$ is defined as in Eq.(6.338)

$$\widehat{N}^{\mathrm{B}}_{\mathrm{cr}\omega} = \frac{1}{i_\omega^2}\frac{\pi^2 \widehat{EI}_\omega}{(kL)^2}. \tag{7.154}$$

Equations (7.153) and (7.154) may be rearranged to yield

$$\widehat{N}_{\mathrm{cr}\psi} = \widehat{N}_{\mathrm{cr}\omega} + \frac{1}{i_\omega^2}\widehat{GI}_{\mathrm{t}}, \tag{7.155}$$

where $\widehat{N}_{\mathrm{cr}\omega}$ is defined as

$$\widehat{N}_{\mathrm{cr}\omega} = \left(\frac{1}{\widehat{N}^{\mathrm{B}}_{\mathrm{cr}\omega}} + \frac{1}{\frac{1}{i_\omega^2}\widehat{S}_{\omega\omega}}\right)^{-1}, \tag{7.156}$$

and where $\widehat{N}^{\mathrm{B}}_{\mathrm{cr}\omega}$ is the buckling load without shear deformation given by Eq. (6.338) with the k values presented in Table 6.11 (page 293). Equation (7.155) is accurate for cases (a), (c), and (d) in Table 6.11 and overestimates the buckling load by less than 6 percent for case (b).

The buckling loads of axially loaded beams with shear deformation are summarized in Appendix B.

7.4.2 Axially Loaded Beams with Symmetrical or Unsymmetrical Cross Sections (Flexural–Torsional Buckling)

We consider orthotropic beams subjected to an axial load. The cross section may be symmetrical or unsymmetrical. The coordinate directions y and z must be in the principal directions (page 208), and, consequently, $\widehat{EI}_{yz} = 0$.

When the cross section of the beam has one axis of symmetry (about the z-axis), it may undergo (a) buckling in the plane of symmetry (x–z plane), or (b) combined flexural–torsional buckling. When the cross section is unsymmetrical, an orthotropic beam undergoes combined flexural–torsional buckling.

In general, for symmetrical and unsymmetrical cross sections, every element of the stiffness matrix must be considered in the calculation of the buckling load. When the off-diagonal terms of the shear stiffness matrix (Eq. 7.36) either are zero (cross section is doubly symmetrical) or are negligible, the buckling load may be approximated by the solution of the following equations[9]

unsymmetrical cross section:

$$\left|\begin{bmatrix} \widehat{N}_{\mathrm{cr}z} & 0 & 0 \\ 0 & \widehat{N}_{\mathrm{cr}y} & 0 \\ 0 & 0 & \widehat{N}_{\mathrm{cr}\psi} i_\omega^2 \end{bmatrix} - \widehat{N}_{\mathrm{cr}} \begin{bmatrix} 1 & 0 & z_{\mathrm{sc}} \\ 0 & 1 & -y_{\mathrm{sc}} \\ z_{\mathrm{sc}} & -y_{\mathrm{sc}} & i_\omega^2 \end{bmatrix}\right| = 0, \tag{7.157}$$

[9] L. P. Kollár, Flexural-Torsional Buckling of Open Section Composite Columns with Shear Deformation. *International Journal of Solids and Structures*, Vol. 38, 7525–7541, 2001.

where || denotes determinant. The buckling load $\widehat{N}_{cr}$ corresponds to flexural–torsional buckling. The solution of Eq. (7.157) results in three values of $\widehat{N}_{cr}$, of which the lowest value is of interest.

symmetrical cross section:

$$\widehat{N}_{cr1} = \widehat{N}_{cry} \tag{7.158}$$

$$\left| \begin{bmatrix} \widehat{N}_{crz} & \\ & \widehat{N}_{cr\psi} i_\omega^2 \end{bmatrix} - \widehat{N}_{cr} \begin{bmatrix} 1 & z_{sc} \\ z_{sc} & i_\omega^2 \end{bmatrix} \right| = 0, \tag{7.159}$$

where $\widehat{N}_{cr1}$ is the buckling load in the x–z plane and $\widehat{N}_{cr}$ corresponds to flexural–torsional buckling. Equation (7.158) yields the value of $\widehat{N}_{cr1}$ and Eq. (7.159) yields two values of $\widehat{N}_{cr}$ denoted by $\widehat{N}_{cr2}$ and $\widehat{N}_{cr3}$. The buckling load of interest is the lowest of these three values.

We observe that the preceding equations (Eqs. 7.157–7.159) are identical to those given for beams without shear deformation (Eqs. 6.343–6.346). The difference is in the expressions used to calculate $\widehat{N}_{crz}$, $\widehat{N}_{cry}$, and $\widehat{N}_{cr\psi}$. Here we use the expressions given by Eqs. (7.136), (7.137), and (7.155).

Equations (7.157)–(7.159) give the exact buckling load when $\widehat{S}_{ij} = 0$ $(i \neq j)$ and either (a) both ends are simply supported, (b) both ends are built-in, or (c) when one end is built-in and the other end is free. When one end is built-in and one is simply supported (case (b) in Table 6.11, page 293) the equations above yield only an approximate value of the buckling load.

The buckling loads of axially loaded beams with shear deformation are summarized in Appendix B.

7.2 Example. *An $L = 0.5$-m-long and $b = 0.1$-m-wide rectangular sandwich beam (Fig. 7.13) is made of a 0.02-m-thick core covered on both sides by graphite epoxy facesheets. The material properties are given in Table 3.6 (page 81). The layup of each face is $[\pm 45_2^t/0_{12}/\pm 45_2^t]$, and the thickness of each facesheet is 0.002 m. The beam, built-in at both ends, is subjected to an axial compressive load. Calculate the buckling load. The core is isotropic ($E_c = 2 \times 10^6$ kN/m^2, $\nu_c = 0.3$).*

Solution. The beam buckles in the x–z plane. With the values of $\widehat{EI}_{yy} = 4\,675$ N·m^2, $\widehat{S}_{zz} = \frac{1}{\widehat{s}_{zz}} = 1\,862$ kN (Eqs. 7.107 and 7.109), and $L = 0.5$ m, the

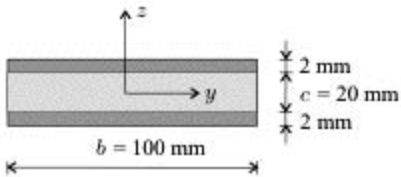

Figure 7.13: The cross section of the sandwich beam in Example 7.2.

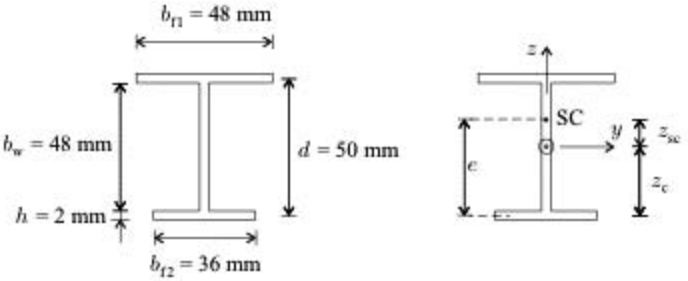

Figure 7.14: The cross-section of the beam in Example 7.3.

buckling load is (see Eqs. 7.136 and 6.337)

$$\widehat{N}_{cry} = \left(\frac{1}{\widehat{N}^{B}_{cry}} + \frac{1}{\widehat{S}_{zz}}\right)^{-1} = \left(\frac{1}{\frac{4\pi^2 \widehat{EI}_{yy}}{L^2}} + \frac{1}{\widehat{S}_{zz}}\right)^{-1}$$
$$= \left(\frac{1}{738} + \frac{1}{1\,862}\right)^{-1} = 529 \text{ kN}. \tag{7.160}$$

7.3 Example. *An $L = 0.5$-m-long I-section beam with the cross section shown in Figure 7.14 is made of graphite epoxy unidirectional plies. The material properties are given in Table 3.6 (page 81). The layup is $[0_{20}]$. The beam is simply supported at each end. Determine the buckling load when the beam is subjected to a compressive axial load.*

Solution. The shear compliances of symmetrical I-beams are given in Table A.8. The layup of the web and the flanges is identical. For a symmetrical layup, $(\alpha^{v}_{66})_f$ and $(\alpha^{v}_{66})_w$ are replaced by a_{66}, and we write

$$\widehat{s}_{yy} = 1.2\left(\frac{a_{66}}{b_{f1}(1+\delta_{sc})^2} + \frac{a_{66}}{b_{f2}(1+\frac{1}{\delta_{sc}})^2}\right) = 1.681 \times 10^{-6}\frac{1}{\text{N}}$$
$$\widehat{s}_{zz} = \frac{a_{66}}{d} + \frac{1}{12}\frac{a_{66}b_{f1}}{d^2\gamma_1^2} + \frac{1}{12}\frac{a_{66}b_{f2}}{d^2\gamma_2^2} = 2.413 \times 10^{-6}\frac{1}{\text{N}}$$
$$\widehat{s}_{\omega\omega} = \frac{1.2}{d^2}\left(\frac{a_{66}}{b_{f1}} + \frac{a_{66}}{b_{f2}}\right) = 2\,564 \times 10^{-6}\frac{1}{\text{N}\cdot\text{m}^2} \tag{7.161}$$
$$\widehat{s}_{y\omega} = \frac{1.2}{d}\left(-\frac{a_{66}}{b_{f1}(1+\delta_{sc})} + \frac{a_{66}}{b_{f2}(1+\frac{1}{\delta_{sc}})}\right) = -16.906 \times 10^{-6}\frac{1}{\text{N}\cdot\text{m}}$$
$$\widehat{s}_{yz} = \widehat{s}_{z\omega} = 0$$

$$\delta_c = \frac{d-z_c}{z_c} = 0.833 \qquad \gamma_1 = 1 + \frac{1}{3}\frac{(\alpha_{11})_{f1}}{(\alpha_{11})_w}\frac{d}{b_{f1}(1+\frac{1}{\delta_c})} = 1.16$$
$$\delta_{sc} = \frac{d-e}{e} = 0.4219 \qquad \gamma_2 = 1 + \frac{1}{3}\frac{(\alpha_{11})_{f2}}{(\alpha_{11})_w}\frac{d}{b_{f2}(1+\delta_c)} = 1.25. \tag{7.162}$$

The parameter a_{66} for both the web and the flanges is $a_{66} = 109.89 \times 10^{-9} \frac{\text{m}}{\text{N}}$ (Table 3.8, page 85), $b_{\text{fl}} = 0.048$ m, $b_{\text{fl2}} = 0.036$ m, $b_{\text{w}} = 0.048$ m, $d = 0.050$ m, and $e = 0.035\,17$ m (Eq. 6.348). The shear stiffnesses are (Eqs. 7.38 and 7.161)

$$\begin{bmatrix} \widehat{S}_{yy} & \widehat{S}_{yz} & \widehat{S}_{y\omega} \\ \widehat{S}_{yz} & \widehat{S}_{zz} & \widehat{S}_{z\omega} \\ \widehat{S}_{y\omega} & \widehat{S}_{z\omega} & \widehat{S}_{\omega\omega} \end{bmatrix} = \begin{bmatrix} \widehat{s}_{yy} & 0 & \widehat{s}_{y\omega} \\ 0 & \widehat{s}_{zz} & 0 \\ \widehat{s}_{y\omega} & 0 & \widehat{s}_{\omega\omega} \end{bmatrix}^{-1} = \begin{bmatrix} 637.0 & 0 & 4.200 \\ 0 & 414.4 & 0 \\ 4.200 & 0 & 0.4177 \end{bmatrix} \times 10^3. \tag{7.163}$$

From Example 6.8 (page 294) we have $\widehat{N}^{\text{B}}_{\text{cry}} = 713.55$ kN, $\widehat{N}^{\text{B}}_{\text{crz}} = 153.32$ kN, $\widehat{N}^{\text{B}}_{\text{cr}\omega} = 127.96$ kN (Eqs. 6.351 and 6.352), $\widehat{GI}_{\text{t}} = 1.602$ N·m^2 (Eq. 6.348), $i_\omega = 0.024\,99$ m (Eq.6.350). The buckling loads are (Eqs. 7.128, 7.137, 7.155, and 7.156)

$$\begin{aligned} \widehat{N}_{\text{crz}} &= \left(\frac{1}{\widehat{N}^{\text{B}}_{\text{crz}}} + \frac{1}{\widehat{S}_{yy}} \right)^{-1} = 123.57\,\text{kN} \\ \widehat{N}_{\text{cry}} &= \left(\frac{1}{\widehat{N}^{\text{B}}_{\text{cry}}} + \frac{1}{\widehat{S}_{zz}} \right)^{-1} = 262.16\,\text{kN} \\ \widehat{N}_{\text{cr}\psi} &= \widehat{N}_{\text{cr}\omega} + \frac{1}{i_\omega^2} \widehat{GI}_{\text{t}} = 109.98\,\text{kN}, \end{aligned} \tag{7.164}$$

where

$$\widehat{N}_{\text{cr}\omega} = \left(\frac{1}{\widehat{N}^{\text{B}}_{\text{cr}\omega}} + \frac{1}{\frac{1}{i_\omega^2} \widehat{S}_{\omega\omega}} \right)^{-1} = 107.42\,\text{kN}. \tag{7.165}$$

The buckling load $\widehat{N}_{\text{cr1}}$ is (Eq. 7.158)

$$\widehat{N}_{\text{cr1}} = \widehat{N}_{\text{cry}} = 262.16\,\text{kN} \qquad \text{buckling in the } x\text{–}z \text{ plane.} \tag{7.166}$$

$\widehat{N}_{\text{cr2}}$ and $\widehat{N}_{\text{cr3}}$ are the roots of Eq. (7.159),

$$\left| \begin{bmatrix} \widehat{N}_{\text{crz}} & \\ & \widehat{N}_{\text{cr}\psi} i_\omega^2 \end{bmatrix} - \widehat{N}_{\text{cr}} \begin{bmatrix} 1 & -z_{\text{sc}} \\ -z_{\text{sc}} & i_\omega^2 \end{bmatrix} \right| = 0, \tag{7.167}$$

where $z_{\text{sc}} = 0.000\,789$ m (Eq. 6.349). Solution of this equation yields

$$\widehat{N}_{\text{cr2}} = 169.17\,\text{kN} \qquad \widehat{N}_{\text{cr3}} = 87.06\,\text{kN}. \tag{7.168}$$

Calculations that neglect shear deformation give the buckling loads as (Eqs. 6.353 and 6.355)

$$\widehat{N}_{\text{cr1}} = 713.55\,\text{kN} \qquad \widehat{N}_{\text{cr2}} = 208.88\,\text{kN} \qquad \widehat{N}_{\text{cr3}} = 106.43\,\text{kN}. \tag{7.169}$$

We now compare these values with the buckling loads calculated above, taking shear deformation into account. The buckling loads calculated with and without shear deformation differ significantly.

7.4.3 Lateral–Torsional Buckling of Beams with Symmetrical Cross Section

We consider orthotropic beams. The cross section of the beam is symmetrical with respect to the z-axis ($\widehat{EI}_{yz} = 0$). The beam is simply supported at each end. At the simple support the beam is restrained from rotating about the x-axis, but the cross section is free to rotate about the y- and z-axes and free to warp.

The beam is subjected to two equal and opposite bending moments at the two ends (Fig. 6.86, top), a uniformly distributed load p in the plane of symmetry (Fig. 6.86, middle), or a concentrated force P in the plane of symmetry at the midspan of the beam (Fig. 6.86, bottom). The distance between the shear center and the point where the load acts is denoted by Δ.

At a certain applied load the beam buckles laterally while the cross sections of the beam rotate (Fig. 6.87). This phenomenon is called lateral buckling or lateral–torsional buckling.

In general, for symmetrical cross sections, every element of the shear stiffness matrix must be considered in the calculation of the buckling load. When the off-diagonal terms of the shear stiffness matrix (Eq. 7.36) either are zero (cross section is doubly symmetrical) or are negligible, the buckling load may be approximated by the following equation[10]:

$$\widehat{Q}_{cr} = F_1 \widehat{N}_{crz} \left(F_2 \Delta + F_3 \beta_1 \pm \sqrt{(F_2 \Delta + F_3 \beta_1)^2 + \frac{\widehat{N}_{cr\psi} i_\omega^2}{\widehat{N}_{crz}}} \right), \tag{7.170}$$

where $\widehat{Q}_{cr}$ is the critical value of the bending moment and is related to the applied loads, as shown in Table 6.12 (page 298). The positive sign before the square root results in a positive load (which acts upward), whereas the negative sign results in a negative load (which acts downward). The values of the constants F_1, F_2, F_3 are also listed in Table 6.12. The parameter β_1 depends on the shape of the cross section (Eq. 6.360).

We observe that Eq. (7.170) is identical to that given for beams without shear deformation (Eq. 6.359). The difference is in the expressions used to calculate $\widehat{N}_{crz}$ and $\widehat{N}_{cr\psi}$. Here we use the expressions given by Eqs. (7.137) and (7.155). These equations contain $\widehat{N}^{B}_{crz}$ and $\widehat{N}^{B}_{cr\psi}$, which are to be calculated by Eq. (6.337) with $k = 1$.

7.4 Example. *An $L = 0.5$-m-long I-section beam with the cross section shown in Figure 7.14 is made of graphite epoxy unidirectional plies. The material properties*

[10] A. Sapkás and L. P. Kollár, Lateral-Torsional Buckling of Composite Beams. *International Journal of Solids and Structures*, Vol. 39, 2939–2963, 2002.

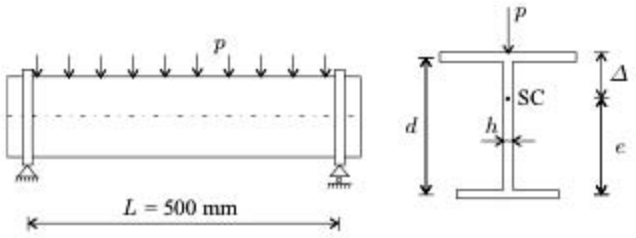

Figure 7.15: The beam in Example 7.4.

are given in Table 3.6 (page 81). The layup is $[0_{20}]$. *The beam, simply supported at each end, is subjected to a distributed load along the top flange (Fig. 7.15). Determine the buckling load.*

Solution. For a transversely loaded beam the buckling load is (Table 6.12, page 298)

$$p_{cr} = \frac{8\widehat{Q}_{cr}}{L^2}, \tag{7.171}$$

where $\widehat{Q}_{cr}$ is given by Eq. (7.170) as follows:

$$\widehat{Q}_{cr} = F_1 \widehat{N}_{crz}\left(F_2\Delta + F_3\beta_1 - \sqrt{(F_2\Delta + F_3\beta_1)^2 + \frac{\widehat{N}_{cr\psi} i_\omega^2}{\widehat{N}_{crz}}}\right). \tag{7.172}$$

The sign before the square root is negative because the load is downward. The parameters are $F_1 = 1.13$, $F_2 = 0.45$, $F_3 = 0.267$ (Table 6.12, page 298), $\Delta = 0.015\,84$ m, (Example 6.9, page 298), $\widehat{N}_{crz} = 123.57$ kN, $\widehat{N}_{cr\psi} = 109.98$ kN (Eq. 7.164), $i_\omega = 0.024\,99$ m (Eq. 6.350), and $\beta_1 = -0.017\,86$ m (Eq. 6.369).

With these values $\widehat{Q}_{cr}$ is

$$\widehat{Q}_{cr} = -2\,979\ \text{N}\cdot\text{m}. \tag{7.173}$$

Equations (7.171) and (7.173) give

$$p_{cr} = \frac{8\widehat{Q}_{cr}}{L^2} = -95\,320\ \frac{\text{N}}{\text{m}}. \tag{7.174}$$

Calculations that neglect shear deformation give the buckling load as $p_{cr} = -115\,407$ N/m (Eq. 6.372). The buckling load calculated with and without shear deformation differs significantly.

7.4.4 Summary

In summary, when the cross section is such that the off-diagonal elements of the stiffness matrix are negligible ($\widehat{S}_{ij} = 0, i \neq j$), the buckling loads may be approximated by the expressions derived for beams without shear deformation by the

following substitutions:

No shear deformation With shear deformation

$$\widehat{N}^{\mathrm{B}}_{\mathrm{cr}z} \Longrightarrow \left(\frac{1}{\widehat{N}^{\mathrm{B}}_{\mathrm{cr}z}} + \frac{1}{\widehat{S}_{yy}}\right)^{-1}$$

$$\widehat{N}^{\mathrm{B}}_{\mathrm{cr}y} \Longrightarrow \left(\frac{1}{\widehat{N}^{\mathrm{B}}_{\mathrm{cr}y}} + \frac{1}{\widehat{S}_{zz}}\right)^{-1} \tag{7.175}$$

$$\widehat{N}^{\mathrm{B}}_{\mathrm{cr}\omega} \Longrightarrow \left(\frac{1}{\widehat{N}^{\mathrm{B}}_{\mathrm{cr}\omega}} + \frac{1}{\frac{1}{i_0^2}\widehat{S}_{\omega\omega}}\right)^{-1}.$$

Numerical examples[11,12] show that these substitutions are reasonable even when $\widehat{S}_{ij} \neq 0$.

7.5 Free Vibration of Beams

In this section we present the circular frequencies ω of orthotropic beams. The parameter ω is related to the period of vibration T and to the natural frequency f by

$$T = \frac{2\pi}{\omega} \qquad f = \frac{\omega}{2\pi}. \tag{7.176}$$

7.5.1 Beams with Doubly Symmetrical Cross Sections

The cross section of the beam has two axes of symmetry y and z. The mass is symmetrical with respect to these axes, and, accordingly, the center of mass coincides with the origin of the y–z coordinate system.

A beam with two cross-sectional planes of symmetry may undergo flexural vibration in either of the two planes of symmetry and torsional vibration (Fig. 6.94). There are three sets of vibrations modes[13],

$$\omega_1 = \omega_y \qquad \omega_2 = \omega_z \qquad \omega_3 = \omega_\psi, \tag{7.177}$$

where ω_y and ω_z correspond to vibration in the x–z and x–y planes, respectively, and ω_ψ corresponds to the torsional mode.

Vibration in the x–z plane. We recall the equilibrium equations of beams subjected to transverse loads (Eqs. 7.83 and 7.84):

$$-\widehat{EI}\frac{d^3\chi}{dx^3} + p = 0 \tag{7.178}$$

$$\widehat{EI}\frac{d^2\chi}{dx^2} + \widehat{S}\left(\frac{dw}{dx} - \chi\right) = 0. \tag{7.179}$$

[11] Ibid.

[12] L. P. Kollár, Flexural-Torsional Vibration of Open Section Composite Beams with Shear Deformation. *International Journal of Solids and Structures*, Vol. 38, 7543–7558, 2001.

[13] W. Weaver, S. P. Timoshenko, and D. H. Young, *Vibration Problems in Engineering*. 5th edition. John Wiley & Sons, New York, 1990, pp. 422–432.

In writing these equations we used the symbols specified in Eq. (7.80). In the present context p is the inertia force given by

$$p = \rho\omega^2 w, \tag{7.180}$$

where ρ is the mass per unit length. Equations (7.178)–(7.180) may be rearranged to yield

$$\frac{1}{\rho\omega^2}\frac{d^4\chi}{dx^4} + \frac{1}{\widehat{S}}\frac{d^2\chi}{dx^2} - \frac{1}{\widehat{EI}}\chi = 0 \tag{7.181}$$

$$w = \frac{\widehat{EI}}{\rho\omega^2}\frac{d^3\chi}{dx^3}. \tag{7.182}$$

The solution of the first of these equations is[14]

$$\chi = C_1 \cosh\frac{\nu}{L}x + C_2 \sinh\frac{\nu}{L}x + C_3 \cos\frac{\mu}{L}x + C_4 \sin\frac{\mu}{L}x. \tag{7.183}$$

We substitute this expression into Eq. (7.182). The result is

$$w = \frac{\widehat{EI}_{yy}}{\rho\omega^2}\left(C_1\frac{\nu^3}{L^3}\sinh\frac{\nu}{L}x + C_2\frac{\nu^3}{L^3}\cosh\frac{\nu}{L}x + C_3\frac{\mu^3}{L^3}\sin\frac{\mu}{L}x - C_4\frac{\mu^3}{L^3}\cos\frac{\mu}{L}x\right), \tag{7.184}$$

where L is the length of the beam, C_1–C_4 are constants determined from the boundary conditions, and μ and ν are parameters defined as

$$\mu = L\sqrt{\left(\frac{\rho\omega^2}{2\widehat{S}}\right) + \sqrt{\left(\frac{\rho\omega^2}{2\widehat{S}}\right)^2 + \frac{\rho\omega^2}{\widehat{EI}}}} \tag{7.185}$$

$$\nu = L\sqrt{-\left(\frac{\rho\omega^2}{2\widehat{S}}\right) + \sqrt{\left(\frac{\rho\omega^2}{2\widehat{S}}\right)^2 + \frac{\rho\omega^2}{\widehat{EI}}}}. \tag{7.186}$$

From the first of these equations, we have

$$\frac{1}{\omega^2} = \rho\left[\left(\frac{L}{\mu}\right)^4\frac{1}{\widehat{EI}} + \left(\frac{L}{\mu}\right)^2\frac{1}{\widehat{S}}\right]. \tag{7.187}$$

By combining Eqs. (7.185) and (7.186), we obtain

$$\mu^2 - \frac{\widehat{EI}}{\widehat{S}L^2}\mu^2\nu^2 - \nu^2 = 0. \tag{7.188}$$

Equations (7.183), (7.184), (7.187), and (7.188) together with the boundary conditions provide the circular frequencies. The process by which ω is determined is illustrated by two examples: a beam simply supported at both ends and a beam built-in at both ends.

[14] E. Kreyszig, *Advanced Engineering Mathematics*. 7th edition. John Wiley & Sons, New York, 1993, pp. 136–138.

Both ends simply supported. When both ends of the beam are simply supported, at the ends the deflection w and the first derivative of χ are zero (Table 7.1, page 321) as follows:

$$w(L) = 0 \qquad \frac{d\chi(L)}{dx} = 0 \qquad w(0) = 0 \qquad \frac{d\chi(0)}{dx} = 0. \tag{7.189}$$

By substituting w and χ (given by Eqs. 7.183 and 7.184) into these boundary conditions, we obtain

$$\begin{bmatrix} \nu^3 \sinh \nu & \nu^3 \cosh \nu & \mu^3 \sin \mu & -\mu^3 \cos \mu \\ \nu \sinh \nu & \nu \cosh \nu & -\mu \sin \mu & \mu \cos \mu \\ 0 & \nu^3 & 0 & -\mu^3 \\ 0 & \nu & 0 & \mu \end{bmatrix} \begin{Bmatrix} C_1 \\ C_2 \\ C_3 \\ C_4 \end{Bmatrix} = \begin{Bmatrix} 0 \\ 0 \\ 0 \\ 0 \end{Bmatrix}. \tag{7.190}$$

For the deflection to be nonzero, at least one of the constants C_1–C_4 must be nonzero. Therefore, Eq. (7.190) is satisfied only when the determinant of the matrix is zero. This requirement is met when

$$\mu^2 \nu^2 (\nu^2 + \mu^2)^2 \sinh \nu \sin \mu = 0. \tag{7.191}$$

This equation requires that the sine term be zero. This condition is satisfied when

$$\mu = \mu_i = i\pi. \tag{7.192}$$

Equations (7.187) and (7.192) give the following expression for the circular frequencies of the beam vibrating in the plane of symmetry:

$$\frac{1}{\omega_i^2} = \rho \left[\frac{1}{\widehat{EI}} \left(\frac{L}{i\pi} \right)^4 + \frac{1}{\widehat{S}} \left(\frac{L}{i\pi} \right)^2 \right]. \tag{7.193}$$

Both ends built-in. When both ends of the beam are built-in, the displacement and the rotation of the cross section at each end are zero (Table 7.1, page 321) as follows:

$$w(L) = 0 \qquad \chi(L) = 0 \qquad w(0) = 0 \qquad \chi(0) = 0. \tag{7.194}$$

By substituting w and χ (given by Eqs. 7.183 and 7.184) into these boundary conditions, we obtain

$$\begin{bmatrix} \nu^3 \sinh \nu & \nu^3 \cosh \nu & \mu^3 \sin \mu & -\mu^3 \cos \mu \\ \cosh \nu & \sinh \nu & \cos \mu & \sin \mu \\ 0 & \nu^3 & 0 & -\mu^3 \\ 1 & 0 & 1 & 0 \end{bmatrix} \begin{Bmatrix} C_1 \\ C_2 \\ C_3 \\ C_4 \end{Bmatrix} = \begin{Bmatrix} 0 \\ 0 \\ 0 \\ 0 \end{Bmatrix}. \tag{7.195}$$

Table 7.4. The equations to determine the circular frequencies ω of beams with shear deformation. For vibration in the x–z plane $\widehat{EI} = \widehat{EI}_{yy}$, and $\widehat{S} = \widehat{S}_{zz}$. For vibration in the x–y plane $\widehat{EI} = \widehat{EI}_{zz}$, and $\widehat{S} = \widehat{S}_{yy}$.

$$\frac{1}{\omega_i^2} = \left(\frac{L}{\mu_i}\right)^4 \frac{\rho}{\widehat{EI}} + \left(\frac{L}{\mu_i}\right)^2 \frac{\rho}{\widehat{S}}$$

Geometry	μ_i
(a) 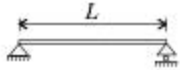	$\sin\mu = 0$ (solution : $\mu_i = i\pi$)
(b) 	$\nu^3 \tanh\nu - \mu^3 \tan\mu = 0$ $\mu^2 - \frac{\widehat{EI}}{\widehat{S}L^2}\mu^2\nu^2 - \nu^2 = 0$
(c) 	$\cos\mu\cosh\nu + \frac{1}{2}\left[\left(\frac{\nu}{\mu}\right)^3 - \left(\frac{\mu}{\nu}\right)^3\right]\sin\mu\sinh\nu - 1 = 0$ $\mu^2 - \frac{\widehat{EI}}{\widehat{S}L^2}\mu^2\nu^2 - \nu^2 = 0$
(d) 	$2 + \left(\frac{\nu}{\mu} - \frac{\mu}{\nu}\right)\sin\mu\sinh\nu$ $+\left[\left(\frac{\nu}{\mu}\right)^2 + \left(\frac{\mu}{\nu}\right)^2\right]\cos\mu\cosh\nu = 0$ $\mu^2 - \frac{\widehat{EI}}{\widehat{S}L^2}\mu^2\nu^2 - \nu^2 = 0$
(e)	$-\cos\mu\cosh\nu + \frac{1}{2}\left(\frac{\nu}{\mu} - \frac{\mu}{\nu}\right)\sin\mu\sinh\nu + 1 = 0$ $\mu^2 - \frac{\widehat{EI}}{\widehat{S}L^2}\mu^2\nu^2 - \nu^2 = 0$

For the deflection to be nonzero, at least one of the constants C_1–C_4 must be nonzero. Thus, Eq. (7.195) is satisfied only when the determinant of the matrix is zero. This requirement is met when

$$\cos\mu\cosh\nu + \frac{1}{2}\left[\left(\frac{\nu}{\mu}\right)^3 - \left(\frac{\mu}{\nu}\right)^3\right]\sin\mu\sinh\nu = 1. \tag{7.196}$$

We now recall Eq. (7.188) as follows:

$$\mu^2 - \frac{\widehat{EI}}{\widehat{S}L^2}\mu^2\nu^2 - \nu^2 = 0. \tag{7.197}$$

Equations (7.196) and (7.197) can be solved numerically for μ and ν; the resulting values are denoted by μ_i and ν_i. The circular frequencies ω_i are then calculated from Eq. (7.187).

Different types of end supports. The equations needed to calculate μ (and the circular frequencies, Eq. 7.187) of beams with different end supports can be obtained in a similar manner. The results are summarized in Table 7.4. The calculation of the circular frequencies requires a numerical procedure except when both ends are simply supported.

Approximate solution. The analysis just described requires a numerical procedure to calculate the circular frequencies. In the following an approximate solution is presented, which results in a closed-form expression for the circular frequencies.

We apply Föppl's theorem developed for estimating the buckling load of elastic structures,[15] and write the circular frequency ω as

$$\frac{1}{\omega^2} \simeq \left(\frac{1}{\omega^{\mathrm{B}}}\right)^2 + \left(\frac{1}{\omega^{\mathrm{S}}}\right)^2, \tag{7.198}$$

where ω^{B} is the circular frequency of a beam undergoing bending deformation only, and ω^{S} is the circular frequency of a beam undergoing shear deformation only.

We illustrate the use of the preceding equation through the example of a beam with both ends built-in. We then generalize the results to beams with different end supports.

To calculate ω^{B} we recall that, when there is no shear deformation the shear stiffness is infinity ($\widehat{S} \to \infty$). In this limit, Eqs. (7.185) and (7.186) yield

$$\mu = \nu. \tag{7.199}$$

By denoting this value of μ by μ_{B} and by substituting $\mu_{\mathrm{B}} = \mu = \nu$ into Eq. (7.196), we obtain

$$\cos \mu_{\mathrm{B}} \cosh \mu_{\mathrm{B}} = 1. \tag{7.200}$$

Numerical solution of this equation yields

$$\begin{aligned} \mu_{B1} &= 4.730 \\ \mu_{B2} &= 7.853 \\ &\vdots \\ \mu_{Bi} &\simeq (i + 0.5)\pi. \end{aligned} \tag{7.201}$$

With these approximate values of $\mu_{\mathrm{B}i}$ the circular frequencies are (Eq. 7.187 with $\widehat{S} \longrightarrow \infty$)

$$\left(\frac{1}{\omega^{\mathrm{B}}}\right)^2 = \rho \frac{1}{\widehat{EI}} \left(\frac{L}{\mu_{\mathrm{B}i}}\right)^4. \tag{7.202}$$

To determine ω^{S} we note that when there is no bending deformation the bending stiffness is infinity ($\widehat{EI} \longrightarrow \infty$). In this limit Eq. (7.186) yields $\nu = 0$. With this value of ν and with the substitution $\mu = \mu_{\mathrm{S}}$ Eq. (7.196) gives

$$\sin \mu_{\mathrm{S}} = 0. \tag{7.203}$$

[15] T. Tarnai, Summation Theorems Concerning Critical Loads of Bifurcation. In: *Structural Stability in Engineering Practice*. L. Kollár, ed., E & FN Spon, London, 1999, pp. 23–58.

Table 7.5. The circular frequencies of beams with shear deformation only. The equations for calculating μ_{Si} (left column) and the values of μ_{Si} (right column). For vibration in the x–z and x–y planes $\widehat{S}$ is $\widehat{S}_{zz}$ and $\widehat{S}_{yy}$ respectively.

$$(\omega_i^S)^2 = \frac{\widehat{S}}{\rho}\left(\frac{\mu_{Si}}{L}\right)^2$$

Geometry	μ_{Si}	
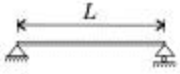	$\sin\mu_S = 0$	$\mu_{Si} = i\pi$
	$\tan\mu_S = 0$	$\mu_{Si} = i\pi$
	$\sin\mu_S = 0$	$\mu_{Si} = i\pi$
	$\cos\mu_S = 0$	$\mu_{Si} = (i-0.5)\pi$
	$-\cos\mu_S + 1 - \frac{\mu_S}{2}\sin\mu_S = 0$	$\mu_{S1} = 6.283$ $\mu_{S2} = 8.987$ $\mu_{S3} = 12.566$ Approximate: $\mu_{Si} \approx (i+1)\pi$

Solutions to this equation are

$$\mu_S = \mu_{Si} = i\pi \qquad i = 1, 2, \ldots. \tag{7.204}$$

With these values of μ_S Eq. (7.187) becomes ($\widehat{EI} \longrightarrow \infty$)

$$\left(\frac{1}{\omega^S}\right)^2 = \rho\left(\frac{L}{\mu_{Si}}\right)^2 \frac{1}{\widehat{S}}. \tag{7.205}$$

Equations (7.198), (7.202), and (7.205) give the circular frequencies in the x–z plane of symmetry of orthotropic beams with built-in ends:

$$\frac{1}{\omega_y^2} \simeq \frac{1}{\left(\omega_y^B\right)^2} + \frac{1}{\left(\omega_y^S\right)^2} = \frac{\rho}{\widehat{EI}_{yy}}\left(\frac{L}{\mu_{Bi}}\right)^4 + \frac{\rho}{\widehat{S}_{zz}}\left(\frac{L}{\mu_{Si}}\right)^2. \tag{7.206}$$

The subscript y is introduced to indicate that the beam vibrates in the x–z plane.

It can be shown that Eq. (7.206) is also applicable to beams with end supports other than ones built-in at both ends provided that the appropriate values of μ_{Bi} and μ_{Si} are used. Values for μ_{Bi} for different end supports are given in Table 6.13 (page 308). Values for μ_{Si} are determined from the expressions given in Table 7.4 (page 350) by setting $\nu = 0$. (Recall that when there is no bending deformation $\widehat{EI} \longrightarrow \infty$ and $\nu = 0$.) The resulting equations are listed in Table 7.5. Solutions of these equations are also given in this table. By comparing the results in Tables 7.5 and 6.13 we see that $\mu_{Si} = \mu_{Gi}$.

Table 7.6. The errors in the circular frequencies (Table 7.4) calculated by the approximate expressions (Eqs. 7.206 and 7.207).

Geometry	$\mathrm{Er} = \frac{\omega^{\text{accurate}} - \omega^{\text{approximate}}}{\omega^{\text{accurate}}} 100$
(a) 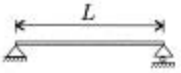	$\mathrm{Er} = 0$
(b) 	$i = 1 \quad 0 \le \mathrm{Er} < 4.2$ $i = 2 \quad 0 \le \mathrm{Er} < 3.1$ $i > 2 \quad 0 \le \mathrm{Er} < 2.4$
(c) 	$i = 1 \quad -0.32 < \mathrm{Er} \le 0$ $i = 2 \quad 0 \le \mathrm{Er} < 4.2$ $i > 2 \quad 0 \le \mathrm{Er} < 3.5$
(d) 	$i = 1 \quad -1.0 < \mathrm{Er} \le 0$ $i = 2 \quad 0 \le \mathrm{Er} < 10.3$ $i > 2 \quad 0 \le \mathrm{Er} < 5.1$
(e)	$i = 1 \quad -0.43 < \mathrm{Er} \le 0$ $i = 2 \quad -0.32 < \mathrm{Er} \le 0$ $i > 2 \quad 0 \le \mathrm{Er} < 2.2$

Circular frequencies of different types of beams were calculated numerically by the accurate (Table 7.4) and by the approximate solutions (Eq. 7.206 or Table B.2). The errors in the approximate solutions are summarized in Table 7.6.

Vibration in the x–y plane. Like vibration in the x–z plane we may express the circular frequency in the x–y plane as

$$\frac{1}{\omega_z^2} \simeq \frac{1}{(\omega_z^{\mathrm{B}})^2} + \frac{1}{(\omega_z^{\mathrm{S}})^2} = \frac{\rho}{\widehat{E}\widehat{I}_{zz}} \left(\frac{L}{\mu_{\mathrm{B}i}}\right)^4 + \frac{\rho}{\widehat{\mathrm{S}}_{yy}} \left(\frac{L}{\mu_{Si}}\right)^2, \tag{7.207}$$

where ω^{B} is the circular frequency of a beam undergoing bending deformation only, and ω^{S} is the circular frequency of a beam undergoing shear deformation only.

Torsional vibration. For a doubly symmetrical beam vibrating about its axis the equilibrium equations are (see Eqs. 7.39 and 7.40)

$$\frac{d\widehat{T}}{dx} + t = 0 \tag{7.208}$$

$$\frac{d\widehat{M}_\omega}{dx} - \widehat{T}_\omega = 0, \tag{7.209}$$

where t is the inertia force defined as[16]

$$t = \Theta\omega^2\psi, \tag{7.210}$$

[16] W. Weaver, S. P. Timoshenko, and D. H. Young, *Vibration Problems in Engineering*. 5th edition. John Wiley & Sons, New York, 1990, pp. 401–402.

where Θ is the polar moment of mass per unit length about the shear center (Eq. 6.402), ψ is the twist of the cross section about the beam's axis, and $\hat{M}_\omega$ is the bimoment; $\hat{T}$ is given by Eq. (7.14) as follows:

$$\hat{T} = \hat{T}_{sv} + \hat{T}_\omega. \tag{7.211}$$

The force–strain relationships are (Eqs. 7.32, 7.34, 7.36)

$$\hat{M}_\omega = -\widehat{EI}_\omega \frac{d\vartheta^B}{dx} \qquad \hat{T}_{sv} = \widehat{GI}_t \vartheta \qquad \hat{T}_\omega = \hat{S}_{\omega\omega} \vartheta^S, \tag{7.212}$$

where ϑ and ϑ^S are (Eqs. 7.6 and 7.7)

$$\vartheta = \frac{d\psi}{dx} \qquad \vartheta^S = \frac{d\psi}{dx} - \vartheta^B. \tag{7.213}$$

Equations (7.208)–(7.213) may be combined to yield

$$\hat{S}_{\omega\omega}\left(\frac{d^2\psi}{dx^2} - \frac{d\vartheta^B}{dx}\right) + \widehat{GI}_t \frac{d^2\psi}{dx^2} + \Theta\omega^2\psi = 0 \tag{7.214}$$

$$-\widehat{EI}_\omega \frac{d^2\vartheta^B}{dx^2} - \hat{S}_{\omega\omega}\left(\frac{d\psi}{dx} - \vartheta^B\right) = 0. \tag{7.215}$$

After algebraic manipulations these equations become

$$\frac{1}{\Theta\omega^2}\frac{d^4\vartheta^B}{dx^4} + \frac{1}{\hat{S}_{\omega\omega}}\frac{d^2\vartheta^B}{dx^2} - \frac{1}{\widehat{EI}_\omega}\vartheta^B - \frac{\widehat{GI}_t}{\Theta\omega^2}\left(\frac{1}{\widehat{EI}_\omega}\frac{d^2\vartheta^B}{dx^2} - \frac{1}{\hat{S}_{\omega\omega}}\frac{d^4\vartheta^B}{dx^4}\right) = 0 \tag{7.216}$$

$$\psi = \frac{1}{\Theta\omega^2}\left[\widehat{EI}_\omega \frac{d^3\vartheta^B}{dx^3} - \widehat{GI}_t\left(\frac{d\vartheta^B}{dx} - \frac{\widehat{EI}_\omega}{\hat{S}_{\omega\omega}}\frac{d^3\vartheta^B}{dx^3}\right)\right]. \tag{7.217}$$

Short beam. For short beams ($\widehat{GI}_t L^2 \ll \widehat{EI}_\omega$) Eqs. (7.216) and (7.217) simplify to *torsional vibration:*

$$\frac{1}{\Theta\omega^2}\frac{d^4\vartheta^B}{dx^4} + \frac{1}{\hat{S}_{\omega\omega}}\frac{d^2\vartheta^B}{dx^2} - \frac{1}{\widehat{EI}_\omega}\vartheta^B = 0 \tag{7.218}$$

$$\psi = \frac{\widehat{EI}_\omega}{\Theta\omega^2}\frac{d^3\vartheta^B}{dx^3}. \tag{7.219}$$

The equations for vibration in the x–z plane are given by Eqs. (7.181) and (7.182) and, for convenience, are repeated here

in-plane vibration:

$$\frac{1}{\rho\omega^2}\frac{d^4\chi}{dx^4} + \frac{1}{\widehat{S}}\frac{d^2\chi}{dx^2} - \frac{1}{\widehat{EI}}\chi = 0 \tag{7.220}$$

$$w = \frac{\widehat{EI}}{\rho\omega^2}\frac{d^3\chi}{dx^3}. \tag{7.221}$$

It can be seen that these equations are identical to Eqs. (7.218) and (7.219) when the following substitutions are made:

Vibration in the x–z plane		Torsional vibration
ρ	$\Longrightarrow$	Θ
$\widehat{EI}$	$\Longrightarrow$	$\widehat{EI}_\omega$
$\widehat{S}$	$\Longrightarrow$	$\widehat{S}_{\omega\omega}$
w	$\Longrightarrow$	ψ
χ	$\Longrightarrow$	ϑ^{B}

(7.222)

For in-plane vibration of short beams the circular frequency is denoted by ω_y, and for torsional vibration by ω_ψ. Thus, the solution for vibration in the x–z plane (Eq. 7.206) is also applicable to torsional vibration of short beams with the following substitutions:

Vibration in the x–z plane		Torsional vibration
ω_y	$\Longrightarrow$	ω_ψ
ρ	$\Longrightarrow$	Θ
$\widehat{EI}$	$\Longrightarrow$	$\widehat{EI}_\omega$
$\widehat{S}$	$\Longrightarrow$	$\widehat{S}_{\omega\omega}$

(7.223)

The parameters w and χ are not included in this equation because they do not appear in the expression for the circular frequency.

For beams with different end supports the circular frequency is given by Eq. (7.206). By replacing ρ, $\widehat{EI}$ $(= \widehat{EI}_{yy})$, and $\widehat{S}$ $(= \widehat{S}_{zz})$ with the expressions in Eq. (7.223), we have

$$\frac{1}{\omega_{\psi i}^2} = \frac{\Theta}{\widehat{EI}_\omega}\left(\frac{L}{\mu_{\mathrm{B}i}}\right)^4 + \frac{\Theta}{\widehat{S}_{\omega\omega}}\left(\frac{L}{\mu_{\mathrm{S}i}}\right)^2 \qquad \begin{matrix}\text{torsional vibration}\\ \text{short beam,}\end{matrix} \tag{7.224}$$

where $\mu_{\mathrm{B}i}$ and $\mu_{\mathrm{S}i}$ $(= \mu_{\mathrm{G}i})$ are given in Tables 6.13 and B.2 (pages 308 and 463).

Long beam. For long beams ($\widehat{GI}_{\mathrm{t}}L^2 \gg \widehat{EI}_\omega$ and $\widehat{S}_{\omega\omega}L^2 \gg \widehat{EI}_\omega$) Eqs. (7.216) and (7.217) simplify to

$$\frac{\widehat{GI}_{\mathrm{t}}}{\Theta\omega^2}\frac{d^2\vartheta^{\mathrm{B}}}{dx^2} + \vartheta^{\mathrm{B}} = 0 \tag{7.225}$$

$$\frac{d\psi}{dx} = \vartheta^{\mathrm{B}}. \tag{7.226}$$

These equations are independent of the torsional shear stiffness $\widehat{S}_{\omega\omega}$ and are identical to the differential equations of long beams without shear deformation.

Hence, the circular frequency is identical to Eq. (6.400):

$$(\omega_{\psi i})^2 = \frac{\widehat{GI}_t}{\Theta}\frac{\mu_{Gi}^2}{L^2} \qquad \begin{matrix}\text{torsional vibration}\\ \text{long beam,}\end{matrix} \tag{7.227}$$

Arbitrary length. We now approximate the torsional circular frequency of a beam of arbitrary length by

$$(\omega_{\psi i})^2 = (\omega_{\psi i})^2\big|_{\text{short}} + (\omega_{\psi i})^2\big|_{\text{long}} \qquad \text{torsional vibration,} \tag{7.228}$$

By using Eqs. (7.224) and (7.227) we have

$$(\omega_{\psi i})^2 = \left[\frac{\Theta}{\widehat{EI}_\omega}\left(\frac{L}{\mu_{\text{B}i}}\right)^4 + \frac{\Theta}{\widehat{S}_{\omega\omega}}\left(\frac{L}{\mu_{\text{S}i}}\right)^2\right]^{-1} + \frac{\widehat{GI}_t}{\Theta}\frac{\mu_{Gi}^2}{L^2}. \tag{7.229}$$

We introduce the notation

$$\frac{1}{\omega_{\omega i}^2} = \frac{1}{\left(\omega_{\omega i}^{\text{B}}\right)^2} + \frac{\Theta}{\widehat{S}_{\omega\omega}}\left(\frac{L}{\mu_{\text{S}i}}\right)^2, \tag{7.230}$$

where $\omega_{\omega i}^{\text{B}}$ is given by (Eq. 6.405)

$$\left(\omega_{\omega i}^{\text{B}}\right)^2 = \frac{\widehat{EI}_\omega}{\Theta}\frac{\mu_{\text{B}i}^4}{L^4}. \tag{7.231}$$

When the notations above are used, Eq. (7.229) becomes

$$(\omega_{\psi i})^2 = \omega_{\omega i}^2 + \frac{\widehat{GI}_t}{\Theta}\frac{\mu_{Gi}^2}{L^2} \qquad \text{torsional vibration,} \tag{7.232}$$

where $\mu_{\text{B}i}$ and $\mu_{\text{S}i}$ $(= \mu_{Gi})$ are given in Table 6.13 (page 308).

Although Eq. (7.232) is an approximation, it is accurate when both ends are simply supported.

The circular frequencies are summarized in Table B.2.

7.5.2 Beams with Symmetrical or Unsymmetrical Cross Sections

We consider freely vibrating orthotropic beams. The cross section may be symmetrical or unsymmetrical. The coordinate directions y and z are in the principal directions (page 208), and, consequently, $\widehat{EI}_{yz} = 0$.

When the cross section of the beam has one axis of symmetry (about the z-axis), it may undergo vibration in the plane of symmetry (x–z plane) or combined flexural–torsional vibration. When the cross section is unsymmetrical, the beam undergoes combined flexural–torsional vibration.

In general, for symmetrical and unsymmetrical cross sections, every element of the stiffness matrix must be considered in the calculation of the circular frequency. When the off-diagonal terms of the shear stiffness matrix (Eq. 7.36) either are zero (cross section is doubly symmetrical) or are negligible, the circular frequency may

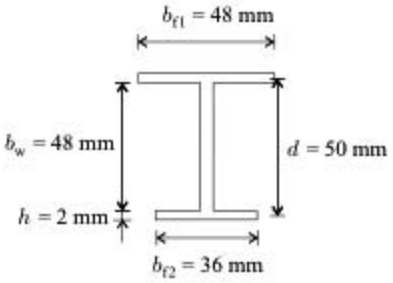

Figure 7.16: The cross section of the beam in Example 7.5.

be approximated by the solution of the following sets of equations[17]:
unsymmetrical cross section:

$$\left|\begin{bmatrix} \omega_z^2 & 0 & 0 \\ 0 & \omega_y^2 & 0 \\ 0 & 0 & \omega_\psi^2 \frac{\Theta}{\rho} \end{bmatrix} - \omega^2 \begin{bmatrix} 1 & 0 & -(z_G - z_{sc}) \\ 0 & 1 & (y_G - y_{sc}) \\ -(z_G - z_{sc}) & (y_G - y_{sc}) & \frac{\Theta}{\rho} \end{bmatrix}\right| = 0, \tag{7.233}$$

where || denotes determinant and ω is the circular frequency corresponding to flexural–torsional vibration. Equation (7.233) yields three sets of ω.
symmetrical cross-section:

$$\omega_1 = \omega_y \tag{7.234}$$

$$\left|\begin{bmatrix} \omega_z^2 & 0 \\ 0 & \omega_\psi^2 \frac{\Theta}{\rho} \end{bmatrix} - \omega^2 \begin{bmatrix} 1 & -(z_G - z_{sc}) \\ -(z_G - z_{sc}) & \frac{\Theta}{\rho} \end{bmatrix}\right| = 0. \tag{7.235}$$

Equations (7.234) and (7.235) yield three sets of ω. The first set is ω_1, which corresponds to the vibration in the x–z plane. The second and third sets of circular frequencies, corresponding to the flexural–torsional vibration, are the two roots of Eq. (7.235), and are denoted by ω_2 and ω_3.

We observe that the preceding equations (Eqs. 7.233–7.235) are identical to those given for beams without shear deformation (Eqs. 6.407–6.410). The difference is in the expressions used to calculate ω_y, ω_z, and ω_ψ. Here these circular frequencies are to be calculated by the expressions that include the shear deformation (Eqs. 7.206, 7.207, and 7.232).

Equations (7.233) and (7.235) give the exact circular frequency when $\widehat{S}_{ij} = 0$ $(i \neq j)$ and the two ends are simply supported (case (a) in Table 6.13, page 308). When both ends are built-in, when one end is built-in and one is simply supported, or when one end is built-in and the other end is free, the equations above yield only approximate values of the circular frequencies.

7.5 Example. *An $L = 0.5$-m-long I-section beam with the cross section shown in Figure 7.16 is made of graphite epoxy unidirectional plies. The material properties are given in Table 3.6 (page 81). The density of the composite is 1.6 g/cm^3. The*

[17] L. P. Kollár, Flexural-Torsional Vibration of Open Section Composite Beams with Shear Deformation. *International Journal of Solids and Structures*, Vol. 38, 7543–7558, 2001.

layup is $[0_{20}]$. *The beam is simply supported at each end. Calculate the natural frequencies of the beam.*

Solution. The circular frequencies are (Eqs. 7.206, 7.207, 7.230, and 7.232)

$$\begin{aligned}
\omega_{y1} &= \sqrt{\left(\frac{1}{\left(\omega_{y1}^{\mathrm{B}}\right)^2}+\frac{1}{\frac{\hat{S}_{zz}}{\rho}\frac{\mu_{\mathrm{S1}}^2}{L^2}}\right)^{-1}} \\
\omega_{z1} &= \sqrt{\left(\frac{1}{\left(\omega_{z1}^{\mathrm{B}}\right)^2}+\frac{1}{\frac{\hat{S}_{yy}}{\rho}\frac{\mu_{\mathrm{S1}}^2}{L^2}}\right)^{-1}} \\
\omega_{\omega 1} &= \sqrt{\left(\frac{1}{\left(\omega_{\omega 1}^{\mathrm{B}}\right)^2}+\frac{1}{\frac{\hat{S}_{\omega\omega}}{\Theta}\frac{\mu_{\mathrm{S1}}^2}{L^2}}\right)^{-1}} \\
\omega_{\psi 1} &= \sqrt{\omega_{\omega 1}^2+\frac{\widehat{GI}_{\mathrm{t}}}{\Theta}\frac{\mu_{G1}^2}{L^2}}.
\end{aligned} \tag{7.236}$$

The parameters are $\omega_{y1}^{\mathrm{B}} = 8\,166\,\frac{1}{\mathrm{s}}, \omega_{z1}^{\mathrm{B}} = 3\,785\,\frac{1}{\mathrm{s}}, \omega_{\omega 1}^{\mathrm{B}} = 3\,458\,\frac{1}{\mathrm{s}}$ (Eq. 6.415), $\widehat{GI}_{\mathrm{t}} = 1.602\ \mathrm{N\cdot m^2}$ (Eq. 6.348), $i_\omega = 0.024\,99$ m (Eq. 6.350), $\mu_{\mathrm{B1}} = \mu_{G1} = \pi$ (Table 6.13, page 308), $\rho = 0.4224\ \frac{\mathrm{kg}}{\mathrm{m}}$ (Eq. 6.412), $\Theta = 0.000\,263\,7\ \mathrm{kg\cdot m}$ (Eq. 6.414), $z_{\mathrm{G}} = 0$ (Eq. 6.413), $z_{\mathrm{sc}} = 0.000\,789$ m (Eq. 6.349). $\hat{S}_{zz} = 414.4 \times 10^3$ N, $\hat{S}_{yy} = 637.0 \times 10^3$ N, $\hat{S}_{\omega\omega} = 0.4177\ \mathrm{Nm^2}$ (Eq. 7.163). With these values we have

$$\omega_{y1} = 4\,950\frac{1}{\mathrm{s}} \qquad \omega_{z1} = 3\,398\frac{1}{\mathrm{s}} \qquad \omega_{\omega 1} = 3\,169\frac{1}{\mathrm{s}} \qquad \omega_{\psi 1} = 3\,206\frac{1}{\mathrm{s}}. \tag{7.237}$$

The circular frequency ω_1 is (Eq. 7.234)

$$\omega_1 = \omega_{y1} = 4\,950\frac{1}{\mathrm{s}}, \tag{7.238}$$

where ω_2 and ω_3 are the roots of Eq. (7.235):

$$\left|\begin{bmatrix}\omega_{z1}^2 & 0\\ 0 & \omega_{\psi 1}^2\frac{\Theta}{\rho}\end{bmatrix} - \omega^2\begin{bmatrix}1 & (z_{\mathrm{G}}-z_{\mathrm{sc}})\\ (z_{\mathrm{G}}-z_{\mathrm{sc}}) & \frac{\Theta}{\rho}\end{bmatrix}\right| = 0. \tag{7.239}$$

Solution of this equation yields

$$\omega_2 = 5\,428\frac{1}{\mathrm{s}} \qquad \omega_3 = 2\,563\frac{1}{\mathrm{s}}. \tag{7.240}$$

The natural frequencies are ($f = \omega/2\pi$)

$$f_1 = 788\ \mathrm{Hz} \qquad f_2 = 864\ \mathrm{Hz} \qquad f_3 = 408\ \mathrm{Hz}. \tag{7.241}$$

Calculations that neglect the shear deformation give the natural frequencies as (Eq. 6.420)

$$f_1 = 1\,300\ \mathrm{Hz} \qquad f_2 = 959\ \mathrm{Hz} \qquad f_3 = 452\ \mathrm{Hz}. \tag{7.242}$$

We can compare these with the circular frequencies calculated above taking shear deformation into account. The circular frequencies calculated with and without shear deformation differ significantly.

7.5.3 Summary

In summary, when the cross section is such that the off-diagonal elements of the stiffness matrix are negligible ($\widehat{S}_{ij} = 0,\ i \neq j$), the circular frequencies may be approximated by the expressions derived for beams without shear deformation by the following substitutions:

No shear deformation	With shear deformation
$(\omega_y^{\mathrm{B}})^2 \Longrightarrow$	$\left(\dfrac{1}{(\omega_y^{\mathrm{B}})^2} + \dfrac{1}{\frac{\widehat{S}_{zz}}{\rho}\frac{\mu_{Sz}^2}{L^2}} \right)^{-1}$
$(\omega_z^{\mathrm{B}})^2 \Longrightarrow$	$\left(\dfrac{1}{(\omega_z^{\mathrm{B}})^2} + \dfrac{1}{\frac{\widehat{S}_{yy}}{\rho}\frac{\mu_{Sy}^2}{L^2}} \right)^{-1}$
$(\omega_\omega^{\mathrm{B}})^2 \Longrightarrow$	$\left(\dfrac{1}{(\omega_\omega^{\mathrm{B}})^2} + \dfrac{1}{\frac{\widehat{S}_{\omega\omega}}{\Theta}\frac{\mu_{S\omega}^2}{L^2}} \right)^{-1}$,

(7.243)

where ω_y^{B}, ω_z^{B}, and $\omega_\omega^{\mathrm{B}}$ are given by Eqs. (6.398), (6.399), and (6.405).

Numerical examples[18] show that the substitutions above are reasonable even for the cases when $\widehat{S}_{ij} \neq 0$.

Circular frequencies of beams with shear deformation are summarized in Appendix B.

7.6 Effect of Shear Deformation

In this section, we show some of the conditions under which shear deformation need to be considered in calculating the maximum deflection, maximum twist, buckling load, and natural frequency. We take into account shear deformation through a parameter α by expressing $\widetilde{w}$, ψ, $\widehat{N}_{\mathrm{cr}}$, and ω in the forms

$$\begin{aligned} \widetilde{w} &= \frac{\widetilde{w}^{\mathrm{B}}}{1-\alpha_w} & \psi &= \frac{\psi^{\mathrm{B}}}{1-\alpha_\psi} \\ \widehat{N}_{\mathrm{cr}} &= \widehat{N}_{\mathrm{cr}}^{\mathrm{B}}(1-\alpha_N) & \omega^2 &= (\omega^{\mathrm{B}})^2(1-\alpha_\omega). \end{aligned} \tag{7.244}$$

As before, $\widetilde{w}^{\mathrm{B}}$, ψ^{B}, $\widehat{N}_{\mathrm{cr}}^{\mathrm{B}}$, and ω^{B} are the values with no shear deformation. The effect of shear deformation is indicated by the magnitude of α. When α is small compared with unity ($\alpha \ll 1$) shear deformation may be neglected, and $\widetilde{w}$, ψ, $\widehat{N}_{\mathrm{cr}}$, and ω may, respectively, be approximated by $\widetilde{w}^{\mathrm{B}}$, ψ^{B}, $\widehat{N}_{\mathrm{cr}}^{\mathrm{B}}$, and ω^{B}. In the following we present expressions for estimating α_w, α_ψ, α_N, and α_ω.

[18] Ibid.

The maximum deflection of a beam with shear deformation is

$$\widetilde{w} = \widetilde{w}^{\mathrm{B}} + \widetilde{w}^{\mathrm{S}} = \frac{\widetilde{w}^{\mathrm{B}}}{1 - \frac{1}{1+\frac{\widetilde{w}^{\mathrm{B}}}{\widetilde{w}^{\mathrm{S}}}}}. \tag{7.245}$$

By comparing Eqs. (7.244) and (7.245), we observe that

$$\alpha_{\mathrm{w}} = \frac{1}{1 + \frac{\widetilde{w}^{\mathrm{B}}}{\widetilde{w}^{\mathrm{S}}}}. \tag{7.246}$$

The ratio $\widetilde{w}^{\mathrm{B}}/\widetilde{w}^{\mathrm{S}}$ is given in Table 7.3 (page 332) for different types of beams. By using the results in this table we may write α_{w} as

$$\alpha_{\mathrm{w}} = \frac{1}{1 + \left[\sqrt{C}\frac{\pi}{k}\right]^2 \frac{(kL)^2}{\pi^2}\frac{\widehat{S}}{\widehat{EI}}}, \tag{7.247}$$

where $\widehat{EI}$ and $\widehat{S}$ represent $\widehat{EI}_{yy}$ and $\widehat{S}_{zz}$ in the x–z plane and $\widehat{EI}_{zz}$ and $\widehat{S}_{yy}$ in the x–y plane and k is the equivalent length factor that depends only on the type of support. Values of k are given in Table 6.11 (page 293); C is a constant in front of $L^2\widehat{S}/\widehat{EI}$ in Table 7.3 (page 332). For the six cases listed in Table 7.3, $\sqrt{C}\pi/k$ ranges from 0.79 to 1.01. For other types of supports and loading, this ratio varies over a similar range. We are interested only in the magnitude of α_{w}. Therefore, we set $\sqrt{C}\pi/k$ equal to unity, and write

$$\alpha_{\mathrm{w}} = \frac{1}{1 + \frac{(kL)^2}{\pi^2}\frac{\widehat{S}}{\widehat{EI}}}. \tag{7.248}$$

The lateral buckling load of a beam is given by Eqs. (7.175) and (6.337). These equation may be rearranged to yield

$$\widehat{N}_{\mathrm{cr}} = \left(\frac{1}{\widehat{N}^{\mathrm{B}}_{\mathrm{cr}}} + \frac{1}{\widehat{S}}\right)^{-1} = \widehat{N}^{\mathrm{B}}_{\mathrm{cr}}\left(1 - \frac{1}{1 + \left(\frac{kL}{\pi}\right)^2 \frac{\widehat{S}}{\widehat{EI}}}\right). \tag{7.249}$$

Equations (7.244) and (7.249) show that α_N is

$$\alpha_N = \frac{1}{1 + \left(\frac{kL}{\pi}\right)^2 \frac{\widehat{S}}{\widehat{EI}}}. \tag{7.250}$$

The circular frequency of a laterally vibrating beam is given by Eq. (7.207). This equation may be written as

$$\omega^2 = \left[\left(\frac{1}{\omega^{\mathrm{B}}}\right)^2 + \left(\frac{1}{\omega^{\mathrm{S}}}\right)^2\right]^{-1} = (\omega^{\mathrm{B}})^2\left(1 - \frac{1}{1 + \left(\frac{\pi\mu_{\mathrm{s}}}{k\mu_{\mathrm{B}}^2}\right)^2 \left(\frac{kL}{\pi}\right)^2 \frac{\widehat{S}}{\widehat{EI}}}\right), \tag{7.251}$$

where μ_{B} and μ_{s} are defined in Tables 6.13 and B.2 (pages 308 and 463). For the types of supports given in Table 6.11 (page 293), the ratio $\pi\mu_{\mathrm{s}}/k\mu_{\mathrm{B}}^2$ ranges from 0.7 to 1.0. We set this ratio equal to unity and approximate α_ω by (see Eqs. 7.244 and 7.251)

$$\alpha_\omega = \frac{1}{1 + \left(\frac{kL}{\pi}\right)^2 \frac{\widehat{S}}{\widehat{EI}}}. \tag{7.252}$$

Equations (7.248), (7.250), and (7.252) show that the effect of shear deformation on the maximum deflection, lateral buckling, and lateral vibration may be estimated by the parameter α ($\alpha = \alpha_w = \alpha_N = \alpha_\omega$):

$$\alpha = \frac{1}{1 + \left(\frac{kL}{\pi}\right)^2 \frac{\hat{S}}{\widehat{EI}}} \qquad \begin{matrix} \text{deflection} \\ \text{lateral buckling} \\ \text{lateral vibration.} \end{matrix} \tag{7.253}$$

where $\widehat{EI}$ and $\hat{S}$ are

$$\begin{matrix} \widehat{EI} = \widehat{EI}_{yy} & \hat{S} = \hat{S}_{zz} & \text{in the } x\text{–}z \text{ plane} \\ \widehat{EI} = \widehat{EI}_{zz} & \hat{S} = \hat{S}_{yy} & \text{in the } x\text{–}y \text{ plane.} \end{matrix} \tag{7.254}$$

The preceding expression for α applies to solid cross sections as well as to thin-walled, open- and closed-section beams. Next, we present α for torsional buckling, torsional vibration and twist of short, thin-walled open-section beams. We only consider short open-section beams because twist and torsion are significantly larger for open-section beams than for closed-section beams, and shear deformation is more pronounced for short than for long beams.

The torsional buckling load is given by Eqs. (7.154)–(7.156). For short, open-section beams, $\widehat{GI}_t \ll \widehat{EI}_\omega / L^2$, and these equations yield

$$\hat{N}_{cr} = \left(\frac{1}{\hat{N}^B_{cr\omega}} + \frac{1}{\frac{1}{i_o^2}\hat{S}_{\omega\omega}} \right)^{-1} = \hat{N}^B_{cr\omega} \left(1 - \frac{1}{1 + \left(\frac{kL}{\pi}\right)^2 \frac{\hat{S}_{\omega\omega}}{\widehat{EI}_\omega}} \right). \tag{7.255}$$

Equations (7.244) and (7.255) show that α_N is

$$\alpha_N = \frac{1}{1 + \left(\frac{kL}{\pi}\right)^2 \frac{\hat{S}_{\omega\omega}}{\widehat{EI}_\omega}}. \tag{7.256}$$

The parameter α can be derived similarly for torsional vibration and for the rate of twist of short, open-section beams. For such beams the following inequality holds: $\widehat{GI}_t \ll \widehat{EI}_\omega / L^2$. With this inequality, and with the approximations $\sqrt{C}\pi/k = 1$, and $\pi\mu_s / k\mu_B^2 = 1$ the expressions for α_ψ and α_ω are identical to that given by Eq. (7.256). Thus, for torsional buckling, torsional vibration and twist of short, open-section beams, α is ($\alpha = \alpha_\psi = \alpha_N = \alpha_\omega$):

$$\alpha = \frac{1}{1 + \left(\frac{kL}{\pi}\right)^2 \frac{\hat{S}_{\omega\omega}}{\widehat{EI}_\omega}} \qquad \begin{matrix} \text{twist} \\ \text{torsional buckling} \\ \text{torsional vibration.} \end{matrix} \tag{7.257}$$

We note the similarity in α given by Eqs. (7.253) and (7.257) and use this similarity to establish the conditions under which shear deformation may be neglected in calculating the deflection, twist, buckling load, and frequency. The error introduced into $\bar{w}$, ψ, $\hat{N}_{cr}$, and ω by neglecting shear deformation is less than 5 percent when α is smaller than 0.05. We now set $\alpha = 0.05$ in Eqs. (7.253) and (7.257). This

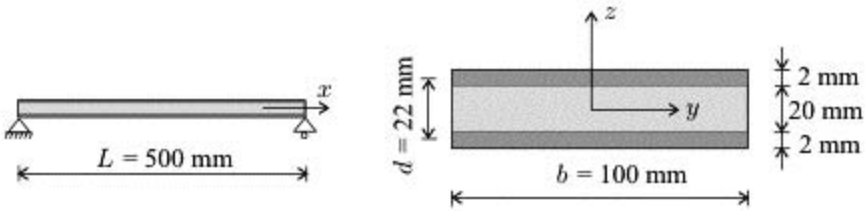

Figure 7.17: The sandwich beam in Example 7.6.

results in the expression

$$0.05 = \frac{1}{1 + \left(\frac{kL}{\pi}\right)^2 \frac{\widehat{S}}{\widehat{EI}}}. \tag{7.258}$$

By rearranging this expression, we obtain ($\alpha = 0.05$):

$$L \gtrless \frac{14}{k}\sqrt{\frac{\widehat{EI}}{\widehat{S}}} \qquad \begin{matrix} \text{shear deformation negligible} \\ \text{shear deformation not negligible.} \end{matrix} \tag{7.259}$$

7.6 Example. *We consider an $L = 0.5$-m-long simply supported sandwich beam. The core is isotropic ($E_c = 2 \times 10^6$ kN/m^2, $\nu_c = 0.3$), and the facesheets are made of graphite epoxy. The material properties are given in Table 3.6 (page 81). The layup of each facesheet is $[\pm 45_2^f/0_{12}/\pm 45_2^f]$. The dimensions are shown in (Fig. 7.17). Transverse or axial load may be applied in the x–z plane. Determine whether or not shear deformation needs be taken into account when calculating the maximum deflection, buckling load, and circular frequency.*

Solution. The beam is orthotropic, the cross section is symmetrical about the z-axis, and the load is in the x–z symmetry plane. Therefore, we only consider α in the x–z plane. The bending stiffness is $\widehat{EI}_{yy} = \frac{b}{\delta_{11}} \approx \frac{bd^2}{2a_{11}^f}$ (see Eq. 7.68 and Table 5.1, page 174), and the shear stiffness is $\widehat{S}_{zz} = \widetilde{S}_{11} b \approx \overline{C}_{55}^c bd$ (see Eqs. 7.62 and 5.32); a_{11}^f is the 11 element of the facesheet's compliance matrix and $\overline{C}_{55}^c = G$ is the shear modulus of the isotropic core. With these expressions, Eq. (7.253) gives ($\alpha = \alpha_w = \alpha_N = \alpha_\omega$):

$$\alpha = \left(1 + \frac{2}{\pi^2} \frac{(kL)^2 a_{11}^f G}{d}\right)^{-1} \qquad \text{in the } x\text{–}z \text{ plane.} \tag{7.260}$$

For the $[\pm 45_2^f/0_{12}/\pm 45_2^f]$ facesheets we have $a_{11}^f = 5.18 \times 10^{-9}$m/N (Table 3.8, page 85), and for the isotropic core $G = E_c/2(1 + \nu_c) = 769 \times 10^3$ kN/m^2. For a simply supported beam, we have $k = 1$ (Table 6.11, page 293). With these values, Eq. (7.260) becomes

$$\alpha_w = \alpha_N = \alpha_\omega = 0.10 \qquad \text{in the } x\text{–}z \text{ plane.} \tag{7.261}$$

For the sandwich beam in this problem we have

$$\frac{14}{k}\sqrt{\frac{\widehat{EI}}{\widehat{S}}} = 10\sqrt{\frac{d}{a_{11}^f G}} = 0.74 \text{ m} \qquad \text{in the } x\text{–}z \text{ plane.}$$

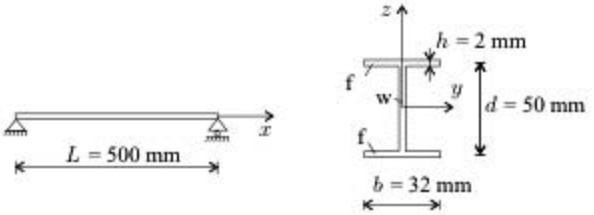

Figure 7.18: The I-beam in Example 7.7.

Thus, shear deformation is negligible when L is greater than 0.74 m. The length of the beam is 0.5 m. Therefore, shear deformation must be considered in calculating the deflection, buckling load, and circular frequency.

7.7 Example. *An $L = 0.5$-m-long doubly symmetrical I-beam is made of graphite epoxy. The material properties are given in Table 3.6 (page 81). The dimensions of the cross section are $b = 32$ mm and $d = 50$ mm (Fig 7.18). The layup of both the flange and the web is $[\pm 45_2^{\mathrm{f}}/0_{12}/\pm 45_2^{\mathrm{f}}]$. Determine whether or not shear deformation needs to be considered in calculating the maximum deflection, twist, buckling load, and circular frequency.*

Solution. The cross section of the I-beam is doubly symmetrical, and the layup of each flange and each web is orthotropic and symmetrical with respect to the midplane of the flange or the web. We approximate the replacement bending and shear stiffnesses by (Tables A.1, A.5, A.8)

$$\begin{aligned}
\widehat{EI}_{yy} &\approx \frac{b}{(a_{11})_{\mathrm{f}}}\frac{d^2}{2} & \widehat{S}_{zz} &\approx d\frac{1}{(a_{66})_{\mathrm{w}}} && \text{in the } x\text{–}z \text{ plane}\\
\widehat{EI}_{zz} &\approx \frac{b^3}{6(a_{11})_{\mathrm{f}}} & \widehat{S}_{yy} &= \frac{2b}{1.2(a_{66})_{\mathrm{f}}} && \text{in the } x\text{–}y \text{ plane}\\
\widehat{EI}_{\omega} &= \frac{1}{(a_{11})_{\mathrm{f}}}\frac{d^2b^3}{24} & \widehat{S}_{\omega\omega} &= \frac{d^2b}{2\times 1.2(a_{66})_{\mathrm{f}}} && \text{in torsion.}
\end{aligned} \tag{7.262}$$

The dimension b and d are shown in Figure 7.18, and a_{11} and a_{66} are the elements of the compliance matrices given in Eq. (3.29). The subscripts f and w refer to the flange and the web. We obtain α by substituting the preceding stiffnesses into Eq. (7.253). For maximum deflection, buckling, and vibration in the x–y and x–z planes, α ($\alpha = \alpha_{\mathrm{w}} = \alpha_N = \alpha_\omega$) is

$$\alpha = \left(1 + \frac{2}{\pi^2}\frac{(kL)^2}{bd}\frac{(a_{11})_{\mathrm{f}}}{(a_{66})_{\mathrm{w}}}\right)^{-1} \qquad \text{in the } x\text{–}z \text{ plane} \tag{7.263}$$

$$\alpha = \left(1 + \frac{10}{\pi^2}\frac{(kL)^2}{b^2}\frac{(a_{11})_{\mathrm{f}}}{(a_{66})_{\mathrm{f}}}\right)^{-1} \qquad \text{in the } x\text{–}y \text{ plane,} \tag{7.264}$$

For the twist, torsional buckling, and torsional vibration α ($\alpha = \alpha_\psi = \alpha_N = \alpha_\omega$) is (see Eqs. 7.257 and 7.262)

$$\alpha = \left(1 + \frac{10}{\pi^2}\frac{(kL)^2}{b^2}\frac{(a_{11})_{\mathrm{f}}}{(a_{66})_{\mathrm{f}}}\right)^{-1} \qquad \text{about the } x\text{-axis,} \tag{7.265}$$

From Table 3.8 (page 85) the relevant elements of the compliance matrix are $(a_{11})_f = (a_{11})_w = 5.18 \times 10^{-9}$m/N, $(a_{66})_f = (a_{66})_w = 27.77 \times 10^{-9}$m/N. For a simply supported beam we have $k = 1$ (Table 6.11, page 293). With these values Eqs. (7.263)–(7.265) give

$$\begin{aligned} \alpha_w &= \alpha_N = \alpha_{\omega} = 0.14 \qquad \text{in the } x\text{–}z \text{ plane} \\ \alpha_w &= \alpha_N = \alpha_{\omega} = 0.02 \qquad \text{in the } x\text{–}y \text{ plane} \\ \alpha_{\psi} &= \alpha_N = \alpha_{\omega} = 0.02 \qquad \text{about the } x\text{-axis.} \end{aligned} \tag{7.266}$$

For the I-beam in this problem we have

$$\begin{aligned} \frac{14}{k}\sqrt{\frac{\widehat{EI}}{\widehat{S}}} &= 14\sqrt{bd}\sqrt{\frac{(a_{66})_w}{(a_{11})_f}} = 1.3\,\text{m} \qquad \text{in the } x\text{–}z \text{ plane} \\ \frac{14}{k}\sqrt{\frac{\widehat{EI}}{\widehat{S}}} &= 4.4b\sqrt{\frac{(a_{66})_f}{(a_{11})_f}} = 0.33\,\text{m} \qquad \text{in the } x\text{–}y \text{ plane} \\ \frac{14}{k}\sqrt{\frac{\widehat{EI}}{\widehat{S}}} &= 4.4b\sqrt{\frac{(a_{66})_f}{(a_{11})_f}} = 0.33\,\text{m} \qquad \text{about the } x\text{-axis.} \end{aligned} \tag{7.267}$$

Thus, shear deformation is negligible when L is greater than 1.3 m. The length of the beam is 0.5 m. Therefore, shear deformation must be taken into account when calculating the deflection, twist, buckling load, and circular frequency.

Shells

In this chapter we consider thin composite shells, which we analyze on the basis of the main assumptions employed in the theory of thin plates. However, there is a major difference in the behavior of plates and shells subjected to external loads. Plates resist transverse loads by bending and by transverse shear forces. On the other hand, thin shells resist the transverse loads mostly by membrane forces, which, at any given point, are in the plane tangential to the reference surface (Fig. 8.1). These membrane forces are determined by the "membrane theory of shells," which neglects bending moments. The resulting stresses, strains, and deformations are reasonable except near supports and in the vicinities of abrupt changes in loads. For thick shells (whose thickness is comparable to the radii of curvature) or when regions near supports or concentrated loads are of interest, more complex analytical solutions or finite element methods must be employed. The decision as to which method to use rests with the individual and depends on his or her experience with analytical solutions and finite element calculations.

Herein we treat thin shells whose thickness h is small compared with all other dimensions and with the radii of curvatures (Fig. 8.2). The membrane forces N_x, N_y, N_{xy}, and N_{yx} acting at the reference surface of an infinitesimal element are[1]

$$N_x = \int_{-h_1}^{h_1} \sigma_x \left(1 + \frac{z}{R_y}\right) dz \qquad N_y = \int_{-h_1}^{h_1} \sigma_y \left(1 + \frac{z}{R_x}\right) dz$$
$$N_{xy} = \int_{-h_1}^{h_1} \tau_{xy} \left(1 + \frac{z}{R_y}\right) dz \qquad N_{yx} = \int_{-h_1}^{h_1} \tau_{yx} \left(1 + \frac{z}{R_x}\right) dz, \tag{8.1}$$

where R_x and R_y are the radii of curvature in the x–z and y–z planes, and x, y, z are local coordinates with x and y in the plane tangential and z perpendicular to the reference surface at the point of interest (Fig. 8.2). The origin of the coordinate system is at the reference surface, which, conveniently, may be taken at the

[1] W. Flügge, *Stresses in Shells*. 2nd edition. Springer, Berlin, 1973, pp. 5–6.

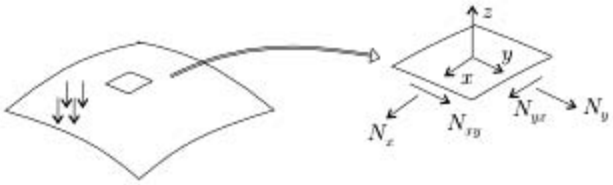

Figure 8.1: Membrane forces in a shell.

midsurface. For thin shells the quantities z/R_y and z/R_x are small with respect to unity, and these expressions reduce to

$$N_x = \int_{-h_b}^{h_t} \sigma_x dz \qquad N_y = \int_{-h_b}^{h_t} \sigma_y dz \qquad N_{xy} = N_{yx} = \int_{-h_b}^{h_t} \tau_{xy} dz. \tag{8.2}$$

In the "membrane theory of shells" the membrane forces depend only on the geometry, on the boundary conditions, and on the applied loads and are independent of the properties of the material. Hence, the membrane forces can be determined by the equations of static equilibrium.

The force–strain relationships are (Eq. 3.21)

$$\begin{Bmatrix} N_x \\ N_y \\ N_{xy} \\ M_x \\ M_y \\ M_{xy} \end{Bmatrix} = \begin{bmatrix} A_{11} & A_{12} & A_{16} & B_{11} & B_{12} & B_{16} \\ A_{12} & A_{22} & A_{26} & B_{12} & B_{22} & B_{26} \\ A_{16} & A_{26} & A_{66} & B_{16} & B_{26} & B_{66} \\ B_{11} & B_{12} & B_{16} & D_{11} & D_{12} & D_{16} \\ B_{12} & B_{22} & B_{26} & D_{12} & D_{22} & D_{26} \\ B_{16} & B_{26} & B_{66} & D_{16} & D_{26} & D_{66} \end{bmatrix} \begin{Bmatrix} \epsilon_x^o \\ \epsilon_y^o \\ \gamma_{xy}^o \\ \kappa_x \\ \kappa_y \\ \kappa_{xy} \end{Bmatrix}. \tag{8.3}$$

One of the major assumptions of the membrane theory is that changes in curvatures do not affect the stresses. With this assumption, from the preceding equation, the strains are

$$\begin{Bmatrix} \epsilon_x^o \\ \epsilon_y^o \\ \gamma_{xy}^o \end{Bmatrix} = \begin{bmatrix} A_{11} & A_{12} & A_{16} \\ A_{12} & A_{22} & A_{26} \\ A_{16} & A_{26} & A_{66} \end{bmatrix}^{-1} \begin{Bmatrix} N_x \\ N_y \\ N_{xy} \end{Bmatrix}, \tag{8.4}$$

where ϵ_x^o, ϵ_y^o, and γ_{xy}^o are the strains of the reference surface. This set of equations applies to symmetrical as well as to unsymmetrical layups even though the *form* of the equations is the same as for symmetrical laminates (Eq. 3.26). In the membrane

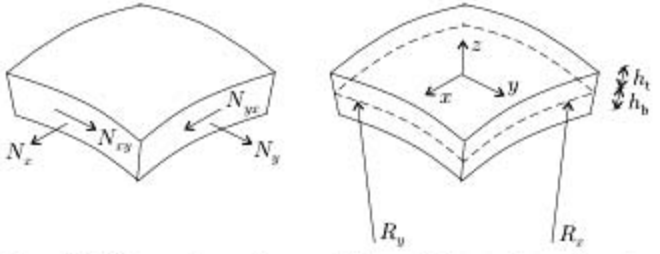

Figure 8.2: The membrane forces and the radii of curvatures of an element.



Figure 8.3: Stresses in an isotropic (left) and composite shell (right).

theory the strains are independent of the moments because the effects of changes in curvatures are neglected. In symmetrical laminates the strains are independent of the moments because the $[B]$ matrix is zero.

We neglect the variations of the strains across the thickness of the shell. Hence, the strains are

$$\begin{Bmatrix} \epsilon_x \\ \epsilon_y \\ \gamma_{xy} \end{Bmatrix} = \begin{Bmatrix} \epsilon_x^o \\ \epsilon_y^o \\ \gamma_{xy}^o \end{Bmatrix}. \tag{8.5}$$

The stresses in each layer are then calculated by Eq. (2.126) as follows:

$$\begin{Bmatrix} \sigma_x \\ \sigma_y \\ \tau_{xy} \end{Bmatrix} = \begin{bmatrix} \overline{Q}_{11} & \overline{Q}_{12} & \overline{Q}_{16} \\ \overline{Q}_{12} & \overline{Q}_{22} & \overline{Q}_{26} \\ \overline{Q}_{16} & \overline{Q}_{26} & \overline{Q}_{66} \end{bmatrix} \begin{Bmatrix} \epsilon_x \\ \epsilon_y \\ \gamma_{xy} \end{Bmatrix}. \tag{8.6}$$

Note that the stress distributions differ in isotropic and composite shells. In an isotropic shell the stress distribution across the thickness is uniform, and the resultant of the stresses is in the midplane (Fig. 8.3). In a composite shell the stresses vary from layer to layer, and the resultant of the stresses generally is not in the midplane.

The stresses and strains resulting from the preceding analysis are used in the design of the membrane section.

Membrane forces for isotropic shells can be found in texts[2] and handbooks. These membrane forces also apply to composite shells. In the next section, we present results for thin composite shells of practical interest.

8.1 Shells of Revolution with Axisymmetrical Loading

A shell of revolution is obtained by rotating a curve, called the meridian, about an axis of revolution. We consider an element of the shell's reference surface formed by two adjacent meridians and two parallel circles (Fig. 8.4).

The load is axisymmetrical, and therefore there are no shear forces ($N_{xy} = 0$), and only N_x and N_y normal forces (per unit length) act. Force balance in the z direction (perpendicular to the surface) gives[3]

$$\frac{N_x}{R_x} + \frac{N_y}{R_y} = p_z, \tag{8.7}$$

where R_x is the radius of curvature of the meridian (Fig. 8.4) and R_y is along a line normal to the meridian with a length that is the distance between the reference

[2] Ibid.
[3] Ibid., p. 23.

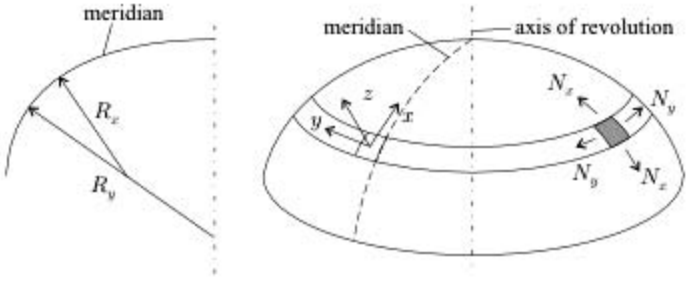

Figure 8.4: Shell of revolution.

surface and the point where the line intersects the axis of rotation; p_z is the component of the load normal to the surface at the point of interest (Fig. 8.5, left).

We now consider the portion of the shell above the parallel circle defined by ϕ (Fig. 8.5, right). We denote by F the resultant of all the loads acting on the shell above the parallel circle. A force balance along the axis of rotation gives

$$F + 2\pi r_0 N_x \sin\phi = 0, \tag{8.8}$$

where r_0 is defined in Figure 8.5. From the preceding equation, N_x is

$$N_x = -\frac{F}{2\pi r_0 \sin\phi}. \tag{8.9}$$

The forces N_y and N_x are calculated from Eqs. (8.7) and (8.9). Expressions for N_x and N_y are given in Table 8.1 for selected problems.

8.2 Cylindrical Shells

We consider thin-walled circular cylinders subjected to pressure p_z (which does not vary circumferentially), axial load $\widehat{N}$, and torque $\widehat{T}$ (Fig. 8.6).

8.2.1 Membrane Theory

By neglecting edge effects, one may calculate the membrane forces (Fig. 8.7) by the membrane theory. Force balances in the x and z directions and moment balance

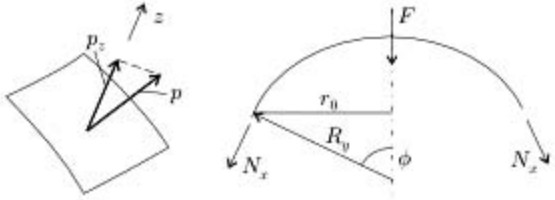

Figure 8.5: Load on an element and the free-body diagram for a shell of revolution.

Table 8.1. Membrane forces in spherical domes subjected to internal pressure (a), self-weight (b), and cones subjected to internal pressure (c); p, p_z, p_{z0} are in N/m^2; p_{z1} is in N/m^3.

(a)

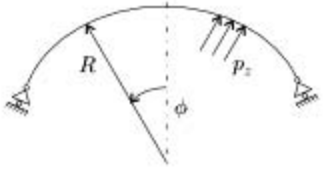

$$N_x = \tfrac{1}{2} p_z R$$
$$N_y = \tfrac{1}{2} p_z R$$

(b)

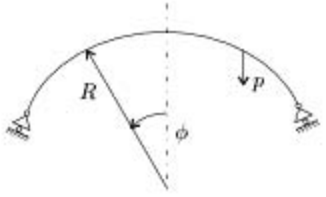

$$N_x = -\frac{pR}{1+\cos\phi}$$
$$N_y = pR\left(\frac{1}{1+\cos\phi} - \cos\phi\right)$$

(c)

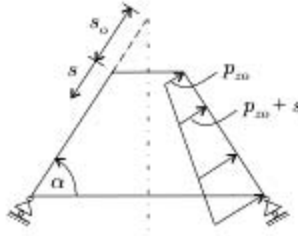

$$N_x = \frac{\cot\alpha}{s+s_o} s\left[p_{z0}\left(s_o + \tfrac{s}{2}\right) + p_{z1} s\left(\tfrac{s_o}{2} + \tfrac{s}{3}\right)\right]$$
$$N_y = (p_{z0} + sp_{z1})(s + s_o)\cot\alpha$$

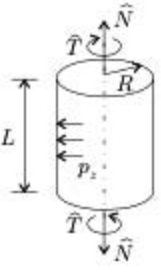

Figure 8.6: Thin cylinder subjected to radial pressure p_z (which does not vary circumferentially), axial load $\widehat{N}$, and torque $\widehat{T}$.

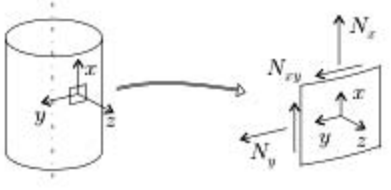

Figure 8.7: The membrane forces in a thin cylinder.

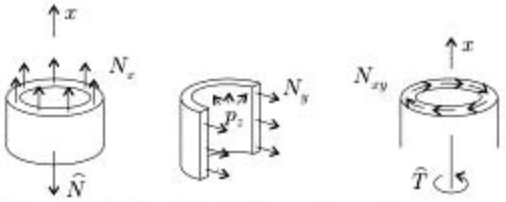

Figure 8.8: The loads and the membrane forces on a cylinder.

about the x-axis yield (Fig. 8.8)

$$\begin{aligned} N_x 2\pi R &= \widehat{N} \\ 2N_y &= p_z 2R \\ (N_{xy}R)\,2\pi R &= \widehat{T}, \end{aligned} \tag{8.10}$$

where R is the radius of the wall's reference surface. From these equations, the membrane forces are

$$N_x = \frac{\widehat{N}}{2\pi R} \qquad N_y = p_z R \qquad N_{xy} = \frac{\widehat{T}}{2\pi R^2}. \tag{8.11}$$

The strains corresponding to these membrane forces are calculated by Eq. (8.4). The axial u^o, radial w^o, and circumferential v^o displacements are

$$u^o = \int \epsilon_x^o dx = x\epsilon_x^o + u_o^o \qquad w^o = R\epsilon_y^o \qquad v^o = \int \gamma_{xy}^o dx = x\gamma_{xy}^o + v_o^o, \tag{8.12}$$

where u_o^o and v_o^o represent rigid-body motion.

8.2.2 Built-In Ends

As we noted previously, near boundary supports the membrane theory is inaccurate, and the forces, moments, and displacements of the shell must be calculated by other means. In the following, we consider thin-walled circular cylinders built-in at each end. The cylinder is subjected to pressure p_z, axial load $\widehat{N}$, and torque $\widehat{T}$

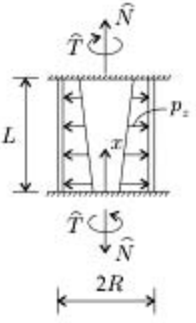

Figure 8.9: Cylinder built-in at both ends subjected to pressure p_z, axial load $\widehat{N}$, and torque $\widehat{T}$.

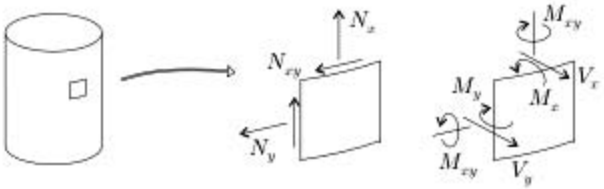

Figure 8.10: Forces and moments inside the wall of a thin cylinder.

(Fig. 8.9). The pressure may vary linearly along the cylinder's axis,

$$p_z = p_{z0} + x p_{z1}, \tag{8.13}$$

where p_{z0} and p_{z1} are specified constants. (For the pressure distribution shown in Fig. 8.9, p_{z1} is negative.) For the applied loads (Fig. 8.9), neither the stresses nor the strains vary circumferentially. Accordingly, the equilibrium equations are[4]

$$\frac{dN_x}{dx} = 0 \tag{8.14}$$

$$\frac{d}{dx}(RN_{xy} + M_{xy}) = 0 \tag{8.15}$$

$$\frac{N_y}{R} - \frac{d^2 M_x}{dx^2} = p_z \tag{8.16}$$

$$V_x = \frac{dM_x}{dx} \tag{8.17}$$

$$V_y = \frac{dM_{xy}}{dx}, \tag{8.18}$$

where the forces N_x, N_y, N_{xy}, the moments M_x, M_{xy}, and the transverse shear forces V_x and V_y are illustrated in Figure 8.10.

The strains and the curvatures of the reference surface are[5]

$$\epsilon_x^o = \frac{du^o}{dx} \qquad \epsilon_y^o = \frac{w^o}{R} \qquad \gamma_{xy}^o = \frac{dv^o}{dx} \tag{8.19}$$

$$\kappa_x = -\frac{d^2 w^o}{dx^2} \qquad \kappa_y = -\frac{w^o}{R^2} \qquad \kappa_{xy} = -\frac{2}{R}\frac{dv^o}{dx}, \tag{8.20}$$

where u^o, v^o, and w^o are the axial, circumferential, and radial displacements of the reference surface.

The force–strain relationships are identical to those of laminated plates and are given by Eq. (8.3).

The equilibrium equations (Eqs. 8.14–8.18), the strain–displacement relationships (Eqs. 8.19–8.20), and the force–strain relationships (Eq. 8.3) provide the forces, moments, and displacements of the wall. In the following we reduce these equations to readily usable forms.

[4] Ibid., pp. 205–206.
[5] Ibid., p. 211.

Table 8.2. The parameters required in the equations

$$[a_1] = \begin{bmatrix} A_{22} - \frac{B_{22}}{R} & B_{12} \\ B_{12} - \frac{D_{12}}{R} & D_{11} \end{bmatrix} \qquad [a_3] = \begin{bmatrix} A_{11} & A_{16} - \frac{2B_{16}}{R} \\ A_{16} + \frac{B_{16}}{R} & A_{66} - \frac{B_{66}}{R} - \frac{2D_{66}}{R^2} \end{bmatrix}$$

$$[a_2] = \begin{bmatrix} A_{12} - \frac{B_{12}}{R} & B_{11} \\ A_{26} - \frac{D_{26}}{R^2} & B_{16} + \frac{D_{16}}{R} \end{bmatrix} \qquad [a_4] = \begin{bmatrix} A_{12} & A_{26} - \frac{2B_{26}}{R} \\ B_{11} & B_{16} - \frac{2D_{16}}{R} \end{bmatrix}$$

$$[H] = \begin{bmatrix} H_{11} & H_{12} \\ H_{21} & H_{22} \end{bmatrix} = [a_1] - [a_4][a_3]^{-1}[a_2]$$

$$\mathbf{g} = \begin{Bmatrix} g_1 \\ g_2 \end{Bmatrix} = [a_4][a_3]^{-1} \begin{Bmatrix} D_1 \\ D_2 \end{Bmatrix}$$

$$f_1 = H_{22} \quad f_2 = -\tfrac{1}{R}(H_{21} + H_{12}) \quad f_3 = \tfrac{H_{11}}{R^2} \quad f_4 = p_{z0} - \tfrac{g_1}{R} \quad f_5 = p_{z1}$$

The starting point of the analysis is the integration of the first two equilibrium equations (Eqs. 8.14 and 8.15). These integrations yield

$$\begin{aligned} D_1 &= N_x \\ D_2 &= N_{xy} + \frac{M_{xy}}{R}, \end{aligned} \tag{8.21}$$

where D_1, D_2 are as yet unknown constants. By substituting the force–strain relationships (Eq. 8.3) into Eq. (8.21) and by introducing Eqs. (8.19) and (8.20) into the resulting equations, we obtain

$$\begin{Bmatrix} D_1 \\ D_2 \end{Bmatrix} = [a_2] \begin{Bmatrix} \frac{w^o}{R} \\ -\frac{d^2 w^o}{dx^2} \end{Bmatrix} + [a_3] \begin{Bmatrix} \frac{du^o}{dx} \\ \frac{dv^o}{dx} \end{Bmatrix}. \tag{8.22}$$

The matrices $[a_2]$ and $[a_3]$ are given in Table 8.2.

From Eq. (8.22) the derivatives of u^o and v^o are

$$\begin{Bmatrix} \frac{du^o}{dx} \\ \frac{dv^o}{dx} \end{Bmatrix} = -[a_3]^{-1}[a_2] \begin{Bmatrix} \frac{w^o}{R} \\ -\frac{d^2 w^o}{dx^2} \end{Bmatrix} + [a_3]^{-1} \begin{Bmatrix} D_1 \\ D_2 \end{Bmatrix}. \tag{8.23}$$

The internal forces N_y and M_x may be expressed as (Eq. 8.3)

$$\begin{Bmatrix} N_y \\ M_x \end{Bmatrix} = \begin{bmatrix} A_{12} & A_{22} & A_{26} & B_{12} & B_{22} & B_{26} \\ B_{11} & B_{12} & B_{16} & D_{11} & D_{12} & D_{16} \end{bmatrix} \begin{Bmatrix} \epsilon_x^o \\ \epsilon_y^o \\ \gamma_{xy}^o \\ \kappa_x \\ \kappa_y \\ \kappa_{xy} \end{Bmatrix}. \tag{8.24}$$

By substituting Eqs. (8.19) and (8.20) into Eq. (8.24), we obtain

$$\begin{Bmatrix} N_y \\ M_x \end{Bmatrix} = [a_1] \begin{Bmatrix} \frac{w^o}{R} \\ -\frac{d^2 w^o}{dx^2} \end{Bmatrix} + [a_4] \begin{Bmatrix} \frac{du^o}{dx} \\ \frac{dv^o}{dx} \end{Bmatrix}. \tag{8.25}$$

The matrices $[a_1]$ and $[a_4]$ are given in Table 8.2. Substitution of Eq. (8.23) into Eq. (8.25) results in

$$\begin{Bmatrix} N_y \\ M_x \end{Bmatrix} = [H] \begin{Bmatrix} \frac{w^o}{R} \\ -\frac{d^2 w^o}{dx^2} \end{Bmatrix} + \begin{Bmatrix} g_1 \\ g_2 \end{Bmatrix}, \tag{8.26}$$

where $[H]$ and $\mathbf{g}$ are given in Table 8.2. This equation can be written as

$$N_y = H_{11} \frac{w^o}{R} - H_{12} \frac{d^2 w^o}{dx^2} + g_1 \tag{8.27}$$

$$M_x = H_{21} \frac{w^o}{R} - H_{22} \frac{d^2 w^o}{dx^2} + g_2, \tag{8.28}$$

where $H_{11}, H_{12}, H_{21}, H_{22}, g_1, g_2$ are the elements of the matrix $[H]$ and the vector $\mathbf{g}$. By introducing Eqs. (8.27) and (8.28) into the third equilibrium equation (Eq. 8.16) we obtain

$$f_1 \frac{d^4 w^o}{dx^4} + f_2 \frac{d^2 w^o}{dx^2} + f_3 w^o = f_4 + x f_5, \tag{8.29}$$

where $f_1, \ldots, f_5$ are given in Table 8.2. We note that f_4 contains the two as yet unknown constants D_1 and D_2.

Solution of this fourth-order differential equation yields the radial displacement of the reference surface[6]

$$w^o = \{e^{-\lambda x}[C_1 \cos(\beta x) + C_2 \sin(\beta x)] + e^{-\lambda(L-x)}[C_3 \cos(\beta(L-x)) + C_4 \sin(\beta(L-x))]\} + \left[\frac{1}{f_3}(f_4 + x f_5)\right], \tag{8.30}$$

where L is the length of the cylinder and λ and β are the real and imaginary parts of the roots of the characteristic polynomial,

$$\begin{aligned} \lambda &= \mathrm{Re}(\gamma) \\ \beta &= \mathrm{Im}(\gamma) \end{aligned} \quad \text{where} \quad \gamma = \sqrt{\frac{-f_2 + \sqrt{f_2^2 - 4 f_1 f_3}}{2 f_1}}. \tag{8.31}$$

Equation (8.30) is the solution of interest. This equation contains six unknown constants D_1, D_2, C_1–C_4. The constant D_1 is given by Eqs. (8.21) and (8.11)

$$D_1 = N_x = \frac{\widehat{N}}{2\pi R}. \tag{8.32}$$

The second equality in this equation is written by virtue of the fact that N_x is per unit length, $\widehat{N}$ is the total force, and $2\pi R$ is the circumference; D_2 is given by

[6] E. Kreyszig, *Advanced Engineering Mathematics*. 7th edition. John Wiley & Sons, New York, 1993, pp. 136–144.

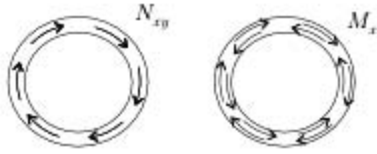

Figure 8.11: The shear force and the twist moment.

Eq. (8.21). The total torque acting at the edge of the cylinder is (Fig. 8.11)

$$\widehat{T} = (N_{xy}R)\,2\pi R + M_{xy}2\pi R. \tag{8.33}$$

Thus, from Eqs. (8.21) and (8.33) D_2 is

$$D_2 = \frac{\widehat{T}}{2\pi R^2}. \tag{8.34}$$

The constants C_1–C_4 are obtained from the boundary conditions, which state that at a built-in end the radial displacement and its slope are zero as follows:

$$\begin{aligned} w^o = 0 \quad \frac{dw^o}{dx} = 0 \quad &\text{at} \quad x = 0 \\ w^o = 0 \quad \frac{dw^o}{dx} = 0 \quad &\text{at} \quad x = L. \end{aligned} \tag{8.35}$$

The derivative of w^o is given in Table 8.4. With the displacement given in Eq. (8.30), the boundary conditions above give

$$\begin{bmatrix} 1 & 0 & Y_{13} & Y_{14} \\ -\lambda & \beta & Y_{23} & Y_{24} \\ Y_{31} & Y_{32} & 1 & 0 \\ Y_{41} & Y_{42} & \lambda & \beta \end{bmatrix} \begin{Bmatrix} C_1 \\ C_2 \\ C_3 \\ C_4 \end{Bmatrix} = - \begin{Bmatrix} \frac{f_4}{f_3} \\ \frac{f_5}{f_3} \\ \frac{f_4 + Lf_5}{f_3} \\ \frac{f_5}{f_3} \end{Bmatrix}, \tag{8.36}$$

where Y_{ij} are listed in Table 8.3. Equations (8.36) provide C_1–C_4. The displacement w^o is calculated with the constants D_1, D_2, C_1–C_4 thus determined.

Table 8.3. The parameters in Eq. (8.36)

$Y_{13} = e^{-\lambda L}\cos\beta L$	$Y_{14} = e^{-\lambda L}\sin\beta L$
$Y_{23} = e^{-\lambda L}(\lambda\cos\beta L + \beta\sin\beta L)$	$Y_{24} = e^{-\lambda L}(-\beta\cos\beta L + \lambda\sin\beta L)$
$Y_{31} = e^{-\lambda L}\cos\beta L$	$Y_{32} = e^{-\lambda L}\sin\beta L$
$Y_{41} = -e^{-\lambda L}(\lambda\cos\beta L + \beta\sin\beta L)$	$Y_{42} = e^{-\lambda L}(\beta\cos\beta L - \lambda\sin\beta L)$

Table 8.4. Displacement w^o of a cylinder, its derivatives, and its integral

$$
\begin{aligned}
w^o &= \tfrac{1}{f_5}(f_4 + x f_5) \\
&\quad + e^{-\lambda x}\cos(\beta x)C_1 \\
&\quad + e^{-\lambda x}\sin(\beta x)C_2 \\
&\quad + e^{-\lambda(L-x)}\cos(\beta(L-x))C_3 \\
&\quad + e^{-\lambda(L-x)}\sin(\beta(L-x))C_4
\end{aligned}
$$

$$
\begin{aligned}
\frac{dw^o}{dx} &= \tfrac{f_5}{f_5} + e^{-\lambda x}\cos(\beta x)(-\lambda C_1 + \beta C_2) \\
&\quad + e^{-\lambda x}\sin(\beta x)(-\beta C_1 - \lambda C_2) \\
&\quad + e^{-\lambda(L-x)}\cos(\beta(L-x))(\lambda C_3 - \beta C_4) \\
&\quad + e^{-\lambda(L-x)}\sin(\beta(L-x))(\beta C_3 + \lambda C_4)
\end{aligned}
$$

$$
\begin{aligned}
\frac{d^2w^o}{dx^2} &= e^{-\lambda x}\cos(\beta x)((\lambda^2-\beta^2)C_1 - 2\lambda\beta C_2) \\
&\quad + e^{-\lambda x}\sin(\beta x)(2\lambda\beta C_1 + (\lambda^2-\beta^2)C_2) \\
&\quad + e^{-\lambda(L-x)}\cos(\beta(L-x))((\lambda^2-\beta^2)C_3 - 2\lambda\beta C_4) \\
&\quad + e^{-\lambda(L-x)}\sin(\beta(L-x))(2\lambda\beta C_3 + (\lambda^2-\beta^2)C_4)
\end{aligned}
$$

$$
\begin{aligned}
\frac{d^3w}{dx^3} &= e^{-\lambda x}\cos(\beta x)(\lambda(3\beta^2-\lambda^2)C_1 + \beta(3\lambda^2-\beta^2)C_2) \\
&\quad + e^{-\lambda x}\sin(\beta x)(-\beta(3\lambda^2-\beta^2)C_1 + \lambda(3\beta^2-\lambda^2)C_2) \\
&\quad + e^{-\lambda(L-x)}\cos(\beta(L-x))(-\lambda(3\beta^2-\lambda^2)C_3 - \beta(3\lambda^2-\beta^2)C_4) \\
&\quad + e^{-\lambda(L-x)}\sin(\beta(L-x))(\beta(3\lambda^2-\beta^2)C_3 - \lambda(3\beta^2-\lambda^2)C_4)
\end{aligned}
$$

$$
\begin{aligned}
\int w^o dx &= \tfrac{1}{f_5}\left(f_4 x + \tfrac{x^2}{2} f_5\right) \\
&\quad + e^{-\lambda x}\cos(\beta x)\tfrac{-\lambda C_1 - \beta C_2}{\lambda^2+\beta^2} \\
&\quad + e^{-\lambda x}\sin(\beta x)\tfrac{\beta C_1 - \lambda C_2}{\lambda^2+\beta^2} \\
&\quad + e^{-\lambda(L-x)}\cos(\beta(L-x))\tfrac{\lambda C_3 + \beta C_4}{\lambda^2+\beta^2} \\
&\quad + e^{-\lambda(L-x)}\sin(\beta(L-x))\tfrac{-\beta C_3 + \lambda C_4}{\lambda^2+\beta^2}
\end{aligned}
$$

The expressions for the axial and circumferential displacements are obtained by integrating Eq. (8.23)

$$
\begin{Bmatrix} u^o \\ v^o \end{Bmatrix} = -[a_3]^{-1}[a_2]\begin{Bmatrix} \frac{\int w^o dx}{R} \\ -\frac{dw^o}{dx} \end{Bmatrix} + x\,[a_3]^{-1}\begin{Bmatrix} D_1 \\ D_2 \end{Bmatrix} + \begin{Bmatrix} u_o^o \\ v_o^o \end{Bmatrix}. \tag{8.37}
$$

The integral of w^o is included in Table 8.4, and u_o^o, v_o^o are rigid-body motions.

Once the displacements are known, all other parameters of interest can be calculated. The strains are calculated by Eqs. (8.19) and (8.20). (The derivatives appearing in these equations are listed in Table 8.4.) The forces and moments per unit length are calculated by Eq. (8.3).

Orthotropic cylinders. For orthotropic cylinders, $A_{16} = A_{26} = B_{16} = B_{26} = D_{16} = D_{26} = 0$, and the parameters in Table 8.2 become simpler, as shown in Table 8.5. With these parameters the radial displacement is given by Eq. (8.30),

Table 8.5. The parameters required in the equations for orthotropic cylinders

$$[a_1]=\begin{bmatrix} A_{22}-\frac{B_{22}}{R} & B_{12} \\ B_{12}-\frac{D_{12}}{R} & D_{11} \end{bmatrix} \qquad [a_3]=\begin{bmatrix} A_{11} & 0 \\ 0 & A_{66}-\frac{B_{66}}{R}-\frac{2D_{66}}{R^2} \end{bmatrix}$$

$$[a_2]=\begin{bmatrix} A_{12}-\frac{B_{12}}{R} & B_{11} \\ 0 & 0 \end{bmatrix} \qquad [a_4]=\begin{bmatrix} A_{12} & 0 \\ B_{11} & 0 \end{bmatrix}$$

$$[H]=\begin{bmatrix} H_{11} & H_{12} \\ H_{21} & H_{22} \end{bmatrix}=[a_1]-[a_4][a_3]^{-1}[a_2]$$

$$\mathbf{g}=\begin{Bmatrix} g_1 \\ g_2 \end{Bmatrix}=[a_4][a_3]^{-1}\begin{Bmatrix} D_1 \\ D_2 \end{Bmatrix}$$

$$f_1=H_{22} \quad f_2=-\tfrac{1}{R}(H_{21}+H_{12}) \quad f_3=\tfrac{H_{11}}{R^2} \quad f_4=p_{20}-\tfrac{g_1}{R} \quad f_5=p_{21}$$

and the axial and circumferential displacements become

$$u^o=\frac{1}{A_{11}}\left[-\left(A_{12}-\frac{B_{12}}{R}\right)\frac{\int w^o dx}{R}+B_{11}\frac{dw^o}{dx}+xD_1\right]+u_o^o \tag{8.38}$$

$$v^o=\frac{x}{A_{66}-\frac{B_{66}}{R}-\frac{2D_{66}}{R^2}}D_2+v_o^o. \tag{8.39}$$

A detailed examination of Eq. (8.37) shows that cylinders with arbitrary layup rotate ($v^o \neq 0$) when subjected to an axial load (Fig. 8.12). On the other hand, orthotropic cylinders do not rotate ($v^o = 0$; see Eq. 8.39) when only an axial load acts.

End effects. We can see from Eq. (8.30) that the effects of the ends are confined to a narrow "boundary layer" and decay exponentially with λx. For example, within a distance $x = 4/\lambda$ from the end, the value of w^o is within 2 percent of the value given by the membrane theory.

For long cylinders the boundary layers extending from each end do not meet (Fig. 8.13) and there is a central region, which may be treated as a membrane. In this membrane region Eq. (8.30) reduces to

$$w^o=\left\{\frac{1}{f_3}(f_4+xf_5)\right\} \qquad L_B < x < L-L_B. \tag{8.40}$$

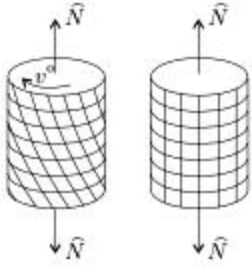

Figure 8.12: Cylinder subjected to axial load. Arbitrary layup (left); orthotropic layup (right).

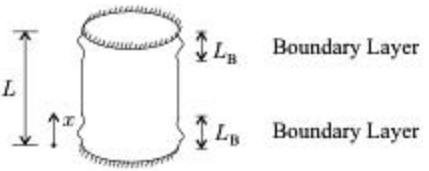

Figure 8.13: Illustration of the boundary layers.

When the two boundary layers do not interact, the support at $x = 0$ does not affect the boundary at $x = L$, and vice versa. Now, Eq. (8.30) becomes simpler, and within each boundary layer the radial displacement is given by

$$w^o = e^{-\lambda x}[C_1 \cos(\beta x) + C_2 \sin(\beta x)] + \left[\frac{1}{f_3}(f_4 + x f_5)\right] \qquad 0 < x < L_B \quad (8.41)$$

$$w^o = e^{-\lambda(L-x)}[C_3 \cos\beta(L-x) + C_4 \sin\beta(L-x)] + \left[\frac{1}{f_3}(f_4 + x f_5)\right] \qquad L - L_B < x < L, \quad (8.42)$$

where L_B is the length of the boundary layer (say, $L_B = 4/\lambda$). When the length of the cylinder is $L > 2L_B$, the boundary layers extending from the two ends do not meet. For $L_B = 4/\lambda$, this gives $L > 8/\lambda$ or $\lambda L > 8$. When $\lambda L > 8$, the parameters Y_{ij} (Table 8.3) are negligible, and the constants C_1 and C_2 are determined from the first two rows, and C_3 and C_4 from the second two rows of Eq. (8.36).

8.1 Example. *An $L = 0.5$-m-long cylinder (inner radius $R_{in} = 0.2$ m) is made of graphite epoxy unidirectional plies. The material properties are given in Table 3.6 (page 81). The layup is $[0_{10}/45_{10}]$. The 0-degree plies are on the inside and are parallel to the cylinder's axis. The thickness of the wall is $h = 0.002$ m. The cylinder is built-in at both ends (Fig. 8.14). An axial load $\widehat{N} = 20\,000$ N is applied to the cylinder. Calculate the displacements along the length.*

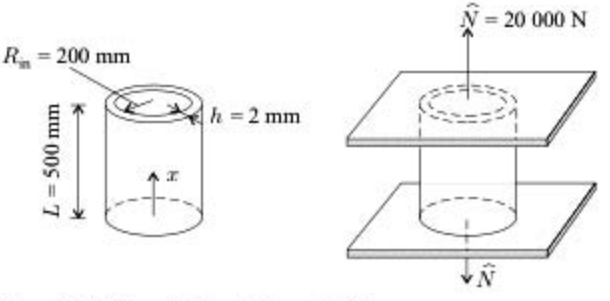

Figure 8.14: The cylinder in Example 8.1.

Solution. The radius of the reference surface, chosen as the midsurface, is

$$R = R_{in} + h/2 = 0.201 \text{ m}, \tag{8.43}$$

where h is the wall thickness ($h = 0.002$ m).

The axial load is $\widehat{N} = 20\,000$ N, and the torque $\widehat{T}$ is zero. The constants D_1 and D_2 are (Eqs. 8.32 and 8.34)

$$D_1 = N_x = \frac{\widehat{N}}{2\pi R} = 15\,836 \frac{\text{N}}{\text{m}} \qquad D_2 = \frac{\widehat{T}}{2\pi R^2} = 0. \tag{8.44}$$

There is no radial load acting on the cylinder, and $p_{z0} = p_{z1} = 0$ (Eq. 8.13). The elements of the $[A]$, $[B]$, and $[D]$ matrices of the wall are given in Eq. (3.54). With the values in Eq. (3.54) the matrices in Table 8.2 (page 372) become

$$[a_1] = \begin{bmatrix} A_{22} - \frac{B_{22}}{R} & B_{12} \\ B_{12} - \frac{D_{12}}{R} & D_{11} \end{bmatrix} = \begin{bmatrix} 55.269 \times 10^6 & 16\,820 \\ 16\,806 & 64.842 \end{bmatrix} \tag{8.45}$$

$$[a_3] = \begin{bmatrix} A_{11} & A_{16} - \frac{2B_{16}}{R} \\ A_{16} + \frac{B_{16}}{R} & A_{66} - \frac{B_{66}}{R} - \frac{2D_{66}}{R^2} \end{bmatrix} = \begin{bmatrix} 194.52 & 34.62 \\ 34.88 & 42.66 \end{bmatrix} \times 10^6 \tag{8.46}$$

$$[a_2] = \begin{bmatrix} A_{12} - \frac{B_{12}}{R} & B_{11} \\ A_{26} - \frac{D_{26}}{R^2} & B_{16} + \frac{D_{16}}{R} \end{bmatrix} = \begin{bmatrix} 39.05 & -0.051\,61 \\ 34.79 & 0.017\,45 \end{bmatrix} \times 10^6 \tag{8.47}$$

$$[a_4] = \begin{bmatrix} A_{12} & A_{26} - \frac{2B_{26}}{R} \\ B_{11} & B_{16} - \frac{2D_{16}}{R} \end{bmatrix} = \begin{bmatrix} 39.46 & 34.62 \\ -0.051\,61 & 0.017\,28 \end{bmatrix} \times 10^6 \tag{8.48}$$

$$[H] = [a_1] - [a_4][a_3]^{-1}[a_2] = \begin{bmatrix} 26.306 \times 10^6 & 7\,069 \\ 6\,987 & 31.755 \end{bmatrix} \tag{8.49}$$

$$\mathbf{g} = [a_4][a_3]^{-1} \begin{Bmatrix} D_1 \\ D_2 \end{Bmatrix} = \begin{Bmatrix} 1\,063 \\ -6.264 \end{Bmatrix}. \tag{8.50}$$

The constants f_1–f_5 are (Table 8.2, page 372)

$$\begin{aligned} f_1 &= H_{22} = 31.76 \qquad f_2 = -\frac{1}{R}(H_{21}+H_{12}) = -69\,931 \\ f_3 &= \frac{H_{11}}{R^2} = 651.13 \times 10^6 \qquad f_4 = p_{z0} - \frac{g_1}{R} = -5\,288 \\ f_5 &= p_{z1} = 0. \end{aligned} \tag{8.51}$$

With these f_i values the root of the characteristic polynomial is (Eq. 8.31)

$$\gamma = \sqrt{\frac{-f_2 + \sqrt{f_2^2 - 4 f_1 f_3}}{2 f_1}} = 53.05 + 41.40\, i. \tag{8.52}$$

The parameters λ and β are

$$\lambda = \text{Re}(\gamma) = 53.05 \qquad \beta = \text{Im}(\gamma) = 41.40. \tag{8.53}$$

The expressions in Table 8.3 (page 374) give

$$\begin{aligned} Y_{13} &= -0.8258 \times 10^{-12} & Y_{14} &= 2.9021 \times 10^{-12} \\ Y_{23} &= 76.319 \times 10^{-12} & Y_{24} &= 188.15 \times 10^{-12} \\ Y_{31} &= -0.8258 \times 10^{-12} & Y_{32} &= 2.9021 \times 10^{-12} \\ Y_{41} &= -76.319 \times 10^{-12} & Y_{42} &= -188.15 \times 10^{-12}. \end{aligned} \tag{8.54}$$

By substituting the preceding values of f_i and Y_{ij} into Eq. (8.36), we obtain

$$\begin{bmatrix} 1 & 0 & Y_{13} & Y_{14} \\ -\lambda & \beta & Y_{23} & Y_{24} \\ Y_{31} & Y_{32} & 1 & 0 \\ Y_{41} & Y_{42} & \lambda & \beta \end{bmatrix} \begin{Bmatrix} C_1 \\ C_2 \\ C_3 \\ C_4 \end{Bmatrix} = \begin{Bmatrix} 8.121 \\ 0 \\ 8.121 \\ 0 \end{Bmatrix} \times 10^{-6}. \tag{8.55}$$

Solution of this set of equations gives the constants

$$\begin{aligned} C_1 &= 8.121 \times 10^{-6} & C_2 &= 10.41 \times 10^{-6} \\ C_3 &= 8.121 \times 10^{-6} & C_4 &= 10.41 \times 10^{-6}. \end{aligned} \tag{8.56}$$

The radial displacement is (Eq. 8.30)

$$\begin{aligned} w^o = &\{e^{-\lambda x}[C_1 \cos(\beta x) + C_2 \sin(\beta x)] \\ &+ e^{-\lambda(L-x)}[C_3 \cos(\beta(L-x)) + C_4 \sin(\beta(L-x))]\} \\ &+ \left[\frac{1}{f_3}(f_4 + x f_5)\right]. \end{aligned} \tag{8.57}$$

With the rigid-body motions neglected, the axial and circumferential displacements are (Eq. 8.37)

$$\begin{Bmatrix} u^o \\ v^o \end{Bmatrix} = -[a_3]^{-1}[a_2] \begin{Bmatrix} \frac{\int w^o dx}{R} \\ -\frac{dw^o}{dx} \end{Bmatrix} + x[a_3]^{-1} \begin{Bmatrix} D_1 \\ D_2 \end{Bmatrix}, \tag{8.58}$$

where $\int w^o dx$ and dw^o/dx are calculated by the expressions given in Table 8.4 (page 375).

The axial, circumferential, and radial displacements are calculated by Eqs. (8.57) and (8.58) together with the constants λ, β, C_1–C_4, f_4, f_5 given in Eqs. (8.51), (8.53), and (8.56). The results are plotted in Figure 8.15. The length of the boundary layer is (page 377) $L_B = 4/\lambda = 0.0754$ m.

8.2.3 Temperature – Built-In Ends

We consider a cylinder with built-in ends on which the mechanical loads p_z, $\widehat{N}$, and $\widehat{T}$ act (Fig. 8.9) and that is subjected to a temperature change ΔT. This ΔT may vary in an arbitrary manner in the radial direction and linearly in the axial direction,

$$\Delta T(x, z) = \Delta T_z(z)(\Delta T_0 + x \Delta T_1), \tag{8.59}$$

where $\Delta T_z(z)$ is the temperature variation across the wall and ΔT_0, ΔT_1 are constants.

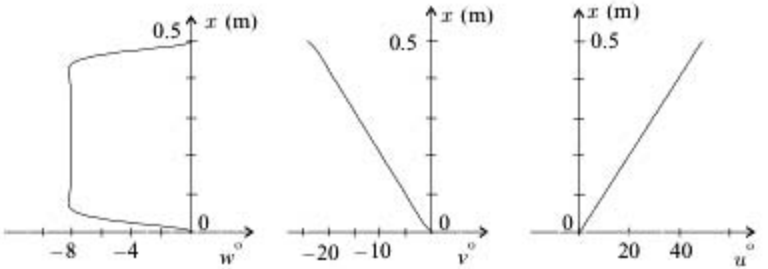

Figure 8.15: The radial w^o, circumferential v^o, and axial u^o displacements of the cylinder wall in Example 8.1. The unit of the displacements is 10^{-6} m.

The equilibrium and strain–displacement relationships are given by Eqs. (8.14)–(8.20), and the relationships between the strains, curvatures, in-plane forces, and moments for plates are given by Eq. (4.251). The radial displacement can be calculated by the steps employed in Section 8.2.2. The resulting expression for w^o is identical to Eq. (8.30), but now f_1, f_2, (which appear through λ), and f_3 are those given in Table 8.2 (page 372), and f_4 and f_5 are those in Table 8.6. The expressions for the axial and circumferential displacements become

$$\begin{Bmatrix} u^o \\ v^o \end{Bmatrix} = -[a_3]^{-1}[a_2] \begin{Bmatrix} \frac{\int w^o dx}{R} \\ -\frac{dw^o}{dx} \end{Bmatrix} + [a_3]^{-1} \left(x \begin{Bmatrix} D_1 \\ D_2 \end{Bmatrix} + \mathbf{b_T} \left(x \Delta T_0 + \frac{x^2}{2} \Delta T_1 \right) \right). \tag{8.60}$$

The vector $\mathbf{b_T}$ is defined in Table 8.6. Once the displacements are known, all other parameters of interest can be calculated. The strains are calculated by Eqs. (8.19) and (8.20), the forces and moments (per unit length) by Eq. (4.251).

8.3 Springback

When an unrestrained isotropic shell is heated to a uniform temperature, its size changes but not its shape. When a laminated shell is heated uniformly, both its size and shape change. This difference in the behavior of isotropic and laminated shells is illustrated in the next section for a cylindrical shell segment.[7]

8.3.1 Springback of Cylindrical Shells

To describe the springback phenomenon we examine a cylindrical shell segment whose temperature is changed uniformly by ΔT_0 (Fig. 8.16). Because of this temperature change the arclengths L_1 and L_2, the thickness h, and the subtended angle γ change to L_1', L_2', h', and γ'. The springback is defined as the change in

[7] N. Zahlan and J. M. O'Neill, Design and Fabrication of Composite Components; the Spring-Forward Phenomenon. *Composites*, Vol. 20, 77–81, 1989.

Table 8.6. The parameters required in Eq. (8.60)

$f_4 = p_{z0} - \frac{g_1}{R} - \Delta T_0 \frac{h_1}{R}$ $f_5 = p_{z1} - \Delta T_1 \frac{h_1}{R}$,

where

$\boldsymbol{h} = \begin{Bmatrix} h_1 \\ h_2 \end{Bmatrix} = [a_4][a_3]^{-1}\mathbf{b}_T - \mathbf{c}_T$, and $[a_3]$, $[a_4]$, g_1 are given in Table 8.2.

$$\mathbf{b}_T = \begin{bmatrix} A_{11} & A_{12} & A_{16} & B_{11} & B_{12} & B_{16} \\ A_{16} + \frac{B_{16}}{R} & A_{26} + \frac{B_{26}}{R} & A_{66} + \frac{B_{66}}{R} & B_{16} + \frac{D_{16}}{R} & B_{26} + \frac{D_{26}}{R} & B_{66} + \frac{D_{66}}{R} \end{bmatrix} \boldsymbol{\Omega}$$

$$\mathbf{c}_T = \begin{bmatrix} A_{12} & A_{22} & A_{26} & B_{12} & B_{22} & B_{26} \\ B_{11} & B_{12} & B_{16} & D_{11} & D_{12} & D_{16} \end{bmatrix} \boldsymbol{\Omega}$$

$\boldsymbol{\Omega}$ is the vector of hygrothermal strains caused by $\Delta T_z(z)$ defined by Eq. (4.250)

$\boldsymbol{\Omega} = \{\epsilon_x^{o,ht} \quad \epsilon_y^{o,ht} \quad \gamma_{xy}^{o,ht} \quad \kappa_x^{ht} \quad \kappa_y^{ht} \quad \kappa_{xy}^{ht}\}^T$

the angle during heating or cooling as follows:

$$\text{springback} = \frac{\gamma' - \gamma}{\gamma}. \tag{8.61}$$

The angle γ is related to the arclengths and the thickness by (Fig. 8.16, left)

$$\gamma = \frac{L_1 - L_2}{h}. \tag{8.62}$$

Similarly, γ' is

$$\gamma' = \frac{L_1' - L_2'}{h'}. \tag{8.63}$$

When the segment is made of a single layer, the thermal strain ϵ^{ht} is $\widetilde{\alpha}\Delta T$. Thus, after deformation, the arclengths of the top and bottom surfaces and the thickness are (Fig. 8.16, right)

$$L_1' = L_1 + \widetilde{\alpha}_y \Delta T_0 L_1 \qquad L_2' = L_2 + \widetilde{\alpha}_y \Delta T_0 L_2 \qquad h' = h + \widetilde{\alpha}_z \Delta T_0 h, \tag{8.64}$$

where $\widetilde{\alpha}_y$ and $\widetilde{\alpha}_z$ are the thermal expansion coefficients in the y and z directions, respectively. Substitution of Eqs. (8.62)–(8.64) into Eq. (8.61) gives the springback

$$\text{springback} = \frac{(\widetilde{\alpha}_y - \widetilde{\alpha}_z)\,\Delta T_0}{1 + \widetilde{\alpha}_z \Delta T_0}. \tag{8.65}$$

When heated, an isotropic material (for which $\widetilde{\alpha}_y = \widetilde{\alpha}_z$) expands equally in every direction. Thus, when heated uniformly, the springback of an isotropic

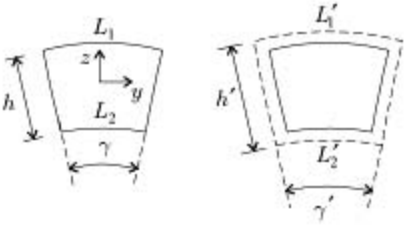

Figure 8.16: Cylindrical shell segment. Undeformed element (left) and the element deformed due to a uniform change in temperature (right).

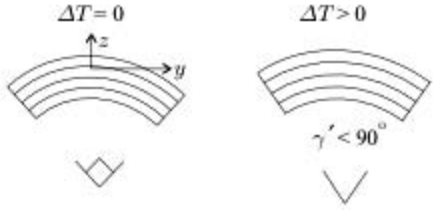

Figure 8.17: Springback of a composite segment made of unidirectional fiber-reinforced matrix.

cylindrical segment is zero; the size of the segment changes but not its shape. On the other hand, in a composite material the thermal expansion coefficient of the matrix differs from that of the fibers. Thus, for example, a heated segment made of identical layers containing fibers in the circumferential direction (Fig. 8.17) expands more in the z direction than in the y direction ($\widetilde{\alpha}_y < \widetilde{\alpha}_z$). In this case the springback is nonzero and the segment bends. (A similar argument holds when the segment is cooled.)

The thermal strains are generally small compared with unity, and the springback may be approximated by

$$\text{springback} = (\widetilde{\alpha}_y - \widetilde{\alpha}_z)\,\Delta T_0 = \epsilon_y^{\text{ht}} - \epsilon_z^{\text{ht}}. \tag{8.66}$$

This expression, derived for a single layer, may also be used for laminated composites with appropriate values of ϵ_y^{ht} and ϵ_z^{ht}. For a laminated composite the average hygrothermal strain perpendicular to the surface is approximated by

$$\epsilon_z^{\text{ht}} = \frac{h' - h}{h} = \frac{\Delta h}{h}, \tag{8.67}$$

where the change in thickness Δh is given by Eq. (4.287). The circumferential hygrothermal strain is approximated by the in-plane hygrothermal strain of a flat laminate given in Eq. (4.250)

$$\epsilon_y^{\text{ht}} = \epsilon_y^{\text{o,ht}} = \{\alpha_{12} \quad \alpha_{22} \quad \alpha_{26} \quad \beta_{12} \quad \beta_{22} \quad \beta_{26}\} \begin{Bmatrix} N_x^{\text{ht}} \\ N_y^{\text{ht}} \\ N_{xy}^{\text{ht}} \\ M_x^{\text{ht}} \\ M_y^{\text{ht}} \\ M_{xy}^{\text{ht}} \end{Bmatrix}. \tag{8.68}$$

When the layup is symmetrical, the springback of a cylindrical segment is given by Eq. (8.66) with the strains in Eqs. (8.67) and (8.68). When the layup is unsymmetrical, an additional term must be included in the springback. This term is arrived at by observing that a flat plate with symmetrical layup does not bend when the plate's temperature is changed uniformly. On the other hand a flat plate with unsymmetrical layup bends when the temperature of the plate is changed uniformly. The change in curvature is κ_y^{ht}. Hence, the total springback of a segment with unsymmetrical layup is

$$\text{springback} = R\kappa_y^{\text{ht}} + \left(\epsilon_y^{\text{o,ht}} - \epsilon_z^{\text{ht}}\right) \qquad \begin{matrix} \text{unsymmetrical} \\ \text{segment.} \end{matrix} \tag{8.69}$$

where κ_y^{ht} is approximated by the hygrothermal curvature of a flat laminate given

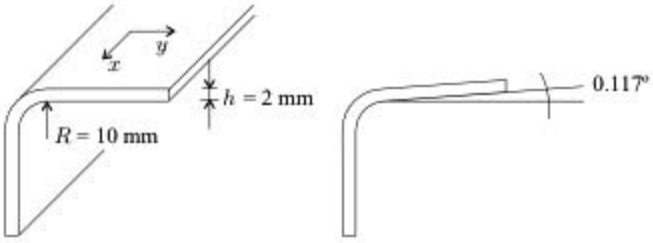

Figure 8.18: L-shaped stiffener in Example 8.2.

by Eq. (4.250) as follows:

$$\kappa_y^{\text{ht}} = \{\beta_{12} \quad \beta_{22} \quad \beta_{26} \quad \delta_{12} \quad \delta_{22} \quad \delta_{26}\} \begin{Bmatrix} N_x^{\text{ht}} \\ N_y^{\text{ht}} \\ N_{xy}^{\text{ht}} \\ M_x^{\text{ht}} \\ M_y^{\text{ht}} \\ M_{xy}^{\text{ht}} \end{Bmatrix}. \tag{8.70}$$

When a cylindrical shell or circular cylinder is analyzed, this springback effect must be included in the hygrothermal force–strain relationship of laminated plates. This is accomplished by making the following replacement in Eq. (4.251):

$$\begin{array}{ll} \text{Laminated plate} & \text{Cylindrical shell} \\ \text{(Eq. 4.251)} & \\ & \kappa_y^{\text{ht}} \Longrightarrow \kappa_y^{\text{ht}} + \dfrac{1}{R}\left(\epsilon_y^{o,\text{ht}} - \epsilon_z^{\text{ht}}\right). \end{array} \tag{8.71}$$

8.2 Example. *An L-shaped stiffener (Fig. 8.18) is made of graphite epoxy unidirectional plies. The material properties are listed in Table 3.6 (page 81). The layup is* $[45_6/0_4]_s$. *The 0-degree plies are along the length of the stiffener. The thickness of the wall is* $h = 0.002$ *m. The temperature is raised by* $80\ ^\circ C$. *Determine the new shape of the stiffener.*

Solution. The springback is (Eqs. 8.66 and 8.67)

$$\text{springback} = \epsilon_y^{\text{ht}} - \frac{\Delta h}{h} = 1.653 \times 10^{-3} - \frac{5.899 \times 10^{-6}}{2 \times 10^{-3}} = -1.297 \times 10^{-3}, \tag{8.72}$$

where h is the thickness of the wall ($h = 0.002$ m), Δh is the change in thickness due to the temperature change ($\Delta h = 5.899 \times 10^{-6}$ m, Eq. 4.295), and ϵ_y^{ht} is the strain in the circumferential direction ($\epsilon_y^{\text{ht}} = 1.653 \times 10^{-3}$, Eq. 4.273).

The change in the angle of the 90-degree stiffener is (Eq. 8.61)

$$\gamma' - \gamma = \text{springback} \times 90^\circ = -0.117^\circ. \tag{8.73}$$

This is illustrated in Figure 8.18, right. The layup of the stiffener is unbalanced and, therefore, the stiffener will also twist.

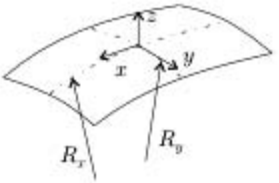

Figure 8.19: Radii of curvatures R_x, R_y of a shell.

8.3.2 Doubly Curved Shells

We generalize the preceding result (Eq. 8.71) and extend it to doubly curved shells with radii of curvatures R_x, R_y in the x–z and y–z planes (Fig. 8.19). In this case, the following replacements must be made in the laminated plate hygrothermal stress–strain relationships (Eq. 4.251):

Laminated plate	Doubly curved shell
κ_x^{ht}	$\Longrightarrow \kappa_x^{\mathrm{ht}} + \dfrac{1}{R_x}\left(\epsilon_x^{\mathrm{o,ht}} - \epsilon_z^{\mathrm{ht}}\right)$
κ_y^{ht}	$\Longrightarrow \kappa_y^{\mathrm{ht}} + \dfrac{1}{R_y}\left(\epsilon_y^{\mathrm{o,ht}} - \epsilon_z^{\mathrm{ht}}\right).$

(8.74)

8.4 Buckling of Shells

We consider a composite shell subjected simultaneously to surface loads on the wall and compressive and shear loads at the edges (Fig. 8.20). When this load set is increased beyond its critical limit, the shell buckles either globally or locally away from the edges. In general, local buckling precedes global buckling. In the following we treat local buckling of laminated composite shells.

We consider a small element away from the edges. The membrane forces acting on this element are (Fig. 8.20, right)

$$N_x = -\lambda N_{x0} \qquad N_y = -\lambda N_{y0} \qquad N_{xy} = -\lambda N_{xy0}, \tag{8.75}$$

where λ is the load parameter. We are interested in the value of λ (denoted by λ_{cr}) at which the shell locally buckles. An analysis describing the local buckling of shells was presented by Kollár.[8] In this analysis the buckling load is derived by representing the short waves arising at the location of the buckling by trigonometric functions. The derivation is long and involved and is not given here. We only quote the results for shells that are shallow[9] in the region where the local buckling occurs, and in this region the shell has constant curvatures (R_x = constant, R_y = constant, and R_{xy} = constant). The reference surface is designated by the function $f(x, y)$ (Table 8.7) and the radii of curvatures are $1/R_x = -\partial^2 f/\partial x^2$,

[8] L. P. Kollár, Buckling of Generally Anisotropic Shallow Sandwich Shells. *Journal of Reinforced Plastics and Composites*, Vol. 9, 549–568, 1990.

[9] W. Flügge, *Stresses in Shells*. 2nd edition. Springer, Berlin, 1973, p. 414.

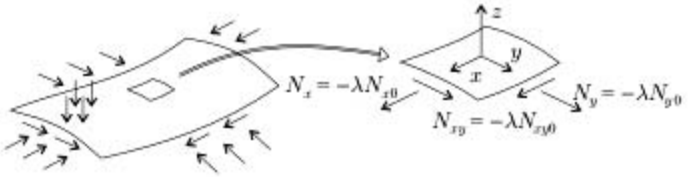

Figure 8.20: Surface and edge loads on a shell and the membrane forces.

$1/R_y = -\partial^2 f/\partial y^2, 1/R_{xy} = -2\partial^2 f/\partial x \partial y$. For such shells, the resulting equation is

$$\left(\begin{bmatrix} O & L \\ L & O \end{bmatrix} \begin{bmatrix} M_o & M_n \\ M_n & M_o \end{bmatrix} \begin{bmatrix} O & L \\ L & O \end{bmatrix}^T - \lambda \begin{bmatrix} \Phi_1[J] & \Phi_2[J] \\ \Phi_2[J] & \Phi_1[J] \end{bmatrix} \right) \begin{Bmatrix} u_1 \\ v_1 \\ w_1 \\ u_2 \\ v_2 \\ w_2 \end{Bmatrix} = 0, \quad (8.76)$$

where u_1, v_1, u_2, v_2 are the in-plane and w_1, w_2 are the out-of-plane amplitudes of the buckling waves. The matrices $[O]$, $[L]$, $[J]$ and the parameters Φ_1, Φ_2 (given in Table 8.8) depend on four constants α, β, c_1, c_2, which characterize the wave pattern of the buckled shape (Fig. 8.21).

Table 8.7. Curvatures of typical shells

	$f(x, y)$	R_x	R_y	R_{xy}
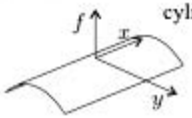 cylinder	$f = -C_1 y^2$	0	$\frac{1}{2C_1}$	0
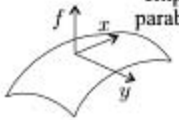 elliptical paraboloid	$f = -C_1 y^2 - C_2 x^2$	$\frac{1}{2C_2}$	$\frac{1}{2C_1}$	0
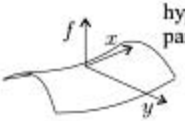 hyperbolic paraboloid	$f = -C_1 y^2 + C_2 x^2$	$-\frac{1}{2C_2}$	$\frac{1}{2C_1}$	0
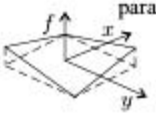 hyperbolic paraboloid	$f = -C_1 xy$	0	0	$\frac{1}{2C_1}$

Table 8.8. The parameters required in Eqs. (8.76) and (8.89). For a cylinder $1/R_x = 1/R_{xy} = 0$ and $R_y = R$

$$[O] = \begin{bmatrix} -\alpha & 0 & \beta & 0 & 0 & 0 \\ 0 & -\beta & \alpha & 0 & 0 & 0 \\ \frac{1}{R_x} & \frac{1}{R_y} & 0 & \alpha^2+\beta^2 c_2^2 & \beta^2+\alpha^2 c_1^2 & -2\alpha\beta\,(1+c_1c_2) \end{bmatrix}$$

$$[L] = \begin{bmatrix} \beta c_2 & 0 & -\alpha c_1 & 0 & 0 & 0 \\ 0 & \alpha c_1 & -\beta c_2 & 0 & 0 & 0 \\ 0 & 0 & \frac{1}{R_{xy}} & -2\alpha\beta c_2 & -2\alpha\beta c_1 & 2(c_1\alpha^2 + c_2\beta^2) \end{bmatrix}$$

$$[M_o] = \begin{bmatrix} A_{11} & A_{12} & 0 & B_{11} & B_{12} & 0 \\ A_{12} & A_{22} & 0 & B_{12} & B_{22} & 0 \\ 0 & 0 & A_{66} & 0 & 0 & B_{66} \\ B_{11} & B_{12} & 0 & D_{11} & D_{12} & 0 \\ B_{12} & B_{22} & 0 & D_{12} & D_{22} & 0 \\ 0 & 0 & B_{66} & 0 & 0 & D_{66} \end{bmatrix} \qquad [M_n] = \begin{bmatrix} A & B \\ B & D \end{bmatrix} - [M_o]$$

$$[J] = \begin{bmatrix} 0 & 0 & 0 \\ 0 & 0 & 0 \\ 0 & 0 & 1 \end{bmatrix}$$

$$\Phi_1 = N_{x0}\left(\alpha^2 + \beta^2 c_2^2\right) + N_{xy0} 2\left(\alpha^2 c_1 + \beta^2 c_2^2\right) + N_{y0}\left(\alpha^2 c_1 + \beta^2\right)$$

$$\Phi_2 = -2\alpha\beta(N_{x0}c_2 + N_{xy0}(1 + c_1c_2) + N_{y0}c_1)$$

The directions of the lines passing through the maxima of the left and right propagating waves are (Fig 8.22)

$$\tan\vartheta_1 = \frac{\alpha + \beta c_2}{\beta + \alpha c_1} \qquad \tan\vartheta_2 = \frac{\alpha - \beta c_2}{\beta - \alpha c_1}. \tag{8.77}$$

The eigenvalues λ_{cr} of Eq. (8.76) are the critical load parameters, which are to be calculated for different values of the constants α, β, c_1, c_2. The lowest value of λ_{cr} resulting from these calculations is the value of interest. In principle, the values of these constants can not be selected arbitrarily, but must be chosen such that the corresponding displacements satisfy the boundary conditions. For short wavelengths, which is the case considered here, the edges do not affect the waves significantly and, hence, the buckling load. Therefore, as an approximation, arbitrary values of α, β, c_1, c_2 may be chosen for calculating λ_{cr}.

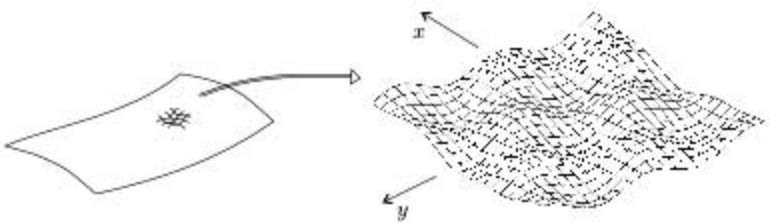

Figure 8.21: Illustration of the buckling pattern at local buckling of a shell.

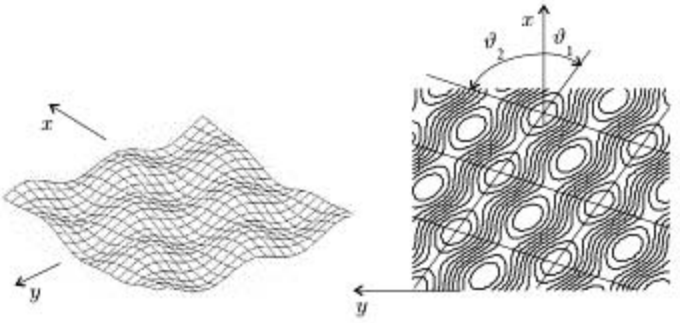

Figure 8.22: The local buckling pattern and the corresponding contour plot.

Once the constants α, β, c_1, and c_2 are known, the deflection perpendicular to the reference surface of the shell is calculated by

$$w_B^0 = w_1 \sin(\alpha(x + c_1 y)) \sin(\beta(y + c_2 x)) + w_2 \sin(\alpha(x + c_1 y)) \cos(\beta(y + c_2 x)). \tag{8.78}$$

8.4.1 Buckling of Cylinders

The buckling analysis presented earlier in this section for thin shallow shells may be applied to the buckling of thin cylinders by setting the radius R equal to the radius R_y of the shell ($R = R_y$), and R_x and R_{xy} to infinity ($1/R_x = 1/R_{xy} = 0$).

8.3 Example. *An $L = 1$-m-long cylinder (inner radius $R_{in} = 0.2$ m) is made of graphite epoxy unidirectional plies. The material properties are given in Table 3.6 (page 81). The layup is $[-30_4/15_4/0_2]_s$. The 0-degree plies are parallel to the cylinder axis. The thickness of the wall is $h = 0.002$ m (Fig. 8.23). An axial load is applied to the cylinder. Calculate the load that causes local buckling.*

Solution. For this cylinder we have

$$\begin{aligned} &R = R_y = R_{in} + h/2 = 0.201 \text{ m} \qquad 1/R_x = 1/R_{xy} = 0 \\ &N_{y0} = N_{xy0} = 0. \end{aligned} \tag{8.79}$$

For N_{x0} we arbitrarily select the value $N_{x0} = 1$. With this value and with the values in Eq. (8.79), the matrices $[O]$ and $[L]$ and the parameters Φ_1, Φ_2 are

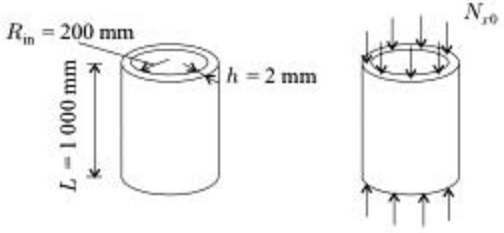

Figure 8.23: The cylinder in Example 8.3.

(Table 8.8, page 386)

$$[O] = \begin{bmatrix} -\alpha & 0 & \beta & 0 & 0 & 0 \\ 0 & -\beta & \alpha & 0 & 0 & 0 \\ 0 & 4.975 & 0 & \alpha^2 + \beta^2 c_2^2 & \beta^2 + \alpha^2 c_1^2 & -2\alpha\beta\,(1 + c_1 c_2) \end{bmatrix} \tag{8.80}$$

$$[L] = \begin{bmatrix} \beta c_2 & 0 & -\alpha c_1 & 0 & 0 & 0 \\ 0 & \alpha c_1 & -\beta c_2 & 0 & 0 & 0 \\ 0 & 0 & 0 & -2\alpha\beta c_2 & -2\alpha\beta c_1 & 2(c_1\alpha^2 + c_2\beta^2) \end{bmatrix} \tag{8.81}$$

$$\Phi_1 = \alpha^2 + \beta^2 c_2^2 \tag{8.82}$$

$$\Phi_2 = -2\alpha\beta c_2. \tag{8.83}$$

The matrices $[M_o]$, $[M_n]$ and $[J]$ (Table 8.8, page 386), with the elements of the $[A]$ and $[D]$ matrices given in Table 3.7 (page 84), are

$$[M_o] = \begin{bmatrix} 235.54 \times 10^6 & 32.74 \times 10^6 & 0 & 0 & 0 & 0 \\ 32.74 \times 10^6 & 27.79 \times 10^6 & 0 & 0 & 0 & 0 \\ 0 & 0 & 36.01 \times 10^6 & 0 & 0 & 0 \\ 0 & 0 & 0 & 65.42 & 16.29 & 0 \\ 0 & 0 & 0 & 16.29 & 11.60 & 0 \\ 0 & 0 & 0 & 0 & 0 & 17.39 \end{bmatrix}$$

$$[M_n] = \begin{bmatrix} 0 & 0 & -10.19 \times 10^6 & 0 & 0 & 0 \\ 0 & 0 & -10.19 \times 10^6 & 0 & 0 & 0 \\ -10.19 \times 10^6 & -10.19 \times 10^6 & 0 & 0 & 0 & 0 \\ 0 & 0 & 0 & 0 & 0 & -18.93 \\ 0 & 0 & 0 & 0 & 0 & -7.74 \\ 0 & 0 & 0 & -18.93 & -7.74 & 0 \end{bmatrix}$$

$$[J] = \begin{bmatrix} 0 & 0 & 0 \\ 0 & 0 & 0 \\ 0 & 0 & 1 \end{bmatrix}.$$

To find λ_{cr}, we refer to Eq. (8.76):

$$\left(\underbrace{\begin{bmatrix} O & L \\ L & O \end{bmatrix} \begin{bmatrix} M_o & M_n \\ M_n & M_o \end{bmatrix} \begin{bmatrix} O & L \\ L & O \end{bmatrix}^T}_{[G]} - \lambda \begin{bmatrix} \Phi_1[J] & \Phi_2[J] \\ \Phi_2[J] & \Phi_1[J] \end{bmatrix} \right) \begin{Bmatrix} u_1 \\ v_1 \\ w_1 \\ u_2 \\ v_2 \\ w_2 \end{Bmatrix} = 0. \tag{8.84}$$

To obtain λ and the displacements we assume different values of the parameters α, β, c_1, c_2. For example, we set $\alpha = 40$, $\beta = 40$, $c_1 = 0$, $c_2 = 0$. With these values

Eq. (8.84) becomes

$$\left([G] - \lambda \begin{bmatrix} 0 & & & & & \\ & 0 & & & & \\ & & 1\,600 & & & \\ & & & 0 & & \\ & & & & 0 & \\ & & & & & 1\,600 \end{bmatrix} \right) \begin{Bmatrix} u_1 \\ v_1 \\ w_1 \\ u_2 \\ v_2 \\ w_2 \end{Bmatrix} = 0, \tag{8.85}$$

where

$$[G] = \begin{bmatrix} 434.49 & 109.99 & -6.5145 & 32.601 & 32.601 & -2.0274 \\ 109.99 & 102.09 & -5.5311 & 32.601 & 32.601 & -2.0274 \\ -6.5145 & -5.5311 & 1.1466 & -2.0274 & -2.0274 & 0.27312 \\ 32.601 & 32.601 & -2.0274 & 434.49 & 109.99 & -6.5145 \\ 32.601 & 32.601 & -2.0274 & 109.99 & 102.09 & -5.5311 \\ -2.0274 & -2.0274 & 0.27312 & -6.5145 & -5.5311 & 1.1466 \end{bmatrix} \times 10^9.$$

Solution of Eq. (8.85) yields

$$\lambda_{cr} = 434\,810 \qquad \text{for} \quad \begin{matrix} \alpha = 40 \\ \beta = 40 \\ c_1 = 0 \\ c_2 = 0\,. \end{matrix}$$

We are interested in the lowest value of λ_{cr}. To find this value we repeat the calculation for different sets of α, β, c_1, c_2 values. The lowest value of λ_{cr} corresponds to $\alpha = 37.5, \beta = 16.4, c_1 = 0.152, c_2 = 1.3$. For these α, β, c_1, c_2 values the results are

$$\lambda_{cr} = 345\,568 \qquad \text{for} \quad \begin{matrix} \alpha = 37.5 \\ \beta = 16.4 \\ c_1 = 0.152 \\ c_2 = 1.3\,. \end{matrix}$$

The buckling load is

$$N_{x,cr} = \lambda_{cr} N_{x0} = 345\,568 \text{ N/m} = 346 \text{ kN/m}. \tag{8.86}$$



Figure 8.24: The buckled shape of the anisotropic cylinder in Example 8.3 (left) and the buckled shape on the assumption that the cylinder is orthotropic (right).

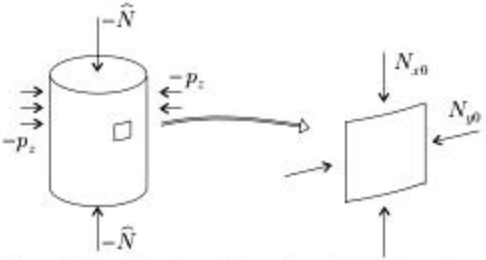

Figure 8.25: Cylinder subjected to axial load and pressure.

The directions of the lines passing through the maxima of the left and right propagating waves are (Eq. 8.77)

$$\vartheta_1 = \arctan \frac{\alpha + \beta c_2}{\beta + \alpha c_1} = 69.4^\circ \qquad \vartheta_2 = \arctan \frac{\alpha - \beta c_2}{\beta - \alpha c_1} = 56.5^\circ. \tag{8.87}$$

Solution of Eq. (8.84) also gives the amplitudes (see Eq. 8.78) of the displacements. For $\alpha = 37.5, \beta = 16.4, c_1 = 0.152$, and $c_2 = 1.3$ the amplitudes of the radial displacements are

$$w_1 = -0.707\,06 \qquad w_2 = 0.707\,06. \tag{8.88}$$

The buckled shape (Eq. 8.78) determined by these amplitudes is shown in Figure 8.24, left.

In the following we consider cylinders subjected to an axial load $-\widehat{N}$ and to a radial pressure $-p_z$ (Fig. 8.25). The membrane forces are $N_{x0} = -\widehat{N}/2\pi R$ and $N_{y0} = -p_z R$.

Orthotropic wall. The layup of the wall of the cylinder is orthotropic, and one of the directions of orthotropy coincides with x. For this case we assume that the cylinder buckles in a checkerboard pattern (Figs. 8.26 and 8.27). For this checkerboard pattern $\vartheta = \vartheta_1 = \vartheta_2 = \arctan \frac{l_x}{l_y}$, and from Eq. (8.77) we have that $c_1 = c_2 = 0$. Equation (8.76) now reduces to

$$([O][M_o][O]^T - \lambda \Phi_1 [J]) \begin{Bmatrix} u_1 \\ v_1 \\ w_1 \end{Bmatrix} = 0, \tag{8.89}$$

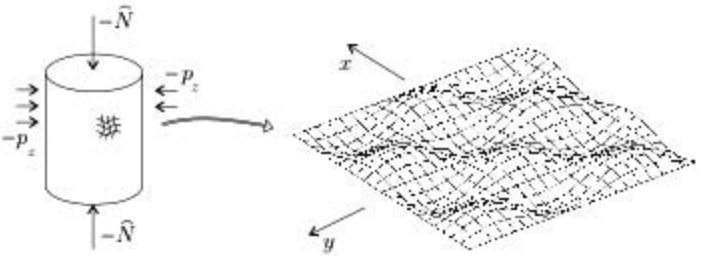

Figure 8.26: Illustration of the checkerboard buckling pattern at local buckling of an orthotropic cylinder subjected to axial load and uniform pressure.

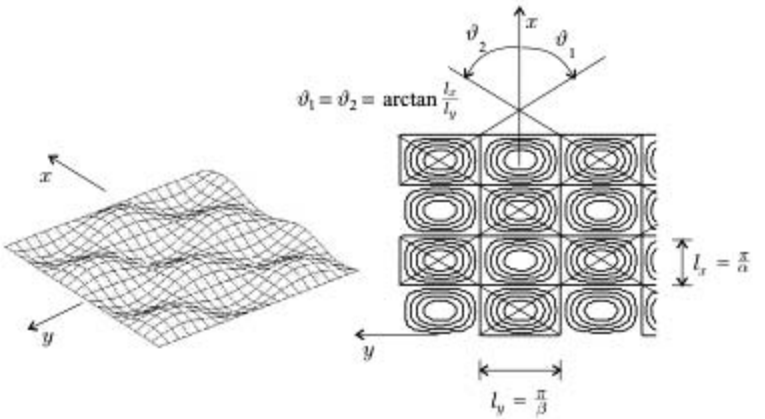

Figure 8.27: The local checkerboard buckling pattern and the corresponding contour plot of an orthotropic cylinder subjected to axial load and uniform pressure.

where the matrix $[O]$ and the parameter Φ_1, given in Table 8.8, are evaluated with $c_1 = c_2 = 0$. The eigenvalues of this equation are

$$\lambda_{cr} = \frac{1}{N_{x0}\alpha^2 + N_{y0}\beta^2} \frac{\begin{vmatrix} F_{11} & F_{12} & F_{13} \\ F_{12} & F_{22} & F_{23} \\ F_{13} & F_{23} & F_{33} \end{vmatrix}}{\begin{vmatrix} F_{11} & F_{12} \\ F_{12} & F_{22} \end{vmatrix}}, \tag{8.90}$$

where $||$ denotes the determinant. The elements F_{ij} $(i, j = 1, 2, 3)$ are given in Table 8.9 (page 392). The critical load parameter λ_{cr} (Eq. 8.90) must be calculated for different values of α and β. The lowest λ_{cr} is the value of interest.

Orthotropic and symmetrical wall. When the wall's layup is orthotropic and symmetrical ($B_{ij} = 0$), Eq. (8.90) simplifies to[10]

$$\lambda_{cr} = \frac{1}{N_{x0}\alpha^2 + N_{y0}\beta^2} \left\{ \left[\frac{\frac{\alpha^4}{R^2}\left(1 - \frac{A_{12}^2}{A_{11}A_{22}}\right)}{\frac{\alpha^4}{A_{22}} + \alpha^2\beta^2\left(\frac{1}{A_{66}} - \frac{A_{12}(A_{12}+2A_{66})}{A_{11}A_{22}A_{66}}\right) + \frac{\beta^4}{A_{11}}} \right] \right.$$
$$\left. + D_{11}\alpha^4 + 2(D_{12} + 2D_{66})\beta^2\alpha^2 + D_{22}\beta^4 \right\}, \tag{8.91}$$

where λ_{cr} (Eq. 8.91) must be calculated for different values of α and β. The lowest λ_{cr} is the value of interest. When $R = \infty$, the term in parentheses is zero, and the expression above reduces to that for flat plates (Eq. 4.121).

8.4 Example. *An $L = 1$-m-long cylinder (inner radius $R_{in} = 0.2$ m) is made of graphite epoxy unidirectional plies (Fig. 8.28). The material properties are given in*

[10] R. M. Jones, Buckling of Circular Cylindrical Shells with Multiple Orthotropic Layers and Eccentric Stiffeners. *AIAA Journal*, Vol. 6, 2301–2305, 1968.

Table 8.9. The parameters required in Eqs. (8.90) and (8.96).

$$F_{11} = A_{11}\alpha^2 + A_{66}\beta^2 \qquad F_{12} = (A_{12} + A_{66})\,\alpha\beta$$
$$F_{13} = -A_{12}\tfrac{\alpha}{R} - B_{11}\alpha^3 - B_{12}\alpha\beta^2 - 2B_{66}\alpha\beta^2$$
$$F_{22} = A_{22}\beta^2 + A_{66}\alpha^2$$
$$F_{23} = -B_{22}\beta^3 - B_{12}\alpha^2\beta - 2B_{66}\alpha^2\beta - A_{22}\tfrac{\beta}{R}$$
$$F_{33} = D_{11}\alpha^4 + 2(D_{12} + 2D_{66})\,\beta^2\alpha^2 + D_{22}\beta^4 + \tfrac{1}{R}\left(A_{22}\tfrac{1}{R} + 2B_{22}\beta^2 + 2B_{12}\alpha^2\right)$$

Table 3.6 (page 81). The layup is $[-30_4/15_4/0_2]_s$. *The 0-degree plies are parallel to the cylinder axis. The thickness of the wall is* $h = 0.002$ *m. An axial load is applied to the cylinder. Calculate the buckling load that causes local buckling.*

Solution. The layup follows the 10-percent rule (page 89), and, accordingly, we may treat the cylinder as orthotropic. The layup is symmetrical and λ_{cr} is calculated by Eq. (8.91)

$$\lambda_{cr} = \frac{1}{N_{x0}\alpha^2 + N_{y0}\beta^2}\left\{\left[\frac{\frac{\alpha^4}{R^2}\left(1 - \frac{A_{12}^2}{A_{11}A_{22}}\right)}{\frac{\alpha^4}{A_{22}} + \alpha^2\beta^2\left(\frac{1}{A_{66}} - \frac{A_{12}(A_{12}+2A_{66})}{A_{11}A_{22}A_{66}}\right) + \frac{\beta^4}{A_{11}}}\right]\right.$$
$$\left. + D_{11}\alpha^4 + 2(D_{12} + 2D_{66})\,\beta^2\alpha^2 + D_{22}\beta^4\right\}. \tag{8.92}$$

For this cylinder we have

$$R = R_y = R_{in} + h/2 = 0.201 \text{ m} \qquad 1/R_x = 1/R_{xy} = 0$$
$$N_{y0} = N_{xy0} = 0. \tag{8.93}$$

For N_{x0} we arbitrarily select the value $N_{x0} = 1$.

With these values and with the elements of the $[A]$ and $[D]$ matrices in Table 3.7 (page 84), Eq. (8.92) becomes

$$\lambda_{cr} = \frac{1}{\alpha^2}\left\{\left[\frac{20.7\alpha^4}{(35.98\alpha^4 + 13.22\alpha^2\beta^2 + 4.246\beta^4)\,10^{-9}}\right]\right.$$
$$\left. + 65.42\alpha^4 + 102.1\beta^2\alpha^2 + 11.60\beta^4\right\}. \tag{8.94}$$

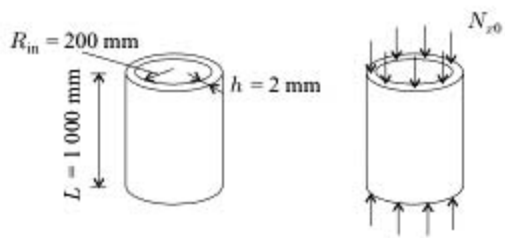

Figure 8.28: The cylinder in Example 8.4.

Table 8.10. The parameters in Eq. (8.96).

$$F_{14} = B_{11}\alpha^2 + B_{66}\beta^2 \qquad F_{15} = (B_{12} + B_{66})\alpha\beta$$
$$F_{24} = (B_{12} + B_{66})\alpha\beta \qquad F_{25} = B_{22}\beta^2 + B_{66}\alpha^2$$
$$F_{34} = -D_{11}\alpha^3 - (D_{12} + 2D_{66})\alpha\beta^2 - \tfrac{1}{R}B_{12}\alpha$$
$$F_{35} = -D_{22}\beta^3 - (D_{12} + 2D_{66})\alpha^2\beta - \tfrac{1}{R}B_{22}\beta$$
$$F_{44} = D_{11}\alpha^2 + D_{66}\beta^2 + \widetilde{S}_{11} \qquad F_{45} = (D_{12} + D_{66})\alpha\beta$$
$$F_{55} = D_{22}\beta^2 + D_{66}\alpha^2 + \widetilde{S}_{22}$$

where λ_{cr} is to be calculated for different of α and β values. We are interested in α and β that result in the lowest value of λ_{cr}. In this case, λ_{cr} is minimum for $\alpha = 54.5$ and $\beta \approx 0$ and has the value $\lambda_{cr} = 388$. Thus, the buckling load is

$$N_{x,cr} = \lambda_{cr} N_{x0} = 388 \text{ kN/m}. \tag{8.95}$$

We also calculated the buckled shape, which is axisymmetrical, as shown in Figure 8.24, right. The buckling load calculated with the assumption that the wall is orthotropic agrees within 12 percent with the result of the "exact" analysis ($N_{x,cr} = 346$ kN, Eq. 8.86).

Sandwich cylinder. When the cylinder's wall is of orthotropic sandwich construction (page 176), λ_{cr} is[11]

$$\lambda_{cr} = \frac{1}{N_{x0}\alpha^2 + N_{y0}\beta^2} \frac{\begin{vmatrix} F_{11} & F_{12} & F_{13} & F_{14} & F_{15} \\ F_{12} & F_{22} & F_{23} & F_{24} & F_{25} \\ F_{13} & F_{23} & F_{33} & F_{34} & F_{35} \\ F_{14} & F_{24} & F_{34} & F_{44} & F_{45} \\ F_{15} & F_{25} & F_{35} & F_{45} & F_{55} \end{vmatrix}}{\begin{vmatrix} F_{11} & F_{12} \\ F_{12} & F_{22} \end{vmatrix} \begin{vmatrix} F_{44} & F_{45} \\ F_{45} & F_{55} \end{vmatrix}}, \tag{8.96}$$

where the elements F_{ij} are given in a Tables 8.9 and 8.10 and λ_{cr} (Eq. 8.96) must be calculated for different values of α and β. The lowest resulting value of λ_{cr} is the value of interest. For $R = \infty$ this expression reduces to that for flat sandwich plates (Eq. 5.91).

When the cylinder wall is of isotropic or quasi-isotropic sandwich construction (page 176), Eq. (8.96) simplifies to

$$\lambda_{cr} = \frac{1}{N_{x0}\alpha^2 + N_{y0}\beta^2} \left\{ A^{iso}(1 - (\nu^{iso})^2) \frac{\left(\frac{\alpha^2}{R}\right)^2}{(\alpha^2 + \beta^2)^2} + \left[\frac{1}{D^{iso}(\alpha^2 + \beta^2)^2} + \frac{1}{\widetilde{S}(\alpha^2 + \beta^2)} \right]^{-1} \right\}, \tag{8.97}$$

[11] L. P. Kollár, Buckling of Generally Anisotropic Shallow Sandwich Shells. *Journal of Reinforced Plastics and Composites*, Vol. 9, 549–568, 1990.

where ν^{iso}, A^{iso}, and D^{iso} are given in Table 5.2 (page 178) and $\widetilde{S}$ is given by Eq. (5.39). When the cylinder is subjected to axial compression only ($N_{y0} = 0$, see Eq. 8.11), the cylinder buckles axisymmetrically[12] ($\beta = 0$) and Eq. (8.97) becomes

$$\lambda_{cr} = \frac{1}{N_{x0}} \left[A^{iso}(1 - (\nu^{iso})^2) \frac{1}{R^2} \frac{1}{\alpha^2} + \left(\frac{1}{D^{iso}\alpha^2} + \frac{1}{\widetilde{S}} \right)^{-1} \right]. \tag{8.98}$$

The lowest value of λ_{cr} is obtained from the condition

$$\frac{\partial \lambda_{cr}}{\partial \alpha} = 0. \tag{8.99}$$

[12] I. Hegedűs, Buckling of Axially Compressed Cylindrical Sandwich Shells. *Acta Technica Hungarica*, Vol. 89, 377–387, 1979.

Finite Element Analysis

The finite element method offers a practical means of calculating the deformations of, and stresses and strains in, complex structures. A detailed description of the finite element method is beyond the scope of this book. Instead, we focus on those features specific to composite materials.

Finite element analysis consists of the following major steps:

1. A mesh encompassing the structure is generated (Fig. 9.1).
2. The stiffness matrix $[k]$ of each element is determined.
3. The stiffness matrix $[K]$ of the structure is determined by assembling the element stiffness matrices.
4. The loads applied to the structure are replaced by an equivalent force system such that the forces act at the nodal points.
5. The displacements of the nodal points $\mathbf{d}$ are calculated by

$$[K]\mathbf{d} = \mathbf{f}, \tag{9.1}$$

where $\mathbf{f}$ is the force vector representing the equivalent applied nodal forces (Fig. 9.1).

6. The vector $\mathbf{d}$ is subdivided into subvectors δ, each δ representing the displacements of the nodal points of a particular element.
7. The displacements at a point inside the element are calculated by

$$\mathbf{u} = [N]\delta, \tag{9.2}$$

where the vector $\mathbf{u}$ represents the displacements and $[N]$ is the matrix of the shape vectors.

8. The strains at a point inside the elements are calculated by

$$\varepsilon = [B]\delta, \tag{9.3}$$

where $[B]$ is the strain–displacement matrix.

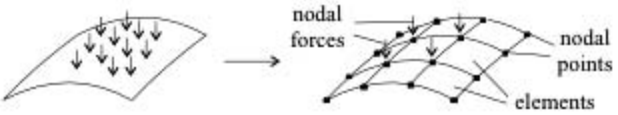

Figure 9.1: Structure and its finite element mesh.

9. The stresses at a point inside the element are calculated by

$$\sigma = [E]\,\varepsilon, \tag{9.4}$$

where $[E]$ is the stiffness matrix characterizing the material.

The element stiffness matrix, referred to in Step 2, is defined as

$$[k]\,\delta = \mathbf{f}_e, \tag{9.5}$$

where $\mathbf{f}_e$ represents the forces acting at the nodal points of the element. The element stiffness matrix is[1]

$$[k] = \int_{(V)} [B]^T [E] [B]\, dV, \tag{9.6}$$

where V is the volume of the element.

The preceding steps apply to structures made of either isotropic or composite materials. The only difference between isotropic and composite structures is in the material stiffness matrix $[E]$. In the following we present expressions for $[E]$.

9.1 Three-Dimensional Element

The stress–strain relationships for a three-dimensional element are (Eq. 2.20)

$$\begin{Bmatrix} \sigma_x \\ \sigma_y \\ \sigma_z \\ \tau_{yz} \\ \tau_{xz} \\ \tau_{xy} \end{Bmatrix} = \underbrace{\begin{bmatrix} \overline{C}_{11} & \overline{C}_{12} & \overline{C}_{13} & \overline{C}_{14} & \overline{C}_{15} & \overline{C}_{16} \\ \overline{C}_{21} & \overline{C}_{22} & \overline{C}_{23} & \overline{C}_{24} & \overline{C}_{25} & \overline{C}_{26} \\ \overline{C}_{31} & \overline{C}_{32} & \overline{C}_{33} & \overline{C}_{34} & \overline{C}_{35} & \overline{C}_{36} \\ \overline{C}_{41} & \overline{C}_{42} & \overline{C}_{43} & \overline{C}_{44} & \overline{C}_{45} & \overline{C}_{46} \\ \overline{C}_{51} & \overline{C}_{52} & \overline{C}_{53} & \overline{C}_{54} & \overline{C}_{55} & \overline{C}_{56} \\ \overline{C}_{61} & \overline{C}_{62} & \overline{C}_{63} & \overline{C}_{64} & \overline{C}_{65} & \overline{C}_{66} \end{bmatrix}}_{[E]} \begin{Bmatrix} \epsilon_x \\ \epsilon_y \\ \epsilon_z \\ \gamma_{yz} \\ \gamma_{xz} \\ \gamma_{xy} \end{Bmatrix}, \tag{9.7}$$

where $[E]$ is the stiffness matrix for a three-dimensional element.

[1] R. D. Cook, D. S. Malkus, and M. E. Plesha, *Concepts and Applications of Finite Element Analysis*. 3rd edition. John Wiley and Sons, New York, 1989, p. 110.

9.2 Plate Element

In the absence of shear deformation, the force–strain relationships for a thin-plate element are (Eq. 3.21)

$$\begin{Bmatrix} N_x \\ N_y \\ N_{xy} \\ M_x \\ M_y \\ M_{xy} \end{Bmatrix} = \underbrace{\begin{bmatrix} A_{11} & A_{12} & A_{16} & B_{11} & B_{12} & B_{16} \\ A_{12} & A_{22} & A_{26} & B_{12} & B_{22} & B_{26} \\ A_{16} & A_{26} & A_{66} & B_{16} & B_{26} & B_{66} \\ B_{11} & B_{12} & B_{16} & D_{11} & D_{12} & D_{16} \\ B_{12} & B_{22} & B_{26} & D_{12} & D_{22} & D_{26} \\ B_{16} & B_{26} & B_{66} & D_{16} & D_{26} & D_{66} \end{bmatrix}}_{[E]} \begin{Bmatrix} \epsilon_x^o \\ \epsilon_y^o \\ \gamma_{xy}^o \\ \kappa_x \\ \kappa_y \\ \kappa_{xy} \end{Bmatrix}, \tag{9.8}$$

where $[E]$ is the stiffness matrix for a plate element without shear deformations. In the presence of shear deformation, the force–strain relationships are (Eqs. 5.13–5.15)

$$\begin{Bmatrix} N_x \\ N_y \\ N_{xy} \\ M_x \\ M_y \\ M_{xy} \\ V_x \\ V_y \end{Bmatrix} = \underbrace{\begin{bmatrix} A_{11} & A_{12} & A_{16} & B_{11} & B_{12} & B_{16} & 0 & 0 \\ A_{12} & A_{22} & A_{26} & B_{12} & B_{22} & B_{26} & 0 & 0 \\ A_{16} & A_{26} & A_{66} & B_{16} & B_{26} & B_{66} & 0 & 0 \\ B_{11} & B_{12} & B_{16} & D_{11} & D_{12} & D_{16} & 0 & 0 \\ B_{12} & B_{22} & B_{26} & D_{12} & D_{22} & D_{26} & 0 & 0 \\ B_{16} & B_{26} & B_{66} & D_{16} & D_{26} & D_{66} & 0 & 0 \\ 0 & 0 & 0 & 0 & 0 & 0 & \widetilde{S}_{11} & \widetilde{S}_{12} \\ 0 & 0 & 0 & 0 & 0 & 0 & \widetilde{S}_{12} & \widetilde{S}_{22} \end{bmatrix}}_{[E]} \begin{Bmatrix} \epsilon_x^o \\ \epsilon_y^o \\ \gamma_{xy}^o \\ \kappa_x \\ \kappa_y \\ \kappa_{xy} \\ \gamma_{xz} \\ \gamma_{yz} \end{Bmatrix}, \tag{9.9}$$

where $[E]$ is the stiffness matrix for a plate element with shear deformations.

Frequently, the behavior of shells can be described by replacing the curved surface with small, flat elements. The stiffness matrices above are applicable to such flat shell elements.

9.3 Beam Element

For a beam element, the force–strain relationships are

arbitrary layup, no shear deformation, no restrained warping (Eq. 6.2)

$$\begin{Bmatrix} \widehat{N} \\ \widehat{M}_y \\ \widehat{M}_z \\ \widehat{T} \end{Bmatrix} = \underbrace{\begin{bmatrix} P_{11} & P_{12} & P_{13} & P_{14} \\ P_{12} & P_{22} & P_{23} & P_{24} \\ P_{13} & P_{23} & P_{33} & P_{34} \\ P_{14} & P_{24} & P_{34} & P_{44} \end{bmatrix}}_{[E]} \begin{Bmatrix} \epsilon_x^o \\ \frac{1}{\rho_y} \\ \frac{1}{\rho_z} \\ \vartheta \end{Bmatrix} \tag{9.10}$$

orthotropic, no shear deformation, no restrained warping (Eq. 6.8)

$$\begin{Bmatrix} \widehat{N} \\ \widehat{M}_y \\ \widehat{M}_z \\ \widehat{T} \end{Bmatrix} = \underbrace{\begin{bmatrix} \widehat{EA} & 0 & 0 & 0 \\ 0 & \widehat{EI}_{yy} & \widehat{EI}_{yz} & 0 \\ 0 & \widehat{EI}_{yz} & \widehat{EI}_{zz} & 0 \\ 0 & 0 & 0 & \widehat{GI}_t \end{bmatrix}}_{[E]} \begin{Bmatrix} \epsilon_x^o \\ \frac{1}{\rho_y} \\ \frac{1}{\rho_z} \\ \vartheta \end{Bmatrix} \tag{9.11}$$

orthotropic, no shear deformation, restrained warping (Eqs. 6.8 and 6.233)

$$\begin{Bmatrix} \widehat{N} \\ \widehat{M}_y \\ \widehat{M}_z \\ \widehat{M}_\omega \\ \widehat{T}_{sv} \end{Bmatrix} = \underbrace{\begin{bmatrix} \widehat{EA} & 0 & 0 & 0 & 0 \\ 0 & \widehat{EI}_{yy} & \widehat{EI}_{yz} & 0 & 0 \\ 0 & \widehat{EI}_{yz} & \widehat{EI}_{zz} & 0 & 0 \\ 0 & 0 & 0 & \widehat{EI}_\omega & 0 \\ 0 & 0 & 0 & 0 & \widehat{GI}_t \end{bmatrix}}_{[E]} \begin{Bmatrix} \epsilon_x^o \\ \frac{1}{\rho_y} \\ \frac{1}{\rho_z} \\ -\frac{d\vartheta}{dx} \\ \vartheta \end{Bmatrix} \tag{9.12}$$

orthotropic, shear deformation, restrained warping (Eqs. 7.30, 7.32, 7.34, 7.36)

$$\begin{Bmatrix} \widehat{N} \\ \widehat{M}_y \\ \widehat{M}_z \\ \widehat{M}_\omega \\ \widehat{T}_{sv} \\ \widehat{V}_y \\ \widehat{V}_z \\ \widehat{T}_\omega \end{Bmatrix} = \underbrace{\begin{bmatrix} \widehat{EA} & 0 & 0 & 0 & 0 & 0 & 0 & 0 \\ 0 & \widehat{EI}_{yy} & \widehat{EI}_{yz} & 0 & 0 & 0 & 0 & 0 \\ 0 & \widehat{EI}_{yz} & \widehat{EI}_{zz} & 0 & 0 & 0 & 0 & 0 \\ 0 & 0 & 0 & \widehat{EI}_\omega & 0 & 0 & 0 & 0 \\ 0 & 0 & 0 & 0 & \widehat{GI}_t & 0 & 0 & 0 \\ 0 & 0 & 0 & 0 & 0 & \widehat{S}_{yy} & \widehat{S}_{yz} & \widehat{S}_{y\omega} \\ 0 & 0 & 0 & 0 & 0 & \widehat{S}_{yz} & \widehat{S}_{zz} & \widehat{S}_{z\omega} \\ 0 & 0 & 0 & 0 & 0 & \widehat{S}_{y\omega} & \widehat{S}_{z\omega} & \widehat{S}_{\omega\omega} \end{bmatrix}}_{[E]} \begin{Bmatrix} \epsilon_x^o \\ -\frac{d\chi_z}{dx} \\ -\frac{d\chi_y}{dx} \\ -\frac{d\vartheta^R}{dx} \\ \vartheta \\ \gamma_y \\ \gamma_z \\ \vartheta^S \end{Bmatrix}, \tag{9.13}$$

where $[E]$ is the stiffness matrix for a beam element.

9.4 Sublaminate

A laminate consisting of several plies may be analyzed by either plate (flat shell) or three-dimensional elements (Fig. 9.2). For thick laminates neither of these

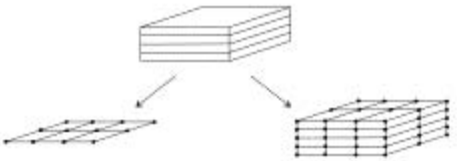

Figure 9.2: Thick laminate (top), analysis with plate elements (left), analysis with three-dimensional elements (right).

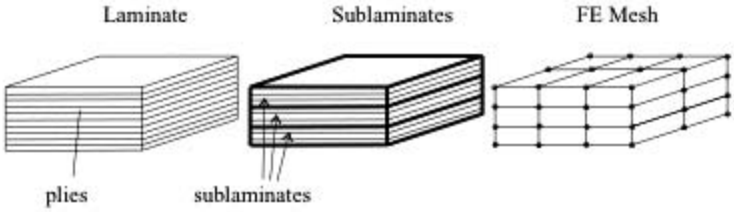

Figure 9.3: Thick laminate (left), sublaminates (middle), and the finite element mesh (right).

is practical. Plate elements give inaccurate results. Three-dimensional elements require that the material be uniform throughout the element, and, hence, an element must contain a single layer or adjacent identical layers. This may result in a very large number of elements, making the numerical computation difficult and often infeasible.

We can overcome these difficulties by dividing the laminate into sublaminates (Fig. 9.3). Each layer in the sublaminate may be monoclinic, orthotropic, transversely isotropic, or isotropic. The thickness of each element is the same as the thickness of the corresponding sublaminate. The stiffness matrix $[E]$ of such a sublaminate is defined by the relationship

$$\begin{Bmatrix} \overline{\sigma}_x \\ \overline{\sigma}_y \\ \overline{\sigma}_z \\ \overline{\tau}_{yz} \\ \overline{\tau}_{xz} \\ \overline{\tau}_{xy} \end{Bmatrix} = [E] \begin{Bmatrix} \overline{\epsilon}_x \\ \overline{\epsilon}_y \\ \overline{\epsilon}_z \\ \overline{\gamma}_{yz} \\ \overline{\gamma}_{xz} \\ \overline{\gamma}_{xy} \end{Bmatrix}. \tag{9.14}$$

The bar denotes average stresses and strains. It is convenient to represent this expression in terms of the compliance matrix $[J]$

$$\begin{Bmatrix} \overline{\epsilon}_x \\ \overline{\epsilon}_y \\ \overline{\epsilon}_z \\ \overline{\gamma}_{yz} \\ \overline{\gamma}_{xz} \\ \overline{\gamma}_{xy} \end{Bmatrix} = \underbrace{\begin{bmatrix} J_{11} & J_{12} & J_{13} & J_{14} & J_{15} & J_{16} \\ J_{21} & J_{22} & J_{23} & J_{24} & J_{25} & J_{26} \\ J_{31} & J_{32} & J_{33} & J_{34} & J_{35} & J_{36} \\ J_{41} & J_{42} & J_{43} & J_{44} & J_{45} & J_{46} \\ J_{51} & J_{52} & J_{53} & J_{54} & J_{55} & J_{56} \\ J_{61} & J_{62} & J_{63} & J_{64} & J_{65} & J_{66} \end{bmatrix}}_{[J]} \begin{Bmatrix} \overline{\sigma}_x \\ \overline{\sigma}_y \\ \overline{\sigma}_z \\ \overline{\tau}_{yz} \\ \overline{\tau}_{xz} \\ \overline{\tau}_{xy} \end{Bmatrix}, \tag{9.15}$$

where

$$[E] = [J]^{-1}. \tag{9.16}$$

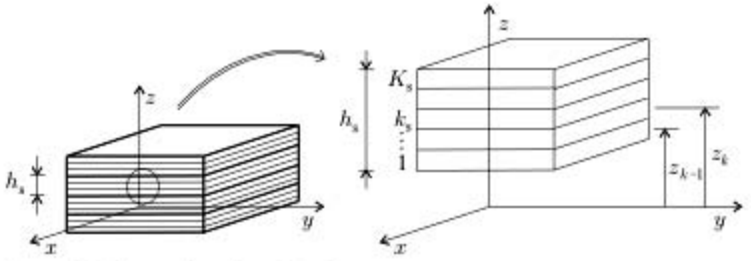

Figure 9.4: Illustration of a sublaminate.

The x,y,z coordinate system is shown in Figure 9.4. The average stresses are defined as

$$\begin{aligned}
\overline{\sigma}_x &= \frac{1}{h_s}\int_{(h_s)} \sigma_x dz = \frac{1}{h_s} N_x \qquad & \overline{\sigma}_z &= \sigma_z \\
\overline{\sigma}_y &= \frac{1}{h_s}\int_{(h_s)} \sigma_y dz = \frac{1}{h_s} N_y \qquad & \overline{\tau}_{yz} &= \tau_{yz} \\
\overline{\tau}_{xy} &= \frac{1}{h_s}\int_{(h_s)} \tau_{xy} dz = \frac{1}{h_s} N_{xy} \qquad & \overline{\tau}_{xz} &= \tau_{xz}.
\end{aligned} \tag{9.17}$$

The second equalities in the left-hand column are written by virtue of Eq. (3.9). The average strains are

$$\begin{aligned}
\overline{\epsilon}_z &= \frac{1}{h_s}\int_{(h_s)} \epsilon_z dz \qquad & \overline{\epsilon}_x &= \epsilon_x \\
\overline{\gamma}_{yz} &= \frac{1}{h_s}\int_{(h_s)} \gamma_{yz} dz \qquad & \overline{\epsilon}_y &= \epsilon_y \\
\overline{\gamma}_{xz} &= \frac{1}{h_s}\int_{(h_s)} \gamma_{xz} dz \qquad & \overline{\gamma}_{xy} &= \gamma_{xy},
\end{aligned} \tag{9.18}$$

where h_s is the thickness of the sublaminate (Fig. 9.4). The terms in the right-hand columns of Eqs. (9.17) and (9.18) show that the stresses σ_z, τ_{yz}, τ_{xz} and the strains ϵ_x, ϵ_y, γ_{xy} do not vary across the thickness.

In the following we derive the elements of the compliance matrix.

9.4.1 Step 1. Elements of [J] due to In-Plane Stresses

In this step we determine the elements in the first, second, and sixth columns of the matrix $[J]$. To this end, we impose the average in-plane stresses $\overline{\sigma}_x$, $\overline{\sigma}_y$, and $\overline{\tau}_{xy}$ on the sublaminate (Fig. 9.5, top). Since $\overline{\sigma}_z$, $\overline{\tau}_{yz}$, $\overline{\tau}_{xz}$ are zero, the stress–strain

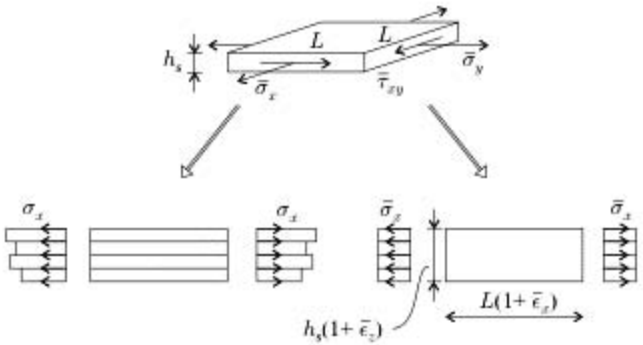

Figure 9.5: Illustration of Step 1. The ply stress and the corresponding average stress on the sublaminate.

relationship (Eq. 9.15) may be written as

$$\begin{Bmatrix} \bar{\epsilon}_x \\ \bar{\epsilon}_y \\ \bar{\gamma}_{xy} \end{Bmatrix} = \begin{bmatrix} J_{11} & J_{12} & J_{16} \\ J_{21} & J_{22} & J_{26} \\ J_{61} & J_{62} & J_{66} \end{bmatrix} \begin{Bmatrix} \bar{\sigma}_x \\ \bar{\sigma}_y \\ \bar{\tau}_{xy} \end{Bmatrix} \tag{9.19}$$

$$\{\bar{\epsilon}_z\} = [J_{31} \quad J_{32} \quad J_{36}] \begin{Bmatrix} \bar{\sigma}_x \\ \bar{\sigma}_y \\ \bar{\tau}_{xy} \end{Bmatrix} \tag{9.20}$$

$$\begin{Bmatrix} \bar{\gamma}_{yz} \\ \bar{\gamma}_{xz} \end{Bmatrix} = \begin{bmatrix} J_{41} & J_{42} & J_{46} \\ J_{51} & J_{52} & J_{56} \end{bmatrix} \begin{Bmatrix} \bar{\sigma}_x \\ \bar{\sigma}_y \\ \bar{\tau}_{xy} \end{Bmatrix}. \tag{9.21}$$

The strains are uniform across the thickness (Eq. 9.18). Under these conditions $\kappa_x, \kappa_y, \kappa_{xy}$ are zero, and we have (see Eqs. 3.21 and 3.7)

$$\begin{Bmatrix} N_x \\ N_y \\ N_{xy} \end{Bmatrix} = [A] \begin{Bmatrix} \epsilon_x^o \\ \epsilon_y^o \\ \gamma_{xy}^o \end{Bmatrix} = [A] \begin{Bmatrix} \epsilon_x \\ \epsilon_y \\ \gamma_{xy} \end{Bmatrix}, \tag{9.22}$$

where $[A]$ is the tensile stiffness matrix of the sublaminate. (The summation in Eq. 3.20 is performed from 1 to K_s, where K_s is the number of layers or ply groups in the sublaminate; see Fig. 9.4). For the sublaminate Eqs. (9.17), (9.18), and (9.22) yield

$$\begin{Bmatrix} \bar{\epsilon}_x \\ \bar{\epsilon}_y \\ \bar{\gamma}_{xy} \end{Bmatrix} = \underbrace{h_s [A]^{-1}}_{\begin{bmatrix} J_{11} & J_{12} & J_{16} \\ J_{21} & J_{22} & J_{26} \\ J_{61} & J_{62} & J_{66} \end{bmatrix}} \begin{Bmatrix} \bar{\sigma}_x \\ \bar{\sigma}_y \\ \bar{\tau}_{xy} \end{Bmatrix}. \tag{9.23}$$

By comparing Eqs. (9.19) and (9.23), we have

$$\begin{bmatrix} J_{11} & J_{12} & J_{16} \\ J_{21} & J_{22} & J_{26} \\ J_{61} & J_{62} & J_{66} \end{bmatrix} = h_s [A]^{-1}. \tag{9.24}$$

Owing to the Poisson effect, the in-plane forces introduce a normal strain ϵ_z in the z direction. For a single layer this strain is (see Eq. 2.133)

$$\epsilon_z = [\overline{S}_{13} \quad \overline{S}_{23} \quad \overline{S}_{36}] \begin{Bmatrix} \sigma_x \\ \sigma_y \\ \tau_{xy} \end{Bmatrix}, \tag{9.25}$$

where σ_x, σ_y, and τ_{xy} are the stresses in the plies. The average normal stress $\overline{\sigma}_x$ across the laminate and the normal ply stress σ_x are illustrated in Figure 9.5 (bottom). The stresses in a single layer are (Eq. 3.13)

$$\begin{Bmatrix} \sigma_x \\ \sigma_y \\ \tau_{xy} \end{Bmatrix} = [\overline{Q}] \begin{Bmatrix} \epsilon_x \\ \epsilon_y \\ \gamma_{xy} \end{Bmatrix}. \tag{9.26}$$

Equations (9.25), (9.26), (9.23), and (9.18) give

$$\epsilon_z = [\overline{S}_{13} \quad \overline{S}_{23} \quad \overline{S}_{36}][\overline{Q}] h_s [A]^{-1} \begin{Bmatrix} \overline{\sigma}_x \\ \overline{\sigma}_y \\ \overline{\tau}_{xy} \end{Bmatrix}. \tag{9.27}$$

By combining Eqs. (9.18) and (9.27), and by replacing the integral with a summation, for the sublaminate we obtain

$$\overline{\epsilon}_z = \underbrace{\sum_{k=1}^{K_s} ([\overline{S}_{13} \quad \overline{S}_{23} \quad \overline{S}_{36}](z_k - z_{k-1})[\overline{Q}]_k)[A]^{-1}}_{[J_{31} \quad J_{32} \quad J_{36}]} \begin{Bmatrix} \overline{\sigma}_x \\ \overline{\sigma}_y \\ \overline{\tau}_{xy} \end{Bmatrix}. \tag{9.28}$$

By comparing Eqs. (9.20) and (9.28), we have

$$[J_{31} \quad J_{32} \quad J_{36}] = \sum_{k=1}^{K_s} ([\overline{S}_{13} \quad \overline{S}_{23} \quad \overline{S}_{36}]_k (z_k - z_{k-1})[\overline{Q}]_k)[A]^{-1}, \tag{9.29}$$

where z_k, z_{k-1} are illustrated in Figure 9.4. Since $\overline{\tau}_{yz} = \overline{\tau}_{xz} = 0$, we have that γ_{yz} and γ_{xz} are zero (Eqs. 2.26 and 2.21), and Eq. (9.21) now becomes

$$\begin{Bmatrix} 0 \\ 0 \end{Bmatrix} = \begin{bmatrix} J_{41} & J_{42} & J_{46} \\ J_{51} & J_{52} & J_{56} \end{bmatrix} \begin{Bmatrix} \overline{\sigma}_x \\ \overline{\sigma}_y \\ \overline{\tau}_{xy} \end{Bmatrix}. \tag{9.30}$$

To satisfy this equation, the preceding elements of the compliance matrix must be zero:

$$\begin{bmatrix} J_{41} & J_{42} & J_{46} \\ J_{51} & J_{52} & J_{56} \end{bmatrix} = \begin{bmatrix} 0 & 0 & 0 \\ 0 & 0 & 0 \end{bmatrix}. \tag{9.31}$$

9.4.2 Step 2. Elements of [J] due to Out-of-Plane Normal Stresses

In this step we determine the elements in the third column of the matrix $[J]$. To accomplish this we consider a sublaminate in which there are only σ_z stresses. To form such a sublaminate, first we consider a sublaminate restrained along its edges ($\epsilon_x = \epsilon_y = \gamma_{xy} = 0$) and apply a uniform stress $\sigma_z = \overline{\sigma}_z$ (Stage 1, Fig. 9.6), which introduces in-plane stresses $\overline{\sigma}_x$, $\overline{\sigma}_y$, $\overline{\tau}_{xy}$. Second, we apply in-plane stresses $-\overline{\sigma}_x$, $-\overline{\sigma}_y$, $-\overline{\tau}_{xy}$ (Stage 2, Fig. 9.6). Third, we superimpose Stages 1 and 2 and arrive at the sublaminate inside which the in-plane average stresses $\overline{\sigma}_x$, $\overline{\sigma}_y$, $\overline{\tau}_{xy}$ and the transverse shear stresses $\overline{\tau}_{yz}$, $\overline{\tau}_{xz}$ are zero and the stress–strain relationships (Eq. 9.15) are

$$\begin{Bmatrix} \overline{\epsilon}_x \\ \overline{\epsilon}_y \\ \overline{\gamma}_{xy} \end{Bmatrix} = \begin{bmatrix} J_{13} \\ J_{23} \\ J_{63} \end{bmatrix} \overline{\sigma}_z \tag{9.32}$$

$$\overline{\epsilon}_z = J_{33}\overline{\sigma}_z \tag{9.33}$$

$$\begin{Bmatrix} \overline{\gamma}_{yz} \\ \overline{\gamma}_{xz} \end{Bmatrix} = \begin{bmatrix} J_{43} \\ J_{53} \end{bmatrix} \overline{\sigma}_z. \tag{9.34}$$

Stage 1. Following the outline above, we apply σ_z to the sublaminate, which is restrained along the edges ($\epsilon_x = \epsilon_y = \gamma_{xy} = 0$). For a single layer, Eqs. (2.27) and

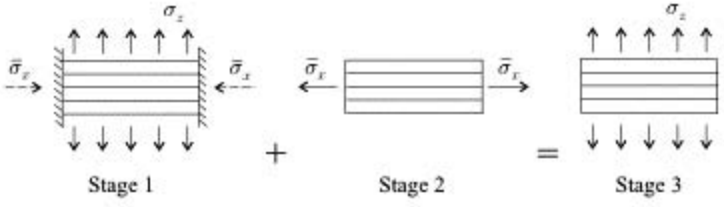

Figure 9.6: Illustration of Step 2. Sublaminate restrained along its edges subjected to σ_z and the resulting stress $\overline{\sigma}_x$ (Stage 1); unrestrained sublaminate subjected to $\overline{\sigma}_x$ (Stage 2); unrestrained sublaminate subjected to σ_z (Stage 3); ($\overline{\sigma}_y$ and $\overline{\tau}_{xy}$ are not shown).

(2.20) give

$$\sigma_z = \overline{C}_{33}\epsilon_z \tag{9.35}$$

$$\begin{Bmatrix} \sigma_x \\ \sigma_y \\ \tau_{xy} \end{Bmatrix} = \begin{Bmatrix} \overline{C}_{13} \\ \overline{C}_{23} \\ \overline{C}_{63} \end{Bmatrix} \epsilon_z. \tag{9.36}$$

These equations may be rearranged to yield

$$\epsilon_z = \frac{1}{\overline{\overline{C}}_{33}}\sigma_z \tag{9.37}$$

$$\begin{Bmatrix} \sigma_x \\ \sigma_y \\ \tau_{xy} \end{Bmatrix} = \begin{Bmatrix} \overline{C}_{13} \\ \overline{C}_{23} \\ \overline{C}_{63} \end{Bmatrix} \frac{1}{\overline{\overline{C}}_{33}}\sigma_z. \tag{9.38}$$

By combining Eqs. (9.37) and (9.18), and by replacing the integrals by summations, for the sublaminate we obtain

$$\overline{\epsilon}_z = \frac{1}{h_s}\sum_{k=1}^{K_s}\left(\frac{z_k - z_{k-1}}{(\overline{\overline{C}}_{33})_k}\right)\sigma_z. \tag{9.39}$$

Equations (9.38) and (9.18) yield

$$\begin{Bmatrix} \overline{\sigma}_x \\ \overline{\sigma}_y \\ \overline{\tau}_{xy} \end{Bmatrix} = \frac{1}{h_s}\sum_{k=1}^{K_s}\left(\begin{Bmatrix} \overline{C}_{13} \\ \overline{C}_{23} \\ \overline{C}_{63} \end{Bmatrix}_k \frac{z_k - z_{k-1}}{(\overline{\overline{C}}_{33})_k}\right)\sigma_z. \tag{9.40}$$

This equation gives the in-plane stresses in the restrained sublaminate.

Stage 2. We apply the equal and opposite of the stresses, calculated by Eq. (9.40), to the sublaminate. The corresponding strains are obtained from Eqs. (9.28), (9.23), and (9.40). Equations (9.28) and (9.40) result in

$$\begin{aligned}\overline{\epsilon}_z &= -\begin{bmatrix} J_{31} & J_{32} & J_{36} \end{bmatrix}\begin{Bmatrix} \overline{\sigma}_x \\ \overline{\sigma}_y \\ \overline{\tau}_{xy} \end{Bmatrix} \\ &= -\begin{bmatrix} J_{31} & J_{32} & J_{36} \end{bmatrix}\frac{1}{h_s}\sum_{k=1}^{K_s}\left(\begin{Bmatrix} \overline{C}_{13} \\ \overline{C}_{23} \\ \overline{C}_{63} \end{Bmatrix}_k \frac{z_k - z_{k-1}}{(\overline{\overline{C}}_{33})_k}\right)\sigma_z.\end{aligned} \tag{9.41}$$

Equations (9.23) and (9.40) give

$$\begin{aligned}\begin{Bmatrix} \overline{\epsilon}_x \\ \overline{\epsilon}_y \\ \overline{\gamma}_{xy} \end{Bmatrix} &= -\begin{bmatrix} J_{11} & J_{12} & J_{16} \\ J_{21} & J_{22} & J_{26} \\ J_{61} & J_{62} & J_{66} \end{bmatrix}\begin{Bmatrix} \overline{\sigma}_x \\ \overline{\sigma}_y \\ \overline{\tau}_{xy} \end{Bmatrix} \\ &= -\begin{bmatrix} J_{11} & J_{12} & J_{16} \\ J_{21} & J_{22} & J_{26} \\ J_{61} & J_{62} & J_{66} \end{bmatrix}\frac{1}{h_s}\sum_{k=1}^{K_s}\left(\begin{Bmatrix} \overline{C}_{13} \\ \overline{C}_{23} \\ \overline{C}_{63} \end{Bmatrix}_k \frac{z_k - z_{k-1}}{(\overline{\overline{C}}_{33})_k}\right)\sigma_z.\end{aligned} \tag{9.42}$$

Stage 3. We combine Eqs. (9.39), (9.41), and (9.42) to obtain the strains of a sublaminate subjected only to the out-of-plane stress σ_z

$$\bar{\epsilon}_z = \left(\frac{1}{h_s} \sum_{k=1}^{K_s} \left(\frac{z_k - z_{k-1}}{(\bar{C}_{33})_k} \right) - [J_{31} \quad J_{32} \quad J_{36}] \frac{1}{h_s} \sum_{k=1}^{K_s} \left(\begin{Bmatrix} \bar{C}_{13} \\ \bar{C}_{23} \\ \bar{C}_{63} \end{Bmatrix}_k \frac{z_k - z_{k-1}}{(\bar{C}_{33})_k} \right) \right) \sigma_z \tag{9.43}$$

$$\begin{Bmatrix} \bar{\epsilon}_x \\ \bar{\epsilon}_y \\ \bar{\gamma}_{xy} \end{Bmatrix} = - \begin{bmatrix} J_{11} & J_{12} & J_{16} \\ J_{21} & J_{22} & J_{26} \\ J_{61} & J_{62} & J_{66} \end{bmatrix} \frac{1}{h_s} \sum_{k=1}^{K_s} \left(\begin{Bmatrix} \bar{C}_{13} \\ \bar{C}_{23} \\ \bar{C}_{63} \end{Bmatrix}_k \frac{z_k - z_{k-1}}{(\bar{C}_{33})_k} \right) \sigma_z. \tag{9.44}$$

Comparisons of Eqs. (9.32) and (9.33) with Eqs. (9.43) and (9.44) yield

$$\begin{bmatrix} J_{13} \\ J_{23} \\ J_{63} \end{bmatrix} = - \begin{bmatrix} J_{11} & J_{12} & J_{16} \\ J_{21} & J_{22} & J_{26} \\ J_{61} & J_{62} & J_{66} \end{bmatrix} \frac{1}{h_s} \sum_{k=1}^{K_s} \left(\begin{Bmatrix} \bar{C}_{13} \\ \bar{C}_{23} \\ \bar{C}_{63} \end{Bmatrix}_k \frac{z_k - z_{k-1}}{(\bar{C}_{33})_k} \right) \tag{9.45}$$

$$J_{33} = \frac{1}{h_s} \sum_{k=1}^{K_s} \left(\frac{z_k - z_{k-1}}{(\bar{C}_{33})_k} \right) - [J_{31} \quad J_{32} \quad J_{36}] \frac{1}{h_s} \sum_{k=1}^{K_s} \left(\begin{Bmatrix} \bar{C}_{13} \\ \bar{C}_{23} \\ \bar{C}_{63} \end{Bmatrix}_k \frac{z_k - z_{k-1}}{(\bar{C}_{33})_k} \right). \tag{9.46}$$

Since $\bar{\tau}_{yz} = \bar{\tau}_{xz} = 0$, we have that γ_{yz} and γ_{xz} are zero (Eqs. 2.26 and 2.21), and Eq. (9.34) becomes

$$\begin{Bmatrix} 0 \\ 0 \end{Bmatrix} = \begin{bmatrix} J_{43} \\ J_{53} \end{bmatrix} \bar{\sigma}_z. \tag{9.47}$$

To satisfy this equation, the preceding elements of the compliance matrix must be zero

$$\begin{bmatrix} J_{43} \\ J_{53} \end{bmatrix} = \begin{bmatrix} 0 \\ 0 \end{bmatrix}. \tag{9.48}$$

9.4.3 Step 3. Elements of [J] due to Out-of-Plane Shear Stresses

In this step we determine the elements in the fourth and fifth column of the matrix $[J]$.

To accomplish this we apply the shear stresses τ_{yz}, τ_{xz} on the sublaminate (Fig. 9.7). Since $\bar{\sigma}_x$, $\bar{\sigma}_y$, $\bar{\sigma}_z$, $\bar{\tau}_{xy}$ are zero, the stress–strain relationships are

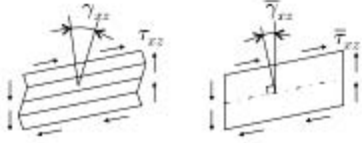

Figure 9.7: Illustration of Step 3. Stress τ_{xz} and strain γ_{xz} on a sublaminate subjected to transverse shear loads (left) and the corresponding average stress $\bar{\tau}_{xz}$ and average strain $\bar{\gamma}_{xz}$ (right).

(Eq. 9.15)

$$\begin{Bmatrix} \overline{\gamma}_{yz} \\ \overline{\gamma}_{xz} \end{Bmatrix} = \begin{bmatrix} J_{44} & J_{45} \\ J_{54} & J_{55} \end{bmatrix} \begin{Bmatrix} \overline{\tau}_{yz} \\ \overline{\tau}_{xz} \end{Bmatrix} \tag{9.49}$$

$$\begin{Bmatrix} \overline{\epsilon}_x \\ \overline{\epsilon}_y \\ \overline{\epsilon}_z \\ \overline{\gamma}_{xy} \end{Bmatrix} = \begin{bmatrix} J_{14} & J_{15} \\ J_{24} & J_{25} \\ J_{34} & J_{35} \\ J_{64} & J_{65} \end{bmatrix} \begin{Bmatrix} \overline{\tau}_{yz} \\ \overline{\tau}_{xz} \end{Bmatrix}. \tag{9.50}$$

For a single layer, we have (see Eqs. 2.26 and 2.21)

$$\begin{Bmatrix} \gamma_{yz} \\ \gamma_{xz} \end{Bmatrix} = \begin{bmatrix} \overline{S}_{44} & \overline{S}_{45} \\ \overline{S}_{45} & \overline{S}_{55} \end{bmatrix} \begin{Bmatrix} \tau_{yz} \\ \tau_{xz} \end{Bmatrix}. \tag{9.51}$$

By combining Eqs. (9.18) and (9.51) and by replacing the integrals by summations, for the sublaminate we obtain

$$\begin{Bmatrix} \overline{\gamma}_{yz} \\ \overline{\gamma}_{xz} \end{Bmatrix} = \frac{1}{h_s} \sum_{k=1}^{K_s} \left((z_k - z_{k-1}) \begin{bmatrix} \overline{S}_{44} & \overline{S}_{45} \\ \overline{S}_{45} & \overline{S}_{55} \end{bmatrix}_k \right) \begin{Bmatrix} \tau_{yz} \\ \tau_{xz} \end{Bmatrix}. \tag{9.52}$$

By comparing Eqs. (9.49) and (9.52), we have

$$\begin{bmatrix} J_{44} & J_{45} \\ J_{54} & J_{55} \end{bmatrix} = \frac{1}{h_s} \sum_{k=1}^{K_s} \left((z_k - z_{k-1}) \begin{bmatrix} \overline{S}_{44} & \overline{S}_{45} \\ \overline{S}_{45} & \overline{S}_{55} \end{bmatrix}_k \right). \tag{9.53}$$

For the sublaminate subjected to transverse shear stresses resulting in $\overline{\gamma}_{yz}$ and $\overline{\gamma}_{xz}$, with all other strains being zero, Eq. (9.50) becomes

$$\begin{Bmatrix} 0 \\ 0 \\ 0 \\ 0 \end{Bmatrix} = \begin{bmatrix} J_{14} & J_{15} \\ J_{24} & J_{25} \\ J_{34} & J_{35} \\ J_{64} & J_{65} \end{bmatrix} \begin{Bmatrix} \overline{\tau}_{yz} \\ \overline{\tau}_{xz} \end{Bmatrix}. \tag{9.54}$$

To satisfy this equation, the preceding elements of the compliance matrix must be zero as follows:

$$\begin{bmatrix} J_{14} & J_{15} \\ J_{24} & J_{25} \\ J_{34} & J_{35} \\ J_{64} & J_{65} \end{bmatrix} = \begin{bmatrix} 0 & 0 \\ 0 & 0 \\ 0 & 0 \\ 0 & 0 \end{bmatrix}. \tag{9.55}$$

Table 9.1. The equations used for calculating the nonzero elements of the $[J]$ compliance matrix

$$\begin{bmatrix} J_{11}\ldots J_{16} \\ \vdots \ddots \vdots \\ J_{61}\ldots J_{66} \end{bmatrix} \Longrightarrow \begin{array}{c} \text{Equation numbers} \\ \hline \begin{bmatrix} 9.24 & 9.24 & 9.45 & - & - & 9.24 \\ 9.24 & 9.24 & 9.45 & - & - & 9.24 \\ 9.29 & 9.29 & 9.46 & - & - & 9.29 \\ - & - & - & 9.53 & 9.53 & - \\ - & - & - & 9.53 & 9.53 & - \\ 9.24 & 9.24 & 9.45 & - & - & 9.24 \end{bmatrix} \end{array}$$

9.4.4 Step 4. The Stiffness Matrix

By combining the results of the preceding three steps, we obtain the following strain–stress relationship:

$$\begin{Bmatrix} \overline{\epsilon}_x \\ \overline{\epsilon}_y \\ \overline{\epsilon}_z \\ \overline{\gamma}_{yz} \\ \overline{\gamma}_{xz} \\ \overline{\gamma}_{xy} \end{Bmatrix} = \underbrace{\begin{bmatrix} J_{11} & J_{12} & J_{13} & 0 & 0 & J_{16} \\ J_{21} & J_{22} & J_{23} & 0 & 0 & J_{26} \\ J_{31} & J_{32} & J_{33} & 0 & 0 & J_{36} \\ 0 & 0 & 0 & J_{44} & J_{45} & 0 \\ 0 & 0 & 0 & J_{54} & J_{55} & 0 \\ J_{61} & J_{62} & J_{63} & 0 & 0 & J_{66} \end{bmatrix}}_{[J]=[E]^{-1}} \begin{Bmatrix} \overline{\sigma}_x \\ \overline{\sigma}_y \\ \overline{\sigma}_z \\ \overline{\tau}_{yz} \\ \overline{\tau}_{xz} \\ \overline{\tau}_{xy} \end{Bmatrix}, \tag{9.56}$$

where $[J]$ is the compliance matrix of the sublaminate. The stiffness matrix is

$$[E] = [J]^{-1}. \tag{9.57}$$

We note that both $[J]$ and $[E]$ are symmetrical. The equations to be used for calculating the elements of $[J]$ are summarized in Table 9.1.

Under plane-stress condition, the strain–stress relationship is

$$\begin{Bmatrix} \overline{\epsilon}_x \\ \overline{\epsilon}_y \\ \overline{\gamma}_{xy} \end{Bmatrix} = \begin{bmatrix} J_{11} & J_{12} & J_{16} \\ J_{21} & J_{22} & J_{26} \\ J_{61} & J_{62} & J_{66} \end{bmatrix} \begin{Bmatrix} \overline{\sigma}_x \\ \overline{\sigma}_y \\ \overline{\tau}_{xy} \end{Bmatrix}. \tag{9.58}$$

Therefore, under plane–stress condition we need to determine only those elements that appear in this expression.

9.1 Example. *Calculate the stiffness matrix $[J]$ of a sublaminate made of graphite epoxy unidirectional plies. The material properties are given in Table 3.6 (page 81). The layup is $[0_2/45_2/0_2/45_2]$ (Fig. 9.8). The thickness of the sublaminate is $h_s =$ 0.0008 m.*

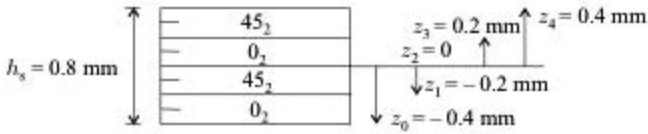

Figure 9.8: The sublaminate in Example 9.1.

Solution. First, we determine the stiffness and compliance matrices. The stiffness matrices $[\overline{Q}]^0$ and $[\overline{Q}]^{45}$ for the plies are given by Eqs. (3.49) and (3.52) as follows:

$$[\overline{Q}]^0 = \begin{bmatrix} 148.87 & 2.91 & 0 \\ 2.91 & 9.71 & 0 \\ 0 & 0 & 4.55 \end{bmatrix} 10^9 \frac{\text{N}}{\text{m}^2} \quad [\overline{Q}]^{45} = \begin{bmatrix} 45.65 & 36.55 & 34.79 \\ 36.55 & 45.65 & 34.79 \\ 34.79 & 34.79 & 38.19 \end{bmatrix} 10^9 \frac{\text{N}}{\text{m}^2}. \tag{9.59}$$

The compliance matrix for the 0-degree ply is (Eq. 2.224)

$$[S] = [\overline{S}]^0 = \begin{bmatrix} 6.76 & -2.03 & -2.03 & 0 & 0 & 0 \\ -2.03 & 103.63 & -62.18 & 0 & 0 & 0 \\ -2.03 & -62.18 & 103.63 & 0 & 0 & 0 \\ 0 & 0 & 0 & 331.61 & 0 & 0 \\ 0 & 0 & 0 & 0 & 219.78 & 0 \\ 0 & 0 & 0 & 0 & 0 & 219.78 \end{bmatrix} 10^{-12} \frac{\text{m}^2}{\text{N}}. \tag{9.60}$$

The compliance matrix for the 45-degree ply is (Eq. 2.194, $[S']$ is replaced by $[\overline{S}]$) as follows:

$$[\overline{S}]^{45} = [\hat{T}_\epsilon^r][S][\hat{T}_\sigma^r]^{-1}. \tag{9.61}$$

The transformation matrices $[\hat{T}_\sigma^r]$ and $[\hat{T}_\epsilon^r]$ are given in Tables 2.15 (page 51) and 2.16 (page 53). The angle is 45°; hence, we have $c_r = \cos 45^\circ = s_r = \sin 45^\circ = 0.707$. The elements of the $[\overline{S}]^{45}$ matrix are

$$[\overline{S}]^{45} = \begin{bmatrix} 81.53 & -28.36 & -32.10 & 0 & 0 & -48.44 \\ -28.36 & 81.53 & -32.10 & 0 & 0 & -48.44 \\ -32.10 & -32.10 & 103.63 & 0 & 0 & 60.15 \\ 0 & 0 & 0 & 275.69 & -55.91 & 0 \\ 0 & 0 & 0 & -55.91 & 275.69 & 0 \\ -48.44 & -48.44 & 60.15 & 0 & 0 & 114.44 \end{bmatrix} 10^{-12} \frac{\text{m}^2}{\text{N}}. \tag{9.62}$$

The stiffness matrices are ($[\overline{C}] = [\overline{S}]^{-1}$)

$$[\overline{C}]^0 = \begin{bmatrix} 152.47 & 7.46 & 7.46 & 0 & 0 & 0 \\ 7.46 & 15.44 & 9.41 & 0 & 0 & 0 \\ 7.46 & 9.41 & 15.44 & 0 & 0 & 0 \\ 0 & 0 & 0 & 3.016 & 0 & 0 \\ 0 & 0 & 0 & 0 & 4.55 & 0 \\ 0 & 0 & 0 & 0 & 0 & 4.55 \end{bmatrix} 10^9 \frac{\text{N}}{\text{m}^2} \tag{9.63}$$

$$[\overline{C}]^{45} = \begin{bmatrix} 50.26 & 41.16 & 8.43 & 0 & 0 & 34.26 \\ 41.16 & 50.26 & 8.43 & 0 & 0 & 34.26 \\ 8.43 & 8.43 & 15.44 & 0 & 0 & -0.98 \\ 0 & 0 & 0 & 3.783 & 0.767 & 0 \\ 0 & 0 & 0 & 0.767 & 3.783 & 0 \\ 34.26 & 34.26 & -0.98 & 0 & 0 & 38.25 \end{bmatrix} 10^9 \frac{\text{N}}{\text{m}^2}. \tag{9.64}$$

The stiffness matrix $[A]$ is (Table 3.9, page 86)

$$[A] = \begin{bmatrix} 77.81 & 15.79 & 13.92 \\ 15.79 & 22.14 & 13.92 \\ 13.92 & 13.92 & 17.10 \end{bmatrix} 10^6 \frac{\text{N}}{\text{m}}. \tag{9.65}$$

We now proceed to determine the elements of the $[J]$ matrix. Equation (9.24) yields

$$\begin{bmatrix} J_{11} & J_{12} & J_{16} \\ J_{21} & J_{22} & J_{26} \\ J_{61} & J_{62} & J_{66} \end{bmatrix} = h_s [A]^{-1} = \begin{bmatrix} 12.38 & -5.10 & -5.92 \\ -5.10 & 76.08 & -57.78 \\ -5.92 & -57.78 & 98.65 \end{bmatrix} 10^{-12} \frac{\text{m}^2}{\text{N}}. \tag{9.66}$$

From Eq. (9.29) we have

$$[J_{31} \quad J_{32} \quad J_{36}] = \sum_{k=1}^{K_s} ([\overline{S}_{13} \quad \overline{S}_{23} \quad \overline{S}_{36}]_k (z_k - z_{k-1}) [\overline{Q}]_k)[A]^{-1}, \tag{9.67}$$

where K_s is the total number of ply groups ($K_s = 4$) and z_k is the distance from the midplane to the ply (Fig. 9.8). Substitution of the numerical values into Eq. (9.67) yields

$$[J_{31} \quad J_{32} \quad J_{36}] = [-3.608 \quad -43.162 \quad 39.554] \times 10^{-12} \frac{\text{m}^2}{\text{N}}. \tag{9.68}$$

Equation (9.45) is

$$\begin{bmatrix} J_{13} \\ J_{23} \\ J_{63} \end{bmatrix} = -\begin{bmatrix} J_{11} & J_{12} & J_{16} \\ J_{21} & J_{22} & J_{26} \\ J_{61} & J_{62} & J_{66} \end{bmatrix} \frac{1}{h_s} \sum_{k=1}^{K_s} \left(\left\{ \begin{matrix} \overline{C}_{13} \\ \overline{C}_{23} \\ \overline{C}_{63} \end{matrix} \right\}_k \frac{z_k - z_{k-1}}{(\overline{C}_{33})_k} \right)$$

$$= \begin{bmatrix} -3.608 \\ -43.162 \\ 39.554 \end{bmatrix} 10^{-12} \frac{\text{m}^2}{\text{N}}. \tag{9.69}$$

Equation (9.46) gives

$$J_{33} = \frac{1}{h_s} \sum_{k=1}^{K_s} \left(\frac{z_k - z_{k-1}}{(\overline{C}_{33})_k} \right) - [J_{31} \quad J_{32} \quad J_{36}] \frac{1}{h_s} \sum_{k=1}^{K_s} \left(\left\{ \begin{matrix} \overline{C}_{13} \\ \overline{C}_{23} \\ \overline{C}_{63} \end{matrix} \right\}_k \frac{z_k - z_{k-1}}{(\overline{C}_{33})_k} \right)$$

$$= 92.80 \times 10^{-12} \frac{\text{m}^2}{\text{N}}. \tag{9.70}$$

Equation (9.53) yields

$$\begin{bmatrix} J_{44} & J_{45} \\ J_{54} & J_{55} \end{bmatrix} = \frac{1}{h_s} \sum_{k=1}^{K_s} \left((z_k - z_{k-1}) \begin{bmatrix} \overline{S}_{44} & \overline{S}_{45} \\ \overline{S}_{45} & \overline{S}_{55} \end{bmatrix}_k \right) \tag{9.71}$$

$$= \begin{bmatrix} 303.65 & -27.96 \\ -27.96 & 247.74 \end{bmatrix} 10^{-12} \frac{\text{m}^2}{\text{N}}. \tag{9.72}$$

The $[J]$ matrix is

$$[J] = \begin{bmatrix} 12.38 & -5.10 & -3.61 & 0 & 0 & -5.92 \\ -5.10 & 76.08 & -43.16 & 0 & 0 & -57.78 \\ -3.61 & -43.16 & 92.80 & 0 & 0 & 39.55 \\ 0 & 0 & 0 & 303.65 & -27.96 & 0 \\ 0 & 0 & 0 & -27.96 & 247.74 & 0 \\ -5.92 & -57.78 & 39.55 & 0 & 0 & 98.65 \end{bmatrix} 10^{-12} \frac{\text{m}^2}{\text{N}}. \tag{9.73}$$

The stiffness matrix of the sublaminate is

$$[E] = [J]^{-1} = \begin{bmatrix} 101.35 & 24.32 & 7.95 & 0 & 0 & 17.14 \\ 24.32 & 32.84 & 8.92 & 0 & 0 & 17.11 \\ 7.95 & 8.92 & 15.44 & 0 & 0 & -0.489 \\ 0 & 0 & 0 & 3.33 & 0.376 & 0 \\ 0 & 0 & 0 & 0.376 & 4.08 & 0 \\ 17.14 & 17.11 & -0.489 & 0 & 0 & 21.39 \end{bmatrix} 10^{9} \frac{\text{N}}{\text{m}^2}. \tag{9.74}$$

Failure Criteria

Failure of fiber-reinforced composites may be caused by fiber buckling, fiber breakage, matrix cracking, delamination, or by a combination of these factors (Fig. 10.1). Local fiber buckling, or microbuckling, reduces the compressive stiffness and strength of the laminate. Microbuckling does not necessarily lead to immediate failure because the surrounding matrix supports the fibers. The properties of the fibers and the matrix greatly affect the onset and magnitude of fiber buckling and the resulting losses in the compressive properties of the laminate.

One of the main roles of the fibers is to carry tensile loads. When dry fibers (with no matrix surrounding them) break, they, of course, can no longer carry tensile loads. When the fibers are embedded in a matrix, the matrix acts as a bridge about the break and transmits the load across the gap created by the breakage as well from the broken to the adjacent fibers. Fiber bridging, as this phenomenon is called, is the main reason that the tensile strengths of unidirectional, continuous fiber-reinforced composites are higher than the tensile strengths of dry fiber bundles.

Matrix cracking frequently occurs in composite laminates. In itself, matrix cracking generally does not result in ultimate failure of a laminate. Nonetheless, matrix cracks have many detrimental effects: they facilitate moisture absorbtion, reduce the matrix-dominated stiffnesses of the laminate and, last but not least, may propagate into the interface between adjacent layers, initiating delamination.

Delamination is a separation of adjacent layers that may be introduced either during manufacture or subsequently by loads applied to the laminate. For example, loads due to transverse impact by an object on the laminate are a frequent cause of delamination. Delamination reduces the bending stiffness and strength as well as the load carrying capability of the laminate under compression. Significantly, under repeated loading the size of the delamination may increase to a critical point. Like the behavior of a crack in metal, once the critical size is reached, the growth of the delamination becomes unstable, leading to a rapid loss of compressive strength.

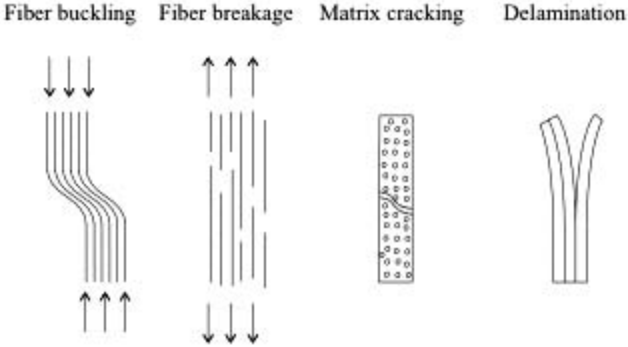

Figure 10.1: Typical failure modes of composites.

Designers would be well served by mechanism-based (physical) theories that would indicate the load at which failure occurs as well as the mode of failure. Although such theories have been proposed,[1,2] none is as yet at the stage where it could be applied in practical engineering design. Instead, frequently, ply–stress-based failure theories are used.[3,4] According to these theories the criterion for failure in any one of the plies is

$$f(\sigma_1, \sigma_2, \sigma_3, \tau_{23}, \tau_{13}, \tau_{12}, F_1, F_2, \ldots) \begin{cases} < 1 & \text{no failure} \\ = 1 & \text{failure limit}, \\ > 1 & \text{failure} \end{cases} \tag{10.1}$$

where $\sigma_1, \ldots, \tau_{12}$ are the stresses in the ply and $F_1, F_2, \ldots$ are strength parameters. The criterion expressed by Eq. (10.1) is established in every ply, and failure is taken to occur when any one of the plies fails (first-ply failure).

Here, we present three failure criteria for composites based on the aforementioned concept: the quadratic, the maximum stress, and the maximum strain failure criteria. These criteria offer results that are sufficiently accurate for many (but by no means all) problems of practical interest. For this reason, in spite of their shortcomings, they are relevant to the engineer. Nonetheless, the reader is warned to be cognizant of the following significant limits of the criteria listed above:

- Each criterion provides only the load at which first-ply failure occurs, that is, the load at which the linear load-displacement curve first changes (Fig. 10.2). Under the load set that causes first-ply failure, the laminate does not necessarily fail because other undamaged plies can still carry load. As the applied loads

[1] R. F. Gibson, *Principles of Composite Material Mechanics*. McGraw-Hill, New York, 1994, pp. 114–126, 244–249, and 356–367.

[2] S. R. Swanson, *Advanced Composite Materials*. Prentice-Hall, Upper Saddle River, New Jersey, 1997, pp. 91–120, 123–147.

[3] R. E. Rowlands, Strength (Failure) Theories and Their Experimental Correlation. In: *Handbook of Composites*, Vol. 3. G. C. Sih and A. M. Skudra, eds., Elsevier, Amsterdam, 1985, pp. 71–125.

[4] M. N. Nahas, Survey of Failure and Post-Failure Theories of Laminated Fiber Reinforced Composites. *Journal of Composites Technology and Research*, Vol. 8, 138–153, 1986.

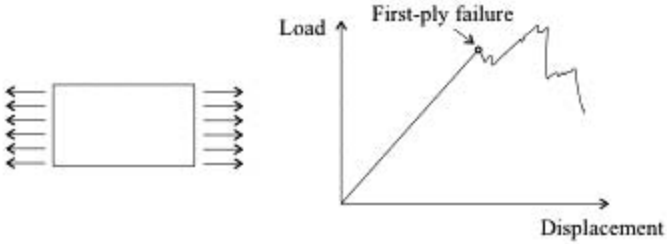

Figure 10.2: Load-displacement curve of a composite part.

are increased beyond those at which first-ply failure occurs, there will be a sequence of ply failures until the load set is reached at which every ply has failed. The loads at ultimate failure may be considerably higher than at first-ply failure. Therefore, criteria based on first-ply failure are conservative.

- None of the criteria sheds light on the failure mechanism or indicates the mode of failure.
- None of the criteria provides acceptable results for every condition of practical interest.
- Each criterion requires data, some of which are difficult to measure.
- Each criterion applies in regions inside the composite away from discontinuities such as holes, cracks, and edges. (Criteria applicable to plates containing a hole or a notch are given in Section 10.4.)

10.1 Quadratic Failure Criterion

The quadratic failure criterion includes stresses up to the second power. In its most general form the quadratic failure criterion states that no failure occurs when the inequality below (Eq. 10.2) is satisfied. This criterion and some of its simplified forms are variously referred to as Tsai-Wu, Hill, or Tsai–Hill failure criterion.

$$\begin{aligned} &F_1\sigma_1 + F_2\sigma_2 + F_3\sigma_3 + F_4\tau_{23} + F_5\tau_{13} + F_6\tau_{12} + \\ &F_{11}\sigma_1^2 + F_{22}\sigma_2^2 + F_{33}\sigma_3^2 + F_{44}\tau_{23}^2 + F_{55}\tau_{13}^2 + F_{66}\tau_{12}^2 + \\ &2(F_{12}\sigma_1\sigma_2 + F_{13}\sigma_1\sigma_3 + F_{14}\sigma_1\tau_{23} + F_{15}\sigma_1\tau_{13} + F_{16}\sigma_1\tau_{12} + \\ &F_{23}\sigma_2\sigma_3 + F_{24}\sigma_2\tau_{23} + F_{25}\sigma_2\tau_{13} + F_{26}\sigma_2\tau_{12} + F_{34}\sigma_3\tau_{23} + \\ &F_{35}\sigma_3\tau_{13} + F_{36}\sigma_3\tau_{12} + F_{45}\tau_{23}\tau_{13} + F_{46}\tau_{23}\tau_{12} + F_{56}\tau_{13}\tau_{12}) < 1, \end{aligned} \tag{10.2}$$

where $\sigma_1, \sigma_2, \ldots, \tau_{12}$ are the components (in the x_1, x_2, x_3 coordinate system) of the stress at the point of interest, that is, the stress that results from the applied loads, and the F's are strength parameters that depend on the material. No failure occurs when the left-hand side of Eq. (10.2) is less then unity. This means that the resultant stress is inside the failure surface (Fig. 10.3, left). On the failure surface (Fig. 10.3, middle), where the stress components are denoted by $\sigma_1^f, \sigma_2^f, \ldots, \tau_{12}^f$.

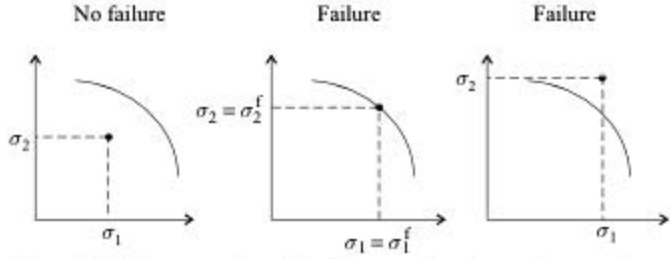

Figure 10.3: Representation of the failure surface when only σ_1 and σ_2 stresses are applied.

Eq. (10.2) is

$$F_1\sigma_1^f + F_2\sigma_2^f + F_3\sigma_3^f + F_4\tau_{23}^f + F_5\tau_{13}^f + F_6\tau_{12}^f + F_{11}\left(\sigma_1^f\right)^2 + F_{22}\left(\sigma_2^f\right)^2 + F_{33}\left(\sigma_3^f\right)^2 + F_{44}\left(\tau_{23}^f\right)^2 + F_{55}\left(\tau_{13}^f\right)^2 + F_{66}\left(\tau_{12}^f\right)^2 + 2\left(F_{12}\sigma_1^f\sigma_2^f + F_{13}\sigma_1^f\sigma_3^f + \cdots + F_{56}\tau_{13}^f\tau_{12}^f\right) = 1. \quad (10.3)$$

The strength parameters must be determined by tests. For generally anisotropic and monoclinic materials, 27 and 17 types of tests are required, respectively. This makes the use of the quadratic failure criterion impractical for structures made of generally anisotropic or monoclinic materials. The criterion becomes more manageable when the material is orthotropic or transversely isotropic. Therefore, in the following the criterion is presented only for these two types of materials.

10.1.1 Orthotropic Material

An orthotropic material has three planes of symmetry (Figs. 2.11 and 2.12). We select the x_1, x_2, x_3 coordinate system with axes perpendicular to these symmetry planes.

First, we consider only the shear–stress component τ_{23} acting in the plane of symmetry (Fig. 10.4). When only τ_{23} acts, and it is in the positive direction, then

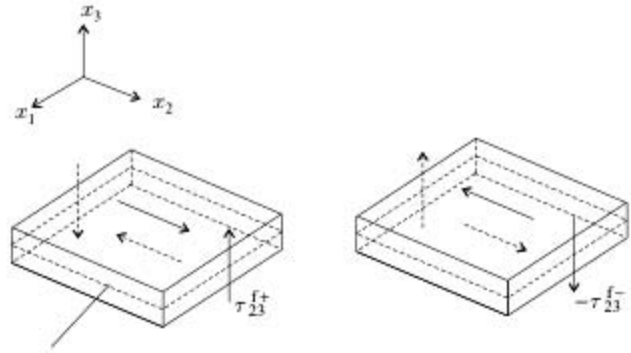

Figure 10.4: The positive and negative shear stresses at failure acting in an orthotropic material; x_1, x_2, and x_3 are perpendicular to the orthotropy planes.

at failure ($\tau_{23} = \tau_{23}^{f+}$) the quadratic failure criterion yields (Eq. 10.3)

$$F_4\tau_{23}^{f+} + F_{44}\left(\tau_{23}^{f+}\right)^2 = 1. \tag{10.4}$$

When only τ_{23} acts in the negative direction, then, at failure ($\tau_{23} = -\tau_{23}^{f-}$) the quadratic failure criterion becomes (Eq. 10.3)

$$-F_4\tau_{23}^{f-} + F_{44}\left(\tau_{23}^{f-}\right)^2 = 1. \tag{10.5}$$

Because of symmetry, the failure stress for positive shear is the same as for negative shear ($\tau_{23}^{f+} = \tau_{23}^{f-}$). The two preceding equations satisfy this condition only if F_4 is zero.

By similar argument it can be shown that F_5, F_6 are zero. Thus, we have

$$F_4 = F_5 = F_6 = 0. \tag{10.6}$$

Next, we apply the normal stresses σ_1, σ_2, σ_3; the shear stresses τ_{12}, τ_{13}; and either a positive or a negative shear stress τ_{23} (Fig. 10.5). For a positive shear stress at failure, $\tau_{23} = \tau_{23}^{f+}$, and we have (Eq. 10.3)

$$\begin{aligned} &F_1\sigma_1^f + F_2\sigma_2^f + F_3\sigma_3^f + F_{11}\left(\sigma_1^f\right)^2 + F_{22}\left(\sigma_2^f\right)^2 + \\ &F_{33}\left(\sigma_3^f\right)^2 + F_{44}\left(\tau_{23}^{f+}\right)^2 + F_{55}\left(\tau_{13}^f\right)^2 + F_{66}\left(\tau_{12}^f\right)^2 + \\ &\qquad 2\left(F_{12}\sigma_1^f\sigma_2^f + F_{13}\sigma_1^f\sigma_3^f + \cdots\right) + \cdots\cdot + \\ &+2\left(F_{14}\sigma_1^f + F_{24}\sigma_2^f + F_{34}\sigma_3^f + F_{45}\tau_{13}^f + F_{46}\tau_{12}^f\right)\tau_{23}^{f+} = 1. \end{aligned} \tag{10.7}$$

For a negative shear stress at failure, $\tau_{23} = -\tau_{23}^{f-}$, and Eq. (10.3) gives

$$\begin{aligned} &F_1\sigma_1^f + F_2\sigma_2^f + F_3\sigma_3^f + F_{11}\left(\sigma_1^f\right)^2 + F_{22}\left(\sigma_2^f\right)^2 + \\ &F_{33}\left(\sigma_3^f\right)^2 + F_{44}\left(\tau_{23}^{f-}\right)^2 + F_{55}\left(\tau_{13}^f\right)^2 + F_{66}\left(\tau_{12}^f\right)^2 + \\ &\qquad 2\left(F_{12}\sigma_1^f\sigma_2^f + F_{13}\sigma_1^f\sigma_3^f + \cdots\right) + \cdots\cdot + \\ &-2\left(F_{14}\sigma_1^f + F_{24}\sigma_2^f + F_{34}\sigma_3^f + F_{45}\tau_{13}^f + F_{46}\tau_{12}^f\right)\tau_{23}^{f-} = 1. \end{aligned} \tag{10.8}$$

Because of symmetry, the failure stress for positive out-of-plane shear is the same as for negative out-of-plane shear ($\tau_{23}^{f+} = \tau_{23}^{f-}$). This condition, together with

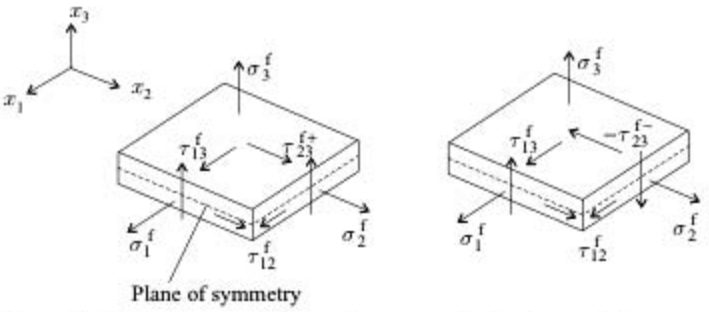

Figure 10.5: The stresses at failure acting on an orthotropic material.

the two preceding equations (Eqs. 10.7 and 10.8), give

$$F_{14} = F_{24} = F_{34} = F_{45} = F_{46} = 0. \tag{10.9}$$

By applying the procedure just given to the other two symmetry planes we find that the following strength parameters are also zero:

$$\begin{aligned} &F_{15} = F_{25} = F_{35} = F_{45} = F_{56} = 0 \\ &F_{16} = F_{26} = F_{36} = F_{46} = F_{56} = 0. \end{aligned} \tag{10.10}$$

For an orthotropic material the quadratic failure criterion (Eq. 10.2) becomes

$$\begin{aligned} &F_1\sigma_1 + F_2\sigma_2 + F_3\sigma_3 + \\ &F_{11}\sigma_1^2 + F_{22}\sigma_2^2 + F_{33}\sigma_3^2 + F_{44}\tau_{23}^2 + F_{55}\tau_{13}^2 + F_{66}\tau_{12}^2 + \\ &2(F_{12}\sigma_1\sigma_2 + F_{13}\sigma_1\sigma_3 + F_{23}\sigma_2\sigma_3) < 1. \end{aligned} \tag{10.11}$$

At failure, where the stress components are designated by the superscript f, Eq. (10.11) is

$$\begin{aligned} &F_1\sigma_1^{\mathrm{f}} + F_2\sigma_2^{\mathrm{f}} + F_3\sigma_3^{\mathrm{f}} + F_{11}\left(\sigma_1^{\mathrm{f}}\right)^2 + F_{22}\left(\sigma_2^{\mathrm{f}}\right)^2 + \\ &F_{33}\left(\sigma_3^{\mathrm{f}}\right)^2 + F_{44}\left(\tau_{23}^{\mathrm{f}}\right)^2 + F_{55}\left(\tau_{13}^{\mathrm{f}}\right)^2 + F_{66}\left(\tau_{12}^{\mathrm{f}}\right)^2 + \\ &2\left(F_{12}\sigma_1^{\mathrm{f}}\sigma_2^{\mathrm{f}} + F_{13}\sigma_1^{\mathrm{f}}\sigma_3^{\mathrm{f}} + F_{23}\sigma_2^{\mathrm{f}}\sigma_3^{\mathrm{f}}\right) = 1. \end{aligned} \tag{10.12}$$

Noninteraction strength parameters. The noninteraction strength parameters are denoted by $F_1, F_2, F_3, F_{11}, F_{22}, F_{33}, F_{44}, F_{55}, F_{66}$. The values of these parameters are obtained from uniaxial and from shear tests.

To obtain F_1 and F_{11} we subject the material to uniaxial tension and compression in the x_1 orthotropy direction (Table 10.1, top left and middle left). At failure, the stresses are $\sigma_1^{\mathrm{f}} = s_1^+$ and $\sigma_1^{\mathrm{f}} = -s_1^-$, where s is the strength of the material and the superscripts $(+)$ and $(-)$ refer to tension and compression. With these stresses, the quadratic failure criterion gives (Eq. 10.12)

$$F_1 s_1^+ + F_{11}(s_1^+)^2 = 1 \qquad -F_1 s_1^- + F_{11}(s_1^-)^2 = 1. \tag{10.13}$$

Solution of these two equations yields

$$F_1 = \frac{1}{s_1^+} - \frac{1}{s_1^-} \qquad F_{11} = \frac{1}{s_1^+ s_1^-}. \tag{10.14}$$

The strength parameters F_2, F_3, F_{22}, F_{33} are obtained in a similar manner and are given in Table 10.2. The tests to determine $s_2^+, s_2^-, s_3^+, s_3^-$ are illustrated in Table 10.1.

To obtain the strength parameter F_{44} we subject the material to shear τ_{23} in the x_2–x_3 orthotropy plane (Table 10.1, bottom left). Because of material symmetry the failure stress is independent of the direction of the shear stress, and at failure $\tau_{23}^{\mathrm{f}} = s_{23} (= s_{23}^+ = s_{23}^-)$. With this stress, Eq. (10.12) gives

$$F_{44}\,(s_{23})^2 = 1, \tag{10.15}$$

Table 10.1. Tests to determine the strengths of orthotropic materials; σ_1, σ_2, σ_3 are perpendicular to the planes of orthotropy.

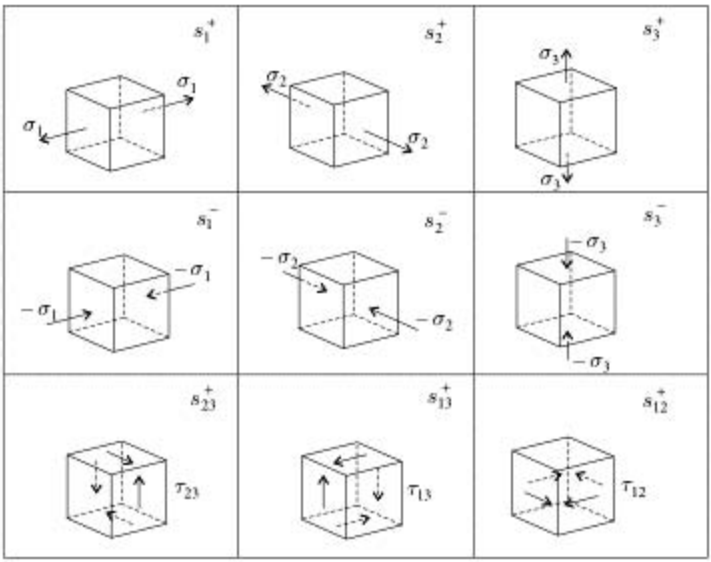

which results in

$$F_{44} = \frac{1}{(s_{23})^2}. \tag{10.16}$$

The strength parameters F_{55}, F_{66} are obtained in a similar manner. These, as well as the other noninteraction strength parameters, are given in Table 10.2.

Interaction strength parameters. The interaction strength parameters F_{12}, F_{13}, and F_{23} can be determined from tests that result in two or more nonzero stress components inside the material. Off-axis uniaxial tests and biaxial tests offer possible means for determining the interaction strength parameters.

Off-axis uniaxial tests. When the interaction strength parameters of orthotropic materials are to be determined by off-axis tests, we take test coupons from each (x_1–x_2, x_2–x_3, and x_1–x_3) orthotropy plane (Fig. 10.6).

Table 10.2. The noninteraction strength parameters in terms of strengths

$F_1 = \frac{1}{s_1^+} - \frac{1}{s_1^-}$	$F_2 = \frac{1}{s_2^+} - \frac{1}{s_2^-}$	$F_3 = \frac{1}{s_3^+} - \frac{1}{s_3^-}$
$F_{11} = \frac{1}{s_1^+ s_1^-}$	$F_{22} = \frac{1}{s_2^+ s_2^-}$	$F_{33} = \frac{1}{s_3^+ s_3^-}$
$F_{44} = \frac{1}{(s_{23})^2}$	$F_{55} = \frac{1}{(s_{13})^2}$	$F_{66} = \frac{1}{(s_{12})^2}$

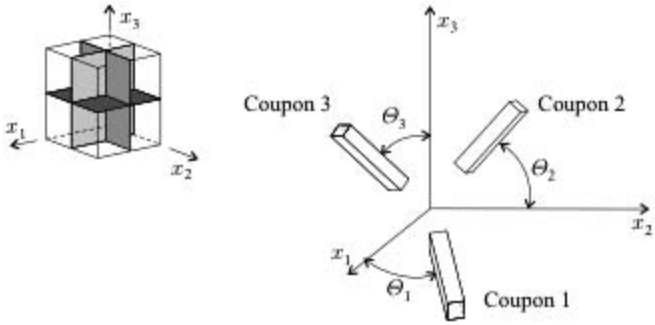

Figure 10.6: Test coupons in the x_1–x_2, x_1–x_3, x_2–x_3 orthotropy planes.

Coupon 1, taken from the x_1–x_2 orthotropy plane, is subjected either to an axial tensile or to an axial compressive stress. At failure the stress is designated by p^{f1}. Superscript 1 indicates Coupon 1. The corresponding stresses in the x_1, x_2 coordinate system are (Eq. 2.182)

$$\sigma_1^{f1} = p^{f1}\cos^2\Theta_1 \qquad \sigma_2^{f1} = p^{f1}\sin^2\Theta_1 \qquad \tau_{12}^{f1} = p^{f1}\cos\Theta_1\sin\Theta_1. \quad (10.17)$$

The angle Θ_1 is shown in Figure 10.6. Substitution of the preceding stresses into Eq. (10.12) results in the expression

$$\begin{aligned} &p^{f1}(F_1\cos^2\Theta_1 + F_2\sin^2\Theta_1) + \\ &(p^{f1})^2(F_{11}\cos^4\Theta_1 + F_{22}\sin^4\Theta_1 + F_{66}\cos^2\Theta_1\sin^2\Theta_1) + \\ &(p^{f1})^2 2F_{12}\cos^2\Theta_1\sin^2\Theta_1 = 1. \end{aligned} \quad (10.18)$$

This equation can be solved for F_{12}. The result is given in Table 10.3. The F_{13}, F_{23} interaction strength parameters are obtained in a similar manner and are also included in Table 10.3.

Biaxial tests. When the interaction strength parameter F_{12} is to be determined from biaxial tests, the specimen is loaded in biaxial tension, resulting in stresses σ_1 and σ_2 (Fig. 10.7). The load is then increased proportionally such that the ratio of the two stresses remains constant. At failure the stresses are denoted by

$$\sigma_1 = \sigma_1^{f(1\text{–}2)} \qquad \sigma_2 = \sigma_2^{f(1\text{–}2)}. \quad (10.19)$$

Table 10.3. The interaction strength parameters obtained from uniaxial tests (orthotropic material). The angles Θ_1, Θ_2, and Θ_3 are shown in Figure 10.6.

$$F_{12} = \frac{1}{2\sin^2\Theta_1\cos^2\Theta_1}\left(\frac{1}{(p^{f1})^2} - \frac{F_1\cos^2\Theta_1 + F_2\sin^2\Theta_1}{p^{f1}} - F_{11}\cos^4\Theta_1 - F_{22}\sin^4\Theta_1\right) - \frac{F_{66}}{2}$$

$$F_{23} = \frac{1}{2\sin^2\Theta_2\cos^2\Theta_2}\left(\frac{1}{(p^{f2})^2} - \frac{F_2\cos^2\Theta_2 + F_3\sin^2\Theta_2}{p^{f2}} - F_{22}\cos^4\Theta_2 - F_{33}\sin^4\Theta_2\right) - \frac{F_{44}}{2}$$

$$F_{13} = \frac{1}{2\sin^2\Theta_3\cos^2\Theta_3}\left(\frac{1}{(p^{f3})^2} - \frac{F_3\cos^2\Theta_3 + F_1\sin^2\Theta_3}{p^{f3}} - F_{33}\cos^4\Theta_3 - F_{11}\sin^4\Theta_3\right) - \frac{F_{55}}{2}$$

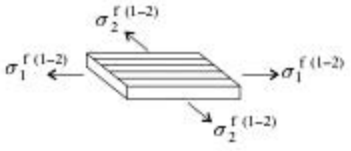

Figure 10.7: Test coupon for biaxial testing in the x_1–x_2 orthotropy plane.

The superscript f refers to the stresses at failure, and the superscript 1–2 identifies the applied biaxial stress components in the x_1–x_2 orthotropy plane. By substituting $\sigma_1^{f(1-2)}$ and $\sigma_2^{f(1-2)}$ into Eq. (10.12), and by setting all other stress components equal to zero, we obtain

$$F_1\sigma_1^{f(1-2)} + F_2\sigma_2^{f(1-2)} + F_{11}\left(\sigma_1^{f(1-2)}\right)^2 + F_{22}\left(\sigma_2^{f(1-2)}\right)^2 + 2F_{12}\sigma_1^{f(1-2)}\sigma_2^{f(1-2)} = 1. \tag{10.20}$$

Equation (10.20) results in

$$F_{12} = \frac{1 - F_1\sigma_1^{f(1-2)} - F_2\sigma_2^{f(1-2)} - F_{11}\left(\sigma_1^{f(1-2)}\right)^2 - F_{22}\left(\sigma_2^{f(1-2)}\right)^2}{2\sigma_1^{f(1-2)}\sigma_2^{f(1-2)}}. \tag{10.21}$$

The other interaction strength parameters, obtained in a similar manner, are

$$F_{ij} = \frac{1 - F_i\sigma_i^{f(i-j)} - F_j\sigma_j^{f(i-j)} - F_{ii}\left(\sigma_i^{f(i-j)}\right)^2 - F_{jj}\left(\sigma_j^{f(i-j)}\right)^2}{2\sigma_i^{f(i-j)}\sigma_j^{f(i-j)}} \quad i, j = 1, 2, 3. \tag{10.22}$$

Approximate expressions for the interaction strength parameters. In practice, it is difficult to perform the tests needed to generate the interaction strength parameters F_{ij}. To eliminate the need for these tests, numerous approximate expressions have been proposed for F_{ij}. One of these expressions is obtained by observing that a quadratic equation is characterized by its discriminants. When all but any two of the normal stresses are zero in the failure criterion (Eq. 10.12), the discriminants are

$$\Delta_{ij} = F_{ii}F_{jj} - F_{ij}^2 \quad i, j = 1, 2, 3 \quad i \neq j. \tag{10.23}$$

For the quadratic equation to represent a closed domain (which in our case is necessary to ensure that the stresses remain finite), every discriminant must be positive. Thus, from Eq. (10.23) we have

$$-\sqrt{F_{ii}F_{jj}} < F_{ij} < \sqrt{F_{ii}F_{jj}}. \tag{10.24}$$

For convenience, we write

$$F_{ij} = f_{ij}\sqrt{F_{ii}F_{jj}}. \tag{10.25}$$

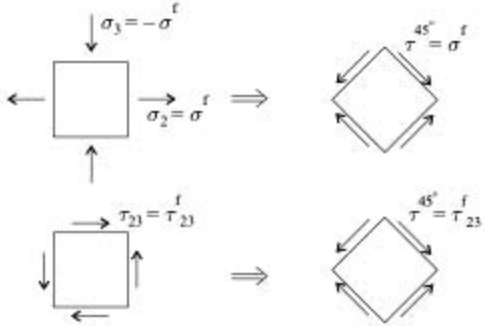

Figure 10.8: Stresses in the x_2–x_3 isotropy plane of a transversely isotropic material.

f_{ij} are constants that may have any value within -1 and $+1$. Tsai and Hahn[5] observed that the quadratic failure criterion for composites reduces to the von Mises quadratic failure criterion for isotropic materials (Section 10.1.3) when $f_{ij} = -0.5$. With this value the interaction strength parameters become

$$F_{12} = -\frac{1}{2}\sqrt{F_{11}F_{22}} \qquad F_{13} = -\frac{1}{2}\sqrt{F_{11}F_{33}} \qquad F_{23} = -\frac{1}{2}\sqrt{F_{22}F_{33}}. \quad (10.26)$$

10.1.2 Transversely Isotropic Material

A transversely isotropic material has three planes of symmetry (Fig. 2.15, page 19). Therefore, the stress parameters, which are zero for an orthotropic material (which also has three planes of symmetry), are also zero for transversely isotropic materials (Eqs. 10.9 and 10.10). In addition, one of the symmetry planes is isotropic. We select this to be the x_2–x_3 plane (Fig. 2.15). Because of isotropy, in this plane the subscripts 2 and 3 are interchangeable, and we can write

$$F_2 = F_3 \qquad F_{22} = F_{33} \qquad F_{13} = F_{12}. \quad (10.27)$$

For the same reason $s_{12} = s_{13}$, and from Table 10.2 (page 417) we have

$$F_{55} = F_{66}. \quad (10.28)$$

We now apply tensile σ_2 and compressive σ_3 stresses of equal magnitude ($\sigma_2 = -\sigma_3$) (Fig. 10.8, top left). At failure, $\sigma_2 = \sigma^f$, $\sigma_3 = -\sigma^f$, and Eq. (10.12) yields

$$F_2\sigma^f - F_3\sigma^f + F_{22}(\sigma^f)^2 + F_{33}(\sigma^f)^2 - 2F_{23}(\sigma^f)^2 = 1. \quad (10.29)$$

By combining Eqs. (10.27)–(10.29), we obtain

$$(\sigma^f)^2 = \frac{1}{2(F_{22} - F_{23})}. \quad (10.30)$$

[5] S. W. Tsai and H. T. Hahn, *Introduction to Composite Materials*. Technomic, Lancester, Pennsylvania, 1980, p. 286.

Next, we apply only the shear stress τ_{23} (Fig. 10.8, bottom left). At failure the value of the shear stress is $\tau_{23} = \tau_{23}^{f}$. Equation (10.12) now yields

$$F_{44}\left(\tau_{23}^{f}\right)^2 = 1. \tag{10.31}$$

We evaluate F_{44} by observing that (a) the biaxial loading (Fig. 10.8, top left) is equivalent to a shear loading τ^{45} in the 45-degree direction (Fig. 10.8, top right), and (b) in the x_2–x_3 isotropy plane the magnitude of the failure shear stress is the same in every direction (Fig. 10.8, bottom). Consequently, at failure, the shear stress is $\tau_{23}^{f} = \sigma^{f}$. By substituting σ^{f} for τ_{23}^{f} in Eq. (10.31) and by using Eq. (10.30), we obtain

$$F_{44} = 2\left(F_{22} - F_{23}\right). \tag{10.32}$$

With these simplifications, for a transversely isotropic material the quadratic failure criterion (Eq. 10.11) becomes

$$\begin{aligned} &F_1\sigma_1 + F_2\left(\sigma_2 + \sigma_3\right) + F_{11}\sigma_1^2 + F_{22}\left(\sigma_2^2 + \sigma_3^2\right) \\ &\quad + 2\left(F_{22} - F_{23}\right)\tau_{23}^2 + F_{66}\left(\tau_{13}^2 + \tau_{12}^2\right) + \\ &\qquad 2F_{12}\left(\sigma_1\sigma_2 + \sigma_1\sigma_3\right) + 2F_{23}\sigma_2\sigma_3 < 1. \end{aligned} \tag{10.33}$$

The noninteraction strength parameters in terms of the strengths are summarized in Table 10.2 (page 417); the interaction strength parameters are given by Eq. (10.26). The strength parameters depend on the strengths. The tests for determining the required strengths $s_1^+, s_1^-, s_2^+, s_2^-, s_{12}$ are illustrated in Figure 10.9.

10.1.3 Isotropic Material

Isotropic materials have an infinite number of symmetry planes, and the strength parameters given in Eqs. (10.9) and (10.10) are zero. In addition, because each symmetry plane is isotropic, the subscripts 1, 2, and 3 are interchangeable. This results in

$$F_1 = F_2 = F_3 \qquad F_{11} = F_{22} = F_{33} \qquad F_{23} = F_{13} = F_{12}. \tag{10.34}$$

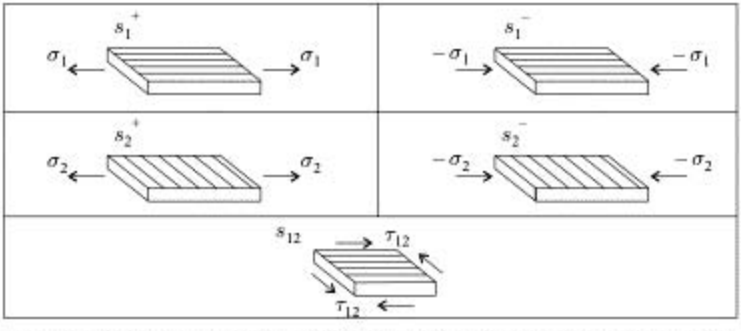

Figure 10.9: Tests to determine the strengths of a transversely isotropic material.

Similarly, $s_{12} = s_{13} = s_{23}$, and from Table 10.2 we have

$$F_{44} = F_{55} = F_{66}. \tag{10.35}$$

where F_{44} is given by Eq. (10.32). With the strength parameters given in Eqs. (10.34) and (10.35), the failure criterion (Eq. 10.11) becomes

$$F_1(\sigma_1 + \sigma_2 + \sigma_3) + F_{11}(\sigma_1^2 + \sigma_2^2 + \sigma_3^2) + 2(F_{11} - F_{12})(\tau_{23}^2 + \tau_{13}^2 + \tau_{12}^2) + 2F_{12}(\sigma_1\sigma_2 + \sigma_1\sigma_3 + \sigma_2\sigma_3) < 1. \tag{10.36}$$

Let us assume now that the compressive and tensile failure strengths are equal ($s_1^+ = s_1^-$). With this assumption, F_1 is zero (Table 10.2)

$$F_1 = 0. \tag{10.37}$$

Furthermore, let us approximate the interaction strength parameter by the expression given in Eq. (10.26) as follows:

$$F_{12} = -\frac{1}{2}\sqrt{F_{11}F_{22}} = -\frac{1}{2}F_{11}. \tag{10.38}$$

By substituting Eqs. (10.38) and (10.37) into Eq. (10.36) and by noting that $F_{11} = 1/(s_1^+)^2$, we obtain

$$\sqrt{\sigma_1^2 + \sigma_2^2 + \sigma_3^2 - \sigma_1\sigma_2 - \sigma_1\sigma_3 - \sigma_2\sigma_3 + 3(\tau_{23}^2 + \tau_{13}^2 + \tau_{12}^2)} < s_1^+. \tag{10.39}$$

This is identical to the von Mises quadratic failure criterion.[6]

10.1.4 Plane-Strain and Plane-Stress Conditions

Under plane-strain condition the equations and the parameters given in Sections 10.1.1–10.1.3 apply.

Under plane-stress condition (where in the x_1–x_2 plane $\sigma_3 = 0, \tau_{23} = 0, \tau_{13} = 0$, see Fig. 2.28) the quadratic failure criterion is simplified. For orthotropic materials and for transversely isotropic materials with x_1 normal to the plane of isotropy, Eqs. (10.12) and (10.33) become

$$F_1\sigma_1 + F_2\sigma_2 + F_{11}\sigma_1^2 + F_{22}\sigma_2^2 + F_{66}\tau_{12}^2 + 2F_{12}\sigma_1\sigma_2 < 1. \tag{10.40}$$

For isotropic materials, Eq. (10.36) reduces to

$$F_1(\sigma_1 + \sigma_2) + F_{11}(\sigma_1^2 + \sigma_2^2) + 2(F_{11} - F_{12})\tau_{12}^2 + 2F_{12}\sigma_1\sigma_2 < 1. \tag{10.41}$$

The strength parameters and the strengths required for the quadratic failure criteria are summarized in Tables 10.4 and 10.5.

[6] N. E. Dowling, *Mechanical Behavior of Materials*. Prentice-Hall, Englewood Cliffs, New Jersey, 1993, p. 245.

Table 10.4. The strength parameters appearing in the quadratic failure criterion for an orthotropic (Eq. 10.11), transversely isotropic (Eq. 10.33), and isotropic material (Eq. 10.36).

	F_1	F_2	F_3	F_{11}	F_{22}	F_{33}	F_{44}	F_{55}	F_{66}	F_{12}	F_{13}	F_{23}
Three-dimensional stresses or plane-strain condition												
Orthotropic	F_1	F_2	F_3	F_{11}	F_{22}	F_{33}	F_{44}	F_{55}	F_{66}	F_{12}	F_{13}	F_{23}
Transversely isotropic	F_1	F_2		F_{11}	F_{22}				F_{66}	F_{12}		F_{23}
Isotropic	F_1			F_{11}						F_{12}		
Plane-stress condition												
Orthotropic or transversely isotropic	F_1	F_2		F_{11}	F_{22}				F_{66}	F_{12}		
Isotropic	F_1			F_{11}						F_{12}		

10.1.5 Proportional Loading – Stress Ratio

We consider a part subjected to a load set $L_1, L_2, \ldots, L_i$. Let us increase (or decrease) the loads proportionally by a factor of $\tilde{R}$ until failure occurs (Fig. 10.10):

$$L_1^f = \tilde{R}L_1 \qquad L_2^f = \tilde{R}L_2 \qquad \ldots \qquad L_i^f = \tilde{R}L_i. \tag{10.42}$$

When the part behaves in a linearly elastic manner, the stresses also increase (or decrease) proportionally. Consequently, each stress component increases (or decreases) by the same proportion until failure occurs. This procedure is expressed as

$$\begin{aligned} \sigma_1^f &= \tilde{R}\sigma_1 \qquad \tau_{23}^f = \tilde{R}\tau_{23} \\ \sigma_2^f &= \tilde{R}\sigma_2 \qquad \tau_{13}^f = \tilde{R}\tau_{13} \\ \sigma_3^f &= \tilde{R}\sigma_3 \qquad \tau_{12}^f = \tilde{R}\tau_{12}. \end{aligned} \tag{10.43}$$

The superscript f refers to the stress components on the failure surface, and $\tilde{R}$ is the factor (called stress ratio) by which each load (and correspondingly each stress component) is multiplied such that the failure surface is reached; $\tilde{R}$ is illustrated in Figure 10.11 for linearly elastic materials. No failure occurs when $\tilde{R} > 1$, and

Table 10.5. The strengths required for evaluating the noninteraction strength parameters (see Tables 10.2 and 10.4)

	s_1^+	s_1^-	s_2^+	s_2^-	s_3^+	s_3^-	s_{12}	s_{13}	s_{23}
Three-dimensional stresses or plane-strain condition									
Orthotropic	s_1^+	s_1^-	s_2^+	s_2^-	s_3^+	s_3^-	s_{12}	s_{13}	s_{23}
Transversely isotropic	s_1^+	s_1^-	s_2^+	s_2^-			s_{12}		
Isotropic	s_1^+	s_1^-							
Plane-stress condition									
Orthotropic or transversely isotropic	s_1^+	s_1^-	s_2^+	s_2^-			s_{12}		
Isotropic	s_1^+	s_1^-							

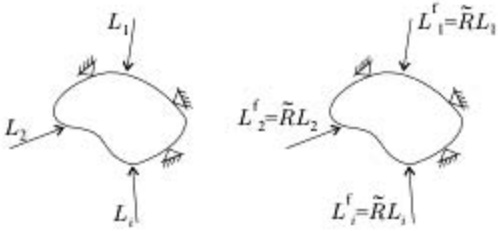

Figure 10.10: Proportional loading.

failure occurs when $\tilde{R} \leq 1$:

$$\begin{array}{ll} \tilde{R} > 1 & \text{no failure} \\ \tilde{R} \leq 1 & \text{failure.} \end{array} \tag{10.44}$$

By substituting Eq. (10.43) into Eq. (10.12), we observe that the quadratic failure criterion for orthotropic materials becomes

$$\begin{aligned} &\tilde{R}(F_1\sigma_1 + F_2\sigma_2 + F_3\sigma_3) + \\ &\tilde{R}^2\left(F_{11}\sigma_1^2 + F_{22}\sigma_2^2 + F_{33}\sigma_3^2 + F_{44}\tau_{23}^2 + F_{55}\tau_{13}^2 + F_{66}\tau_{12}^2\right) + \\ &2\tilde{R}^2(F_{12}\sigma_1\sigma_2 + F_{13}\sigma_1\sigma_3 + F_{23}\sigma_2\sigma_3) = 1. \end{aligned} \tag{10.45}$$

Whether or not failure occurs is indicated by the value of the stress ratio; $\tilde{R}$ is given by the solution of Eq. (10.45) as follows:

$$\tilde{R} = \frac{-b + \sqrt{b^2 + 4a}}{2a}. \tag{10.46}$$

Only the positive sign is applied in front of the square root because $\tilde{R}$, by definition, is positive. The coefficients a and b are given in Table 10.6 for orthotropic, transversely isotropic, and isotropic materials.

Under plane-strain condition the expressions in Table 10.6 apply.

Under plane-stress condition, in the x_1–x_2 plane, σ_3, τ_{23}, τ_{13} are zero ($\sigma_3 = 0$, $\tau_{23} = 0$, and $\tau_{13} = 0$, Fig. 2.28). By setting these stresses equal to zero in Table 10.6, we obtain the a and b parameters listed in Table 10.7.

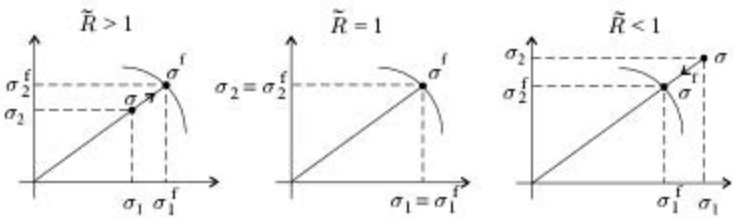

Figure 10.11: Representation of the failure surface when only σ_1 and σ_2 stresses are applied ($\tilde{R} = \sigma_1^f/\sigma_1 = \sigma_2^f/\sigma_2$).

Table 10.6. The stress ratio $\tilde{R}$

Material	*a*	*b*
Orthotropic	$F_{11}\sigma_1^2 + F_{22}\sigma_2^2 + F_{33}\sigma_3^2$ $+ F_{44}\tau_{23}^2 + F_{55}\tau_{13}^2 + F_{66}\tau_{12}^2$ $+ 2(F_{12}\sigma_1\sigma_2 + F_{13}\sigma_1\sigma_3 + F_{23}\sigma_2\sigma_3)$	$F_1\sigma_1 + F_2\sigma_2 + F_3\sigma_3$
Transversely isotropic	$F_{11}\sigma_1^2 + F_{22}(\sigma_2^2 + \sigma_3^2)$ $+ 2(F_{22} - F_{23})\tau_{23}^2 + F_{66}(\tau_{13}^2 + \tau_{12}^2)$ $+ 2F_{12}(\sigma_1\sigma_2 + \sigma_1\sigma_3) + 2F_{23}\sigma_2\sigma_3$	$F_1\sigma_1 + F_2(\sigma_2 + \sigma_3)$
Isotropic	$F_{11}(\sigma_1^2 + \sigma_2^2 + \sigma_3^2)$ $+ 2(F_{11} - F_{12})(\tau_{23}^2 + \tau_{13}^2 + \tau_{12}^2)$ $+ 2F_{12}(\sigma_1\sigma_2 + \sigma_1\sigma_3 + \sigma_2\sigma_3)$	$F_1(\sigma_1 + \sigma_2 + \sigma_3)$
	$\tilde{R} = \frac{-b+\sqrt{b^2+4a}}{2a}$	

10.2 "Maximum Stress" Failure Criterion

Frequently, for orthotropic materials and for transversely isotropic materials under plane-stress condition, a so-called "maximum stress" criterion is used. In applying this criterion we use the x_1, x_2, x_3 coordinate system aligned with the direction of orthotropy (Fig. 2.12, left). The normal stresses in the x_1, x_2, x_3 directions and the shear stresses in the x_1–x_2, x_3–x_1, x_2–x_3 planes are compared with the corresponding strengths. Failure does not occur if none of the stresses exceeds the strengths.

For an orthotropic material, no failure occurs when all of the following conditions are met:

$$\begin{aligned} -s_1^- < \sigma_1 < s_1^+ \qquad & |\tau_{23}| < s_{23} \\ -s_2^- < \sigma_2 < s_2^+ \qquad & |\tau_{13}| < s_{13} \\ -s_3^- < \sigma_3 < s_3^+ \qquad & |\tau_{12}| < s_{12}. \end{aligned} \tag{10.47}$$

For a transversely isotropic material under plane-stress condition, no failure occurs when all of the following conditions are met:

$$-s_1^- < \sigma_1 < s_1^+ \qquad -s_2^- < \sigma_2 < s_2^+ \qquad |\tau_{12}| < s_{12}, \tag{10.48}$$

Table 10.7. The stress ratio $\tilde{R}$ under plane-stress condition

Material	*a*	*b*
Orthotropic or transversely isotropic	$F_{11}\sigma_1^2 + F_{22}\sigma_2^2 + F_{66}\tau_{12}^2$ $+ 2F_{12}\sigma_1\sigma_2$	$F_1\sigma_1 + F_2\sigma_2$
Isotropic	$F_{11}(\sigma_1^2 + \sigma_2^2)$ $+ 2(F_{11} - F_{12})\tau_{12}^2 + 2F_{12}\sigma_1\sigma_2$	$F_1(\sigma_1 + \sigma_2)$
	$\tilde{R} = \frac{-b+\sqrt{b^2+4a}}{2a}$	

where s_i^+ and s_i^- are the tensile and compressive strengths in the i direction and s_{ij}^+ are the shear strengths in the ij $(i, j = 1, 2, 3)$ plane (Table 10.1, page 417).

Two important points are to be made here as follows:

1. The "maximum stress" criterion differs from the quadratic failure criterion.
2. The "maximum stress" failure criterion for composites differs from the maximum (normal or shear) stress criterion used for isotropic materials. The reason is that for isotropic materials the maximum (normal or shear) stress failure criterion is based on the maximum values of the stresses at a point. On the other hand, for composite materials the "maximum stress" failure criterion is based on the stress components in the orthotropy directions where the stresses are not necessarily the highest.

Despite the aforementioned shortcomings, the maximum stress criterion for composites (Eqs. 10.47, 10.48) has the advantage that it does not require knowledge of the interaction strength parameters.

10.3 "Maximum Strain" Failure Criterion

Frequently, for orthotropic materials and for transversely isotropic materials under plane-stress condition, a so-called maximum strain criterion is used. In applying this criterion we use the x_1, x_2, x_3 coordinate system aligned with the direction of orthotropy (Fig. 2.12, left). The normal strains in the x_1, x_2, x_3 directions and the shear strains in the x_1–x_2, x_3–x_1, x_2–x_3 planes are compared with the corresponding maximum allowable strains. Failure does not occur if none of the strains exceeds the allowable strains.

For an orthotropic material, no failure occurs when all of the following conditions are met:

$$\begin{aligned} -\eta_1^- < \epsilon_1 < \eta_1^+ \qquad & |\gamma_{23}| < \eta_{23}^+ \\ -\eta_2^- < \epsilon_2 < \eta_2^+ \qquad & |\gamma_{13}| < \eta_{13}^+ \\ -\eta_3^- < \epsilon_3 < \eta_3^+ \qquad & |\gamma_{12}| < \eta_{12}^+. \end{aligned} \tag{10.49}$$

For a transversely isotropic material, under plane-stress condition no failure occurs when all of the following conditions are met:

$$-\eta_1^- < \epsilon_1 < \eta_1^+ \qquad -\eta_2^- < \epsilon_2 < \eta_2^+ \qquad |\gamma_{12}| < \eta_{12}^+, \tag{10.50}$$

where η_i^+ and η_i^- are the allowable tensile and compressive strains in the x_i direction, and η_{ij}^+ are the allowable shear strains in the x_i–x_j $(i, j = 1, 2, 3)$ planes.

In general, the strain components above do not necessarily correspond to the maximum strain at the point. Therefore, this is not a true maximum strain failure criterion and is not equivalent to the maximum strain failure criterion for isotropic

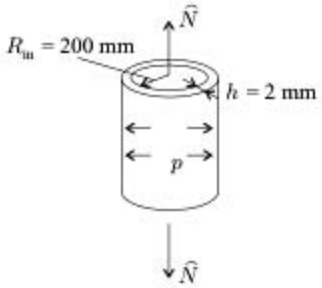

Figure 10.12: The cylinder subjected to internal pressure and axial load in Example 10.1.

materials, where failure is based on the maximum value of the strain components at the point.

Furthermore, the "maximum strain" (Eq. 10.50) failure criterion above is not equivalent to the "maximum stress" failure criterion (Eq. 10.48).

10.1 Example. *A cylinder (inner radius $R_{in} = 0.2$ m, and wall thickness $h = 0.002$ m) is made of woven glass epoxy. The material properties are given in Tables C.3 and C.4 (page 466). The cylinder is subjected to an axial load $\widehat{N} = 500\,000$ N and to an internal pressure $p = 2\,000\,000$ N/m^2 (Fig. 10.12). Determine the stress ratio $\widetilde{R}$.*

Solution. The radius of the reference surface, chosen as the midsurface, is

$$R = R_{in} + h/2 = 0.201 \text{ m}. \tag{10.51}$$

Using the membrane theory of shells, we determine that the membrane forces are (Eq. 8.11, with $p \equiv p_z$)

$$N_x = \frac{\widehat{N}}{2\pi R} = 395\,908 \frac{\text{N}}{\text{m}} \qquad N_y = pR = 402\,000 \frac{\text{N}}{\text{m}} \qquad N_{xy} = \frac{\widehat{T}}{2\pi R^2} = 0. \tag{10.52}$$

The stresses in the wall are

$$\begin{aligned} \sigma_x &= \frac{N_x}{h} = 197.95 \times 10^6 \frac{\text{N}}{\text{m}^2} \\ \sigma_y &= \frac{N_y}{h} = 201.00 \times 10^6 \frac{\text{N}}{\text{m}^2} \\ \tau_{xy} &= \frac{N_{xy}}{h} = 0. \end{aligned} \tag{10.53}$$

The wall of the cylinder consists of a single layer. The coordinates of this layer are x_1, x_2, x_3, and they coincide with the x, y, z coordinates of the cylinder (Fig. 10.12). Thus, the stresses in the layer are

$$\begin{aligned} \sigma_1 &= 197.95 \times 10^6 \frac{\text{N}}{\text{m}^2} \\ \sigma_2 &= 201.00 \times 10^6 \frac{\text{N}}{\text{m}^2} \\ \tau_{12} &= 0. \end{aligned} \tag{10.54}$$

With the strengths listed in Table C.4 ($s_1^+ = 367$ MPa, $s_1^- = 549$ MPa, $s_2^+ = 367$ MPa, $s_2^- = 549$ MPa, $s_{12} = 97$ MPa), the required strength parameters are (Table 10.2, page 417 and Eq. 10.26)

$$\begin{aligned} F_1 &= \frac{1}{s_1^+} - \frac{1}{s_1^-} = 903 \times 10^{-12} \qquad F_{11} = \frac{1}{s_1^+ s_1^-} = 4.96 \times 10^{-18} \\ F_2 &= \frac{1}{s_2^+} - \frac{1}{s_2^-} = 903 \times 10^{-12} \qquad F_{22} = \frac{1}{s_2^+ s_2^-} = 4.96 \times 10^{-18} \\ F_{66} &= \frac{1}{(s_{12})^2} = 106 \times 10^{-18} \qquad F_{12} = -\frac{1}{2}\sqrt{F_{11}F_{22}} = -2.48 \times 10^{-18}. \end{aligned} \tag{10.55}$$

The stress ratio from Table 10.7 (page 425) is

$$a = F_{11}\sigma_1^2 + F_{22}\sigma_2^2 + F_{66}\tau_{12}^2 + 2F_{12}\sigma_1\sigma_2 = 0.1975 \tag{10.56}$$

$$b = F_1\sigma_1 + F_2\sigma_2 = 0.3604 \tag{10.57}$$

$$\widetilde{R} = \frac{-b + \sqrt{b^2 + 4a}}{2a} = 1.52 > 1, \tag{10.58}$$

where $\widetilde{R}$ is greater than unity and the cylinder does not fail.

Next, we establish the failure envelope. At failure the Tsai–Wu criterion is (see Eqs. 10.40 and 10.3)

$$F_1\sigma_1^{\mathrm{f}} + F_2\sigma_2^{\mathrm{f}} + F_{11}\left(\sigma_1^{\mathrm{f}}\right)^2 + F_{22}\left(\sigma_2^{\mathrm{f}}\right)^2 + F_{66}\left(\tau_{12}^{\mathrm{f}}\right)^2 + 2F_{12}\sigma_1^{\mathrm{f}}\sigma_2^{\mathrm{f}} = 1, \tag{10.59}$$

where the superscript f refers to the stresses at failure, which are (Eqs. 10.52 and 10.53)

$$\begin{aligned} \sigma_1^{\mathrm{f}} &= \frac{N_x}{h} = \frac{\widehat{N}^{\mathrm{f}}}{2\pi Rh} = 395.9\widehat{N}^{\mathrm{f}} \\ \sigma_2^{\mathrm{f}} &= \frac{N_y}{h} = \frac{p^{\mathrm{f}}R}{h} = 100.5p^{\mathrm{f}} \\ \tau_{12}^{\mathrm{f}} &= \frac{N_{xy}}{h} = \frac{\widehat{T}}{2\pi R^2 h} = 0, \end{aligned} \tag{10.60}$$

where $\widehat{N}^{\mathrm{f}}$ and p^{f} are the applied loads at failure. In terms of $\widehat{N}^{\mathrm{f}}$ and p^{f}, Eq. (10.59) gives

$$\begin{aligned} 3.58 \times 10^{-7}\widehat{N}^{\mathrm{f}} + 9.08 \times 10^{-8}p^{\mathrm{f}} + 7.78 \times 10^{-13}(\widehat{N}^{\mathrm{f}})^2 + \\ 5.01 \times 10^{-14}(p^{\mathrm{f}})^2 - 1.97 \times 10^{-13}\widehat{N}^{\mathrm{f}}p^{\mathrm{f}} = 1. \end{aligned}$$

The failure envelope along which the $\widehat{N}^{\mathrm{f}}$ and p^{f} values satisfy this condition is plotted in Figure 10.13.

The "maximum stress" failure criterion is (Eq. 10.47)

$$-s_1^- < \sigma_1 < s_1^+ \tag{10.61}$$

$$-s_2^- < \sigma_2 < s_2^+. \tag{10.62}$$

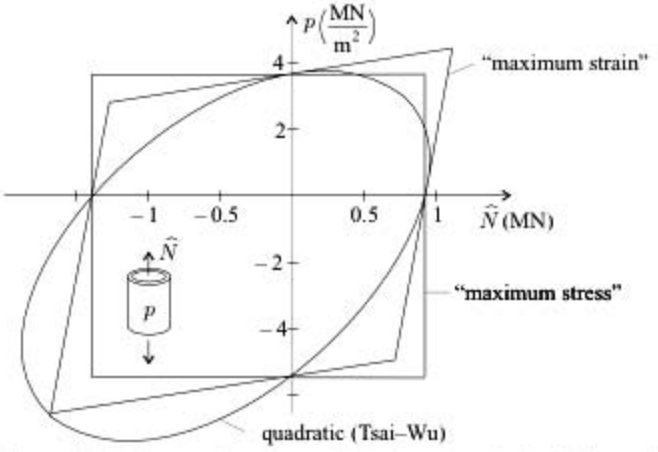

Figure 10.13: The "maximum stress," "maximum strain," and the quadratic (Tsai–Wu) failure envelopes for the cylinder in Example 10.1.

The value of $\sigma_1 = 197.95$ MPa is between $-s_1^- = -549$ MPa and $s_1^+ = 367$ MPa, and $\sigma_2 = 201$ MPa is between $-s_2^- = -549$ MPa and $s_2^+ = 367$ MPa. Hence, the cylinder does not fail.

To establish the failure envelope, we note that failure occurs when any of the following conditions are met:

$$\begin{aligned} -s_1^- = -549 = \sigma_1^{\text{f}} = 395.9\widehat{N}^{\text{f}} \qquad & s_1^+ = 367 = \sigma_1^{\text{f}} = 395.9\widehat{N}^{\text{f}} \\ -s_2^- = -549 = \sigma_2^{\text{f}} = 100.5p^{\text{f}} \qquad & s_2^+ = 367 = \sigma_2^{\text{f}} = 100.5p^{\text{f}}. \end{aligned} \tag{10.63}$$

The failure envelope represented by these equations is included in Figure 10.13.

The "maximum strain" failure criterion is (Eq. 10.49)

$$\begin{aligned} -\eta_1^- < \epsilon_1 < \eta_1^+ \\ -\eta_2^- < \epsilon_2 < \eta_2^+. \end{aligned} \tag{10.64}$$

With the engineering constants $E_1 = E_2 = 29.7 \times 10^9$ N/m^2 (Table C.3, page 466), the maximum allowable strains are

$$\begin{aligned} \eta_1^- = \frac{s_1^-}{E_1} = 0.0185 \qquad & \eta_1^+ = \frac{s_1^+}{E_1} = 0.0124 \\ \eta_2^- = \frac{s_2^-}{E_2} = 0.0185 \qquad & \eta_2^+ = \frac{s_2^+}{E_2} = 0.0124. \end{aligned} \tag{10.65}$$

With S_{ij} given in Table 2.7 (page 15), the strain–stress relationships are (Eq. 2.132)

$$\begin{Bmatrix} \epsilon_1 \\ \epsilon_2 \\ \gamma_{12} \end{Bmatrix} = \begin{bmatrix} \frac{1}{E_1} & -\frac{\nu_{21}}{E_2} & 0 \\ -\frac{\nu_{12}}{E_1} & \frac{1}{E_2} & 0 \\ 0 & 0 & \frac{1}{G_{12}} \end{bmatrix} \begin{Bmatrix} \sigma_1 \\ \sigma_2 \\ \tau_{12} \end{Bmatrix}. \tag{10.66}$$

The engineering constants are $E_1 = E_2 = 29.7 \times 10^9$ N/m^2, $G_{12} = 5.3 \times 10^9$ N/m^2, $\nu_{12} = 0.17$ (Table C.3). Thus, we have

$$\begin{Bmatrix} \epsilon_1 \\ \epsilon_2 \\ \gamma_{12} \end{Bmatrix} = \begin{bmatrix} 33.67 & -5.72 & 0 \\ -5.72 & 33.67 & 0 \\ 0 & 0 & 188.68 \end{bmatrix} \times 10^{-12} \begin{Bmatrix} 197.95 \\ 201.00 \\ 0 \end{Bmatrix} \times 10^6$$
$$= \begin{Bmatrix} 0.005\,51 \\ 0.005\,63 \\ 0 \end{Bmatrix}. \tag{10.67}$$

The value $\epsilon_1 = 0.005\,51$ is between $-\eta_1^- = -0.018\,5$ and $\eta_1^+ = 0.012\,4$, and $\epsilon_2 = 0.005\,63$ is between $-\eta_2^- = -0.018\,5$ and $\eta_2^+ = 0.012\,4$. Therefore, the cylinder does not fail.

To establish the failure envelope, we note that failure occurs when any of the following conditions is met:

$$\begin{aligned} -\eta_1^- &= \epsilon_1^{\mathrm{f}} \quad \eta_1^+ = \epsilon_1^{\mathrm{f}} \\ -\eta_2^- &= \epsilon_2^{\mathrm{f}} \quad \eta_2^+ = \epsilon_2^{\mathrm{f}}, \end{aligned} \tag{10.68}$$

where ϵ_1^{f} and ϵ_2^{f} are the strains at failure, which, in terms of $\widehat{N}^{\mathrm{f}}$ and p^{f}, are (Eqs. 10.66 and 10.60)

$$\begin{aligned} \epsilon_1^{\mathrm{f}} &= (13.3\widehat{N}^{\mathrm{f}} - 0.575p^{\mathrm{f}}) \times 10^{-9} \\ \epsilon_2^{\mathrm{f}} &= (-2.27\widehat{N}^{\mathrm{f}} + 3.38p^{\mathrm{f}}) \times 10^{-9}. \end{aligned} \tag{10.69}$$

From Eqs. (10.65), (10.68), and (10.69) we have

$$\begin{aligned} -0.0185 \times 10^9 &= 13.3\widehat{N}^{\mathrm{f}} - 0.575p^{\mathrm{f}} \qquad 0.0124 \times 10^9 = 13.3\widehat{N}^{\mathrm{f}} - 0.575p^{\mathrm{f}} \\ -0.0185 \times 10^9 &= -2.27\widehat{N}^{\mathrm{f}} + 3.38p^{\mathrm{f}} \qquad 0.0124 \times 10^9 = -2.27\widehat{N}^{\mathrm{f}} + 3.38p^{\mathrm{f}}. \end{aligned} \tag{10.70}$$

The failure envelope represented by these equations is included in Figure 10.13.

Figure 10.13 shows that the failure envelopes are markedly different for the quadratic (Tsai–Wu), the "maximum stress," and the "maximum strain" failure criteria. Thus, although in this example all three failure criteria indicate that there is no failure, there may be conditions under which they give contradictory results.

10.4 Plate with a Hole or a Notch

The quadratic, maximum stress, and maximum strain failure criteria are inapplicable when failure is initiated by localized disturbances such as imperfections, cracks, holes, notches, or free edges. If any of these criteria were evaluated using the stresses near the disturbance (where the stresses are high), the criteria would underestimate the failure load. On the other hand, if the criteria were evaluated using the stresses in the farfield (where the stresses are significantly lower than the nearfield stresses), the criteria would overestimate the failure load. To

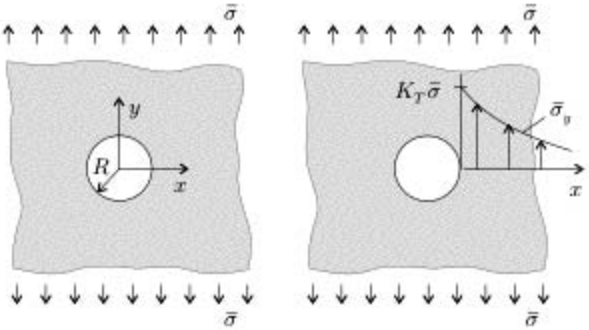

Figure 10.14: Unidirectionally loaded plate contaning a circular hole and the average stress distribution along the x-axis near the hole.

predict the failure in the presence of a disturbance we would need an understanding of the fracture behavior of the material and appropriate fracture models. To date, there is no simple, comprehensive model that describes failure of different composite systems largely because different systems exhibit different damage mechanisms and failure modes. One model, which is applicable in engineering design, is Whitney and Nuismer's[7,8] model for predicting failure of laminates with local stress concentrations. In the following we illustrate the concept underlying this model via the failure of laminates containing a circular hole or a notch.

10.4.1 Plate with a Circular Hole

Let us consider a large plate containing a circular hole of radius R (Fig. 10.14, left). The plate is subjected to a uniformly distributed average tensile stress $\bar{\sigma}$. Under the action of this stress the through-the-thickness average of the normal stress along the x axis is $\bar{\sigma}_y$ (Fig. 10.14, right).

Whitney and Nuismer proposed two failure criteria, one referred to as the point-stress the other as the average stress criterion.

According to the *point stress criterion*, failure occurs when, at a fixed distance d_0 from the hole along the x-axis (Fig. 10.15), $\bar{\sigma}_y$ is equal to or greater than the stress at failure of the "solid" plate (i.e., the plate *without* the hole),

$$\bar{\sigma}_y(R+d_0,0) \geq \bar{\sigma}_0^f \qquad \text{failure}, \tag{10.71}$$

where $\bar{\sigma}_0^f$ is the strength of the solid plate (Fig. 10.16).

According to the *average stress criterion*, failure occurs when the stress $\bar{\sigma}_y$, averaged over a fixed distance a_0 along the x-axis, is equal to or greater than the

[7] J. M. Whitney and R. J. Nuismer, Stress Fracture Criteria for Laminated Composites Containing Stress Concentrations. *Journal of Composite Materials*, Vol. 8, 253–265, 1974.

[8] R. J. Nuismer and J. M. Whitney, Uniaxial Failure of Composite Laminates Containing Stress Concetrations. In: *Fracture Mechanics of Composites*. ASTM STP 593, American Society for Testing and Materials, Philadelphia, 1975, pp. 117–142.

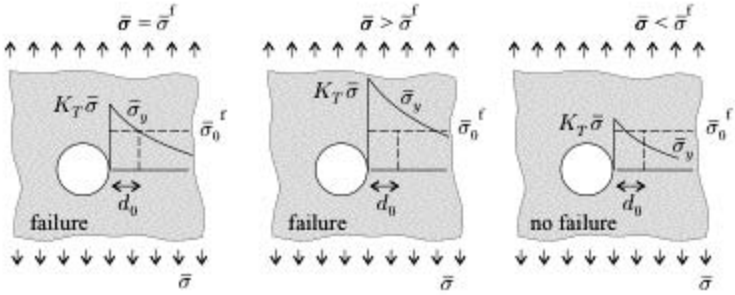

Figure 10.15: Illustration of the failure of a plate with a circular hole according to the point stress failure criterion.

failure stress of the "solid" plate:

$$\frac{1}{a_0}\int_R^{R+a_0} \bar{\sigma}_y(x,0)\,dx \geq \bar{\sigma}_0^f \qquad \text{failure.} \tag{10.72}$$

To apply either of the criteria above, the strength $\bar{\sigma}_0^f$ of the solid plate (Fig. 10.16) and the stress distribution $\bar{\sigma}_y$ (Fig. 10.15) must be known. The strength is to be obtained by tests. The stress distribution must be determined numerically.

Orthotropic plate. For orthotropic plates (with the x- and y-axes in the directions of orthotropy) the stress distribution along the x-axis is given by Eq. (4.305). With the definitions $\bar{\sigma}_y = N_y/h$ and $\bar{\sigma} = N_y^\infty/h$, we write Eq. (4.305) as

$$\bar{\sigma}_y(x,0) = \frac{\bar{\sigma}}{2}\left\{2 + \left(\frac{R}{x}\right)^2 + 3\left(\frac{R}{x}\right)^4 - (K_T - 3)\left[5\left(\frac{R}{x}\right)^6 - 7\left(\frac{R}{x}\right)^8\right]\right\}, \tag{10.73}$$

where $\bar{\sigma}$ is the applied uniform tensile stress (Fig. 10.14) and K_T is the stress intensity factor ($K_T = \bar{\sigma}_y(R,0)/\bar{\sigma}$). From Eq. (4.304), K_T is

$$K_T = 1 + \sqrt{\frac{2}{A_{11}}\left(\sqrt{A_{11}A_{22}} - A_{12} + \frac{A_{11}A_{22} - A_{12}^2}{2A_{66}}\right)}. \tag{10.74}$$

where A_{ij} are the elements of the stiffness matrix in the x–y coordinate system (Eq. 3.20). At failure $\bar{\sigma}$ is denoted by $\bar{\sigma}^f$ (Fig. 10.16). With this notation, Eqs. (10.71)

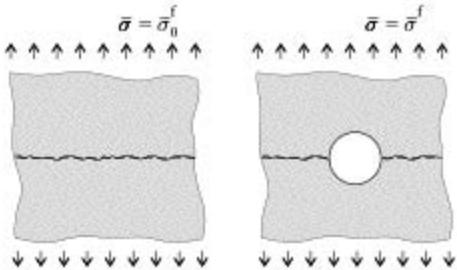

Figure 10.16: The applied stress at failure of a plate without and with the hole.

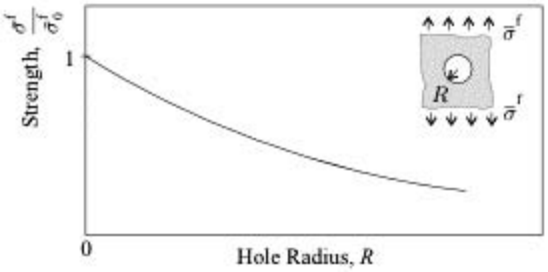

Figure 10.17: The strength of a composite plate with a hole as the function of the hole size.

and (10.73) yield

$$\frac{\bar{\sigma}^f}{\bar{\sigma}_0^f} = \frac{2}{2+r^2+3r^4-(K_T-3)(5r^6-7r^8)} \qquad \begin{matrix}\text{orthotropic plate} \\ \text{with hole.}\end{matrix} \tag{10.75}$$

The parameter r is defined as

$$r = \frac{R}{R+d_0}. \tag{10.76}$$

The expression using the average stress criterion is not given because Whitney and Nuismer have shown that the point stress and average stress criteria yield very similar results.

Equation (10.75) shows the hole size effect, which has also been observed experimentally: when subjected to tension, plates with larger holes have lower strengths than plates with smaller holes (Fig. 10.17). To explain this phenomenon, we observe that the high stresses in the vicinity of the hole are confined to a region that is narrower for smaller holes than for larger holes (Fig. 10.18). One possible explanation for the hole size effect is that, in this narrower region, there are fewer flaws (failure initiation sites) that could initiate damage growth, resulting in reduced strength.

It has also been argued that plates with smaller holes are stronger because stress gradients near the hole can better distribute for small holes (where the stress gradients are high) than for large holes (where the stress gradients are smaller).

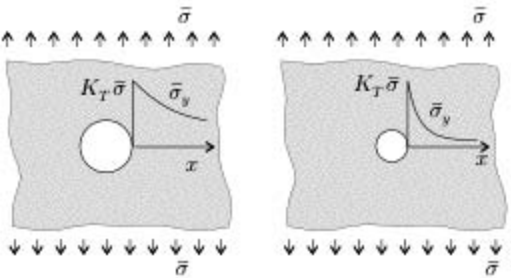

Figure 10.18: The stress distribution along the x-axis for two different hole sizes.

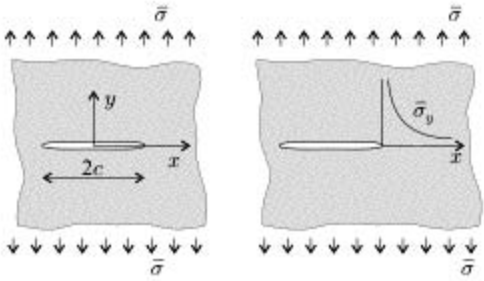

Figure 10.19: Unidirectionally loaded plate contaning a notch and the stress distribution along the x-axis near the notch.

10.4.2 Plate with a Notch

We now apply the Whitney–Nuismer point stress criterion to a large symmetric orthotropic plate containing a through-the-width notch of length $2c$ (Fig. 10.19, left). The notch is aligned with one of the orthotropy axes. When this plate is subjected to a uniform tensile stress $\bar{\sigma}$, the through-the-thickness average of the normal stress along the x-axis $\bar{\sigma}_y$ (Fig. 10.19, right) is given by Whitney and Nuismer[9] as

$$\bar{\sigma}_y(x,0) = \frac{\bar{\sigma}x}{\sqrt{x^2 - c^2}}. \tag{10.77}$$

Substitution of Eq. (10.77) into Eq. (10.71) (R replaced by c) yields

$$\frac{\bar{\sigma}^f}{\bar{\sigma}_0^f} = \sqrt{1 - \left(\frac{c}{c + d_0}\right)^2} \qquad \begin{matrix}\text{plate} \\ \text{with notch.}\end{matrix} \tag{10.78}$$

The average stress criterion can be obtained similarly. It is not given here because it yields results similar to the point stress criterion.

10.4.3 Characteristic Length

The usefulness of the Whitney–Nuismer point stress and average stress failure criteria is predicated on the assumption that the characteristic lengths d_0 or a_0 are independent of the hole or notch size – at least for a given laminate made of a particular material system. In such a case, the characteristic lengths can be determined through one test for one hole or one notch size. Obviously, the model would be even more useful if the characteristic lengths were to remain constant for all laminates (layups) made of different types of fiber-reinforced composites. There is evidence that the values of the characteristic lengths do not vary appreciably

[9] J. M. Whitney and R. J. Nuismer, Stress Fracture Criteria for Laminated Composites Containing Stress Concentrations. *Journal of Composite Materials*, Vol. 8, 253–265, 1974.

over a wide range of conditions. For example, Nuismer and Whitney[10] have found that the values $d_0 = 1.0$ mm and $a_0 = 3.8$ mm fit the data for cross-ply and quasi-isotropic glass–epoxy and graphite epoxy laminates containing a circular hole or a notch well. Although the existing data are not all conclusive, the Whitney–Nuismer point stress and average stress criteria, together with the characteristic length values just cited, should be useful at least for the purpose of preliminary design.

[10] R. J. Nuismer and J. M. Whitney, Uniaxial Failure of Composite Laminates Containing Stress Concetrations. In: *Fracture Mechanics of Composites*. ASTM STP 593, American Society for Testing and Materials, Philadelphia, 1975, pp. 117–142.

Micromechanics

Micromechanics is used to estimate the mechanical and hygrothermal properties of composite materials from the known values of the properties of the fiber and the matrix. There are three major categories of micromechanical approaches: (i) mechanics of material models based on simplifying assumptions that make it unnecessary to specify in detail the stress–strain distributions, (ii) elasticity models requiring that the stresses and strains be determined at the micromechanical level, and (iii) empirical expressions resulting from curve-fitting elasticity solutions or data.

It is not our intent to discuss the numerous available models. Instead, we focus on two mechanics of materials models, namely on the "rule of mixtures" and the "modified rule of mixtures." The rule of mixtures is the simplest and most intuitive approach and is useful for introducing concepts. However, it fails to represent some of the properties with reasonable accuracy. The modified rule of mixtures is an improvement over the rule of mixtures, and predicts the properties with better accuracies.

Methods to predict strength – though available – are not presented because they are less accurate than the models predicting elastic and hygrothermal properties.

11.1 Rule of Mixtures

We consider the volume V of an element shown in Figure 11.1. The volume of this element is

$$V = V_f + V_m + V_v, \tag{11.1}$$

where the subscripts f, m and v refer to the fiber, the matrix, and the void. It is convenient to introduce the volume fractions as follows:

$$v_f \equiv \frac{V_f}{V} \qquad v_m \equiv \frac{V_m}{V} \qquad v_v \equiv \frac{V_v}{V}. \tag{11.2}$$

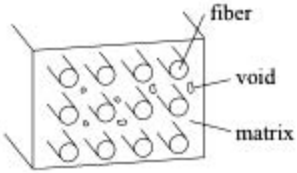

Figure 11.1: Illustration of the matrix, fiber, and void volumes.

Equations (11.1) and (11.2) give

$$v_f + v_m + v_v = 1. \tag{11.3}$$

When the void fraction is negligible ($v_v = 0$), we have

$$v_m = 1 - v_f. \tag{11.4}$$

The mass of the element in Figure 11.1 is

$$M = M_f + M_m + M_v. \tag{11.5}$$

By neglecting the mass of the void, we can write this equation as

$$M = \rho_f V_f + \rho_m V_m, \tag{11.6}$$

where ρ_f and ρ_m are the fiber and the matrix densities, respectively. The density of the composite is

$$\rho_{comp} = \frac{M}{V} = v_f \rho_f + v_m \rho_m. \tag{11.7}$$

In the following, we treat unidirectional, fiber-reinforced composites without voids. We derive the properties using two types of elements (Fig. 11.2). Element 1 contains a single fiber bundle of circular cross section. Element 2 consists of a fiber layer sandwiched between two layers of matrix material. In Element 2, the

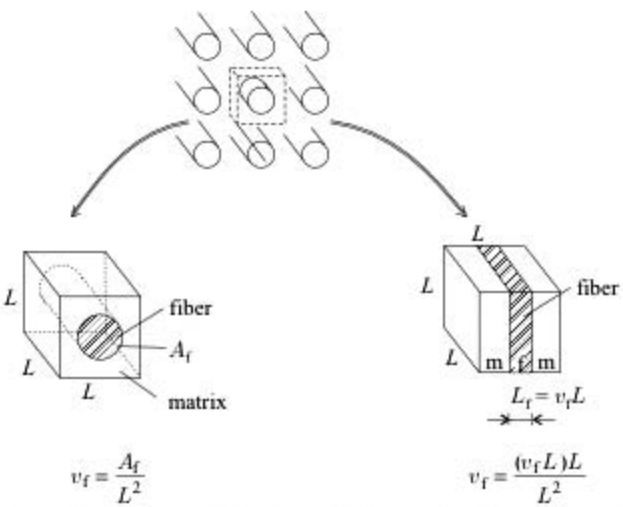

Figure 11.2: Representative elements. Element 1 (left) and Element 2 (right).

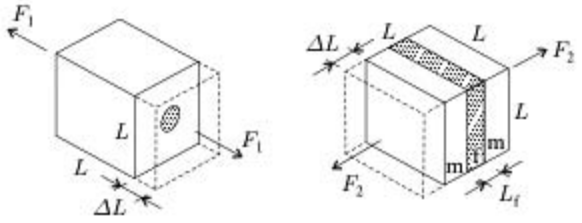

Figure 11.3: Element 1 subjected to a force in the fiber direction (left), and Element 2 subjected to a force in the transverse direction (right).

fiber and matrix volumes are the same as in Element 1. Hence, the thickness of the fiber layer in Element 2 is $v_f L$.

11.1.1 Longitudinal Young Modulus E_1

Element 1 is subjected to a force F_1 in the fiber direction. The force, distributed over the surface, is (Fig. 11.3)

$$F_1 = \sigma_1 A, \tag{11.8}$$

where σ_1 is the average normal stress across the entire cross-sectional area A ($A = L^2$). Part of the force is carried by the fibers and part by the matrix. Thus, we write

$$\sigma_1 A = A_f \sigma_{f1} + A_m \sigma_{m1}, \tag{11.9}$$

A_f and A_m are the cross-sectional areas of the fiber bundle and the matrix, respectively. When the Poisson effect is neglected, the normal stresses in the composite σ_1, in the fiber bundle σ_{f1}, and in the matrix σ_{m1} are

$$\sigma_1 = \epsilon_1 E_1 \qquad \sigma_{f1} = \epsilon_{f1} E_{f1} \qquad \sigma_{m1} = \epsilon_{m1} E_m, \tag{11.10}$$

where E_1 and E_{f1} are the composite and the fiber longitudinal Young moduli and E_m is the matrix Young modulus, respectively. Equations (11.9) and (11.10) give

$$\epsilon_1 E_1 = \frac{A_f}{A} \epsilon_{f1} E_{f1} + \frac{A_m}{A} \epsilon_{m1} E_m. \tag{11.11}$$

The elongations ΔL and, hence, the longitudinal normal strains of the composite ϵ_1, the matrix ϵ_{m1}, and the fiber ϵ_{f1} are equal:

$$\epsilon_1 = \epsilon_{f1} = \epsilon_{m1}. \tag{11.12}$$

The volume fractions are

$$v_f = \frac{A_f}{A} \qquad v_m = \frac{A_m}{A}. \tag{11.13}$$

Equations (11.11)–(11.13) result in the following expression for the longitudinal Young modulus of the composite in terms of the fiber and matrix moduli:

$$E_1 = v_f E_{f1} + v_m E_m = v_f E_{f1} + (1 - v_f) E_m. \tag{11.14}$$

11.1.2 Transverse Young Modulus E_2

We consider a rectangular element with sides L made up of three layers (Element 2, Fig. 11.3). The inner layer is a sheet of fiber with the same volume as the fiber bundle in Element 1. The length and the transverse (x_2 direction) Young modulus of this inner layer are L_f and E_{f2}, respectively, and the length and the Young modulus of the outer layers are $L_m = (L - L_f)/2$ and E_m. The element is subjected to a force F_2. The force is distributed uniformly across the surface $A\,(A = L^2)$. The normal stress in the transverse direction is $\sigma_2 = F_2/A$, which can be expressed as

$$\sigma_2 = \epsilon_2 E_2, \tag{11.15}$$

where E_2 is the transverse Young modulus of the element and ϵ_2 is the average transverse normal strain

$$\epsilon_2 = \frac{\Delta L}{L}. \tag{11.16}$$

The change in the length of the element is

$$\Delta L = 2L_m \epsilon_{m2} + L_f \epsilon_{f2}, \tag{11.17}$$

where ϵ_{m2} and ϵ_{f2} are the transverse normal strains in the matrix and fiber layers. By neglecting the Poisson effect, we have

$$\epsilon_{m2} = \frac{\sigma_{m2}}{E_m} \qquad \epsilon_{f2} = \frac{\sigma_{f2}}{E_{f2}}. \tag{11.18}$$

By introducing Eqs. (11.17) and (11.18) into Eq. (11.16), we obtain

$$\epsilon_2 = \frac{\Delta L}{L} = \frac{2L_m}{L}\frac{\sigma_{m2}}{E_m} + \frac{L_f}{L}\frac{\sigma_{f2}}{E_{f2}}. \tag{11.19}$$

The transverse normal stresses in the composite σ_2, the matrix σ_{m2}, and the fiber σ_{f2} layers are equal as follows:

$$\sigma_2 = \sigma_{m2} = \sigma_{f2}. \tag{11.20}$$

The matrix and fiber volume fractions are

$$v_f = \frac{L_f}{L} \qquad v_m = \frac{2L_m}{L}. \tag{11.21}$$

By substituting Eqs. (11.20), (11.21), and $\epsilon_2 = \sigma_2/E_2$ into Eq. (11.19), we obtain the transverse Young modulus

$$E_2 = \left(\frac{v_f}{E_{f2}} + \frac{v_m}{E_m}\right)^{-1} = \left(\frac{v_f}{E_{f2}} + \frac{1 - v_f}{E_m}\right)^{-1}. \tag{11.22}$$

11.1.3 Longitudinal Shear Modulus G_{12}

We consider Element 2. The length and the longitudinal shear modulus of the inner layer are L_f and G_{f12} respectively, and the length and the shear modulus of the outer layers are $L_m = (L - L_f)/2$ and G_m. The element is subjected to a

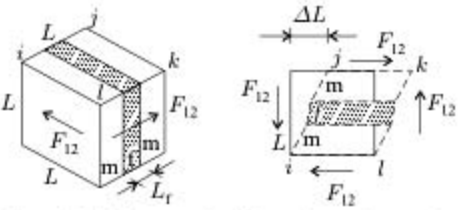

Figure 11.4: Element 2 subjected to a shear force (left) and deformation of the "top" (*ijkl*) surface (right).

shear force F_{12} (Fig. 11.4) distributed uniformly across the surface A ($A = L^2$). The shear stress $\tau_{12} = F_{12}/A$ is

$$\tau_{12} = \gamma_{12} G_{12}, \tag{11.23}$$

where G_{12} is the longitudinal shear modulus of the element and γ_{12} is the average shear strain,

$$\gamma_{12} \cong \tan \gamma_{12} = \frac{\Delta L}{L}, \tag{11.24}$$

where ΔL is due to the shear deformations of the matrix and fiber layers,

$$\Delta L = 2L_m \gamma_{m12} + L_f \gamma_{f12}, \tag{11.25}$$

where γ_{m12} and γ_{f12} are the shear strains in the matrix and fiber layers as follows:

$$\gamma_{m12} = \frac{\tau_{m12}}{G_m} \qquad \gamma_{f12} = \frac{\tau_{f12}}{G_{f12}}. \tag{11.26}$$

The shear stresses in the composite, the matrix, and the fiber layers are equal:

$$\tau_{12} = \tau_{m12} = \tau_{f12}. \tag{11.27}$$

By combining Eqs. (11.21) and (11.23)–(11.27), we obtain the longitudinal shear modulus:

$$G_{12} = \left(\frac{v_f}{G_{f12}} + \frac{v_m}{G_m} \right)^{-1} = \left(\frac{v_f}{G_{f12}} + \frac{1 - v_f}{G_m} \right)^{-1}. \tag{11.28}$$

11.1.4 Transverse Shear Modulus G_{23}

We again consider Element 2 made up of three layers (Fig. 11.4). The transverse shear modulus G_{23} of this element is derived in the same way as the longitudinal shear modulus G_{12}. The result is

$$G_{23} = \left(\frac{v_f}{G_{f23}} + \frac{1 - v_f}{G_m} \right)^{-1}. \tag{11.29}$$

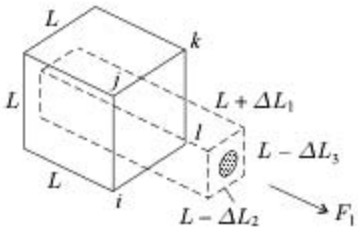

Figure 11.5: Deformation of Element 1 subjected to an axial force in the x_1 direction.

11.1.5 Longitudinal Poisson Ratio ν_{12}

Element 1, shown in Figure 11.2, is subjected to a force F_1 in the longitudinal x_1 direction. Because of this force the element deforms, as illustrated in Figure 11.5. The sides of the deformed element are $(L + \Delta L_1)$, $(L - \Delta L_2)$, and $(L - \Delta L_3)$. The change in the cross-sectional area A of the face $ijkl$ is

$$\Delta A = A - (L - \Delta L_2)(L - \Delta L_3). \tag{11.30}$$

By definition, the normal strains in the x_2 and x_3 directions are

$$\epsilon_2 = -\frac{\Delta L_2}{L} \qquad \epsilon_3 = -\frac{\Delta L_3}{L}. \tag{11.31}$$

Owing to symmetry, $\Delta L_2 = \Delta L_3$ and, consequently, we have

$$\epsilon_2 = \epsilon_3. \tag{11.32}$$

By neglecting higher-order terms, we find that Eqs. (11.30)–(11.32) give

$$\Delta A = A(\epsilon_2 + \epsilon_3) = 2A\epsilon_2. \tag{11.33}$$

By similar arguments, the changes in the matrix and fiber areas are

$$\Delta A_f = 2A_f\epsilon_{f2} \qquad \Delta A_m = 2A_m\epsilon_{m2}. \tag{11.34}$$

The change in the total area is the sum of the changes of the fiber and matrix areas:

$$\Delta A = \Delta A_f + \Delta A_m. \tag{11.35}$$

Under the action of the longitudinal normal stress $\sigma_1 = F_1/A$, the transverse normal strains are related to the longitudinal normal strain by

$$\epsilon_2 = -\nu_{12}\epsilon_1 \qquad \epsilon_3 = -\nu_{13}\epsilon_1. \tag{11.36}$$

By virtue of Eqs. (11.32) and (11.36), we have

$$\nu_{12} = \nu_{13}. \tag{11.37}$$

From Eqs. (11.36) and (11.33) we obtain

$$\nu_{12} = -\frac{\epsilon_2}{\epsilon_1} = -\frac{\Delta A}{2A}\frac{1}{\epsilon_1}. \tag{11.38}$$

By combining Eqs. (11.35) and (11.38) and introducing Eq. (11.34) into the resulting expression, we obtain

$$\nu_{12} = -\frac{2A_f\epsilon_{f2} + 2A_m\epsilon_{m2}}{2A}\frac{1}{\epsilon_1} = -\frac{A_f}{A}\frac{\epsilon_{f2}}{\epsilon_1} - \frac{A_m}{A}\frac{\epsilon_{m2}}{\epsilon_1}. \tag{11.39}$$

The changes in the lengths of the fiber, the matrix, and the composite are equal. Consequently, in the x_1 direction the normal strains in the composite, in the fiber, and in the matrix are equal as follows:

$$\epsilon_1 = \epsilon_{f1} = \epsilon_{m1}. \tag{11.40}$$

With the definitions

$$v_f = \frac{A_f}{A} \qquad v_m = \frac{A_m}{A} \qquad \nu_{f12} = -\frac{\epsilon_{f2}}{\epsilon_{f1}} \qquad \nu_m = -\frac{\epsilon_{m2}}{\epsilon_{m1}}, \tag{11.41}$$

Eqs. (11.39)–(11.41) give the following expression for the longitudinal Poisson ratio:

$$\nu_{12} = v_f\nu_{f12} + v_m\nu_m. \tag{11.42}$$

11.1.6 Transverse Poisson Ratio ν_{23}

For a transversely isotropic material (which is under consideration here), the transverse shear and the Young moduli are related by the following expression (Eq. 2.34):

$$G_{23} = \frac{E_2}{2(1+\nu_{23})}. \tag{11.43}$$

By rearranging this expression, we obtain the transverse Poisson ratio

$$\nu_{23} = \frac{E_2}{2G_{23}} - 1. \tag{11.44}$$

More accurate expressions for E_2 and G_{23} are obtained by the modified rule of mixtures (Section 11.2). These expressions are included in Table 11.1, below.

Table 11.1. Expressions for the engineering constants

Longitudinal Young modulus	$E_1 = v_f E_{f1} + v_m E_m$
Transverse Young modulus	$E_2 = \left(\frac{\sqrt{v_f}}{E_{h2}} + \frac{1-\sqrt{v_f}}{E_m}\right)^{-1}$ where $E_{h2} = \sqrt{v_f}E_{f2} + (1-\sqrt{v_f})E_m$
Longitudinal shear modulus	$G_{12} = \left(\frac{\sqrt{v_f}}{G_{h12}} + \frac{1-\sqrt{v_f}}{G_m}\right)^{-1}$ where $G_{h12} = \sqrt{v_f}G_{f12} + (1-\sqrt{v_f})G_m$
Transverse shear modulus	$G_{23} = \left(\frac{\sqrt{v_f}}{G_{h23}} + \frac{1-\sqrt{v_f}}{G_m}\right)^{-1}$ where $G_{h23} = \sqrt{v_f}G_{f23} + (1-\sqrt{v_f})G_m$
Longitudinal Poisson ratio	$\nu_{12} = v_f\nu_{f12} + v_m\nu_m$
Transverse Poisson ratio	$\nu_{23} = \frac{E_2}{2G_{23}} - 1$

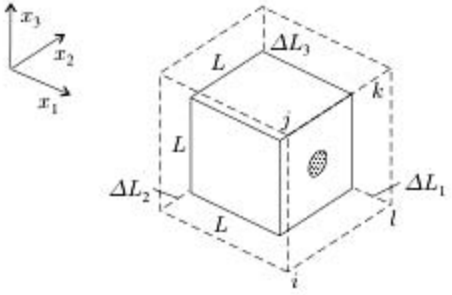

Figure 11.6: Deformation of Element 1 subjected to a uniform temperature change ΔT.

11.1.7 Thermal Expansion Coefficients

When the unrestrained Element 1 is subjected to a ΔT temperature change, its volume changes (Fig. 11.6). The new length, width, and height are $(L+\Delta L_1)$, $(L+\Delta L_2)$, and $(L+\Delta L_3)$, and the corresponding normal strains are

$$\epsilon_1 = \frac{\Delta L_1}{L} \qquad \epsilon_2 = \frac{\Delta L_2}{L} \qquad \epsilon_3 = \frac{\Delta L_3}{L}. \tag{11.45}$$

The longitudinal $\widetilde{\alpha}_1$ and transverse $\widetilde{\alpha}_2, \widetilde{\alpha}_3$ thermal expansion coefficients are defined as

$$\widetilde{\alpha}_1 = \frac{\epsilon_1}{\Delta T} \qquad \widetilde{\alpha}_2 = \frac{\epsilon_2}{\Delta T} \qquad \widetilde{\alpha}_3 = \frac{\epsilon_3}{\Delta T}. \tag{11.46}$$

Owing to symmetry, the transverse thermal expansion coefficients are equal ($\widetilde{\alpha}_2 = \widetilde{\alpha}_3$), and the transverse normal strains are equal ($\epsilon_2 = \epsilon_3$).

Equations (11.45) and (11.46) refer to the element.

For the fiber and the matrix, the strain–stress relationships are (Eqs. 2.162 and 2.163 and Table 2.7, page 15)

$$\epsilon_{f1} - \widetilde{\alpha}_{f1}\Delta T = \frac{\sigma_{f1}}{E_{f1}} \qquad \epsilon_{m1} - \widetilde{\alpha}_m \Delta T = \frac{\sigma_{m1}}{E_m} \tag{11.47}$$

$$\epsilon_{f2} - \widetilde{\alpha}_{f2}\Delta T = \frac{-\nu_{f12}}{E_{f1}}\sigma_{f1} \qquad \epsilon_{m2} - \widetilde{\alpha}_m \Delta T = \frac{-\nu_m}{E_m}\sigma_{m1}. \tag{11.48}$$

These equations are written with the assumptions that the longitudinal normal stress σ_1 dominates and is the only stress needed to be considered.

Longitudinal thermal expansion coefficient. When Element 1 is subjected to a temperature change ΔT, in the x direction the fiber and the matrix elongate the same amount as the composite. Hence, the normal strains in the x_1 direction are equal

$$\epsilon_1 = \epsilon_{f1} = \epsilon_{m1}. \tag{11.49}$$

From Eq. (11.47) the longitudinal normal stress (in the x_1 direction) in the fiber and the matrix may be written as (Eqs. 11.47 and 11.49)

$$\sigma_{f1} = (\epsilon_1 - \widetilde{\alpha}_{f1}\Delta T)E_{f1} \qquad \sigma_{m1} = (\epsilon_1 - \widetilde{\alpha}_m \Delta T)E_m. \tag{11.50}$$

The total force acting on the *ijkl* face (Fig. 11.6) is the sum of the forces acting on the fiber and the matrix:

$$F_1 = F_f + F_m. \tag{11.51}$$

Since there is no net force on the *ijkl* face, we write

$$F_f + F_m = \sigma_{f1} A_f + \sigma_{m1} A_m = 0. \tag{11.52}$$

By introducing Eq. (11.50) into (11.52) and by noting that $v_f = A_f/A$ and $v_m = A_m/A$, we obtain

$$\epsilon_1 (E_{f1} v_f + E_m v_m) - (\tilde{\alpha}_{f1} E_{f1} v_f + \tilde{\alpha}_m E_m v_m) \Delta T = 0. \tag{11.53}$$

By combining Eqs. (11.46, left) and (11.53), and by noting that $E_{f1} v_f + E_m v_m = E_1$ (Eq. 11.14), we obtain

$$\tilde{\alpha}_1 = \frac{v_f E_{f1}}{E_1} \tilde{\alpha}_{f1} + \frac{v_m E_m}{E_1} \tilde{\alpha}_m. \tag{11.54}$$

Transverse thermal expansion coefficient. When the temperature of Element 1 is changed by ΔT, the cross-sectional area of the face *ijkl* as well as the fiber and matrix areas change (Fig. 11.5). The changes in these areas are (Eqs. 11.33–11.34)

$$\Delta A = 2A\epsilon_2 \qquad \Delta A_f = 2A_f \epsilon_{f2} \qquad \Delta A_m = 2A_m \epsilon_{m2}. \tag{11.55}$$

The change in the total area is the sum of the changes of the fiber and matrix areas:

$$\Delta A = \Delta A_f + \Delta A_m. \tag{11.56}$$

By combining Eqs. (11.55) and (11.56) and by noting that $v_f = A_f/A$ and $v_m = A_m/A$, we obtain

$$\epsilon_2 = \frac{\Delta A}{2A} = v_f \epsilon_{f2} + v_m \epsilon_{m2}. \tag{11.57}$$

From Eq. (11.48), the transverse normal strains in the fiber and the matrix may be written as (x_2 direction)

$$\epsilon_{f2} = -\nu_{f12} \frac{\sigma_{f1}}{E_{f1}} + \tilde{\alpha}_{f2} \Delta T \qquad \epsilon_{m2} = -\nu_m \frac{\sigma_{m1}}{E_m} + \tilde{\alpha}_m \Delta T. \tag{11.58}$$

By introducing Eqs. (11.47) into these expressions and observing that $\epsilon_1 = \epsilon_{f1} = \epsilon_{m1} = \tilde{\alpha}_1 \Delta T$, we obtain

$$\epsilon_{f2} = -\nu_{f12}(\tilde{\alpha}_1 - \tilde{\alpha}_{f1})\Delta T + \tilde{\alpha}_{f2} \Delta T \qquad \epsilon_{m2} = -\nu_m (\tilde{\alpha}_1 - \tilde{\alpha}_m)\Delta T + \tilde{\alpha}_m \Delta T. \tag{11.59}$$

Equations (11.46, middle), (11.57), and (11.59) yield

$$\tilde{\alpha}_2 = v_f \tilde{\alpha}_{f2} + v_m \tilde{\alpha}_m + v_f \nu_{f12} (\tilde{\alpha}_{f1} - \tilde{\alpha}_1) + v_m \nu_m (\tilde{\alpha}_m - \tilde{\alpha}_1), \tag{11.60}$$

where $\tilde{\alpha}_1$ is given by Eq. (11.54).

11.1.8 Moisture Expansion Coefficients

We assume that the moisture content of the interface is negligible. Further, we consider composites in which the fibers do not absorb moisture and the moisture is uniformly distributed throughout the matrix. The moisture content of Element 1 is the sum of the moisture contents of the fiber and the matrix

$$cV = c_f V_f + c_m V_m, \tag{11.61}$$

where V is the volume, c the moisture concentration, and, as before, f and m refer to the fiber and the matrix. Since here we treat composites in which the fiber moisture content is zero ($c_f = 0$), we have

$$c = \frac{c_m V_m}{V} = c_m v_m. \tag{11.62}$$

The moisture-induced strains of Element 1 are

$$\epsilon_1 = \tilde{\beta}_1 c \qquad \epsilon_2 = \tilde{\beta}_2 c \qquad \epsilon_3 = \tilde{\beta}_3 c, \tag{11.63}$$

where $\tilde{\beta}_1$ is the longitudinal and $\tilde{\beta}_2$ and $\tilde{\beta}_3$ are the transverse moisture expression coefficients. Owing to symmetry, the transverse moisture expansion coefficients are equal ($\tilde{\beta}_2 = \tilde{\beta}_3$).

The moisture expansion coefficients of the fiber and the matrix are ($i = 1, 2, 3$)

$$\tilde{\beta}_{fi} = \frac{\epsilon_{fi}}{c_f} = \frac{c}{c_f}\frac{\epsilon_{fi}}{c} \qquad \tilde{\beta}_{mi} = \frac{\epsilon_{mi}}{c_m} = \frac{c}{c_m}\frac{\epsilon_{mi}}{c}. \tag{11.64}$$

We now compare the definitions of the thermal and moisture expansion coefficients as follows:

$$\begin{aligned} \tilde{\alpha}_i &= \frac{\epsilon_i}{\Delta T} & \tilde{\beta}_i &= \frac{\epsilon_i}{c} \\ \tilde{\alpha}_{fi} &= \frac{\epsilon_{fi}}{\Delta T} & \frac{c_f}{c}\tilde{\beta}_{fi} &= \frac{\epsilon_{fi}}{c} \\ \tilde{\alpha}_m &= \frac{\epsilon_{mi}}{\Delta T} & \frac{c_m}{c}\tilde{\beta}_m &= \frac{\epsilon_{mi}}{c}. \end{aligned} \tag{11.65}$$

From these equations we note the analogy between the thermal and moisture expansion coefficients. The temperature change ΔT corresponds to the moisture concentration c, and the thermal expansion coefficients correspond to the moisture expansion coefficients as follows:

$$\begin{aligned} \tilde{\alpha}_i &\Longrightarrow \tilde{\beta}_i \\ \tilde{\alpha}_{fi} &\Longrightarrow \frac{c_f}{c}\tilde{\beta}_{fi} \\ \tilde{\alpha}_m &\Longrightarrow \frac{c_m}{c}\tilde{\beta}_m. \end{aligned} \tag{11.66}$$

Since $c_f = 0$, Eqs. (11.66) and (11.62) give the following correspondence between the thermal and moisture expansion coefficients:

$$\begin{aligned} \widetilde{\alpha}_i &\Longrightarrow \widetilde{\beta}_i \\ \widetilde{\alpha}_{fi} &\Longrightarrow 0 \\ \widetilde{\alpha}_m &\Longrightarrow \frac{\widetilde{\beta}_m}{v_m}. \end{aligned} \tag{11.67}$$

Longitudinal moisture expansion coefficient. The longitudinal moisture expansion coefficient is obtained by replacing in Eq. (11.54) $\widetilde{\alpha}_1$ by $\widetilde{\beta}_1$, and $\widetilde{\alpha}_m$ by $\widetilde{\beta}_m/v_m$, and by setting $\widetilde{\alpha}_{f1} = 0$ as follows:

$$\widetilde{\beta}_1 = \frac{E_m}{E_1}\widetilde{\beta}_m. \tag{11.68}$$

Transverse moisture expansion coefficient. The transverse moisture expansion coefficient is obtained by replacing in Eq. (11.60) $\widetilde{\alpha}_i$ by $\widetilde{\beta}_i$, $\widetilde{\alpha}_m$ by $\widetilde{\beta}_m/v_m$, and by setting $\widetilde{\alpha}_{fi} = 0$:

$$\widetilde{\beta}_2 = \widetilde{\beta}_m + v_f v_{f12}(-\widetilde{\beta}_1) + v_m(\widetilde{\beta}_m - v_m\widetilde{\beta}_1). \tag{11.69}$$

11.1.9 Thermal Conductivity

The heat conducted (per unit time) in the longitudinal and transverse directions is given by Fourier's law

$$q_1 = A(K_1)\left(-\frac{\partial T}{\partial x_1}\right) \qquad q_2 = A(K_2)\left(-\frac{\partial T}{\partial x_2}\right). \tag{11.70}$$

where A is the cross-sectional area, $\partial T/\partial x$ is the temperature gradient, and K_1, K_2 are the longitudinal and transverse heat conduction coefficients, respectively.

The longitudinal and transverse normal forces are related to the longitudinal and transverse normal strains by Hooke's law as follows:

$$F_1 = A(E_1)(\epsilon_1) \qquad F_2 = A(E_2)(\epsilon_2). \tag{11.71}$$

Equations (11.70) and (11.71) show the analogy between Fourier's and Hooke's laws. This analogy is used to obtain the micromechanical expressions for the thermal conductivities. The heat-conducted q corresponds to the force F, the thermal conductivity K to the Young modulus E and the temperature gradient $\partial T/\partial x$ to the strain ϵ.

$$\begin{aligned} q &\Longrightarrow F \\ K &\Longrightarrow E \\ \frac{\partial T}{\partial x} &\Longrightarrow \epsilon. \end{aligned} \tag{11.72}$$

Longitudinal thermal conductivity. The longitudinal thermal conductivity is obtained by replacing in Eq. (11.14) E_{f1} by K_{f1} and E_m by K_m. The resulting expression is

$$K_1 = v_f K_{f1} + v_m K_m \tag{11.73}$$

Transverse thermal conductivity. The transverse thermal conductivity is obtained by replacing in Eq. (11.22) E_{f2} by K_{f2} and E_m by K_m. The resulting expression is

$$K_2 = \left(\frac{v_f}{K_{f2}} + \frac{v_m}{K_m}\right)^{-1}. \tag{11.74}$$

11.1.10 Moisture Diffusivity

Moisture diffusion in the longitudinal and transverse directions are assumed to follow Fick's law

$$\dot{m}_1 = A(D_1)\left(-\frac{\partial c}{\partial x_1}\right) \qquad \dot{m}_2 = A(D_2)\left(-\frac{\partial c}{\partial x_2}\right), \tag{11.75}$$

where $\dot{m}$ is the mass of moisture being transported (per unit time) across the surface A, $\partial c/\partial x$ is the moisture concentration gradient, and D_1, D_2 are the longitudinal and transverse diffusivities, respectively.

Equations (11.70) and (11.75) show the analogy between Fourier's and Fick's laws. This analogy is used to obtain the micromechanical expressions for the moisture diffusivities. The heat conduction q corresponds to the moisture transport $\dot{m}$, the thermal conductivity K to the diffusivity D, and the temperature gradient $\partial T/\partial x$ to the moisture gradient $\partial c/\partial x$ as follows:

$$\begin{aligned} q &\Longrightarrow m \\ K &\Longrightarrow D \\ \frac{\partial T}{\partial x} &\Longrightarrow \frac{\partial c}{\partial x}. \end{aligned} \tag{11.76}$$

Longitudinal moisture diffusivity. The longitudinal moisture diffusivity is obtained by replacing in Eq. (11.73) K_{f1} by D_{f1} and K_m by D_m. The resulting expression is

$$D_1 = v_f D_{f1} + v_m D_m. \tag{11.77}$$

When the diffusivity of the fibers is negligible, we have

$$D_1 = v_m D_m. \tag{11.78}$$

Transverse moisture diffusivity. The transverse moisture diffusivity is obtained by replacing in Eq. (11.74) K_{f2} by D_{f2} and K_m by D_m. The resulting expression is

$$D_2 = \left(\frac{v_f}{D_{f2}} + \frac{v_m}{D_m}\right)^{-1}. \tag{11.79}$$

When the diffusivity of the fibers is small ($D_{f2} \to 0$), this expression gives that $D_2 \to 0$, and Eq. (11.79) should not be used.

11.1.11 Specific Heat

When the temperature of Element 1 is raised from a specific datum T_0 to T, the heat contents of the composite, the fiber, and the matrix are

$$H = \rho C V (T - T_0) \qquad H_f = \rho_f C_f V_f (T - T_0) \qquad H_m = \rho_m C_m V_m (T - T_0), \tag{11.80}$$

where C, C_f, C_m are the specific heats of the composite, the fiber, and the matrix, respectively. The total heat content of the composite is

$$H = H_f + H_m. \tag{11.81}$$

Thus, the specific heat is

$$C = C_f \frac{\rho_f v_f}{\rho} + C_m \frac{\rho_m v_m}{\rho}. \tag{11.82}$$

By substituting the expression for the density ρ given by Eq. (11.7), we obtain

$$C = \frac{C_f \rho_f v_f + C_m \rho_m v_m}{\rho_f v_f + \rho_m v_m}. \tag{11.83}$$

11.2 Modified Rule of Mixtures

The modified rule of mixtures is somewhat more complex than the rule of mixtures, but it gives the transverse properties with better accuracy. We illustrate the main features of the model through the derivation of the transverse Young modulus.

The basic building block is an element in which the fiber bundle is taken to be of rectangular cross section (Fig. 11.7).[1] The volume fraction of this rectangular fiber bundle is the same as the volume fraction of the corresponding circular fiber bundle.

As a first step we replace this element with a rectangular "box" with three layers. The two outer layers consist of the matrix whereas, for now, the middle layer is taken to consist of a fictitious homogeneous material. This "box" is compared with Element 2 shown in Figure 11.2. For the present "box" the middle layer (designated by b) corresponds to the middle fiber sheet in Element 2. Thus, the transverse Young modulus of the "box" is given by Eq. (11.22) with the subscript f replaced by b

$$E_2 = \left(\frac{v_b}{E_{b2}} + \frac{1 - v_b}{E_m} \right)^{-1}. \tag{11.84}$$

[1] D. A. Hopkins and C. C. Chamis, A Unique Set of Micromechanical Equations for High Temperature Metal Matrix Composites. In: *Testing Technology of Metal Matrix Composites*, ASTM STP 964, American Society for Testing and Materials, Philadelphia, 1988, pp. 159–176.

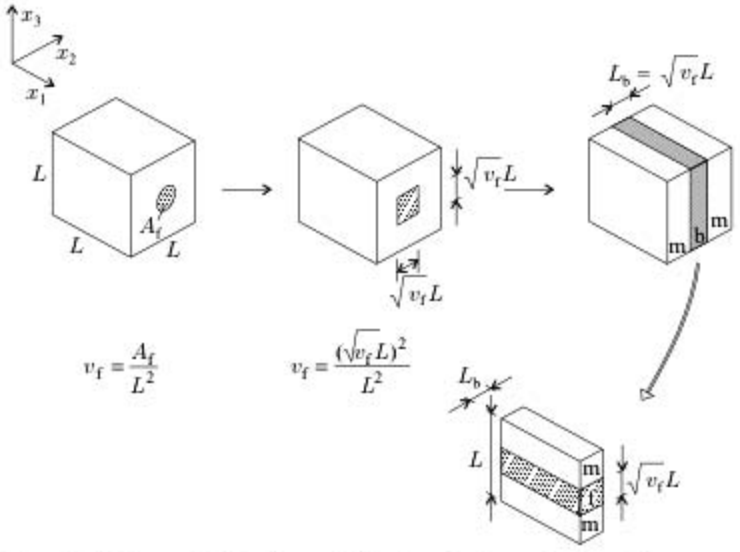

Figure 11.7: The model for the modified rule of mixtures (top) and the representation of the middle "b" layer (bottom).

The volume fraction of the middle layer v_b is determined as follows. The width of the middle layer L_b is the same as the width of the rectangular fiber bundle. Thus, v_b is

$$v_b = \frac{(L)(L_b)}{L^2} = \frac{L\sqrt{v_f}}{L} = \sqrt{v_f}, \tag{11.85}$$

where v_f is the fiber volume fraction of the entire box ($v_f = (\sqrt{v_f}L)^2/L^2$, Fig. 11.7, middle).

The Young modulus E_{b2} of the middle layer is obtained by replacing this homogenized fictional layer by a layer consisting of the rectangular fiber bundle surrounded by matrix (Fig. 11.7, bottom). The volume fraction of the fiber bundle in this middle layer is $\frac{(\sqrt{v_f}L)L_b}{LL_b} = \sqrt{v_f}$. We now apply the longitudinal rule of mixtures (Eq. 11.14) to the middle layer. The result is

$$E_{b2} = \sqrt{v_f}E_{f2} + (1 - \sqrt{v_f})\,E_m. \tag{11.86}$$

Equations (11.84) and (11.86) give the transverse Young modulus. Other properties may be obtained similarly. Details of the derivations are not given here. The results are included in Tables 11.1 and 11.2.

11.3 Note on the Micromechanics Models

The various available micromechanics approaches yield similar results, except for the rule of mixtures, which underestimates the shear moduli and the transverse properties. This is illustrated by the examples in Figure 11.8, where the transverse Young modulus and the longitudinal shear modulus are shown as calculated by

Table 11.2. Expressions for the hygrothermal properties

Thermal expansion coefficients	$\tilde{\alpha}_1 = \frac{v_f E_{f1}}{E_1}\tilde{\alpha}_{f1} + \frac{v_m E_m}{E_1}\tilde{\alpha}_m$
	$\tilde{\alpha}_2 = v_f\tilde{\alpha}_{f2} + v_m\tilde{\alpha}_m + v_f v_{f12}(\tilde{\alpha}_{f1} - \tilde{\alpha}_1) + v_m v_m(\tilde{\alpha}_m - \tilde{\alpha}_1)$
Moisture expansion coefficients ($c_f = 0$)	$\tilde{\beta}_1 = \frac{E_m}{E_1}\tilde{\beta}_m$
	$\tilde{\beta}_2 = \tilde{\beta}_m + v_f v_{f12}(-\tilde{\beta}_1) + v_m(\tilde{\beta}_m - v_m\tilde{\beta}_1)$
Longitudinal thermal conductivity	$K_1 = v_f K_{f1} + v_m K_m$
Transverse thermal conductivity	$K_2 = \left(\frac{\sqrt{v_f}}{K_{b2}} + \frac{1-\sqrt{v_f}}{K_m}\right)^{-1}$ where $K_{b2} = \sqrt{v_f}K_{f2} + (1-\sqrt{v_f})K_m$
Longitudinal moisture diffusivity	$D_1 = v_f D_{f1} + v_m D_m$
	$D_1 = v_m D_m$ when $D_{f1} = 0$
Transverse moisture diffusivity	$D_2 = \left(\frac{\sqrt{v_f}}{D_{b2}} + \frac{1-\sqrt{v_f}}{D_m}\right)^{-1}$ where $D_{b2} = \sqrt{v_f}D_{f2} + (1-\sqrt{v_f})D_m$
	$D_2 = D_m\left(\frac{1}{1-\sqrt{v_f}} - \sqrt{v_f}\right)^{-1}$ when $D_{f2} = 0$
Specific heat	$C = C_f\frac{\rho_f v_f}{\rho} + C_m\frac{\rho_m v_m}{\rho} = \frac{C_f\rho_f v_f + C_m\rho_m v_m}{\rho_f v_f + \rho_m v_m}$

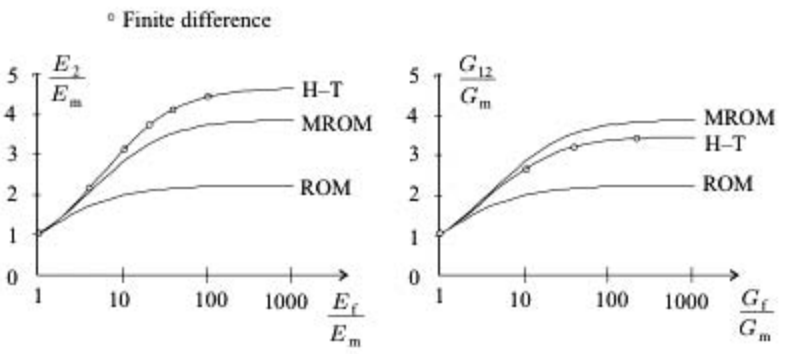

Figure 11.8: The transverse Young and shear moduli calculated by the rule of mixtures (ROM), the modified rule of mixtures (MROM), the Halpin–Tsai (H–T) equations, and the finite difference solutions (circles) of Adams and Doner ($v_f = 0.55$).

Table 11.3. The engineering constants in Example 11.1

	E_1 (GPa)	E_2 (GPa)	G_{12} (GPa)	ν_{12}
Nominal ($v_f = 0.6$)	148	9.65	4.55	0.300
Back calculated ($v_f = 0.55$)				
Rule of mixtures	136	–	–	0.304
Modified rule of mixtures	–	9.00	4.14	–

(i) mechanics of materials models (rule of mixtures, modified rule of mixtures), (ii) the elasticity solutions of Adams and Doner,[2,3] and (iii) the Halpin–Tsai[4] semiempirical expressions.

Even when property values predicted by various micromechanics expressions are by and large similar, they should not be relied upon for design purposes because of inaccuracies introduced by approximations in the models, by uncertainties in constituents properties, and by manufacturing variances. Rather, it is recommended that the ply properties be determined by testing the ply itself.

Micromechanics expressions are useful for estimating the changes in ply properties with small changes in the volume fraction or in the properties of the fiber and the matrix. The procedure for estimating the changes in ply properties is referred to as "back calculation" and is illustrated in the following example.

11.1 Example. *The nominal engineering constants of a unidirectional graphite epoxy ply are given in Table 11.3 for a fiber volume fraction of 60 percent. The fiber volume is reduced to 55 percent. Estimate the engineering constants for this reduced fiber volume fraction.*

Solution. Generally, the matrix properties are known reasonably accurately, whereas the fiber properties are not. Therefore, the fiber properties are back calculated.

The ply's longitudinal Young modulus is (Eq. 11.14)

$$E_1 = v_f E_{f1} + v_m E_m. \tag{11.87}$$

The fiber's longitudinal Young modulus with the matrix properties in Table C.2 ($E_m = 4.1$ GPa, $G_m = 1.5$ GPa, $\nu_m = 0.35$) is

$$E_{f1} = \frac{1}{v_f}(E_1 - v_m E_m) = \frac{1}{0.6}(148 - 0.4 \times 4.1) = 244 \text{ GPa}.$$

With this value of E_{f1} the longitudinal Young modulus for $v_f = 0.55$ is (Eq. 11.87)

$$E_1^{0.55} = v_f E_{f1} + v_m E_m = 0.55 \times 244 + 0.45 \times 4.1 = 136 \text{ GPa}.$$

[2] D. F. Adams and D. R. Doner, Transverse Normal Loading of a Unidirectional Composite. *Journal of Composite Materials*, Vol. 1, 152–164, 1967.

[3] D. F. Adams and D. R. Doner, Longitudinal Shear Loading of a Unidirectional Composite. *Journal of Composite Materials*, Vol. 1, 4–17, 1967.

[4] J. C. Halpin and S. W. Tsai, *Effects of Environmental Factors on Composite Materials*. Air Force Material Laboratory, Wright–Patterson Air Force Base, Dayton, Ohio. TR–67–423, 1969.

The ply's longitudinal Poisson ratio υ_{f12} is obtained similarly by the rule of mixtures. The result is given in Table 11.3.

The ply's transverse Young modulus is (Eqs. 11.84 and 11.85)

$$E_2 = \left(\frac{\sqrt{\upsilon_f}}{E_{b2}} + \frac{1 - \sqrt{\upsilon_f}}{E_m} \right)^{-1}. \tag{11.88}$$

By rearranging this expression, we obtain ($\upsilon_f = 0.6$)

$$E_{b2} = \sqrt{\upsilon_f} \left(\frac{1}{E_2} - \frac{1 - \sqrt{\upsilon_f}}{E_m} \right)^{-1} = \sqrt{0.6} \left(\frac{1}{9.65} - \frac{1 - \sqrt{0.6}}{4.1} \right)^{-1} = 15.92 \text{ GPa}.$$

From (Eq. 11.86) we have

$$E_{b2} = \sqrt{\upsilon_f} E_{f2} + (1 - \sqrt{\upsilon_f})\, E_m. \tag{11.89}$$

From this expression the transverse fiber Young modulus is ($\upsilon_f = 0.6$)

$$\begin{aligned} E_{f2} &= \frac{1}{\sqrt{\upsilon_f}} (E_{b2} - (1 - \sqrt{\upsilon_f}) E_m) \\ &= \frac{1}{\sqrt{0.6}} (15.92 - (1 - \sqrt{0.6})(4.1)) = 19.36 \text{ GPa}. \end{aligned}$$

With this value of E_{f2}, Eq. (11.89) gives

$$E_{b2}^{0.55} = \sqrt{0.55}(19.36) + (1 - \sqrt{0.55})(4.1) = 10.73 \text{ GPa}.$$

The ply's transverse Young modulus for $\upsilon_f = 0.55$ is (Eq. 11.88)

$$E_2^{0.55} = \left(\frac{\sqrt{0.55}}{10.73} + \frac{1 - \sqrt{0.55}}{4.1} \right)^{-1} = 9.00 \text{ GPa}.$$

The shear modulus G_{12} is calculated by the modified rule of mixtures in a similar manner. The back-calculated engineering constants are tabulated in Table 11.3.

Cross-Sectional Properties of Thin-Walled Composite Beams

In the following tables a_{11} and d_{11} are the elements of the compliance matrix of symmetrical laminates (Eqs. 3.29 and 3.30) evaluated at the midsurface; α_{ij}, β_{ij}, δ_{ij} are the elements of the compliance matrix of nonsymmetrical laminates (Eq. 3.23). These properties are evaluated at each wall segment's "neutral" plane. In the main text these elements are identified by the superscript ϱ. To simplify the notation, in this Appendix the superscript ϱ is omitted.

The subscripts f1, f2, and w refer to flange 1, flange 2 and the web, respectively.

The modified material properties are

$$\bar{\alpha}_{11} = \left(\alpha_{11} - \frac{(\beta_{16})^2}{\delta_{66}}\right) \qquad \hat{\alpha}_{11} = \left(\alpha_{11} - \frac{\beta_{12}^2}{\delta_{22}}\right)$$

$$\bar{\beta}_{11} = \left(\beta_{11} - \frac{\beta_{16}\delta_{16}}{\delta_{66}}\right) \qquad \hat{\beta}_{11} = \left(\beta_{11} - \frac{\beta_{12}\delta_{12}}{\delta_{22}}\right)$$

$$\bar{\delta}_{11} = \left(\delta_{11} - \frac{(\delta_{16})^2}{\delta_{66}}\right) \qquad \hat{\delta}_{11} = \left(\delta_{11} - \frac{\delta_{12}^2}{\delta_{22}}\right).$$

The location of the "neutral" plane with respect to the midplane is

$$\tilde{\varrho} = -\frac{\beta_{11}^{MP}}{\delta_{11}^{MP}} \qquad \begin{matrix}\text{open section}\\ \text{orthotropic unsymmetrical layup}\\ \text{arbitrary cross section}\end{matrix} \tag{A.1}$$

$$\bar{\varrho} = -\frac{\bar{\beta}_{11}^{MP}}{\bar{\delta}_{11}^{MP}} \qquad \begin{matrix}\text{open section}\\ \text{arbitrary layup}\\ \text{symmetrical cross section}\end{matrix} \tag{A.2}$$

$$\hat{\varrho} = -\frac{\hat{\beta}_{11}^{MP}}{\hat{\delta}_{11}^{MP}} \qquad \begin{matrix}\text{closed section}\\ \text{orthotropic unsymmetrical layup}\\ \text{arbitrary cross section.}\end{matrix} \tag{A.3}$$

β_{11}^{MP} and δ_{11}^{MP} are evaluated at the midplanes.

The stiffness α_{66}^{v} is (Eq. 6.196)

$$\alpha_{66}^{v} = \alpha_{66} - \frac{\beta_{66}^2}{\delta_{66}}, \tag{A.4}$$

where α_{66}, β_{66}, and δ_{66} are evaluated at the "neutral" plane.

Table A.1. The tensile and bending stiffnesses and the coordinates of the centroid. The layup of each wall segment is orthotropic and symmetrical. The properties are evaluated at each wall segment's "neutral" plane, which is at the midplane.

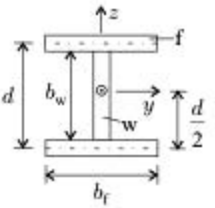

$$\widehat{EA} = \frac{2b_f}{(a_{11})_f} + \frac{b_w}{(a_{11})_w}$$

$$\widehat{EI}_{yy} = \frac{b_f}{(a_{11})_f}\frac{d^2}{2} + \frac{2b_f}{(d_{11})_f} + \frac{b_w^3}{12(a_{11})_w}$$

$$\widehat{EI}_{zz} = \frac{b_w}{(d_{11})_w} + \frac{2b_f^3}{12(a_{11})_f}$$

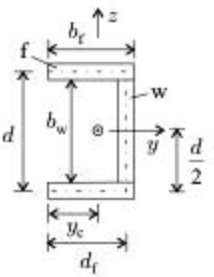

$$\widehat{EA} = \frac{2b_f}{(a_{11})_f} + \frac{b_w}{(a_{11})_w}$$

$$y_c = \frac{1}{\widehat{EA}}\left(\frac{2b_f}{(a_{11})_f}\frac{b_f}{2} + \frac{b_w}{(a_{11})_w}d_f\right)$$

$$\widehat{EI}_{yy} = \frac{b_f}{(a_{11})_f}\frac{d^2}{2} + \frac{2b_f}{(d_{11})_f} + \frac{b_w^3}{12(a_{11})_w}$$

$$\widehat{EI}_{zz} = \frac{b_w}{(a_{11})_w}(d_f - y_c)^2 + \frac{b_w}{(d_{11})_w} + \frac{2}{(a_{11})_f}\left(\frac{y_c^3}{3} + \frac{(b_f - y_c)^3}{3}\right)$$

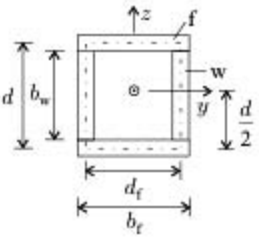

$$\widehat{EA} = \frac{2b_f}{(a_{11})_f} + \frac{2b_w}{(a_{11})_w}$$

$$\widehat{EI}_{yy} = \frac{b_f}{(a_{11})_f}\frac{d^2}{2} + \frac{2b_f}{(d_{11})_f} + \frac{2b_w^3}{12(a_{11})_w}$$

$$\widehat{EI}_{zz} = \frac{b_w}{(a_{11})_w}\frac{d_f^2}{2} + \frac{2b_w}{(d_{11})_w} + \frac{2b_f^3}{12(a_{11})_f}$$

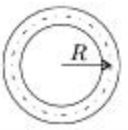

$$\widehat{EA} = \frac{2R\pi}{a_{11}}$$

$$\widehat{EI}_{yy} = \widehat{EI}_{zz} = \pi\left(\frac{R^3}{a_{11}} + \frac{R}{d_{11}}\right)$$

Table A.2. The tensile and bending stiffnesses and the coordinates of the centroid. The layup of each wall segment is orthotropic and unsymmetrical. The properties α_{11} and δ_{11} are evaluated at each wall segment's "neutral" plane, which is at $\tilde{\varrho}$.

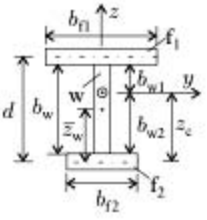

$$\widehat{EA} = \frac{b_{f1}}{(\alpha_{11})_{f1}} + \frac{b_{f2}}{(\alpha_{11})_{f2}} + \frac{b_w}{(\alpha_{11})_w}$$

$$z_c = \frac{1}{\widehat{EA}}\left(\frac{b_{f1}}{(\alpha_{11})_{f1}} d + \frac{b_w}{(\alpha_{11})_w}\bar{z}_w\right)$$

$$\widehat{EI}_{zz} = \frac{b_w}{(d_{11})_w} + \frac{1}{(\alpha_{11})_{f1}}\frac{b_{f1}^3}{12} + \frac{1}{(\alpha_{11})_{f2}}\frac{b_{f2}^3}{12}$$

$$\widehat{EI}_{yy} = \frac{b_{f1}}{(\alpha_{11})_{f1}}(d - z_c)^2 + \frac{b_{f2}}{(\alpha_{11})_{f2}} z_c^2 + \frac{b_{f1}}{(\delta_{11})_{f1}} + \frac{b_{f2}}{(\delta_{11})_{f2}} + \frac{1}{(\alpha_{11})_w}\left(\frac{b_{w1}^3 + b_{w2}^3}{3}\right)$$

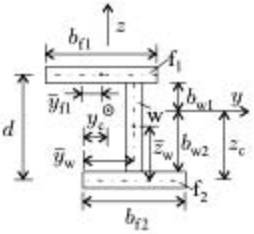

$$\widehat{EA} = \frac{b_{f1}}{(\alpha_{11})_{f1}} + \frac{b_{f2}}{(\alpha_{11})_{f2}} + \frac{b_w}{(\alpha_{11})_w}$$

$$z_c = \frac{1}{\widehat{EA}}\left(\frac{b_{f1}}{(\alpha_{11})_{f1}} d + \frac{b_w}{(\alpha_{11})_w}\bar{z}_w\right)$$

$$y_c = \frac{1}{\widehat{EA}}\left(\frac{b_{f1}}{(\alpha_{11})_{f1}}\bar{y}_{f1} + \frac{b_{f2}}{(\alpha_{11})_{f2}}\frac{b_{f2}}{2} + \frac{b_w}{(\alpha_{11})_w}\bar{y}_w\right)$$

$$\widehat{EI}_{yy} = \frac{b_{f1}}{(\alpha_{11})_{f1}}(d - z_c)^2 + \frac{b_{f2}}{(\alpha_{11})_{f2}} z_c^2 + \frac{b_{f1}}{(\delta_{11})_{f1}} + \frac{b_{f2}}{(\delta_{11})_{f2}} + \frac{1}{(\alpha_{11})_w}\left(\frac{b_{w1}^3 + b_{w2}^3}{3}\right)$$

$$\widehat{EI}_{zz} = \frac{b_w}{(\alpha_{11})_w}(\bar{y}_w - y_c)^2 + \frac{b_w}{(\delta_{11})_w} + \frac{1}{(\alpha_{11})_{f1}}\frac{b_{f1}^3}{12} + \frac{1}{(\alpha_{11})_{f2}}\frac{b_{f2}^3}{12} + \frac{b_{f1}}{(\alpha_{11})_{f1}}(y_c - \bar{y}_{f1})^2 + \frac{b_{f2}}{(\alpha_{11})_{f2}}\left(y_c - \frac{b_{f2}}{2}\right)^2$$

$$\widehat{EI}_{yz} = \frac{b_{f1}}{(\alpha_{11})_{f1}}(\bar{y}_{f1} - y_c)(d - z_c) - \frac{b_{f2}}{(\alpha_{11})_{f2}}\left(\frac{b_{f2}}{2} - y_c\right) z_c + \frac{b_w}{(\alpha_{11})_w}(\bar{y}_w - y_c)\left(\frac{b_w}{2} - z_c\right)$$

Table A.3. The tensile and bending stiffnesses. The layup of each wall segment is orthotropic and unsymmetrical. Doubly symmmetrical cross section. The property $\widehat{\alpha}_{11}$ is evaluated at each wall segment's "neutral" plane, which is at $\widehat{\varrho}$. The properties α_{11} and δ_{11} are evaluated at each wall segment's "neutral" plane, which is at $\tilde{\varrho}$.

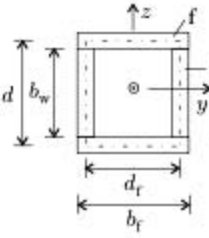

$$\widehat{EA} = \frac{2b_f}{(\widehat{\alpha}_{11})_f} + \frac{2b_w}{(\widehat{\alpha}_{11})_w}$$

$$\widehat{EI}_{yy} = \frac{b_f}{(\alpha_{11})_f}\frac{d^2}{2} + \frac{2b_f}{(\delta_{11})_f} + \frac{2b_w^3}{12(\alpha_{11})_w}$$

$$\widehat{EI}_{zz} = \frac{b_w}{(\alpha_{11})_w}\frac{d_f^2}{2} + \frac{2b_w}{(\delta_{11})_w} + \frac{2b_f^3}{12(\alpha_{11})_f}$$

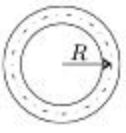

$$\widehat{EA} = 2R\pi\frac{1}{\widehat{\alpha}_{11}}$$

$$\widehat{EI}_{yy} = \widehat{EI}_{zz} = \pi\left(R^3\frac{1}{\alpha_{11}} + R\frac{1}{\delta_{11}}\right)$$

Table A.4. The tensile and bending stiffnesses and the coordinates of the centroid. The cross section is symmetrical about the z-axis. The layup of each wall segment is arbitrary. The properties $\overline{\alpha}_{11}$ and $\overline{\delta}_{11}$ are evaluated at each wall segment's "neutral" plane, which is at $\overline{\varrho}$.

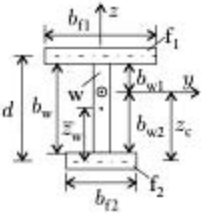

$$\widehat{EA} = \frac{b_{f1}}{(\overline{\alpha}_{11})_{f1}} + \frac{b_{f2}}{(\overline{\alpha}_{11})_{f2}} + \frac{b_w}{(\alpha_{11})_w}$$

$$z_c = \frac{1}{\widehat{EA}}\left(\frac{b_{f1}}{(\overline{\alpha}_{11})_{f1}} d + \frac{b_w}{(\alpha_{11})_w}\bar{z}_w\right)$$

$$\widehat{EI}_{yy} = \frac{b_{f1}}{(\overline{\alpha}_{11})_{f1}}(d - z_c)^2 + \frac{b_{f2}}{(\overline{\alpha}_{11})_{f2}} z_c^2 + \frac{b_{f1}}{(\overline{\delta}_{11})_{f1}} + \frac{b_{f2}}{(\overline{\delta}_{11})_{f2}} + \frac{1}{(a_{11})_w}\left(\frac{b_{w1}^3 + b_{w2}^3}{3}\right)$$

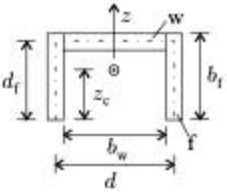

$$\widehat{EA} = \frac{2b_f}{(\overline{\alpha}_{11})_f} + \frac{b_w}{(\overline{\alpha}_{11})_w}$$

$$z_c = \frac{1}{\widehat{EA}}\left(\frac{2b_f}{(\overline{\alpha}_{11})_f}\frac{b_f}{2} + \frac{b_w}{(\overline{\alpha}_{11})_w} d_f\right)$$

$$\widehat{EI}_{yy} = \frac{2}{(\overline{\alpha}_{11})_f}\frac{b_f^3}{12} + \frac{2}{(\overline{\alpha}_{11})_f} b_f\left(\frac{b_f}{2} - z_c\right)^2 + \frac{b_w}{(\overline{\alpha}_{11})_w}(d_f - z_c)^2 + \frac{b_w}{(\overline{\delta}_{11})_w}$$

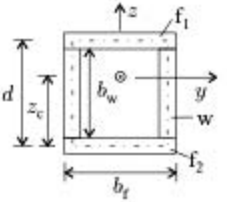

$$\widehat{EA} \approx \frac{b_{f1}}{(\overline{\alpha}_{11})_{f1}} + \frac{b_{f2}}{(\overline{\alpha}_{11})_{f2}} + \frac{2b_w}{(\overline{\alpha}_{11})_w}$$

$$z_c \approx \frac{1}{\widehat{EA}}\left(\frac{b_f}{(\overline{\alpha}_{11})_{f1}} d + \frac{2b_w}{(\overline{\alpha}_{11})_w}\frac{d}{2}\right)$$

$$\widehat{EI}_{yy} \approx \frac{b_{f1}}{(\overline{\delta}_{11})_{f1}} + \frac{b_{f2}}{(\overline{\delta}_{11})_{f2}} + \frac{2b_w^3}{12(\overline{\alpha}_{11})_w}$$
$$+ \frac{b_{f1}}{(\overline{\alpha}_{11})_{f1}}(d - z_c)^2 + \frac{b_{f2}}{(\overline{\alpha}_{11})_{f2}} z_c^2 + \frac{2b_w}{(\overline{\alpha}_{11})_w}\left(\frac{d}{2} - z_c\right)^2$$

Table A.5. The warping and torsional stiffnesses and the location of the shear center. The layup of each wall segment is orthotropic and unsymmetrical. The properties δ_{66} and δ_{11} are evaluated at each wall segment's "neutral" plane, which is at $\tilde{\varrho}$.

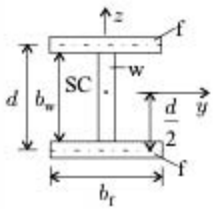

$$\widehat{GI}_t = 4\left(\frac{2b_f}{(\delta_{66})_f} + \frac{b_w}{(\delta_{66})_w}\right)$$

$$\widehat{EI}_\omega = \frac{1}{(\sigma_{11})_f}\frac{d^2 b_f^3}{24}$$

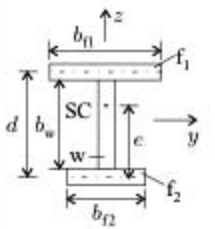

$$\widehat{GI}_t = 4\left(\frac{b_{f1}}{(\delta_{66})_{f1}} + \frac{b_{f2}}{(\delta_{66})_{f2}} + \frac{b_w}{(\delta_{66})_w}\right)$$

$$\widehat{EI}_\omega = \frac{\frac{b_{f2}^3}{(\sigma_{11})_{f2}}}{12}ed \qquad e = d\frac{\frac{b_{f1}^3}{(\sigma_{11})_{f1}}}{\frac{b_{f1}^3}{(\sigma_{11})_{f1}} + \frac{b_{f2}^3}{(\sigma_{11})_{f2}}}$$

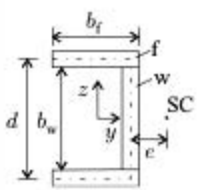

$$\widehat{GI}_t = 4\left(\frac{2b_f}{(\delta_{66})_f} + \frac{b_w}{(\delta_{66})_w}\right) \qquad e = \frac{\frac{3b_f^2}{(\sigma_{11})_f}}{\frac{6b_f}{(\sigma_{11})_f} + \frac{d}{(\sigma_{11})_w}}$$

$$\widehat{EI}_\omega = \frac{b_f^3 d^2}{12}\frac{\frac{1}{(\sigma_{11})_f}}{\frac{\frac{3b_f}{(\sigma_{11})_f} + \frac{2d}{(\sigma_{11})_w}}{\frac{6b_f}{(\sigma_{11})_f} + \frac{d}{(\sigma_{11})_w}}}$$

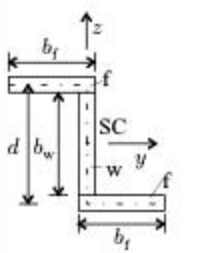

$$\widehat{GI}_t = 4\left(\frac{2b_f}{(\delta_{66})_f} + \frac{b_w}{(\delta_{66})_w}\right)$$

$$\widehat{EI}_\omega = \frac{b_f^3 d^2}{12(2b_f+d)^2}\left(2\frac{\left(b_f^2+b_f d+d^2\right)}{(\sigma_{11})_f} + 3\frac{b_f d}{(\sigma_{11})_w}\right)$$

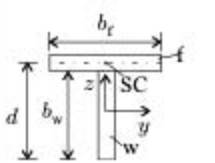

$$\widehat{GI}_t = 4\left(\frac{b_f}{(\delta_{66})_f} + \frac{b_w}{(\delta_{66})_w}\right)$$

$$\widehat{EI}_\omega = 0$$

Table A.6. The warping and torsional stiffnesses of closed-section beams. The layup of each wall segment is orthotropic and unsymmetrical. α_{66}^{v} is given by Eq. (A.4).

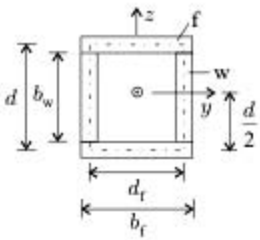

$$\widehat{GI}_t = \frac{2d_f^2 d^2}{(\alpha_{66}^v)_f d_f + (\alpha_{66}^v)_w d}$$

$$\widehat{EI}_\omega \approx 0$$

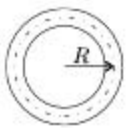

$$\widehat{GI}_t = \frac{2R^3\pi}{\alpha_{66}^v}$$

$$\widehat{EI}_\omega = 0$$

Table A.7. Shear compliances of closed-section beams. The layup of each wall segment is orthotropic and unsymmetrical. The properties $\widetilde{\delta}_{66}$ and $\widetilde{\delta}_{11}$ are evaluated at each wall segment's "neutral" plane, which is at $\widetilde{\varrho}$. α_{66}^{v} is given by Eq. (A.4).

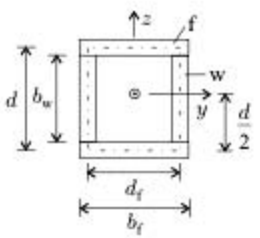

$$\widehat{s}_{zz} = \frac{(\alpha_{66}^v)_w}{2d} + \frac{1}{6}\frac{(\alpha_{66}^v)_f d_f}{d^2 \gamma_z^2}$$

$$\widehat{s}_{yy} = \frac{(\alpha_{66}^v)_f}{2d_f} + \frac{1}{6}\frac{(\alpha_{66}^v)_w d}{d_f^2 \gamma_y^2}$$

$$\widehat{s}_{yz} = 0$$

$$\gamma_z = 1 + \frac{1}{3}\frac{(\alpha_{11})_f}{(\alpha_{11})_w}\frac{d}{d_f} \qquad \gamma_y = 1 + \frac{1}{3}\frac{(\alpha_{11})_w}{(\alpha_{11})_f}\frac{d_f}{d}$$

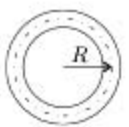

$$\widehat{s}_{zz} = \widehat{s}_{yy} = \frac{\alpha_{66}^v}{R\pi}$$

$$\widehat{s}_{yz} = 0$$

Table A.8. Shear compliances. The layup of each wall segment is orthotropic and unsymmetrical. The coordinates of the centroid y_c, z_c are given in Tables A.1 through A.4, and the coordinate of the shear center e in Table A.5. The properties are evaluated at each wall segment's "neutral" plane, which is at $\tilde{\rho}$. α_{66}^{v} is given by Eq. (A.4).

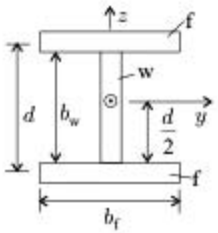

$$\widehat{s}_{yy} = 1.2\frac{\left(\alpha_{66}^{v}\right)_f}{2b_f}$$

$$\widehat{s}_{zz} = \frac{\left(\alpha_{66}^{v}\right)_w}{d} + \frac{1}{6}\frac{\left(\alpha_{66}^{v}\right)_f b_f}{d^2\gamma^2}$$

$$\widehat{s}_{\omega\omega} = \frac{2.4}{d^2}\frac{\left(\alpha_{66}^{v}\right)_f}{b_f}$$

$$\widehat{s}_{yz} = \widehat{s}_{y\omega} = \widehat{s}_{z\omega} = 0$$

where $\gamma = 1 + \frac{1}{6}\frac{(\alpha_{11})_f}{(\alpha_{11})_w}\frac{d}{b_f}$

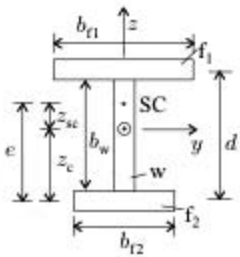

$$\widehat{s}_{yy} = 1.2\left(\frac{\left(\alpha_{66}^{v}\right)_{f1}}{b_{f1}(1+\delta_{sc})^2} + \frac{\left(\alpha_{66}^{v}\right)_{f2}}{b_{f2}\left(1+\frac{1}{\delta_{sc}}\right)^2}\right)$$

$$\widehat{s}_{zz} = \frac{\left(\alpha_{66}^{v}\right)_w}{d} + \frac{1}{12}\frac{\left(\alpha_{66}^{v}\right)_{f1} b_{f1}}{d^2\gamma_1^2} + \frac{1}{12}\frac{\left(\alpha_{66}^{v}\right)_{f2} b_{f2}}{d^2\gamma_2^2}$$

$$\widehat{s}_{\omega\omega} = \frac{1.2}{d^2}\left(\frac{\left(\alpha_{66}^{v}\right)_{f1}}{b_{f1}} + \frac{\left(\alpha_{66}^{v}\right)_{f2}}{b_{f2}}\right)$$

$$\widehat{s}_{y\omega} = \frac{1.2}{d}\left(-\frac{\left(\alpha_{66}^{v}\right)_{f1}}{b_{f1}(1+\delta_{sc})} + \frac{\left(\alpha_{66}^{v}\right)_{f2}}{b_{f2}\left(1+\frac{1}{\delta_{sc}}\right)}\right)$$

$$\widehat{s}_{yz} = \widehat{s}_{z\omega} = 0$$

where $\delta_c = \frac{d-z_s}{z_c}$ $\quad \delta_{sc} = \frac{d-e}{e}$

$$\gamma_1 = 1 + \frac{1}{3}\frac{(\alpha_{11})_{f1}}{(\alpha_{11})_w}\frac{d}{b_{f1}\left(1+\frac{1}{\delta_c}\right)} \qquad \gamma_2 = 1 + \frac{1}{3}\frac{(\alpha_{11})_{f2}}{(\alpha_{11})_w}\frac{d}{b_{f2}(1+\delta_c)}$$

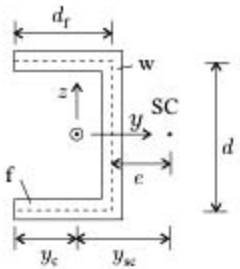

$$\widehat{s}_{yy} = \frac{\rho_y}{2}\frac{\left(\alpha_{66}^{v}\right)_f}{d_f} + d\frac{1}{3}q_{yu}^2\left(\alpha_{66}^{v}\right)_w$$

$$\widehat{s}_{zz} = \frac{\left(\alpha_{66}^{v}\right)_w}{d} + \frac{2}{3}\frac{\left(\alpha_{66}^{v}\right)_f d_f}{d^2\gamma^2}$$

$$\widehat{s}_{\omega\omega} = 2\rho_\omega\frac{1}{d^2}\frac{\left(\alpha_{66}^{v}\right)_f}{d_f} + d\frac{1}{5}q_{\omega u}^2\left(\alpha_{66}^{v}\right)_w$$

$$\widehat{s}_{z\omega} = \frac{\left(\alpha_{66}^{v}\right)_f}{d^2}\frac{2(5-3\delta_\omega)}{\gamma(8-4\delta_\omega)}$$

$$\widehat{s}_{yz} = \widehat{s}_{y\omega} = 0$$

where $\gamma = 1 + \frac{1}{6}\frac{(\alpha_{11})_f}{(\alpha_{11})_w}\frac{d}{d_f}$

$$\delta_y = \frac{d_f - y_c}{y_c} \qquad \delta_\omega = \frac{1}{\frac{d_f}{e}-1} \qquad \rho_y = \frac{3}{5}\frac{8-9\delta_y+3\delta_y^2}{(2-\delta_y)^2} \approx 1.2$$

$$q_{yu} = \frac{1}{2d_f}\frac{3-3\delta_y}{2-\delta_y} \qquad q_{\omega u} = \frac{1}{dd_f}\frac{3-3\delta_\omega}{2-\delta_\omega} \qquad \rho_\omega = \frac{3}{5}\frac{8-9\delta_\omega+3\delta_\omega^2}{(2-\delta_\omega)^2} \approx 1.2$$

Table A.9. Shear compliances. The layup of each wall segment is orthotropic and unsymmetrical. The coordinate of the centroid z_c is given in Table A.2. The properties are evaluated at each wall segment's "neutral" plane, which is at $\tilde{\varrho}$. α^{ν}_{66} is given by Eq. (A.4).

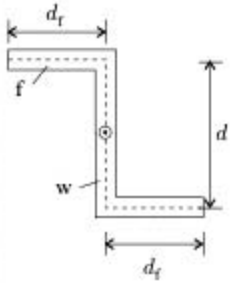

$$\widehat{s}_{yy} = 0.6\frac{(\alpha^{\nu}_{66})_f}{d_f} + d\tfrac{1}{5}q^2_{yz}(\alpha^{\nu}_{66})_w$$
$$\widehat{s}_{zz} = \frac{(\alpha^{\nu}_{66})_w}{d} + \frac{4}{15}\frac{(\alpha^{\nu}_{66})_f d_f}{d^2\beta^2}$$
$$\widehat{s}_{\omega\omega} = 2.4\frac{1}{d^2}\frac{(\alpha^{\nu}_{66})_f}{d_f} + d\tfrac{1}{3}q^2_{\omega z}(\alpha^{\nu}_{66})_w$$
$$\widehat{s}_{yz} = -\frac{(\alpha^{\nu}_{66})_f}{d\beta}\frac{2-3\delta_y}{20-10\delta_y} + \frac{(\alpha^{\nu}_{66})_w}{5}\left(1-\tfrac{1}{\beta}\right)q_{yz}$$
$$\widehat{s}_{y\omega} = \widehat{s}_{z\omega} = 0$$

where

$$\gamma = 1 + \tfrac{1}{6}\frac{(\alpha_{11})_f}{(\alpha_{11})_w}\frac{d}{d_f} \qquad \beta = 4\gamma - 3$$
$$q_{yz} = \tfrac{3}{4d_f}\left(1-\tfrac{1}{\beta}\right) \qquad \delta_\omega = \frac{1}{1+\frac{(\alpha_{11})_f}{(\alpha_{11})_w}\frac{d}{d_f}}$$
$$q_{\omega z} = \tfrac{1}{dd_f}\frac{3-3\delta_\omega}{2-\delta_\omega} \qquad \delta_y = \frac{3-4q_{yz}d_f}{3-2q_{yz}d_f}$$

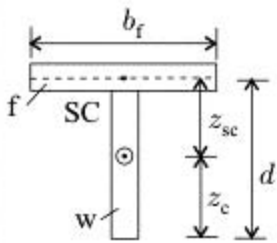

$$\widehat{s}_{yy} = 1.2\frac{(\alpha^{\nu}_{66})_f}{b_f}$$
$$\widehat{s}_{zz} = \rho\frac{(\alpha^{\nu}_{66})_w}{b_w} + \tfrac{1}{12}(\alpha^{\nu}_{66})_f b_f q^2_{zf}$$
$$\widehat{s}_{\omega\omega} = \infty$$
$$\widehat{s}_{yz} = \widehat{s}_{y\omega} = \widehat{s}_{z\omega} = 0$$

where

$$q_{zf} = \tfrac{1}{d}\frac{3-3\delta_z}{2-\delta_z} \qquad \delta_z = \frac{d-z_c}{z_c} \qquad \rho = \tfrac{3}{5}\frac{8-9\delta_z+3\delta_z^2}{(2-\delta_z)^2} \approx 1.2$$

Buckling Loads and Natural Frequencies of Orthotropic Beams with Shear Deformation

The buckling loads $\widehat{N}_{cr}$ of beams with doubly symmetrical cross section are given in Table B.1.

The buckling loads $\widehat{N}_{cr}$ of beams with unsymmetrical cross section, where the coordinate directions y and z are in the principal directions ($\widehat{EI}_{yz} = 0$, page 208), are given by the solution of the following equation:

$$\left| \begin{bmatrix} \widehat{N}_{crz} & 0 & 0 \\ 0 & \widehat{N}_{cry} & 0 \\ 0 & 0 & \widehat{N}_{cr\psi} i_\omega^2 \end{bmatrix} - \widehat{N}_{cr} \begin{bmatrix} 1 & 0 & z_{sc} \\ 0 & 1 & -y_{sc} \\ z_{sc} & -y_{sc} & i_\omega^2 \end{bmatrix} \right| = 0, \tag{B.1}$$

where $||$ denotes determinant. The buckling loads $\widehat{N}_{cry}$, $\widehat{N}_{crz}$, $\widehat{N}_{cr\psi}$ are calculated by the expressions in Table B.1, y_{sc} and z_{sc} are the coordinates of the shear center with respect to the centroid, and i_ω is the polar radius of gyration

$$i_\omega^2 = z_{sc}^2 + y_{sc}^2 + \frac{\widehat{EI}_{zz} + \widehat{EI}_{yy}}{\widehat{EA}}. \tag{B.2}$$

The circular frequencies ω of beams with doubly symmetrical cross sections are given in Table B.2. The circular frequencies ω of beams with unsymmetrical cross section, where the coordinate directions y and z are in the principal directions ($\widehat{EI}_{yz} = 0$, page 208), are given by the solution of the following equation:

$$\left| \begin{bmatrix} \omega_z^2 & 0 & 0 \\ 0 & \omega_y^2 & 0 \\ 0 & 0 & \omega_\psi^2 \frac{\Theta}{\rho} \end{bmatrix} - \omega^2 \begin{bmatrix} 1 & 0 & -(z_G - z_{sc}) \\ 0 & 1 & (y_G - y_{sc}) \\ -(z_G - z_{sc}) & (y_G - y_{sc}) & \frac{\Theta}{\rho} \end{bmatrix} \right| = 0, \tag{B.3}$$

where ω_y, ω_z, and ω_ψ are given in Table B.2, y_{sc} and z_{sc} are the coordinates of the shear center, ρ is the mass per unit length, y_G and z_G are the coordinates of the center of mass (Fig. 6.95), and Θ is the polar moment of mass about the shear center (Eq. 6.411).

Table B.1. Buckling loads of beams. For buckling in the x–z plane $\widehat{N}_{cry} = \widehat{N}_{cr}$, $\widehat{EI} = \widehat{EI}_{yy}$, and $\widehat{S} = \widehat{S}_{zz}$. For buckling in the x–y plane $\widehat{N}_{crz} = \widehat{N}_{cr}$, $\widehat{EI} = \widehat{EI}_{zz}$, and $\widehat{S} = \widehat{S}_{yy}$. For torsional buckling $\widehat{N}_{cr\psi} = \widehat{N}_{cr} + \frac{1}{i_c^2}\widehat{GI}_t$, $\widehat{EI} = \frac{1}{i_c^2}\widehat{EI}_\omega$, and $\widehat{S} = \frac{1}{i_c^2}\widehat{S}_{\omega\omega}$.

Geometry, loading	Buckling load: No shear deformation	Buckling load: With shear deformation
(a) 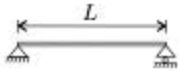	$\widehat{N}_{cr}^B = \frac{\pi^2 \widehat{EI}}{L^2}$	$\frac{1}{\widehat{N}_{cr}} = \frac{1}{\widehat{N}_{cr}^B} + \frac{1}{\widehat{S}}$
(b) 	$\widehat{N}_{cr}^B = \frac{\pi^2 \widehat{EI}}{(0.7L)^2}$	$\frac{1}{\widehat{N}_{cr}} \simeq \frac{1}{\widehat{N}_{cr}^B} + \frac{1}{\widehat{S}}$
(c) 	$\widehat{N}_{cr}^B = \frac{\pi^2 \widehat{EI}}{(0.5L)^2}$	$\frac{1}{\widehat{N}_{cr}} = \frac{1}{\widehat{N}_{cr}^B} + \frac{1}{\widehat{S}}$
(d) 	$\widehat{N}_{cr}^B = \frac{\pi^2 \widehat{EI}}{(2L)^2}$	$\frac{1}{\widehat{N}_{cr}} = \frac{1}{\widehat{N}_{cr}^B} + \frac{1}{\widehat{S}}$

Table B.2. Circular frequencies of beams. $i = 1, 2, 3, \ldots$, where $i = 1$ belongs to the first mode. For vibration in the x-z plane $\omega_{yi} = \omega_i$, $\widehat{EI} = \widehat{EI}_{yy}$, and $\widehat{S} = \widehat{S}_{zz}$. For vibration in the x-y plane $\omega_{zi} = \omega_i$, $\widehat{EI} = \widehat{EI}_{zz}$, and $\widehat{S} = \widehat{S}_{yy}$. For torsional vibration $(\omega_{\psi i})^2 = \omega_i^2 + \frac{\widehat{GI}_t}{\widehat{\Theta}}\left(\frac{\mu_{Gi}}{L}\right)^2$, $\frac{\widehat{EI}}{\rho} = \frac{\widehat{EI}_{yy}}{\widehat{\Theta}}$, and $\frac{\widehat{S}}{\rho} = \frac{\widehat{S}_{zzz}}{\widehat{\Theta}}$.

$$\frac{1}{\omega_i^2} \simeq \frac{1}{\left(\omega_i^B\right)^2} + \frac{1}{\left(\omega_i^S\right)^2}$$

Geometry	No shear deformation $\left(\omega_i^B\right)^2 = \frac{\widehat{EI}}{\rho}\left(\frac{\mu_{Bi}}{L}\right)^4$	No bending deformation $\left(\omega_i^S\right)^2 = \frac{\widehat{S}}{\rho}\left(\frac{\mu_{Si}}{L}\right)^2$
(a) 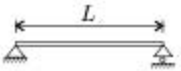	$\mu_{Bi} = i\pi$	$\mu_{Si} = \mu_{Gi} = i\pi$
(b) 	$\mu_{B1} = 3.927$ $\mu_{B2} = 7.069$ $\mu_{Bi} \simeq (i + 0.25)\pi$	$\mu_{Si} = \mu_{Gi} = i\pi$
(c) 	$\mu_{B1} = 4.730$ $\mu_{B2} = 7.853$ $\mu_{Bi} \simeq (i + 0.5)\pi$	$\mu_{Si} = \mu_{Gi} = i\pi$
(d) 	$\mu_{B1} = 1.875$ $\mu_{B2} = 4.694$ $\mu_{Bi} \simeq (i - 0.5)\pi$	$\mu_{Si} = \mu_{Gi} = (i - 0.5)\pi$
(e)	$\mu_{B1} = 4.730$ $\mu_{B2} = 7.853$ $\mu_{B3} = 10.996$ $\mu_{Bi} \simeq (i + 0.5)\pi$	$\mu_{S1} = \mu_{G1} = 6.283$ $\mu_{S2} = \mu_{G2} = 8.987$ $\mu_{S3} = \mu_{G3} = 12.566$ $\mu_{Si} = \mu_{Gi} \simeq (i + 1)\pi$

Typical Material Properties

The properties of typical materials are given in Tables C.1–C.5. These properties are nominal only in that they may vary owing to variations in the material and in the manufacturing process.

Typical thickness of a graphite epoxy ply is 0.127 mm (0.005 in.).

Fiber

E_{f1}	longitudinal Young's modulus
G_{f12}	longitudinal shear modulus
ν_{f12}	longitudinal Poisson's ratio
s_{f1}	tensile strength
η_{f1}	maximum elongation
$\widetilde{\alpha}_{f1}$	longitudinal thermal expansion coefficient
$\widetilde{\alpha}_{f2}$	transverse thermal expansion coefficient
ρ_f	density

Matrix

E_m	Young's modulus
G_m	shear modulus
ν_m	Poisson's ratio
s_m	tensile strength
η_m	maximum elongation
ρ_m	density

Composite ply

v_f	fiber volume fraction
ρ_{comp}	density
E_1, E_2	longitudinal and transverse Young's moduli
G_{12}	longitudinal shear modulus
ν_{12}	longitudinal Poisson's ratio

ν_{23} transverse Poisson's ratio
s_1^+, s_1^- tensile and compression strengths in the fiber direction
s_2^+, s_2^- tensile and compression strengths perpendicular to the fibers
s_{12} shear strengths
$\tilde{\alpha}_1, \tilde{\alpha}_2$ longitudinal and transverse thermal expansion coefficients
$\tilde{\beta}_1, \tilde{\beta}_2$ longitudinal and transverse moisture expansion coefficients

Table C.1. Fiber properties

Material	E_{f1} GPa	G_{f12} GPa	ν_{f12}	s_{f1} MPa	η_{f1} %	$\tilde{\alpha}_{f1}$ $10^{-6}/°C$	$\tilde{\alpha}_{f2}$	ρ_f $\frac{g}{cm^3}$
Glass								
E-glass	72	33	0.09	3103	4.3	5–5.4	–	2.6
S-glass	87	37	0.18	3792	4.4	1.6–2.9	–	2.49
Aramid						–		
Kevlar 29	83	29	0.44	3620	4.4	–	–	1.44
Kevlar 49	124	43	0.45	3620	2.9	–2	59	1.44
Kevlar 149	172	65	0.33	3448	2.0	–	–	1.44
Graphite								
AS4	234	93	0.26	3930	1.7	–0.9	–	1.8
IM6	276	109	0.26	5102	1.8	–	–	1.74
IM7	276	109	0.26	5309	1.9	–	–	1.77
IM8	303	120	0.26	5447	1.8	–	–	1.8
PANEX	228	–	0.25	3600	1.6	–	–	1.72
T300	231	91	0.27	3241	1.4	–0.6	7–12	1.77
T40	283	107	0.32	5654	2.0	–	–	1.8
T50	393	159	0.24	2413	0.6	–	–	1.8
T55	379	142	0.33	1724	0.5	–	–	1.99
T75	517	204	0.27	2069	0.4	–	–	1.99
Boron	400	–	0.2	3160	0.79	4.5	0.2	2.57

Table C.2. Matrix properties

Material	E_m GPa	G_m GPa	ν_m	s_m MPa	η_m %	ρ_m $\frac{g}{cm^3}$
Epoxy						
Der 332	3.4	1.2	0.35	64	1.9	1.22
934	4.1	1.5	0.35	83	2.0	1.3
Epon	2.8	1.0	0.35	83	3.0	1.30
3501	4.4	1.6	0.36	69	1.6	1.26
5208	3.9	1.4	0.35	50	1.3	1.27
1962	3.7	1.4	0.35	–	–	1.27
Vinylester						
1222	3.2	–	–	79	2.5	1.3
Polyester						
7241	3.3	–	–	79	2.4	1.38

Table C.3. Ply properties

Material	v_f %	ρ_{comp} $\frac{g}{cm^3}$	E_1 GPa	E_2 GPa	G_{12} GPa	ν_{12}	ν_{23}
Graphite/Epoxy							
T300/5208	70	1.6	181	10.3	7.17	0.28	0.59
AS/3501	66	1.6	138	8.96	7.1	0.3	0.59
H-IM6/epoxy	–	–	203	11.2	8.4	0.32	–
AS4/APC2	–	1.6	134	8.9	5.1	0.28	0.66
T300/934							
tape	–	–	148	9.65	4.55	0.3	0.6
cloth (13mil)	–	–	74	74	4.55	0.05	–
cloth (7mil)	–	–	66	66	4.1	0.04	–
Glass/Epoxy							
Scotchply 1002	45	1.8	38.6	8.27	4.14	0.26	–
S-glass/Epoxy	50	2.0	43	8.9	4.5	0.27	0.40
WovenGl/Epoxy	45	2.2	29.7	29.7	5.3	0.17	–
Aramid/Epoxy							
Kevlar 49	60	1.5	76	5.5	2.3	0.34	0.37
Boron/Epoxy							
B(4)/5505	50	2.0	204	18.5	5.59	0.23	–
B5.6/5505	50	2.0	201	21.7	5.4	0.17	–
E-glass/Vinylester	–	–	24.4	6.87	2.89	0.32	–

Table C.4. Ply properties

Material	S_1^+ MPa	S_1^- MPa	S_2^+ MPa	S_2^- MPa	S_{12} MPa
Graphite/Epoxy					
T300/5208	1500	1500	40	246	68
AS/3501	1447	1447	52	206	93
H-IM6/epoxy	3500	1540	56	150	98
AS4/APC2	2130	1100	80	200	160
T300/934					
tape	1314	1220	43	168	48
cloth (13mil)	499	352	458	352	46
cloth (7mil)	375	279	368	278	46
Glass/Epoxy					
Scotchply 1002	1062	610	31	118	72
S-glass/Epoxy	1280	690	49	158	69
WovenGl/Epoxy	367	549	367	549	97
Aramid/Epoxy					
Kevlar 49	1400	235	12	53	34
Boron/Epoxy					
B(4)/5505	1260	2500	61	202	67
B5.6/5505	1380	1600	56	125	62
E-glass/Vinylester	548	803	43	187	64

Table C.5. Ply properties

Material	$\tilde{\alpha}_1$ $10^{-6}/C^\circ$	$\tilde{\alpha}_2$	β_1	β_2
Graphite/Epoxy				
T300/5208	−0.7	25.0	0	0.6
AS/3501	−0.7	29.0	0	0.4
Glass/Epoxy	8.6	22.1	0	0.6
Aramid/Epoxy				
Kevlar 49	−4.0	79.0	0	0.6
Boron/Epoxy				
B(4)/5505	6.1	30.3	0	0.6

Conversion Factors between U.S. Customary Units and SI Units

To convert from	To	Multiply by
inches (in.)	millimeters (mm)	25.400
inches (in.)	meters (m)	0.0254
foot (ft)	meters (m)	0.3048
square inches ($in.^2$)	square meters (m^2)	0.000 645
square feet (ft^2)	square meters (m^2)	0.092 903
cubic feet (ft^3)	cubic meters (m^3)	0.028 317
cycles per second	hertz (Hz)	1.0
pound-mass (lb)	kilograms (kg)	0.453 592
pound-force (lbf)	newtons (N)	4.448 222
kilopound-force (kip)	kilonewtons (kN)	4.448 222
pound-force per square foot (psf)	newtons/$meter^2$ ($\frac{N}{m^2} = Pa$)	47.880
pound-force per square inch (psi)	kilonewtons/$meter^2$ ($\frac{kN}{m^2} = kPa$)	6.894 757
kilopound-force per square inch (ksi)	meganewtons/$meter^2$ ($\frac{MN}{m^2} = MPa$)	6.894 757
inch-pound force (in.-lbf)	newton-meter ($N \cdot m$)	0.112 985
foot-pound force (ft-lbf)	newton-meter ($N \cdot m$)	1.355 818

SI Unit Prefixes

Multiplication Factor	Prefix	Symbol
$1\,000\,000\,000\,000 = 10^{12}$	terra	T
$1\,000\,000\,000 = 10^{9}$	giga	G
$1\,000\,000 = 10^{6}$	mega	M
$1\,000 = 10^{3}$	kilo	k
$100 = 10^{2}$	hecto	h
10	deka	da
$0.1 = 10^{-1}$	deci	d
$0.01 = 10^{-2}$	centi	c
$0.001 = 10^{-3}$	milli	m
$0.000\,001 = 10^{-6}$	micro	μ
$0.000\,000\,001 = 10^{-9}$	nano	n
$0.000\,000\,000\,001 = 10^{-12}$	pico	p

Index

A matrix, 70–3, 80
Amplification factor, 302
Average stress criterion, 431–2

Back calculation of engineering constants, 451
  example, 451
B-matrix, 70–3, 80
Beams
  applied loads, 203–4
  bending, 206–10
  bending stiffness, 206, 207, 208, 209, 210
  boundary conditions, 205, 206, 264
  box-beams. *See* Box-beams
  buckling. *See* Buckling of beams; Buckling of beams with shear deformation
  C-section beams. *See* C-beams
  centroid, 203
  with circular cross section. *See* Beams with circular cross section
  compliance, 209–10
  coordinate system, 203
  coupling. *See* Coupling
  curvature, 204
  equilibrium, 204
  force–strain relationship, 204, 206–8, 209
  governing equations, 203–5
  I-beams. *See* I-beams
  internal forces, 203–5
  isotropic beams, 206
  L-beams. *See* L-beams
  neutral plane, 213. *See also* Neutral plane
  orthotropic beams, 207–8
  rate of twist, 204
  rectangular solid cross section. *See* Solid-section beams under axial load and bending
  reference plane, 213. *See also* Reference plane
  replacement stiffness, 210
  restrained-warping-induced torque, 263, 318–19, 339, 354
  sandwich. *See* Sandwich beams
  shear center. *See* Shear center
  shear deformation. *See* Beams with shear deformation; Sandwich beams
  shear force, 203
  stiffness, 204–8
  strain-displacement relationship, 204
  summary of equations, 311
  with symmetrical cross section, 206–7
  tensile stiffness, 206, 207, 208, 210
  thin-walled beams. *See* Closed-section beams under axial load and bending; Open-section beams under axial load and bending; Stiffened beams; Thin-walled beams under axial load, bending, and torsion; Torsion of thin-walled beams
  torque neutral surface, 254, 258
  torsional stiffness, 206, 208, 210
  transversely loaded. *See* Transversely loaded beams; Transversely loaded beams with shear deformation
  T-section beams. *See* T-beams
  twist, 203
  vibration. *See* Vibration
  warping stiffness. *See* Warping stiffness
  Z-section beams. *See* Z-beams
Beam element, 397–8
Beam equations, summary of, 311
Beams with circular cross section, 454, 455, 458
Beams with shear deformation, 313–64. *See also* Sandwich beams; Transversely loaded beams with shear deformation
  bending moment, 319
  bending stiffness, 322
  boundary conditions, 321
  buckling. *See* Buckling of beams with shear deformation

Beams with shear deformation (*continued*)
coordinate system, 313
deflection, 313, 330–4
deformation, 313–14
effects of shear deformation, 359–64
equations, summary of, 320–1
equilibrium, 320
force–strain relationship, 315–19
governing equations, 314–21
I-beams, 315–18, 324–5
rate of twist, 314, 315, 317
restrained-warping-induced torque, 319
rotation of the cross-section, 313, 314
Saint-Venant torque, 317–19
shear compliance, 320, 321–6
shear force, 319–20
shear stiffness 320, 321, 322, 325–6
strain–displacement relationship, 315
strain energy, 322
tensile stiffness, 322
torsional stiffness, 322
transverse shear strain, 313
vibration, 347–59
warping stiffness, 322
Bending–bending coupling, 73
Bending moment. *See* Moment
Bending–shear coupling, 73
Bending stiffness
of beams with shear deformation, 322
of box-beams, 256, 258, 454, 455, 456
of C-beams, 285, 454, 456
of circular cross-section beams, 454, 455
of closed-section beams, 231, 232, 234, 235, 246
of I-beams, 295, 454, 455, 456
of L-beams, 223–5
of open-section beams, 230, 231, 232, 234, 235, 236
of sandwich beams, 327, 328, 333, 334
of stiffened beams, 289
of T-beams, 219–21, 240
Bending stiffness parameter, 100
Bending–twist coupling, 72–3, 76
Bernoulli–Navier hypothesis, 203, 227, 267, 313
Biaxial test, 418–19
Bimoment, 262, 317, 318, 319, 354
Boundary conditions, 47–8
beams, 205, 206, 264
beams with shear deformation, 321
plates, 92, 101, 113, 145
sandwich plates, 172–3, 183
torsion of beams, 264
Box-beams, 255–60, 272–4, 300–3
bending stiffness, 256, 258, 454, 455, 456
centroid, 274, 454, 456
compliance, 274
deflection, 257, 259
elongation, 260, 274
examples, 255, 257, 272, 304
local buckling, 300–3, 304–5
neutral surface, 258, 259
parameter of restraint, 304
reference surface, 259
shear compliance, 458
spring constant, 304
stiffness, 256, 258, 259, 273
tensile stiffness, 259, 454, 455, 456
torque neutral surface, 258
torsion, 255–7, 257–9
torsional stiffness, 256, 258, 458
twist, 257, 259, 274
warping stiffness, 458
Bredt–Batho formula, 253
Buckling amplification factor, 302
Buckling constant, 292–3
Buckling length. *See* Buckling of plates
Buckling load parameter. *See* Load parameter
Buckling load. *See* Buckling of: beams; beams with shear deformation; cylinders; plates; shells
Buckling of beams, 290–306, 461–2
effective length factor, 292, 293
examples, 294, 298, 304, 305
flexural–torsional, 291–6
force–strain relationship, 291
lateral–torsional, 296–300
local buckling, 300–5
orthotropic beams, 290–1
spring constant, 301–4
Buckling of beams with shear deformation, 334–47
equilibrium, 335, 339
examples, 342, 343, 345
flexural, 335–9
flexural–torsional, 341–4
lateral–torsional, 345
shear deformation effects, 359–62
torsional, 339–41
Buckling of cylinders, 387–94
buckled shape, 389
buckling pattern, 387, 390–1
examples, 387, 391
with orthotropic wall, 390–3
with sandwich wall, 393–4
Buckling of plates, 112–41
under biaxial load, 112–15, 118–22, 187
buckled shape, 122, 125, 127, 136
buckling length, 135
buckling load, 123, 125, 136
with built-in and simply supported edges, 118–24
equilibrium, 132
examples, 115, 116, 121, 126, 130
examples, long plates, 133, 138, 139
examples, sandwich plates, 186, 188, 195
face wrinkling, 190–6
with free edge, 124–7

Buckling of plates (*continued*)
under linearly varying load, 140
load parameter, 112, 119
long plates with various edge supports, 132–41
potential energy, 118, 125
potential of external forces, 113
principle of stationary potential energy, 113, 118
Ritz method, 113, 118, 183, 188
with rotationally restrained edges, 127–31
sandwich plates, 185–8
shear load, under, 140–1
with simply supported edges, 112–18
strain energy, 112
under uniaxial load, 122, 123, 124–39
Buckling of shells, 384–7
buckled shape, 386, 389
buckling pattern, 386, 387, 390, 391
examples, 387, 391

C-beams, 284–8
bending stiffness, 285, 454, 456
centroid, 285, 454, 456
coordinate system, 285
deflection, 286
examples, 284, 287
shear center, 286, 457
shear compliance, 459
tensile stiffness, 285, 454, 456
torsional stiffness, 286, 457
twist, 286–7, 288
warping stiffness, 288, 457
Center of mass, 309, 310
Center of gravity, 203, 213
Center of twist, 252
Centroid, 203
of box-beams, 274, 454, 456
of C-beams, 285, 454, 456
of closed-section beams, 231, 232, 234, 235
of I-beams, 295, 454, 455, 456
of L-beams, 223
of open-section beams, 230, 231, 232, 234, 235, 236
of sandwich beams, 328
of solid-section beams, 213
of stiffened beams, 289
of T-beams, 219, 240
of thin-walled beams with arbitrary layup, 271
Characteristic length, 431–2, 434–5
Circular frequency, 141. *See also* Vibration
of beams, 306, 350, 352, 463
of plates, 141, 196
Closed-section beams under axial load and bending, 243–8. *See also* Box beams
bending stiffness, 231, 232, 234, 235, 246
centroid, 231, 232, 234, 235
compatibility condition, 245–6
compliance, 247
coordinate system, 243, 269
displacements, 243–7
force-strain relationship, 247, 267
neutral surface, 453
tensile stiffness, 231, 232, 234, 235, 247
transversely loaded, 278–80, 282–3
Compliance. *See also* Shear compliance
of beams, 209–10
of closed-section beams, 247, 254, 266–8, 273, 274
constraint on, 56, 58–61
example, 21
of isotropic material, 12, 14–15, 21, 35, 42
of generally anisotropic material, 9–11, 29, 30, 36
of laminates, 71–2, 74, 76, 77–9, 81–8
of monoclinic material, 12–15, 32–3
in new reference plane, 81
of open-section beams, 266–8
of orthotropic material, 12, 14–15, 34, 41
under plane-strain, 30, 32, 33, 34–5
under plane-stress, 39, 41, 42
of solid-section beams, 212–13, 214, 250
transformation, 53–4
of transversely isotropic material, 12, 14–15, 20, 35, 42
of woven fabric, 44
Conservation of energy, 145, 323
Constitutive equations. *See* Stress–strain relationship, Force–strain relationship
Continuity condition, 48–9
Conversion factors, 467
Coordinate system, 3–4
of beams, 203, 211, 313
of C-beams, 221
of closed section beams, 243, 265, 267, 268–9
of isotropic material, 20
of laminates, 63–4, 66
of monoclinic material, 11
of open-section beams, 226–7, 265, 266, 267, 268, 269
of orthotropic material, 14, 16
under plane-strain, 22
under plane-stress, 38
of plates, 90
of T-beams, 217
transformation, 49–50
of transversely isotropic material, 19
Core, 169, 170, 326
Coupling
in balanced laminates, 75
in beams in torsion, 248
in beams with symmetrical cross section, 206–7
in cylinders, 376
in isotropic laminates, 78
in laminates, 72, 73
in monoclinic material, 12
in orthotropic beams, 207–8
in orthotropic closed-section beams, 243

Coupling (*continued*)
in orthotropic laminates, 75, 76, 77
in orthotropic material, 17
in orthotropic open-section beams, 226, 229
in orthotropic solid-section beams, 213, 214
in quasi-isotropic laminates, 80
in sandwich beams, 333
in sandwich plates, 176
in solid-section beams, 212, 214
in thin rectangular cross-section beams, 250
transversely loaded thin-walled beams, 275, 276
Critical load parameter
for cylinders, 386, 388–9, 391, 392, 393, 394
for plates, 112, 115, 118, 121
for sandwich plates, 188
Curvature, 67–8
of beams, 204
of cylinders, 371
of laminates, 67–8
of open-section beams, 227, 234, 235, 251
of plates, 90, 94, 95
of radius, 365–6
of shells, 365–6, 385
of solid-section beams, 211, 215, 216
Cylindrical deformation, 94, 132, 142, 301
Cylindrical shells, 368–80. *See also* Buckling of shells
with built-in ends, 370–5
coupling, 376
curvature, 371
displacement, 375–6
end effects, 376–7
equilibrium, 371
examples, 377, 387, 391, 427
membrane forces, 369, 370
membrane theory, 366, 368–70
with orthotropic walls, 375–6, 390–1
strain-displacement relationship, 371
temperature effects, 379–80

D matrix, 70–3, 80
Deflection
of beams, 313, 332
of beams with shear deformation, 313, 330–4
of box-beams, 257, 259
of C-beams, 286
of long plates, 96–100
of plates, 93–4, 100–7, 107–12
of sandwich plates, 180, 182–4
shear deformation effects, 359–62
of T-beams, 241
Deformation under plane strain, 27, 31, 35, 36
Delamination, 167, 411–12
Density, 437
Displacement, 3–4
of closed-section beams, 243–7, 265–7, 273–4
of cylindrical shells, 375–6
of I-beams, 316
of laminates, 66–7
of L-beams, 221
of open-section beams, 226, 265–7
under plane-strain, 25–8, 30, 33, 34, 35, 37
of plates, 91
of sandwich plates, 169, 170, 199, 200
of solid-section beams, 210–14
summary, 57–8
of T-beams, 217–18
Displacement function of vibrating beams, 119

Effective length factor, 292, 293
Engineering constants
constraint on, 61
example, back calculation, 451
of isotropic material, 13, 16, 20
micromechanics expression, 442
of monoclinic material, 13, 16
of orthotropic material, 13, 16
of transversely isotropic material, 13, 16, 19
of woven fabric, 44
Engineering strain, 3, 5, 6
Equilibrium equations, 6–8
for beams, 204, 276, 280
for beams with shear deformation, 320, 335, 339, 353
for buckling of plates, 132
for cylindrical shells, 371
for long plates, 95–6, 132
under plane-strain, 29, 32
under plane-stress, 39–40
for plates, 91, 142, 197
for sandwich plates, 179, 197
summary of, 57
Examples
back calculation of engineering constants, 451
beam under lateral load, 215, 239, 255
box-beam, 255, 257, 272, 304
C-beam, 284, 287
constraints on compliances and engineering constants, 61
cylinder, 377, 427
cylinder buckling, 387, 391
face wrinkling, 195
failure, 427
hygrothermal effects, 156, 159, 162, 383
I-beam buckling, 294, 298, 305, 343, 345, 363
I-beam vibration, 310, 357
laminate compliance and stiffness, 81, 83, 87
local buckling, 304, 305, 387, 391
long plate buckling, 133, 138, 139
plate buckling, 115, 116, 121, 126, 130
plate under lateral load, 96, 103, 105, 111
plate vibration, 143, 147, 148, 150
ply compliance and stiffness, 21, 42, 43
sandwich beam, 334, 342, 362
sandwich plate, 180
sandwich plate buckling, 186, 188, 195
sandwich plate vibration, 198, 201

Examples (*continued*)
shear center, 284, 294
shear flow, 239
shear deformation effects on beams, 362, 363
springback, 383
sublaminate stiffness, 407
T-beam, 239
woven fabric, 43
Extension-extension coupling, 73
Extension-shear coupling, 72–3, 76
Extension-twist coupling, 72–3, 76

Fabric. *See* Woven fabric
Facesheet, 169, 326
Face wrinkling, 190–6
Failure envelope, 428–30
example, 427
Failure modes, 411–12
Failure surface, 424
Failure theories, 411–35
applicability of, 412–13
Fiber failure, 411–12
Fibers, 1
properties, 465
Filament wound layer, 41
Finite element, 395–410
beam element stiffness, 397–8
example, 407
formulation, 395–6
plate element stiffness, 397
sublaminate element stiffness, 398–410
three-dimensional element stiffness, 396
First order shear theory, 313
First ply failure, 412
Flexural rigidity. *See* Bending stiffness
Force–strain relationship
for beams, 204, 206–8, 209
for beams with shear deformation, 315–19
for buckling of beams, 291
for closed-section beams, 247
hygrothermal, 153, 154, 155
for laminates, 71, 74, 75
for open-section beams, 228, 236, 237, 238, 239
for plates, 91
for sandwich plates, 172
for shells, 366
for solid-section beams under axial load and bending, 211, 212, 213, 214, 215
for T-beams, 242
for thin-walled beams under axial load and bending, 266, 269
for torsion of beams, 250, 255
Free edge effect, 166–8, 210
Free vibration. *See* Vibration
Frequency. *See* Natural frequency; Circular frequency

Generalized displacement in beams with shear deformation, 320
Generalized force, 71
in beams with shear deformation, 320
Generalized force-strain relationship, 71
Generalized strain, 71
in beams with shear deformation, 315, 320
Generally anisotropic material
compliance, 9–11, 29, 30, 36
description, 8
under plane-strain, 28–30, 35–6
under plane-stress, 38–40
stiffness, 9–11
stress–strain relationship, 8–11
Governing equations, 57
of beams, 203–5, 314–21
of plates, 90–2
of sandwich plates, 170–2
summary of, 57

Halpin–Tsai, 450–1
Hill failure criterion, 412
Hole size effect, 433
Honeycomb core, 169, 326
Huber orthotropy, 108–12
Hygrothermal, 44–7, 151–63, 379–84
examples, 156, 159, 162, 383
force, 152, 154, 155, 156
force–strain relationship, 153–6
under plane–strain, 47
under plane–stress, 47
properties, 450, 467
strain, 44–7, 153
strain–displacement relationship, 44–7
stress, 152
stress–strain relationship, 45–6, 47, 152
thickness change, 161–3

I-beams
bending moment, 316
bending stiffness, 295, 454, 455, 456
bimoment, 262, 318
buckling, 294–6, 298–300, 305–6, 343–5, 346
center of mass, 310
centroid, 295, 454, 455, 456
displacement, 316
example, effect of shear deformation, 363
examples, buckling, 294, 298, 305, 343, 345
examples, vibration, 310, 357
local buckling, 303, 305–6
parameter of restraint, 305
polar moment of mass, 310
polar radius of gyration, 295
rate of twist, 317
restrained warping, 261–4
restrained warping induced torque, 263, 318
Saint-Venant torque, 263, 317
shear center, 295, 457
shear compliance, 324–5, 343–4, 459
shear deformation effects, 363–4

I-beams (*continued*)
with shear deformation, 315–18
shear flow, 241
shear stiffness, 318
spring constant, 305
strain–displacement relationship, 316
tensile stiffness, 295, 454, 455, 456
transverse shear force, 316
torque, 261, 262, 263, 316
torsion, 261–4, 315–18
torsional stiffness, 295, 457
vibration, 310–12, 357–9
warping stiffness, 262–4, 295, 318, 457
Inertia force, 142, 348, 353
In-plane-out-of-plane coupling, 72–3, 76
Interaction strength parameters, 417–20, 423
Interlaminar stresses, 166–8, 210
Isotropic material
compliance, 12, 14–15, 21, 35, 42
coordinate system, 20
description, 20
engineering constants, 13, 16, 20
under plane-strain, 34–5, 38
under plane-stress, 42
Poisson's ratio, 20
shear modulus, 20
stiffness, 21, 35, 42
Young's modulus, 20

Kinetic energy, 144–5
Kirchhoff hypothesis, 66, 169

Lamina, 1, 2
Laminate plate theory, 65–72
Laminates, 63–88
angle-ply, 65
balanced, 65, 75
compliance, 71–2, 74, 75, 76, 77–9, 81–8
coordinate system, 63–4, 66
coupling, 72–3, 75, 76, 77, 78, 80
cross-ply, 65
curvature, 67–8
curved, 81
displacements, 66–7
examples, 81, 83, 87
force-strain relationship, 71, 74, 75
in-plane forces, 67–8, 70, 74
isotropic, 78, 79
laminate code, 63
moments, 67–8, 70, 74
neutral plane, 66
normal shear force, 67
orthotropic, 75–8, 207
$\pi/4$ laminate, 65, 79–80
quasi-isotropic, 79–80, 177
reference plane, 66–7, 68, 69, 80–1
rotation, 66
stiffness, 70–3, 74, 75, 76, 78, 79, 81–8
strain-displacement, 66–7, 75
stress, 65–6
symmetric, 63, 64–5, 74–5, 84, 85
transverse shear force, 68
unsymmetric, 86
L-beams, 221–5
displacement, 221
centroid, 223
bending stiffness, 223–5
tensile stiffness, 223
Load parameter, 112, 118, 187, 384. *See also* Critical load parameter
Local buckling
of cylinders, 387, 390–1
example, box-beam, 304
example, I-beam, 305
examples, cylinders, 387, 391
of thin-walled beams, 300–4
Long plates, 94–100. *See also* Buckling of plates; Sandwich plates
applicability of theory in bending, 94–5, 97
applicability of theory in buckling, 116, 132, 190
applicability of theory in vibration, 148, 202
curvature, 95
cylindrical deformation, 94
deflection, symmetrical layup, 96
deflection, unsymmetrical layup, 98–100
description, 94
equilibrium, 95–6, 132, 142
examples, 96, 133, 180, 198
vibration, 141–4, 196–9

Mass, 437
Material properties. *See* Properties
Matrix cracking, 411–12
Matrix properties, 465
Maximum strain criterion, 426–7
example, 427
Maximum stress criterion, 425–6
example, 427
Membrane forces, 365–70
Membrane theory, 365, 366, 368–70
Meridian, 367
Micromechanics, 436–52
engineering constants, summary of, 442
hygrothermal properties, summary of, 450
Modified rule of mixtures, 448–9
Moisture concentration, 44, 445
Moisture diffusivity, 447–8, 450
Moisture expansion coefficient, 44, 46, 445–6, 450
Moment
in beams, 210, 211, 316, 327, 332
in laminates, 67, 70, 74
in plates, 91, 96, 99–100, 108, 109
Moment couple. *See* Bimoment
Moment of inertia, 208, 261

Monoclinic material
compliance, 12–15, 32–3
coordinate system, 11
description, 11
engineering constants, 13, 16
under plane-strain, 30–4, 36–8
under plane-stress, 40–1
Poisson's ratio, 13
shear modulus, 13
stiffness, 14, 41
stress–strain relationship, 17
Young's modulus, 13
Monocoque beam, 311

Natural frequency, 141. *See also* Vibration
Neutral plane (surface), 230, 231, 254
in box-beams, 258, 259
in closed-section beams, 453
in open-section beams, 230, 231, 233, 453
in sandwich beams, 328
in sandwich plates, 177
in solid-section beams, 213
Noninteraction strength parameters, 416–17, 420, 421, 423

Off-axis unidirectional test, 417–18
Open-section beams, 217–43. *See also* C-beams; I-beams; L-beams; T-beams; Torsion of thin-walled beams; Transversely loaded thin-walled beams
bending stiffness, arbitrary cross section, 230, 231, 232, 234, 235, 236
centroid, 230, 231, 232, 234, 235, 236
coordinate system, 226–7
curvature, 227, 234, 235
displacement, 226
example, 239
force-strain relationship, 228, 236, 237, 238, 239
neutral surface, 230, 231, 233, 453
reference surface, 230, 233
segmented wall, 233
shear flow, 234, 241, 275, 278
strain, 234, 235, 237, 269
tensile stiffness, arbitrary cross section, 229, 231, 232, 234, 235, 236
torsion, 250–2
transversely loaded, 276–8, 280
Orthotropic material
compliance, 12, 14–15, 34, 41
coordinate system, 14, 16
description, 14
engineering constants, 13, 16
under plane-strain, 34–5, 38
under plane-stress, 41
Poisson's ratio, 13
shear modulus, 13
stiffness, 17, 34, 41
stress–strain relationship, 17
Young's modulus, 13
Out-of-plane shear force. *See* Shear force

Parallel axis theorem, 80
Parameter of restraint, 128, 304–5
Period of vibration, 141
Plane–strain, 22–38, 267
body force, 22, 24
compliance, 30, 32, 33, 34–5
coordinate system, 22
definition, 22–5
deformation, 27, 31, 35, 36
displacement, 25–8, 30, 33, 34, 35, 37
end loads, 24–5
end supports, 23
equilibrium, 29, 32
fiber orientation, 23–4
geometry, 23
generally anisotropic material, 28–30, 35–6
hygrothermal, 47
isotropic material, 34–5, 38
monoclinic material, 30–4, 36–8
orthotropic material, 34–5, 38
stiffness, 30, 33, 34–5
strain–displacement relationship, 25–6, 28, 30, 33, 35, 37
stress–strain relationship, 29–30, 32, 33, 36, 37, 38
surface force, 22, 24
transversely isotropic material, 34–5, 38
Plane–stress, 38–44, 66
compliance, 39, 41, 42
coordinate system, 38
definition, 38
equilibrium, 39–40
examples, 42, 43
generally anisotropic material, 38–40
hygrothermal, 47
isotropic material, 42
monoclinic material, 40–1
orthotropic material, 41
stiffness, 39–40, 41, 42–3
stress, 38, 39
stress-strain relationship, 39–40
transversely isotropic material, 42–3
Plate element, 397
Plates, 89–94, 100–12. *See also* Long plates; Sandwich plates
bending moment, 91, 108, 109
boundary conditions, 92, 101, 113, 145
buckling. *See* Buckling of plates
coordinate system, 90
curvature, 90, 94
deflection of built-in plates, 107–12
deflection of simply supported plates, 100–7
deflection under pure bending and in-plane loads, 93–4

Plates (*continued*)
equilibrium, 91
examples, 103, 105, 111
force-strain relationship, 91
governing equations, 90–2
hygrothermal effects. *See* Hygrothermal
in-plane forces, 91
potential energy, 107, 108, 109, 118, 125
potential of external forces, 101
principle of stationary potential energy, 101, 113, 118
reference plane, 99
Ritz method, 101
shear force, 91
strain–displacement relationship, 90
strain energy, 92, 93, 101
strain energy, plate buckling, 112
strain energy, vibrating plate, 144, 149–50
twist moment, 91
vibration, 144–51
Plates with a hole, 163–6, 431–4
Plate with a notch, 434
Ply, 1, 2
example, compliance and stiffness, 21, 42, 43
orientation, 63
properties, 466–7
stiffness, 69–70
stress–strain relationship, 39, 68–9
thickness, 464
Ply group, 63
Ply stress-based failure criterion, 412
Point stress failure criterion, 431–4
Poisson's ratio, 13, 19, 20, 178, 441–2
major and minor, 62
Polar moment of mass, 307, 309, 310, 354, 361
Polar radius of gyration, 292, 295, 339, 461
Potential energy, 55
for plates, 107, 108, 109
for plate buckling, 118, 125
Potential of external forces, 55
for plates, 101, 183
for plate buckling, 113
Principle direction, 208–9
Principle of stationary potential energy, 56
for plates, 101, 184
for plate buckling, 113, 118
Properties, 464–7
used in the examples, 81
Proportional loading, 423–25

Quadratic failure criterion, 413–25
applicability of, 412–13
example, 427
for isotropic material, 421–2
for orthotropic material, 414–20
under plane-strain, 422
under plane-stress, 422
under proportional loading, 424–5
for transversely isotropic material, 420–1
Quasi-homogeneous material, 3

Radius of curvature, 365–6
Rate of twist, 26, 248
of beams, 204, 315, 316, 317
of closed-section beams, 253–4, 260, 279, 280
of I-beams, 317
shear deformation effects, 359–62
of solid-section beams, 212, 214
of thin rectangular cross section beams, 249
of transversely loaded beams, 212, 214, 275–6
Rayleigh energy method, 145, 149
Rayleigh principle, 145, 200
Reduced bending stiffness, 90
Reference plane (surface)
for closed-section beams, 254, 259
for laminates, 66–7, 68, 69, 80–1
for long plates, 99
for open-section beams, 230, 231, 233
for sandwich plates, 170–1, 177
for solid-section beams, 213
Reinforced beams. *See* Stiffened beams
Replacement shear force, 92
Replacement stiffness, 210, 291
Representative element, 437–8
Restrained warping, 261–64, 271, 288
Restrained-warping-induced torque, 263, 318–19, 339, 354
Ritz method, 55–6, 101, 113, 118, 183, 188
Rotation, 26
of beams with shear deformation, 313, 314
of laminates, 66
of sandwich plates, 169, 179, 183, 199, 200
Rotational shear stiffness, 318–20
Rotational spring constant. *See* Spring constant
Rule of mixtures, 436–9

Saint-Venant torque, 263, 317–19, 339, 354
Sandwich beams, 326–9. *See also* Buckling of beams with shear deformation
bending stiffness, 327, 328, 333, 334
centroid, 328
core, 326
coupling, 333
examples, 334, 342, 362, 363
neutral plane, 328
shear center, 328
shear compliance, 327, 329, 334
shear deformation effects, 362–3
shear force, 326–7, 333
shear stiffness, 329, 333, 334
tensile stiffness, 328
torsional stiffness, 329
transversely loaded, 331–4
warping stiffness, 328
Sandwich plates, 169–202
boundary conditions, 172–3, 183

Sandwich plates (*continued*)
buckling of long plates, 185–7
buckling of simply supported plates, 187–8
core, 169, 170
core stiffness, 175
coupling, 176
deflection of long plates, 178–80
deflection of simply supported plates, 182–4
deformation, 171, 175–6
displacements, 169, 170, 199, 200
equilibrium, 179, 197
example, 180
examples, buckling, 186, 188, 195
examples, vibration, 198, 201
facesheet, 169
face wrinkling, 190–6
force-strain relationship, 172
governing equations, 170–2
isotropic plates, 176–8
long plates, 178–82
neutral plane, 177
orthotropic plates, 176
Poisson's ratio, 178
potential of external forces, 183
quasi-isotropic, 178
reference plane, 170–1, 177
rotation, 169, 179, 183, 199, 200
shear force, 171–2, 175, 176
shear stiffness, 172, 176, 178
stiffness, 174–8
strain, 182
strain-displacement relationship, 170–1
strain energy, 173–4, 182–3, 199–200
stress-strain relationship, 171, 175
transverse shear strain, 170
vibration, 196–202
Semimonocoque beams. *See* Stiffened beams
Shear center, 252, 283–4
of C-beams, 286, 457
example, 284
of I-beams, 295, 457
of sandwich beams, 328
of transversely loaded beams, 275, 283–4
Shear compliance
of beams with shear deformation, 320, 321–6
of box-beams, 458
of C-beams, 459
of circular cross-section beams, 458
of I-beams, 324–5, 343–4, 459
of sandwich beams, 327, 329, 334
of T-beams, 460
of Z-beams, 460
Shear deformation, effects of, 359–64
examples, 362, 363
Shear flow, 234, 275
in closed-section beams, 253, 260, 278–80, 282–3
example, 239
in I-beams, 241
in open-section beams, 276–8, 281
in stiffened beams, 290
in transversely loaded beams, 275–83
Shear force
in beams, 204
in beams with shear deformation, 319–20, 331
in laminates, 67, 68
in plates, 91
in sandwich plates, 171–2, 175, 176
in sandwich beams, 126–7, 333
Shear modulus, 13, 19, 20, 439–40, 442
Shear strain in thin-walled beams, 251, 253–4, 279
Shear stiffness
of beams with shear deformation, 320, 321, 322, 325–6
of I-beams, 318
of sandwich beams, 326, 329, 333, 334
of sandwich plates, 172, 176, 178
Shells, 365–8. *See also* Buckling of shells; Cylindrical shells
coordinate system, 365–6
curvature, 385
force-strain relationship, 366
membrane forces, 365–8, 369
membrane theory, 365, 366
meridian, 367, 368
radii of curvature, 365–6
strain, 367
stress–strain relationship, 367
Shells of revolution, 367–8
SI unit prefixes, 467
Solid-section beams under axial load and bending, 210–15
axial force, 211
bending moment, 211
centroid, 213
compliance, 212–13, 214
coordinate system, 211
curvature, 211, 215, 216
displacement, 211–14
equations, summary of, 311
example, 215
force–strain relationship, 211, 212, 213, 214, 215
neutral plane, 213
rate of twist, 212, 214
reference plane, 213
strain, 215
stress, 215
stress-strain relationship, 215
Specific heat, 448, 450
Springback, 380–4
example, 383
Spring constant, 128, 301–4, 305
Stiffened beams, 288–90
axial force, 289
bending stiffness, 289
centroid, 289

Stiffened beams (*continued*)
shear flow, 290
tensile stiffness, 289
torsion, 290
Stiffness. *See also* Bending stiffness; Shear stiffness; Torsional stiffness; Warping stiffness
of beams, 204–8
of box-beams, 273–4
constraint on, 56, 58–61
example, 21, 42
of filament wound layer, 41
of generally anisotropic material, 9, 11
of isotropic material, 21, 35, 42
of laminates, 70–3, 74, 75, 76, 78, 79, 81–8
of monoclinic material, 14, 41
of orthotropic material, 17, 34, 41
under plane-strain, 30, 33, 34–5
under plane-stress, 39–40, 41, 42–3
of ply, 69–70
of sandwich plates, 174–8
of thin-walled beams with arbitrary layup, 266–8
transformation, 53–4
of transversely isotropic material, 20, 35, 42
of woven fabric, 41
Stiffness parameter, 108, 129
Strain, 3
closed-section beams, 269, 274
hygrothermal, 44–7, 153
notation, 6
open-section beams, 234, 235, 237, 268–70, 274
sandwich plates, 182
shells, 367
solid-section beams, 215
torsion of beams, 251
summary, 57–8
transformation, of, 52–3
Strain–displacement relationship, 4–6
beams, 204, 315
cylindrical shells, 371
equations, summary of, 57
I-beams, 316
laminates, 66–7
plane-strain, 25–6, 28, 30, 33, 35, 37
plates, 90
sandwich plates, 170–1
thin-walled section beams under axial load, bending and torsion, 265
Strain energy, 55
of beams with shear deformation, 322
of buckling of plates, 112
of plates, 92, 93, 101
of sandwich plates, 173–4, 182–3
of vibrating plates, 144, 149–50, 199–200
Strength, 416, 417, 421, 423
Strength parameter, 412, 413, 416, 423
Stress, 3, 5, 6
closed-section beams, 268–70
hygrothermal, 152
laminates, 65–6
notation, 5
open-section beams, 268–70
plane-stress, 38, 39
sign convention, 4
solid-section beams under axial load and bending, 215
summary, 57–8
transformation, 49–51
Stress intensity factor, 165, 432
Stress ratio, 423–5, 428
Stress–strain relationship. *See also* Force–strain relationship
equations, summary of, 57
generally anisotropic material, 8–11
hygrothermal, 45–6, 47, 152
plane-strain, 29–30, 32, 33, 36, 37, 38
plane-stress, 39–40
sandwich plates, 171, 175
shells, 367
solid-section beams, 215, 217
torsion of beams, 251
monoclinic material, 17
orthotropic material, 17
ply, 39, 68–9
Sublaminate element, 398–410
example, 407
Surface force, 22, 24

T-beams, 217–21
bending stiffness, 219–21, 240
centroid, 219, 240
coordinate system, 217
deflection, 241
displacement, 217–18
example, 239
force–strain relationship, 242
shear compliance, 460
shear flow, 241
tensile stiffness, 219, 240, 456
torsional stiffness, 457
warping stiffness, 457
Ten percent rule, 89–90, 117, 149, 392
Tensile stiffness
of beams, 206, 207, 208, 210, 322
of box-beams, 259, 454, 455, 456
of C-beams, 285, 454, 456
of circular cross-section beams, 454, 455
of closed-section beams, 231, 232, 234, 235, 247
of I-beams, 295, 454, 455, 456
of L-beams, 223
of open-section beams, 229, 231, 232, 234, 235, 236
of sandwich beams, 328

Tensile stiffness (*continued*)
of stiffened beams, 289
of T-beams, 219, 240
Tensorial strain, 3, 6
Thermal conductivity, 446–7, 450
Thermal expansion coefficient, 44, 46, 152, 443–4, 450
Thickness, change in, 161–3
Thin plates. *See* Plates
Thin-walled beams under axial load, bending and torsion, 265–74
centroid, 271, 274
compliance, 266–8, 273–4
coordinate system, 265, 266, 267, 268
displacement, 265–7, 274
example, 272
force-strain relationship, 266, 269, 271
rate of twist, 274
restrained warping, 271
segmented wall, 265
stiffness, 266, 267, 268
strain–displacement relationship, 265
strain, 268–70, 274
stress, 268–70
Three-dimensional element, 396
Timoshenko beam, 313
Torque, 203, 253, 261, 262, 263–4
Torque neutral surface, 254, 258
Torsional stiffness
of beams, 206, 208, 210, 322
of box-beams, 256, 258, 458
of C-beams, 286, 457
of circular cross-section beams, 458
of closed-section beams, 254
of I-beams, 295, 457
of open-section beams, 250
of sandwich beams, 329
of solid section beams, 249, 250
of T-beams, 457
of beams in torsion, 249, 250, 254
of Z-beams, 457
Torsion of thin-walled beams, 248–265
boundary conditions, 264
box-beams, 255–60, 272–4
closed-section, multicell, 260–1
closed-section, single cell, 252–60
compliance, 250, 254
curvature, 251
examples, 255, 257, 272
force-strain relationship, 250, 255
I-beams, 261–4, 315–18
open-section beams, 250–2
rate of twist, 248, 249, 253, 254, 260
restrained warping, 261–4
shear flow, 253, 260
shear strain, 251, 253–4, 314, 322
stiffened beams, 290
stress–strain relationship, 251
thin rectangular cross-section beams, 248–250
torque, 253
torque neutral surface, 254, 258
torsional stiffness, 249, 250, 254
warping, 251–2
warping stiffness, 262–4
Transformations, 49–54, 69
Transversely isotropic material
compliance, 12, 14–15, 20, 35, 42–3
coordinate system, 19
description, 19
engineering constants, 13, 16, 19
under plane-strain, 34–5, 38
under plane-stress, 42–3
Poisson's ratio, 13, 19
shear modulus, 13, 19
stiffness 20, 35, 42–3
Young's modulus, 13, 19
Transversely loaded beams with shear deformation, 329–34
bending moment, 332
bending stiffness, 333
deflection, 330–4
equilibrium, 329
example, 334
sandwich beams, 331, 334
shear force, 331
shear stiffness, 333
Transversely loaded thin-walled beams, 274–80
applied loads, 274
axial force, 277
C-beams, 284–8
closed-section beams, multicell, 279–80
closed-section beams, single cell, 278–9, 282–3
equilibrium, 276, 280
examples, 284, 287
internal forces, 275–6
open-section beams, 276–8, 281
rate of twist, 275–6, 279, 280
shear center, 283–4, 275
shear flow, 275–83
shear strain, 279
Transverse shear force. *See* Shear force
Tsai–Wu failure criterion, 413
Twist
of box-beams, 257, 259, 274
of C-beams, 286–7, 288
of solid-section beams, 203
Twist moment. *See* Moments

Unidirectional test, 417–18

Vibration
of beams, 306–10
of beams with shear deformation, 347–59
circular frequencies of beams with shear deformation, 350, 352, 353, 359

Vibration (*continued*)
deflection of vibrating plates, 145, 199
equilibrium of vibrating beams, 353
equilibrium of vibrating plates, 142, 197
examples, I-beam, 310, 357
examples, plates, 143, 147, 148, 150, 198, 201
force-strain relationship, beam, 354
I-beams, of, 310–11, 357–9
inertia force, 141, 348, 353
kinetic energy of plate, 144–5
of long plates, 141–4
of long sandwich plates, 196–9
shear deformation effects, 359–62
of simply supported plates, 144–51
of simply supported sandwich plates, 199–201
strain energy of vibrating plates, 144, 149–50, 199–200
Volume, 436–7
Volume fraction, 436–7
Von Mises failure criterion, 420, 422

Warping, 251–2
Warping stiffness
of beams with shear deformation, 322
of box-beams, 458
of C-beams, 288, 457
of circular cross-section beams, 458
of I-beams, 261–4, 295, 318, 457
of sandwich beams, 328
of T-beams, 457
of Z-beams, 457
Whitney-Nuismer failure criterion, 430–4
Work done by external forces, 323
Woven fabric, 1, 2, 41–2, 43–4
example, 43

Young's modulus, 13, 19, 20
micromechanics expressions, 438–9, 442, 448–9, 450, 451–2

Z-beams, 457, 460